

AD A017201

CTU13

DS

IITRI Project J6324

Final Technical Report

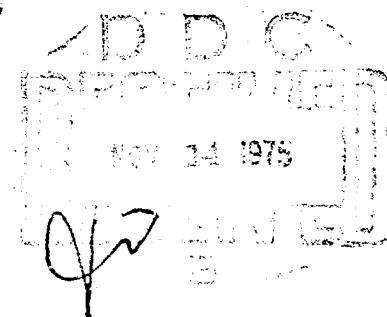
IITRI J-TR-74-6324

THERMAL MODEL OF LASER-INDUCED  
EYE DAMAGE

Contract F41609-74-C-0005

October 8, 1974

4



Approved for public release; distribution unlimited.

IITRI

Advanced concepts are being used by IIT Research Institute to solve research, development, and design problems for industry and government through contract research. Our services encompass virtually all of the physical and biological sciences. Principal areas are: chemistry, computer sciences, electronics, engineering mechanics, life sciences, mechanics of materials, medical engineering, metals, and management and social science research.

The interdisciplinary approach at IITRI brings the latest technology to bear upon the problem-solving process.

*Principal office:*

10 West 35th Street  
Chicago, Illinois 60616

Engineering Mechanics Division  
IIT Research Institute  
10 West 35th Street  
Chicago, Illinois 60616

IITRI Project J6324

Final Technical Report  
IITRI J-TR-74-6324  
THERMAL MODEL OF LASER-INDUCED  
EYE DAMAGE

Contract F41609-74-C-0005

October 8, 1974

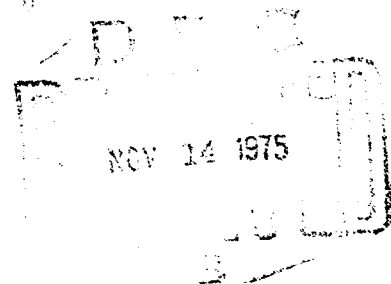
Approved for public release; distribution unlimited.

Prepared by

A. N. Takata  
L. Goldfinch  
J. K. Hinds  
L. P. Kuan  
N. Thomopoulos  
A. Weigandt

for

Aerospace Medical Division (AFSC)  
Brooks AFB, Texas 78235



UNCLASSIFIED

SECURITY CLASSIFICATION OF THIS PAGE (When Data Entered)

REPORT DOCUMENTATION PAGE		READ INSTRUCTIONS BEFORE COMPLETING FORM
1. REPORT NUMBER 14 IITRI-J-TR-74-6324	2. GOVT ACCESSION NO.	3. RECIPIENT'S CATALOG NUMBER 11 8 Oct 74
4. TITLE (and Subtitle) THERMAL MODEL OF LASER-INDUCED EYE DAMAGE		5. TYPE OF REPORT & PERIOD COVERED Final Report. Oct 1973 - Sep 1974
7. AUTHOR(s) A. N. Takata L. P. Kuan L. Goldfinch N. Thomopoulos J. K. Hinds A. Weigandt		6. PERFORMING ORG. REPORT NUMBER IITRI-J6324
9. PERFORMING ORGANIZATION NAME AND ADDRESS Engineering Mechanics Division IIT Research Institute 10 West 35th Street Chicago, Illinois 60616		8. CONTRACT OR GRANT NUMBER(s) F41609-74-C-0005
11. CONTROLLING OFFICE NAME AND ADDRESS USAF School of Aerospace Medicine (RAL) Aerospace Medical Division (AFSC) Brooks Air Force Base, Texas 78235		10. PROGRAM ELEMENT, PROJECT, TASK AREA & WORK UNIT NUMBERS 62202F 6301-00-48
14. MONITORING AGENCY NAME & ADDRESS (if different from Controlling Office) 16 AF-6301 IITRI-J6324		12. REPORT DATE September 1974
		13. NUMBER OF PAGES 398
		15. SECURITY CLASS. (of this report) Unclassified
		15a. DECLASSIFICATION/DOWNGRADING SCHEDULE
16. DISTRIBUTION STATEMENT (of this Report) Approved for public release; distribution unlimited. 17 6301001 12 411		
17. DISTRIBUTION STATEMENT (of the abstract entered in Block 20, if different from Report)		
18. SUPPLEMENTARY NOTES		
19. KEY WORDS (Continue on reverse side if necessary and identify by block number) Ocular Damage Laser Effects Thermal Model Temperature Rise Prediction Retinal, Corneal, Lenticular Damage		
20. ABSTRACT (Continue on reverse side if necessary and identify by block number) This report describes the development of computerized models for predicting the temperatures and thermal damage (protein denaturation) caused by the exposure of eyes to laser beams. The extent of thermal damage or the threshold level for thermal damage may be predicted either for the cornea, lens or retina of the eye -- wherever the energy deposition is greatest. Included in the report is (continued)		

DD FORM 1 JAN 73 1473 EDITION OF 1 NOV 65 IS OBSOLETE

UNCLASSIFIED

SECURITY CLASSIFICATION OF THIS PAGE (When Data Entered)

404 502



UNCLASSIFIED

SECURITY CLASSIFICATION OF THIS PAGE(When Data Entered)

Item 20. continued *fr*

*P1473A)*

a description of the models and data for predicting the thermal damage to monkey and human eyes for known laser exposures.

*1000.*

Model predictions were found to be in reasonably good agreement with experimental results for pulse durations ranging from about  $10^{-7}$  sec to  $10^3$ . However, major discrepancies arise with pulses less than about  $10^{-7}$  sec. With such short pulses, the predicted temperature rises are much too small to cause thermal damage. Therefore, some other damage mechanism appears responsible for the damage caused by the very short pulse. At present, the mechanism of damage has not been identified.

*10 to the minus 7th power*

*10 to the minus 7th power*

UNCLASSIFIED

SECURITY CLASSIFICATION OF THIS PAGE(When Data Entered)

## PREFACE

This report describes the development of the Corneal and Retinal models for predicting the temperature rises and thermal damage produced in the eye by laser exposures. IIT Research Institute personnel involved in the program were A. N. Takata, L. Goldfinch, J. K. Hinds, L. P. Kuan, Y. Shikari and A. Weigandt. The project monitor was Capt. D. Egbert of the AMD School of Aerospace Medicine's Radiobiology Division, Laser Effects Branch (SAM/RAL) at Brooks AFB, San Antonio, Texas.

Work presented in this report represents the combined efforts of IITRI with various Brooks AFB personnel. Particularly notable is the excellent guidance and support efforts provided by Dr. Ralph Allen and Capt. David Egbert of Brooks AFB.

## TABLE OF CONTENTS

	<u>Page</u>
1. INTRODUCTION	1
2. LITERATURE	6
3. OPTICAL STUDIES	7
3.1 Irradiance Profiles Produced by Refraction of Laser Beam by Cornea	8
3.2 Retinal Image	10
3.3 Check of Optical Analysis	12
4. THERMAL STUDIES	15
4.1 Grid System	15
4.2 Energy Deposition	17
4.3 Use of Implicit Explicit Alternating Direction Technique for Predicting Transient Temperatures	17
4.4 Blood Flow	19
4.5 Melanin Granules	20
4.6 Typical Temperature Rises	22
5. DAMAGE CRITERIA	25
5.1 Thermal Damage	25
5.2 Mechanical Damage	26
6. OPTICAL, THERMAL, AND LESION DATA	27
6.1 Optical Properties Associated with the Eyes of Man and the Rhesus Monkey	27
6.1.1 Absorption and Reflection Coefficients	27
6.1.2 Index of Reflection	33
6.2 Thermal Property Data	33
6.3 Thicknesses of Eye Media	34
6.4 Experimental Ocular Threshold Data	35
7. COMPUTER CODES	40
7.1 Retinal Model	41
7.1.1 Main Program for Retinal Model	41
7.1.2 Subroutine Grid for Retinal Model	55
7.1.3 Subroutine Image of Retinal Model	57

## TABLE OF CONTENTS (contd)

	<u>Page</u>
7.1.4 Subroutine HTXDEP of Retinal Model	60
7.1.5 Subroutine MXGRAN of Retinal Model	63
7.1.6 Subroutine BLOOD of Retinal Model	66
7.2 Corneal Model	68
7.2.1 Main Program for Corneal Model	68
7.2.2 Subroutine GRID for Corneal Model	82
7.2.3 Subroutine IMAGE of Corneal Model	83
7.2.4 Subroutine HTXDEP of Corneal Model	86
7.2.5 Subroutine MXGRAN for Corneal Model	88
7.3 Description of Code for Preparing 2D and 3D Illustrations	88
8. MODEL PREDICTIONS, AND SENSITIVITY AND ERROR ANALYSES	89
8.1 Model Predictions of Laser Power Necessary to Cause Given Lesion Sizes	89
8.1.1 Predictions of Corneal Damage	89
8.1.2 Predictions of Retinal Damage	93
8.2 Sensitivity Runs	94
8.2.1 Corneal Model	95
8.2.2 Retinal Model	100
8.3 Assessment of Frequency Distribution of Errors Associated with Predicted Laser Power	101
9. SUMMARY AND CONCLUSIONS	108
9.1 Consequence of Parametric Errors	108
9.2 Comparison of Model Predictions with Experimental Data	109
9.3 Problem Areas	110
REFERENCES	111
APPENDIX A - Computational Scheme for Predicting Eye Temperatures	
APPENDIX B - Thermal Effects Caused by Blood Flow	
APPENDIX C - Decay of Normalized Temperature Rises of Melanin Granules with Time	
APPENDIX D - Assessment of Temperatures Caused by Multiple Pulses Using Single-Pulse Temperature Predictions	
APPENDIX E - Choice of Time Intervals	

## TABLE OF CONTENTS (concl)

- APPENDIX F - Heat Deposition Analyses
- APPENDIX G - Optical Properties of Eyes of Man and Rhesus Monkey
- APPENDIX H - Retinal Irradiance Profile
- APPENDIX I - Grid System
- APPENDIX J - Measuring Uncertainties in Predicted Laser Powers to Cause Damage
- APPENDIX K - Nomenclature, Sample Data, Code Listing, and Sample Run for Retinal Model
- APPENDIX L - Nomenclature, Sample Data, Code Listing, and Sample Run for Corneal Model
- APPENDIX M - User Manual for Preparing 2D and 3D Illustrations of Temperature Rise Profiles
- APPENDIX N - Literature Bibliography

# LIST OF FIGURES

<u>Figure</u>		<u>Page</u>
1	Schematic Illustration of Principal Components of Eye	5
2	Nomenclature for Determining Laser Profile after Corneal Refraction	9
3	Schematic for Evaluating W	13
4	Grid System Used by Corneal and Retinal Models	16
5	Decay of Normalized Temperature Rises of Melanin Granules Following an Instantaneous Deposition of Energy	21
6	Axial Temperature Profiles at End of Single Pulses	23
7	Radial Temperature Profiles at End of Single Pulses	24
8	Schematic Illustration of Principal Routines of Retinal Model	42
9	Flow Diagram of Main Program of Retinal Model	43
10	Schematic Illustration of Principal Routines of Corneal Model	69
11	Flow Diagram of Main Program of Corneal Model	70
12	Frequency Distribution of Errors in Predicted Power for Corneal Model for Beam Size of 0.0350 cm	103
13	Frequency Distribution of Errors in Predicted Power for Corneal Model for Beam Size of 0.0250 cm	104
14	Frequency Distribution of Errors in Predicted Power for Retinal Model for Beam Size of 0.0300 cm	105
15	Frequency Distribution of Errors in Predicted Power for Retinal Model for Beam Size of 0.0025 cm	106

# LIST OF TABLES

<u>Table</u>		<u>Page</u>
1	Physiological Parameters Required for Optical Analysis	14
2	Comparison of Predicted and Experimental Retinal Image Radii for Gaussian Laser Profiles	14
3	Summary of Optical Data for Retinal Model (Rhesus Monkey)	28
4	Summary of Optical Data for Retinal Model (Caucasian)	29
5	Summary of Optical Data for Retinal Model (Negro)	30
6	Absorption Constants for Water	31
7	Index of Refraction Versus Wavelength for Water	33
8	Thickness of Eye Media	34
9	Experimental Data for Retinal Damage in Rhesus Monkey Eyes	36
10	Experimental Data for Corneal Damage in Rhesus Monkey Eyes	39
11	Comparison Between Computer and Experimental Laser Powers (Total) and Lesion Sizes Associated with Corneal Damage	90
12	Comparison Between Predicted and Experimental Laser Powers (Total) to Cause Specified Lesions on Retina	91
13	Effect of Varying Individual Parameters on Total Laser Power to Initiate Corneal Damage for Four Different Laser Exposures ( $\lambda = 2727 \text{ nm}$ )	96
14	Effect of Varying Individual Parameters on Total Laser Power to Initiate Retinal Damage for Four Different Laser Exposures ( $\lambda = 1060 \text{ nm}$ )	97
15	Rates of Thermal Damage Versus Temperature	99
16	Confidence Intervals Associated with Predicted Laser Power	102

## THERMAL MODEL OF LASER-INDUCED EYE DAMAGE

### 1. INTRODUCTION

This is the final report of the contract entitled "Thermal Model of Laser-Induced Eye Damage" and covers the work performed by IIT Research Institute (IITRI) from October 1973 through September 1974. The principal objective of the program was to select and develop mathematical models for predicting eye damage caused by exposure to lasers. The laser exposures of concern involve various wavelengths, beam geometries and intensities, as well as pulse lengths, number of pulses, and repetition rates. Predictions of eye damage involve either threshold lesions or the extent of damage. These capabilities were achieved by

- Reviewing the literature for pertinent
  - thermal and optical analytical techniques
  - optical and thermal property data
  - experimental temperature and damage data
- Developing a model (Retinal model) for predicting temperatures and damage in and about the retina
- Developing a model (Corneal model) for predicting the temperatures and damage to the cornea and lens
- Checking models by comparing predictions against experimental data
- Assessing sensitivity of predictions to input variables
- Evaluating consequences of estimated errors in input variables on total laser power necessary to cause eye damage

These models allow for variations in laser exposures described in terms of

- wavelength
- pulse duration
- repetition rate
- number of pulses



- beam profile
- laser power on the cornea
- beam divergence

Major assumptions used to develop the models are:

- simulation of eye geometries by polar coordinates
- use of retinal image at all depths of the eye in the Retinal model
- all reflected radiation considered to move along axial directions
- use of rates of damage pertaining to skin for retinal, corneal and lens damage
- radiation is coherent and defocus can be calculated via geometric optics

A summary of the model capabilities is presented below:

#### Input

1. User inputs thermal, optical, and physiological properties of desired layers for human or monkey
2. User specifies beam characteristics, at the cornea (or at the retina if desired): total power, beam diameter, divergence (or the distance from the nearest beam waist)
3. User specifies the range of spatial coordinates for damage calculations, printouts of temperature rise histories and/or 3D plotting of temperature rises

#### Output

1. Damage thresholds at specified spatial coordinates
2. Prediction of the extent of damage for input power as a function of depth and radius
3. Prediction of temperature-rise time histories as a function of depth and radial position
4. Prediction of thresholds for preselected peak temperature rises in the pigment granules
5. 3D or 2D plots of temperature rises
6. Retinal image distribution calculated by optical routine

Innovations Compared to Original Tech. Inc. Model  
(Refs. 1, 52)

1. Damage is predicted by integrating a damage rate function over the time history of the temperature rises of selected points to determine their threshold levels and then the extent of damage
2. Possible to validate model predictions with threshold, extent of lesion and temperature measurements
3. Automated optimum selection of temporal and spatial grid elements, their extent and configuration for input physiological and beam parameters, to include automated handling of repetitive pulse exposures
4. Optical routine available to predict retinal or lenticular beam characteristics based on beam description at the cornea and distance of the last beam waist
5. Blood flow in chorio-capillary and surrounding tissue incorporated into heat flow - temperature rise calculations
6. Granular structure provided in pigment epithelial layer to simulate the melanin granule absorption. The same structure is available but not used for the cornea
7. Able to adjust the position and thickness of the melanin granule structures within the PE to accommodate simulation of both human and monkey retina
8. Simple selection of spatial coordinates for temperature rise history and threshold predictions output
9. Documented collection of appropriate thermal, optical, and physiological parameter values necessary to determine damage to human and monkey eyes.
10. Calculated predictions comparable with representative threshold data for retina and cornea
11. Can run a number of test exposures at once where pulse repetition rate and numbers of pulses (or train length) can be varied

In the remainder of this report all aspects of the development of computer codes for the thermal models are discussed and a comparison is made between predictions with experimental results. Detailed analytical studies and information are included in appendices as well as documentation of a code developed by IITRI for preparing 2D and 3D illustrations of the temperature rise profiles.

Figure 1 illustrates principal components of the eye. Except for the pigment epithelium and the underlying chorio-capillaris, all components have relatively substantial thicknesses. Periodically within this report, we shall refer to these eye media.

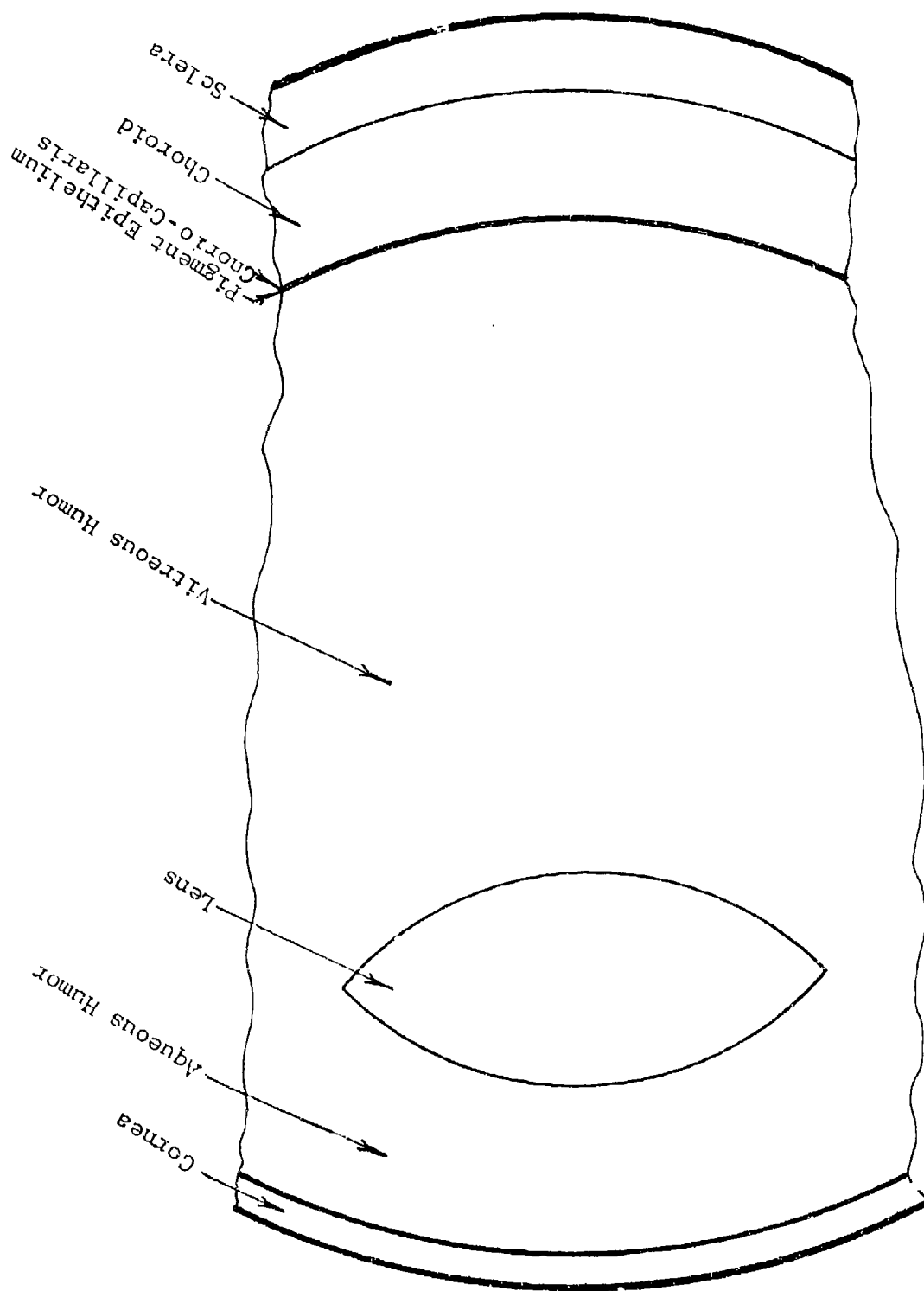


Fig. 1 SCHEMATIC ILLUSTRATION OF PRINCIPAL COMPONENTS OF EYE

## 2. LITERATURE

Before formalizing the computer codes, the literature was searched for means and information with which to base the models. This literature search pertained to

- Schemes for predicting laser deposition of energy within eye
- Schemes for predicting the transfer of heat within the eye by heat conduction or the flow of blood
- Thermal and optical property data for human and animal eyes
- Experimental laser-induced temperature and threshold damage data with which to check and refine predictions

The literature study involved searching for recent articles of interest and using the resultant lists of references to identify earlier articles. All reference titles have been placed on computer cards to speed revision and listing of articles pertaining to important subject areas. The result is the list of references shown in Appendix N, arranged according to the following subjects:

- thermal models
- optical models
- thermal properties
- optical properties
- blood effects
- threshold damage criteria
- experimental temperature data
- experimental damage data
- melanin granules
- miscellaneous

A very significant portion of the models is based on information found in the literature as well as that provided by SAM/RAL of Brooks Air Force Base.

### 3. OPTICAL STUDIES

Due to differences in the absorption constants of the various media of the eye with wavelength, there are considerable differences in the locations at which the lasers deposit their energy within the eye. Peak depositions may occur either in the cornea, lens or retina. For this reason, two models were developed -- one for retina damage (Retinal model), and one for cornea and lens damage (Corneal model).

In each model, the optical calculations are initiated by a determination of the refraction of the laser beam by the cornea. The result is a description of the irradiance as a function of radius and depth from the anterior surface of the cornea to the pupil and beyond. The resultant irradiance profile is then used directly by the Corneal model with appropriate provisions for absorption and reflection to assess the rate of energy deposition in the cornea, aqueous humor, lens and vitreous humor.

On the other hand the Retinal model utilizes the above analysis to assess the irradiance profile at the pupil of the eye. This profile is then used by the optical analysis described in Section 3.2 to determine the retinal profile. The resultant irradiance distribution of the retinal image is preserved at all depths of the eye and tissues analyzed by the Retinal model. Each model will accept any symmetric laser profile at the cornea. This includes uniform, gaussian or irregular profiles.

In the Retinal model, the user has two options for the irradiance profile at the retina. The first is to calculate the irradiance profile using parameters describing the incident laser beam and the eye; while the second is to use experimental measurements of the profiles. Similarly, two options are provided in the Corneal model, depending on whether one wishes to assess cornea or lens damage. In order to ensure accurate burn predictions, each model concentrates the finer mesh grid in the region of the eye at which the greatest temperatures and temperature gradients are anticipated.

In the remainder of this section we shall discuss means for calculating irradiance profiles from the cornea to the lens. Then we shall discuss imaging the laser beam onto the retina accounting for spherical and chromatic aberrations.

### 3.1 Irradiance Profiles Produced by Refraction of Laser Beam by Cornea

Laser beams can be reduced in diameter by as much as a factor of 1.2 in traveling from the cornea to the lens due to refraction by the cornea. This can cause an appreciable increase in the peak irradiance incident upon the lens and thereby increase the possibility for lens burns. Also, if the beam is appreciably reduced in size at the pupil, significant changes can occur in the retinal image.

The first step in analyzing the effect of the cornea on the beam is to determine the imaginary depth at which the beam would be focused solely by cornea. This depth exceeds the depth of the retina as illustrated by Fig. 2. The depth  $z_f$  shown in this figure is given by

$$z_f = n \cdot z_o \cdot f_c / (n \cdot z_o - f_c) \quad (1)$$

subject to the condition that  $n \cdot z_o > f_c$ , where

$f_c$  = focal length of cornea

$n$  = index of refraction of ocular media

$z_o$  = distance between laser's waist and pupil

Here  $z_o$  may be approximated by dividing the beam diameter at the cornea by the total beam divergence expressed in radians. More accurate determinations of  $z_o$  require measurements of the width of the beam at 2 or more axial locations. The above condition has been found to hold for all AFSC experiments to date.

To determine the irradiance profiles between the cornea and lens, we shall neglect the curvature of the cornea and utilize linear interpolation based on the triangle formed by the two entrance points and the imaginary focal point. Here it is readily

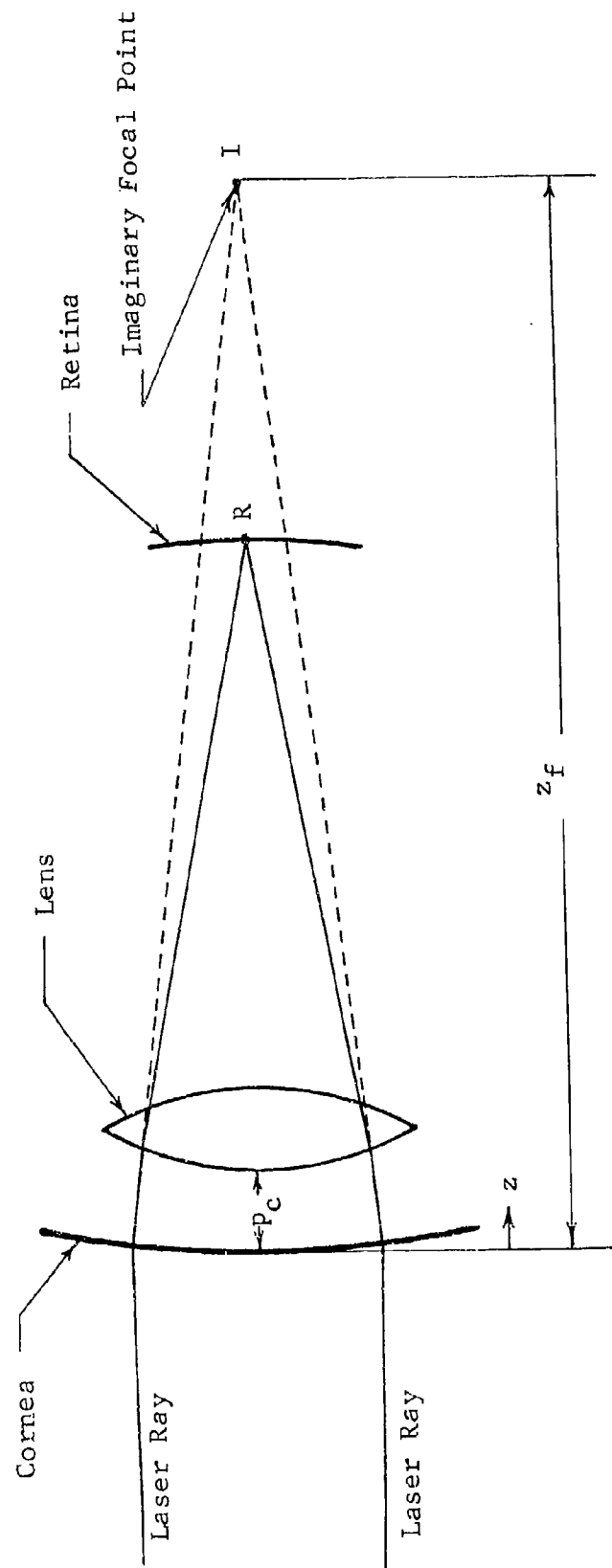


Fig. 2 NOMENCLATURE FOR DETERMINING LASER PROFILE AFTER CORNEAL REFRACTION



seen that incident rays at a radial distance  $r$  are displaced to radial distances  $\xi \cdot r$  upon entering the eye where  $\xi$  depends on the depth  $z$  as follows

$$\xi = 1 - z/z_f \quad (2)$$

This means that a laser profile of  $P_c(r)$  at the surface of the cornea will assume a shape  $P_c(r/\xi)$  upon entering the eye, where  $\xi > 0$ . Moreover, conservation of energy for the case of no absorption requires that the total power in the incident beam equals that of the refracted beam. Thus, if the refracted beam is described by  $C' \cdot P_c(r/\xi)$ , then

$$\begin{aligned} \int P_c(r) \cdot 2 \cdot \pi \cdot r \, dr &= C' \cdot \int P_c(r/\xi) \cdot 2 \cdot \pi \cdot r \, dr \\ &= C' \cdot \xi^2 \int P_c(r') \cdot 2 \cdot \pi \cdot r' \, dr' \end{aligned} \quad (3)$$

so that the constant  $C'$  is given by

$$C' = 1/\xi^2 \quad (4)$$

Based on the above, the irradiance  $P(r,z)$  at points  $r,z$  is given by

$$P(r,z) = P_c(r/\xi)/\xi^2 \quad (5)$$

Thus to determine the profile at a depth  $z$ , one first evaluates  $z_f$  and  $\xi$  using Eqs. 1 and 2, and then substitutes the resulting value for  $\xi$  into Eq. 5.

### 3.2 Retinal Image

The first step in computing the distribution of the irradiance  $H(r)$  at the retina is the determination of the profile  $P_p(r)$  at the pupil plane given by

$$P_p(r) = P_c(r/\xi)/\xi^2 \quad (6)$$

where

$$\xi = 1 - p_c/z_f$$

$p_c$  = distance of pupil from cornea (see Fig. 2)

The normalized irradiance at the retina is then given by (Appendix H)

$$\frac{H(r)}{H(0)} = \left| \frac{1}{\lambda \cdot f'} \int_0^a \sqrt{P_p(\rho)} \cdot J_0\left(\frac{2\pi \cdot r \cdot \rho}{\lambda \cdot f'}\right) \cdot F_1(\rho) \cdot F_2(\rho) \cdot \rho \, d\rho \right|^2 \quad (7)$$

where

$a$  = pupil radius, cm

$f' = f_0 - p$

$f_0$  = second principal focal length at a reference wavelength of  $\lambda_0$

$F_1(\rho)$  = function accounting for defocusing (chromatic and geometric)

$F_2(\rho)$  = function accounting for spherical aberration

$J_0$  = zero order Bessel function of first kind

$p$  = distance of pupil from second principal plane, cm

$r$  = radial distance in retinal plane, cm

$\lambda$  = wavelength, nm

$\rho$  = radial distance in pupil plane, cm

In Eq. 7 the functions  $F_1(\rho)$  and  $F_2(\rho)$  are given by:

$$F_1(\rho) = \exp(i \cdot C_0 \cdot \rho^2) \quad (8)$$

$$F_2(\rho) = \exp(i \cdot C_2 \cdot \rho^4) \quad (9)$$

while the constants  $C_0$  and  $C_2$  are given by

$$C_0 = \frac{2\pi n}{\lambda \cdot a^2} W = \frac{2\pi n}{\lambda \cdot a^2} [-f' - \Delta z \cdot (1 - \cos \alpha) + (f'^2 - \Delta z^2 \sin^2 \alpha)^{\frac{1}{2}}] \quad (10)$$

$$C_2 = -3 \cdot 10^6 / \lambda$$

where

$\alpha$  = angle between the refracted beam at the cornea and the axis of the eye

$n$  = index of refraction at wavelength  $\lambda$

$p$  = distance of pupil from second principal plane

$z_0$  = distance of pupil from waist of laser beam, cm

The incremental distances  $W$  and  $\Delta z$ , the angle  $\alpha$ , and the focal length  $f$  are illustrated in Fig. 3. The distance  $W$  is expressed by Eq. 10 while  $\alpha$ ,  $\Delta z$  and  $f$  may be obtained from the following equations:

$$f = f_0 \cdot n(n_0 - 1) / n_0(n - 1) \quad (11)$$

$$\tan \alpha = a / (f' + \Delta z) \quad (12)$$

$$\Delta z = \frac{n \cdot z_0 \cdot (f/f_0)}{n \cdot (z_0/f_0) - (f/f_0)} - f_0 \quad (13)$$

where

$f$  = focal length at laser's wavelength, cm

$n_0$  = index of refraction at a reference wavelength  $\lambda_0$ , cm

Constants required for the optical analyses are presented in Tables 1 and 7.

### 3.3 Check of Optical Analysis

To ensure a comprehensive check of the optical analysis, eight experiments were chosen representing a wide variety of conditions. Experimental and predicted results for the image radius ( $1/e^2$  point) are given in Table 2.



TABLE 1  
PHYSIOLOGICAL PARAMETERS  
REQUIRED FOR OPTICAL ANALYSES (derived from Ref. 17)

Parameter	Values of Parameters, cm	
	<u>Human Eye</u>	<u>Monkey Eye</u>
a	0.35	0.35
$f_o$ (at $\lambda_o = 500$ nm)	2.24	1.68
p	0.135	0.12
$f_c$	3.12	2.43
$p_c$	0.31	0.29

TABLE 2  
COMPARISON OF PREDICTED AND EXPERIMENTAL  
RETINAL IMAGE RADII FOR GAUSSIAN LASER PROFILES

Run Number*	Beam Radius, at Cornea ( $1/e^2$ points), cm	$z_o$ , cm	$\lambda$ , nm	Image Radius, at $1/e^2$ points, cm	
				Exp.	Calc.
11	0.135	270.	530.0	.0025	.0013
51	0.075	118.	514.5	.0025	.0009
52	0.180	600.	514.5	.0025	.0009
59	0.144	533.	520.8	.0025	.0009
60	0.124	310.	647.1	.0025	.0024
61	0.125	12.8	647.1	.0140	.0179
64	0.125	7.50	647.1	.0225	.0288
66	0.125	3.17	647.1	.0525	.0523

\*See Table 9 for a description of experiments.

From a comparison of the experimental and calculated image radii, one can see that all five predictions of the radii of the smaller experimental images are less than their experimental counterparts of 25  $\mu$ m. The source of this discrepancy is not known. Very appreciable changes in the constant  $C_2$  (which could be in error by as much as 50 percent) had a negligible effect on the small images.

#### 4. THERMAL STUDIES

In this section we shall review means for calculating the deposition and transport of heat starting with a knowledge of the laser's profile within the eye which has been covered in Section 3 and Appendix H. Each model

- selects the grid network for predicting the deposition and transport of heat which consists of a network of points located at various radii and depths,
- computes the deposition rates of energy per unit volume at each of the grid points,
- computes the transport of heat by thermal conduction.

In addition the Retinal model

- computes the absorption and transport of heat by blood flow
- computes the temperature rises of melanin granules in the pigment epithelium (PE)

##### 4.1 Grid System

The grid system chosen for performing the temperature calculation is shown in Fig. 4. Here the front of the eye is located at the left-hand side of the network while the axis of the eye is located at  $R(1)=0$ . In each model, the fine portions of the grid are located at regions of greatest temperature rise. In the Retinal model this region would be at the retina while in the Corneal model the region would either be in the cornea or lens depending on where the temperatures are greatest. Within the finer grid, each of the spacial steps DR and DZ are uniform. Beyond this region the spacial increments are sequentially increased by the constant factors  $R_1$  and  $R_2$  as illustrated below

$$\begin{aligned} Z(i+1)-Z(i) &= R_1 \cdot (Z(i)-Z(i-1)) \\ R(j+1)-R(j) &= R_2 \cdot (R(j)-R(j-1)) \end{aligned} \tag{14}$$

The choice of a constantly expanding network away from the region of highest temperature was made to conserve on computational time. In addition the size of the smallest elements was varied according to the magnitude of the anticipated temperature gradients.

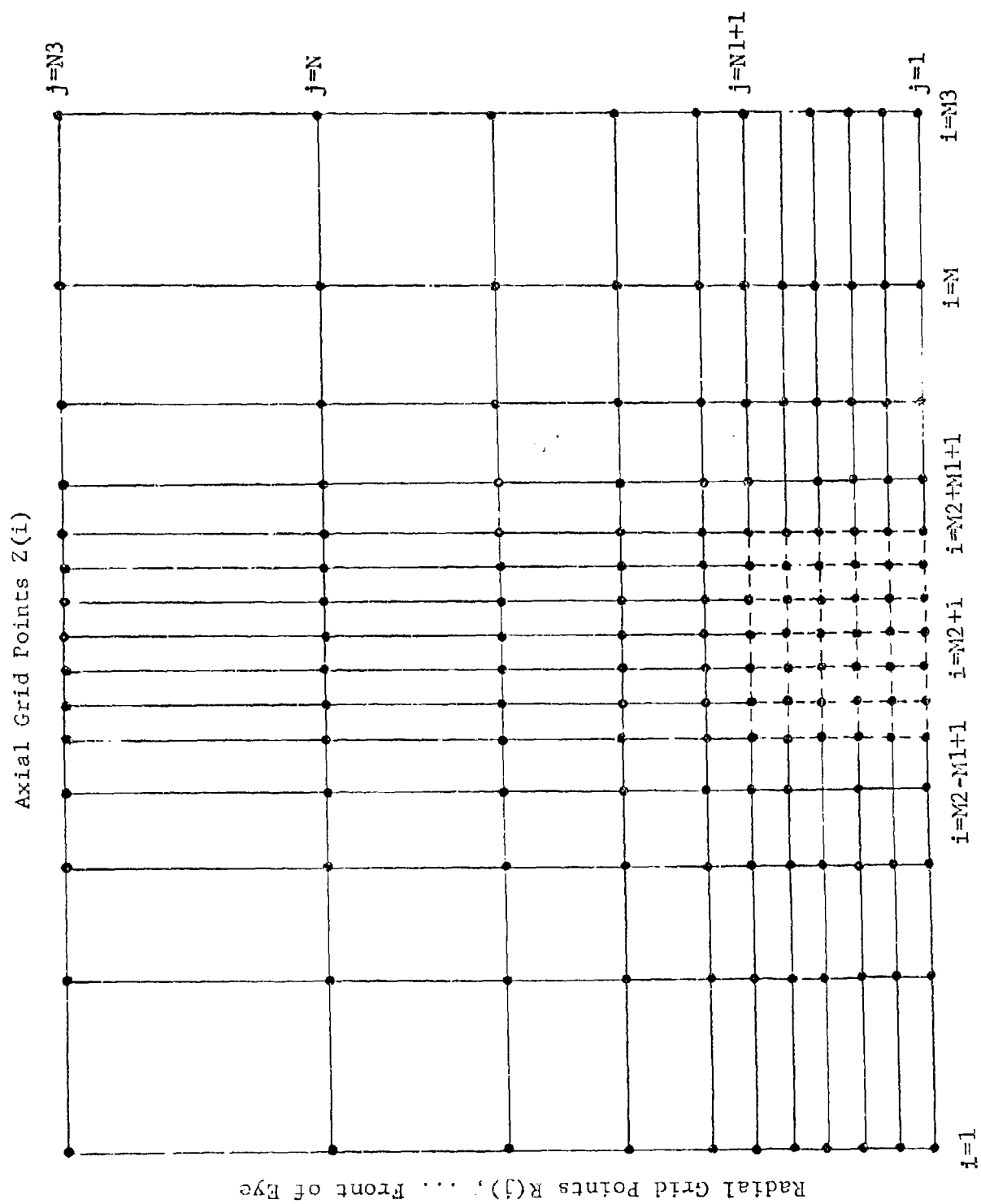


Figure 4 GRID SYSTEM USED BY CORNEAL AND RETINAL MODELS

In this regard the spacial increments are increased in size with the pulse duration. Moreover, in the Corneal model the increments are decreased with increased absorption coefficients. A detailed description of the means used to arrive at the grid system is given in Appendix I.

#### 4.2 Energy Deposition

Having established the shape of the laser beam within the eye, the next problem is to determine where the laser's energy is deposited within the eye. With this purpose in mind six different eye media are provided in each model. These eye media are distinguished according to:

- thicknesses
- absorption coefficients
- total reflections at the various interfaces

All reflected radiation is considered to move in axial directions. Multiple reflections are considered of secondary importance and neglected. Energy deposition is computed using Lamberts Law at the various grid points described in the previous section. The deposition of energy is considered to be uniformly dispersed throughout each spacial increment. A description of the means used to calculate the rates of energy deposition is presented in Appendix F.

#### 4.3 Use of Implicit Explicit Alternating Direction Technique for Predicting Transient Temperatures

Temperature predictions for single pulses are made using the scheme developed by Technology, Inc. (Refs. 1,52). This scheme is based on the work of Peaceman (Ref. 2) and evaluates the consequence of heat conduction using finite-difference solutions of parabolic equations. This is accomplished by solving the finite-difference equation explicitly in  $z$  (axial direction) and implicitly in  $r$  (radial direction) for odd time steps; and implicitly in  $z$  and explicitly in  $r$  for even time steps. The implicit representation of the thermal gradients involves using future temperatures while the explicit representation of the thermal gradients involves using existing temperatures. The result is two sets of equations which are solved using ordinary matrix algebra.



The primary advantage of this method is that the time steps may be one or more orders of magnitude larger than those required by standard explicit methods. Solutions are stable provided the time steps are not excessively large during periods of sudden changes in the deposition of energy, such as at the start and end of a pulse. To ensure accurate temperature predictions, the time steps and spacial steps must be chosen consistent with the thermal gradients (See Appendix E). This finite-difference technique is used to predict temperature rises at specific locations of the eye during and following a single pulse.

In order to minimize the execution times of the computer codes, it is important to use the largest time intervals possible consistent with accurate temperature predictions. For this reason an analysis was conducted to establish how these time intervals should be chosen. This analysis is described in Appendix E and indicates that progressively larger time intervals may be used as the temperature gradients diminish with time. As shown in Appendix E these time intervals may be increased sequentially by a factor XC as illustrated below:

$$\Delta t_{k+1} = XC \cdot \Delta t_k \quad (15)$$

where the first time interval  $\Delta t_1$  should be chosen such that it is of the order of the times required by purely explicit finite-difference solutions and the factor XC may assume values from 1 to 1.4 (See Appendix E).

The above technique for computing the time intervals guards against excessively large errors that may not be obvious to the user in that the alternating-direction, implicit, explicit technique is usually stable even for excessively large time steps.

A major limitation of using constantly expanding time steps occurs when one considers multiple pulses. Direct application of the method to multiple pulses would require regular time steps during each pulse. Use of regular time steps throughout the exposure will cause enormous computational times because of the relatively large times between pulses. Thus, the finite-difference predictions of the temperature rise are confined to single pulse exposures.

Instead, a more efficient method was developed for computing the temperature rises from multiple pulses. This method is described in Appendix D and involves adding the temperature contributions from each pulse provided by the finite-difference computations. Here, of course, it is necessary to account for the differences in elapsed time. To illustrate the method used for multiple pulses, let us represent the temperature rise prediction from a single pulse at a particular point by  $T(t)$ . Then the temperature rise following a second pulse is given by

$$T(t) + T(t-\tau) \quad (16)$$

where  $\tau$  represents the time period from the start of the first pulse to the start of the second pulse. Temperature rises from the various pulses can be added because all the terms in the heat conduction and its subsidiary equations are linear in  $T$  (See Appendix D)

When the times  $t$  are less than the interval  $\tau$ , the second term of Eq. 16 is zero and the temperature is  $T(t)$ . For exceptionally large time intervals  $\tau$  wherein  $T(\tau) \neq 0$ , the temperatures during the second pulse are essentially the same as those during the first pulse.

#### 4.4 Blood Flow

In the Retinal model account is also made for the transport of heat by blood flow. Two regions of blood flow are considered. The first is the chorio-capillaris layer beneath the pigment epithelium, while the second is the blood flow through tissues surrounding the eye.

Blood is considered to enter the chorio-capillaris layer through major blood vessels at the ambient temperatures of the eye. Once blood enters the chorio-capillaris it is diverted into numerous small blood vessels of various sizes and paths. Thereafter, thermal equilibrium is considered to exist between the blood and tissues through which it flows. The immediate effect of the blood flow is to abstract sufficient heat to raise its temperature to that of the spacial increment within which it enters. Additionally,

radial blood flows can transport heat as they move through regions of differing temperatures. The resultant radial transport of heat depends upon the flow of blood, the temperature gradients and the specific heat of blood. Radial flows are controlled through values assigned the artificial blood flows entering and leaving the chorio-capillaris at various radial distances.

Consideration is also given to the thermal effects of blood flow within tissues surrounding the eye. In this case the blood is assumed to enter the tissues at the ambient temperatures of the tissue and leave at the temperature of the tissue. Here the transport of heat between grid elements by blood flow is of secondary importance and therefore is neglected.

#### 4.5 Melanin Granules

To estimate the temperatures of the melanin granules within the pigment epithelium (PE), it is necessary to take advantage of the fact that the granules lose their temperature much more rapidly than the PE grid increments within which they lie. This allows one to treat the granules separately from the PE grid increments. To predict the granule temperatures, calculations are made describing how an increment's heat is partitioned between the granules and its surroundings with respect to time.

To provide such determinations, two sets of calculations must be made. The first is to subdivide the pulse into a number of incremental pulses short enough so that essentially no heat is transferred from the granule to its surroundings during the incremental pulse. For this purpose we have chosen a time of  $0.3 \cdot 10^{-8}$  sec for the incremental pulses. If no further heat were deposited into the granules, then their normalized temperature rise would decay in time as shown in Fig. 5. After a relatively short time of about  $5 \cdot 10^{-7}$  sec there would be essentially no difference between the temperatures of the granules and their immediate surroundings.

To account for additional heat deposition from several incremental pulses, it is necessary to add the temperature contributions

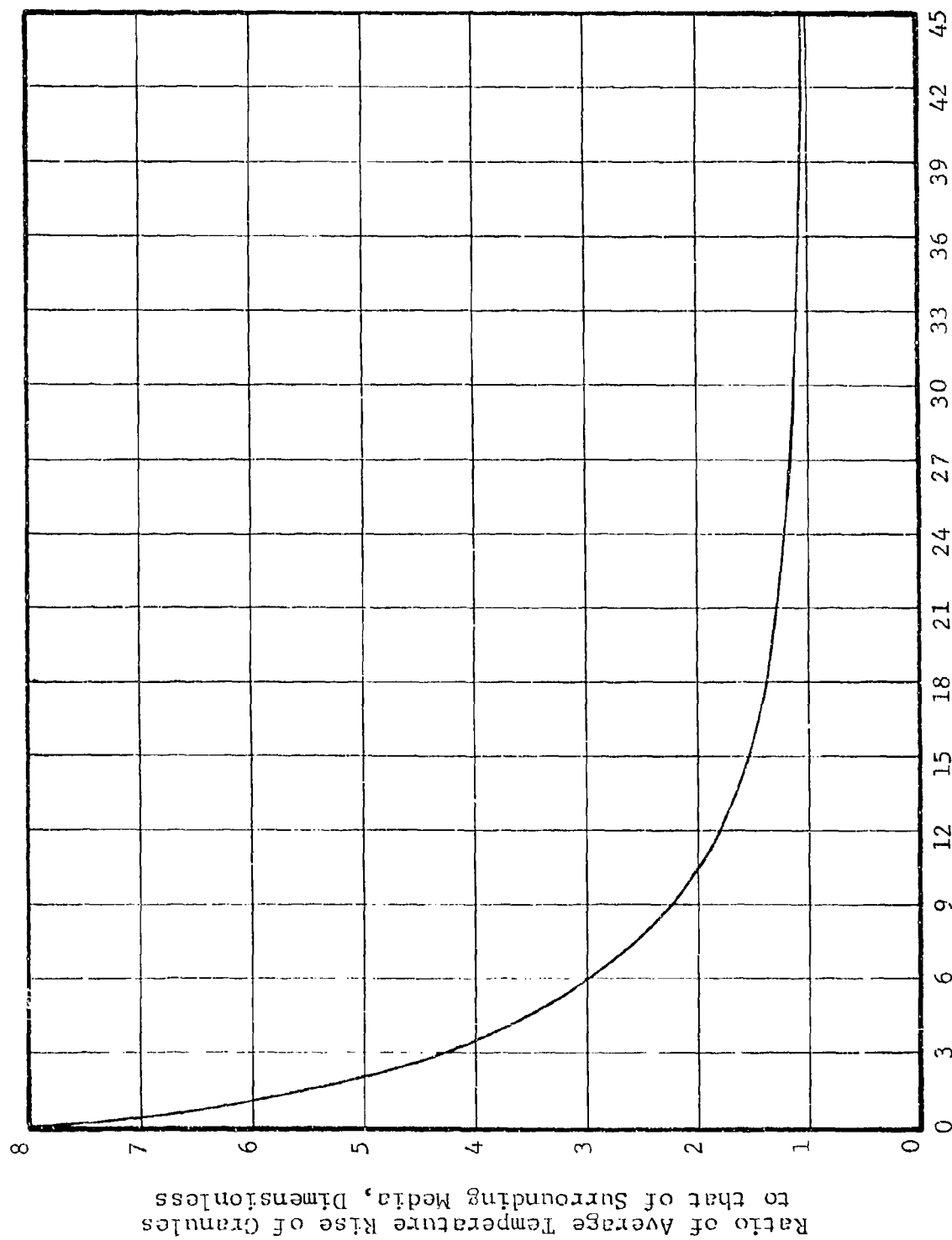


Fig. 5 DECAY OF NORMALIZED TEMPERATURE RISES OF MELANIN GRANULES FOLLOWING AN INSTANTANEOUS DEPOSITION OF ENERGY

from each incremental pulse allowing for differences of elapsed time. These time-dependent results are then divided by the number of incremental pulses and multiplied by the temperature rise of the spacial increment to arrive at the actual temperature rise of the granules.

#### 4.6 Typical Temperature Rises

To acquaint the reader with the magnitude of the temperature rises needed to thermally damage the eye, we have chosen three widely different pulse durations. The temperature rises at the end of the pulses are shown in Figs. 6 and 7. Figure 6 shows the temperature profiles in the axial direction at the end of pulses of duration  $1.5 \cdot 10^{-8}$ ,  $4.0 \cdot 10^{-2}$ , and 1000 sec. Figure 7 shows the corresponding temperature profiles in the radial direaction.

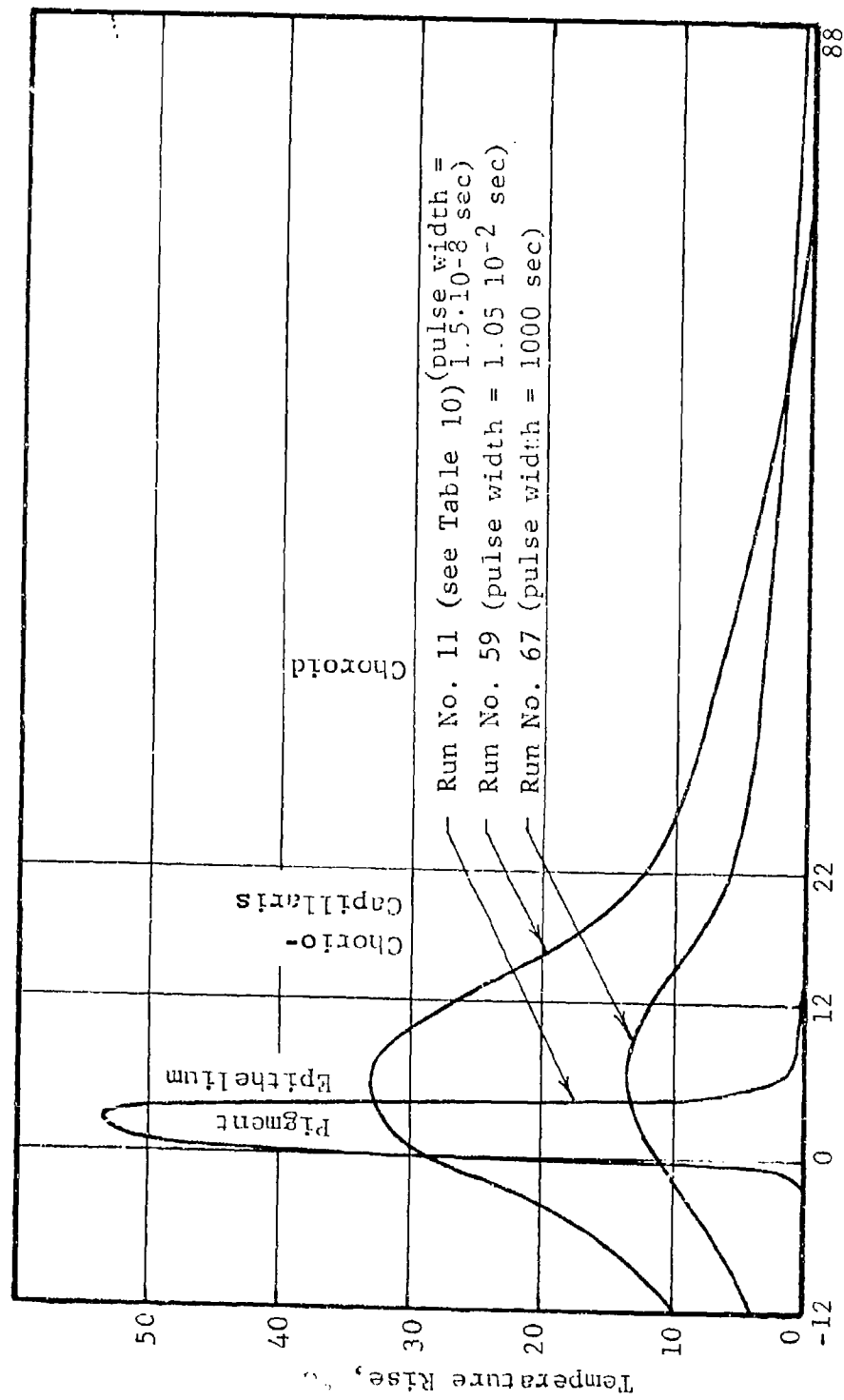


Figure 6 AXIAL TEMPERATURE PROFILES AT END OF SINGLE PULSE

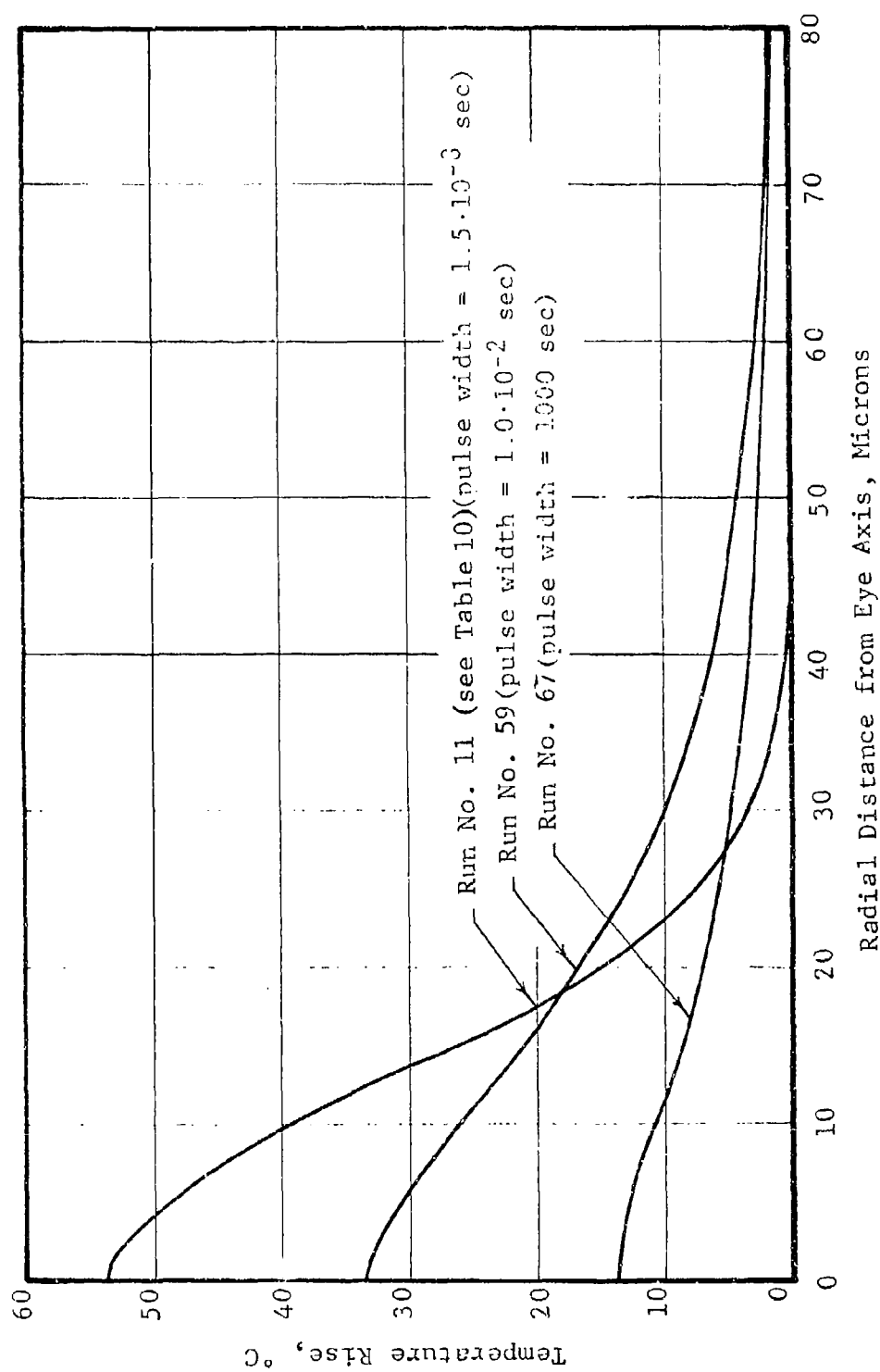


Figure 7 RADIAL TEMPERATURE PROFILES AT FRONT OF PE  
AT END OF SINGLE PULSE

## 5. DAMAGE CRITERIA

There are at least two modes by which lasers can cause eye damage. These are

- thermal damage causing protein denaturation
- mechanical damage caused by acoustic and/or shock waves

Thermal damage is produced by pulses in excess of roughly  $10^{-7}$  to  $10^{-8}$  sec while pressure waves may be a primary cause of damage by shorter pulses. Here we shall briefly review each damage mechanism.

### 5.1 Thermal Damage

Thermal damage is an accumulative process which depends both on the temperatures and their duration (Ref. 3). Damage commences at a temperature of 43 C. To compute the damage  $\Omega$ , one must first convert the predicted temperature rises  $VC(z,r,t)$  at the points  $r,z$  into absolute temperature  $VC(z,r,t)$  in degrees Kelvin and use the following expression

$$\Omega(z,r) = \sum_{\text{time}} \Delta\Omega(z,r,t) = \sum_{\text{time}} C_1 \exp(-C_2/VC(z,r,t)) \Delta t \quad (17)$$

For skin, the constants  $C_1$  and  $C_2$  are as follows (Ref. 3)

$$\left. \begin{array}{l} C_1 = 4.322 \cdot 10^{64} / \text{sec} \\ C_2 = 50,000^\circ \text{K} \end{array} \right\} \text{ for tissue temperatures } \leq (50 + 273)^\circ \text{K} \quad (18)$$

$$\left. \begin{array}{l} C_1 = 9.389 \cdot 10^{104} / \text{sec} \\ C_2 = 80,000^\circ \text{K} \end{array} \right\} \text{ for tissue temperatures } \geq (50 + 273)^\circ \text{K} \quad (19)$$

Here  $\Delta t$  represents the time interval in seconds over which the damage is being summed. Once the accumulated damage  $\Omega(z,r)$  achieves a value of 1 the tissue is irreversibly damaged. These damage determinations are made for all ocular media except for the 6  $\mu\text{m}$  thick tear layer on the cornea.



Because of the large magnitude of  $C_1$  and the small magnitude of the exponentials, it is most efficient to use logarithms to evaluate the incremental damage  $\Delta\Omega$ . Thus

$$\Delta\Omega(z,r,t) = \exp(\ln C_1 - C_2/VC(z,r,t) + \ln \Delta t_k) \quad (20)$$

In the two codes the values for  $\ln C_1$  and  $C_2$  are stored in the array DAMAGE.

## 5.2 Mechanical Damage

With the shorter pulses appreciable pressures can result due to the lack of time for energy losses either by thermal conduction, wave propagation, or media displacement.

Studies covering the generation of acoustic waves by the uniform radiant exposure of a semi-infinite body are presented in Ref. 4. This study shows that pressure of the order of a hundred psi can cause damage. Unfortunately, much has to be learned regarding the

- generation of acoustic waves by non-uniform heat deposition,
- shock waves caused by extremely short pulses, and
- criteria of mechanical damage.

Until such knowledge is available, damage predictions can only be made for pulses in excess of roughly  $10^{-7}$  to  $10^{-8}$  sec wherein the damage is primarily thermal in origin.

## 6. OPTICAL, THERMAL, AND LESION DATA

In this section we shall present input data required by the codes, and summarize experimental data acquired from corneal and retinal burns of the rhesus monkey.

### 6.1 Optical Properties Associated with the Eyes of Man and the Rhesus Monkey

Amongst the more important data needed to predict damage to the eye by laser exposures are the optical properties of the various eye media. Optical data for man and the rhesus monkey are presented in Appendix G.

In this section, we shall discuss the optical data and present our best estimates of the absorptance, reflectance and transmission data for use in the models. Before presenting these data, it should be emphasized that the published data are incomplete and a number of inconsistencies have been found in examining the data. The reasons for the discrepancies are apparently due to

- differences in experimental technique
- differences in terminology
- specimen variations
- limited number of experiments

#### 6.1.1 Absorption and Reflection Coefficients

Optical data, derived primarily from the work of Coogan (Ref. 5), Boettner (Refs. 6,10), Geeraets (Refs. 7,8,9,11), and Smith (Ref. 42) are presented for the rhesus monkey, caucasian, and negro in Tables 3 through 5 respectively at several selected wavelengths.

For the Corneal model one should use the values of the absorption coefficients for water shown in Table 6. These values were derived from transmission measurements of Hale (Ref. 12).

Table 3  
SUMMARY OF OPTICAL DATA FOR RETINAL MODEL (RHESUS MONKEY)\*

Wavelength nm (WAVEL)*	Total Transmission from Cornea to Retina (TON) (Ref. 6)	Absorption Coefficient For Pigment Epithelium, cm <sup>-1</sup> (APE) (Ref. 5)	Absorption Coefficient for Choroid, cm <sup>-1</sup> (ACH) (Ref. 6)	Reflection from Cornea (RCO) (IITRI calc.)	Reflection from Retina (RRT) (Ref. 6,9)	Reflection from Sclera (RSC) (Ref. 6)
400.0	.077	1852.	187.	.025	.080	.360
500.0	.826	1545.	169.	.025	.070	.325
514.5	.836	1485.	166.	.025	.070	.318
520.8	.841	1460.	164.	.025	.070	.315
530.0	.847	1425.	163.	.025	.070	.310
600.0	.877	1194.	151.	.025	.070	.265
647.1	.882	1108.	145.	.025	.075	.242
694.3	.887	1028.	141.	.025	.079	.231
700.0	.887	1019.	140.	.025	.080	.230
800.0	(.892)**	838.	123.	.025	.095	.250
900.0	(.878)	605.	114.	.025	.144	.245
1000.0	(.790)	434.	110.	.025	.210	.240
1060.0	(.814)	363.	108.	.025	.252	.252
1064.0	(.816)	258.	108.	.025	.255	.253
1100.0	(.830)	313.	107.	.025	.280	.260
1200.0	(.315)	303.	100.	.025	.260	.215

\* Results derived from data presented in Appendix G,  
computer symbols presented in parentheses

\*\* Extrapolated values

Table 4  
SUMMARY OF OPTICAL DATA FOR RETINAL MODEL (CAUCASIAN)\*

Wavelength nm (WAVEL)*	Total Transmission from Cornea to Retina (TOM) (Ref. 6,10)	Absorption Coefficient for Pigment Epithelium, cm <sup>-1</sup> (APE) (Ref. 6,8,9,10)	Absorption Coefficient for Choroid, cm <sup>-1</sup> (ACH) (Ref. 6,8,9,10)	Reflection from Cornea (RCO) IITRI Computation	Reflection from Retina (RRT) (Ref. 9)	Reflection from Sclera (RSC) (Ref. 42)
400.0	.094	1838.	240.	.025	.078	-
500.0	.763	1827.	106.	.025	.091	.530
514.5	.777	1745.	99.	.025	.097	.543
520.8	.782	1711.	97.	.025	.099	.549
530.0	.791	1664.	93.	.025	.104	.557
600.0	.823	1371.	68.	.025	.133	.620
647.1	.848	1253.	61.	.025	.160	.620
694.3	.853	1144.	54.	.025	.186	.620
700.0	.854	1132.	53.	.025	.189	.620
800.0	.840	974.	43.	.025	.289	.580
900.0	.763	524.	36.	.025	.398	.520
1000.0	.394	373.	32.	.025	.409	.450
1060.0	.492	247.	31.	.025	.450	.426
1064.0	.499	238.	31.	.025	.453	.421
1100.0	.562	164.	30.	.025	.478	.410
1200.0	.082	191.	29.	.025	.394	.320

\* Values derived from Appendix G,  
computer symbols presented in parentheses

Table 5  
SUMMARY OF OPTICAL DATA FOR RETINAL MODEL (NEGRO)\*

Wavelength nm (WAVELENGTH)*	Total Transmission from Cornea to Retina (TOY) (Ref. 6,10)	Absorption Coefficient for Pigment Epithelium cm <sup>-1</sup> (APE) (Ref. 6,8,9,10)	Absorption Coefficient for Choroid, cm <sup>-1</sup> (ACH) (Ref. 6,8,9,10)	Reflection from Cornea (RCO) (Ref. 9)	Reflection from Retina (RRT) (Ref. 9)	Reflection from Sclera (RSC) (Ref. 42)
400.0	.094	1838.	240.	.025	.078	-
500.	.763	1355.	203.	.025	.091	.530
514.5	.777	1261.	195.	.025	.097	.543
520.8	.782	1223.	194.	.025	.099	.549
530.0	.791	1170.	192.	.025	.104	.557
600.0	.823	850.	179.	.025	.133	.620
647.1	.848	743.	168.	.025	.160	.620
694.3	.853	643.	159.	.025	.186	.620
700.0	.854	632.	158.	.025	.189	.620
800.0	.840	433.	136.	.025	.289	.580
900.0	.763	271.	120.	.025	.398	.520
1000.0	.394	205.	109.	.025	.409	.450
1060.0	.492	131.	106.	.025	.450	.426
1064.0	.499	126.	105.	.025	.453	.424
1100.0	.562	79.—	103.	.025	.478	.410
1200.0	.082	223.	100.	.025	.394	.320

\* Values derived from Appendix G,  
computer symbols in parentheses

Table 6  
ABSORPTION CONSTANTS OF WATER (Ref. 12)

$\lambda (\mu\text{m})$	$\alpha (\text{cm}^{-1})$	$\lambda (\mu\text{m})$	$\alpha (\text{cm}^{-1})$	$\lambda (\mu\text{m})$	$\alpha (\text{cm}^{-1})$
0.200	$6.9115 \cdot 10^{-2}$	0.900	$6.7858 \cdot 10^{-2}$	3.400	$7.2072 \cdot 10^2$
0.225	$2.7367 \cdot 10^{-2}$	0.925	$1.4400 \cdot 10^{-1}$	3.450	$4.8080 \cdot 10^2$
0.250	$1.6839 \cdot 10^{-2}$	0.950	$3.8757 \cdot 10^{-1}$	3.500	$3.3750 \cdot 10^2$
0.275	$1.0739 \cdot 10^{-2}$	0.975	$4.4852 \cdot 10^{-1}$	3.600	$1.7977 \cdot 10^2$
0.300	$6.7021 \cdot 10^{-3}$	1.000	$3.6317 \cdot 10^{-1}$	3.700	$1.2227 \cdot 10^2$
0.325	$4.1759 \cdot 10^{-3}$	1.200	1.0357	3.800	$1.1244 \cdot 10^2$
0.350	$2.3338 \cdot 10^{-3}$	1.400	$1.2387 \cdot 10^{+1}$	3.900	$1.2244 \cdot 10^2$
0.375	$1.1729 \cdot 10^{-3}$	1.600	6.7152	4.000	$1.4451 \cdot 10^2$
0.400	$5.8434 \cdot 10^{-4}$	1.800	8.0285	4.100	$1.7225 \cdot 10^2$
0.425	$3.8438 \cdot 10^{-4}$	2.000	$6.9115 \cdot 10^{+1}$	4.200	$2.0585 \cdot 10^2$
0.450	$2.8484 \cdot 10^{-4}$	2.200	$1.6508 \cdot 10^{+1}$	4.300	$2.4694 \cdot 10^2$
0.475	$2.4736 \cdot 10^{-4}$	2.400	$5.0056 \cdot 10^{+1}$	4.400	$2.9417 \cdot 10^2$
0.500	$2.5133 \cdot 10^{-4}$	2.600	$1.5321 \cdot 10^{+2}$	4.500	$3.7420 \cdot 10^2$
0.525	$3.1595 \cdot 10^{-4}$	2.650	$3.1772 \cdot 10^2$	4.600	$4.0158 \cdot 10^2$
0.550	$4.4782 \cdot 10^{-4}$	2.700	$8.8430 \cdot 10^2$	4.700	$4.1977 \cdot 10^2$
0.575	$7.8676 \cdot 10^{-4}$	2.750	$2.6961 \cdot 10^3$	4.800	$3.9270 \cdot 10^2$
0.600	$2.2829 \cdot 10^{-3}$	2.800	$5.1612 \cdot 10^3$	4.900	$3.5135 \cdot 10^2$
0.625	$2.7948 \cdot 10^{-3}$	2.850	$8.1571 \cdot 10^3$	5.000	$3.1165 \cdot 10^2$
0.650	$3.1706 \cdot 10^{-3}$	2.900	$1.1613 \cdot 10^4$	5.100	$2.7350 \cdot 10^2$
0.675	$4.1516 \cdot 10^{-3}$	2.950	$1.2694 \cdot 10^4$	5.200	$2.4408 \cdot 10^2$
0.700	$6.0139 \cdot 10^{-3}$	3.000	$1.1394 \cdot 10^4$	5.300	$2.3236 \cdot 10^2$
0.725	$1.5860 \cdot 10^{-2}$	3.050	$9.8883 \cdot 10^3$	5.400	$2.3969 \cdot 10^2$
0.750	$2.6138 \cdot 10^{-2}$	3.100	$7.7830 \cdot 10^3$	5.500	$2.6504 \cdot 10^2$
0.775	$2.3998 \cdot 10^{-2}$	3.150	$5.3856 \cdot 10^3$	5.600	$3.1865 \cdot 10^2$
0.800	$1.9635 \cdot 10^{-2}$	3.200	$3.6285 \cdot 10^3$	5.700	$4.4754 \cdot 10^2$
0.825	$2.7722 \cdot 10^{-2}$	3.250	$2.3586 \cdot 10^3$	5.800	$7.1498 \cdot 10^2$
0.850	$4.3317 \cdot 10^{-2}$	3.300	$1.4013 \cdot 10^3$	5.900	$1.3248 \cdot 10^3$
0.875	$5.6154 \cdot 10^{-2}$	3.350	$9.7905 \cdot 10^2$	6.000	$2.2410 \cdot 10^3$

Table 6  
ABSORPTION CONSTANTS OF WATER (Concl)

$\lambda(\mu\text{m})$	$\alpha(\text{cm}^{-1})$	$\lambda(\mu\text{m})$	$\alpha(\text{cm}^{-1})$	$\lambda(\mu\text{m})$	$\alpha(\text{cm}^{-1})$
6.100	$2.6987 \cdot 10^3$	9.800	$6.1421 \cdot 10^2$	27.000	$1.6011 \cdot 10^3$
6.200	$1.7836 \cdot 10^3$	10.000	$6.3837 \cdot 10^2$	28.000	$1.5169 \cdot 10^3$
6.300	$1.1370 \cdot 10^3$	10.500	$7.9228 \cdot 10^2$	29.000	$1.4430 \cdot 10^3$
6.400	$8.8161 \cdot 10^2$	11.000	$1.1058 \cdot 10^3$	30.000	$1.3739 \cdot 10^3$
6.500	$7.5785 \cdot 10^2$	11.500	$1.5517 \cdot 10^3$	32.000	$1.2724 \cdot 10^3$
6.600	$6.7782 \cdot 10^2$	12.000	$2.0839 \cdot 10^3$	34.000	$1.2162 \cdot 10^3$
6.700	$6.3207 \cdot 10^2$	12.500	$2.6038 \cdot 10^3$	36.000	$1.1973 \cdot 10^3$
6.800	$6.0430 \cdot 10^2$	13.000	$2.9483 \cdot 10^3$	38.000	$1.1938 \cdot 10^3$
6.900	$5.8643 \cdot 10^2$	13.500	$3.1928 \cdot 10^3$	40.000	$1.2095 \cdot 10^3$
7.000	$5.7446 \cdot 10^2$	14.000	$3.3211 \cdot 10^3$	42.000	$1.2237 \cdot 10^3$
7.100	$5.6637 \cdot 10^2$	14.500	$3.3626 \cdot 10^3$	44.000	$1.2452 \cdot 10^3$
7.200	$5.6025 \cdot 10^2$	15.000	$3.3678 \cdot 10^3$	46.000	$1.2621 \cdot 10^3$
7.300	$5.5430 \cdot 10^2$	15.500	$3.3564 \cdot 10^3$	48.000	$1.2776 \cdot 10^3$
7.400	$5.5020 \cdot 10^2$	16.000	$3.3144 \cdot 10^3$	50.000	$1.2918 \cdot 10^3$
7.500	$5.4622 \cdot 10^2$	16.500	$3.2596 \cdot 10^3$	60.000	$1.2294 \cdot 10^3$
7.600	$5.4234 \cdot 10^2$	17.000	$3.1712 \cdot 10^3$	70.000	$1.0340 \cdot 10^3$
7.700	$5.4019 \cdot 10^2$	17.500	$3.0806 \cdot 10^3$	80.000	$8.5923 \cdot 10^2$
7.800	$5.3971 \cdot 10^2$	18.000	$2.9740 \cdot 10^3$	90.000	$7.4840 \cdot 10^2$
7.900	$5.3924 \cdot 10^2$	18.500	$2.8597 \cdot 10^3$	100.000	$6.6853 \cdot 10^2$
8.000	$5.3878 \cdot 10^2$	19.000	$2.7382 \cdot 10^3$	110.000	$6.0661 \cdot 10^2$
8.200	$5.3790 \cdot 10^2$	19.500	$2.6035 \cdot 10^3$	120.000	$5.5083 \cdot 10^2$
8.400	$5.4006 \cdot 10^2$	20.000	$2.4693 \cdot 10^3$	130.000	$4.9686 \cdot 10^2$
8.600	$5.4357 \cdot 10^2$	21.000	$2.2859 \cdot 10^3$	140.000	$4.4880 \cdot 10^2$
8.800	$5.4978 \cdot 10^2$	22.000	$2.1306 \cdot 10^3$	150.000	$4.1469 \cdot 10^2$
9.000	$5.5711 \cdot 10^2$	23.000	$2.0052 \cdot 10^3$	160.000	$3.8956 \cdot 10^2$
9.200	$5.6685 \cdot 10^2$	24.000	$1.8902 \cdot 10^3$	180.000	$3.4837 \cdot 10^2$
9.400	$5.7886 \cdot 10^2$	25.000	$1.7895 \cdot 10^3$	190.000	$3.3136 \cdot 10^2$
9.600	$5.9429 \cdot 10^2$	26.000	$1.6916 \cdot 10^3$	200.000	$3.1667 \cdot 10^2$

### 6.1.2 Index of Refraction

For computing the laser profiles, the indexes of refraction are taken equivalent to those of water as shown below. The index of refraction for water for wavelengths greater than  $1.4\mu\text{m}$  can be obtained from Ref. 12.

Table 7

#### INDEX OF REFRACTION VERSUS WAVELENGTH FOR WATER (Refs. 48 and 49)

Wavelength, nm	Index of Refraction	Wavelength, nm	Index of Refraction
350	1.357	900	1.328
400	1.346	950	1.327
450	1.341	1000	1.326
500	1.336	1050	1.325
550	1.334	1100	1.324
600	1.332	1150	1.3235
650	1.331	1200	1.323
700	1.330	1250	1.322
750	1.329	1300	1.321
800	1.328	1350	1.320
850	1.327	1400	1.320

The only exceptions are for wavelengths 350, 400, and 450 nm where the index of refraction is taken as 1.357, 1.346, and 1.341, respectively (see Appendix H).

### 6.2 Thermal Property Data

Property data associated with the conduction and storage of heat are taken as:

$$\text{Density} = 1.0 \text{ gm/cm}^3$$

$$\text{Specific Heat} = 1.0 \text{ cal/gm-}^\circ\text{C}$$

$$\text{Thermal Conductivity} = 0.0012 \text{ cal/cm-sec-}^\circ\text{C}$$

The above value of thermal conductivity was estimated based on values associated with organic media such as (Ref. 13)

Dermis	.00088 cal/cm-sec- $^\circ\text{C}$	
Blood	.0012	"
Egg white	.0013	"
Beef vitreous humor	.0014	"
Beef aqueous humor	.0014	"



Different values of blood flow were used for the chorio-capillaris, and for tissues surrounding the eye. Total blood flow to the chorio-capillaris was taken as 0.024 ml/sec (Ref. 14) and was distributed uniformly throughout the chorio-capillaris. The result is a flow of 0.016 gm/sec per unit radial area of the chorio-capillaris. Blood flow to tissues surrounding the eye was assumed as  $0.001 \text{ gm/cm}^3\text{-sec}$ . In both cases, the specific heat of blood was taken  $0.9 \text{ cal/gm-}^\circ\text{C}$  Ref (15).

### 6.3 Thicknesses of Eye Media

Thicknesses of various eye media for rhesus monkeys and humans are presented in Table 8.

Table 8  
THICKNESSES OF EYE MEDIA\*

	<u>Thicknesses in cm</u>	
	Monkey	Man
Tear Layer	$6 \cdot 10^{-4}$	$6 \cdot 10^{-4}$
Cornea	$5.16 \cdot 10^{-2}$	$5.86 \cdot 10^{-2}$
Aqueous Humor	$2.9 \cdot 10^{-1}$	$3.1 \cdot 10^{-1}$
Lens	$3.5 \cdot 10^{-1}$	$3.6 \cdot 10^{-1}$
Vitreous Humor	1.157	1.697
Pigment Epithelium	$1.2 \cdot 10^{-3}$	$1.4 \cdot 10^{-3}$
Chorio-Capillaris	$1.0 \cdot 10^{-3}$	$1.2 \cdot 10^{-3}$
Choroid	$1.68 \cdot 10^{-2}$	$1.42 \cdot 10^{-2}$
Sclera	$1.0 \cdot 10^{-1}$	$1.0 \cdot 10^{-1}$
Corneal Surface to Second Principal Plane	$1.70 \cdot 10^{-1}$	$1.75 \cdot 10^{-1}$
Corneal Surface to Pupil	$2.9 \cdot 10^{-1}$	$3.1 \cdot 10^{-1}$

\*Refs. 5, 16, 17, and 18

#### 6.4 Experimental Ocular Threshold Damage

To ensure a comprehensive check of the two models, experimental data were acquired by Brooks Air Force Base. These data are associated with retinal and corneal damage and are presented in Tables 9 and 10, respectively. Later, in Section 8 we shall use selected experiments to verify the two models.

Table 9  
EXPERIMENTAL DATA FOR RETINAL DAMAGE IN RHESUS MONKEY EYES

Run No. (RUN)*	Wavelength, nm (WAVE)	Beam Radius** (1/e <sup>2</sup> point) at Cornea, cm (RIM)	Full Angle Divergence at Cornea, Milli-Radians	Image Radius (1/e <sup>2</sup> point), cm (RIM)	Total Power of Laser, Watts (POW)	Pulse Width, Sec (DPULSE)	Number of Pulses (NPULSE)	Repetition Rate, Pulses/Sec (REPET)	Lesion Radius, cm (LESION)
2 (19)	1060.0	.175		.0025	$1.67 \cdot 10^1$	$5.00 \cdot 10^{-12}$	12	$1.45 \cdot 10^8$	.0010
3 (20)	694.3	---	(U)	.0025	$2.48 \cdot 10^5$	$4.50 \cdot 10^{-11}$	7	$7.25 \cdot 10^7$	.0020
4 (21)	594.3	---	(U)	.0025	$2.75 \cdot 10^3$	$8.00 \cdot 10^{-9}$	1		.0010
5 (22)	1060.0	.15 (M)		.0025	$1.20 \cdot 10^4$	$1.00 \cdot 10^{-8}$	20	$2.00 \cdot 10^1$	.0010
6 (22)	1060.0	.150 (M)		.0025	$1.22 \cdot 10^4$	$1.00 \cdot 10^{-8}$	10	$2.00 \cdot 10^1$	.0010
7 (22)	1060.0	.150 (M)		.0025	$1.37 \cdot 10^4$	$1.00 \cdot 10^{-8}$	10	$1.00 \cdot 10^1$	.0010
8 (22)	1060.0	.150 (M)		.0025	$1.57 \cdot 10^4$	$1.00 \cdot 10^{-8}$	5	$1.00 \cdot 10^1$	.0010
9 (22)	1060.0	.150 (M)		.0025	$1.64 \cdot 10^4$	$1.00 \cdot 10^{-8}$	1		.0010
10 (20)	694.3	---	(U)	.0025	$2.20 \cdot 10^3$	$1.00 \cdot 10^{-8}$	1		.0010
11 (23)	530.0	.135 (U)	1.0	.0025	$2.01 \cdot 10^2$	$1.50 \cdot 10^{-8}$	1		.0010
12 (24)	1060.0	.150		.0325	$1.21 \cdot 10^5$	$1.50 \cdot 10^{-8}$	1		.0010
13 (24)	1060.0	.150		.0707	$2.11 \cdot 10^4$	$1.50 \cdot 10^{-8}$	1		.0010
14 (24)	1060.0	.150		.0707	$7.73 \cdot 10^3$	$1.50 \cdot 10^{-8}$	1		.0010
15 (23)	530.0	.135		.0025	$1.13 \cdot 10^1$	$1.50 \cdot 10^{-8}$	600	5.00	.0010
16 (23)	530.0	.135 (U)		.0025	$3.40 \cdot 10^1$	$1.50 \cdot 10^{-8}$	150	5.00	.0010
17 (23)	530.0	.135 (U)		.0025	$2.60 \cdot 10^1$	$1.50 \cdot 10^{-8}$	150	5.00	.0010
19 (25)	1060.0	---	(U)	.0045	$9.66 \cdot 10^3$	$3.00 \cdot 10^{-8}$	1		.0010
20 (26)	1060.0	---		.0044	$9.33 \cdot 10^3$	$3.00 \cdot 10^{-8}$	1		.0010
21 (25)	1060.0	---		.0030	$7.33 \cdot 10^3$	$3.00 \cdot 10^{-8}$	1		.0010
22 (25)	1060.0	---		.0045	$5.00 \cdot 10^3$	$3.00 \cdot 10^{-8}$	1		.0010
23 (27)	694.3	.400		.0025	$8.70 \cdot 10^2$	$3.00 \cdot 10^{-8}$	1		.0010
24 (28)	694.3	.395		.00495	$8.4 \cdot 10^2$	$3.00 \cdot 10^{-8}$	1		.0010
25 (29)	694.3	.150		.0025	$6.00 \cdot 10^2$	$3.00 \cdot 10^{-8}$	1		.0010

Table 9  
EXPERIMENTAL DATA FOR RETINAL DAMAGE IN RHESUS MONKEY EYES (contd)

Run No. (NRUN)	Wave Length, nm (WAVE)	Beam Radius at Cornea, cm (RM)	Full Angle Divergence at Cornea, Milli-Radians	Image Radius (1/e <sup>2</sup> point), cm (RM)	Total Power of Laser, Watts (PW)	Pulse Width, Sec (DPULSE)	Number of Pulses (NPULSE)	Repetition Rate, Pulses/Sec (REFET)	Lesion Radius, cm (LESION)
26(28)	694.3	.150		.0028	5.63·10 <sup>2</sup>	3.00·10 <sup>-8</sup>	1		.0010
27(28)	694.3	.150		.00495	4.27·10 <sup>2</sup>	3.00·10 <sup>-8</sup>	1		.0010
28(27)	694.3	.400		.0025	4.33·10 <sup>2</sup>	3.00·10 <sup>-8</sup>	1		.0010
29(28)	694.3	.150		.0028	3.27·10 <sup>2</sup>	3.00·10 <sup>-8</sup>	1		.0010
30(27)	694.3	.150		.0025	3.00·10 <sup>2</sup>	3.00·10 <sup>-8</sup>	1		.0010
31(30)	530.0	--- (U)		.0025	3.33·10 <sup>2</sup>	5.00·10 <sup>-8</sup>	1		.0010
32(30)	530.0	--- (U)		.0025	1.66·10 <sup>2</sup>	3.00·10 <sup>-8</sup>	1		.0010
33	1064.0	<.20	1.2	.0025	1.08·10 <sup>2</sup>	3.00·10 <sup>-7</sup>	1		.0010
34	1064.0	<.20	1.2	.0025	9.70	3.00·10 <sup>-7</sup>	500	1.00·10 <sup>2</sup>	.0010
35	530.0	<.20	5.0	.0025	6.00	3.00·10 <sup>-7</sup>	1		.0010
36	1064.0	<.20	1.2	.0025	2.10·10 <sup>1</sup>	3.00·10 <sup>-7</sup>	2	4.00	.0010
37	1064.0	<.20	1.2	.0025	2.00·10 <sup>1</sup>	3.00·10 <sup>-7</sup>	5	1.00·10 <sup>1</sup>	.0010
38	1064.0	<.20	1.2	.0025	2.40·10 <sup>1</sup>	3.00·10 <sup>-7</sup>	5	1.00	.0010
39	1064.0	<.20	1.2	.0025	1.50·10 <sup>1</sup>	3.00·10 <sup>-7</sup>	50	1.00·10 <sup>2</sup>	.0010
40	1064.0	<.20	1.2	.0025	9.20	3.00·10 <sup>-7</sup>	50	1.00·10 <sup>1</sup>	.0010
41	1064.0	<.20	1.2	.0025	6.60	3.00·10 <sup>-7</sup>	500	1.00·10 <sup>3</sup>	.0010
42	1064.0	---		.0025	8.00	3.00·10 <sup>-7</sup>	5000	1.00·10 <sup>3</sup>	.0010
43	1064.0	<.20	1.2	.0025	9.70	3.00·10 <sup>-7</sup>	500	1.00·10 <sup>2</sup>	.0010
44	1064.0	.090		.0025	1.09	7.34·10 <sup>-7</sup>	5000	1.00·10 <sup>4</sup>	.0010
45	1064.0	---		.0025	5.70·10 <sup>-1</sup>	7.74·10 <sup>-7</sup>	50000	1.00·10 <sup>4</sup>	.0010
46	514.5	.075	0.8	.0025	1.80·10 <sup>-1</sup>	1.00·10 <sup>-5</sup>	1	1.00·10 <sup>1</sup>	.0010
47	514.5	.075	0.8	.0025	6.80·10 <sup>-2</sup>	1.00·10 <sup>-5</sup>	5	1.00·10 <sup>2</sup>	.0010
48	514.5	.075	0.8	.0025	2.10·10 <sup>-2</sup>	1.00·10 <sup>-5</sup>	50	1.00·10 <sup>2</sup>	.0010
49	514.5	.075	0.8	.0025	1.50·10 <sup>-1</sup>	1.00·10 <sup>-5</sup>	500	1.00·10 <sup>3</sup>	.0010
50	514.5	.18	0.6	.0025	5.00·10 <sup>-2</sup>	4.00·10 <sup>-5</sup>	1		.0010

Table 9  
EXPERIMENTAL DATA FOR RETINAL DAMAGE IN RUESUS MONKEY EYES (concl)

Run No. (NRUN)	Wavelength, nm (WAVEL)	Beam Radius at Cornea, cm (RIM)	Full Angle Divergence at Cornea, Milli-Radians	Image Radius (1/e <sup>2</sup> point), cm (RIM)	Total Power of Laser, Watts (POM)	Pulse Width, Sec (DPULSE)	Number of Pulses (NFULSE)	Repetition Rate, Pulses/Sec (REFET)	Lesion Radius, cm (LESION)
51	514.5	.075	0.8	.0025	3.00·10 <sup>-2</sup>	4.00·10 <sup>-5</sup>	5	1.00·10 <sup>1</sup>	.0010
52	514.5	.18	0.5	.0025	5.00·10 <sup>-2</sup>	4.00·10 <sup>-5</sup>	10	1.00·10 <sup>2</sup>	.0010
53	514.5	.18	0.6	.0025	2.40·10 <sup>-2</sup>	4.00·10 <sup>-5</sup>	50	1.00·10 <sup>2</sup>	.0010
54	514.5	.18	0.6	.0025	1.10·10 <sup>-2</sup>	4.00·10 <sup>-5</sup>	150	1.00·10 <sup>2</sup>	.0010
55	514.5	.18	0.6	.0025	2.50·10 <sup>-2</sup>	4.00·10 <sup>-5</sup>	500	1.00·10 <sup>3</sup>	.0010
56	514.5	.075	0.8	.0025	2.10·10 <sup>-2</sup>	1.00·10 <sup>-3</sup>	1	1.00·10 <sup>1</sup>	.0010
57	514.5	.075	0.8	.0025	1.90·10 <sup>-2</sup>	1.00·10 <sup>-3</sup>	5	1.00·10 <sup>1</sup>	.0010
58	514.5	.075	0.8	.0025	1.50·10 <sup>-2</sup>	1.00·10 <sup>-3</sup>	50	1.00·10 <sup>2</sup>	.0010
59	520.8	.144	0.54	.0025	1.05·10 <sup>-2</sup>	4.00·10 <sup>-2</sup>	1	1.00·10 <sup>1</sup>	.0010
60	647.1	.124	0.8	.0025	1.20·10 <sup>-2</sup>	4.00·10 <sup>-2</sup>	1	1.00·10 <sup>1</sup>	.0010
61	647.1	.125	19.6	.0140	3.86·10 <sup>-2</sup>	2.50·10 <sup>-1</sup>	1	1.00·10 <sup>1</sup>	.0010
62	520.8	.125	19.6	.0140	3.77·10 <sup>-2</sup>	2.50·10 <sup>-2</sup>	1	1.00·10 <sup>1</sup>	.0010
63	647.1	.125	7.8	.0090	2.00·10 <sup>-1</sup>	1.00·10 <sup>-1</sup>	1	1.00·10 <sup>1</sup>	.0115
64	647.1	.125	33.4	.0225	3.20·10 <sup>-1</sup>	5.00·10 <sup>-1</sup>	1	1.00·10 <sup>1</sup>	.0342
65	647.1	.125	63.3	.0425	4.25·10 <sup>-1</sup>	1.00	1	1.00·10 <sup>1</sup>	.0525
66	647.1	.125	78.9	.0525	4.25·10 <sup>-1</sup>	4.00	1	1.00·10 <sup>1</sup>	.0895
67	514.5	---		.0025	1.63·10 <sup>-3</sup>	1000.	1	1.00·10 <sup>1</sup>	.0010

\* Reference numbers given in parentheses, otherwise test data are from Brooks AFB.

\*\* U = uniform and M = multimode, otherwise profile has a gaussian shape

Table 10

## EXPERIMENTAL DATA FOR CORNEAL DAMAGE IN RHESUS MONKEY EYES

Run No. (NRUN)*	Wavelength, m (WAVEL)	Beam Radius at Cornea, cm (RIM)	Total Power of Laser, Watts (POW)	Pulse Width, Sec (DPULSE)	Number of Pulses (NPULSE)	Repetition Rate, Pulses/Sec (REPET)	Lesion Radius, cm (LESION)
1(31)	2735	.029	$1.80 \cdot 10^4$	$4.50 \cdot 10^{-8}$	1	-	.045
2(31)	3765	.034	$2.74 \cdot 10^4$	$1.00 \cdot 10^{-7}$	1	-	.053
3(32)	10600	.177	$3.93 \cdot 10^1$	$1.00 \cdot 10^{-3}$	1	-	.140
4(32)	10600	.177	$2.37 \cdot 10^1$	$2.00 \cdot 10^{-3}$	1	-	.140
5(32)	10600	.177	7.36	$6.00 \cdot 10^{-3}$	1	-	.140
6(31)	2795	.064	$5.50 \cdot 10^{-1}$	$1.00 \cdot 10^{-2}$	1	-	.045
7(32)	10600	.177	3.56	$1.00 \cdot 10^{-2}$	1	-	.140
8(31)	2727	.064	$4.00 \cdot 10^{-1}$	$2.50 \cdot 10^{-2}$	1	-	.045
9(33)	10600	.280	2.76	$5.50 \cdot 10^{-2}$	1	-	.140
10(31)	2795	.064	$1.32 \cdot 10^{-1}$	$1.00 \cdot 10^{-1}$	1	-	.045
11(31)	2727	.064	$1.80 \cdot 10^{-1}$	$1.00 \cdot 10^{-1}$	1	-	.045
12(32)	10600	.177	1.21	$1.00 \cdot 10^{-1}$	1	-	.010
13(31)	3715	.075	$3.25 \cdot 10^{-1}$	$1.25 \cdot 10^{-1}$	1	-	.052
14(31)	2795	.064	$6.09 \cdot 10^{-2}$	$5.00 \cdot 10^{-1}$	1	-	.045
15(31)	2727	.064	$9.00 \cdot 10^{-2}$	$5.00 \cdot 10^{-1}$	1	-	.045
16(31)	3715	.075	$1.35 \cdot 10^{-1}$	$5.00 \cdot 10^{-1}$	1	-	.053
17(32)	10600	.177	$3.78 \cdot 10^{-1}$	1.00	1	-	.140
18(32)	10600	.177	$1.47 \cdot 10^{-1}$	5.00	1	-	.140

\* Reference numbers given in parentheses

\*\* Lesion was estimated

## 7. COMPUTER CODES

In this section we shall describe the Retinal and Corneal models used to predict thermal damage to the retina, cornea and lens. Listings, nomenclature, and sample data for the two codes are presented in Appendices K and L. Basic analytical studies used to develop the codes are presented in Appendices A, B, C, D, E, F, H, and I. In this section we shall describe the two codes with particular emphasis being given to the users needs. First, we shall cover the major aspects of the codes, and then examine each code in detail.

Each code starts with a description of the laser exposure as presented below

- wavelength
- total power in the laser beam on the cornea
- shape of laser beam profile
- distance of laser's waist from pupil
- pulse duration
- number of pulses
- repetition rate

Then these input data are used to establish how the laser's beam is refracted into the eye (See Section 3 ). Next, the resultant laser profile and power are used in conjunction with the thicknesses and absorption coefficients of the various eye media, to determine the deposition of energy into the eye (See Appendix F) at select points in the grid system indicated by Fig. 4. Here we have chosen polar coordinates in  $r$  and  $z$  (See Appendix A) to identify the various locations of the eye.

To calculate the transient temperatures within the eye resulting from a single laser pulse, we have used a finite-difference method formulated by Tech. Inc. (Refs. 1,52) using the work of Peaceman (Ref. 2). This method represents an alternating explicit implicit technique for computing the temperature rises that allows use of constantly expanding time steps.

Temperature predictions for multiple pulses (See Appendix D) are made using the resultant temperature predictions for a single pulse. Total damage is predicted by integrating the rates of damage over the times at which the rates of damage are significant.

Based on the damage criterion of Ref. 3, the codes compute the total laser powers required to damage each of the specified locations within the eye. After the threshold powers are found for the specified points, the codes predict the region damaged by the particular laser power specified by the user. The damaged region is found by interpolating the radial extent of damage at various depths, as well as the axial extent of damage along the axis of the eye.

Having briefly reviewed the principal features of the two models, let us now examine each code in detail.

#### 7.1 Retinal Model

The Retinal model consists of a main program plus five subroutines. Principal features of the code are illustrated in Fig. 8. Here we shall describe each part of the Retinal model using the listing presented in Appendix K. Throughout this discussion we shall refer to the sequence numbers at the left-hand side of the listing. Included in Appendix K is a description of the variables, sample data, and output results.

All input data required by the code are read in the main program and subroutine IMAGE. The order in which the data are read in is indicated by the numbers at the right-hand side of the listing. Read statements with asterisks are executed only for irregular laser profiles.

##### 7.1.1 Main Program for Retinal Model

Figure 9 illustrates key portions of the Main Program. Numbers in the boxes refer to the sequence numbers of the listing. The symbols  $i$ ,  $j$ ,  $k$  refer to the grid positions  $Z(i)$ ,  $R(j)$  and times  $XT(k)$ , respectively.



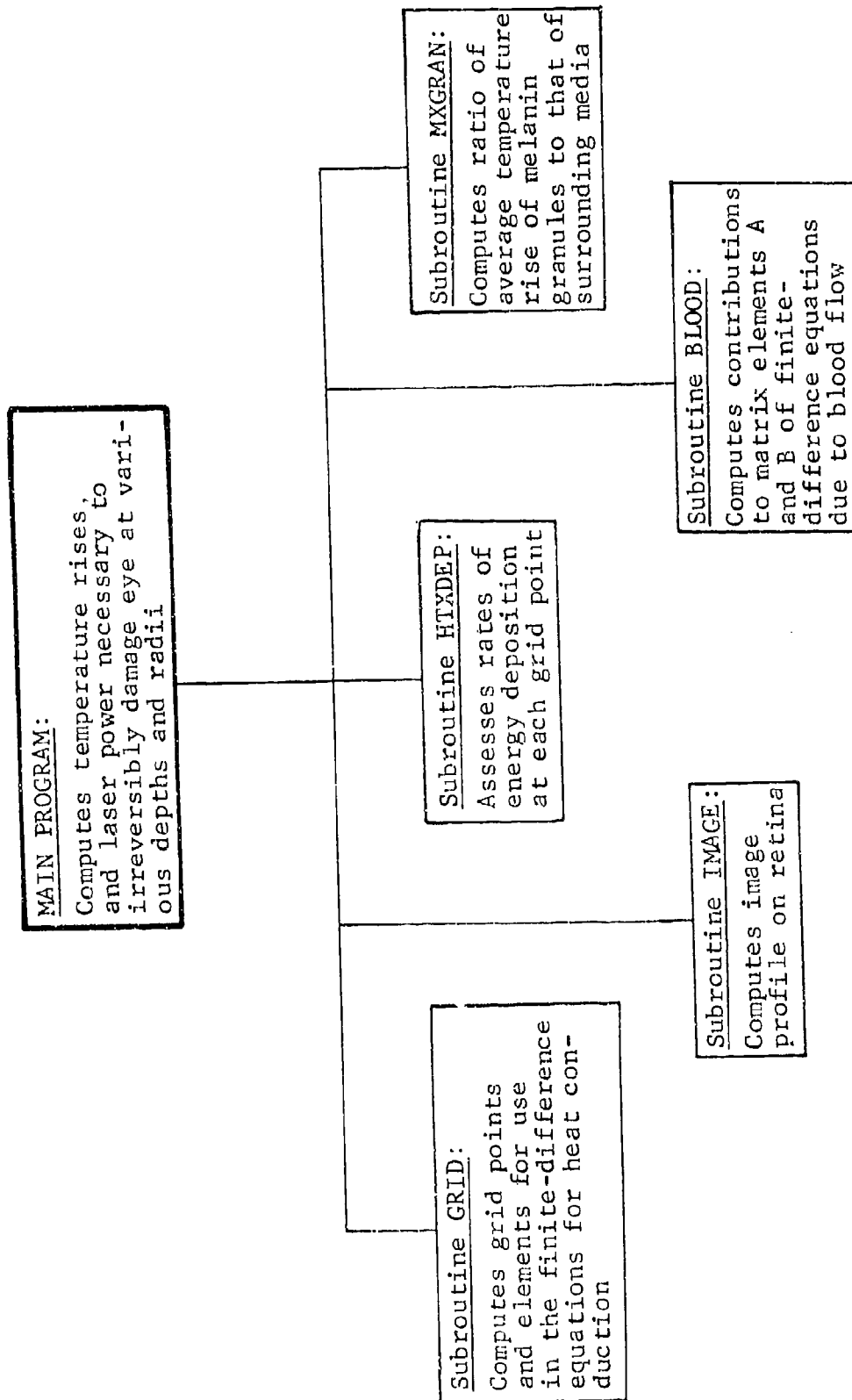


Fig. 8 SCHEMATIC ILLUSTRATION OF PRINCIPAL ROUTINES OF RETINAL MODEL

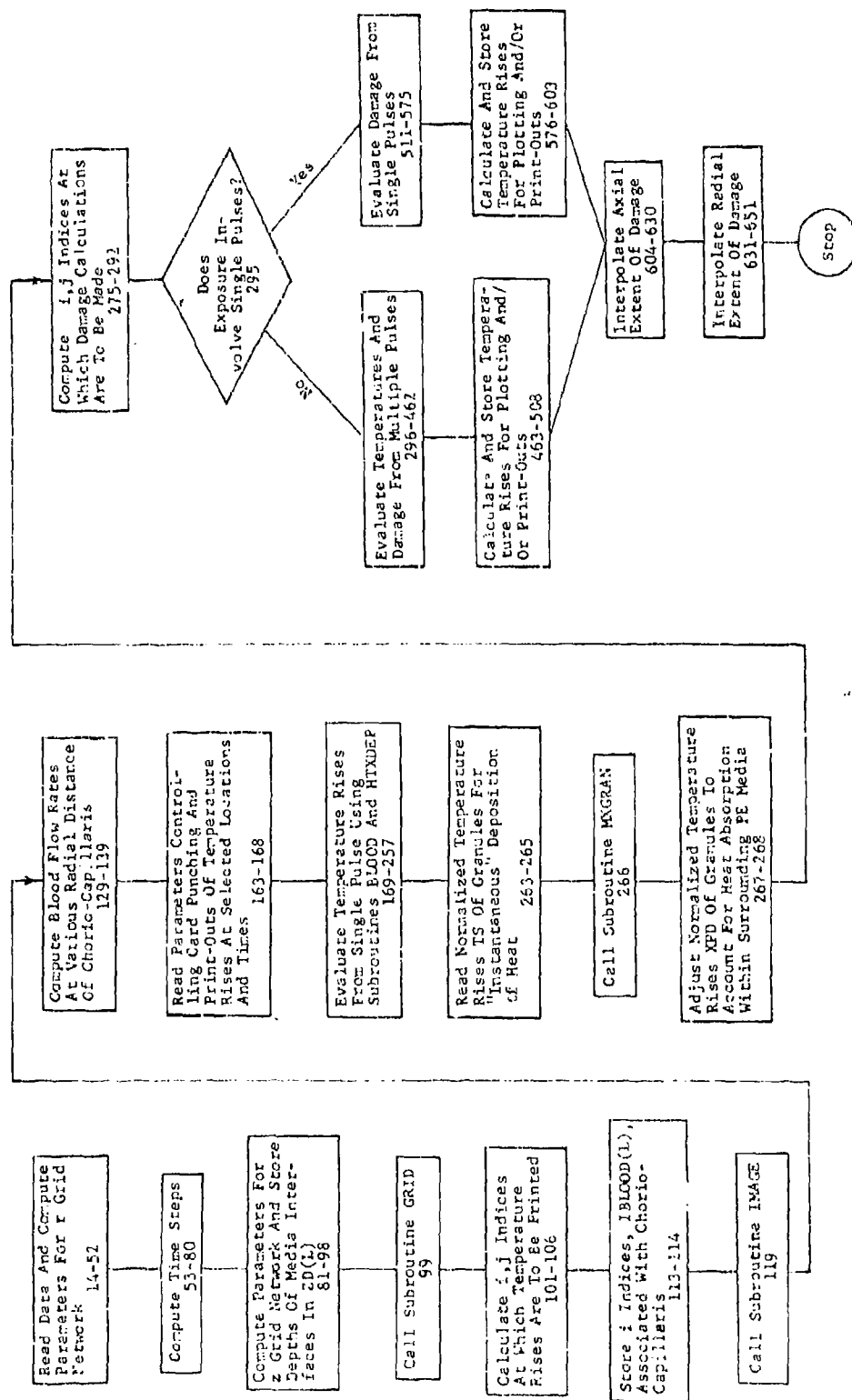


Fig. 9 FLOW DIAGRAM OF MAIN PROGRAM OF RETINAL MODEL

#### Retinal Main: Sequence Numbers 1-52

Sequence numbers 25 through 27 define the number  $N1$  of uniform grid increments, and the total number  $N3$  of grid points in the radial grid. Here  $N1$  must be less than  $N3$ . The size of the smallest radial grid increments  $DR$  is established at sequence numbers 30 and 31. For gaussian or irregular laser profiles,  $DR$  is found by subdividing the lesion radius  $LESION$  into an integer number  $LIM$  of increments. For uniform profiles,  $DR$  is found by subdividing the profile radius  $RIM$  into  $(LIM-.5)$  increments. At present, all values of  $DR$  should be larger than about  $0.0003$  cm to avoid temperature instability. To use smaller  $DR$  values, the size of the initial time steps  $DT$  must be decreased and the dimension  $KT$  increased in the appropriate arrays (see Appendix K). If one wishes to reduce  $DR$  by a factor  $\xi$ , then  $DT$  should be decreased by the factor  $\xi^2$ .

At sequence numbers 37 and 38, the index  $LPX$  is set equal to 0 or 1 according to whether the laser exposure involves single or multiple pulses, respectively. This index is used to control the course of the computations. At sequence numbers 42 and 43, the laser power and pulse duration are altered when the pulse duration is less than  $0.3 \cdot 10^{-8}$  sec. In these alterations, the total energy is preserved. These changes save on computational time and reflect the fact that the conduction of heat is insignificant during times less than  $0.3 \cdot 10^{-8}$  sec.

#### Retinal Main: Sequence Numbers 54-63

At sequence numbers 54 through 63, the time step  $DT$  and the total time  $TIME$  are computed using the arrays  $XCT$ ,  $NPT$ , and  $KTT$ . Specific values for  $XC$ ,  $NP$  and  $KT$  are selected from these arrays as a function of the pulse duration  $DPULSE$ . The array  $XCT$  presents values for the expansion factor  $XC$  by which successive time steps are increased;  $NPT$  the number of time steps  $NP$  contained within  $DPULSE$ ; and  $KTT$  the total number of time steps  $KT$ . The values assigned these arrays are given in the sample data cards 18, 17 and 19 presented in Appendix K. The result of these computations is time steps  $DT$ ,  $XC \cdot DT$ ,  $XC^2 \cdot DT, \dots, XC^{(KT-1)} \cdot DT$ , where the total time  $TIME$  is given by

$$\text{TIME} = \sum_{n=0}^{KT-1} (\text{XC})^n \cdot \text{DT} = \text{DT} \cdot \frac{\text{XC}^{KT} - 1}{\text{XC} - 1} = \text{XT}(KT) \quad (21)$$

The elapsed time from the start of a pulse to the K-th time step is represented by XT(K+1). Here XT(1)=0. At the end of a pulse of duration DPULSE,

$$\text{XT}(KM) = \text{DPULSE} \quad (22)$$

#### Retinal Main: Sequence Numbers 66-77

At sequence numbers 66 through 77, the code computes TIME, DT, KT and KM for multiple-pulsed exposures. Here the expansion factor XC is set equal to the relatively large value of 1.4 so that the total time TIME brackets all the pulses without resorting to large numbers of time steps. The total time TIME is determined by first evaluating the train length, and then multiplying the result by the value selected from the array FTIME. To provide maximum flexibility the array FTIME is described by input data as a function of pulse duration. Elements of FTIME should always be greater than 1.

If the temperature rises from a pulse do not approach zero in the allotted time, then one should increase the particular element of the array FTIME corresponding to DPULSE.

To integrate damage over each pulse, DPULSE is subdivided into NP uniform time steps of magnitude PTIME (See Appendix D). For more refined damage calculations, one can increase the number of intervals bearing in mind that it will require increases in the dimensions of arrays with arguments KT and KX (See Appendix K). Here KX equals the total number of time intervals used to evaluate damage from pulse to pulse and presently equals NP+3 (see sequence number 331).

#### Retinal Main: Sequence Numbers 82-89

At sequence numbers 82 through 89, the indices for grid points along the Z axis, i, are chosen along with the size of the smallest increment DZ along the z axis. To conserve on computational time, DZ is increased with the pulse duration DPULSE.

At sequence number 87, the first grid point in the pigment epithelium designated by IPE is located at the second uniform grid point shown in Fig. 4. Also, the first grid point in the cornea designated by IPA is located at the second grid point.

#### Retinal Main: Sequence Numbers 91-100

From sequence numbers 91 through 98, the distances ZD of the various interfaces from the cornea are computed using the assigned thicknesses for the various media. Here ZD(8) is set equal to an exceptionally large value to ensure it contains Z(M3), the last grid point on the Z axis.

At sequence number 99, subroutine GRID is called to compute

- the locations of all grid points Z(i), R(j),
- the indices for the various eye media, and
- other spacially-dependent thermal properties.

A discussion of this subroutine is given in Section 7.1.2.

At sequence number 100, the number of grid points NVL in the chorio-capillaris for any specified value of J is calculated using the first grid point IPV and last point LPV in the layer.

#### Retinal Main: Sequence Numbers 102-106

Here the i,j indices, at which temperature print outs are desired, are computed. These points are chosen according to the values assigned ID1, ID2, JD1 and JD2 on data card no. 11.

#### Retinal Main: Sequence Numbers 113-114

Here the i indices associated with points in the vascular layer are computed and stored in the array IBLOOD.

#### Retinal Main: Sequence Numbers 116-121

In this section the normalized irradiance profile HR is set to zero and subroutine IMAGE called to evaluate HR at the retina. In this regard, two options are available to the user. Either one can input the retinal image directly by setting IFIL=0, or compute the image as described in Section 3 and Appendix H by setting IFIL=1.

When IFIL equals zero, the program sets the image equal to the profile described by input data on cards 4 and 6 of the main program (for gaussian and uniform profiles), or cards 19A\*, 19A\*\* and 19A\*\*\* of subroutine IMAGE (for irregular profiles). Otherwise these profiles are considered to be at the cornea and the retinal images are calculated in subroutine IMAGE.

Retinal Main: Sequence Numbers 131-139

Here the blood flows entering (IFLOWI) and leaving (XFLOWO) the chorio-capillaris are specified at various radial distances DFLOW. These blood flows are all on a unit area basis and are distributed uniformly over a circular area of radius RVL such that the total flow equals CFLOW. Presently the incoming and exiting flows are set equal. This means that there is no net radial flow. However, the code is structured so that one can easily vary the incoming and exiting flows with radius as more detailed information is acquired.

Retinal Main: Sequence Numbers 144-146

In this section the initial temperature rises are set to an insignificantly nonzero value ( $10^{-10}$ ), to prevent underflow. Computer installations without library routines to handle underflow will not tolerate temperature rises of the order of  $1 \cdot 10^{-37}$  that are other than zero.

Retinal Main: Sequence Numbers 172-257

This part of the code assesses temperature rises caused by a single pulse as described by Appendix A. Here heat is deposited at a rate of  $S(i,j)$  per unit volume at each point  $Z(i), R(j)$  during the pulse, i.e. at times of  $XT(1), XT(2) \dots XT(KM)$ . After the pulse,  $S(i,j)$  is set equal to zero by subroutine HTXDEP.

Two provisions are left to the discretion of the user. The first is that one can subdivide the time intervals used to compute the temperature rises without changing the time steps  $XT(K) - XT(K-1)$ . This involves changing the integer IKX which provides for  $2 \cdot IKX$  time intervals of size  $(XT(K) - XT(K-1)) / (2 \cdot IKX)$ . For this purpose, IKX may be altered by adjusting the values of EDT1 and EDT2 assigned

as input data on card no. 12. This provision is included so that one can improve accuracy or eliminate instability without having to increase the number of time steps  $KT$ . Except for long pulse times, a value of 1 for  $IKX$  is usually adequate. To reflect the fact that  $IKX$  should be greater than 1 for pulse widths of the order of 1000 sec or more,  $DPULSE$  has been included in the evaluation of  $IKX$ .

The second option is the times at which temperature printouts are desired. This option is provided by the value assigned  $ITYPE$  in the input data. If one wishes print outs at each time  $XT$ , then one merely sets  $ITYPE = 1$ . If one wishes printouts at every  $n$ -th  $XT$ , then  $ITYPE$  should be set equal to  $n$ . Print outs will always be provided at the conclusion of the pulse as well as at the last time  $XT(KT)$ .

#### Retinal Main: Sequence Numbers 263-268

Here we complete the evaluation of the array  $XPD(K)$  describing the ratio of the average temperature of the granules to the average temperature of the region of the pigment epithelium in which they lie. The values for  $XPD(K)$  are given at times of  $XT(K)$  and approach 1 after the conclusion of a pulse. This reflects the fact that the excess heat in the granules is dissipated to its immediate surroundings following a pulse.

#### Retinal Main: Sequence Numbers 275-294

Here we select the points  $ID(L)$ ,  $JD(L)$  at which damage calculations are to be made. Two input parameters are required to specify the points. The first is the radial distance  $RMAX$  over which damage assessments are desired. Here the code assesses damage for all grid points starting at  $R(1)$  and ending at the first point beyond  $RMAX$ , namely  $R(JM)$ .

The second control one has in selecting the points is in the value assigned  $LIMAX$ . Knowing this variable, the code establishes the depth  $Z(IMAX)$  of greatest temperature rise, and then assess the damage from  $Z(IMAX-LIMAX)$  to  $Z(IMAX+LIMAX)$ . Thus when  $LIMAX$  is set equal to zero, damage is only evaluated at the depth of highest temperature.

The number of points at which damage is to be evaluated is given by LIJ. If LIJ is larger than the allotted dimension for the arrays associated with LIJ then the computations will stop. Moreover, care should be exercised not to designate more points than needed -- first, because points remote from the region of greatest temperature require considerable time to heat and cool, and secondly because of the appreciable increase of storage required when LIJ is increased.

Retinal Main: Sequence Numbers 299-403

In this section the temperature rises caused by multiple pulses are computed using the temperature predictions for a single pulse. Also, the array ZTT is evaluated for subsequent computations of the damage.

First, the temperature rises at the points, at which damage calculations are desired, are stored in the array VE(L,K,n). In the array VE the point is at LD(L), JD(L), the time is XT(K), and n=1 when VE represents the temperature rise of the region around the point while n=2 when VE represents the average temperature rise of the granules. When the point is not in the pigment epithelium, the two temperatures VE for n=1 and 2 are the same.

As may be noted at sequence number 315, provisions have been made to evaluate NTEST exposures during a single computer run. These exposures may differ only in their repetition rate or number of pulses.

The basis for the multiple-pulse computations is presented in Appendix D. First the temperatures are interpolated at select interpulse times during and between pulses. The interpulse times differ from the times XT(K). The total number of interpulse times from one pulse to the next, is given by KX -- where NP interpulse times are uniformly spaced across each pulse and three are uniformly spaced across the interval between pulses. Measured from the beginning of each pulse, the interpulse times for the thermal damage calculations are stored in ZTX(L3) while the interpulse times for predicting the granule temperatures are stored in ZT(L3). Then the temperatures VE for a single pulse are used to compute the temperature rises VZ from multiple pulses.



Temperatures are stored in VZ for each pulse only when the number of pulses is less than 20. Otherwise the code groups the pulses into an odd number of IN pulses, and stores the temperatures associated with the middle pulse of each groups of pulses. Later these temperatures will be used to assess the damage caused by each group. The number of groups of pulses during the exposure is INX, while the number of groups in the time TIME is represented by INXX. Generally, TIME exceeds the train length so more pulses are considered than actually exist. The reason for using more pulses than exist is to provide for temperature predictions following the exposure (see Appendix D). This point will be returned to later in this section.

In order to relate the interpulse times to the times XT, it is first necessary to add the interpulse times ZTX and ZT to the product of the number of prior pulses and the time interval TC from pulse to pulse. These times are designated by X3 and are calculated at sequence numbers 367 and 371, where L7 equals the number of pulses started during the times of interest.

From sequence numbers 363 to 378, the temperatures during the middle pulse of the first group of pulses are evaluated and stored in VZ(L,L6,L3,n) where L indicates the point ID(L), JD(L) at which the temperatures are calculated; L6 labels the groups of pulses concerned; L3 designates particular interpulse times, and n indicates whether the temperatures are for the media or granules.

To interpolate the temperatures at time X3, it is first necessary to determine which pair of XT(K) bracket X3. To this end it should be remembered that the times XT are given by

$$\begin{aligned} XT(1) &= 0 \\ XT(K) &= DT \cdot \frac{XC^{K-1} - 1}{XC - 1}, \quad K \geq 2 \end{aligned} \tag{23}$$

To find the time XT(K) just prior to X3, one merely substitutes X3 for XT(K) and solves for the integer value of K. In this manner X3 is located between XT(K) and XT(K+1). Linear interpolation is then used to find the temperature at time X3.

From sequence numbers 379 through 397, the computations are continued for the 2nd, 3rd...INXX group of pulses ( $L6=2,3...$ ). In each case the computations start with the pulse following the last pulse considered and end with the middle pulse of the succeeding group. In the process the temperature contributions are added sequentially for all pulses. The result is a description VZ of the temperature rises during and immediately following selected pulses for a total of  $IN \cdot INXX$  pulses.

As mentioned previously the number of pulses  $IN \cdot INXX$  considered exceeds the number of pulses  $IN \cdot INX$  in the exposure. Therefore, for times exceeding the total exposure time, one must subtract the temperature contributions from the last  $IN \cdot (INXX - INX)$  pulses. This operations is performed at sequence numbers 398 through 402.

#### Retinal Main: Sequence Numbers 404-462

Here we compute the damage caused by temperatures from multiple pulses. Damage is evaluated at the points with indices  $ID(L)$ ,  $JD(L)$ . For each point, an initial estimate is made of the factor CQ by which the input laser power POW must be multiplied to cause irreversible damage. This operation is conducted from sequence numbers 413 through 416. This estimate of CQ is purely empirical based on the pulse duration DPULSE and the peak temperature rise at the conclusion of the last pulse. The computations are aborted if the temperature rise is below  $0.001^\circ\text{C}$ . This provision is included to prevent examination of remote points wherein there is no temperature rise. In such situations an arbitrary threshold power of  $10^{20}$  is printed for the points  $ID(L)$ ,  $JD(L)$ .

Having made an initial estimate of the laser power, the next step is to set the control indices LLT and LGT to 0. These indices become 1 when the assumed laser power is below or above the predicted threshold value, respectively. We will return to this point later.

The damage calculations are made from sequence numbers 421 through 432. Two criteria are used to assess damage. The first

is the use of an arbitrary temperature TSTEAM of the melanin granules. If the temperature rise of the granules VZ(L,L6,L3,2) exceeds TSTEAM-T0, where T0 represents the initial temperature, then irreversible damage is assumed. For the computer runs considered, the granule temperatures are high enough to cause damage. However, the fact that the experimental damage results are more in line with the thermal denaturation criteria suggests that any damage caused by steam is too localized to be observable. Within a time increment of say  $\Delta t$ , the incremental damage  $\Delta\Omega$  caused by thermal denaturation is (see Section 5)

$$\Delta\Omega = C_1 \exp(-C_2/T_a(t)) \Delta t \quad (24)$$

where  $C_1$  and  $C_2$  are constants and  $T_a(t)$  is the absolute temperature. Irreversible damage occurs if and when

$$\int_0^t \Delta\Omega \cdot d\tau \geq 1 \quad (25)$$

Being that  $C_1$  is a very large number and the exponential is a very small number, it is advisable to evaluate the damage using logarithms. Therefore, taking the log of Eq. 24 yields

$$\ln(\Delta\Omega) = \ln C_1 - C_2/T_a(t) + \ln \Delta t \quad (26)$$

To assess the incremental damage one merely sums the exponentials of the logarithm of  $\Delta\Omega$ . The accumulated damage DAMC is therefore given by

$$\text{DAMC} = \sum_t \exp(X1) \quad (27)$$

where  $X1 = \ln C_1 - C_2/T_a(t) + \ln \Delta t$ . When groups of pulses are considered,  $\Delta t$  is multiplied by the number of pulses IN per group.

After the damage has been evaluated for the assumed laser power, CQ is either increased or decreased by 4% according to whether DAMC is less than or greater than 1, respectively. In the process LLT is set equal to one if  $\text{DAMC} < 1$  or LGT is set equal to one if  $\text{DAMC} > 1$ . Once both LLT and LGT are equal to 1, the

damage calculations are completed in that one has crossed over the threshold value. One half of the last 4% correction is then returned to CQ so that one can be assured that the predicted value is accurate to within 2%. To separate the predictions of laser power caused by the two criteria, TSTEAM is progressively increased until the last two sets of power predictions are the same. To determine when this occurs one of the predicted laser powers is stored in XQ so it can be compared with its subsequent prediction.

As a result, the last two sets of power predictions are associated with thermal damage while earlier predictions indicate the laser power necessary to raise the granule temperature above TSTEAM. One word of caution is needed at this point. Damage assessments are only made over the time TIME. At regions far removed from the region of greatest energy deposition, the assigned TIME may not be adequate. The adequacy of the time may be judged by examining the temperature print-outs. If the temperature peaks, and then drops by more than roughly 5°C, then the predicted power is satisfactory. Otherwise, one should increase TIME through the array FTIME and increase dimensions of arrays containing the time index KT.

#### Retinal Main: Sequence Numbers 463-508

This section provides data cards for plotting the temperatures at times specified by the user. Here the temperature rises from multiple pulses are calculated at points with indices i ranging from I11 through I12 and j indices ranging from J11 through J12. The times at which the temperatures are desired are input by the user in the array TIMEX. These times are measured from the start of the first pulse and may assume any value from 0 to TIME. These calculations are essentially the same as those of sequence numbers 361 through 403.

In addition to the temperature rises, the plotting routine must know the range of the points over which plots are desired as well as the peak temperature rise RGV of the profile. Also to aid in identifying the curves, a provision has been included to label a particular curve. The curve to be labeled will have an i index corresponding to the assigned value for I13.

In addition to providing data cards for plotting, provisions are also made for print-outs of the data. Three options are available in this regard. If KTYPE is assigned a value of 0, then no cards or print-outs will be provided. If KTYPE=n and KTYPEO=1 the code will only print the temperature rises at n times TIMEX(n). Values of KTYPE=n and KTYPEO=0 will provide both cards as well as print-outs.

Retinal Main: Sequence Numbers 523-564

This portion of the code computes the damage from single pulses. The basic difference from the damage calculations for multiple pulses is the use of the temperatures at the times XT(K). Here the code assesses the damage from the KM time intervals, i.e. XT(2)-XT(1), XT(3)-XT(2), etc., during the pulse as well as an additional (KT-KM) time intervals following the pulse. As with multiple pulses, damage is evaluated by using the temperatures at the mid-points of the above time intervals. Other than the difference in time intervals the computations are identical to those for multiple pulse and the same observations apply.

Retinal Main: Sequence Numbers 578-603

Here provisions are made for preparing data cards for constructing 3-D and 2-D profiles of the temperature at selected locations and times. Except for the use of a single pulse, the computations are identical to those used for multiple pulses.

Retinal Main: Sequence Numbers 605-653

In the final portion of the main program, the predicted threshold powers QD for specified points are used to assess the region damaged by the particular laser power specified by the user.

To assess the axial extent of the damage, the computer first scans the predicted powers to find the i indices at which the predicted powers bracket the specified power POX=POW. For minimum depths of damage the i indices are I5 and I6 while for maximum depths of damage the i indices are I7 and K8. If POW is lower than all the QD(i,1), then I6 assumes the value 0 and all remaining computations are aborted.

If POW exceeds all the QD(I,1), then the computer prints a message indicating this fact and all future axial computations are aborted.

To interpolate the depths where QD=POW, the following equation is used

$$QD = X1 \cdot \exp(X2 \cdot z) \quad (28)$$

where QD represents the power, z represents the axial distance and X1 and X2 are constants to be evaluated. By substituting the two laser powers, say QD<sub>1</sub> and QD<sub>2</sub>, that bracket POW into Eq. 28 along with their axial distances, say z<sub>1</sub> and z<sub>2</sub>, one can solve the resultant equations for X1 and X2. The result is

$$X1 = QD_1 / \exp(X2 \cdot z_1) \quad (29)$$

$$X2 = \log(QD_2 / QD_1) / (z_2 - z_1) \quad (30)$$

Thus, substituting X1 and X2 back into Eq. 28, replacing QD by POW, and solving for the threshold depth z yields

$$z = \log(POW / X1) / X2 \quad (31)$$

By using the pair of laser powers found for small i values and for large i values, one arrives at the minimum and maximum depths of damage along the eye's axis.

Starting at sequence number 632, a similar set of computations is made to assess the radial extent of damage for the depths at which the predicted power exceeds POX or POW. Except for the use of r instead of z, the same analysis is used as exemplified by Eqs. 28 through 31. This then completes the description of the main program.

#### 7.1.2 Subroutine Grid for Retinal Model

Subroutine grid establishes the values for Z(i) and R(j) subject to the values assigned N, N1, N3, DR, RVL, M, M1, M2, M3, TAV, and DZ in the main program. Also the subroutine evaluates the matrix elements A and B for the finite-difference solution of the heat conduction equation. Moreover, the subroutine determines

the location of the  $i$  indices associated with the first and last points of each eye media. Finally, the subroutine stores the assigned thermal conductivities  $CON(i)$  and heat capacities  $VSH(i)$  at the appropriate depths  $Z(i)$ .

Appendix I describes the techniques used to develop the grid network.

#### Retinal Grid: Sequence Numbers 15-21

Here the subroutine evaluates the expansion factor by which the radial grid steps are sequentially increased starting at  $j=N1$ . The grid is selected so that the radial extent  $RVL$  of the eye is located at

$$RVL = (R(N-1)+R(N))/2 \quad (32)$$

For more details the reader is referred to Appendix I.

#### Retinal Grid: Sequence Numbers 27-32

In this section the radial distances of the radial points  $R(j)$  are evaluated and assigned.

#### Retinal Grid: Sequence Numbers 34-52

Here the matrix elements  $B(j,1)$ ,  $B(j,2)$  and  $B(j,3)$  are evaluated for the finite-difference solution of the heat conduction equation. A description of this evaluation is presented in Appendix A.

#### Retinal Grid: Sequence Numbers 54-61

This portion of the code computes the expansion factor  $R1$  for the  $z$  grid. The surface of the cornea is located halfway between  $Z(1)$  and  $Z(2)$ , while the surface of the pigment epithelium is located halfway within the first uniform element. This element is bounded by the points  $Z(M2-M1+1)$  and  $Z(M2-M1+2)$ .

#### Retinal Grid: Sequence Numbers 64-76

Here the subroutine computes and assigns the values for the various  $Z(i)$  using the expansion factor  $R1$ .

#### Retinal Grid: Sequence Numbers 80-100

Here the subroutine uses the depths of the various interfaces to locate the initial and last grid points in each media. The resulting  $i$  values are stored in the arrays  $IX$  and  $LX$  and then assigned to  $IPV$ ,  $IPC$ , ...  $LPS$ ,  $LPT$ .

#### Retinal Grid: Sequence Numbers 102-118

To provide for the possibility that the various eye media may have different thermal conductivities CONX and heat capacities VSHX, provisions are made for such variations. To this end, the assigned thermal properties are stored with depth in the arrays CON(i) and VSH(i).

#### Retinal Grid: Sequence Numbers 121-126

Here the matrix elements A(i,1), A(i,2) and A(i,3) are evaluated for use in the finite-difference equations of the heat conduction equation discussed in Appendix A. These elements were chosen so that there is no heat flow from the cornea to the environmental air. In this regard, no consideration was given to the effects of blinking.

#### 7.1.3 Subroutine Image of Retinal Model

This subroutine performs two major functions. These are to determine the

- normalized image profile HR at the retina (normalized profiles have a value of 1 at the eye's axis)
- irradiance QP on the eye's axis by which the normalized profile HR must be multiplied to obtain the irradiance across the image prior to any internal reflections or absorption. The latter is accounted for in subroutine HTXDEP.

#### Retinal Image: Sequence Numbers 16-17

Here the number of radial increments for the spread function (see Appendix H) integration is specified. The integration is made across the entire laser beam or pupil radius -- whichever is the smaller. In situations in which the beam is smaller than the pupil, LII becomes less than LI.

For most exposures, 500 increments are adequate. The one exception is when much of the laser's energy is beyond about 0.1 cm from the center of the pupil. In such situations, it is advisable to increase the number of increments. A very crude rule of thumb is to use an LI value of 5000 times the radius wherein most of the



energy is contained. This is necessary to decrease the intervals of the argument of the Bessel Function at larger radial distances  $r$ .

Retinal Image: Sequence Numbers 25-26

Any shape of laser profile may be accommodated by the code. The most obvious profiles are the gaussian (IPROF=1) and the uniform (IPROF=0). Other profile shapes may be handled by assigning a value of 2 for IPROF on data card 6 of the main program.

Retinal Image: Sequence Numbers 29-48

For irregular profiles (other than gaussian or uniform), the user must specify the profile's shape on a point by point basis. This is accomplished by first assigning the number of points LR on data card 19A. Then the profile values PX and associated radial distances RX are read on data cards 19A\*\* and 19A\*\*\*. The numbers for the profile values need only be relative.

From sequence numbers 35 through 48 the code normalizes the profile values PX and then integrates the profile over it's radial area. The normalized power incident on the pupil is represented by X5 and the normalized power beyond the pupil is represented by X6. In order to account for the possibility that only a portion of the laser's energy may enter the eye, we have used XX to represent the fraction of the laser's power entering the eye.

Two additional determinations are made. The first is the determination of the irradiance QP entering the eye on the eye's axis. This value of irradiance is only used when one wishes to image the profile directly onto the retina. This is accomplished by assigning a value of 0 to IFIL on data card 4 of the main program. For such cases the entire energy in the profile is used. When the radius RX(LR) of the profile is less than the pupil radius, the number of radial increments LLI is reduced accordingly.

Retinal Image: Sequence Numbers 49-59

Here the magnitudes of the irregular profile are evaluated at radial increments of RINT and stored in the array for future use.

#### Retinal Image: Sequence Numbers 61-80

In this part of the subroutine, the code evaluates QP and XX for gaussian profiles. When the user indicates a desire to place the profile directly onto the retina, the computer evaluates the normalized image profile and stores the results in PR(j) for future use. On the other hand, if the profile represents the beam profile (signified by setting IFIL=1), then the code evaluates the normalized profile at radial increments of RINT and stores the results in the array FX.

#### Retinal Image: Sequence Numbers 82-93

Here the subroutine treats uniform profiles in a similar fashion as the gaussian profiles are handled at sequence numbers 61-80.

#### Retinal Image: Sequence Numbers 98-119

This section images irregular profiles directly onto the retina. Here the array PR is determined by first evaluating the accumulated radial area and associated power between  $r=0$  and  $L \cdot RINT$ . The accumulated area is stored in the array FA(L), while the accumulated power is stored in the array FP(L). These arrays are then used to establish the laser's intensity at the points R(j).

#### Retinal Image: Sequence Numbers 122-210

Here the beam profile is optically imaged onto the retina. The method used to determine the image is described in Section 3 and Appendix H. The spread function calculations apply to all profiles. Wherever different symbols are used in the code from those of the text we shall inject an 'or' between symbols. The first symbol is used in the code.

The first portion of this section evaluates the index of refraction NC or n, the second principal focal length FL or f and the incremental distance XO or  $\Delta z$ . Then the beam profile (described by the array FX) is refracted onto the pupil yielding a profile FY.

From sequence number 148 through 158 the real and imaginary parts of the integrand of Eq. 7 are evaluated exclusive of the Bessel Function. The real part of the integrand is stored in XF1(L) at

radial distances of  $(L-1) \cdot RINT$  while the imaginary part is stored in  $XF2(L)$ . From sequence numbers 167 through 190, the Bessel Function is evaluated and stored in  $X7$ . Then the integrals of the real and imaginary parts are determined using the radial increments  $RINT$ . The two integrals are represented by  $X2$  and  $X3$ . Finally at sequence number 191, the resultant integrals are squared and added together to yield the shape of the image profile  $HR$ . Before using  $HR$ , it is normalized so that it has a value of 1 at  $r=0$ .

From sequence numbers 195 through 210 the normalized image profile  $HR$  is integrated over the radial area. The result is represented by  $X4$ . Then the total laser power  $POX$  is used in conjunction with  $X4$  to arrive at the irradiance  $QP$  on the retina at  $r=0$  presuming no internal reflections or absorption. Reflections and absorption are considered in subroutine  $HTXDEP$ .

#### Retinal Image: Sequence Numbers 217-218

In cases in which the specified profile is to be projected directly onto the retina (by setting  $IFIL=0$ ),  $HR(j)$  is set equal to the specified profile  $PR(j)$ . After the above computations are completed, subroutine  $IMAGE$  is never reentered.

#### 7.1.4 Subroutine $HTXDEP$ of Retinal Model

This subroutine assesses the rate of energy deposition into the various regions of the eye on a per unit volume basis. A discussion of the techniques used is given in Appendix F. The primary advantage of this analysis is that the eye's interfaces need not coincide with the boundaries between grid increments.

To determine the rates of energy deposition, the subroutine starts with the image profile and assumes that it exists at all depths of the eye. This assumption is reasonable in the vicinity of the retina where much of the heat is concentrated. Discrepancies will increase with distance from the retina. However, at depths far removed from the retina, errors are of secondary importance because of the relatively low rates of energy deposition.

#### Retinal HTXDEP: Sequence Numbers 13-15

These statements control the course of the calculations. Initially, the control index IHT is set equal to two in the main program while QP has a value exceeding  $1 \cdot 10^{-10}$ . Therefore, the heat deposition rates  $S(i,j)$  are evaluated following the first entry of the subroutine. After these computations are completed, IHT is set equal to 1 so that the same  $S(i,j)$  values are used throughout the pulse. This means, of course, that the laser power is constant during the pulse. Once the pulse is over, QP is set equal to 0 in the main program causing the subroutine to set IHT and all the  $S(i,j)$  equal to zero. Once IHT assumes a value of zero, all future entries are aborted.

#### Retinal HTXDEP: Sequence Numbers 16-32

Here the subroutine sets LZ equal to the number eye media + 1. Moreover, LZ0 is set equal to the number of eye media. LZ1 is set equal to the number of interfaces in the eye and underlying tissue. Then the boundarys ZH(i) of the z increments are evaluated, and the arrays II, IZ, AB, REF and REFL are initialized to zero. These arrays will be discussed as they are evaluated. Finally, the reflection coefficients REF are assigned values at the retina and sclera. Here REF(1) has been set to 0 since corneal reflection is accounted for in the irradiance QP.

#### Retinal HTXDEP: Sequence Numbers 37-47

Then the code uses the known absorption coefficients APE and ACH for the pigment epithelium and choroid, respectively, to assess the absorption coefficient for the portion of the PE containing granules and the portion void of granules. To distinguish between the two portions of the PE, the user must assign a value for the fractional distance RPE of their interface from the front of the PE. This datum is read in on data card 13 of the main program. The coefficient for the front portion of the PE is represented by APE1 while the coefficient for the rear portion of the PE is represented by APE2. In monkeys, the granules are at the front of the PE while in humans the granules are at the rear. To accommodate this difference, ICX should be assigned a value of 0 when considering

monkeys, and a value of 1 when considering humans. This index is read in on data card 4 of the main program.

To evaluate the coefficients APE1 and APE2, the portion of the PE void of granules is assumed to have an absorption coefficient equal to that of the choroid. The absorption coefficient of the remaining portion of the PE is then selected consistent with the absorption of energy by the entire PE. This condition requires that the sum of the products of the absorption coefficients and PE thicknesses are equal for the two cases.

Next, a determination is made of the fraction AP of the granulated PE's energy absorbed by the granules. This evaluation is made by first computing the energies absorbed by granulated PE and by an equivalent thickness of choroid. Then the fraction AP is found by dividing the difference by the energy absorbed by the granulated PE. The fraction AP is later combined with computations of subroutine MXGRAN to predict how the average temperature of the granules decay in time. Finally, the i index IG of the first point in the granulated PE is assigned.

#### Retinal HTXDEP: Sequence Numbers 50-102

After assigning the absorption coefficients to the array ABS, the subroutine evaluates the arrays AB, II, IZ and ABR. For details of this analysis the reader is referred to Appendix F. Here  $AB(i,L)$  represents the product of the absorption coefficient and thickness of each eye media in the increment containing  $Z(i)$ . The index L ranges from 1 to the total number of media contained within the element. To identify which media interfaces are located within the increments, the array  $II(i)$  is used to represent the number of interfaces within the i-th increment plus 1, while  $IZ(L)$  represents the argument of the first interface ZD within the increment. The array  $ABR(i,L1)$  represents the sum of the  $AB(i,1)$ ,  $AB(i,2)$ ... associated with each media between  $ZH(i-1)$  and  $ZD(L1)$ .

In order to prevent the possibility of underflow due to excessively large values of AB or ABR, they were limited to a value of 10. This value was chosen since it means that practically all the energy will be absorbed within the particular element.

#### Retinal HTXDEP: Sequence Numbers 104-122

In this portion of the subroutine, the incoming irradiance is followed through each media to find rates at which energy is being deposited into each increment. Here X3 represents the irradiance entering an increment; X2 represents irradiance entering the next increment; and X4 represents the irradiance reflected away. To account for irradiance changes with radius, the resultant values are multiplied by the normalized image profile. To arrive at the rates of energy deposition  $S(i,j)$  per unit volume, the above product is divided by the increment's depth, i.e.  $ZH(i)-ZH(i-1)$ .

To guard against the possibility of underflow,  $S(i,j)$  is set equal to zero when it becomes excessively small ( $10^{-10}/DPULSE$ ).

#### Retinal HTXDEP: Sequence Numbers 125-145

From sequence number 125 through 131, the reflected intensities REFL are evaluated for each of the interfaces. Immediately thereafter, each of the reflected irradiances are followed through the eye to arrive at the rates of energy deposition into each increment. Here we have assumed the rays move in an axial direction, and have neglected multiple reflections.

#### Retinal HTXDEP: Sequence Numbers 151-154

As mentioned earlier, after the pulse is over,  $S(i,j)$  and IHT are set to zero. Thereafter, all subsequent calculations by this subroutine are aborted.

#### 7.1.5 Subroutine MXGRAN of Retinal Model

In this subroutine the granule temperatures are calculated neglecting

- heat absorbed by changes of state
- energy losses due to pressure waves and mechanical displacements

Thus all granule temperature predictions represent upper bounds. The subroutine starts with a description of how the average temperature rise of the granules decays with time following the instantaneous deposition of heat. These results were obtained from

the analysis of Appendix C and are placed on data cards at time intervals of  $3.0 \cdot 10^{-8}$  sec. During intervals of  $0.3 \cdot 10^{-8}$  sec, heat conduction from the granules is insignificant. These temperature rises are represented by TS, and were computed by placing a given quantity of heat in the granules and using the finite-difference equations of Appendix C to determine the transient temperatures. The quantity of heat was chosen so that the average temperature rise of the granules and their immediate environment is  $1^\circ\text{C}$ .

Most laser pulses are sufficiently long (i.e.  $> 10^{-8}$  sec) to allow significant heat conduction from the granules to their immediate surroundings during the pulse. Such cases may be treated by subdividing the pulse into LPT incremental pulses of  $0.3 \cdot 10^{-8}$  sec duration, and adding the temperature contributions from each incremental pulse. The incremental pulse duration of  $0.3 \cdot 10^{-8}$  sec is represented by BT. If the normalized temperature rise from a single incremental pulse is TS(t), then the normalized temperature rise T(t) produced by LPT incremental pulses is:

$$T(t) = \sum_{n=1}^{LPT} TS(t-(n-1)BT)/LPT \quad (32)$$

With time, both TS and T approach  $1^\circ\text{C}$ . When T equals one there is no temperature difference between the granules and their immediate environment.

To relate the above results to the temperature rises of the PE, one must account for the fact that only a portion of the PE's energy is deposited into the granules. This fact is accounted for in the main program by use of the factor AP. To arrive at the actual granule temperature rises, the normalized temperature rises are multiplied by the temperature rise of the PE volume within which they lie.

Here the temperature rises are evaluated at the times XT(K), and the results stored in XPD(K). To conserve on computational time the summation is made only when the contributions from TS

are significantly greater than  $1^{\circ}\text{C}$ . In this regard, the incremental pulses cease to be important after a time  $\text{LTMAX} \cdot \text{BT}$ .

Retinal MXGRAN: Sequence Numbers 12-30

If the pulse duration  $\text{DPULSE}$  is greater than  $1 \cdot 10^{-5}$  sec, the peak temperature achieved by the granules will not exceed that of its immediate surroundings. Therefore, for such exposures the transient temperature calculations are aborted. In addition this section assigns values to  $\text{BT}$  and  $\text{LPT}$ , and evaluates  $\text{TS}$  at each  $\text{BT}$  interval using the data provided  $\text{TS}$  at intervals of  $10 \cdot \text{BT}$ .

Retinal MXGRAN: Sequence Numbers 33-62

In order to conserve on computational time, the subroutine distinguishes between short pulses in which the pulse duration  $\text{LPT} \cdot \text{BT}$  is less than the time for heat dissipation following the first incremental pulse, namely  $\text{LTMAX} \cdot \text{BT}$ .

In this portion of the code  $\text{LPT}$  is less than  $\text{LTMAX}$  so that all  $\text{LPT}$  temperature contributions are significant during the pulse. After the pulse, an increasing number  $\text{PO}$  of the incremental pulses cease to be important while  $(\text{LPT} - \text{PO})$  are significant.

Therefore, at sequence numbers 57 through 59 the sum of the temperature contribution  $\text{X2}$  is first set equal to  $\text{PO}$ . Then the remaining contributions are added to  $\text{X2}$  on a one by one basis. Finally the sum  $\text{X2}$  is divided by the total number of contributions considered.

Retinal MXGRAN: Sequence Numbers 65-87

In this section, the subroutine performs the calculations for cases in which the pulse duration  $\text{LPT} \cdot \text{BT}$  exceeds  $\text{LTMAX} \cdot \text{BT}$ . Here the only difference from the earlier case is the manner by which the significant contributions are identified. Otherwise, the determinations of  $\text{XPD}(\text{K})$  are the same.

Retinal MXGRAN: Sequence Numbers 90-92

When the granule temperatures do not differ from those of their surroundings, all subsequent values of  $\text{XPD}(\text{K})$  are set equal to 1. After printing the values for  $\text{XPD}$ , the subroutine calculations are completed and never repeated thereafter.



#### 7.1.6 Subroutine BLOOD of Retinal Model

Subroutine BLOOD considers blood flow both in the chorio-capillaris and in tissues surrounding the eye. To this end we have used the analysis described in Appendix B to determine the changes needed in the matrix elements  $A(i,2)$ ,  $B(j,1)$ ,  $B(j,2)$  and  $B(j,3)$  to account for blood flow. The elements  $A$  and  $B$  represent the factors by which various differences of temperature rises must be multiplied to account for heat conduction. The coefficients  $B$  are associated with heat conduction along radial directions while the coefficients  $A$  are associated with heat conduction in the axial direction.

##### Retinal BLOOD: Sequence Numbers 19-21

Here we determine the interfaces between the radial points  $R(j)$  needed to assess the rates of blood flow entering and leaving each radial increment of the chorio-capillaris.

##### Retinal BLOOD: Sequence Numbers 22-31

Here determinations are made of the blood flows, entering  $XI(j)$  and leaving  $XO(j)$  the chorio-capillaris at points  $R(j)$ . These flows are on a per unit area basis and are interpolated using the flows  $XFLOW1(L2)$  and  $XFLOWO(L2)$  specified at radial distances of  $OFLOW(L2)$ .

##### Retinal BLOOD: Sequence Numbers 32-46

Next the arrays  $XFLOWX(j)$ ,  $FLOWI(j)$  and  $RD(j)$  are evaluated. For a description of these arrays see Appendix B.

##### Retinal BLOOD: Sequence Numbers 54-77

At sequence numbers 54-61 the necessary changes  $BV$  and  $BB$  of the matrix elements  $A$  and  $B$  are evaluated using Eq. B-17. Following these computations, the arrays  $IV(i)$  and  $IAB(i,j)$  designating the locations of the two blood flows are specified. The array  $IV(i)$  is set to 1 for all  $i$  values corresponding to points in the chorio-capillaris and 0 otherwise; the array  $IAB(i,j)$  is set to 1 for all  $i,j$  values corresponding to points in the tissues surrounding the eye and 0 otherwise. Blood flow is not

considered at a particular location  $i,j$  of the eye when both arrays are zero.

Because of the possibility for rapidly changing temperatures, this subroutine is reentered at each time step used in the single pulse calculations of the main program.

## 7.2 Corneal Model

The Corneal model computes damage either on the cornea or lens and consists of a main program plus four subroutines. Principal features of the code are illustrated in Fig. 10. Here we shall describe each part of the Corneal model using the listing presented in Appendix L. Throughout this discussion we shall refer to the sequence numbers at the left-hand side of the listing. Included in Appendix L is a description of the variables and sample data used in the code.

All input data required by the code are read in the main program. The order in which the data are read in is indicated by the numbers at the right-hand side of the listing. Read statements with asterisks are executed only for irregular laser profiles.

Some of this discussion is a repeat of that for the Retinal model due to the many similarities between the two models.

### 7.2.1 Main Program for Corneal Model

Figure 11 illustrates key portions of the main program. Numbers in the boxes refer to the sequence numbers of the listing.

#### Corneal Main: Sequence Numbers 1-52

Sequence numbers 24 through 26 define the number N1 of uniform grid increments, and the total number N3 of grid points in the radial grid. Here N1 must be less than N3. The size of the smallest radial grid increments DR is established at sequence numbers 29 and 30. For gaussian or irregular laser profiles, DR is found by subdividing the lesion radius LESION into an integer number LIM of increments. For uniform profiles, DR is found by subdividing the profile radius RIM into (LIM-.5) increments. The latter choice was made so that the boundary of the radial increments would coincide with RIM. At present all values of DR should be larger than about 0.0003 cm to avoid temperature instability. To use smaller DR values, the size of the initial time steps DT must be decreased and the dimension KT increased in the appropriate arrays (see Appendix L). If one wishes to reduce DR by a factor  $\xi$ , then DT should be decreased by the factor  $\xi^2$ .

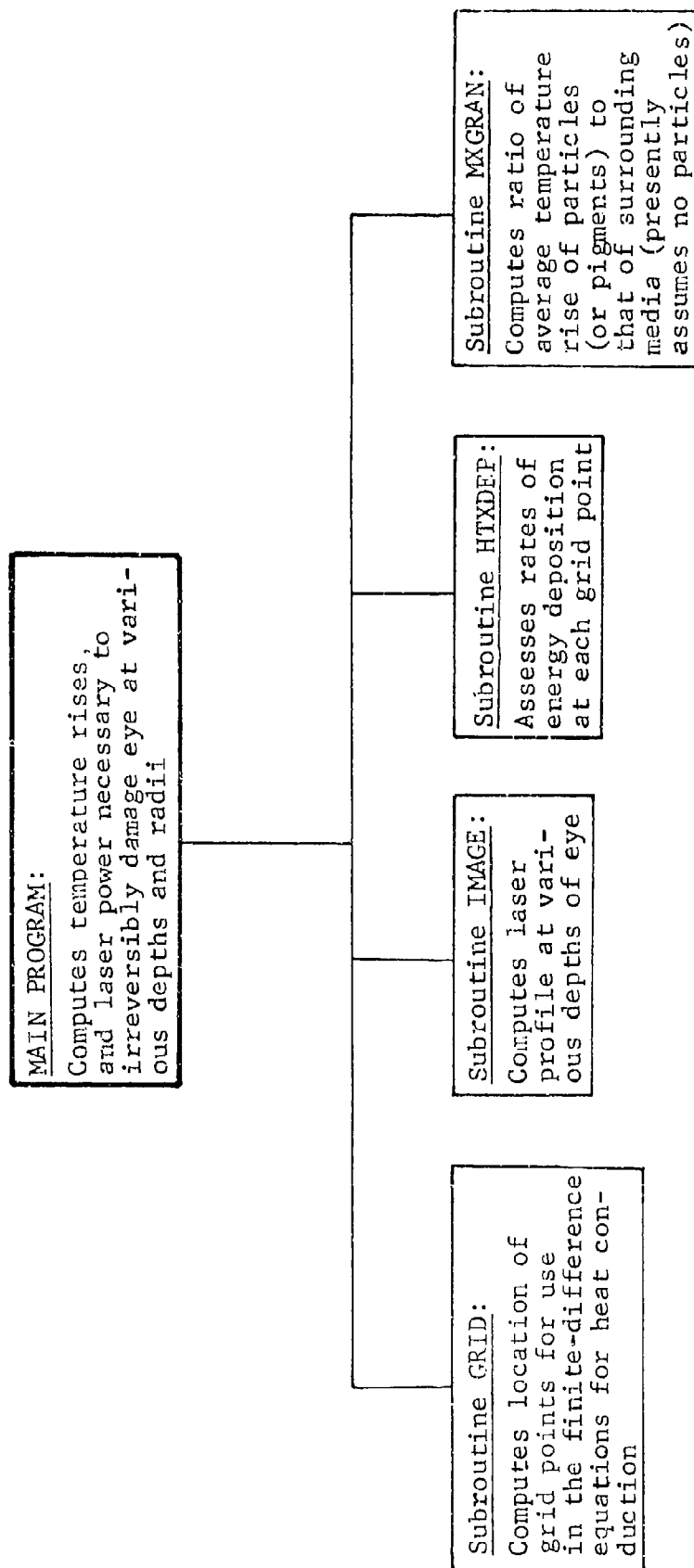


Fig. 10 SCHEMATIC ILLUSTRATION OF PRINCIPAL ROUTINES OF CORNEAL MODEL

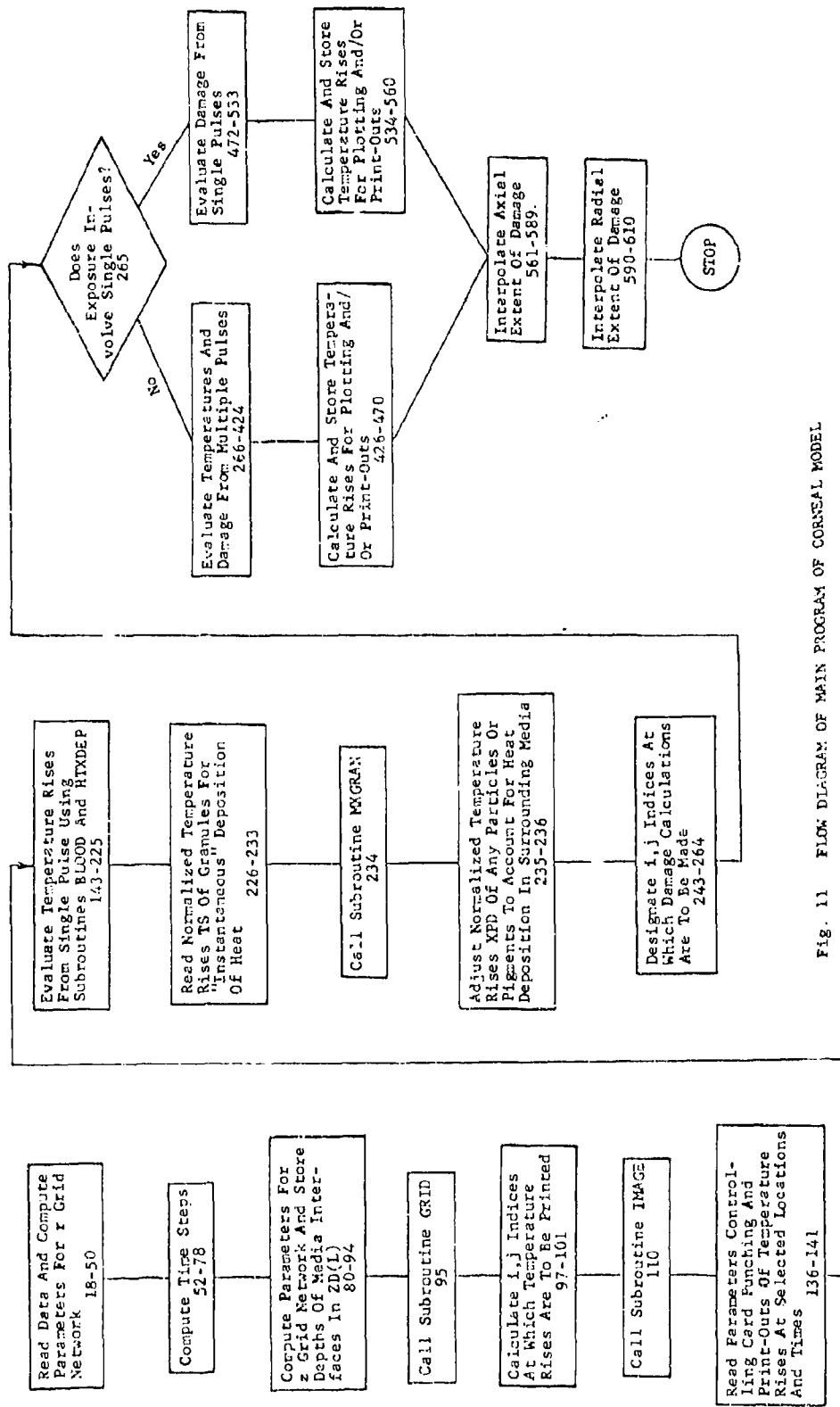


Fig. 11 FLOW DIAGRAM OF MAIN PROGRAM OF CORNEAL MODEL

At sequence numbers 36 and 37, the index LPX is set equal to 0 or 1 according to whether the laser exposure involves single or multiple pulses, respectively. This index is used to control the course of the computations. At sequence numbers 41 and 42, the laser power and pulse duration are altered when the pulse duration is less than  $0.3 \cdot 10^{-8}$  sec. In these alterations, the total energy is preserved. These changes save on computational time and reflect the fact that the conduction of heat over dimensions of 0.0001 cm is insignificant during times less than  $0.3 \cdot 10^{-8}$  sec.

Corneal Main: Sequence Numbers 57-61

At sequence numbers 57 through 61, the time step DT and the total time TIME are computed for single-pulse exposures using the arrays XCT, NPT, and KTT as a function of the pulse duration DPULSE. The expansion factor XC by which successive time steps are increased is selected from the values of the array XCT. The number of time steps NP within DPULSE is selected from values in the array NPT; and the total number of time steps KT is selected from the values in the array KTT. The values assigned these arrays are given on data cards 18, 17, and 19, respectively. The result of these computations is time steps, DT,  $XC \cdot DT$ ,  $XC^2 \cdot DT$ , ...,  $XC^{(KT-1)} \cdot DT$ , where the total time TIME is given by

$$TIME = \sum_{n=0}^{KT-1} (XC)^n \cdot DT = DT \cdot \frac{XC^{KT} - 1}{XC - 1} = XT(KT) \quad (34)$$

The elapsed time from the start of a pulse to the K-th time step is represented by  $XT(K+1)$ . Here  $XT(1)=0$ . At the end of a pulse of duration DPULSE,

$$XT(KM) = DPULSE \quad (35)$$

Corneal Main: Sequence Numbers 64-75

At sequence numbers 64 through 73, the code computes TIME, and DT for multiple-pulsed exposures. Also the expansion factor XC is set equal to the relatively large value of 1.4 so that the total time TIME brackets all the pulses without resorting to large numbers of time steps. The total time TIME is determined by first evaluating the train length and then multiplying the result by

the value found in the array FTIME for the pulse width. To provide maximum flexibility the array FTIME is described by input data as a function of pulse duration. Elements of FTIME should always be greater than 1.

If the temperature rises from a pulse do not approach zero in the allotted time, then one should increase the particular element of the array FTIME corresponding to DPULSE.

At sequence number 73, DPULSE is subdivided into NP uniform time steps of magnitude PTIME (see Appendix D) for subsequent damage evaluations. For more refined damage calculations, one can increase the number of intervals bearing in mind that it will require increases in the dimensions of arrays with arguments KT and KX (see Appendix L). Here KX equals the total number of time intervals used to evaluate damage from pulse to pulse and presently equals NP+3 (see sequence number 294).

At sequence numbers 74 and 75 the final values for KT and KM are specified for single or multiple-pulsed exposures.

#### Corneal Main: Sequence Numbers 80-85

At sequence numbers 80 through 85, the  $i$  indices for the axial grid points are chosen along with the size of the smallest increment DZ on the  $z$  axis. Here DZ is chosen according to the pulse duration DPULSE, absorption coefficient (ABS(1) for corneal damage or ABS(4) for lens damage) and the constants DZ1 and DZ2 assigned on card no. 1. To ensure DZ is not too large, the user should examine the temperature results for excessive temperature changes. Such cases may be remedied by altering the values assigned DZ1 and DZ2.

#### Corneal Main: Sequence Numbers 87-95

From sequence numbers 87 through 94, the distances ZD of the various interfaces from the cornea are computed using the assigned thicknesses TH for the various media. Here ZD(8) is set equal to an exceptionally large value to ensure it contains Z(M3), the last grid point on the  $Z$  axis.

At sequence number 95, subroutine GRID is called to compute

- the locations of all grid points  $Z(i)$ ,  $R(j)$ ,

- the indices for the various eye media, and
- other spatially-dependent thermal properties.

A discussion of this subroutine is given in Section 7.2.2.

#### Corneal Main: Sequence Numbers 97-101

Here the  $i, j$  indices, at which temperature print-outs are desired, are computed. These points are chosen according to the values assigned ID1, ID2, JD1 and JD2 on data card no. 11. Temperature print-outs are provided for  $i$  indices ranging from IP1+ID1 (input) to IP1+ID2 (input), where IP1 refers to first point in the cornea regardless of the value assigned ILENS.

#### Corneal Main: Sequence Number 110

In this section subroutine IMAGE is called to store the normalized irradiance profile (corneal) in the array HR(j) and to assess how the profile is altered in depth by corneal refraction. This subject will be returned to in Sections 7.2.2 and 7.2.3. Input data describing gaussian and uniform profiles are to be placed on data cards 4 and 6, while other profiles may be designated by using data cards 1C\*\*, 19\*\* and 19A\*\*\* of subroutine IMAGE.

#### Corneal Main: Sequence Numbers 113-123

In this section the initial temperature rises are set to an insignificantly small non-zero ( $10^{-10}$ ) value. This provision is provided to prevent subsequent underflow. Computer installations without library routines to handle underflow will not tolerate temperature rises of the order of  $1 \cdot 10^{-37}$  that are other than zero.

#### Corneal Main: Sequence Numbers 145-225

This part of the code assesses temperature rises caused by a single pulse as described by Appendix A. Here heat is deposited at a rate of  $S(i, j)$  per unit volume at each point  $Z(i)$ ,  $R(j)$  during the pulse, i.e. at times of XT(1), XT(2)...XT(KM). Immediately after the pulse,  $S(i, j)$  is set equal to zero by subroutine HTXDEP.

Two provisions are left to the discretion of the user. The first is that one can reduce the time intervals used to compute the temperature rises without changing the time steps XT(K)-XT(K-1).



This involves changing the integer IKX which provides for  $2 \cdot IKX$  time intervals of size  $(XT(K) - XT(K-1)) / (2 \cdot IKX)$ .

IKX may be altered by adjusting the values assigned EDT1 and EDT2 on data card no. 12. This provision is included so that one can improve accuracy or eliminate instability without having to increase the number of time steps KT and storage. Except for long pulse times, a value of 1 for IKX is usually adequate. To reflect the fact that IKX should be greater than 1 for pulse widths of the order of 1000 sec or more, DPULSE has been included in the evaluation of IKX.

The second option is the times at which temperature print-outs are desired. This option is provided by the value assigned ITYPE in the input data. If one wishes print-outs at each of the times  $XT(K)$ , then one merely sets  $ITYPE = 1$ . If one wishes print-outs at every n-th  $XT(K)$  then ITYPE should be set equal to n. Print-outs will always be provided at the conclusion of the pulse as well as at the last time  $XT(KT)$ .

#### Corneal Main: Sequence Numbers 231-236

This part of the code is provisional in that it applies only if there are any particles in the eye. At present, no particles are considered so that subroutine MXGRAN sets both XPD and AP equal to one. The above discussion also applies to the arrays  $VE(L, K, 2)$  and  $VZ(L, L6, L3, 2)$  which will be discussed later in this section.

#### Corneal Main: Sequence Numbers 243-262

Here we select the points  $ID(L)$ ,  $JD(L)$  at which damage calculations are to be made. Two input parameters are required to specify the points. The first is the radial distance RMAX over which damage assessments are desired. Damage is evaluated for all grid points starting at  $R(1)$  and ending at the first point beyond RMAX, namely  $R(JM)$ .

The second control one has in selecting the points is in the value assigned LIMAX. Knowing this variable, the code establishes the depth  $Z(IMAX)$  of greatest temperature rise beyond the tear layer

and the assesses the damage from  $Z(IMAX-LIMAX)$  to  $Z(IMAX+LIMAX)$ . Thus when LIMAX is set equal to zero, damage is evaluated only at the depth of highest temperature.

The number of points at which damage is to be evaluated is given by LIJ. If LIJ is larger than the allotted dimension for the arrays associated with LIJ, then the computations are halted. Moreover, care should be exercised to limit the number of points -- first, because points remote from the region of greatest temperature require considerable time to heat and cool, and secondly because of the appreciable increase of storage required when LIJ is increased.

#### Corneal Main: Sequence Numbers 269-366

In this section the temperature rises caused by multiple pulses are computed using the temperature predictions for a single pulse. Also, the array ZTT is evaluated for subsequent computations of the damage.

First, the temperature rises at the grid points,  $ID(L)$  and  $JD(L)$  at which damage calculations are desired at times  $XT(K)$  are stored in the array  $VE(L,K,n)$ . The index  $n$  is provided to distinguish between any particles and their immediate surroundings. At present this provision of the code is not used so that the temperatures  $VE$  for  $n=1$  and  $n=2$  are identical. As may be noted at sequence number 283, provisions have been made to evaluate NTEST exposures during a single computer run. These exposures may differ only in their repetition rate or number of pulses.

The basis for the multiple-pulse computations is presented in Appendix D. First temperatures are interpolated at a number of select interpulse times during and between successive pulses since the interpulse times differ from the times  $XT(K)$ . The total number of interpulse times from one pulse to the next, is given by  $KX$  -- where  $NP$  interpulse times are uniformly spaced across each pulse and three are uniformly spaced across the interval between pulses. Measured from the beginning of each pulse, the interpulse times for the thermal damage calculations are represented by  $ZTX(L3)$  while the interpulse times associated with any particle

temperatures are represented by  $ZT(L3)$ . For a description of these times the reader is referred to Appendix D.

Temperatures are stored in VZ for each pulse only when the number of pulses is less than 20. Otherwise the code groups the pulses into an odd number of IN pulses, and stores the temperatures associated with the middle pulse of each group of pulses. Later these temperatures are used to assess the damage caused by each group. The number of groups of pulses during the exposure is INX, while the number of groups of pulses contained in time TIME is represented by INXX. In order to account for the fact that the time TIME exceeds the train length, more pulses are considered than actually exist. The reason for using more pulses than exist is to provide for temperature predictions following the exposure (see Appendix D). This point will be returned to later in this section.

In order to relate the interpulse times to the times XT, it is first necessary to add the interpulse times ZTX and ZT to the product of the number of prior pulses and the time interval TC from pulse to pulse. These times are designated by X3 and are calculated at sequence numbers 331 and 335, where L7 equals the number of pulses started during the times of interest.

From sequence numbers 326-341, the temperatures during the middle pulse of the first group of pulses are evaluated and stored in  $VZ(L,L6,L3,n)$ , where L indicates the point  $ID(L)$ ,  $JD(L)$  at which the temperatures are calculated; L6 equals one for the first group of pulses; L3 designates particular interpulse times and n indicates whether the temperatures are for the media or any particles.

To interpolate the temperatures at time X3, it is first necessary to determine which pair of  $XT(K)$  bracket X3. To this end it should be remembered that the times XT are given by

$$\begin{aligned} XT(1) &= 0 \\ XT(K) &= DT \cdot \frac{XC^{K-1} - 1}{XC - 1}, \quad K \geq 2 \end{aligned} \quad (36)$$

To find the time  $XT(K)$  just prior to  $X3$ , one merely substitutes  $X3$  for  $XT(K)$  and solves for the integer value of  $K$ . In this manner  $X3$  is located between  $XT(K)$  and  $XT(K+1)$ . Linear interpolation is then used to find the temperature at time  $X3$ .

From sequence numbers 342 through 360, the computations are continued for subsequent groups of pulses i.e.  $L6=2, 3, \dots, INXX$ . In each case the computations start with the pulse following the last pulse considered, and end with the middle pulse of the succeeding group. These temperature contributions are then summed for each of the previous pulses. The result is a description  $VZ$  of the temperature rises during and following selected pulses for a total of  $IN \cdot INXX$  pulses.

As mentioned previously the number of pulses  $IN \cdot INXX$  considerably exceeds the number of pulses  $IN \cdot INX$  in the exposure. Therefore, for times exceeding the total exposure time, one must subtract the temperature contributions from the last  $IN \cdot (INXX - INX)$  pulses. This operation is performed at sequence numbers 361 through 366.

#### Corneal Main: Sequence Numbers 368-424

Here we compute the damage caused by temperatures from multiple pulses. Damage is evaluated at the points with indices  $ID(L)$ ,  $JD(L)$ . For each point, an initial estimate is made of the factor  $CQ$  by which the input laser power  $POW$  is to be multiplied to arrive at the threshold power. This operation is conducted from sequence numbers 376 through 379. The relationships used to estimate  $CQ$  are peak temperature rise achieved at the point in question. Damage computations for points having a negligible temperature rise of  $0.001^\circ C$  are aborted and the threshold power  $QD(i,j)$  set to the arbitrary value of  $10^{20}$ . Without this provision the computer could run without end in attempting to find the threshold laser power.

Having made an initial estimate of the laser power, the next step is to set the control indices LLT and LGT to 0. Later the index LLT is assigned the value 1 when the assumed laser power is less than the threshold value, while LGT is assigned the value 1 when the assumed laser power exceeds the threshold value. We will return to this subject.

The damage calculations are made from sequence numbers 384 through 395. Two criteria are used to assess damage. The first is the use of an arbitrary temperature TSTEAM. If the temperature rise VZ exceeds TSTEAM-T0, where T0 represents the initial temperature, then irreversible damage is assumed. For the computer runs considered, peak eye temperature is a poor criteria of damage. The second and more meaningful damage criteria is thermal denaturation. The latter criterion is the one used in this report. Over a time increment of say  $\Delta t$ , this criterion predicts incremental damage  $\Delta\Omega$  (see page 152) of

$$\Delta\Omega = \exp [\ln C_1 - C_2/T_a(t) + \ln \Delta t] \quad (37)$$

where  $C_1$  and  $C_2$  are constants and  $T_a(t)$  is the absolute temperature. To assess the incremental damage one merely sums the exponentials of the logarithm of  $\Delta\Omega$ . The accumulated damage DAMC is therefore given by

$$\text{DAMC} = \sum_t \exp(X_1) \quad (38)$$

where  $X_1 = \ln C_1 - C_2/T_a(t) + \ln \Delta t$ . When groups of pulses are considered,  $\Delta t$  is multiplied by the number of pulses  $1N$  per group as may be seen by examining the array ZTT back at sequence numbers 309, 316 and 319.

These damage calculations involve all ocular media other than the 6 $\mu$ m tear layer over the cornea. This layer is not considered since it consists essentially of water.

After the damage has been evaluated for the assumed laser power, CQ is either increased or decreased by 4% according to whether DAMC is less than or greater than 1, respectively. In the process LLT is set equal to one if DAMC < 1 while LGT is set equal to one if DAMC > 1. Once both LLT and LGT equal 1, the damage calculations are completed since the assumed power has crossed over the threshold value. Then one-half of the last 4% correction is returned to CQ so that one can be assured that the predicted value is accurate to within 2%.

To separate the predictions of laser power caused by the two criteria, TSTEAM is progressively increased until the last two sets of power predictions are the same. To determine when this occurs, one of the predicted laser powers is selected and stored in XQ so it may be compared with its subsequent value.

Thus, the last two sets of power predictions are associated with thermal damage while earlier predictions indicate the laser powers necessary to produce temperature in excess of TSTEAM. One word of caution is needed at this point. Damage assessments are only made over the time TIME. At regions far removed from the region of greatest energy deposition considerable time is required to heat and cool such regions and the assigned time TIME may not be adequate. The adequacy of the time may be judged by examining the temperature print-outs. If the temperature peaks and then drops by more than about 5°C, then the predicted power is satisfactory. Otherwise, one should increase TIME through the array FTIME and increase dimensions of arrays containing the time index KT.

#### Corneal Main: Sequence Numbers 426-470

This section provides data cards for plotting the temperatures at time specified by the user. Here the temperature rises from multiple pulses are calculated at points with axial indices  $i$  ranging

from II1 through II2 and radial indices j ranging from JJ1 through JJ2. The times at which the temperatures are desired are inputted by the user in the array TIMEX. These times are measured from the start of the first pulse and may assume any value from 0 to TIME.

In addition to being provided with the temperature rises, the plotting routine must know the range of the points over which plots are desired as well as the peak temperature rise RGV of the profile. Also to aid in identifying the curves a provision has been included to label one of the curves. In this regard the plotting routine will index the curve having an assigned value II3 for i.

In addition to providing data cards for plotting, provisions are also made for print-outs of the data. Three options are available to the user. If KTYPE is assigned a value of 0, then no cards or print-outs will be provided. If KTYPE=n and KTYPEO=1 the code will only print the temperature rises at n times TIMEX(n). Values of KTYPE=n and KTYPEO=0 will provide cards as well as print-outs.

#### Corneal Main: Sequence Numbers 482-533

This portion of the code computes the damage from single pulses. The basic difference from the damage calculations for multiple pulses is the use of the temperatures at the time XT(K). Here the code assesses the damage from the KM time intervals, i.e. XT(2)-XT(1), XT(3)-XT(2), etc., during the pulse as well as an additional (KT-KM) time intervals following the pulse. As with multiple pulses, damage is evaluated by using the temperatures at the mid-points of the time intervals. Other than the difference in time intervals the computations are identical to those for multiple pulse and the same observations apply.

#### Corneal Main: Sequence Numbers 536-560

Here provisions are made for preparing data cards for constructing 3-D and 2-D profiles of the temperature at selected locations and times. Except for the use of a single pulse, the computations are identical to those used for multiple pulses.

### Corneal Main: Sequence Numbers 561-610

In the final portion of the main program, the predicted laser power QD for the specified points are used to assess the region damaged by the particular laser power specified by the user.

To assess the axial extent of the damage, the computer first scans the predicted power to find the i indices at which the predicted powers bracket the specified power  $POX=POW$ . For minimum depth of damage (low i values) the indices are I5 and I6 while for maximum depth of damage (high i values) the indices are I7 and I8. If POW is lower than all the  $QD(i,1)$ , then I6 assumes the value 0 and all remaining computations are aborted. If POW exceeds all the  $QD(i,1)$ , then the computer prints out a message indicating this fact and all future axial computations are aborted.

To interpolate the depths where  $QD=POW$ , the following equation is used

$$QD = X1 \cdot \exp(X2 \cdot z) \quad (39)$$

where QD represents the power, z represents the axial distance and X1 and X2 are constants to be evaluated. By substituting the two laser powers, say  $QD_1$  and  $QD_2$ , that bracket POW into Eq. 39 along with their axial distances, say  $z_1$  and  $z_2$ , one can solve the resultant equations for X1 and X2. The result is

$$\begin{aligned} X1 &= QD_1 / \exp(X2 \cdot z_1) \\ X2 &= \log(QD_2 / QD_1) / (z_2 - z_1) \end{aligned} \quad (40)$$

Thus, substituting X1 and X2 back into Eq. 39, replacing QD by POW, and solving for the threshold depth z yields

$$z = \log(POW/X1)/X2 \quad (41)$$

By using the pair of laser powers found for small i values and for large i values, one arrives at the minimum and maximum depths of damage along the eye's axis.

Starting at sequence number 590 a similar set of computations is made to assess the radial extent of damage for the depths at which the predicted power exceeds POX or POW. Except for the use



of r instead of z, the same analysis is used as exemplified by Eqs. 39 through 41. This then completes the description of the main program of the Corneal model.

#### 7.2.2 Subroutine GRID for Corneal Model

Subroutine GRID establishes the values for Z(i) and R(j) subject to the values assigned N, N1, N3, D1, RVL, M, M1, M2, M3, TH, and DZ in the main program. Also the subroutine evaluates the matrix elements A and B for the finite-difference solution of the heat conduction equation. Moreover, the subroutine determines the location of the i indices associated with the first and last points of each eye media. Finally, the subroutine stores the assigned thermal conductivities CON(i) and heat capacities VSH(i) at the appropriate depths Z(i).

Appendix I describes the techniques used to develop the grid network.

##### Corneal GRID: Sequence Numbers 13-19

Here the subroutine evaluates the expansion factor R2 by which the radial grid steps are sequentially increased starting at j=N1. The grid is selected such that the radial extent RVL of the eye is located at

$$RVL = (R(N-1)+R(N))/2 \quad (42)$$

For more details the reader is referred to Appendix I.

##### Corneal GRID: Sequence Numbers 27-32

In this section the radial distances of the radial points R(j) are evaluated and assigned.

##### Corneal GRID: Sequence Numbers 34-52

Here the matrix elements B(j,1), B(j,2) and B(j,3) are evaluated for the finite-difference solution of the heat conduction equation. A description of these elements and their use is given in Appendix A.

##### Corneal GRID: Sequence Numbers 54-63

This portion of the code assesses the expansion factor R1 for the z grid. Two different grids are chosen depending on

whether damage occurs at the cornea or lens. For the corneal case the anterior tear surface is located midway between the first uniform increment at  $(Z(IP1-1)+Z(IP1))/2$  while the sixth eye media extends to a depth of  $Z(M3)$ .

To assess lens damage the fine grid work starts at the depth  $ZD(4)$  of the anterior surface of the lens. This means this surface is midway between the first uniform increment located at  $(Z(M2+1-M1)+Z(M2+2-M1))/2$  while the anterior surface of the tear layer is midway between  $Z(3)$  and  $Z(4)$ .

#### Corneal GRID: Sequence Numbers 71-83

Here the subroutine computes and assigns the values for the various  $Z(i)$  using the expansion factor  $R1$ .

#### Corneal GRID: Sequence Numbers 84-108

Here the subroutine uses the depths of the various interfaces to locate the initial and last grid points in each media. The resulting  $i$  values are stored in the arrays  $IX$  and  $LX$  and then assigned to  $IP2, IP3...IP6, LP1, LP2...LP6$ .

#### Corneal GRID: Sequence Numbers 110-127

Here provisions are made for the eye media having different thermal conductivities  $CONX$  and heat capacities  $VSHX$ . To accommodate any differences, the assigned thermal properties are stored with depth in the arrays  $CON(i)$  and  $VSH(i)$ .

#### Corneal GRID: Sequence Numbers 129-136

Here the matrix elements  $A(i,1)$ ,  $A(i,2)$  and  $A(i,3)$  are evaluated for use in the finite-difference equations of the heat conduction equation discussed in Appendix A. These elements were chosen so that there is no heat flow from the cornea to the environmental air. In this regard, the effects of blinking have been neglected. This effect could be important for pulses in excess of 0.1 sec.

### 7.2.3 Subroutine IMAGE of Corneal Model

This subroutine performs two major functions. These are to determine the

- normalized laser profile at various depths of the eye (normalized means profiles have a value of 1 at the eye's axis).
- irradiance QP on the eye's axis by which the normalized profile HR must be multiplied to obtain the irradiance across the beam prior to any internal reflections or absorption. The latter are accounted for in subroutine HTXDEP.

#### Corneal IMAGE: Sequence Numbers 10-20

Here the number of radial increments is specified for determining how the profile is altered in depth by corneal refraction. The increments have a radius RINT and extend across the pupil or beam radius, whichever is smaller. The number of increments across the pupil radius PUPIL is (LI-1). The radial increments RINT are chosen accordingly. Later if the beam proves smaller than the pupil, the number of increments is reduced and stored in LII.

#### Corneal IMAGE: Sequence Numbers 21-22

Any symmetric laser profile may be accommodated by the code. The most obvious profiles are the gaussian (IPROF=1) and the uniform (IPROF=0). Other profile shapes may be handled by assigning a value of 2 for IPROF on data card 6 of the main program.

#### Corneal IMAGE: Sequence Numbers 25-41

For irregular profiles (other than gaussian or uniform), the user must specify the profile's shape on a point by point basis. This is accomplished by first assigning the number of points LR on data card 19A. Then the profile values PX and associated radial distances RX are read on data cards 19A.\* and 19A\*\*\*. The numbers used to describe the profile intensities need only be relative.

From sequence numbers 30 through 39 the code normalizes the profile values PX and then integrates the profile over it's radial area. The integral of the normalized profile is represented by X5.

Two additional determinations are made in this portion of the subroutine. The first is the determination of the irradiance QP entering the eye on the eye's axis. The second is to determine

whether or not the profile extends beyond the pupil. When the radius  $R_X(LR)$  of the profile is less than the radius of the pupil, the number of radial increments  $LII$  is reduced accordingly.

Corneal IMAGE: Sequence Numbers 42-51

Here the magnitudes of the irregular profile are evaluated at radial increments of  $RINT$  and stored in the array  $FX$  for future use.

Corneal IMAGE: Sequence Numbers 57-62

In this part of the subroutine, the code evaluates gaussian profiles at the points  $R(j)$  as well as the irradiance  $QP$ .

Corneal IMAGE: Sequence Numbers 65-67

Here the subroutine stores the values of uniform profiles at  $R(j)$ . In addition the irradiance  $QP$  is evaluated.

Corneal IMAGE: Sequence Numbers 71-95

This section is reserved for irregular profiles. Here we have avoided interpolation of the intensities at  $R(j)$  in that it could cause appreciable errors in the energy deposition. Instead an evaluation is first made of the radial area and laser power between  $r=0$  and the radial distances  $(L-5) \cdot RINT$ . The areas are stored in the array  $FA(L)$ , while the accumulated powers are stored in the array  $FP(L)$ . These arrays are then used to find the average intensity of the laser beam from  $(R(j-1)-R(j))/2$  to  $(R(j)+R(j+1))/2$  and stored in  $HR(j)$ . Then the profile is normalized at sequence numbers 93 through 95.

Corneal IMAGE: Sequence Numbers 96-116

In all the previous computations the irradiance profile  $HR$  has the same shape as that of the laser beam at the cornea. This section computes the alteration of the profile  $HR$  by corneal refraction. A discussion of the means by which this is accomplished is presented in Section 3. Here we have evaluated the array  $ZCON(i,j)$  by which  $HR(j)$  is to be multiplied to arrive at the resultant profile as a function of depth. The resultant profile becomes more compact with depth due to convergence of the beam's rays.

I

In the next section we shall discuss how subroutine HTXDEP utilizes the arrays HR and ZCON to compute the rates of energy deposition per unit volume at each of the grid points. For this purpose, one must know the absorption and reflection coefficients of the various eye media.

#### 7.2.4 Subroutine HTXDEP of Corneal Model

This subroutine assesses the rate of energy deposition into the various regions of the eye on a per unit volume basis. A discussion of the techniques used is given in Appendix F. The primary advantage of this analysis is that the eye's interfaces need not coincide with the boundaries between grid increments.

To determine the rates of energy deposition, the subroutine projects the beam rays refracted at the cornea to all depths of the eye. Refraction by the lens is not considered since it has a negligibly small effect on corneal or lens burns. Due to corneal refraction the beam converges with depth as may be seen by examining Fig. 2.

##### Corneal HTXDEP: Sequence Numbers 10-12

These statements control the course of the calculations. Initially, the control index IHT is set equal to two in the main program while QP has a value exceeding  $1 \cdot 10^{-10}$ .

The heat deposition rates  $S(i,j)$  are evaluated following the first entry of the subroutine. After these computations are completed, IHT is set equal to 1 so that the same  $S(i,j)$  values are used throughout the pulse. This means, of course, that the laser power is constant during the pulse. Once the pulse is over, QP is set equal to 0 in the main program causing a subroutine to set IHT and all the  $S(i,j)$  equal to zero. Once IHT assumes a value of zero, all future entries are aborted.

##### Corneal HTXDEP: Sequence Numbers 14-26

Here the subroutine sets LZ equal to the number eye media + 1. Moreover, LZ0 is set equal to the number of eye media while LZ1 is set equal to the number of interfaces in the eye and underlying tissue.

Then the boundaries  $ZH(i)$  of the  $z$  increments are evaluated, and the arrays  $II$ ,  $IZ$ ,  $AB$ ,  $REF$  and  $REFL$  are initialized to zero. These arrays will be discussed as they are evaluated.

#### Corneal HTXDEP: Sequence Numbers 29-74

Next the subroutine evaluates the arrays  $AB$ ,  $II$ ,  $IZ$  and  $ABR$ . For details of this analysis the reader is referred to Appendix F. Here  $AB(i,L)$  represents the product of the absorption coefficient and thickness of each eye media in the increment containing  $Z(i)$ . The index  $L$  ranges from 1 to the total number of media contained within the element. To identify which media interfaces are located within the increments, the array  $II(i)$  is used to represent the number of interfaces within the  $i$ -th increment plus 1, while  $IZ(i)$  is used to represent the argument of the first interface  $ZD$  within the increment. The array  $ABR(i,L)$  represents the sum of the  $AB(i,1)$ ,  $AB(i,2)$ ... associated with each media between  $ZH(i-1)$  and  $ZD(L)$ .

In order to prevent the possibility of underflow due to excessively large values of  $AB$  or  $ABR$ , they were limited to a value of 10. This value was chosen since it means that practically all the energy will be absorbed within the particular element.

#### Corneal HTXDEP: Sequence Numbers 75-94

In this portion of the subroutine, the incoming irradiance is followed through each media to find rates of energy deposition in each increment. Here  $X3$  represents the irradiance entering an increment;  $X2$  represents irradiance entering the next increment; and  $X4$  represents the irradiance reflected away. To account for irradiance changes with radius, the resultant values are multiplied by the profile shape  $HR(i,j) \cdot ZCON(i,j)$ . To arrive at the rates of energy deposition  $S(i,j)$  per unit volume, the above product is divided by the increment's depth, i.e.  $ZH(i) - ZH(i-1)$ .

To guard against the possibility of underflow,  $S(i,j)$  is set equal to zero whenever the rates of energy deposition become excessively small ( $10^{-10}/DPULSE \text{ cal/cm}^3\text{-sec}$ ).

#### Corneal HTXDEP: Sequence Numbers 97-120

From sequence number 97 through 103, the reflected intensities REFL are evaluated for each of the interfaces. Immediately thereafter, each of the reflected irradiances are followed through the eye to arrive at the rates of energy deposition per unit volume at each of the grid points  $Z(i)$ ,  $R(j)$ . The results are then added to the deposition rates from the incoming beam to arrive at the total rates of energy deposition.

#### Corneal HTXDEP: Sequence Numbers 123-126

As mentioned earlier, after the pulse is over,  $S(i,j)$  and IHT are set to zero. Thereafter, all subsequent calculations by this subroutine are aborted.

#### 7.2.5 Subroutine MXGRAN for Corneal Model

This subroutine is a remnant from the Retinal model for assessing temperature rises of PE granules. Since no particles are presently considered in the Corneal model, the normalized particle temperature rises  $XPD(K)$  have been set to one. If at some future date, one wishes to examine the effect of any particles, one merely substitutes a modified version of the subroutine used in the Retinal model.

#### 7.3 Description of Code for Preparing 2D and 3D Illustrations

This code utilizes the temperature rise predictions from the models to display two and three dimensional temperature rise profiles as a function of the radial and axial coordinates, and of the times from the start of the laser exposure. Provisions are made in the code for varying the angles from which the profiles are viewed as well as the dimensions of the profiles. Appendix M presents a user manual for the code along with its listing.

## 8. MODEL PREDICTIONS, AND SENSITIVITY AND ERROR ANALYSES

### 8.1 Model Predictions of Laser Power Necessary to Cause Given Lesion Sizes

A total of 18 cases were run covering corneal damage, and a total of 32 cases were run covering retinal damage. In the corneal calculations, the laser beam was refracted at the cornea so that the beam radius decreases progressively with depth. In the retinal studies, the image was identical to that estimated experimentally. Results of the two sets of computer runs are given in Tables 11 and 12 for the Corneal and Retinal models, respectively.

In both tables, the experiments are referred to by run numbers and ordered in terms of increasing pulse widths. Experimental data associated with the run numbers are presented in Tables 9 and 10 of Section 6.

#### 8.1.1 Predictions of Corneal Damage

Two criteria were used to assess the accuracy of the Corneal model -- one involving predictions of the laser power necessary to cause the given experimental lesion, and one involving predictions of the size of lesion for the given experimental laser power. From an examination of the corneal results shown in Table 11, it may be observed that with one exception, the predicted laser power always exceeds the experimental values. This discrepancy is particularly pronounced with the short pulse times of  $10^{-7}$  to  $10^{-8}$  sec. The fact that the discrepancy is much greater than can be attributed to errors in the prediction of thermal damage suggests the damage is caused by some other mechanism other than thermal or that the estimated lesion size is in error.

One likely candidate for causing the damage is the generation of compressive and tensile waves due to thermal expansion. This hypothesis is based on the fact that the energy is delivered in sufficiently small times to produce pressure waves of the order of 100 psi. The fact that the anomaly arises with short pulses probably reflects the fact that when similar quantities of energy



Table 11

COMPARISON BETWEEN COMPUTED AND EXPERIMENTAL LASER POWERS (TOTAL)  
AND LESION SIZES ASSOCIATED WITH CORNEAL DAMAGE\*

Run No.	Pulse Width, Sec	Beam Radius at Cornea (1/e <sup>2</sup> points) cm	Total Laser Power to Cause		Ratio of Calc. to Exp. Power	Lesion Radius for		Ratio of Calc. to Exp. Lesion Radius
			Exp.	Calc.		Exp.	Calc.	
1	4.50 · 10 <sup>-8</sup>	0.029	1.80 · 10 <sup>4</sup>	7.28 · 10 <sup>5</sup>	40.44	0.045	0.029	0.64
2	1.00 · 10 <sup>-7</sup>	0.034	2.70 · 10 <sup>4</sup>	2.56 · 10 <sup>6</sup>	94.81	0.053	0.010	0.20
3	1.00 · 10 <sup>-3</sup>	0.177	3.93 · 10 <sup>1</sup>	7.61 · 10 <sup>1</sup>	1.94	0.140	0.091	0.65
4	2.00 · 10 <sup>-3</sup>	0.177	2.37 · 10 <sup>1</sup>	4.13 · 10 <sup>1</sup>	1.74	0.140	0.103	0.74
5	6.00 · 10 <sup>-2</sup>	0.177	7.36 · 10 <sup>-1</sup>	1.69 · 10 <sup>-1</sup>	2.30	0.140	0.078	0.56
6	1.00 · 10 <sup>-2</sup>	0.064	5.50 · 10 <sup>-1</sup>	6.26 · 10 <sup>-1</sup>	1.14	0.045	0.042	0.93
7	1.00 · 10 <sup>-2</sup>	0.177	3.56 · 10 <sup>-1</sup>	1.12 · 10 <sup>-1</sup>	3.15	0.140	0.036	0.26
8	2.50 · 10 <sup>-2</sup>	0.064	4.00 · 10 <sup>-1</sup>	5.33 · 10 <sup>-1</sup>	1.33	0.045	0.037	0.82
9	5.50 · 10 <sup>-1</sup>	0.280	2.76 · 10 <sup>-1</sup>	3.70 · 10 <sup>-1</sup>	1.34	0.140	0.089	0.64
10	1.00 · 10 <sup>-1</sup>	0.064	1.32 · 10 <sup>-1</sup>	2.14 · 10 <sup>-1</sup>	1.62	0.045	0.031	0.69
11	1.00 · 10 <sup>-1</sup>	0.064	1.80 · 10 <sup>-1</sup>	2.23 · 10 <sup>-1</sup>	1.24	0.045	0.039	0.86
12	1.00 · 10 <sup>-1</sup>	0.177	1.21 · 10 <sup>-1</sup>	6.27 · 10 <sup>-1</sup>	0.52	0.010	0.013	1.30
13	1.25 · 10 <sup>-1</sup>	0.075	3.25 · 10 <sup>-1</sup>	3.84 · 10 <sup>-1</sup>	1.18	0.052	0.046	0.88
14	5.00 · 10 <sup>-1</sup>	0.064	6.09 · 10 <sup>-2</sup>	9.03 · 10 <sup>-2</sup>	1.48	0.045	0.033	0.73
15	5.00 · 10 <sup>-1</sup>	0.064	9.00 · 10 <sup>-1</sup>	9.21 · 10 <sup>-2</sup>	1.02	0.045	0.044	0.98
16	5.00 · 10 <sup>-1</sup>	0.075	1.35 · 10 <sup>-1</sup>	1.55 · 10 <sup>-1</sup>	1.15	0.053	0.047	0.89
17	1.00	0.177	3.78 · 10 <sup>-1</sup>	5.58 · 10 <sup>-1</sup>	1.48	0.140	0.113	0.81
18	5.00	0.177	1.47 · 10 <sup>-1</sup>	2.25 · 10 <sup>-1</sup>	1.53	0.140	0.103	0.74

\* All corneal exposures consist of single pulses

Table 12

COMPARISON BETWEEN PREDICTED AND EXPERIMENTAL LASER POWERS (TOTAL)  
TO CAUSE SPECIFIED LESIONS ON RETINA

Run No.	Pulse Width, Sec	No. of Pulses	Exp.		Ratio of Calc. to Exp. Power
			Image Radius (1/e <sup>2</sup> point) cm	Lesion Radius, cm	
3	$4.50 \cdot 10^{-11}$	7	0.0025	0.0010	$5.30 \cdot 10^3$
4	$8.00 \cdot 10^{-9}$	1	0.0025	0.0010	$2.45 \cdot 10^2$
10	$1.00 \cdot 10^{-8}$	1	0.0025	0.0010	$1.96 \cdot 10^2$
11	$1.50 \cdot 10^{-8}$	1	0.0025	0.0010	$7.31 \cdot 10^1$
19	$3.00 \cdot 10^{-8}$	1	0.0045	0.0010	$7.70 \cdot 10^2$
23	$3.00 \cdot 10^{-8}$	1	0.0025	0.0010	$4.72 \cdot 10^1$
29	$3.00 \cdot 10^{-8}$	1	0.0028	0.0010	$5.55 \cdot 10^1$
31	$3.00 \cdot 10^{-8}$	1	0.0025	0.0010	$5.69 \cdot 10^1$
32	$3.00 \cdot 10^{-8}$	1	0.0025	0.0010	$5.69 \cdot 10^1$
34	$3.00 \cdot 10^{-7}$	500	0.0025	0.0010	$1.61 \cdot 10^1$
35	$3.00 \cdot 10^{-7}$	1	0.0025	0.0010	3.93
36	$3.00 \cdot 10^{-7}$	2	0.0025	0.0010	$2.01 \cdot 10^1$
37	$3.00 \cdot 10^{-7}$	5	0.0025	0.0010	$1.93 \cdot 10^1$
40	$3.00 \cdot 10^{-7}$	50	0.0025	0.0010	$9.20$
42	$3.00 \cdot 10^{-7}$	5000	0.0025	0.0010	$8.00$
44	$7.34 \cdot 10^{-7}$	5000	0.0025	0.0010	1.09
45	$7.74 \cdot 10^{-7}$	50000	0.0025	0.0010	$5.70 \cdot 10^{-1}$
49	$1.00 \cdot 10^{-5}$	500	0.0025	0.0010	$1.50 \cdot 10^{-1}$
					$0.02$
					$0.09$
					$0.09$
					$0.36$
					$0.08$
					$0.05$
					$0.17$
					$0.17$
					$0.34$
					$1.66$
					$0.66$
					$0.96$
					$0.96$
					$0.55$
					$1.35$
					$0.81$
					$1.24$
					$0.62$

Table 12 (concl)

COMPARISON BETWEEN PREDICTED AND EXPERIMENTAL LASER POWERS (TOTAL)  
TO CAUSE SPECIFIED LESIONS ON RETINA

Run No.	Pulse Width, Sec	No. of Pulses	Exp.		Exp. Lesion Radius, cm	Total Laser Power, Watts		Ratio of Calc. to Exp. Power
			Image Radius (1/e <sup>2</sup> point) cm	Radius cm		Exp.	Calc.	
51	4.00·10 <sup>-5</sup>	5	0.0025	0.0010	0.0010	3.00·10 <sup>-2</sup>	4.44·10 <sup>-2</sup>	1.48
54	4.00·10 <sup>-5</sup>	100	0.0025	0.0010	0.0010	1.10·10 <sup>-2</sup>	3.88·10 <sup>-2</sup>	3.53
56	1.00·10 <sup>-3</sup>	1	0.0025	0.0010	0.0010	2.10·10 <sup>-2</sup>	7.63·10 <sup>-3</sup>	0.36
57	1.00·10 <sup>-3</sup>	5	0.0025	0.0010	0.0010	1.90·10 <sup>-2</sup>	7.63·10 <sup>-3</sup>	0.39
58	1.00·10 <sup>-3</sup>	50	0.0025	0.0010	0.0010	1.50·10 <sup>-2</sup>	6.18·10 <sup>-3</sup>	0.41
59	4.00·10 <sup>-2</sup>	1	0.0025	0.0010	0.0010	1.05·10 <sup>-2</sup>	3.20·10 <sup>-3</sup>	0.30
60	4.00·10 <sup>-2</sup>	1	0.0025	0.0010	0.0010	1.20·10 <sup>-2</sup>	3.37·10 <sup>-3</sup>	0.28
61	2.50·10 <sup>-1</sup>	1	0.0140	0.0010	0.0010	3.86·10 <sup>-2</sup>	1.58·10 <sup>-2</sup>	0.41
62	2.50·10 <sup>-1</sup>	1	0.0140	0.0010	0.0010	3.77·10 <sup>-2</sup>	1.52·10 <sup>-2</sup>	0.40
63	1.00·10 <sup>-1</sup>	1	0.0090	0.0115	0.0115	2.00·10 <sup>-1</sup>	5.05·10 <sup>-2</sup>	0.25
64	5.00·10 <sup>-1</sup>	1	0.225	0.0342	0.0342	3.20·10 <sup>-1</sup>	2.13·10 <sup>-1</sup>	0.67
65	1.00	1	0.7425	0.0525	0.0525	4.25·10 <sup>-1</sup>	3.91·10 <sup>-1</sup>	0.92
66	4.00	1	0.0525	0.0895	0.0895	4.25·10 <sup>-1</sup>	6.79·10 <sup>-1</sup>	1.60
67	1000.	1	0.0025	0.0010	0.0010	1.60·10 <sup>-3</sup>	1.30·10 <sup>-3</sup>	0.81

are delivered over longer times, the pressure waves are of reduced intensity. Much, however, remains to be learned about the interaction of pressure waves with eye media. In this regard, it is suspected that to irreversibly damage a particular region of the eye, one need only damage some of the critical components within the region -- not necessarily all components in the region. Identification and modeling of the critical components is no simple task.

Next let us explore the fact that most of the power predictions are higher than their experimental counterparts. The immediate thought which comes to mind is whether or not the depths at which damage are predicted are consistent with the minimum depth at which damage must occur in order to be observable. Unfortunately, this argument is not very convincing in that the predicted depths of damage vary considerably -- ranging from a few microns to tens of microns in going from short to long pulses. A more likely possibility is that thermal damage proceeds more rapidly in the cornea than in the retina. This possibility should be explored experimentally.

Finally, let us compare the size of the experimentally determined lesion with the lesion size predicted using the experimental laser power. As may be anticipated from the above discussion, the predicted lesion sizes are, with one exception, all smaller than the experimentally determined lesion sizes. While this discrepancy is not large, it is consistent enough to be of concern. The cause of the excessively small predicted lesion sizes is probably the same as the cause of the excessively large predicted laser power. In this regard, it is suspected that the rates of thermal damage for the cornea are somewhat larger than those developed for skin.

#### 8.1.2 Predictions of Retinal Damage

Results of the computer runs corresponding to experiments involving retinal damage are presented in Table 12. Notice that for pulses exceeding  $1 \cdot 10^{-7}$  sec, that the predicted laser powers necessary to cause the specified lesions fluctuate above and below their experimental counterparts. Slightly better agreement is had with the exposures involving the largest images.

namely run numbers 61, 62, 64, 65, and 66. Over this range of pulse durations, the errors appear random and therefore not suggestive of any particular source of error.

The next observation is the fact that the predicted power for the short duration pulses ( $1 \cdot 10^{-7}$  sec or less) are with one exception very low. Here we refer to run numbers 3, 4, 10, 19, 23, 29, 31, and 32. In these computer runs the image radius ranged from 0.0025 to 0.0045 cm at the  $1/e^2$  point of a gaussian profile. Much of the above discrepancy is believed due to errors in the experimentally determined image size. For example, when the image size was calculated for run number 23, the  $1/e^2$  image radius was predicted to be 0.0075 cm rather than the estimated value of 0.0025 cm used in Table 12. Using the 0.0075 cm image size, the laser power was computed to be  $1.12 \cdot 10^3$  watts which compares quite favorably with the experimental value of  $0.87 \cdot 10^3$  watts found experimentally. This, of course, raises the possibility that the discrepancies for the shorter pulses may in large part be attributable to errors in the estimated image size. Unfortunately, time did not allow this question to be explored further. The fact that the major discrepancies occur primarily with exposures having short pulses is consistent with the observation that errors in the image size have their greatest effect on predictions involving short pulses.

## 8.2 Sensitivity Runs

In order to better appreciate the consequence of parametric errors on the predictions of total laser power, four representative single-pulse exposures were first selected for the Corneal model and four representative exposures were selected for the Retinal model. Next, a set of key parameters was selected for study for each model, and estimates made of the limiting errors associated with each parameter. Finally, the computer codes were used to assess the effect of the errors on the predicted laser power necessary to initiate irreversible damage at the axis of the eye.

In these studies, all parameters were held at their nominal values except for the particular parameter being considered. Results of the sensitivity analyses are shown in Tables 13 and 14 for the Corneal and Retinal models, respectively.

#### 8.2.1 Corneal Model

Parameters varied in the Corneal model were the absorption coefficient, thermal conductivity and heat capacity plus the size of the incident laser beam, and the rates at which thermal damage occurs. A description of the nominal and limiting values chosen for each parameter is presented at the bottom of Table 13.

Four exposures were used to assess the effect of the limiting errors. These exposures involved combinations of small and large beam size, and small and large pulse durations. To better appreciate the consequence of the errors, the predicted laser powers were divided by the predicted laser power for the case when all parameters are held at their nominal values.

Examination of Table 13 shows that errors in the absorption coefficient have their greatest effect on short duration exposures, and are of minor or negligible importance for long duration exposures. This result is for the most part independent of beam size, and indicates that during extended pulses the differences in heat deposition tend to be negated by thermal conduction. In fact over extended exposures, the temperatures are most sensitive to the thermal conductivity as may be seen by examination of Table 13.

Errors in the heat capacity have their largest effect for exposures involving short pulses and small beams. This result is a consequence of the very steep and transient temperature profiles produced by the above exposures. In such exposures, the temperatures associated with threshold damage are higher than those required by longer pulses and/or larger beams. As a result, errors in the heat capacity produce greater changes in the predicted temperatures as well as thermal damage for exposures involving short pulses

Table 13

EFFECT OF VARYING INDIVIDUAL PARAMETERS ON TOTAL LASER POWER  
TO INITIATE CORNEAL DAMAGE FOR FOUR DIFFERENT LASER EXPOSURES ( $\lambda=2727$  nm)

Individual Parameters Varied From Nominal Values	Total Laser Power Necessary to Initiate Damage at Axis of Eye, Watts					
	Predicted Power For RIM=0.035cm, PW=10sec, Watts	Ratio of Power To That For Nominal Values	Predicted Power For RIM=0.035cm, PW=10 <sup>7</sup> /sec, Watts	Ratio of Power To That For Nominal Values	Predicted Power for RIM=0.025cm, PW=10sec, Watts	Ratio of Power To That For Nominal Value
None	$3.02 \cdot 10^2$	1.000	$2.66 \cdot 10^{-1}$	1.000	$1.54 \cdot 10^3$	$6.97 \cdot 10^{-3}$
ABS <sub>L</sub>	$3.49 \cdot 10^5$	1.156	$2.66 \cdot 10^{-1}$	1.000	$1.78 \cdot 10^3$	$7.00 \cdot 10^{-3}$
ABS <sub>H</sub>	$2.66 \cdot 10^5$	0.881	$2.66 \cdot 10^{-1}$	1.000	$1.36 \cdot 10^3$	$6.95 \cdot 10^{-3}$
CON <sub>L</sub>	$3.02 \cdot 10^5$	1.000	$2.41 \cdot 10^{-1}$	0.906	$1.54 \cdot 10^3$	$5.96 \cdot 10^{-3}$
CON <sub>H</sub>	$3.02 \cdot 10^5$	1.000	$2.91 \cdot 10^{-1}$	1.094	$1.54 \cdot 10^3$	$7.98 \cdot 10^{-3}$
VSH <sub>L</sub>	$2.71 \cdot 10^5$	0.897	$2.56 \cdot 10^{-1}$	0.962	$1.38 \cdot 10^3$	$6.95 \cdot 10^{-3}$
VSH <sub>H</sub>	$3.31 \cdot 10^5$	1.096	$2.76 \cdot 10^{-1}$	1.038	$1.69 \cdot 10^3$	$6.99 \cdot 10^{-3}$
CUT <sub>L</sub>	$2.80 \cdot 10^5$	0.927	$2.50 \cdot 10^{-1}$	0.940	$1.43 \cdot 10^3$	$6.61 \cdot 10^{-3}$
CUT <sub>H</sub>	$3.40 \cdot 10^5$	1.126	$2.84 \cdot 10^{-1}$	1.068	$1.65 \cdot 10^4$	$7.27 \cdot 10^{-3}$
DAMAGE <sub>L</sub>	$3.45 \cdot 10^5$	1.176	$3.54 \cdot 10^{-1}$	1.331	$1.81 \cdot 10^2$	$9.67 \cdot 10^{-3}$
DAMAGE <sub>H</sub>	$2.46 \cdot 10^5$	0.815	$1.77 \cdot 10^{-1}$	0.665	$1.25 \cdot 10^2$	$4.27 \cdot 10^{-3}$

ABS = Absorption coefficient for cornea; ABS<sub>L</sub> = 1583/cm, ABS<sub>H</sub> = 1863/cm, ABS<sub>N</sub> = 2142/cm

CON = Thermal conductivity of cornea; CON<sub>L</sub> = 0.00102 cal/cm-sec-°C, CON<sub>H</sub> = 0.00120 cal/cm-sec-°C, CON<sub>N</sub> = 0.00138 cal/cm-sec-°C

VSH = Heat capacity of cornea; VSH<sub>L</sub> = 0.9 cal/cm<sup>3</sup>-°C, VSH<sub>H</sub> = 1.0 cal/cm<sup>3</sup>-°C, VSH<sub>N</sub> = 1.1 cal/cm<sup>3</sup>-°C

CUT = Value of normalized beam profile (-1 at r=0) at r = RIM, CUT<sub>L</sub> = 0.225, CUT<sub>H</sub> = 0.250, CUT<sub>N</sub> = 0.275

DAMAGE = Temperature coefficients describing rate of thermal damage; DAMAGE<sub>L</sub> = 0.01 times nominal value and DAMAGE<sub>H</sub> = 100. times nominal value

RIM = Beam radius, cm

PW = Pulse width, sec

Table 14

EFFECT OF VARYING INDIVIDUAL PARAMETERS ON TOTAL LASER POWER  
TO INITIATE RETINAL DAMAGE FOR FOUR DIFFERENT LASER EXPOSURES ( $\lambda=1060$  nm)

Individual Parameters Varied From Nominal Values	Total Laser Power Necessary to Initiate Damage at Axis of Eye, Watts				Predicted Power For RIM=0.025cm, PW=100sec, Watts	Ratio of Power To That For Nominal Value	Ratio of Power To That For Nominal Value
	Predicted Power For RIM=0.025cm, PW=100sec, Watts	Ratio of Power To That For Nominal Values	Predicted Power For RIM=0.025cm, PW=100sec, Watts	Ratio of Power To That For Nominal Values	Predicted Power For RIM=0.025cm, PW=100sec, Watts	Ratio of Power To That For Nominal Values	Ratio of Power To That For Nominal Value
None	$7.28 \cdot 10^4$	1.000	$3.67 \cdot 10^{-2}$	1.000	$5.06 \cdot 10^2$	1.000	$3.69 \cdot 10^{-3}$
ABS <sub>L</sub>	$8.80 \cdot 10^4$	1.209	$3.67 \cdot 10^{-2}$	1.000	$6.11 \cdot 10^2$	1.208	$3.94 \cdot 10^{-3}$
ABS <sub>H</sub>	$6.24 \cdot 10^4$	0.857	$2.65 \cdot 10^{-2}$	.995	$4.33 \cdot 10^2$	0.856	$3.48 \cdot 10^{-3}$
CON <sub>L</sub>	$7.28 \cdot 10^4$	1.00	$3.25 \cdot 10^{-2}$	.836	$5.06 \cdot 10^2$	1.000	$3.16 \cdot 10^{-3}$
CON <sub>H</sub>	$7.28 \cdot 10^4$	1.00	$4.09 \cdot 10^{-2}$	1.114	$5.06 \cdot 10^2$	1.000	$4.21 \cdot 10^{-3}$
VSH <sub>L</sub>	$6.55 \cdot 10^4$	0.900	$3.67 \cdot 10^{-2}$	1.000	$4.55 \cdot 10^2$	0.899	$3.69 \cdot 10^{-3}$
VSH <sub>H</sub>	$8.01 \cdot 10^4$	1.100	3.67	1.000	$5.56 \cdot 10^2$	1.099	$3.69 \cdot 10^{-3}$
CFLON <sub>L</sub>	$7.28 \cdot 10^4$	1.000	$3.21 \cdot 10^{-2}$	.875	$5.06 \cdot 10^2$	1.00	$3.57 \cdot 10^{-3}$
CFLON <sub>H</sub>	$7.28 \cdot 10^4$	1.000	$4.50 \cdot 10^{-2}$	1.226	$5.06 \cdot 10^2$	1.00	$3.87 \cdot 10^{-3}$
RPE <sub>L</sub>	$5.78 \cdot 10^4$	0.794	$3.67 \cdot 10^{-2}$	1.000	$4.01 \cdot 10^2$	0.793	$3.69 \cdot 10^{-3}$
RPE <sub>H</sub>	$8.43 \cdot 10^4$	1.158	$3.67 \cdot 10^{-2}$	1.000	$5.85 \cdot 10^2$	1.156	$3.69 \cdot 10^{-3}$
CUT <sub>L</sub>	$6.77 \cdot 10^4$	.930	$3.52 \cdot 10^{-2}$	.959	$3.92 \cdot 10^2$	0.775	$3.48 \cdot 10^{-3}$
CUT <sub>H</sub>	$7.62 \cdot 10^4$	1.074	$3.83 \cdot 10^{-2}$	1.044	$7.15 \cdot 10^2$	1.413	$4.04 \cdot 10^{-3}$
DAMAGE <sub>L</sub>	$6.57 \cdot 10^4$	1.177	$5.30 \cdot 10^{-2}$	1.444	$5.95 \cdot 10^2$	1.176	$5.32 \cdot 10^{-3}$
DAMAGE <sub>H</sub>	$5.95 \cdot 10^4$	0.817	$1.76 \cdot 10^{-2}$	0.480	$4.12 \cdot 10^2$	0.814	$1.77 \cdot 10^{-3}$

\*ABS = Absorption coefficient for pigment epithelium; ABS<sub>L</sub> = 309/cm, ABS<sub>H</sub> = 419/cm

CON = Thermal conductivity; CON<sub>L</sub> = 0.00102 cal/cm-sec-°C, CON<sub>H</sub> = 0.00120 cal/cm-sec-°C, CON<sub>H</sub> = 0.00138 cal/cm-sec-°C

VSH = Heat capacity; VSH<sub>L</sub> = 0.9 cal/cm<sup>3</sup>-°C, VSH<sub>H</sub> = 1.0 cal/cm<sup>3</sup>-°C, VSH<sub>H</sub> = 1.1 cal/cm<sup>3</sup>-°C

CFLON = blood flow to choroid-cap illaris; CFLON<sub>L</sub> = 0.012 gm/sec, CFLON<sub>H</sub> = 0.024 gm/sec, CFLON<sub>H</sub> = 0.025 gm/sec

RPE = Fraction of pigment epithelium containing retinal granules; RPE<sub>L</sub> = 0.250, RPE<sub>H</sub> = .333, RPE<sub>H</sub> = 0.400

CUT = Value of normalized image profile (=1 at r=0) at retina for r=RIM; CUT<sub>L</sub> = .167 for RIM = 0.0025 cm, = .225 for RIM = 0.0300 cm;

CUT<sub>H</sub> = .275; CUT<sub>H</sub> = .375 for RIM = 0.0025 cm, = .275 for RIM = 0.0300 cm

DAMAGE = Temperature coefficients describing rate of thermal damage; DAMAGE<sub>L</sub> = 0.01 times nominal value and DAMAGE<sub>H</sub> = 100 times nominal value

RIM = image radius, cm

P<sub>L</sub> = image width, sec



and small beams. This explains why errors in the heat capacity have their greatest effect on predictions involving exposures with short pulses and small beams.

Beam size is controlled by the parameter CUT which describes the magnitude of the normalized gaussian beam at  $r=RIM$ . Beam size increases with the value of CUT. Errors in the beam size have their greatest effect on predictions for exposures involving the shorter laser pulses. This result can be explained by the fact that in such exposures the temperatures are highly transient. In such cases, damage is more dependent on the deposition of energy than on its dissipation by thermal conduction.

Perhaps the most important parameters studied is the rate at which thermal damage proceeds with temperature. Here the rates were increased or decreased by a factor of 100 over the entire range of temperatures. At first glance, one would suspect that such a factor is excessively large. This is in part true at temperatures up to  $60^{\circ}C$  wherein the rates were determined. Over this range of temperatures, the factor should be closer to 10 rather than 100. On the other hand, above  $60^{\circ}C$  the factor of 100 is probably unduely conservative. To appreciate the significance of using a factor of 100 one should examine how rapidly the rates of damage change as shown in Table 15.

From an examination of Table 13, it may be observed that the predicted laser power is very sensitive to errors in the rate of thermal damage. This is true for all four cases considered.

If one were to rate the parameters in need of more refined measurement one would rank them in priority as follows:

- Rate of thermal damage
- Absorption coefficient and beam size
- Heat capacity
- Thermal conductivity

Table 15

## RATES OF THERMAL DAMAGE VERSUS TEMPERATURE

Temperature, °C	Rate of Damage, 1/sec	Temperature, °C	Rate of Damage, 1/sec
44	$1.62 \cdot 10^{-4}$	82	$1.70 \cdot 10^7$
46	$4.35 \cdot 10^{-4}$	84	$6.00 \cdot 10^7$
48	$1.16 \cdot 10^{-3}$	86	$2.09 \cdot 10^8$
50	$3.03 \cdot 10^{-3}$	88	$7.19 \cdot 10^8$
52	$1.57 \cdot 10^{-2}$	90	$2.44 \cdot 10^9$
54	$7.08 \cdot 10^{-2}$	92	$8.16 \cdot 10^9$
56	$3.13 \cdot 10^{-1}$	94	$2.69 \cdot 10^{10}$
58	1.36	96	$8.78 \cdot 10^{10}$
60	5.81	98	$2.82 \cdot 10^{11}$
62	$2.44 \cdot 10^1$	100	$8.97 \cdot 10^{11}$
64	$1.01 \cdot 10^2$	102	$2.82 \cdot 10^{12}$
66	$4.08 \cdot 10^2$	104	$8.74 \cdot 10^{12}$
68	$1.63 \cdot 10^3$	106	$2.68 \cdot 10^{13}$
70	$6.40 \cdot 10^3$	108	$8.11 \cdot 10^{14}$
72	$2.47 \cdot 10^4$	110	$2.43 \cdot 10^{14}$
74	$9.41 \cdot 10^4$	112	$7.18 \cdot 10^{14}$
76	$3.53 \cdot 10^5$	114	$2.10 \cdot 10^{15}$
78	$1.30 \cdot 10^6$	116	$6.08 \cdot 10^{15}$
80	$4.74 \cdot 10^6$	118	$1.74 \cdot 10^{16}$

### 8.2.2 Retinal Model

As with the Corneal model, four laser exposures were chosen to study the effect of the limiting parametric errors on the predicted laser power necessary to initiate retinal damage. The exposures chosen involve combinations of image radii of 0.0025 and 0.0300 cm, and pulse durations of  $10^{-8}$  and 100 sec. Parameters chosen for this study were identical to those chosen for the Corneal model except for the use of the image rather than the beam profile; and the added consideration of blood flow CFLOW in the chorio-capillaris, and the fraction RPE of the pigment epithelium containing the melanin granules.

As with the Corneal model, errors in the absorption coefficient and heat capacity have their greatest impact on exposures involving short pulses. These results can be explained by the fact that the temperatures necessary to cause damage are higher with the shorter pulses. In such situations, errors in the absorption coefficient and/or heat capacity result in greater changes in the predicted temperature than achieved with long duration pulses. The result is greater changes in the rate of damage with shorter pulses, and hence in predictions of the total laser power.

The effects of errors in the blood flow are most apparent for exposures involving large images and long pulses. Here, long exposures provide greater time for the transport of heat by the blood. On the other hand, large images create less transient temperatures which in turn extend the period over which damage occurs as well as the period over which blood can remove critical heat from those portions of the eye being damaged.

Errors in the fraction RPE of the pigment epithelium containing melanin granules are most important with short pulses. The reason for this behavior is the same as advanced for errors in the absorption coefficient and heat capacity -- namely that such errors bring about greater temperature changes with the shorter pulses.

Image size was varied by varying the parameter CUT which describes the magnitude of the gaussian profile at  $r=RIM$ . In this study the limiting errors were chosen considering that large images are more precisely known percentage-wise than small images. Examination of Table 14 shows that errors in the image size are significant in all four cases considered, and are most important with exposures involving small images and short pulses. With such exposures, changes in the image size have their greatest effect on the predicted peak temperatures, rates of thermal damage, and total laser power. From an examination of Table 14, it may be observed that errors in the rate of damage have the greatest effect on the predicted laser power -- assuming the estimated limiting errors are accurate. This result is true for all four cases considered.

According to the need for more accurate measurements, the parameters are ranked as follows:

- Rates of thermal damage
- Image size
- Absorption coefficients
- Fraction of PE containing granules
- Thermal conductivity
- Blood flow
- Heat capacity

### 8.3 Assessment of Frequency Distribution of Errors Associated with Predicted Laser Power

Having gained an appreciation of how individual errors affect the predicted laser power, let us now examine the effect of all the errors on the predicted power. Here we have used Beta functions along with the limiting values of the errors to arrive at the frequency distribution of the errors for each parameter. Then these results were used along with the power predictions from the sensitivity analysis to arrive at the frequency distributions associated with the predicted laser power. This exercise was performed for each of the four cases for each of the two models.

The results are illustrated by Figs. 12 and 13 for the Corneal model, and by Figs. 14 and 15 for the Retinal model. Confidence intervals for the four cases of each model are presented below

Table 16  
CONFIDENCE INTERVALS  
ASSOCIATED WITH PREDICTED LASER POWER

Exposure	<u>Confidence Intervals</u>			
	50%	75%	90%	99%
Case 1, Cornea	.89-1.13	.81-1.21	.75-1.27	.64-1.43
Case 2, "	.84-1.14	.74-1.23	.65-1.31	.56-1.44
Case 3, "	.88-1.10	.81-1.16	.75-1.24	.64-1.37
Case 4, "	.80-1.17	.68-1.27	.61-1.36	.50-1.47
Case 1, Retina	.86-1.12	.75-1.23	.66-1.31	.53-1.48
Case 2, "	.91-1.14	.83-1.22	.76-1.30	.62-1.44
Case 3, "	.86-1.20	.72-1.33	.62-1.45	.45-1.69
Case 4, "	.92-1.13	.84-1.20	.78-1.28	.65-1.40

Here cases 1 through 4 refer to the exposures of Tables 13 and 14, reading from left to right.

The first observation to be noted from the figures is that the power predictions are slightly more accurate with the shorter pulses for the cornea and with the longer pulses for the retina. One possible cause for this difference is uncertainties in the beam profile at the retina. This source of error would have its greatest effect on retinal burns produced by short pulses, and would be of negligible importance for corneal burns. When this error is small, one would expect the damage predictions to be more accurate for the shorter pulses. The second observation is that the power predictions are slightly more accurate with exposures involving large irradiated areas for both models. One may anticipate this result in that, when the laser's energy is deposited over larger areas, errors in the optical data and thermal conduction are of lesser importance.

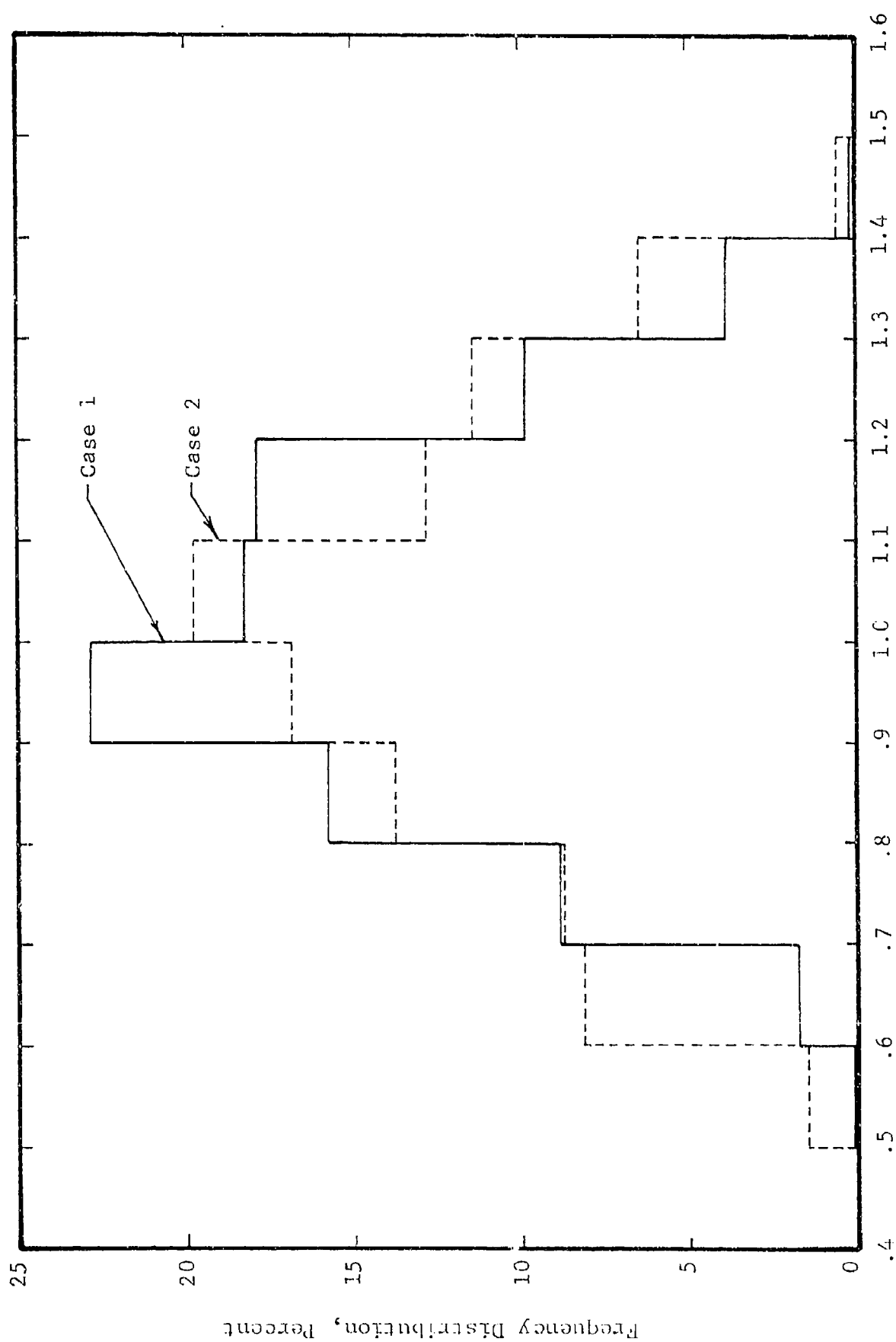


Fig. 12 FREQUENCY DISTRIBUTION OF ERRORS IN PREDICTED POWER  
FOR CORNEAL MODEL FOR BEAM SIZE OF 0.0350 CM

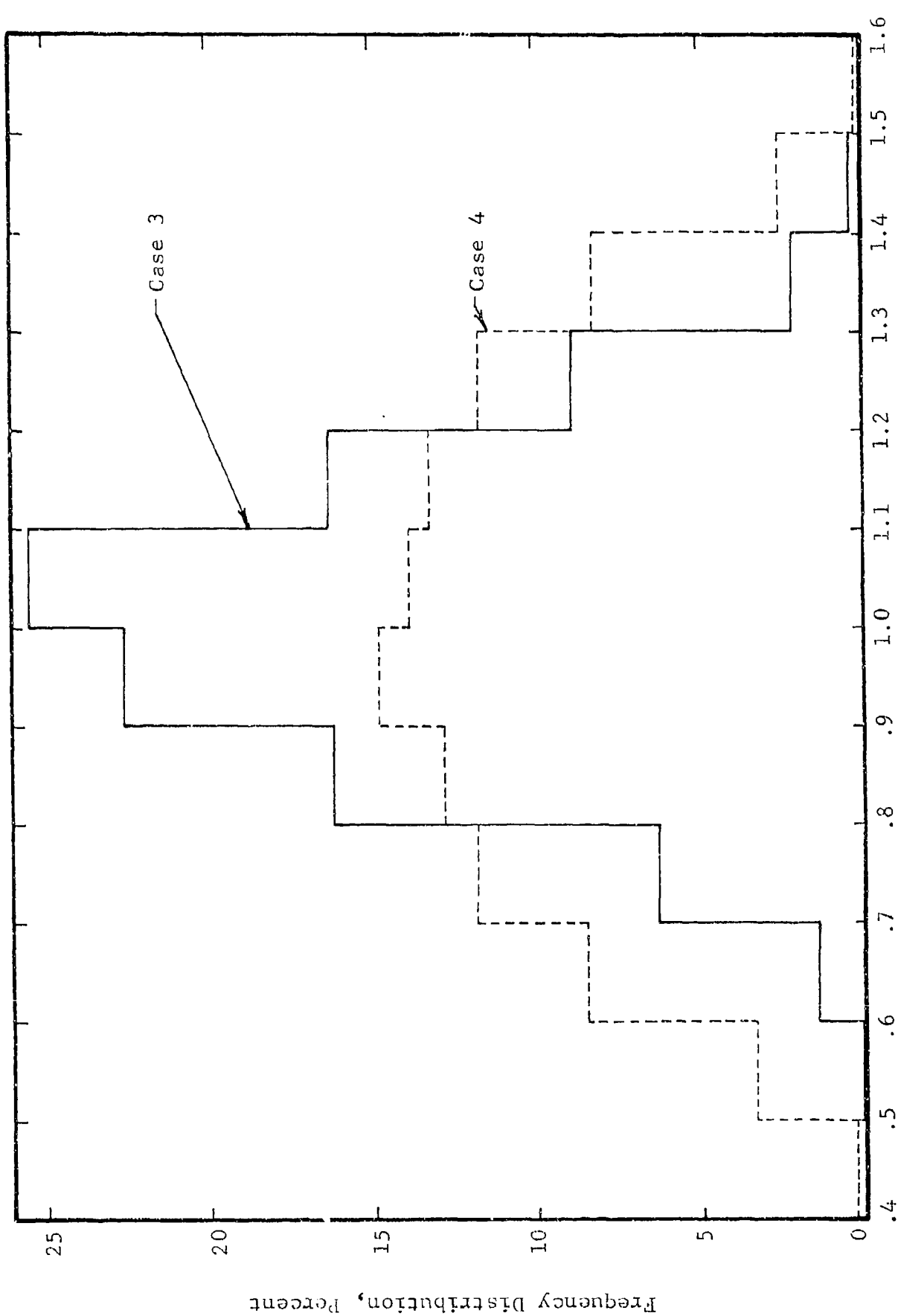


Fig. 13 FREQUENCY DISTRIBUTION OF ERRORS IN PREDICTED POWER  
FOR CORNEAL MODEL FOR BEAM SIZE OF 0.0250 CM

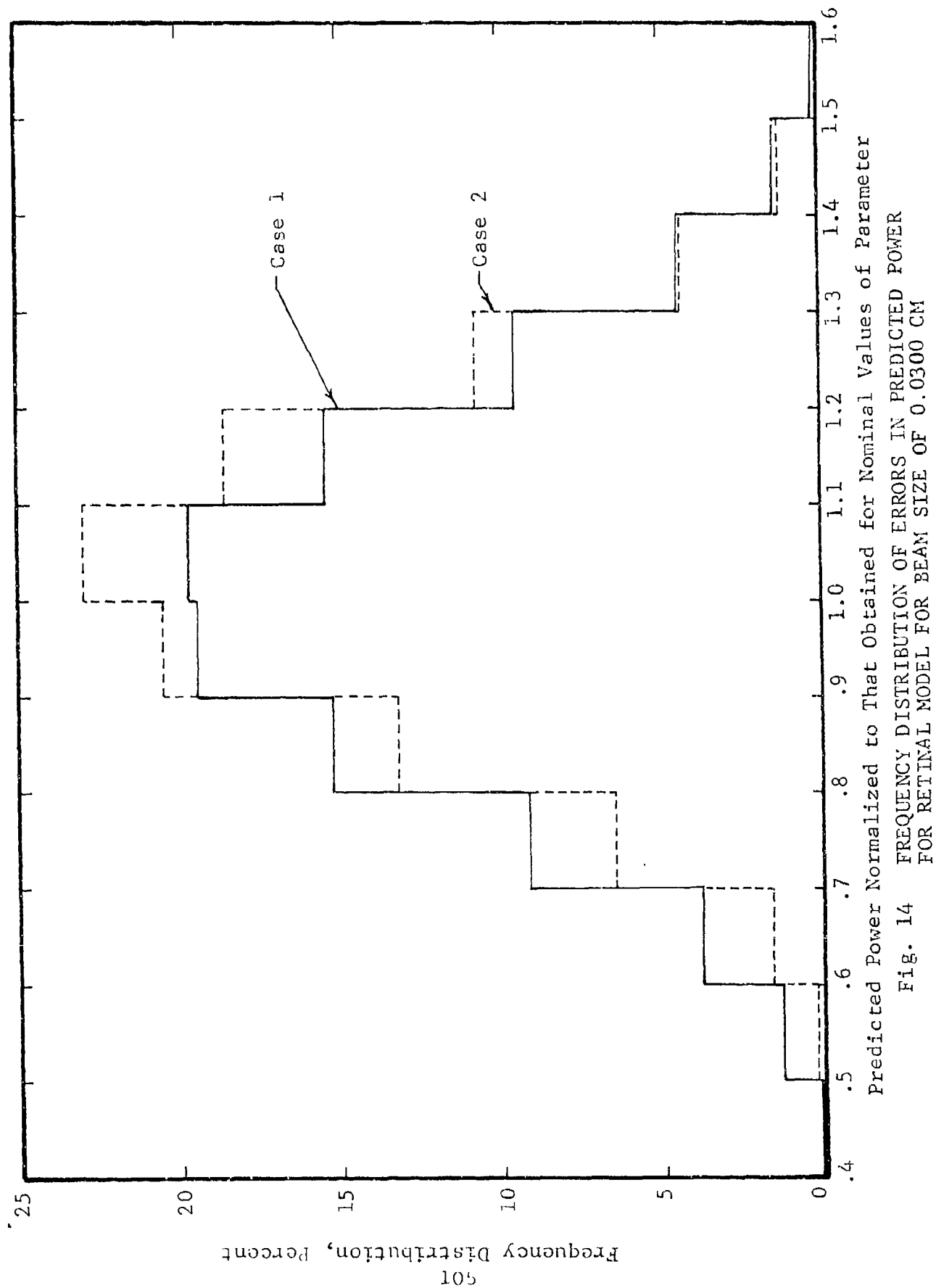


Fig. 14 FREQUENCY DISTRIBUTION OF ERRORS IN PREDICTED POWER FOR RETINAL MODEL FOR BEAM SIZE OF 0.0300 CM



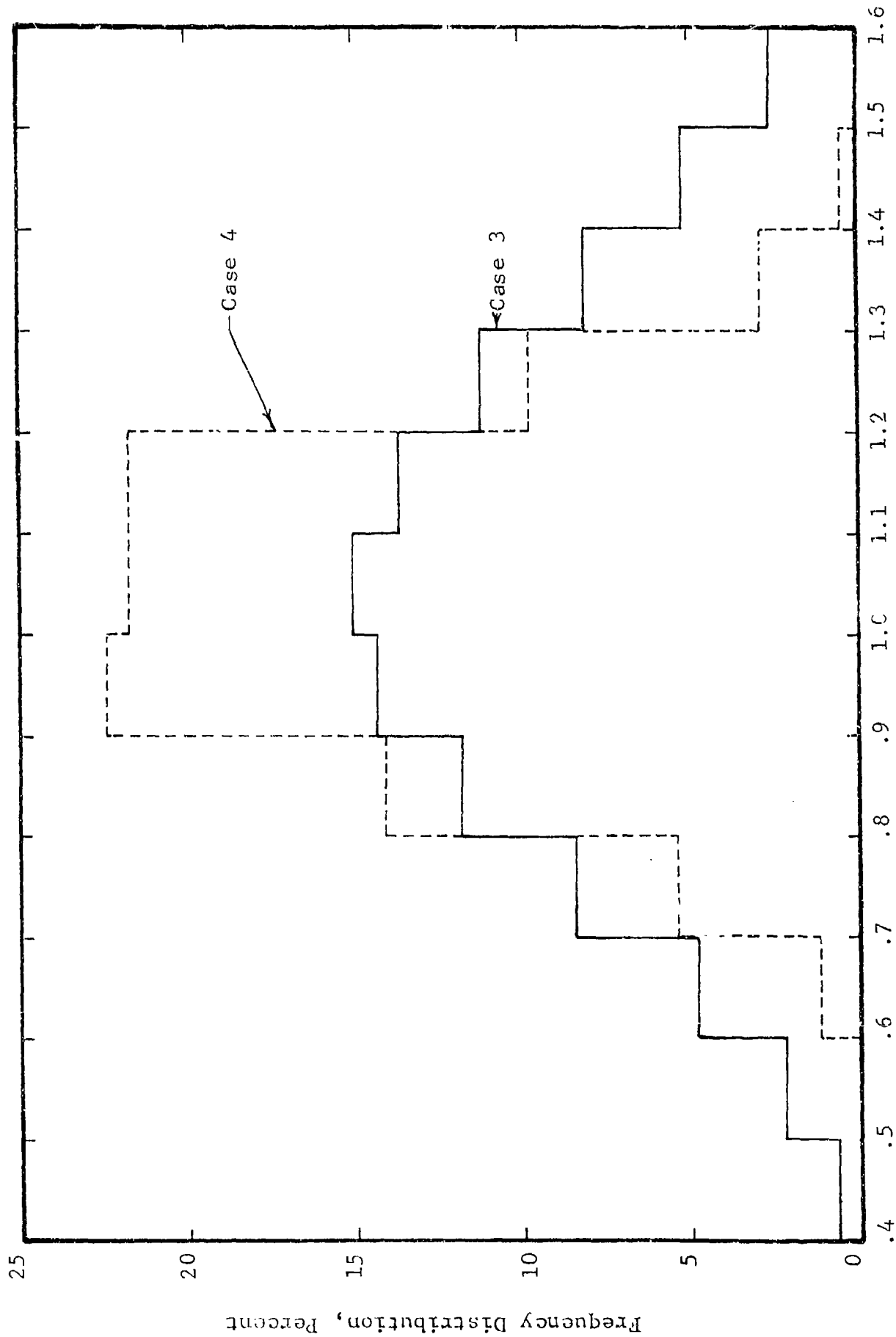


Fig. 15 FREQUENCY DISTRIBUTION OF ERRORS IN PREDICTED POWER FOR RETINAL MODEL FOR BEAM SIZE OF 0.0025 CM

As would be expected the Corneal model provides more accurate power predictions than the Retinal model. This is attributable to the fact that there are fewer variables in the Corneal model.

## 9. SUMMARY AND CONCLUSIONS

During the course of this program two codes, namely the Corneal and Retinal models, were developed to assess the temperatures and thermal damage produced in eyes by exposure to lasers. These models differ according to where one wishes to examine damage. Corneal or lens burns are treated by the Corneal model while retinal burns are treated by the Retinal model. Computer times for the models range from about 10 to 20 sec on the UNIVAC 1108 computer.

Predictions of thermal damage were made using the damage criterion presented in Ref. 3 for skin tissues. Two means were used to assess the capabilities of the models for providing accurate predictions. These were to

- assess the error in the predicted laser power due to estimated uncertainties in the input data
- compare model predictions with experimental results

### 9.1 Consequence of Parametric Errors

To assess the effect of parametric errors on the predicted laser powers, seven key parameters were chosen. Most sensitive and those requiring additional accuracy are in order of priority, for the cornea:

- Rates of thermal damage
- Absorption coefficient and beam size
- Heat capacity
- Thermal conductivity

and for the retina:

- Rates of thermal damage
- Image size
- Absorption coefficients
- Fraction of PE containing granules
- Thermal conductivity
- Blood flow
- Heat capacity

Based on estimated errors associated with each parameter two conclusions were drawn. These are that the accuracy of the predicted laser powers is approximately  $\pm 14$  percent for a 50 percent confidence interval. Of all the parameters, estimated errors for the rate of thermal damage has the greatest impact on the predictions.

## 9.2 Comparison of Model Predictions with Experimental Data

Two additional means were used to assess the capabilities of the models for providing accurate burn predictions. These involved

- 1) comparing predicted and experimental laser power for the given lesion size.
- 2) comparing predicted and experimental lesion size for the given experimental laser power.

For the retina, the agreement between predictions and experimental determinations is reasonably good for pulse durations of the order of  $10^{-6}$  sec or greater. Poorer agreement is had for pulses of  $10^{-8}$  to  $10^{-7}$  sec. The latter may be caused by errors in the image size. Of greatest concern is that with picosecond pulses (run 1 of Table 10), damage is inflicted with extremely low energies. In fact the experimental laser energies will only produce temperature rises of the order of  $10^{-3}$  C in the retina. Hence thermal damage may be discarded as a credible cause of damage for picosecond pulses. The most likely cause of damage is shocks produced within the melanin granules due to the very rapid deposition of energy. During such short deposition times the energies cannot escape either by thermal or mechanical means. The result is very pronounced concentrations of energy that lead to very steep fronted pressure waves. Whether or not such waves represent a primary cause of damage remains to be seen.

For the cornea, the predicted laser powers were almost always higher than their experimental counterparts. This discrepancy is particularly pronounced for pulses of the order of  $10^{-7}$  sec or less. Here the predicted laser powers were some 40 to 90 times larger than the experimental values. This discrepancy suggests that some other damage mechanism other than thermal is involved, such as acoustic

pressure waves. Literature studies (Ref. 4) suggest that the latter is a credible mechanism of damage. On the other hand, the discrepancy at the longer pulses suggests that the rates of thermal damage for the cornea are higher than those of the skin.

### 9.3 Problem Areas

From the above results it should be apparent that there is a serious need for information regarding the

- 1) rates at which the cornea is thermally damaged,
- 2) generation, movement and damage capabilities of shock waves,
- 3) generation, movement and damage capabilities of acoustic waves.

Measurements of the rates of thermal damage in the cornea should very substantially improve the accuracy of the predictions of corneal burns. Such studies would require a combined experimental and analytical effort -- the experiments to establish the damage and associated temperatures in the corneal and the analytical work to establish the rates of thermal damage from the experimental results.

Items 2 and 3 appear to be a likely cause of damage at the shorter pulses. To resolve this question feasibility studies are needed. Such studies should not only establish whether the above discrepancies can be attributed to pressure waves, but also identify situations in which pressure waves could cause extensive damage. Only by knowing the extent of damage caused by various phenomena can one identify the prime cause of damage.

1. White, T.J., "Observer Distances for Nuclear Events," 1, Model for Observer Distances for Retinal Burn Criteria, Report DASIAC SR 125 prepared by General Electric for Defense Nuclear Agency under Contract DASA 01-70-C-0035, NWED Subtask DC0001-04 (Mar. 1973)
2. Peaceman, "The Parabolic and Elliptic Differential Equations," J. Soc. Indust. Appl. Math. 3, pp 28-41 (1955)
3. Takata, A.N., "Development of Criterion for Skin Burns," Aerospace Medicine, pp 634-637 (June 1974)
4. Cleary, S.F. and P.E. Hamrik, "Laser-Induced Acoustic Transients in the Mammalian Eye," J. Acous. Soc. Amer. 46(2), pp 1037 (Oct. 1969)
5. Coogan, P.S., W.F. Hughes and J. Mollsen, Histologic and Spectrophotometric Comparisons of the Human and Rhesus Monkey Retina and Pigmented Ocular Fundus, Final Report on Contract AF 41(609)-71-C-0006 for USAF School of Aerospace Medicine, Rush-Presbyterian St. Luke's Medical Center (Jan. 1974)
6. Boettner, E.A., Spectral Transmission of the Eye, Final Report on Contract AF 41(609)-2966 for the USAF School of Aerospace Medicine, The University of Michigan (July 1967)
7. Geeraets, et al., "The Loss of Light Energy in Retina and Choroid," AMA Arch. Ophth. 64V, pp 606-615 (1960)
8. Geeraets, et al., "The Relative Absorption of Thermal Energy in Retina and Choroid," Invest. Ophth. 1, pp 340 (1962)
9. Geeraets and Berry, "Ocular Spectral Characteristics as Related to Hazards from Lasers and Other Light Sources," Amer. J. Ophth. 66(1) (July 1968)
10. Boettner, et al., "Transmission of the Ocular Media," Invest. Ophth. 1, pp 776-783 (1962)
11. Geeraets, et al., "Light Reflectance from the Ocular Fundus," AMA Arch. Ophth. 69, pp 612 (1963)
12. Hale, G.M. and M.R. Querry, "Optical Constants of Water in 200 nm to 200  $\mu$ m Wavelength Region," Appl. Optics 12(3), pp 555-563 (Mar. 1973)
13. Chas, B.T., Advanced Heat Transfer, University of Illinois Press, Urbana, Chicago, London (1969)

14. Wilson, T.M., et al., "The Measurement of the Choroidal Blood Flow in the Rabbit Using 85-Krypton," Exp. Eye Res. 16, pp 421-425 (1973)
15. "Thermal Problems in Biotechnology," American Society of American Engineers, New York, N.Y. (Dec. 3, 1968)
16. Maurice, D.M. "The Cornea and Sclera," The Eye 1, Davson Academic Press, New York, N.Y. (1919)
17. Gallagher, J.T., personal communication to Brooks AFB (July 1974)
18. Bruce, R., personal communication to Brooks AFB (1973)
19. Taboada, J. and R.W. Ebbers, "Ocular Tissue Damage Study for 1060 nm Ultrashort Laser Pulse Train" Post Deadline Paper OSA meeting (Apr. 24, 1974)
20. Vassiliadis, A., et al., "Investigations of Laser Damage to Ocular Tissues," AFAL TR-67-170, AFA Lab WPAFB (Mar. 1967)
21. Zweng, H.C., et al., "Experimental Q-Switched Ruby Laser Retinal Damage," Arch. Ophth. 78 (Nov. 1967)
22. Ebbers, R.W. and I.L. Dunskey, "Retinal Damage Thresholds for Multiple Pulse Lasers," Aerospace Medicine 44(3) pp 317 (Mar. 1973)
23. Gibbons, W.D., "Retinal Burn Thresholds for Exposure to a Frequency-Doubled Neodymium Laser," SAM-TR-73-45, School of Aerospace Medicine, Brooks AFB (Nov. 1973)
24. Beatrice, E.S. and P.D. Shawaluk, "Q-Switched Neodymium Laser Retinal Damage in Rhesus Monkey," Memo Report M73-9-1, Frankford Arsenal, Philadelphia, Pa. (Mar. 1967)
25. Vassiliadis, A., et al., Research on Ocular Laser Thresholds, SRI Report on contract for F41609-68-C-0041 (Aug. 1969)
26. Vassiliadis, A., et al., Investigation of Laser Damage to Ocular Tissues, SRI Report on contract F33615-67-C-1752 (Mar. 1968)
27. Beatrice, E.S., et al., Retinal Damage Thresholds Comparison of 3mm and 8mm Diameter Q-Switched Ruby Laser, Report R-1956 Frankford Arsenal, Philadelphia, Pa. (Apr. 1970)
28. Beatrice, E.S. and C.S. Steinke, Q-Switched Ruby Retinal Damage in Rhesus Monkey, Report R-2051, Frankford Arsenal, Philadelphia, Pa. (Sept. 1972)
29. Frisch, G.D., et al., "Comparative Study of Argon and Ruby Retinal Damage Thresholds," Memo Report M71-9-1, Frankford Arsenal, Philadelphia, Pa. (Apr. 1971)

30. Vassiliadis, A., Ocular Laser Threshold Investigation, SRI Report on contract F41609-70-C-0002 (Jan. 1971)
31. Dunskey, I.L. and D.E. Egbert, "Corneal Damage Thresholds for Hydrogen Fluoride and Deuterium Fluoride Chemicals," USAF School of Aerospace Medicine, Brooks AFB, Texas, SAM-TR-73-51 (Dec. 1973)
32. Stuck, "Corneal Damage Thresholds for Carbon Dioxide Laser Irradiation, Ottawa, Canada, pp 19-23 (June 1972)
33. Vassiliadis, A., Investigations of Laser Damage to Ocular Tissues, SRI Report, Contract No. F53505-67-C-1752 (Mar. 1968)
34. Cooper, et al., "The Yellow Colour of the Lens of Man and Other Primates," Jour. Physiol. 230, pp 414-417 (1969)
35. Said, F., et al., "The Variation with Age of the Spectral Transmissivity of the Living Human Crystalline Lens," Gerontologia 3, pp 2-3 (1939)
36. Ludvig, et al., "Absorption of the Visible Light by the Refractive Media of the Human Eye," Arch. Ophth., pp 20-37 (1937)
37. Alpern, et al., "Spectral Transmittance of Visible Light by Human Eye," Jour. Opt. Soc. Am. 55, pp 723-727 (1965)
38. Ruddock, R.H., "The Effect of Age Upon Colour Vision II. Changes with Age in Light Transmission of the Ocular Media," Vision Res. 5, pp 47-55 (1964)
39. Sliney, et al., "Evaluation of Optical Radiation Hazards," Appl. Optics 21(1) (Jan. 1973)
40. Norren, D., "Literature Review of Human Ocular Absorption in the Visible," Institute for Perception RVO-TVO, Report LZP-1972-S.
41. Coogan, et al., "A Histological Comparison of the Human and Rhesus Monkey Retinas and its Relation to Laser Photocoagulation," USAF School of Aerospace Medicine, Aerospace Medical Division of Brooks Air Force Base, SAM-TR.
42. Smith, et al., "Ocular Hazards of Transscleral Laser Radiation," Amer. Jour. Ophthal. 66, pp 21 (1968)
43. Goodman, Z.W., Introduction to Fourier Optics, McGraw-Hill, pp 60 (1968)
44. Born, M. and E. Wolf, Principles of Optics, third ed., Pergamon Press (1965)



45. Lotmar, W., Jour. Opt. Soc. Am. 61, pp 1522 (1971)
46. Van Meeteren, A., Optica Acta 21, pp 395 (1974)
47. el Hage, S.G. and F. Berny, Jour. Opt. Soc. Am. 63, pp 205 (1973)
48. Irvine, W.H. and J.B. Pollack, Icarus 8, pp 324 (1968)
49. Palmer, K.F. and D. Williams, Jour. Opt. Soc. Am. 64, pp 1107 (1974)
50. Wald, G. and D.R. Griffin, Jour. Opt. Soc. Am. 37, pp 321 (1947)
51. Douglas, Jr., and T.M. Gallie, Jr., "Variable Time Steps in the Solution of the Heat Flow Equation by a Difference Equation," J. Soc. Indust. Appl. Math. 3 (1955)
52. Mainster, M.A., T.S. White, J.H. Tips and P.W. Wilson, "Transient Thermal Behavior in Biological Systems," Bull. of Math. Biophysics 32(303) (1970)

APPENDIX A

COMPUTATIONAL SCHEME FOR PREDICTING EYE TEMPERATURES

## APPENDIX A

### COMPUTATIONAL SCHEME FOR PREDICTING EYE TEMPERATURES

#### 1. INTRODUCTION

In this appendix we shall describe the method used to compute temperatures within the eye as developed by Technology, Inc. (1,52) and modified by IIT Research Institute. In essence the method involves the use of finite-difference equations to assess the transient temperatures within the eye produced by exposures to a laser beam. Because the usual explicit techniques require a minimum size of time element for stable solutions, an explicit-implicit alternating direction technique was used. Here we shall briefly discuss the disadvantages of standard explicit techniques for the problem at hand and then develop the equations associated with the explicit-implicit alternating-direction method.

#### 2. DISADVANTAGES OF STANDARD EXPLICIT TECHNIQUES FOR SOLVING FINITE-DIFFERENCE EQUATIONS

Explicit techniques involve using existing temperatures to calculate future temperatures. While the equations are relatively simple, it is necessary to use a minimum size of time increment to prevent the fluxes and temperatures from oscillating with progressively increasing magnitudes. These oscillations are caused by the temperature differences and fluxes being maintained for longer times than is possible, causing exceptionally large or small temperature rises. At the next time interval, the process will be reversed and exceptionally large temperature rises will become exceptionally small, or vice versa.

Pure explicit techniques require very small time intervals and relatively large computational times to prevent such temperature fluctuations. The method described in this appendix circumvents the need for using very small time intervals by the simultaneous use of implicit and explicit techniques.

### 3. EXPLICIT-IMPLICIT ALTERNATING DIRECTION TECHNIQUE FOR SOLVING FINITE-DIFFERENCE EQUATIONS

One method by which stable solutions may be achieved by use of large time intervals is the explicit-implicit alternating-direction technique. This method is based on the work of Peaceman (2) and involves the simultaneous use of present and future temperature uses to assess future fluxes and temperature rises. This is accomplished by treating the fluxes explicitly in one direction while the fluxes are being treated implicitly in the other direction. At succeeding time steps the process is reversed.

#### 3.1 Formulation of Equations for Explicit-Implicit Alternating-Direction Technique

Here we shall develop the equations for the explicit-implicit alternating-direction techniques for polar coordinates, where  $r$  represents radial displacements and  $z$  represents axial displacements. Differences in the composition of the eye are accounted for by varying the thermal conductivities and heat capacities with depth in each model. In order to account for blood flow in the Retinal model, provisions have been made for adjusting the matrix elements derived from this analysis. This subject is covered in Appendix B.

Within each eye media, heat conduction can be described using the standard heat-conduction equation

$$(\rho \cdot C) \frac{dv}{dt} = q(z, r, t) + K \left[ \frac{1}{r} \cdot \frac{\partial v}{\partial r} + \frac{\partial^2 v}{\partial r^2} \right] + \frac{\partial}{\partial z} (K \cdot \frac{\partial v}{\partial z}) \quad (A-1)$$

where

$C$  = specific heat

$K$  = thermal conductivity

$q$  = rate of heat deposition from laser

$r$  = radial distance

$t$  = time

$v$  = temperature rise above initial temperature

$z$  = axial distance

$\rho$  = density

This equation provides for variations of thermal conductivity with depth.

Just prior to exposure to the laser beam,

$$v(z,r,0) = 0 \quad (A-2)$$

Beyond some radial and axial distance away from the region at which appreciable energy is deposited, the temperature rises will remain insignificant over the times in which damage is inflicted. Moreover, because the temperatures are symmetric about the  $z$  axis, there is no heat transfer across the  $z$  axis. Mathematically these facts may be expressed by:

$$\begin{aligned} \frac{\partial v}{\partial r} &= 0 \quad \text{at } r = 0; \text{ and} \\ v &= 0 \quad \text{at } r = RN, \quad z = 0 \quad \text{and } z = 2 \cdot ZM \end{aligned} \quad (A-3)$$

where  $z$  is measured from the outer surface of the cornea; and  $RN$  and  $2 \cdot ZM$  represent radial and axial distances, respectively, beyond which there is no temperature rise during the times at which damage is being inflicted.

To achieve stable solutions two sets of finite-difference equations are employed to represent the heat fluxes. The first involves treating the fluxes explicitly in  $z$  and implicitly in  $r$ , which is termed COLUMN; and the second involves treating the fluxes implicitly in  $z$  and explicitly in  $r$ , which is termed ROW. For reasons which will be evident later in this section each set of calculations involve the use of two time steps each of size  $\Delta t/2$ , where  $\Delta t$  represents the time increment for one complete cycle.

Increments of  $z$ ,  $r$  and  $t$  are represented by  $z_{i+1} - z_i$ ,  $r_{j+1} - r_j$ , and  $t_{k+1} - t_k$ , respectively, where  $i, j, k = 1, 2, 3, \dots$ , and where  $t_1 = 0$ . To conserve on computational time the size of the spacial elements is progressively increased with distance from the region of appreciable energy deposition while the time intervals are progressively increased with time.

Using time steps of  $\Delta t_k/2$ , the finite-difference approximations of the heat fluxes of Eq. A-1 are as follows:

$$\rho \cdot C \frac{dv}{dt} \approx -\frac{(\rho \cdot C)_i}{\Delta t_k} \left[ v_{i,j,k+k4} - v_{i,j,k+k3} \right] \quad (A-4)$$

$$q(z,r,t) = q_{i,j,k+1/2} \quad (A-5)$$

$$\frac{K}{r} \frac{\partial v}{\partial r} \approx \frac{K_i}{r_j} \left[ \frac{v_{i,j+1,k+k1} - v_{i,j-1,k+k1}}{r_{j+1} - r_{j-1}} \right] \quad (A-6)$$

$$K \frac{\partial^2 v}{\partial r^2} \approx \frac{K_i}{r_{j+1} - r_{j-1}} \left[ \frac{v_{i,j+1,k+k1} - v_{i,j,k+k1}}{r_{j+1} - r_j} - \frac{v_{i,j,k+k1} - v_{i,j-1,k+k1}}{r_j - r_{j-1}} \right] \quad (A-7)$$

$$\frac{\partial}{\partial z} (K \frac{\partial v}{\partial z}) \approx \frac{K_i}{z_{i+1} - z_{i-1}} \left[ \frac{v_{i+1,j,k+k2} - v_{i,j,k+k2}}{z_{i+1} - z_i} - \right. \quad (A-8)$$

$$\left. \frac{v_{i,j,k+k2} - v_{i-1,j,k+k2}}{z_i - z_{i-1}} \right] + \frac{K_{i+1} - K_{i-1}}{z_{i+1} - z_{i-1}} \left[ v_{i+1,j,k+k2} - v_{i-1,j,k+k2} \right]$$

Equations A-4 through A-8 hold at all points within the eye except on the z axis and at the outer surface of the cornea at  $z=0$  wherein the radial heat flux is zero. At  $r=0$

$$\frac{K}{r} \frac{\partial v}{\partial r} \approx K \frac{\partial^2 v}{\partial r^2} \approx \frac{K_i}{r_2^2} \left[ v_{i,2,k+k1} - v_{i,1,k+k1} \right] \quad (A-9)$$

At  $z=0$ , the following condition holds

$$K \frac{\partial v}{\partial z} = 0 \quad (A-10)$$

Table A-1

VARIATIONS OF THE  $k_1$ ,  $k_2$ ,  $k_3$  and  $k_4$ \* WITH THE TIME INTERVAL

k	Values*	Column Computations	Row Computations
		First $\Delta t_k/2$	Second $\Delta t_k/2$
	$k_1$	1/2	1/2
	$k_2$	0	1
	$k_3$	0	1/2
	$k_4$	1/2	1

\* For use in Eqs. A-4 through A-9

Here the COLUMN computations are performed during the first time interval  $\Delta t_k/2$  while the ROW computations are performed during the final time step.

### 3.2 Formulation of Grid Network

In view of the fact that much of the laser's energy is deposited within relatively small regions of the eye, it is desirable to vary the size of spacial elements so that small uniform elements are used in regions of high energy absorption, and progressively larger elements are used for more remote regions. To achieve this end the first  $N_1+1$  radial grid points are spaced  $\Delta r$  apart starting at  $r = 0$  wherein the energy deposition is most intense. Thereafter the spacing is sequentially increased by a factor  $R_2$  for a total of  $N$  intervals or  $N+1$  grid points. This choice of  $r$  intervals is illustrated graphically in Fig. A-1 and mathematically as follows:

$$r_{j+1} - r_j = \begin{cases} \Delta r & 1 \leq j \leq N_1 \\ \Delta r \cdot (R_2)^{j-N_1} & N_1+1 \leq j \leq N \end{cases} \quad (A-11)$$

For the  $z$  axis, a total of  $M_1+1$  grid points are spaced at uniform intervals on either side of the midpoint  $z = ZM$

Axial Displacements, cm

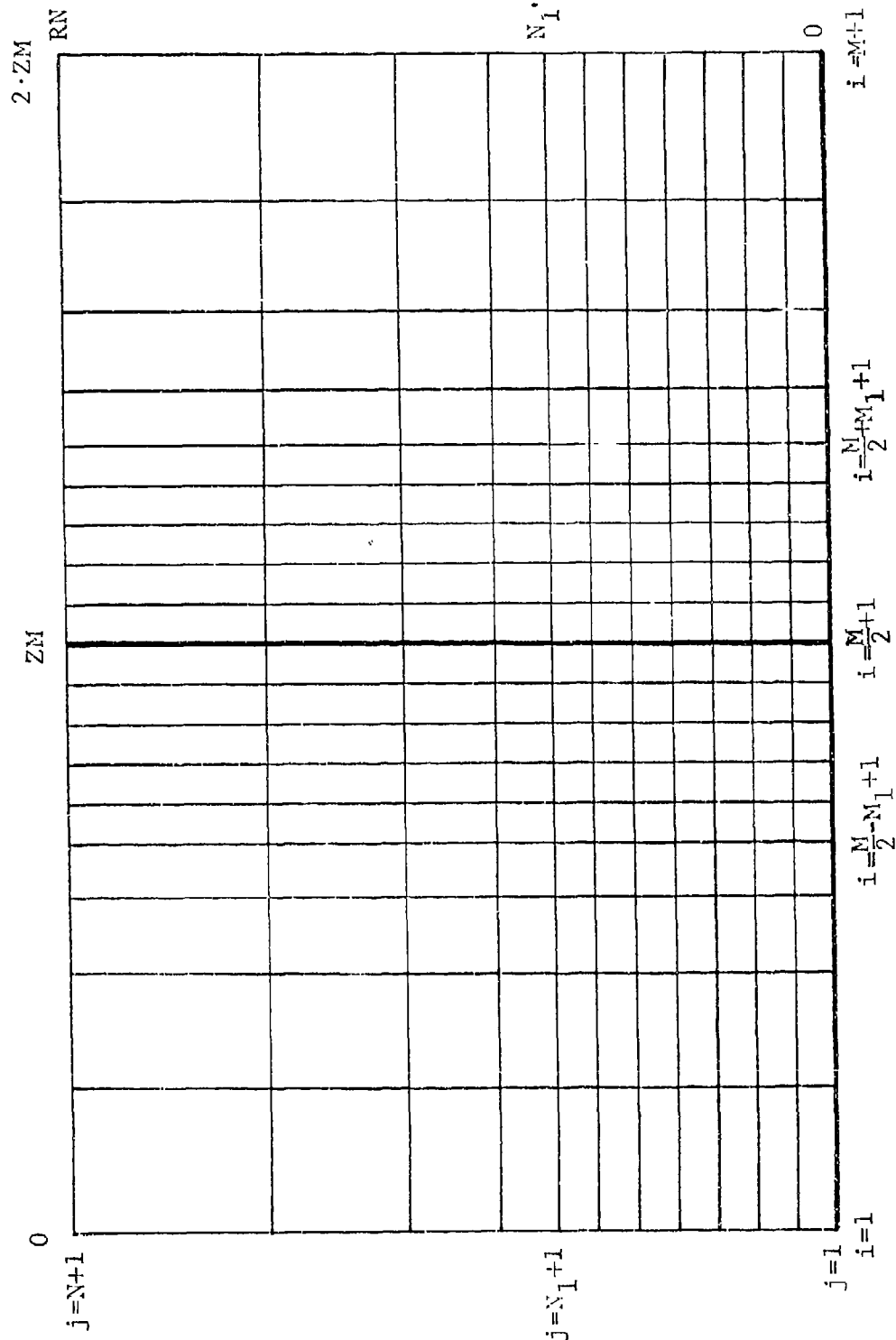


Figure A-1 GRID SCHEME USED IN FINITE-DIFFERENCE EQUATIONS



At shallower and deeper depths the spacing is progressively increased by a factor  $R_1$ , to yield a total of  $M+1$  grid points or  $M$  intervals along the  $z$  axis. This choice of  $z$  intervals is illustrated graphically in Fig. A-1 and represented mathematically by

$$z_{i+1} - z_i = \begin{cases} \Delta z \cdot (R_1)^{\frac{M}{2} - M_1 - i + 1} & 1 \leq i \leq \frac{M}{2} - M_1 \\ \Delta z & \frac{M}{2} - M_1 + 1 \leq i \leq \frac{M}{2} + M_1 \\ \Delta z \cdot (R_1)^{i - \frac{M}{2} - M_1} & \frac{M}{2} + M_1 + 1 \leq i \leq M \end{cases} \quad (A-12)$$

To determine the various grid points it is first necessary to specify the maximum values of  $z$  and  $r$  represented by  $2 \cdot ZM$  and  $RN$ , respectively, along with the number of uniformly spaced grid points  $M_1$  and  $N_1$  and the total number of grid spaces  $M$  and  $N$ . Values of the ratios  $R_1$  and  $R_2$  are then determined such that the proper number of increments are provided within the distances  $2 \cdot ZM$  and  $RN$ . Here we shall illustrate the method for assessing the ratios for the case of  $R_1$ .

Given the designated values for  $ZM$ ,  $M_1$ ,  $M$ , and  $\Delta z$ , it is necessary that

$$\frac{ZM}{\Delta z} - M_1 + 1 = \sum_{m=0}^{M/2 - M_1} R_1^m = \frac{R_1^{M/2 - M_1 + 1} - 1}{R_1 - 1}$$

Setting  $\frac{ZM}{\Delta z} - M_1 + 1$  equal to  $c_p$ , and  $M/2 - M_1 + 1$  equal to  $c_k$  and simplifying Eq. A-13 yields

$$c_p \cdot R_1 - c_p + 1 = R_1^{c_k} \quad (A-14)$$

Taking logarithms of both sides of Eq. A-14 yields

$$\log(c_p \cdot R_1 - c_p + 1) = c_k \cdot \log R_1 \quad (A-15)$$

Finally rearrangement of Eq. A-15 yields

$$R_1 = \exp \left[ \frac{\log(c_p \cdot R_1 - c_p + 1)}{c_k} \right] \quad (A-16)$$

In view of the fact that factor  $R_1$  is present on both sides of Eq. A-16 it is necessary to determine  $R_1$  by successive approximations. This is accomplished by first setting  $R_1$  equal to an initial value of say 2, and then evaluating the right-hand side of Eq. A-16 for the first trial value for  $R_1$ . If with this  $R_1$ , Eq. A-16 is not satisfied, then  $R_1$  is set equal to the value found for the right-hand side of the equation and the process repeated until Eq. A-16 is satisfied.

To evaluate the ratio  $R_2$  for the  $r$  coordinate one merely replaces  $ZM$ ,  $i$ ,  $M_1$ ,  $M/2$  and  $\frac{\Delta z}{\Delta r}$  by  $RN$ ,  $j$ ,  $N_1$ ,  $N$  and  $\Delta r$ , respectively. With these changes  $c_p$  becomes  $\frac{RN}{\Delta r} - N_1 + 1$  and  $c_k$  becomes  $N - N_1 + 1$ .

### 3.3 Matrix Representation of Finite-Difference Equations

Generally the most efficient method for solving simultaneous finite-difference equations involves the use of matrix representation of the appropriate equations. In this regard we are concerned with solutions for two problems -- the first for COLUMN in which the heat transfer in the  $z$  direction is treated explicitly while the heat transfer in the  $r$  direction is treated implicitly; and the second for ROW in which the heat transfer in the  $z$  direction is treated implicitly while the heat transfer in the  $r$  direction is treated explicitly.

To determine the finite-difference equations appropriate for each set of computations one must first substitute the finite-difference expressions given by Eqs. A-4 through A-9 for the various partial derivatives of temperature rise  $v$  presented by Eq. A-1. The result is two sets of finite-difference equations -- one for COLUMN and one for ROW.

After collecting like terms in  $v_{i,j,k}$  one arrives at the following equations.

COLUMN:

$$\begin{aligned}
 & -K_i \cdot B_{j,1} \cdot v_{i,j-1,k+1/2} + (K_i \cdot B_{j,2} + \frac{2 \cdot \rho_i \cdot C_i}{\Delta t_k}) v_{i,j,k+1/2} - K_i \cdot B_{j,3} v_{i,j+1,k+1/2} \\
 & = A_{i,1} \cdot v_{i-1,j,k} - (A_{i,2} - \frac{2 \cdot \rho_i \cdot C_i}{\Delta t_k}) v_{i,j,k} + A_{i,3} \cdot v_{i+1,j,k} + S_{i,j,k+1/2}
 \end{aligned}
 \tag{A-17}$$

ROW:

$$\begin{aligned}
 & -A_{i,1} \cdot v_{i-1,j,k+1} + (A_{i,2} + \frac{2 \cdot \rho_i \cdot C_i}{\Delta t_k}) v_{i,j,k+1} - A_{i,3} \cdot v_{i+1,j,k+1} \\
 & = K_i \cdot B_{j,1} \cdot v_{i,j-1,k+1/2} - (K_i \cdot B_{j,2} - \frac{2 \cdot \rho_i \cdot C_i}{\Delta t_k}) v_{i,j,k+1/2} + K_i \cdot B_{j,3} \cdot v_{i,j+1,k+1/2} \\
 & + S_{i,j,k+1/2}
 \end{aligned}
 \tag{A-18}$$

where  $\Delta t_k$  = difference in elapsed times given by  $XT(k+1) - XT(k)$  (10);  
 $i = 2, 3 \dots M$ ;  $j = 2, 3 \dots N$ ; and where at the boundaries

$$\begin{aligned}
 v_{2,j,k} &= v_{1,j,k} \\
 v_{M+1,j,k} &= 0 \\
 v_{k,N+1,k} &= 0
 \end{aligned}
 \tag{A-19}$$

For the case of COLUMN, the index  $i$  is held constant while the index  $j$  is varied to yield the matrix presented in Fig. A-2. For the initial time interval  $\Delta t_k/2$ ,  $i$  is first set equal to 2 while the temperature rises  $v_{2,j,k+1/2}$  are being evaluated. Then  $i$  is set equal to 3 to determine the temperature rises  $v_{3,j,k+1/2}$  etc. Finally,  $i$  is set equal to  $M$  to yield  $v_{M,j,k+1/2}$ .

For the case of ROW, the index  $j$  is held constant while the index  $i$  is varied to yield the matrix presented in Fig. A-3. For the second time interval  $\Delta t_k/2$ ,  $j$  is first set equal to 1 while the temperature rises  $v_{i,1,k+1}$  are being evaluated. Then  $j$  is increased to 2 while  $v_{i,2,k+1}$  is being evaluated, etc.

Values for the coefficients  $A_{i,1}, A_{i,2}, A_{i,3}, B_{j,i}, B_{j,2}$  and  $B_{j,3}$  are given in Table A-2.

### 3.4 Solution of Matrix Representation of Finite-Difference Equations

Having established the matrices for performing the COLUMN and ROW calculations, the next step is the evaluation of the temperature rises  $v_{i,j,k}$ . In this regard it is important to observe that the coefficient matrices shown in Figs. A-2 and A-3 are tridiagonal in that all elements are zero except for those on the main diagonal and on either side of the diagonal. To solve these equations, a very efficient algorithm is available which involves an elimination procedure.

To illustrate this procedure consider the simplified version of the equations presented below:

$$\begin{bmatrix} b_1 & c_1 & 0 & 0 & \dots & 0 \\ a_2 & b_2 & c_2 & 0 & & 0 \\ 0 & a_3 & b_3 & c_3 & & 0 \\ 0 & 0 & a_4 & b_4 & & \\ \vdots & 0 & 0 & & & \\ 0 & 0 & 0 & & a_p & b_p \end{bmatrix} \cdot \begin{bmatrix} v_1 \\ v_2 \\ \vdots \\ v_p \end{bmatrix} = \begin{bmatrix} x_1 \\ x_2 \\ \vdots \\ x_p \end{bmatrix} \quad (A-20)$$

Table A-2 VALUES OF COEFFICIENTS A AND B

i Indices	$A_{i,1}$	$A_{i,2} = A_{i,1} + A_{i,3}$	$A_{i,3}$
$2 \leq i \leq \frac{M}{2} - M_1 + 1$	$\frac{R_1 K_{i-1} + 2(R_1 + 1)K_i - R_1 K_{i+1}}{(\Delta z)^2 (R_1 + 1)^2 R_1^{M-2i-2M_1+3}}$	$\frac{2K_i}{(\Delta z)^2 (R_1)^{M-2i-2M_1+3}}$	$\frac{K_{i+1} + 2(R_1 + 1)K_i - K_{i-1}}{(\Delta z)^2 (R_1 + 1)^2 R_1^{M-2i-2M_1+2}}$
$\frac{M}{2} - M_1 + 2 \leq i \leq \frac{M}{2} + M_1$	$\frac{K_{i-1} + 4K_i - K_{i+1}}{4(\Delta z)^2}$	$\frac{2K_i}{(\Delta z)^2}$	$\frac{K_{i+1} + 4K_i - K_{i-1}}{4(\Delta z)^2}$
$\frac{M}{2} + M + 1 \leq i \leq M$	$\frac{K_{i-1} + 2(R_1 + 1)K_i - K_{i+1}}{(\Delta z)^2 (R_1 + 1)^2 R_1^{2i-M-2M_1-2}}$	$\frac{2K_i}{(\Delta z)^2 R_1^{2i-M-2M_1-1}}$	$\frac{R_1 K_{i+1} + 2(R_1 + 1)K_i - R_1 K_i}{(\Delta z)^2 (R_1 + 1)^2 R_1^{2i-M-2M_1}}$
j Indices	$B_{j,1}$	$B_{j,2} = B_{j,1} + B_{j,3}$	$B_{j,3}$
$j = 1$	0	$\frac{4}{(\Delta x)^2}$	$\frac{4}{(\Delta x)^2}$
$2 \leq j \leq N_1$	$\frac{1}{(\Delta x)^2} \frac{(2j-3)}{(2j-2)}$	$\frac{2}{(\Delta x)^2}$	$\frac{1}{(\Delta x)^2} \frac{(2j-1)}{(2j-2)}$
$N_1 + 1 \leq j \leq N$	$\frac{2/R_2}{(\Delta x)^2 (R_2 + 1) R_2^{j-1-N_1}} \frac{R_2^{j-1-N_1}}{j-1-N_1 + \sum_{n=1}^{j-1-N_1} R_2^n}$	$\frac{2}{(\Delta x)^2 R_2^{2j-1-N_1}}$	$\frac{2/(j-N_1) + 1/(N_1 + \sum_{n=1}^{j-1-N_1} R_2^n)}{(\Delta x)^2 (R_2 + 1) R_2^{j-1-N_1}}$

$K_1 \cdot B_{1,2} + \frac{2 \cdot \rho_1 \cdot C_1}{\Delta t_k}$	$-K_1 \cdot B_{1,3}$	0	0	0	$v_{1,1,k+k_1}$	$b_1$
$-K_1 \cdot B_{2,1}$	$K_1 \cdot B_{2,2} + \frac{2 \cdot \rho_1 \cdot C_1}{\Delta t_k}$	$-K_1 \cdot B_{2,3}$	0	0	$v_{1,2,k+k_1}$	$b_2$
0	$-K_1 \cdot B_{3,1}$	$K_1 \cdot B_{3,2} + \frac{2 \cdot \rho_1 \cdot C_1}{\Delta t_k}$	$-K_1 \cdot B_{3,3}$	0	$v_{1,3,k+k_1}$	$b_3$
0	0	$-K_1 \cdot B_{4,1}$	$K_1 \cdot B_{4,2} + \frac{2 \cdot \rho_1 \cdot C_1}{\Delta t_k}$	0	$v_{1,4,k+k_1}$	$b_4$
0	0	0	0	$-K_1 \cdot B_{N-1,3}$	0	0
0	0	0	$-K_1 \cdot B_{N,1}$	$K_1 \cdot B_{N,2} + \frac{2 \cdot \rho_1 \cdot C_1}{\Delta t_k}$	$v_{1,N,k+k_1}$	$b_N$

where:  $b_j = A_{1,1} \cdot v_{1-1,j,k+k_2} + (-A_{1,2} + \frac{2 \cdot \rho_1 \cdot C_1}{\Delta t_k}) \cdot v_{1,j,k+k_2} + A_{1,3} \cdot v_{1+1,j,k+k_2} + q_{1,j,k+k_1/2}$  and values for

$A_{1,1}, A_{1,2}, A_{1,3}, B_{1,1}, B_{1,2}$  and  $B_{1,3}$  are presented in Table A-2.

Figure A-2 MATRIX REPRESENTATION OF EQUATIONS FOR COLUMN COMPUTATIONS

$$\begin{bmatrix}
 A_{2,2} + \frac{2 \cdot P_2 \cdot C_2}{\Delta E_k} & -A_{2,3} & 0 & 0 & \dots & 0 \\
 -A_{3,1} & A_{3,2} - \frac{2 \cdot P_3 \cdot C_3}{\Delta E_k} & -A_{3,3} & 0 & \dots & 0 \\
 0 & -A_{4,1} & A_{4,2} + \frac{2 \cdot P_4 \cdot C_4}{\Delta E_k} & -A_{4,4} & \dots & 0 \\
 0 & 0 & -A_{5,1} & A_{5,2} + \frac{2 \cdot P_5 \cdot C_5}{\Delta E_k} & \dots & 0 \\
 \vdots & \vdots & \vdots & \vdots & \ddots & \vdots \\
 0 & 0 & 0 & -A_{M,1} & A_{M,2} + \frac{2 \cdot P_M \cdot C_M}{\Delta E_k} & -A_{M-1,3}
 \end{bmatrix}
 \cdot
 \begin{bmatrix}
 v_{2,j,k+k_2} \\
 v_{3,j,k+k_2} \\
 v_{4,j,k+k_2} \\
 v_{5,j,k+k_2} \\
 \vdots \\
 v_{M,j,k+k_2}
 \end{bmatrix}
 =
 \begin{bmatrix}
 b_2 \\
 b_3 \\
 b_4 \\
 b_5 \\
 \vdots \\
 b_M
 \end{bmatrix}$$

where:  $b_i = K_i \cdot B_{j,1} \cdot v_{i,j-1,k+k_1} + (-K_i \cdot B_{j,2} + \frac{2 \cdot P_i \cdot C_i}{\Delta E_k}) v_{i,j,k+k_1} + K_i \cdot B_{j,3} \cdot v_{i,j+1,k+k_1} + q_{i,j,k+1/2}$

and values for  $A_{i,1}, A_{i,2}, A_{i,3}, B_{i,1}, B_{i,2}$  and  $B_{i,3}$  are presented in Table A-2.

Figure A-3 MATRIX REPRESENTATION OF EQUATIONS FOR ROW COMPUTATIONS

The procedure is as follows. The first equation, namely

$$b_1 \cdot v_1 + c_1 \cdot v_2 = x_1 \quad (\text{A-21})$$

is solved for  $v_1$  which is then employed to eliminate  $v_1$  from the second equation, namely

$$a_2 \cdot v_1 + b_2 \cdot v_2 + c_2 \cdot v_3 = x_2 \quad (\text{A-22})$$

The resulting equation is then solved for  $v_2$  and used to eliminate  $v_2$  from the third equation, namely

$$a_3 \cdot v_2 + b_3 \cdot v_3 + c_3 \cdot v_4 = x_3 \quad (\text{A-23})$$

This process is repeated for all of the equations and results in the following set of simultaneous equations

$$\begin{aligned} v_1 + \frac{c_1}{F_1} \cdot v_2 &= D_1 \\ v_2 + \frac{c_2}{F_2} \cdot v_3 &= D_2 \\ v_3 + \frac{c_3}{F_3} \cdot v_4 &= D_3 \\ \vdots & \\ v_{p-1} + \frac{c_{p-1}}{F_{p-1}} \cdot v_p &= D_{p-1} \\ v_p &= D_p \end{aligned} \quad (\text{A-24})$$

where

$$F_1 = b_1, \quad D_1 = \frac{x_1}{F_1}, \quad \text{and}$$

$$C_m = \frac{c_m}{F_m}$$

$$F_m = b_m - a_m \cdot C_{m-1}$$

$$D_m = \frac{x_m - a_m \cdot D_{m-1}}{F_m}$$

for  $m = 1, 2, 3 \dots p$

(A-25)



To solve for  $v_m$  one first evaluates  $C_m$ ,  $D_m$  and  $F_m$  and then evaluates the  $v_m$  sequentially starting with  $v_p$ . The result is as follows:

$$\begin{aligned}
 v_p &= D_p \\
 v_{p-1} &= D_{p-1} - \frac{c_{p-1}}{F_{p-1}} v_p \\
 v_{p-2} &= D_{p-2} - \frac{c_{p-2}}{F_{p-2}} v_{p-1} \\
 &\vdots \\
 v_2 &= D_2 - \frac{c_2}{F_2} v_3 \\
 v_1 &= D_1 - \frac{c_1}{F_1} v_2
 \end{aligned}
 \tag{A-26}$$

To use the above set of equations, one must first evaluate the expressions for  $a_m$ ,  $b_m$ , and  $c_m$  for the COLUMN computations presented by Fig. A-2 and for the ROW computations by Fig. A-3 using the results of Table A-2. Then the resultant values for  $a_m$ ,  $b_m$  and  $c_m$  are used to evaluate the parameters  $C_m$ ,  $D_m$  and  $F_m$  given by Eq. A-25.

APPENDIX B

THERMAL EFFECTS CAUSED BY BLOOD FLOW  
WITHIN CHORIO-CAPILLARIS  
AND TISSUES SURROUNDING EYE

## APPENDIX B

### THERMAL EFFECTS CAUSED BY BLOOD FLOW WITHIN CHORIO-CAPILLARIS AND TISSUES SURROUNDING EYE

#### 1. INTRODUCTION

Blood flow occurs in a diffuse and pulsating fashion through many sizes of blood vessels within the chorio-capillaris of the eye as well as within tissues surrounding the eye. During and after exposure to a laser beam the flow of blood shall act to dissipate heat from surrounding tissue and thereby moderate thermal damage. Such heat dissipation occurs as a result of two effects. The initial effect of the blood is to act as a heat sink, while the second effect is to transport heat from regions of high temperature to regions of low temperature. Both effects are considered in assessing the consequence of blood flow in the chorio-capillaris. On the other hand blood flow within tissues surrounding the eye is treated purely as a heat sink.

Recognizing that the problem is inherently complex because of the multitude of blood vessels, some assumptions must be made to achieve tractable solutions. To this end we shall assume that

- the blood reaches the chorio-capillaris or tissues through the main blood vessels at its normal temperature
- the temperature of blood within the smaller blood vessels of the vascular layer equals that of surrounding tissue
- the flow of blood is not altered by temperature changes

Moreover, we shall consider the transport of heat by the blood in the chorio-capillaris only along directions of changing radii. Axial heat transport is neglected in view of the shallow depth of the chorio-capillaris.

## 2. CHORIO-CAPILLARIS

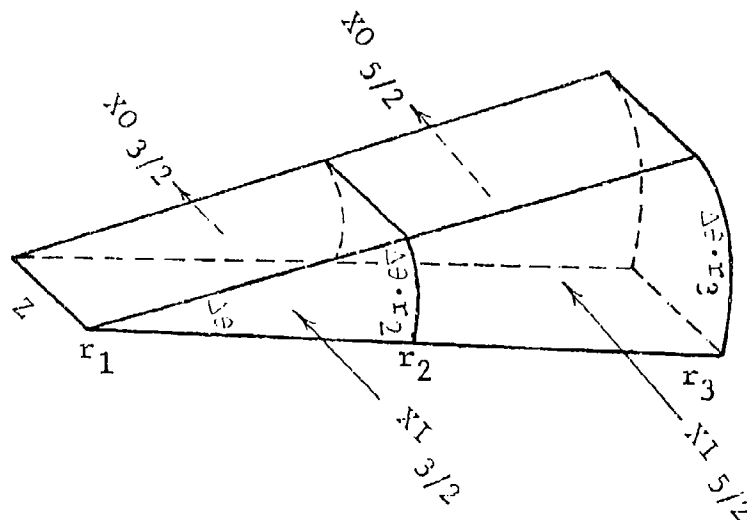
### 2.1 Radial Grid Coordinates for Analyzing Blood Flow in Chorio-Capillaris

To remain consistent with the scheme for predicting eye temperatures described in Appendix A, we shall use the same grid system shown in Fig. A-1. In this scheme, temperatures are specified at radial distances  $r_j$  starting with  $r_1=0$  at the axis of the eye. To minimize the number of radial elements, the first  $N_1$  spacings are kept uniform and then allowed to progressively increase in size by a factor  $R_2$ . A similar scheme is used for the axial elements  $\Delta z$ . The vascular layer is considered to lie within the region of uniform spacing between one or more of the incremental depths  $\Delta z$ .

Due to the fact that only a small number of volume elements are in the vascular layer, we shall utilize explicit finite-difference equations to predict the transport and loss of heat caused by blood flow. These heat transfer predictions shall be made for each time interval  $\Delta t_k = XT(k+1) - XT(k)$  considered in the Technology, Inc. scheme for predicting temperatures. The result of this analysis shall be predictions of the incremental changes of heat to each of the elements of the vascular layer during each of the intervals of time.

### 2.2 Representation of Blood Flows in Chorio-Capillaris

In order to describe the flow of blood into and out of various elements of the vascular layer, the flows to and from unit areas of the two boundary surfaces of the vascular layer will be represented by  $X_{1j}$  and  $X_{0j}$ , respectively. Variations of the flows  $X_{1j}$  and  $X_{0j}$  with radial distance  $r$  will be accounted for by delineating the flows at several select radial distances. An illustration of these flows is shown below.



Differences in the quantities of blood entering and leaving various radial sections of the vascular layer will move either inward or outward in the radial direction. If the radial flows at  $r_j$  are designated by  $FR_j$ , then the radial flows are given by

$$\begin{aligned} FR_1 &= 0 \\ FR_2 &= (XI_{3/2} - XO_{3/2}) \cdot \Delta O \cdot r_2^2 / 2 \\ FR_3 &= FR_2 + (XI_{5/2} - XO_{5/2}) \cdot \Delta O \cdot (r_3^2 - r_2^2) / 2 \\ &\vdots \end{aligned} \quad (B-2)$$

or in general

$$FR_j = \sum_{n=2}^{j-1} (XI_{n-1/2} - XO_{n-1/2}) \cdot \Delta O \cdot (r_n^2 - r_{n-1}^2) / 2 \quad (B-3)$$

Since these flows pass through crosssectional areas of

$$Z \cdot \Delta O \cdot r_j \quad (B-4)$$

it is necessary to divide each flow  $FR_j$  by the area through which it flows to assess the rates per unit area. The resultant radial flows per unit area at  $N_j$  are given by

$$\begin{aligned} FLOWR_j &= FR_j / (Z \cdot \Delta O \cdot r_j) \\ &= \sum_{n=2}^{j-1} (XI_{n-1/2} - XO_{n-1/2}) (r_n^2 - r_{n-1}^2) / (2 \cdot Z \cdot r_j) \end{aligned} \quad (B-5)$$

for  $j \geq 2$ . These flows will transport heat along radial lines.

To assess the cooling effects of the incoming blood, one must first determine the blood flows entering unit volumes of the chorionicapillaris. This is accomplished by dividing the flows  $XI_j$  by the thickness  $Z$  of the vascular layer to yield

$$FLOWI_j = XI_j / Z \quad (B-6)$$

### 2.3 Analysis of Thermal Effects Caused by Blood Flow in Chorio-Capillaris

In this section we shall consider the thermal effects of blood apart from the effects of heat conduction treated in Appendix A. The results shall be a description of the temperature changes caused by blood flow during the given time interval  $\Delta t_k = XT(k+1) - XT(k)$ .

The differential equation requiring solution is

$$\rho \cdot C \cdot \frac{\partial v}{\partial t} = - \frac{C_b}{r} \frac{\partial}{\partial r} (r \cdot \text{FLOWR} \cdot v) - \text{FLOWI} \cdot v \cdot C_b \quad (\text{B-7})$$

If  $r \cdot \text{FLOWR}$  is represented by  $\text{FLOWX}$  then Eq. B-7 becomes

$$\rho \cdot C \cdot \frac{\partial v}{\partial t} = - \frac{C_b}{r} \frac{\partial}{\partial r} (\text{FLOWX} \cdot v) - \text{FLOWI} \cdot v \cdot C_b \quad (\text{B-8})$$

In terms of the indices  $i, j, k$  for  $z, r$  and time  $t$ , respectively, the finite-difference solution of Eq. B-8 is

$$\begin{aligned} v_{i,j,k+1/2} = & v_{i,j,k} + \frac{c}{r_j \cdot (r_{j+1} - r_{j-1})} \cdot \text{FLOWX}_j \cdot (v_{i,j-1,k} - v_{i,j+1,k}) \\ & + v_{i,j,k} \cdot (\text{FLOWX}_{j-1} - \text{FLOWX}_{j+1}) - c \cdot \text{FLOWI} \cdot v_{i,j,k} \end{aligned} \quad (\text{B-9})$$

where  $c = \Delta t_k \cdot C_b / (2 \cdot \rho \cdot C)$

The term involving the bracket reflects temperature changes of the tissue caused by the radial flow of blood while the last term reflects temperature changes of the tissue caused by instantaneous heating of the blood as it enters the chorio-capillaris through small capillaries.

Using the following substitution

$$\text{RD}(j) = \frac{1}{r_j \cdot (r_{j+1} - r_{j-1})} \quad (\text{B-10})$$

Eq. B-9 becomes

$$\frac{(\rho C)}{\Delta t_k/2} (v_{i,j,k+1/2} - v_{i,j,k}) = C_b \cdot RD(j) \cdot FLOWX_j (v_{i,j-1,k} - v_{i,j+1,k}) + \left[ C_b \cdot RD(j) (FLOWX_{j-1} - FLOWX_{j+1}) - C_b \cdot FLOWI_j \right] v_{i,j,k} \quad (B-11)$$

Within the Retinal Model the coefficients on the right-hand side of Eq. B-11 are represented by

$$BV(j,1) = C_b \cdot RD(j) \cdot FLOWX_j \quad (B-12)$$

$$2 \cdot BV(j,2) = C_b \cdot RD(j) (FLOWX_j - FLOWX_{j+1}) - C_b \cdot FLOWI_j \quad (B-13)$$

$$BV(j,3) = -C_b \cdot RD(j) \cdot FLOWX_j \quad (B-14)$$

The terms on the left-hand side of the above equations are to be added or subtracted from the corresponding matrix elements  $B(j,1)$ ,  $B(j,2)$ ,  $B(j,3)$  and  $A(i,2)$  used to compute the temperatures (see Appendix A). In other words

$$\begin{aligned} B(j,1) &\rightarrow B(j,1) + BV(j,1) \cdot IV(i) \\ B(j,2) &\rightarrow B(j,2) - BV(j,2) \cdot IV(i) \\ B(j,3) &\rightarrow B(j,3) + BV(j,3) \cdot IV(i) \\ A(i,2) &\rightarrow A(i,2) - BV(j,2) \cdot IV(i) \end{aligned} \quad (B-15)$$

Here IV equals one when the point is in the chorio-capillaris and equals zero otherwise. Here the contribution from  $2 \cdot BV(j,2)$  has been partitioned equally between  $B(j,2)$  and  $A(i,2)$  for purposes of temperature stability.

#### 2.4 Blood Flow in Tissues

In tissues surrounding the eye, blood is considered only as a heat sink. If XFLOW represents the rate of blood flow per unit volume, then the rate of heat loss from tissues having a temperature rise  $v_{i,j,k}$  is

$$C_b \cdot XFLOW \cdot v_{i,j,k} \quad (B-16)$$

In the Retinal model the coefficient of  $v$  is represented by  $-2 \cdot BB$ .

To include these heat losses as well as the effects of blood flow in the chorio-capillaris, the matrix elements A and B must be changed as follows:

$$\begin{aligned} B(j,1) &\rightarrow B(j,1) + BV(j,1) \cdot IV(i) \\ B(j,2) &\rightarrow B(j,2) - BV(j,2) \cdot IV(i) - BB \cdot IAB(i,j) \\ B(j,3) &\rightarrow B(j,3) + BV(j,3) \cdot IV(i) \\ A(i,2) &\rightarrow A(i,2) - BV(j,2) \cdot IV(i) - BB \cdot IAB(i,j) \end{aligned} \tag{B-17}$$

where IAB equals one when the point is in the tissues surrounding the eye and equals zero otherwise. As with the  $BV(j,2)$  contributions,  $2 \cdot BB$  has been partitioned equally between  $B(j,2)$  and  $A(i,2)$  to improve the stability of the temperature calculations. Otherwise, one could have placed the contributions for  $A(i,2)$  into  $B(j,2)$ .



APPENDIX C

DECAY OF NORMALIZED TEMPERATURE RISES  
OF MELANIN GRANULES WITH TIME

## APPENDIX C

### DECAY OF NORMALIZED TEMPERATURE RISES OF MELANIN GRANULES WITH TIME

#### 1. INTRODUCTION

Melanin granules are better absorbers of radiation than other media within the pigment epithelium within which they are situated. As a result considerable temperature differences can be produced between the granules and the intervening tissue especially by short duration, high-intensity pulses. With very short exposures, steam could be produced within the granules, and the resultant pressures cause damage.

Here of course one must recognize that temperature differences between the granules and intervening media persist only for relatively short times. To identify the laser exposures in which the temperature differences are appreciable, it is necessary to predict the temperature rises at and between granules. In this endeavor, we shall restrict the analysis to very small volumes of the pigment epithelium across which the transmitted radiation is essentially constant. Also we shall neglect energy losses due to

- changes of state
- development and transmission of pressure waves

As a result, all temperature predictions represent upper bounds and should be treated accordingly.

#### 2. FINITE-DIFFERENCE EQUATIONS

To predict the temperature rises we will assume that the granules are cubes which are located at the intersections of a three dimensional cartesian grid of equal linear dimensions. An illustration of a cross section through the center of the granules is shown in Fig. C-1. Here the spacing between granules is taken equal to the diameter of the granules. This spacing is minimal in that the diameter of the granules is about 1 micron while the spacing ranges from 1 micron to 1.5 micron (Ref. 1).

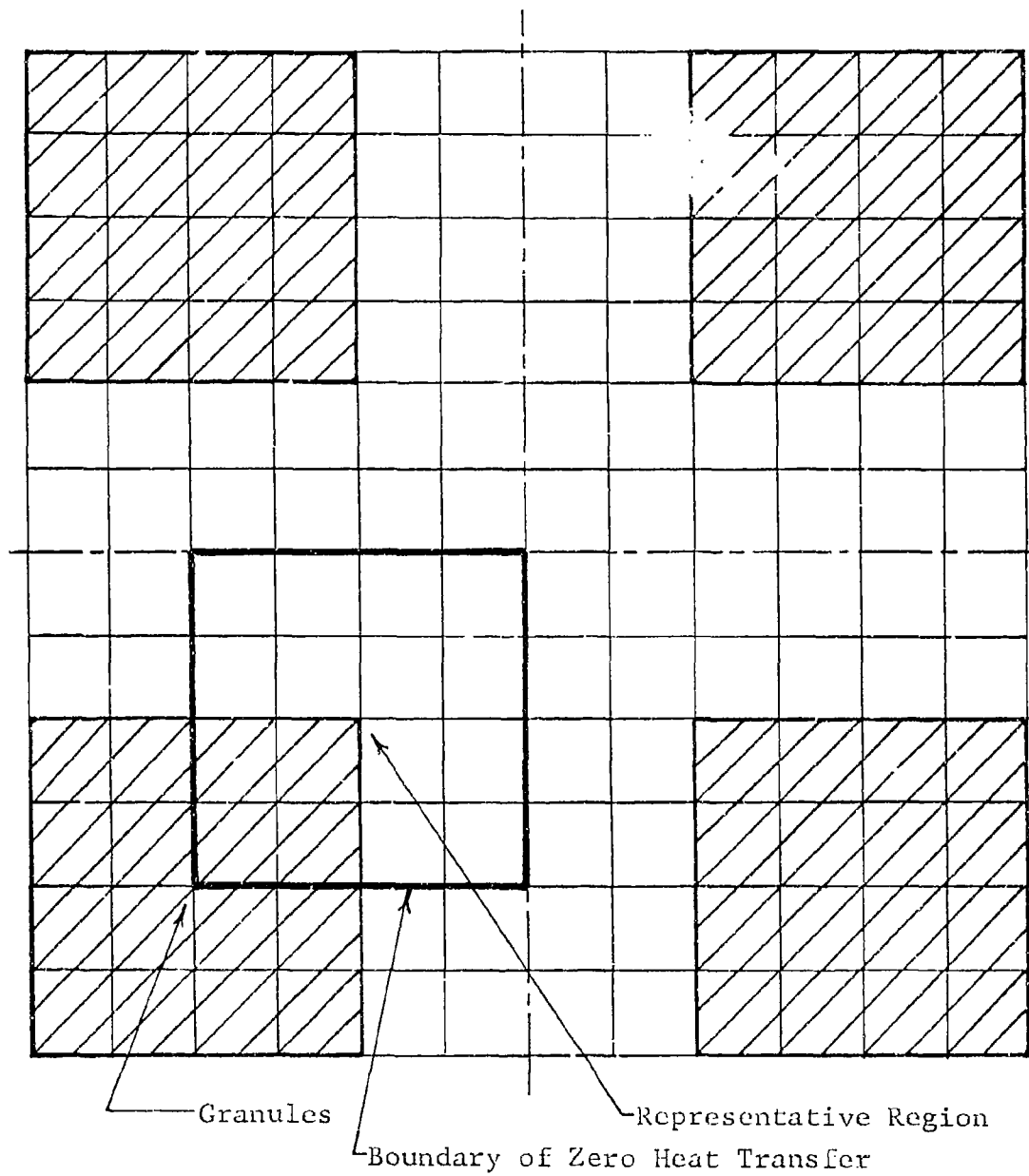


Figure C-1 SCHEMATIC OF CROSS SECTION OF GRANULES AND REPRESENTATIVE REGION FOR ANALYSIS

For the case of maximum spacing one must add two additional elements between the granules.

Due to symmetry one needs to consider only those elements enclosed by the heavy lines. Because of their relatively small dimensions, the surrounding groups of elements will be at essentially the same temperatures.

To perform the necessary calculations we shall employ an explicit finite-difference analysis since the computational times are relatively small. To this end we shall consider a 4·4·4 cube of elements for the case of minimum spacing or a 5·5·5 cube of elements for the case of maximum spacing. In addition, volume elements immediately surrounding the cubes will be included as a convenient means for ensuring that no heat is lost from the cubes.

In the analysis we shall consider the worst case in which all the absorbed energy is deposited within the melanin granules. Moreover we shall normalize the results by depositing just enough heat so that if it were uniformly absorbed without the granules a unit temperature rise would result. This, of course, simplifies the interpretation and ultimate use of the normalized temperatures. To achieve this end, it is necessary that the total quantity of heat deposition be

$$\rho \cdot C \cdot ((n-2) \cdot \Delta x)^3 \cdot 1 \quad (C-1)$$

where:

- C = specific heat of tissue
- n = number of elements
- $\Delta x$  = linear dimension of elements
- $\rho$  = density of tissue

and where the number 2 accounts for the fact that the heat is deposited only within elements beneath the outer ring of elements and the number 1 represents the unit temperature rise. For the case of minimum spacing  $n=6$ , and for the case of maximum spacing  $n=7$ .

This heat will be deposited within a total of  $2^3$  elements corresponding to the portion of the melanin granule under consideration

(see Fig. C-1). If this heat is deposited in an increment of time  $\Delta t$ , then deposition  $q_1$  per unit granule volume is

$$q_1 = \rho \cdot C \cdot ((n-2) \cdot \Delta x)^3 \cdot 1 / (8 \cdot (\Delta x)^3 \cdot \Delta t) = \rho \cdot C (n-2)^3 / (8 \cdot \Delta t) \quad (C-2)$$

Implicit in this analysis is that there is negligible heat transfer during the incremental time  $\Delta t$ . In the remainder of this analysis we shall discuss how the resultant temperatures decay with time at intervals  $\Delta t$ .

For central differences the appropriate finite-difference equation is

$$\rho \cdot C \cdot \frac{v_{i1,j1,k1}^{t+\Delta t} - v_{i1,j1,k1}^t}{\Delta t} = K \left[ v_{i1-1,j1,k1}^t + v_{i1,j1-1,k1}^t + v_{i1,j1,k1-1}^t - 6 v_{i1,j1,k1}^t + v_{i1+1,j1,k1}^t + v_{i1,j1+1,k1}^t + v_{i1,j1,k1+1}^t \right] / (\Delta x)^2 \quad (C-3)$$

where

$i1, j1, k1$  = indices describing the location of the element

$K$  = thermal conductivity of tissue

$t$  = time

$v$  = temperature rises at locations and times indicated by subscripts and superscripts, respectively.

Prior to exposure all the temperature rises  $v$  are zero. The condition of zero heat loss is accounted for by maintaining a zero temperature gradient between the outermost elements and corresponding adjacent elements by use of the following equations:

$$\begin{aligned} v_{1,j1,k1}^t &= v_{2,j1,k1}^t \\ v_{i1,1,k1}^t &= v_{i1,2,k1}^t \\ v_{i1,j1,1}^t &= v_{i1,j1,2}^t \end{aligned} \quad (C-4)$$

$$\begin{aligned}
v_{n,j1,k1}^t &= v_{n-1,j1,k1}^t \\
v_{il,n,k1}^t &= v_{il,n-1,k1}^t \\
v_{il,j1,n}^t &= v_{il,j1,n-1}^t
\end{aligned}
\tag{C-4}$$

where n represents the maximum index of the elements and equals 6 for the case of minimum spacing and 7 for the case of maximum spacing.

To ensure computational stability,  $\Delta t$  should additionally satisfy the following condition

$$\Delta t \leq (\Delta x)^2 \cdot \rho \cdot C / (6 \cdot K) \tag{C-5}$$

Predictions of the temperature rises consists of first setting the  $v_{il,j1,k1}$  to zero. Then Eq. C-3 is used to evaluate the  $v_{il,j1,k1}^{t+\Delta t}$  for  $il, j1$ , and  $k1 = 2, 3, \dots, N-2$  using the previous temperature rises. Then Eqs. C-4 are applied to ensure no heat loss and the process repeated with the new temperature rises to compute the next set of temperature rises.

The result of this analysis is normalized temperature rise histories of the granules assuming all the energy is deposited within an incremental time interval of  $\Delta t$ . When the actual deposition period exceeds  $\Delta t$ , then one must

- divide each of the above temperature rises by the ratio of the deposition time/ $\Delta t$  to ensure the final temperature rises are normalized (i.e. ultimate temperature rises of 1°C)
- superimpose the resultant temperature rises allowing for differences in elapsed time

The above steps are mathematically illustrated by Eq. 32.

APPENDIX D

ASSESSMENT OF TEMPERATURES CAUSED BY MULTIPLE PULSES  
USING SINGLE-PULSE TEMPERATURE PREDICTIONS

## APPENDIX D

### ASSESSMENT OF TEMPERATURES CAUSED BY MULTIPLE PULSES USING SINGLE-PULSE TEMPERATURE PREDICTIONS

#### 1. INTRODUCTION

There are two ways to compute the transient temperatures caused by multiple pulses. The first is to deposit the energies from each pulse at the appropriate times using the scheme for computing temperatures discussed in Appendix A. Unfortunately, this is not practical since the number of pulses could be in the thousands. Moreover, the time intervals would have to be chosen so they would correspond to the beginning and end of each pulse. Regular intervals would, of course, preempt the use of constantly expanding time intervals.

#### 2. ANALYTICAL MEANS FOR PREDICTING TEMPERATURES CAUSED BY MULTIPLE PULSES

A more practical approach may be arrived at by examining the heat conduction equation for the temperature rise  $V$  given below.

$$KV^2V + q(t) + q_b = \rho \cdot C \frac{\partial V}{\partial t} \quad (D-1)$$

where  $V=0$ , at  $t=0$

$$\frac{\partial V}{\partial z} = 0, \text{ at } z=0 \text{ for all } r, t$$

$$V \rightarrow 0, \text{ as } r, z \rightarrow +\infty \text{ for all } t$$

$$q(t) = \begin{cases} q_0(r), & 0 \leq t \leq t_0 \\ 0, & t > t_0 \end{cases}$$

$$q_b = C_1 V + C_2 \frac{\partial V}{\partial r} \text{ for } z \text{ values corresponding to vascular layer. } C_1, C_2 = \text{constants depending on the heat capacity and flow of blood.}$$

and where  $r$  = radial distance

$t$  = time

$t_0$  = pulse duration

$q$  = rate of energy deposition from laser per unit volume

$q_b$  = rate of heat exchange per unit volume due to blood flow



$\rho$  = density  
 $C$  = specific heat  
 $K$  = thermal conductivity  
 $z$  = axial distance

In order to examine the possibilities of making use of the computing temperatures caused by single pulses, let us consider that  $V_1(r, z, t)$  represents the solution of Eq. 1 for a single pulse of duration  $t_0$ . If there are two such pulses, with  $TC$  representing the time from the start of the first pulse to the start of the second pulse, then the solution for times  $t$  less than  $TC$  is obviously the same as that of a single pulse.

Once  $t > TC$ , the solution becomes

$$V_1(t) + V_1(t-TC) \quad (D-2)$$

To validate this solution, let us replace  $V$  of Eq. D-1 by the above expression. The result is

$$KV^2V_1(t) + q(t) + C_1V_1(t) + C_2\frac{\partial V_1(t)}{\partial r} + KV^2V_1(t-TC) + q(t-TC) + C_1V_1(t-TC) + C_2\frac{\partial V_1(t-TC)}{\partial r} = \left[ \frac{\partial V_1(t)}{\partial t} + \frac{\partial V_1(t-TC)}{\partial t} \right] \rho C \quad (D-3)$$

Since  $V_1(t)$  is a solution of Eq. D-1, the first four terms on the left-hand side of Eq. D-3 equal the first term on the right-hand side. Therefore, eliminating these terms and replacing the argument  $t - TC$  by  $t'$  results in

$$KV^2V_1(t') + q(t') + C_1V_1(t') + C_2\frac{\partial V_1(t')}{\partial r} = \frac{\partial V_1(t')}{\partial t} \rho C \quad (D-4)$$

To prove that this equation holds, it is first necessary to establish that  $q(t')$  satisfies the heat deposition condition for Eq. D-1. This means that the following equation should hold:

$$q(t') = \begin{cases} q_0(r), & 0 \leq t' \leq t_0 \\ 0, & t' > t_0 \end{cases} \quad (D-5)$$

At  $t'=0$ ,  $t$  equals  $TC$  which corresponds to the start of the second pulse; while at  $t'=t_0$ ,  $t$  equals  $TC+t_0$  which corresponds to the end of the second pulse. Thus, the heat deposition condition is satisfied.

Let us now examine the initial and boundary conditions associated with Eq. D-1. Since both conditions hold for the first pulse, it is only necessary to examine whether or not the conditions hold for the second pulse which starts at  $t'=0$  or  $t=TC$ . At  $t=TC$

$$V_1(t-TC) = V_1(0) = 0 \quad (D-6)$$

so that the initial condition holds. Also shifting the time scale does not alter either boundary condition, namely  $V \rightarrow 0$  as  $r, z \rightarrow +\infty$  and  $\partial V / \partial z = 0$  at  $z=0$ . Thus, the expression given by Eq. D-2 satisfies the heat conduction equation, and its initial and boundary conditions.

An illustration of the above technique for evaluating the temperature rises caused by two pulses is illustrated in Fig. D-1. Here the temperature rises produced by the pulses are identical -- where the first pulse is represented by the solid curve and the second pulse by the dashed curve. The temperature rise produced by both pulses is represented by the heavy curve, and from Eq. D-2 equals the sum of the contributions from each pulse at the appropriate times.

By extending the argument to additional pulses, it is obvious that the temperature rise  $V(t)$  produced by  $N'$  pulses is given by

$$V(t) = \sum_{n=1}^{N'} V_1(t-(n-1) \cdot TC) \quad (D-7)$$

where  $N'$  equals the number of pulses started prior to time  $t$ . At the culmination of all pulses  $N'=N$ .

### 3. COMPUTERIZED MEANS FOR PREDICTING TEMPERATURES CAUSED BY MULTIPLE PULSES

Having established a rather simple technique for assessing the temperature rises caused by multiple pulses, the next step is the selection of the times between pulses at which temperatures are to be calculated to ensure accurate damage assessments. In this regard it is desirable that the times be sufficiently close to ensure accurate integration of the damage over time.

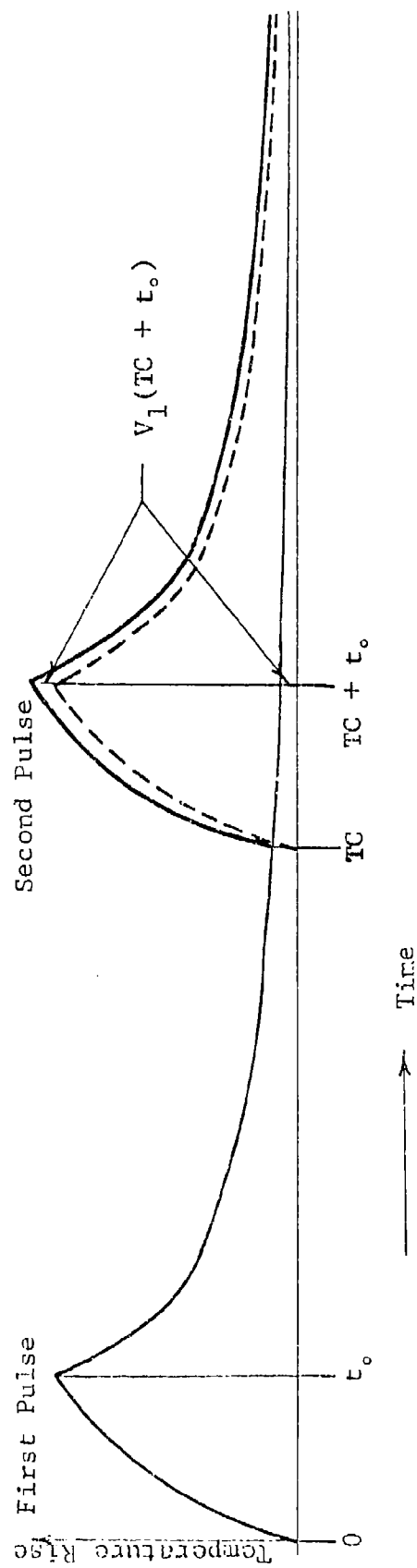


Figure D-1 ILLUSTRATION OF TECHNIQUE FOR EVALUATING  
TEMPERATURE RISES PRODUCED BY MULTIPLE PULSES

For this purpose, five values of the temperature rise (as calculated for the single pulse described in Appendix A) at regularly-spaced time intervals are used to cover the period during each pulse, and three values of the temperature rise at regularly-spaced time steps are used to cover the period from the end of one pulse and the start of the next. An illustration of the time steps is shown by Fig. D-2. Integration of the thermal damage is accomplished using the temperatures at the midpoints of the intervals. On the other hand, the average granule temperatures are calculated at the end of the time intervals to arrive at the peak temperatures.

In the computer codes, the times from the start of each pulse to the midpoints of the intervals are designated by  $ZT(L)$ ; while the times to the end of the intervals are designated by  $ZTX(L)$ . As may be observed from Fig. D-2 the index  $L$  ranges from 1 to 8.

In the remainder of this section we shall elaborate on the technique using the time intervals  $ZT(L)$ . Measured from the start of the first pulse, the times of concern are

$$t = (N'-1) \cdot TC + ZT(L) \quad (D-8)$$

where  $N'$  = number of pulses started prior to time  $t$ . Substitution of this expression into Eq. D-7 yields

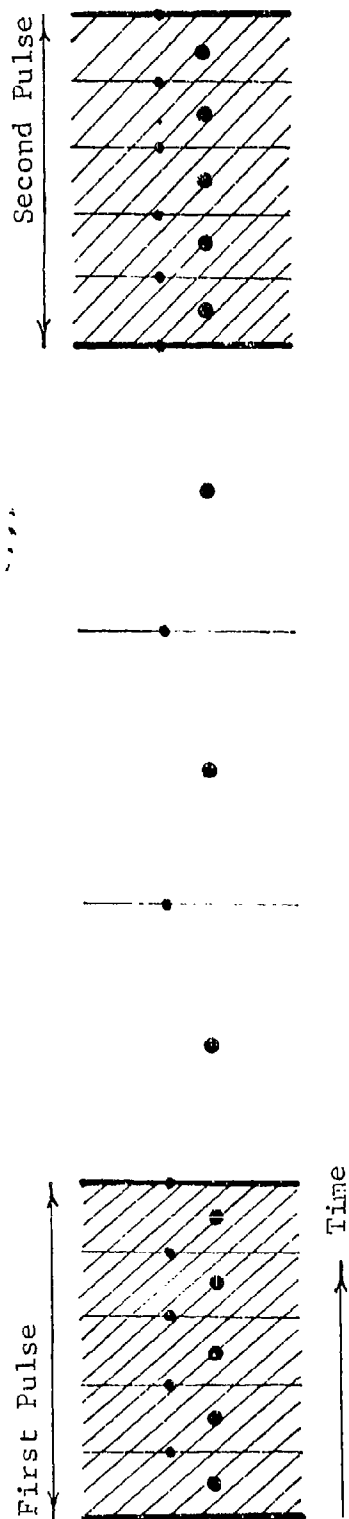
$$V(t) = \sum_{n=1}^{N'} V_1((N'-1) \cdot TC + ZT(L) - (n-1)TC) \quad (D-9)$$

which simplifies to

$$V(t) = \sum_{n=1}^{N'} V_1((n-1)TC + ZT(L)) \quad (D-10)$$

This expression describes temperature rises at times  $ZT(L)$  following the start of the  $N'$ -th pulse. Here, of course,  $N'$  may range over the number of pulses  $N$  used.

To evaluate the temperatures following the exposure at times of say  $(M-1)TC + ZT(L)$  where  $M > N$ , it is necessary to consider the effect of  $M$  hypothetical pulses given by



- Times at which granule temperature rises are calculated
- Times at which eye temperature rises are calculated

Figure D-2 TIMES AND TIME INTERVALS USED FOR TEMPERATURES  
AND DAMAGE EVALUATIONS FOR MULTIPLE PULSES

$$\sum_{n=1}^M V_1((n-1) \cdot TC + ZT(L)) \quad (D-11)$$

Here only the first N of the M pulses are real. In the above summation, these pulses correspond to  $n=M-N+1$  to M. The M-N hypothetical pulses correspond to  $n=1$  to M-N. Eliminating the non-existent contributions from the M-N hypothetical pulses yields

$$\begin{aligned} V(t) &= \sum_{n=1}^M V_1((n-1) \cdot TC + ZT(L)) - \sum_{n=1}^{M-N} V_1((n-1) \cdot TC + ZT(L)) \\ &= \sum_{n=M-N+1}^M V_1((n-1) \cdot TC + ZT(L)) \end{aligned} \quad (D-12)$$

In summary, Eqns. D-10 and D-12 describe the temperatures at the intervals  $ZT(L)$  shown in Fig. D-2 during and following exposure to the laser, respectively. The temperature rises  $V_1$  are linearly interpolated using the computer predictions for a single pulse represented by  $VC(i,j,k)$  at the times  $XT(k)$  at the desired points  $Z(i)$ ,  $R(j)$ .

As long as the number of pulses is minimal, the execution times are reasonably rapid. However, for exposures involving many pulses the execution times can become excessive. Excessive computer execution times are avoided by evaluating the temperatures and damage only at select regularly-spaced pulses when the number of pulses is 20 or more. For example, for exposures of 57 pulses the pulses are subdivided into 29 groups of 3 pulses, with the temperature and damage evaluations made during each of the middle pulses -- i.e. pulses 2, 5, 8...56. Total damage is arrived at by summing the damage produced during each of the select pulses, and multiplying the result by three to account for the remaining pulses.

In this analysis the number of pulses per group is always set equal to an odd number so that the damage occurring during the middle pulse of each group is representative of the average damage of all pulses in the group.

The number of pulses/group is given below.

<u>Total Number of Pulses</u>	<u>Number of Pulses/Group</u>
1 to 19	1
20 to 59	3
60 to 99	5
100 to 139	7
140 to 179	9
180 to 219	11
⋮	⋮
⋮	⋮
⋮	⋮
N to N+39	integer value of $(N/20)+2$

APPENDIX E

CHOICE OF TIME INTERVALS



## APPENDIX E

### CHOICE OF TIME INTERVALS

#### 1. INTRODUCTION

The principal advantage of the Technology, Inc. scheme is that it produces stable temperature solutions for large time intervals. However it does not address itself to the problem of choosing time-intervals so that errors are consistently small. Choice of time intervals is complicated by the fact that excessively small time intervals will cause unnecessarily long computer times while excessively large time intervals will produce excessive errors. As with all finite-difference schemes some compromise must be made between accuracy and execution times. Specifically, we are concerned with selecting the sizes of progressively larger time intervals such that errors are maintained at some consistently small value.

To assess how the error depend on the time increment and on the dimensions of the spacial elements we shall examine the residues that were neglected in approximating the heat conduction equation by means of the finite-difference equations described in Appendix A. This means assessing how well the heat conduction equation

$$\rho C \frac{\partial u}{\partial t} = \frac{K}{r} \frac{\partial u}{\partial r} + K \frac{\partial^2 u}{\partial r^2} + \frac{\partial}{\partial z} \left( K \frac{\partial u}{\partial z} \right) \quad (\text{E-1})$$

is satisfied by use of finite-difference approximations of Appendix A

where  $C$  = specific heat

$K$  = thermal conductivity

$r$  = radial distance

$z$  = axial distance

$u$  = temperature rise

$\rho$  = density

$t$  = time

In Eq. E-1 the temperature rise is represented by  $u$  to distinguish it from the temperature rise  $v$  obtained from the finite-difference solution. Errors in the finite-difference predictions will, of course, be

$$\ell = v - u \quad (\text{E-2})$$

## 2. ANALYSIS OF RESIDUALS NEGLECTED BY FINITE-DIFFERENCE APPROXIMATIONS

In this analysis we shall consider the first and last pair of the two time steps  $\Delta t_{k/2}$  used in the computational scheme described in Appendix A. The result is two time steps each of duration  $\Delta t_{k/2}$  -- in which the COLUMN computations are used for the first time step  $\Delta t_{k/2}$  while the ROW computations are used for the second time step  $\Delta t_{k/2}$ . In each case it is necessary to expand each of the partial derivatives of Eq. E-1 where the first time step  $\Delta t_{k/2}$  corresponding to  $k \rightarrow k+1/2$  will be designated by  $\Delta \tau_k$ . Similarly the second time step  $\Delta t_{k/2}$  corresponding to  $k+1/2 \rightarrow k+1$  will also be of duration  $\Delta \tau_k$ .

For the first time step  $\Delta \tau_k$  the differential equation requiring solution is

$$\rho \cdot C \left. \frac{\partial u}{\partial t} \right|_{i,j,k+1/2} = \frac{K}{r_j} \left. \frac{\partial u}{\partial r} \right|_{i,j,k+1/2} + K \left. \frac{\partial^2 u}{\partial r^2} \right|_{i,j,k+1/2} + K \left. \frac{\partial^2 u}{\partial z^2} \right|_{i,j,k+1/2} \quad (E-3)$$

Since the COLUMN computations involve using existing temperatures for the term in  $z$  and future temperatures for terms in  $r$ , it is necessary to replace the last term of Eq. E-3 by

$$K \left. \frac{\partial^2 u}{\partial z^2} \right|_{i,j,k} + K \left. \frac{\partial^3 u}{\partial t \partial z^2} \right|_{i,j,k} \Delta \tau_k \quad (E-4)$$

The result of the above substitution is

$$\rho \cdot C \left. \frac{\partial u}{\partial t} \right|_{i,j,k+1/2} \approx \frac{K}{r_j} \left. \frac{\partial u}{\partial r} \right|_{i,j,k+1/2} + K \left. \frac{\partial^2 u}{\partial r^2} \right|_{i,j,k+1/2} + K \left[ \left. \frac{\partial^2 u}{\partial z^2} \right|_{i,j,k} + \left. \frac{\partial^3 u}{\partial t \partial z^2} \right|_{i,j,k} \Delta \tau_k \right] \quad (E-5)$$

Reversing the time steps for the ROW computations for the second time step  $\Delta \tau_k$  in which  $k+1/2 \rightarrow k+1$  yields

$$\rho \cdot C \frac{\partial u}{\partial t} \Big|_{i,j,k+1} \approx \frac{K}{r_j} \cdot \left[ \frac{\partial u}{\partial r} \Big|_{i,j,k+1/2} + \frac{\partial u}{\partial t \partial r} \Big|_{i,j,k+1/2} \Delta \tau_k \right] +$$

$$K \left[ \frac{\partial^2 u}{\partial r^2} \Big|_{i,j,k+1/2} + \frac{\partial^3 u}{\partial t \partial r^2} \Big|_{i,j,k+1/2} \Delta \tau_k \right] + K \cdot \frac{\partial^2 u}{\partial z^2} \Big|_{i,j,k+1} \quad (E-6)$$

Next it is necessary to replace the terms of Eqs. E-5 and E-6 by the following series expansions:

$$\frac{\partial u}{\partial t} \Big|_{i,j,k+1/2} \approx \frac{u_{i,j,k+1/2} - u_{i,j,k}}{\Delta \tau_k} + \frac{1}{2} \frac{\partial^2 u}{\partial t^2} \Big|_{i,j,k+1/2} \Delta \tau_k -$$

$$\frac{1}{6} \frac{\partial^3 u}{\partial t^3} \Big|_{i,j,k+1/2} (\Delta \tau_k)^2 \dots \quad (E-7)$$

$$\frac{\partial u}{\partial t} \Big|_{i,j,k+1} \approx \frac{u_{i,j,k+1} - u_{i,j,k+1/2}}{\Delta \tau_k} + \frac{1}{2} \frac{\partial^2 u}{\partial t^2} \Big|_{i,j,k+1/2} \Delta \tau_k -$$

$$\frac{1}{6} \frac{\partial^3 u}{\partial t^3} \Big|_{i,j,k+1/2} (\Delta \tau_k)^2 \dots \quad (E-8)$$

$$\frac{\partial u}{\partial r} \Big|_{i,j,k+1/2} \approx \frac{u_{i,j+1,k+1/2} - u_{i,j-1,k+1/2}}{2 \cdot \Delta r} - \frac{1}{6} \frac{\partial^3 u}{\partial r^3} \Big|_{i,j,k+1/2} (\Delta r)^2 \dots \quad (E-9)$$

$$\frac{\partial^2 u}{\partial r^2} \Big|_{i,j,k+1/2} \approx \frac{u_{i,j+1,k+1/2} - 2 \cdot u_{i,j,k+1/2} + u_{i,j-1,k+1/2}}{(\Delta r)^2} -$$

$$\frac{1}{12} \frac{\partial^4 u}{\partial r^4} \Big|_{i,j,k+1/2} (\Delta r)^2 \dots \quad (E-10)$$

$$\frac{\partial^2 u}{\partial z^2} \Big|_{i,j,k+1/2} \approx \frac{u_{i+1,j,k+1/2} - 2 \cdot u_{i,j,k+1/2} + u_{i-1,j,k+1/2}}{(\Delta z)^2} -$$

$$\frac{1}{12} \frac{\partial^4 u}{\partial z^4} \Big|_{i,j,k+1/2} (\Delta z)^2 \dots \quad (E-11)$$

$$\left. \frac{\partial^2 u}{\partial z^2} \right|_{i,j,k+1} \approx \frac{u_{i+1,j,k+1} - 2 \cdot u_{i,j,k+1} + u_{i-1,j,k+1}}{(\Delta z)^2} - \frac{1}{12} \cdot \left. \frac{\partial^4 u}{\partial z^4} \right|_{i,j,k+1} (\Delta z)^2 - \dots \quad (E-12)$$

Substituting Eqs. E-7 through E-12 into Eq. E-3 along with

$$K \cdot \left. \frac{\partial^3 u}{\partial t \partial z^2} \right|_{i,j,k} \Delta \tau_k \approx K \cdot \left. \frac{\partial^3 u}{\partial t \partial z^2} \right|_{i,j,k+1/2} \Delta \tau_k - K \cdot \left. \frac{\partial^4 u}{\partial t^2 \partial z^2} \right|_{i,j,k+1/2} (\Delta \tau_k)^2 \quad (E-13)$$

yields

$$\begin{aligned} & \left\{ \rho \cdot C \frac{u_{i,j,k+1/2} - u_{i,j,k}}{\Delta \tau_k} \right\} + \left[ \frac{\rho \cdot C}{2} \left. \frac{\partial^2 u}{\partial t^2} \right|_{i,j,k+1/2} \Delta \tau_k \right] - \\ & \quad \frac{2}{3} \left. \frac{\partial^3 u}{\partial t^3} \right|_{i,j,k+1/2} (\Delta \tau_k)^2 \\ & = \left\{ \frac{K}{r_j} \cdot \frac{u_{i,j+1,k+1/2} - u_{i,j-1,k+1/2}}{2 \cdot \Delta r} \right\} - \frac{K}{6 \cdot r_j} \left. \frac{\partial^3 u}{\partial r^3} \right|_{i,j,k+1/2} (\Delta r)^2 + \\ & \quad \left\{ K \cdot \frac{u_{i,j+1,k+1/2} - 2 \cdot u_{i,j,k+1/2} + u_{i,j-1,k+1/2}}{(\Delta r)^2} \right\} - \frac{K}{12} \cdot \left. \frac{\partial^4 u}{\partial r^4} \right|_{i,j,k+1/2} (\Delta r)^2 + \\ & \quad \left\{ K \cdot \frac{u_{i+1,j,k} - 2 \cdot u_{i,j,k} + u_{i-1,j,k}}{(\Delta z)^2} \right\} - \frac{K}{12} \cdot \left. \frac{\partial^4 u}{\partial z^4} \right|_{i,j,k} (\Delta z)^2 + \\ & \quad \left[ K \cdot \left. \frac{\partial^3 u}{\partial t \partial z^2} \right|_{i,j,k+1/2} \Delta \tau_k \right] - K \cdot \left. \frac{\partial^4 u}{\partial t^2 \partial z^2} \right|_{i,j,k+1/2} \Delta \tau_k \quad (E-14) \end{aligned}$$

for the COLUMN computations. The corresponding equation for the ROW computations is obtained by substituting Eqs E-7 through E-12 into Eq. E-4 to yield

$$\begin{aligned}
& \left\{ \rho \cdot C \frac{u_{i,j,k+1} - u_{i,j,k+1/2}}{\Delta \tau_k} \right\} + \left[ \frac{\rho \cdot C}{2} \frac{\partial^2 u}{\partial t^2} \right]_{i,j,k+1/2} \Delta \tau_k - \\
& - \frac{\rho \cdot C}{6} \frac{\partial^3 u}{\partial t^3} \Big|_{i,j,k+1/2} (\Delta \tau_k)^2 = \left\{ \frac{K}{r_j} \frac{u_{k,j+1,k+1/2} - u_{i,j-1,k+1,1/2}}{2 \cdot \Delta r} \right\} - \\
& \frac{K}{6 \cdot r_j} \frac{\partial^3 u}{\partial r^3} \Big|_{i,j,k+1/2} (\Delta r)^2 + \left[ \frac{K}{r_j} \frac{\partial^2 u}{\partial t \partial r} \right]_{i,j,k+1/2} \Delta \tau_k + \\
& \left\{ K \cdot \frac{u_{i,j+1,k+1/2} - 2 \cdot u_{i,j,k+1/2} + u_{i,j-1,k+1/2}}{(\Delta r)^2} \right\} - \frac{K}{12} \frac{\partial^4 u}{\partial r^4} \Big|_{i,j,k+1/2} (\Delta r)^2 + \\
& \left[ K \cdot \frac{\partial^3 u}{\partial t \partial r^2} \right]_{i,j,k+1/2} \Delta \tau_k + \left\{ K \frac{u_{i+1,j,k+1/2} - 2 \cdot u_{i,j,k+1/2} + u_{i-1,j,k+1/2}}{(\Delta z)^2} \right\} - \\
& \frac{K}{12} \frac{\partial^4 u}{\partial z^4} \Big|_{i,j,k+1/2} (\Delta z)^2 \quad (E-15)
\end{aligned}$$

The result of one set of COLUMN and ROW computations would be the sum of Eqs. E-14 and E-15. Therefore, summing the two equations and replacing the terms  $u$  with  $v$  from Eq. E-2 results in

$$\Delta^2 \ell_{i,j,k+1} = \frac{(\rho \cdot C) (\ell_{i,j,k+1} - \ell_{i,j,k})}{\Delta \tau_k} + C_{r,k} (\Delta r)^2 + C_{z,k} (\Delta z)^2 + C_{t,k} (\Delta \tau_k)^2 \quad (E-16)$$

where the terms in the braces and brackets cancel and where

$$\begin{aligned}
\Delta^2 \ell_{i,j,k+1} = & \frac{2}{r_j} \left[ \frac{\ell_{i,j+1,k+1/2} - \ell_{i,j-1,k+1/2}}{2 \cdot \Delta r} \right] + \\
& 2 \cdot K \left[ \frac{\ell_{i,j+1,k+1/2} - 2 \cdot \ell_{i,j,k+1/2} + \ell_{i,j-1,k+1/2}}{(\Delta r)^2} \right] + \\
& K \left[ \frac{\ell_{i+1,j,k+1/2} - 2 \cdot \ell_{i,j,k+1/2} + \ell_{i-1,j,k+1/2}}{(\Delta z)^2} \right] \quad (E-17)
\end{aligned}$$

$$C_{r,k} = - K \cdot \left[ \frac{1}{3 \cdot r_j} \frac{\partial^3 u}{\partial r^3} + \frac{1}{6} \frac{\partial^4 u}{\partial r^4} \right]_{i,j,k+1/2} \quad (E-18)$$

$$C_{z,k} = -K \cdot \frac{1}{6} \frac{\partial^4 u}{\partial z^4} \Big|_{i,j,k+1/2} \quad (E-19)$$

$$C_{t,k} = \frac{\partial}{\partial t^2} \left[ \frac{5}{6} (\rho \cdot C) \frac{\partial u}{\partial t} - K \frac{\partial^2 u}{\partial z^2} \right] \Big|_{i,j,k+1/2} \quad (E-20)$$

Now it has been shown (Ref. 51) that if

$$\Delta^2 y - C_k \cdot y_k = g_k \quad \text{for } k=1, 2, \dots, K-1 \text{ with } y_0 = y_K = 0, \quad (E-21)$$

then

$$\max |y_k| \leq \max \left| \frac{g_k}{C_k} \right| \quad (E-22)$$

Applying Eq. E-22 to Eq. E-15 yields

$$\max |\ell_{i,j,k+1}| \leq \max \left| -\ell_{i,j,k} + \Delta\tau_k \frac{C_{r,k}(\Delta r)^2 + C_{z,k}(\Delta z)^2 + C_{t,k}(\Delta\tau_k)^2}{(\rho \cdot C)} \right| \quad (E-23)$$

Since  $\ell_{i,j,0} = 0$ , Eq. E-23 becomes

$$\max |\ell_{i,j,K}| \leq \sum_{k=1}^{K-1} \Delta\tau_k |C_{r,k}(\Delta r)^2 + C_{z,k}(\Delta z)^2 + C_{t,k}(\Delta\tau_k)^2| \quad (E-24)$$

Equation E-24 shows that errors shall accumulate with time depending on the size of  $\Delta r$ ,  $\Delta z$  and  $\Delta\tau_k$  as well as the various derivatives of temperature rise with respect to  $r$ ,  $z$  and  $t$ . During the early times while the eye is being exposed to the laser, the derivatives associated with  $C_{r,k}$ ,  $C_{z,k}$  and  $C_{t,k}$  will be most pronounced. Therefore, it is obvious that initially  $\Delta\tau_k$  must be relatively small. Subsequently, the time intervals  $\Delta\tau_k = \Delta t_{k/2}$  may be progressively increased with time.

In order to keep the errors small, the first time interval should be such that it satisfies the stability condition for standard explicit finite-difference equations, namely

$$\Delta t_1 \leq \rho \cdot C \cdot \frac{(\Delta r)^2 + (\Delta z)^2}{6 \cdot K} \quad (E-25)$$

To better appreciate how rapidly to increase subsequent intervals, let us examine the last term of Eq. E-24, namely

$$\frac{\partial}{\partial t^2} \left[ \frac{5}{6} (\rho \cdot C) \cdot \frac{\partial u}{\partial t} - K \cdot \frac{\partial^2 u}{\partial z^2} \right] \Big|_{i,j,k+1/2} \frac{(\Delta t_k)^2}{4} \quad (E-26)$$

Along the axis of the eye, wherein the most pronounced temperatures occur, the heat flow approximates one-dimensional flow. Therefore, to gain an appreciation of the above term we will take the second derivative of the one-dimensional heat conduction equation with respect to time. Holding the thermal properties constant, the result is

$$K \frac{\partial^4 u}{\partial t^2 \partial z^2} = \rho \cdot C \frac{\partial^3 u}{\partial t^3} \quad (E-27)$$

Using this relationship, the expression given by Eq. E-26 becomes

$$- \frac{(\rho \cdot C)}{6} \frac{\partial^3 u}{\partial t^3} \Big|_{i,j,k+1/2} \frac{(\Delta t_k)^2}{4} \quad (E-28)$$

For the worst condition, in which heat is supplied at a single depth at a constant rate, the temperature rises at the given depth will approximate

$$u = c_1 \sqrt{t} \quad (E-29)$$

where  $c_1$  is a constant. Differentiating this equation three times with respect to time yields

$$\frac{\partial^3 u}{\partial t^3} = - 3 \cdot c_1 / (8 \cdot t^{5/2}) \quad (E-30)$$

Substituting Eq. E-30 into the expression given by Eq. E-28 along with the subscript  $k$  and dropping all the constants yields

$$\frac{(\Delta t_k)^2}{t_k^{5/2}} \quad (E-31)$$

In order to keep this expression consistently small, it is necessary that

$$\Delta t_k \leq c \cdot t_k^{5/4} \quad (E-32)$$

where  $c$  is a constant. This result indicates that one can expand the time intervals very rapidly with respect to time. However, in view of the various assumptions made in this analysis, it is wise to select time intervals appreciably smaller than indicated by the above condition. One choice which has proven satisfactory is as follows

$$\Delta t_{k+1} = C \cdot \Delta t_k \quad (E-33)$$

where the first time interval  $\Delta t_1$  is given by Eq. E-25. Values for the constant  $C$  used in this study ranged from 1.1 to 1.4.



APPENDIX F  
HEAT DEPOSITION ANALYSES

## APPENDIX F

### HEAT DEPOSITION ANALYSES

#### 1. INTRODUCTION

In order to calculate the deposition of energy within the eye, it is first necessary to determine the laser profile within the eye. To this end each model starts with a determination of the refraction of the laser beam by the cornea as described in Section 3. The result is a description of the normalized profile as a function of radius and depth from the anterior surface of the cornea to the anterior surface of the lens. The resultant irradiance profile is then used directly by the Corneal Model with appropriate provisions for absorption and reflection to assess the rate of energy deposition into various regions of the eye. On the other hand the Retinal Model utilizes the normalized profile at the lens to assess the irradiance profile at the retina as described in Section 3 and Appendix H. The resultant irradiance distribution of the retinal image is preserved at all depths of the eye. This assumption is considered reasonable in that the profile varies only slightly in and about the retina wherein most of the energy is deposited.

In this appendix we shall illustrate the procedures used to compute the deposition of energy from these irradiance profiles at various depths of the eye. Key parameters in this analysis are the absorption and reflection coefficients for the various eye media and interfaces, respectively.

First, it is important to recognize that it is not possible to locate all interfaces (between eye media) at the boundaries  $ZH(i)$  if the  $z$  increments are given by

$$ZH(i) = (Z(i-1) + Z(i))/2 \quad F(1)$$

Only the more important interfaces are located at the above boundaries. These include the front of the eye medium for which damage is being evaluated (see Appendix I for a description of the grid network).

Thus, most of the interfaces do not coincide with the boundaries  $ZH(i)$ . Moreover, in some situations there can be more than one interface within a given increment. To provide for such eventualities we have used the array  $ZD(LI)$  to represent the depths  $z$  associated with the various interfaces between eye media. The absorption coefficients associated with eye medium between  $ZD(LI-1)$  and  $ZD(LI)$  are represented by  $ABS(LI-1)$ . The above coordinates and nomenclature are depicted by Fig. F-1 for a given  $z$  increment, starting at  $ZH(i-1)$  and ending at  $ZH(i)$ . Included are the products  $AB(i,L)$  of the absorption coefficients and thicknesses of various eye media within the given  $z$  increment. The products  $AB(i,L)$  are given by

$$\begin{aligned} AB(i,1) &= ABS(LI-1) \cdot (ZD(LI) - ZH(i-1)) \\ AB(i,2) &= ABS(LI) \cdot (ZH(i) - ZD(LI)) \end{aligned} \quad F(2)$$

If there is one eye medium between  $ZH(i-1)$  and  $ZH(i)$ , then

$$\begin{aligned} AB(i,1) &= ABS(LI-1) \cdot (ZH(i) - ZH(i-1)) \\ AB(i,2) &= 0 \end{aligned} \quad F(3)$$

## 2. ENERGY DEPOSITION FROM INCOMING BEAM

To compute the total energy deposition within an increment, it is first necessary to determine the irradiance  $H(r)$  at the front of the increment. At the anterior surface of the cornea, the entering irradiance is represented by

$$H(r) = QP \cdot HR(r) \quad F(4)$$

Here  $r$  equals the radial distance  $R(j)$  of the radial grid points, where  $j=1,2,\dots,N3$  and  $QP$  represents the irradiance at  $r=0$ .

To arrive at the rate of energy deposition into a given increment  $z$ , it is first necessary to determine how the irradiance changes on passing through the increment allowing for absorption and reflections. For purposes of simplicity, we shall follow the irradiance (at a given radial distance  $R(j)$ ) through each of the media contained in the increment illustrated by Fig. F-1. Here  $X3$  shall represent the incoming irradiance;  $X2$  shall represent the irradiance at various depths, and  $X4$  shall represent the sum of the reflected irradiances.

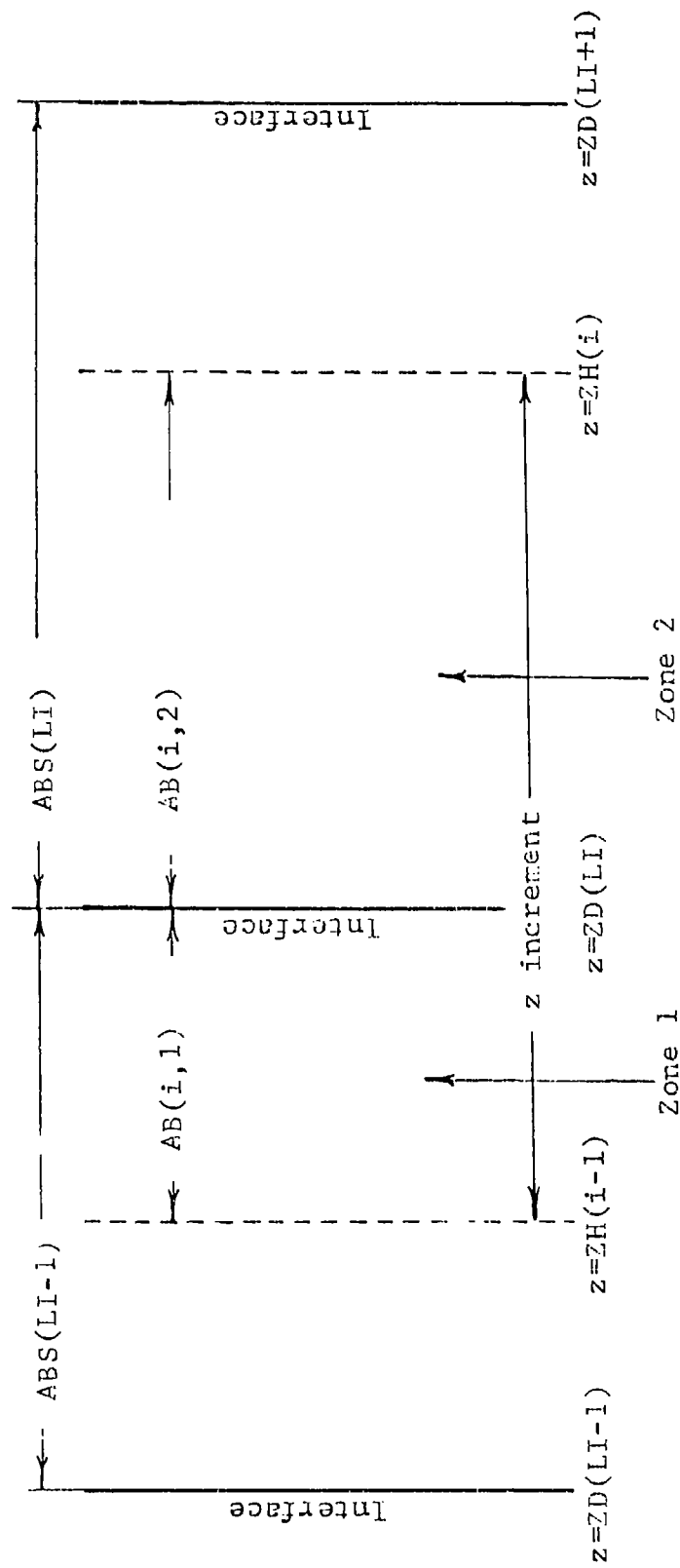


Fig. F-1 NOMENCLATURE USED TO EVALUATE ABSORPTION OF RADIATION WITHIN VARIOUS  $z$  INCREMENTS

After passage through the first zone shown in Fig. F-1, the irradiance is

$$X2 = X3 \cdot \exp(-AB(i,1)) \quad F(5)$$

At the interface at ZD(LI), a portion of the radiation is reflected away given by

$$X4 = REF(LI) \cdot X2 \quad (6)$$

After passage through the second zone shown in Fig. F-1, the irradiance becomes

$$X2' = (1-REF(LI)) \cdot X2 \cdot \exp(-AB(i,2)) \quad F(7)$$

The net rate of energy deposition per unit volume surrounding the point Z(i), R(j) is therefore given by

$$(X3 - X2' - X4) \cdot H(r) / (ZH(i) - ZH(i-1)) \quad F(8)$$

The above result includes only the absorption from the incoming beam. In the next section we shall assess absorption from radiation reflected at the several interfaces.

### 3. ENERGY DEPOSITION FROM REFLECTED RADIATION

In this analysis we shall consider the radiation to be reflected parallel to the axis of the eye. The neglect of diffuse reflections is considered of secondary importance in view of the fact that reflected radiation is of secondary importance. Calculations are also simplified by the neglect of multiple reflections.

To determine the deposition of energy from the reflected radiation, it is first necessary to assess the sums ABR(i,LI) of the products of the absorption coefficients and thicknesses of each eye media within each increment z prior to the depths at which the reflections occur, namely ZD(LI). For the situation illustrated in Fig. F-1, these sums are given by

$$\begin{aligned} ABR(i,LI) &= AB(i,1) \\ ABR(i,LI+1) &= AB(i,1) + AB(i,2) \end{aligned} \quad F(9)$$

To compute the ratio of absorption of the reflected radiation, it is first necessary to determine the intensities of the reflected radiation at each of the interfaces ZD(LI). At the first interface,

ZD(i) beneath the anterior surface of the cornea, the intensity of the reflected radiation REFL(2) is

$$\text{REFL}(2) = H(r) \cdot (1 - \exp(-\text{ABS}(1))) \cdot \text{REF}(2) \quad F(10)$$

At the third interface ZD(3), the reflected irradiance REFL(3) is

$$\begin{aligned} \text{REFL}(3) = H(r) \cdot (1 - \exp(-\text{ABS}(1))) \cdot (1 - \text{REF}(2)) \cdot \\ (1 - \exp(-\text{ABS}(2))) \cdot \text{REF}(3) \end{aligned} \quad F(11)$$

By continuing this process, each of the reflected intensities REFL(LI) may be determined for each of the interfaces.

To determine the rates of energy deposition, it is necessary to consider the reflected radiation from each interface separately. For example, at the interface ZD(LI) shown in Fig. F-1 the reflected irradiance at ZH(i-1) from the ZD(LI) interface is

$$\text{REFL}(LI) \cdot \exp(-\text{ABR}(i, LI)) \quad F(12)$$

and the rate of energy deposition into the z increment is

$$\text{REFL}(LI) (1 - \exp(-\text{ABR}(i, LI))) / (ZH(i) - ZH(i-1)) \quad F(13)$$

Similarly, the rate of energy deposition into the next increment between ZH(i-2) and ZH(i-1) is

$$\text{REFL}(LI) \exp(-\text{ABR}(i, LI)) (1 - \exp(-\text{ABR}(i-1, LI))) / (ZH(i-1) - ZH(i-2)) \quad F(14)$$

By continuing the process for decreasing i, one arrives at the rates of energy deposition into each increment due to reflection at ZD(LI).

To arrive at the total deposition, one merely performs the computations for all interfaces and sums the results for each increment. Then by dividing the sums by the depths ZH(i) - ZH(i-1) of each increment, one arrives at the rates of energy deposition per unit volume at each of the grid points Z(i), R(j). The total deposition, of course, is the sum of the energy depositions from the incoming and reflected beams.

APPENDIX G

OPTICAL PROPERTIES OF EYES OF MAN AND RHESUS MONKEY

## 1. OPTICAL PROPERTIES OF THE RHESUS MONKEY

### 1.1 CORNEA

The rhesus cornea has a refractive index of 1.376 so the calculated reflection coefficient for light incident along the normal is approximately 2.5% for visible wavelengths.

Boettner (6) measured the transmittances of the corneas of young adult rhesus as shown below. The total transmittance includes both the direct beam and forward scattered radiation.



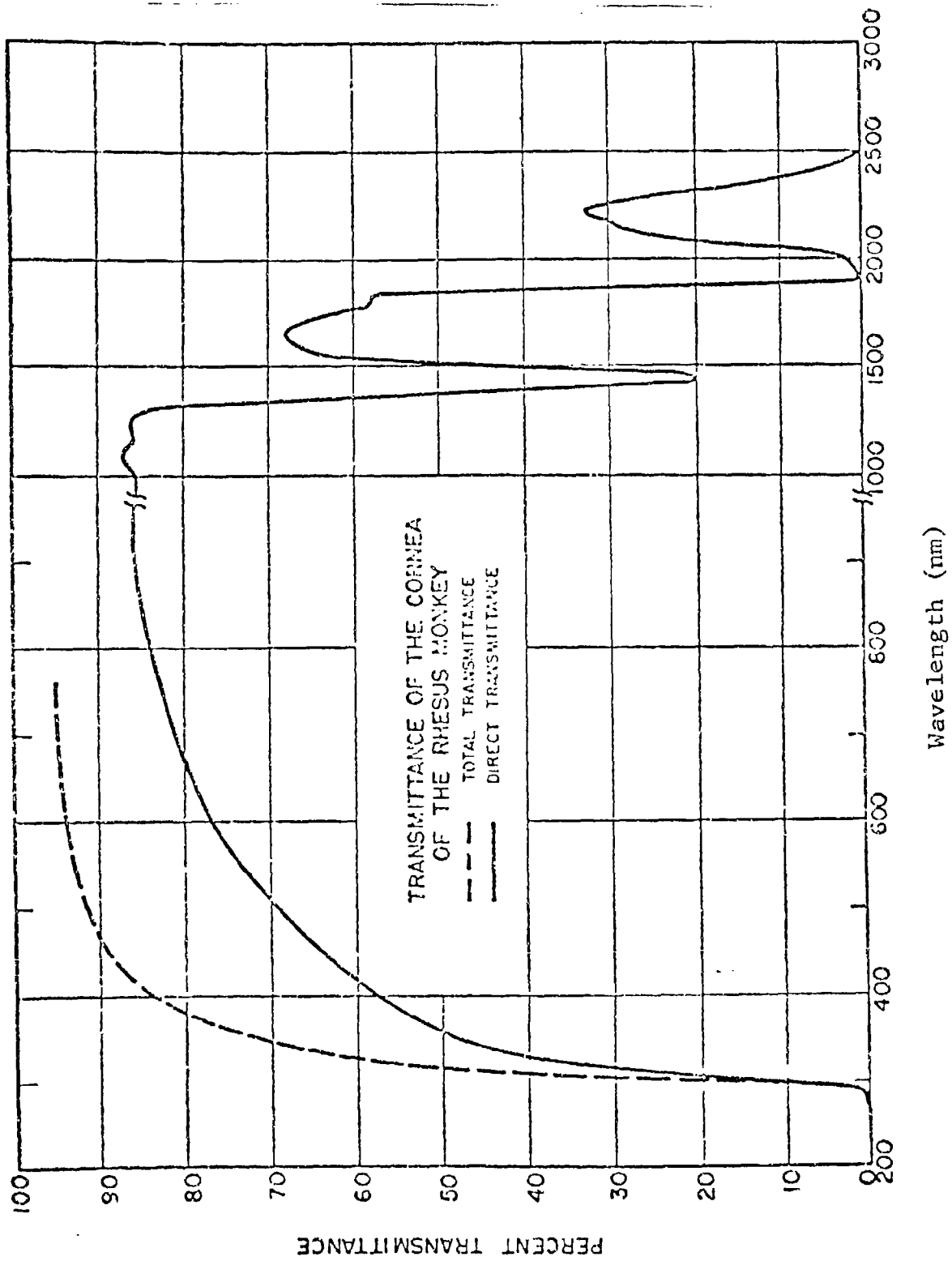


Figure G-1 TRANSMITTANCE OF THE CORNEA OF THE RHESUS MONKEY

## 1.2 AQUEOUS HUMOR

Since the refractive indices of the cornea and aqueous humor are very similar (1.376 and 1.336) the reflection coefficient for normal incidence can be calculated as approximately 0.02% for visible wavelengths.

Boettner's (6) measurements of the transmission of the rhesus aqueous humor are shown in Figure G-2. There is no forward scattering, nor is the transmission age dependent.

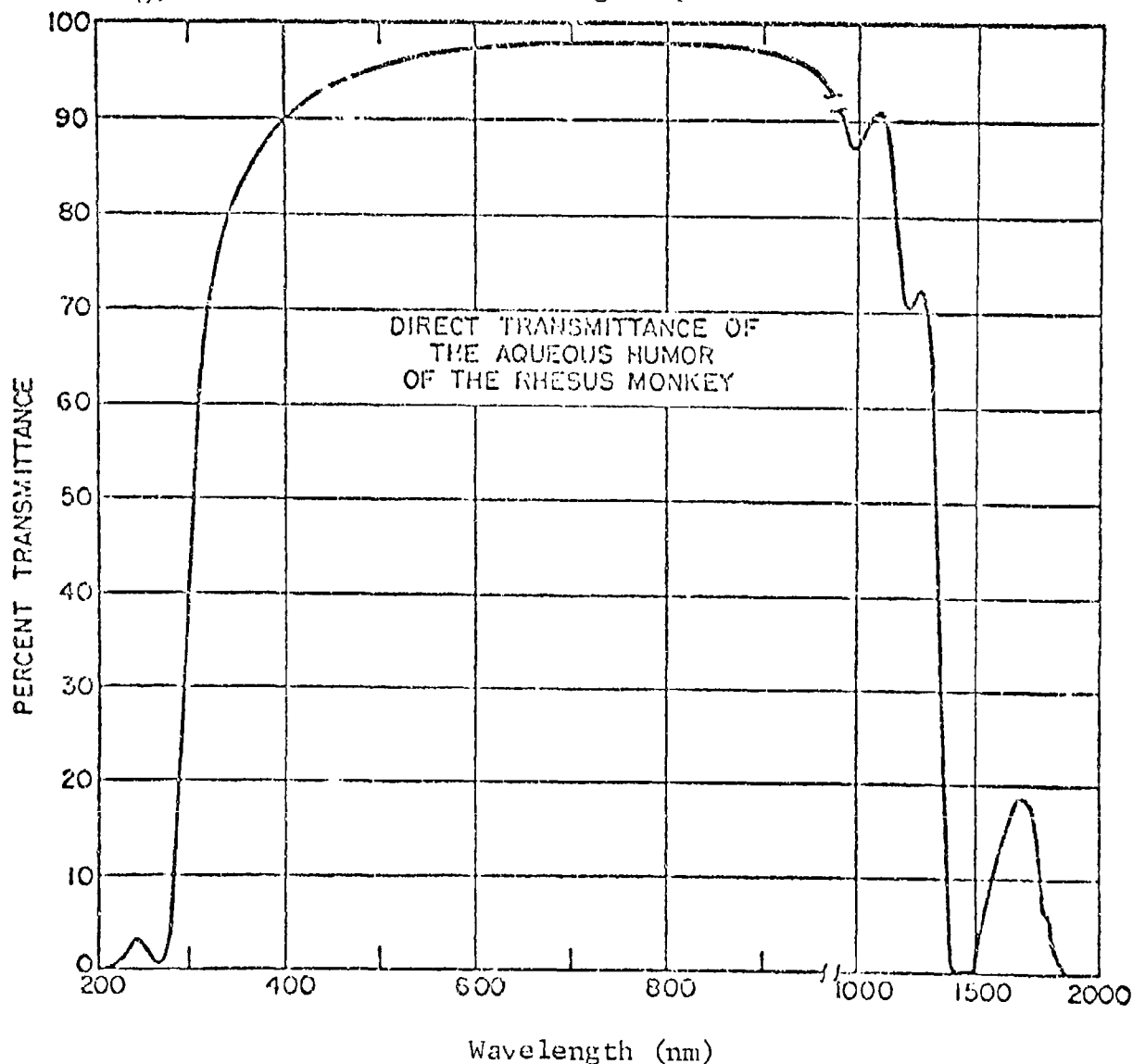


Figure G-2 TRANSMITTANCE OF THE AQUEOUS HUMOR OF THE RHESUS MONKEY

### 1.3 LENS

Since the lens has a graded density the reflection from its surfaces is minimized. Calculation shows that for a lens cortex refractive index of 1.386 and for aqueous and vitreous regions both 1.336, the reflection from each surface is only approximately 0.034% for visible wavelengths. The transmittances of the rhesus monkey lens, with and without forward scattering, measured by Boettner (6) are shown in Figure G-3.

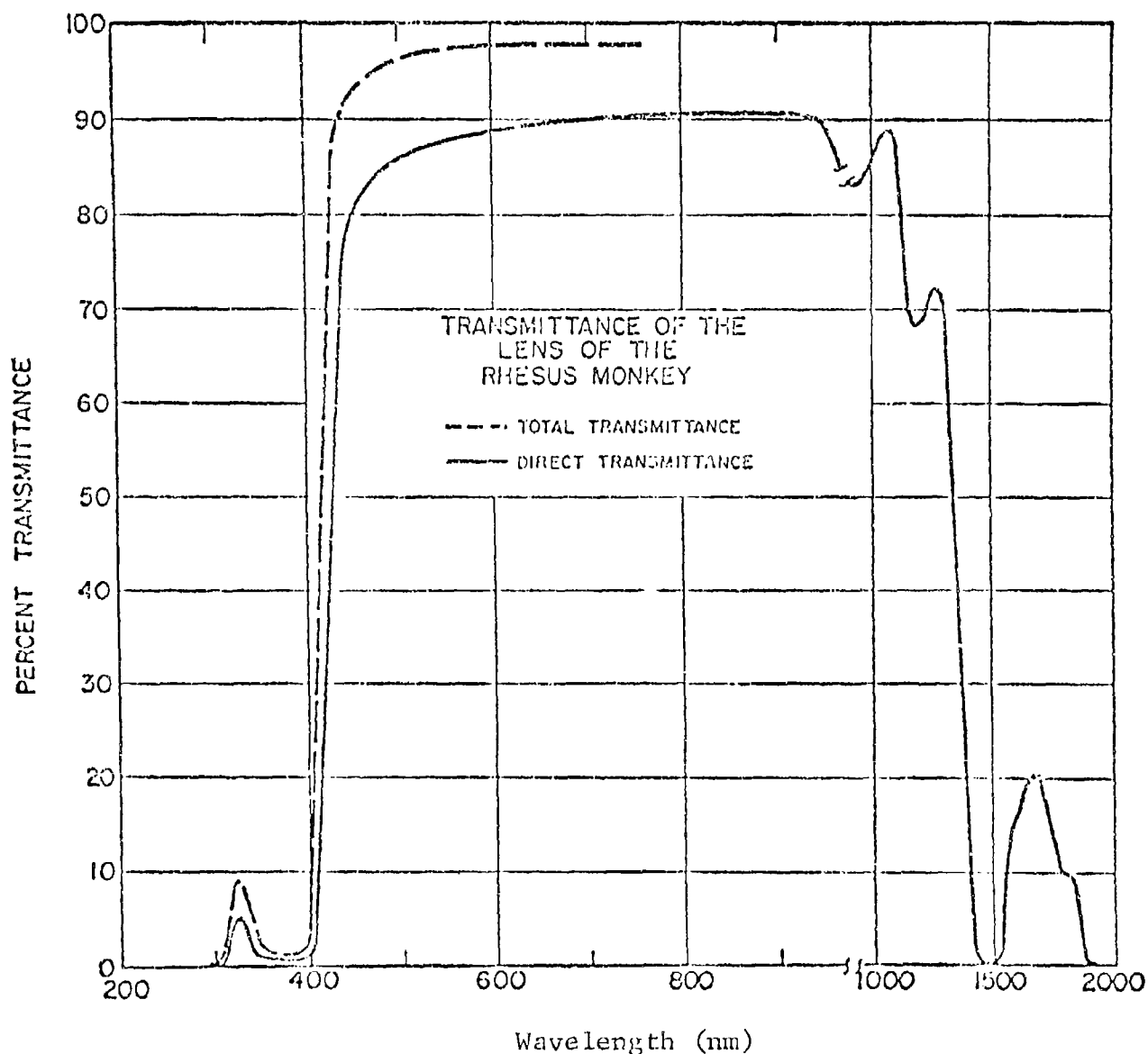


Figure G-3 TRANSMITTANCE OF THE LENS OF THE RHESUS MONKEY

#### 1.4 VITREOUS BODY

The transmission of the rhesus vitreous body shown in Figure G-4 is due to Boettner (6).

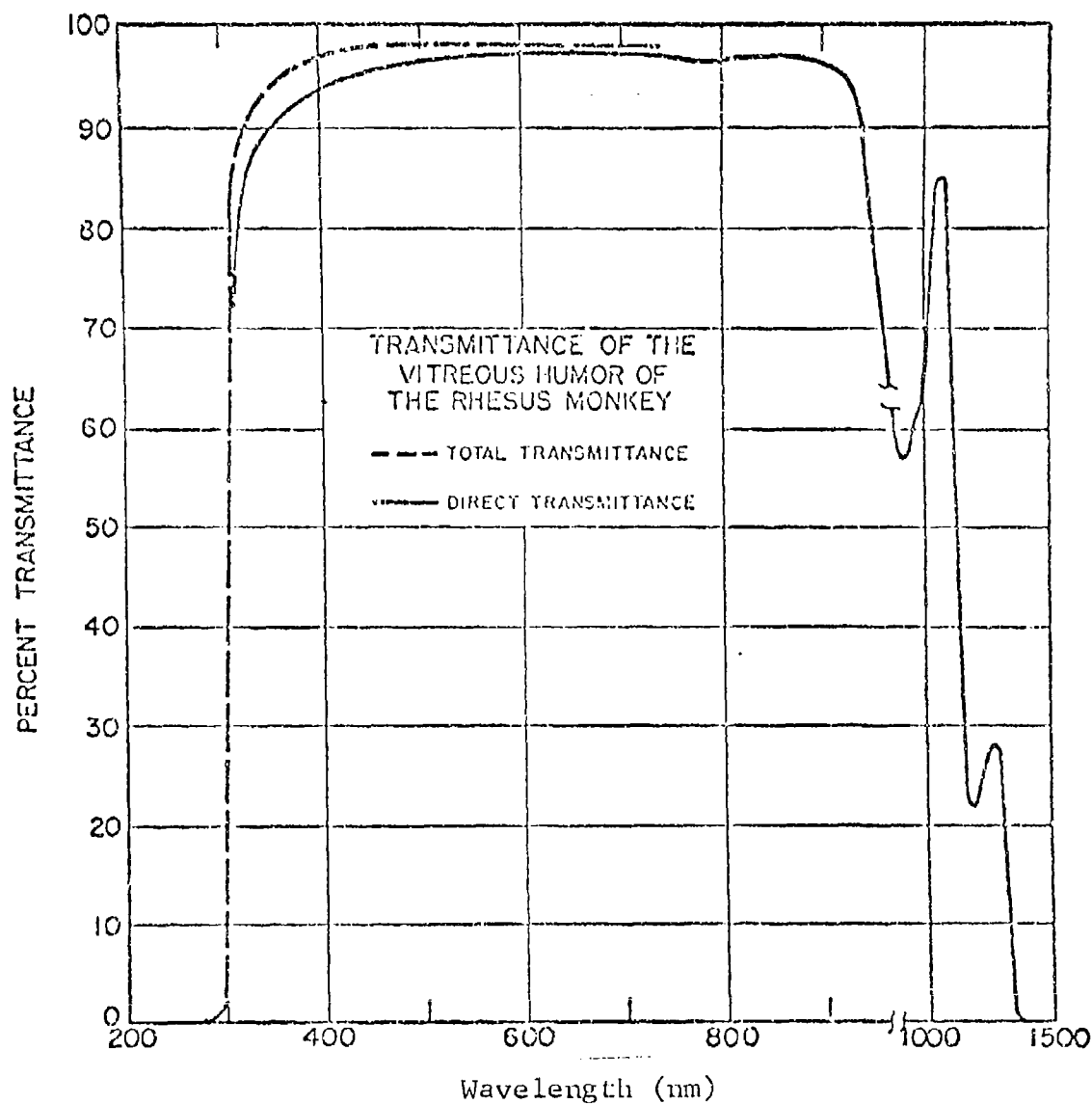


Figure G-4 TRANSMITTANCE OF THE VITREOUS HUMOR  
OF THE RHESUS MONKEY

# 1.5 OCULAR MEDIA

The foregoing measurements by Boettner (6) on the individual components of the ocular media are summarized in Table G-1.

Table G-1

## TRANSMITTANCES OF THE INDIVIDUAL OCULAR MEDIA OF RHESUS MONKEY (%)

Wavelength (nm)	Cornea		Aqueous Direct	Lens		Vitreous	
	Direct	Total		Direct	Total	Direct	Total
200			< 0.1				
220			.2				
240			2.5				
260			1.5				
280	< 0.1	< 0.1	2.0			< 0.1	< 0.1
300	10.	16.	40.	< 0.1	0.5	15.	15.
320	34.	54.	70.	5.	9.	82.	90.
340	45.	67.5	80.	1.	3.	88.5	93.
360	51.5	74.	84.	.5	1.	90.5	94.5
380	54.	80.	87.5	.5	1.	92.5	96.
400	67.5	83.5	89.5	2.	10.	93.5	97.
420	60.5	96.	91.5	35.	62.	94.	97.5
440	63.	88.	93.	71.	90.5	95.	97.5
460	65.	90.	93.5	82.	93.	95.5	98.
480	67.	91.	94.5	84.5	95.5	96.	98.
500	69.	91.5	95.	86.5	96.5	96.5	98.
550	73.5	92.5	96.5	87.5	97.5	97.	98.
600	77.	94.	97.5	89.	97.5	97.5	98.
650	79.	94.5	97.5	89.5	98.	97.5	93.
700	81.	95.	97.5	90.	98.	97.	98.
750	82.5	95.	98.	90.5		97.	98.
800	84.		98.	90.5		96.5	
850	85.		97.5	91.		97.	
900	86.		97.	91.		96.5	
950	86.		95.	89.		80.	
980	85.5		90.5	83.		57.	
1000	85.5		88.	85.5		53.5	
1100	87.		90.5	88.		77.	
1200	86.		70.5	68.5		22.5	
1300	83.5		65.	70.		23.	
1400	38.0		0.5	5.		< 0.1	
1445	20.		0.1	0.1			
1500	38.		0.5	0.5			
1600	66.5		10.5	16.5			
1700	66.5		19.	18.5			
1800	58.		7.	9.5			
1900	0.5		< 0.1	< 0.1			
1950	0.5						
2000	2.0						
2100	22.5						
2200	32.						
2300	23.						
2400	16.5						
2500	0.5						

Table G-2 shows the percentage of the light incident on the cornea which penetrates through the rhesus monkey's eye to the anterior surface of each component of the ocular media. These are values computed using Table G-1. The column headed "retina" shows the percentage transmission of the whole ocular media.

Table G-2

TRANSMISSION THROUGH THE OCULAR MEDIA OF THE RHESUS MONKEY (%)

Wavelength (nm)	Aqueous		Lens		Vitreous		Retina	
	Direct	Total	Direct	Total	Direct	Total	Direct	Total
280	< 0.1	< 0.1	0.0					
300	10.	16.	4.	6.5	0.0	< 0.1	0.0	0.0
320	33.	53.	23.	38.	1.0	3.5	0.8	3.0
340	44.	66.	35.	53.	0.4	1.5	0.3	1.5
360	50.	72.	42.	60.5	0.2	0.6	0.2	0.6
380	52.5	78.	46.	68.	0.2	0.7	0.2	0.7
400	66.	81.5	59.	73.	1.0	7.5	1.0	7.5
420	59.	94.	54.	86.	19.	53.5	18.	52.
440	61.5	86.	57.	80.	40.5	72.5	38.5	70.5
460	63.5	88.	59.5	82.5	49.	76.5	47.	75.
480	65.5	89.	62.	84.	52.5	80.	50.5	78.5
500	67.5	89.5	64.	85.	55.5	82.	53.5	80.5
550	71.5	90.5	69.	87.5	60.5	85.5	58.5	84.
600	75.	92.	73.	89.5	65.	87.	63.5	85.5
650	77.	92.5	75.	90.	67.	88.	65.5	86.
700	79.	93.	77.	90.5	69.5	88.5	67.5	86.5
750	80.5	93.	79.	91.	71.5		69.5	
800	82.		80.5		73.		70.5	
850	83.		81.		73.5		71.5	
900	84.		81.5		74.		71.5	
950	84.		80.		73.		58.5	
980	83.5		75.5		62.5		35.5	
1000	83.5		73.5		63.		40.	
1100	85.		77.		68.		52.5	
1200	84.		59.		40.5		9.	
1300	81.5		53.		37.		8.5	
1400	37.		18.5		3.5		0.0	
1445	19.5		< 0.1		0.0			
1500	37.		0.2		0.0			
1600	65.		8.		1.5			
1700	65.		12.5		2.0			
1800	56.5		4.		0.4			
1900	0.5		< 0.0		< 0.0			
1950	0.5							
2000	2.							
2100	22.							
2200	31.							
2300	22.5							
2400	16.							
2500	0.5							

The data shown graphically in Figs G-6 and G-7 are tabulated below in Table G-3.

Table G-3

TRANSMITTANCE OF THE FUNDUS OF RHESUS MONKEY (%)				
Wavelength (nm)	Nervous Retina		P.E. & Choroid	
	Direct	Total	Direct	Total
300	< 0.1	45.		
325	< 0.1	59.		
350	0.1	63.		
375	0.1	63.		
400	0.1	62.		
425	0.1	65.5		< 0.1
450	0.2	72.		0.1
475	0.2	77		0.5
500	0.2	80.5		1.0
550	0.3	83.		1.0
600	0.4	84.5		1.5
650	0.5	85.		2.0
700	0.6	85.		2.5
750	0.7	85.		4.0
800	0.8	84.5		5.5
850	1.0	85.		8.0
900	1.1	84.		11.
950	1.3	84.5		14.
1000	1.6	85.		17.
1100	2.3	81.		21.5
1200	3.3	83.		26.
1300	4.8	71.		30.
1400	3.7	40.		31.
1445	2.0	27.	0.00	27.5
1500	3.7	35.5	0.03	29.
1600	8.0	66.	0.14	33.5
1700	10.9	69.5	0.23	35.5
1800	10.5	62.	0.22	36.
1900	< 0.1	23.	0.02	34.
1950	< 0.1	< 0.1	0.00	18.
2000	2.0	5.	< 0.01	23.
2100	7.4	32.5	0.09	30.5
2200	10.9	46.	0.20	34.5
2300	8.0		0.11	22.5
2400	3.5		0.03	11.5
2500	< 0.1		< 0.01	7.
2600	0.0			

Figure G-5, due to Geeraets and Berry (9) shows their measurements on the transmission of the whole ocular media of the rhesus monkey with a comparison with the rabbit and man.

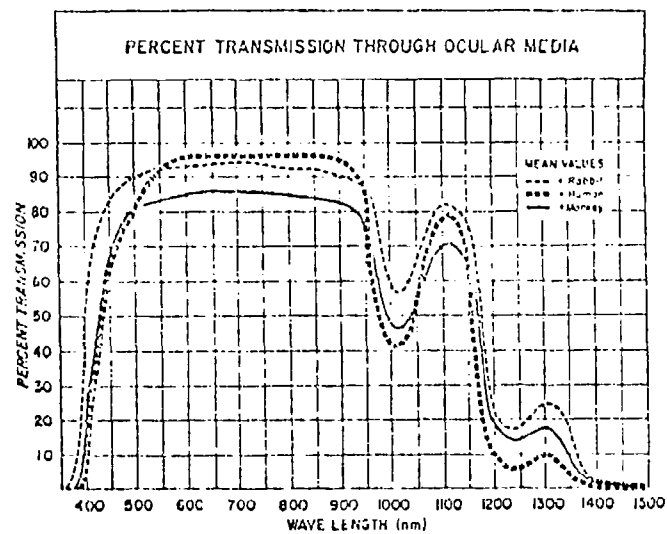


Figure G-5 TRANSMISSION THROUGH THE OCULAR MEDIA FOR RHESUS MONKEY, MAN, AND RABBIT



## 1.6 FUNDUS

Figure G-6, due to Boettner (6), shows the transmission of the nervous retina of the rhesus monkey, without the pigment epithelium.

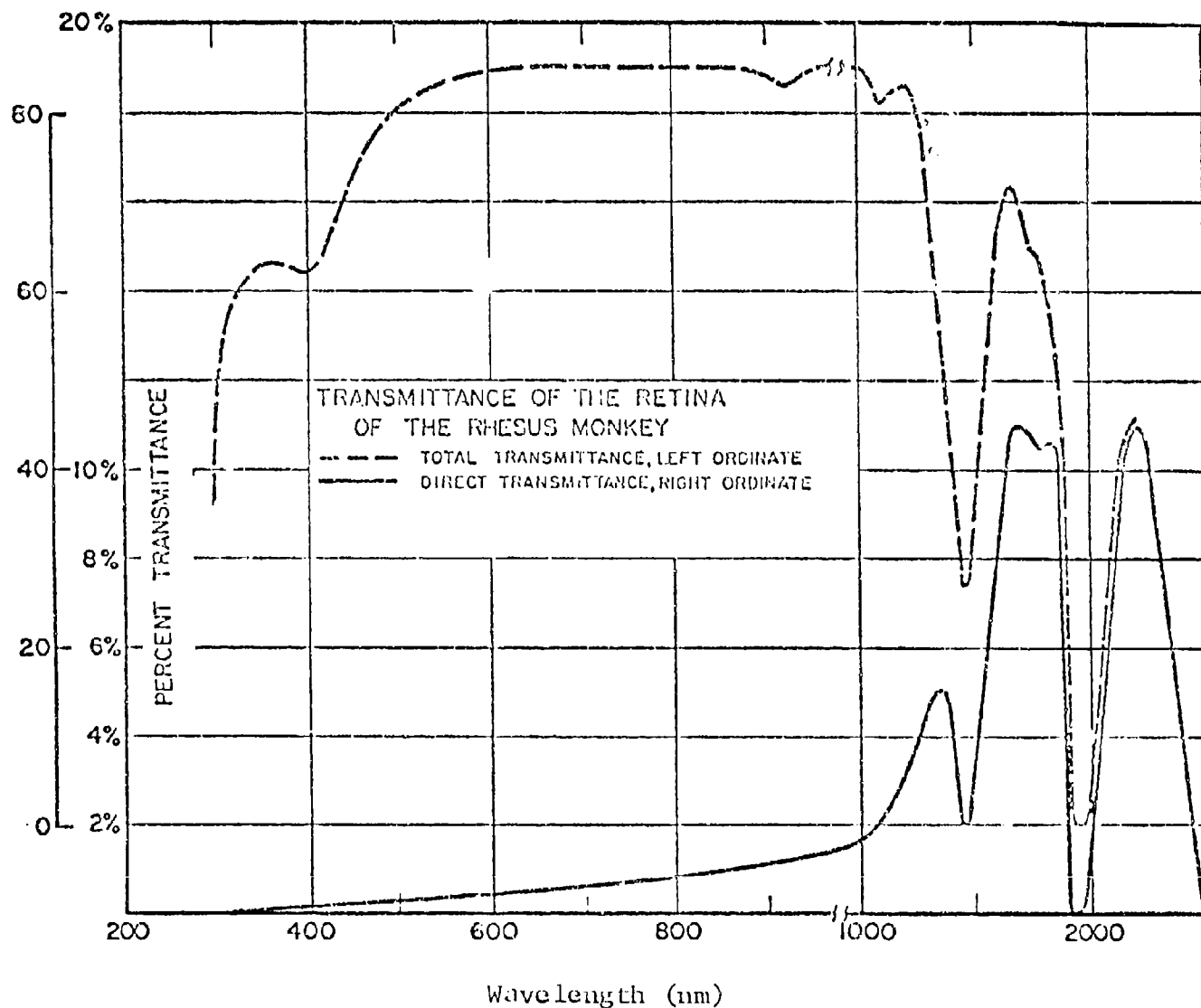


Figure G-6 TRANSMITTANCE OF THE NERVOUS RETINA  
OF THE RHESUS MONKEY

Boettner's measurements of the transmittance of the rhesus monkey pigment epithelium plus choroid are shown in Figure G-7.

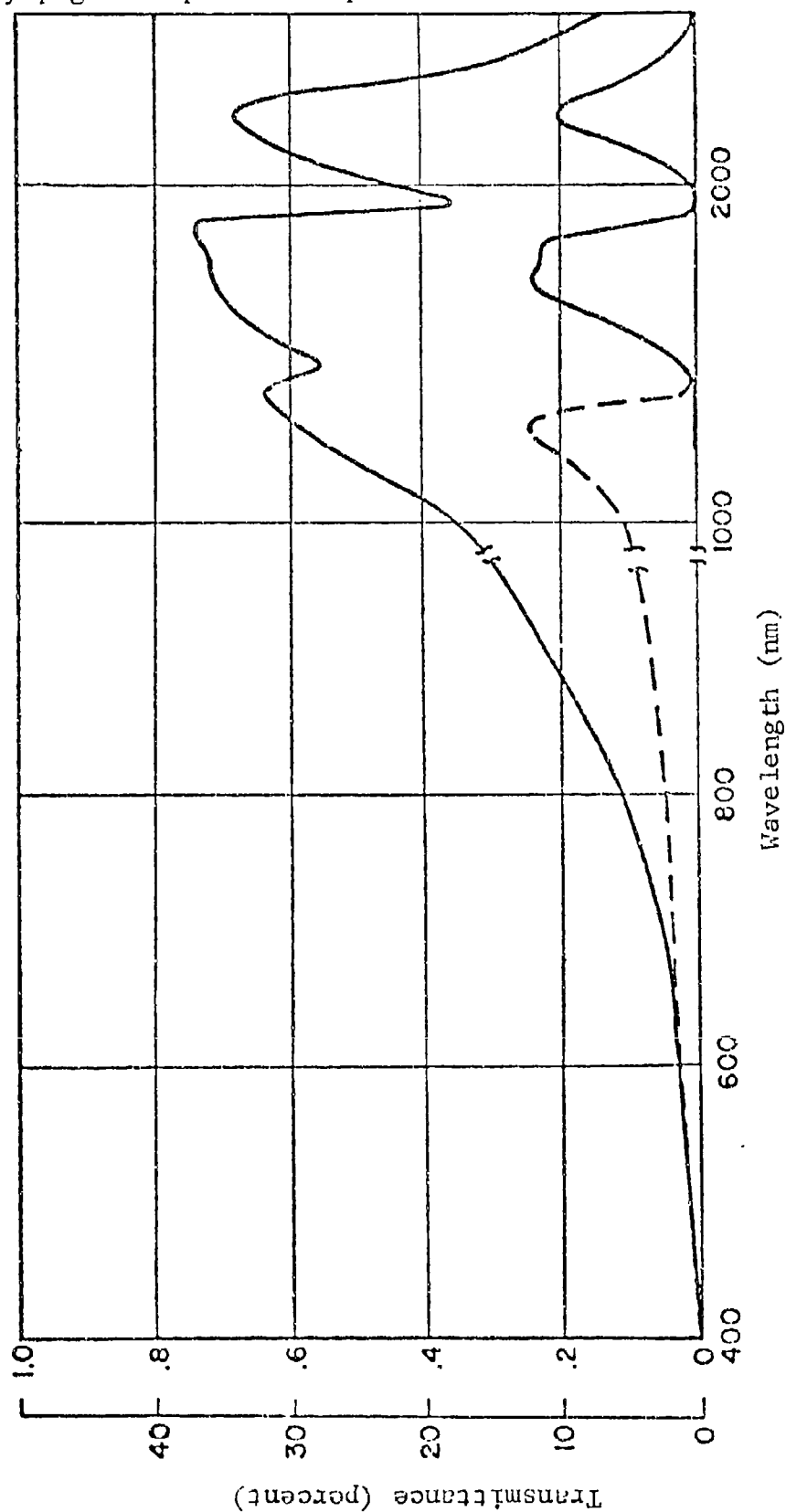


Figure G-7 TRANSMITTANCE OF THE P.E. PLUS CHOROID OF THE RHESUS MONKEY

In Figure G-8 below, Boettner (6) shows the spectral reflectance of the rhesus monkey fundus. The curve labeled fundus was taken on specimens consisting of the whole fundus plus sclera. The curve labeled sclera was taken on sclera alone.

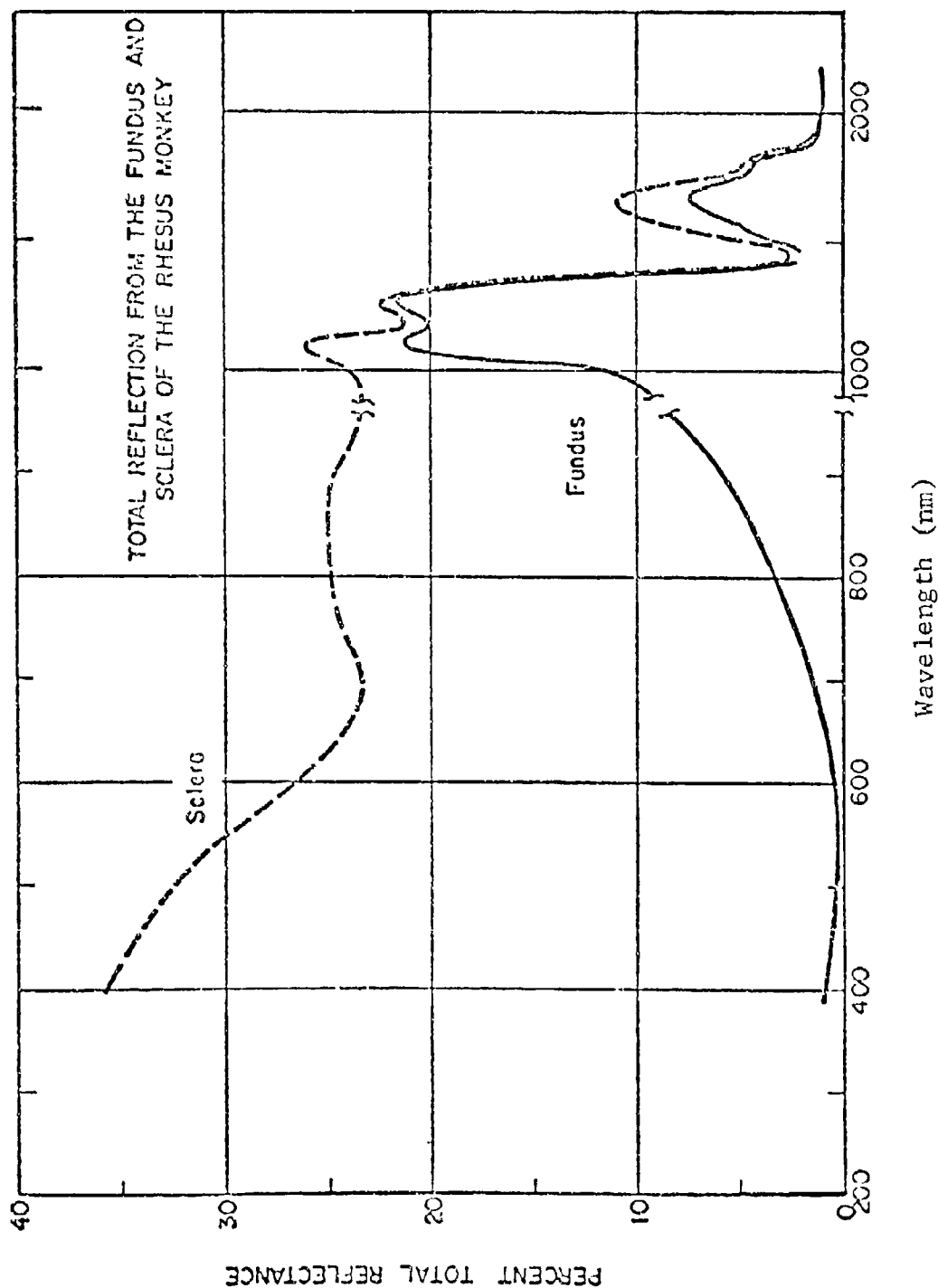


Figure G-8 TOTAL REFLECTANCE OF THE FUNDUS AND SCLERA OF THE RHESUS MONKEY

The reflectance of the sclera of the rhesus monkey is shown in Figure G-8 and Table G-4. These measurements are due to Boettner (6). No other scleral measurements on the rhesus monkey have been found in the open literature.

Table G-4

REFLECTANCE OF SCLERA AND FUNDUS PLUS SCLERA FOR RHESUS MONKEY (%)

Wavelength (nm)	Fundus	Sclera
400	0.8	36.
450	0.5	34.
500	0.3	32.5
550	0.3	30.
600	0.4	26.5
650	0.8	24.
700	1.5	23.
750	2.3	24.
800	3.1	25.
850	4.3	25.
900	5.8	24.5
950	8.	23.5
1000	10.5	24.
1100	22.5	26.
1200	20.5	21.5
1300	20.5	21.5
1400	5.	7.5
1445	2.	2.5
1500	3.	4.
1600	6.	10.
1700	7.	10.
1800	4.5	5.
1900	1.5	1.5
2000	1.	1.
2100	1.	1.

Figure G-9 due to Ceeraets and Berry (9) shows the spectral reflection from the rhesus monkey fundus, with data on the rabbit and man shown for comparison.

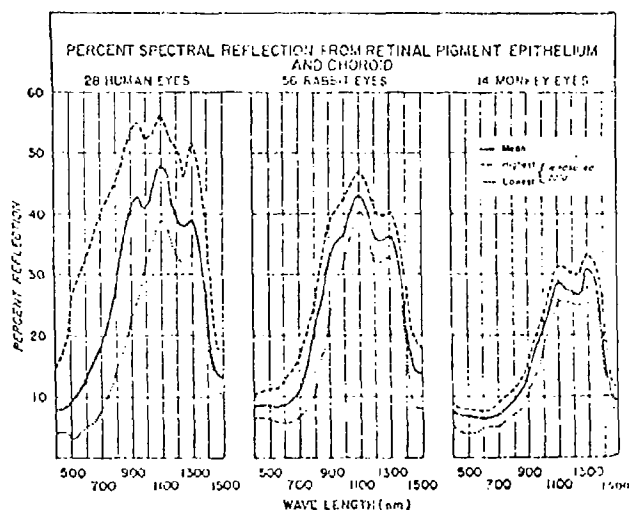


Figure G-9 PERCENT REFLECTION FROM P.E. PLUS CHOROID FOR MAN, RABBIT AND RHESUS MONKEY

Figure G-10, from the same source, shows the absorption in the complete fundus.

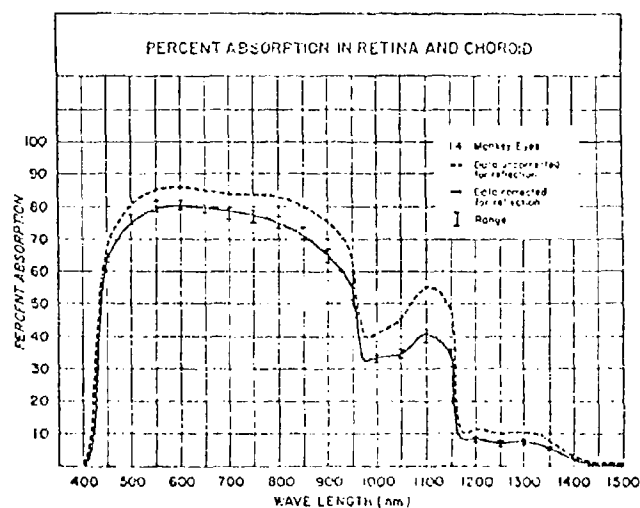


Figure G-10 ABSORPTION IN THE COMPLETE FUNDUS OF RHESUS MONKEY

The total transmission data of Tables G-3 and G-4 have been used to compute the absorption coefficients of the nervous retina and of the combined P.E. and choroid, as shown in Table G-5. It is truncated at 1500 nm since the transmission of the O.M. has fallen to zero by then. The computation is based upon a thickness of 190  $\mu\text{m}$  for the P.E. + ChCp + Ch and 300  $\mu\text{m}$  for the nervous retina, the latter being an arbitrary choice.

In Table G-3 the transmission of the choroid at 500  $\mu\text{m}$  is shown as 11%. This is assumed to be an error and a figure of 1% has been abstracted from Figure G-7. The reflection of the interface between the vitreous body and nervous retina was assumed to be zero.

Table G-5  
ABSORPTION COEFFICIENTS DERIVED FROM BOETTNER'S  
DATA FOR THE RHESUS MONKEY

Wavelength (nm)	Absorption Coefficients ( $\text{cm}^{-1}$ )	
	N.R.	P.E. & Ch.
0.4	15.9	Above 242
0.45	11.0	242
0.5	7.2	242
0.6	5.6	221
0.7	5.4	193
0.8	5.6	151
0.9	5.8	113
1.0	5.4	87
1.1	7.0	68
1.2	6.2	59
1.3	11.4	51
1.4	31.0	59
1.445	-	67
1.5	35.0	64

The Geeraets and Berry (1968) data (Figs. G-5, G-9 and G-10) have been used to derive absorption coefficient for the whole fundus of the rhesus monkey. This has been possible in two ways --- firstly, by using data on the transmittance of the ocular media, the reflectance of the fundus and the combined absorption plus scatter plus reflection of the fundus. Secondly, the calculation has been made using Geeraets computed value for absorption in the fundus, combined with the O.M. transmission and fundus reflection data. These should be equivalent methods, but the Geeraets absorption data is not consistent with the data from which it is ostensibly derived. An additional source of error arises because of the inaccuracies occurring when values are read from several curves then subtracted. Neither method has yielded usable values for 1400 nm or over the range 400-600 nm, and large uncertainties remain in the range 700-1000 nm.

Table G-6

ABSORPTION COEFFICIENTS OF THE RHESUS MONKEY FUNDUS, DERIVED FROM THE DATA OF GEERAETS AND BERRY		
<u>Wavelength</u>	<u>Absorption Coefficients (cm<sup>-1</sup>)</u>	
(nm)	Method 1	Method 2
0.7	-	195
0.8	229	184
0.9	130	127
1.0	89	107
1.1	64	88
1.2	41	49
1.3	45	48

The open literature contains no transmittance data for separate P.E. and Ch so the only available absorption coefficients for these tissues are those derived using Coogan's data (5). These are tabulated below, including data for the whole fundus.

Table G-7

ABSORPTION COEFFICIENTS OF THE RHESUS FUNDUS

Wavelength (nm)	Absorption Coefficients ( $\text{cm}^{-1}$ )		
	Pigment Epithelium (PE) 12 microns thick	Choroid (ch) 168 microns thick	PE+ChCp+Ch 190 microns thick
400	1852	187	210
476.2	1622	189	193
500	1545	169	189
514.5	1485	166	186
520.8	1460	164	186
530	1425	163	184
568.2	1294	165	176
600	1194	151	173
647.1	1108	145	167
700	1019	140	160
1000	434	110	108
1064	358	108	99
1100	313	107	94

The absorption coefficients were calculated using Coogan's transmission data for the nominal thicknesses listed. These values could be in error by as much as 15 to 20 percent.

Figure G-11 shows graphically a comparison between the absorption coefficient computed from the various sources, for the rhesus monkey (P.E. plus choroid). Included in Fig. G-11 are the results of Table G-7, as well as their range of values.



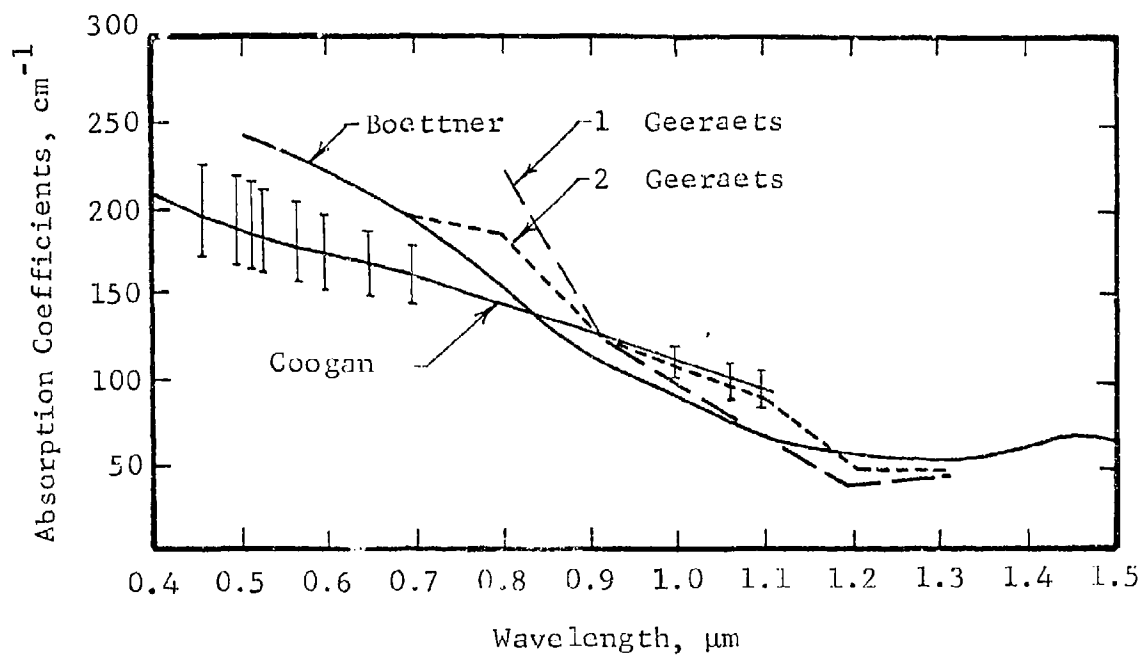


Figure G-11 COMPUTED SPECTRAL DEPENDENCE OF THE ABSORPTION COEFFICIENTS (see text)

## 2.0 OPTICAL PROPERTIES OF MAN

### 2.1 CORNEA

Since the cornea has a refractive index of 1.376 its reflection coefficient for light incident along the normal can be calculated as approximately 2.5% for visible wavelengths.

Measurements of the human corneal transmission, made by Boettner (6) are shown below. The total transmission includes forward scattered radiation, which is age dependent.

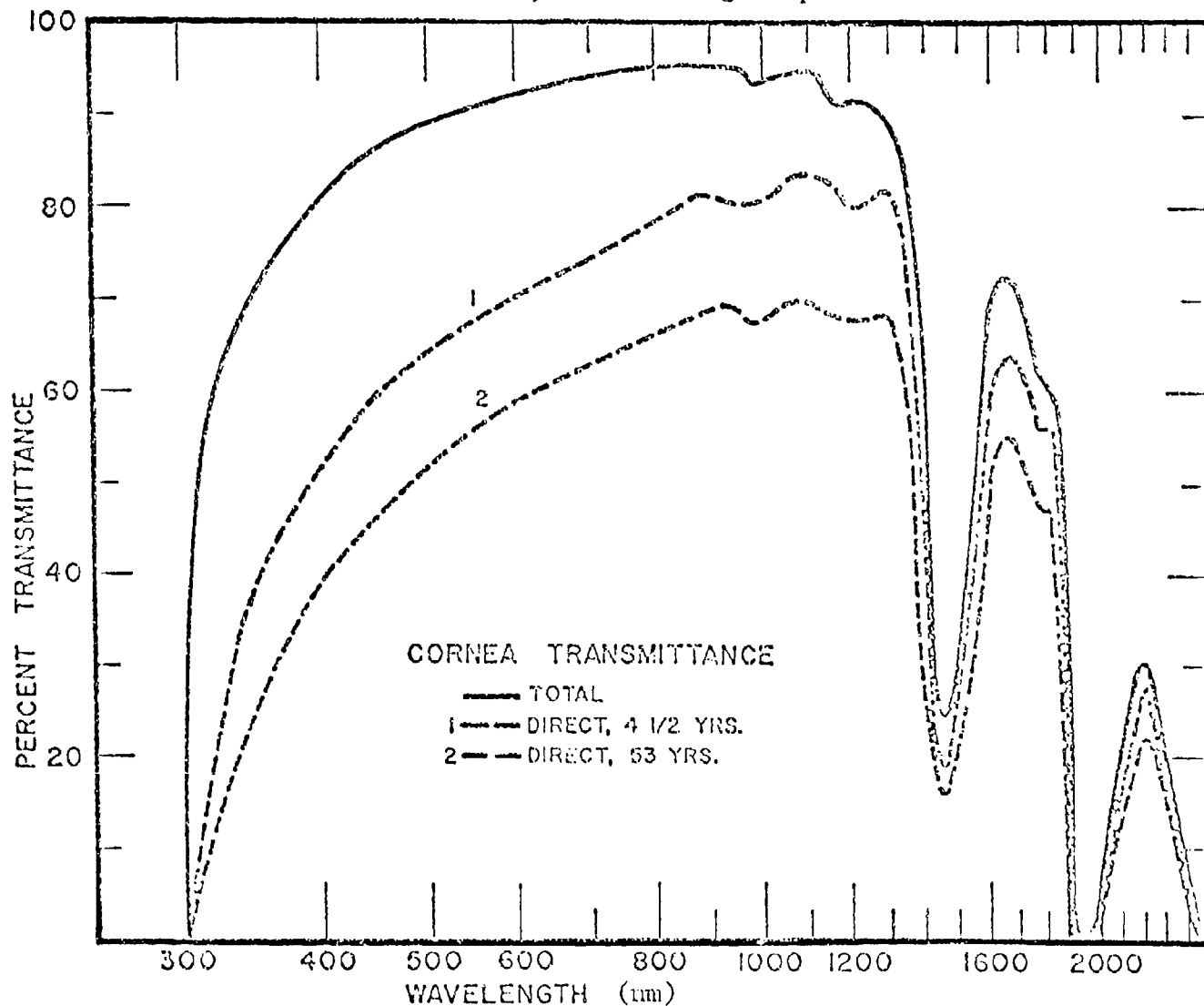


Figure G-12 TRANSMITTANCE OF THE HUMAN CORNEA

## 2.2 AQUEOUS HUMOR

The aqueous humor shows no age effect and no forward scattering. The spectral transmittance of the human aqueous humor as measured by Boettner (6) is shown in Figure G-13.

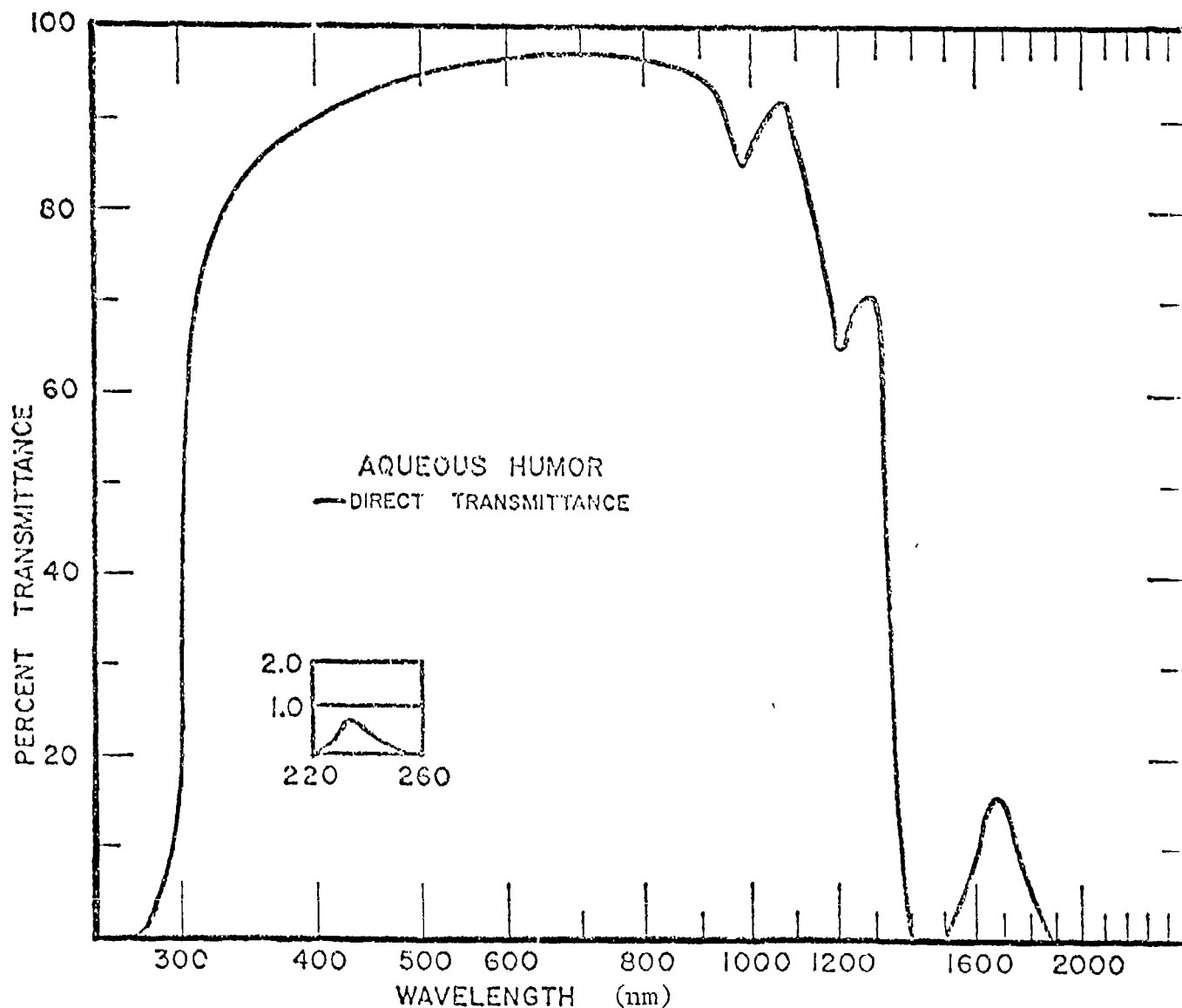


Figure G-13 TRANSMITTANCE OF THE AQUEOUS HUMOR OF MAN

### 2.3 LENS

The human lens increases in optical density with age, particularly at the shorter wavelength. This appears to be due to yellowing of the lens with age due to increasing pigmentation. The density plot below is due to Cooper and Robson (34). It is plotted to emphasize the density in the UV.

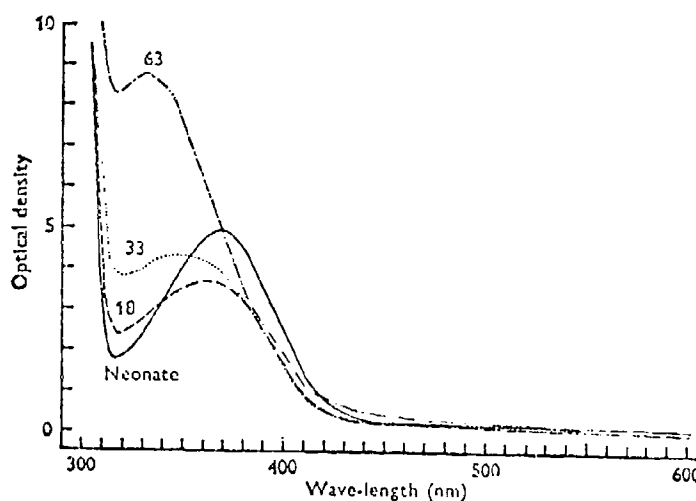


Figure G-14 DENSITY SPECTRA OF INTACT HUMAN LENSES OF VARIOUS AGES. THE AGE IN YEARS IS SHOWN AGAINST THE CURVES.

Said and Weale (35) shows an optical density plot shown in Figure G-15 scaled to show the effect of age upon transmission in the visible. The crosses on this plot show the mean of measurements on two lenses, 48 and 53 years old.

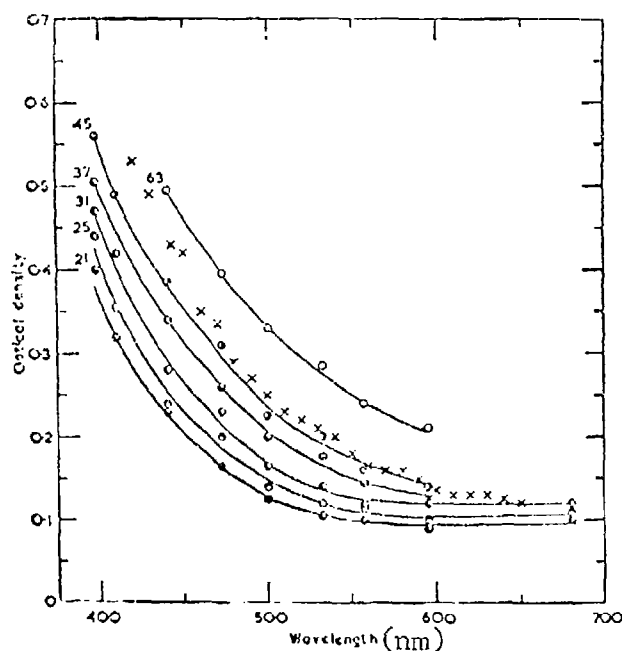


Figure G-15 SPECTRAL DENSITY CURVES OF SOME ENGLISH LENSES OF DIFFERENT AGES

## 2.4 VITREOUS BODY

Boettner's (6,10) data shown in Figure G-17 show the transmittances of the human vitreous body, both with and without the forward scattered light. Boettner reported the possibility that the vitreous humor may have been contaminated with pigment, lowering the values obtained for direct transmission.

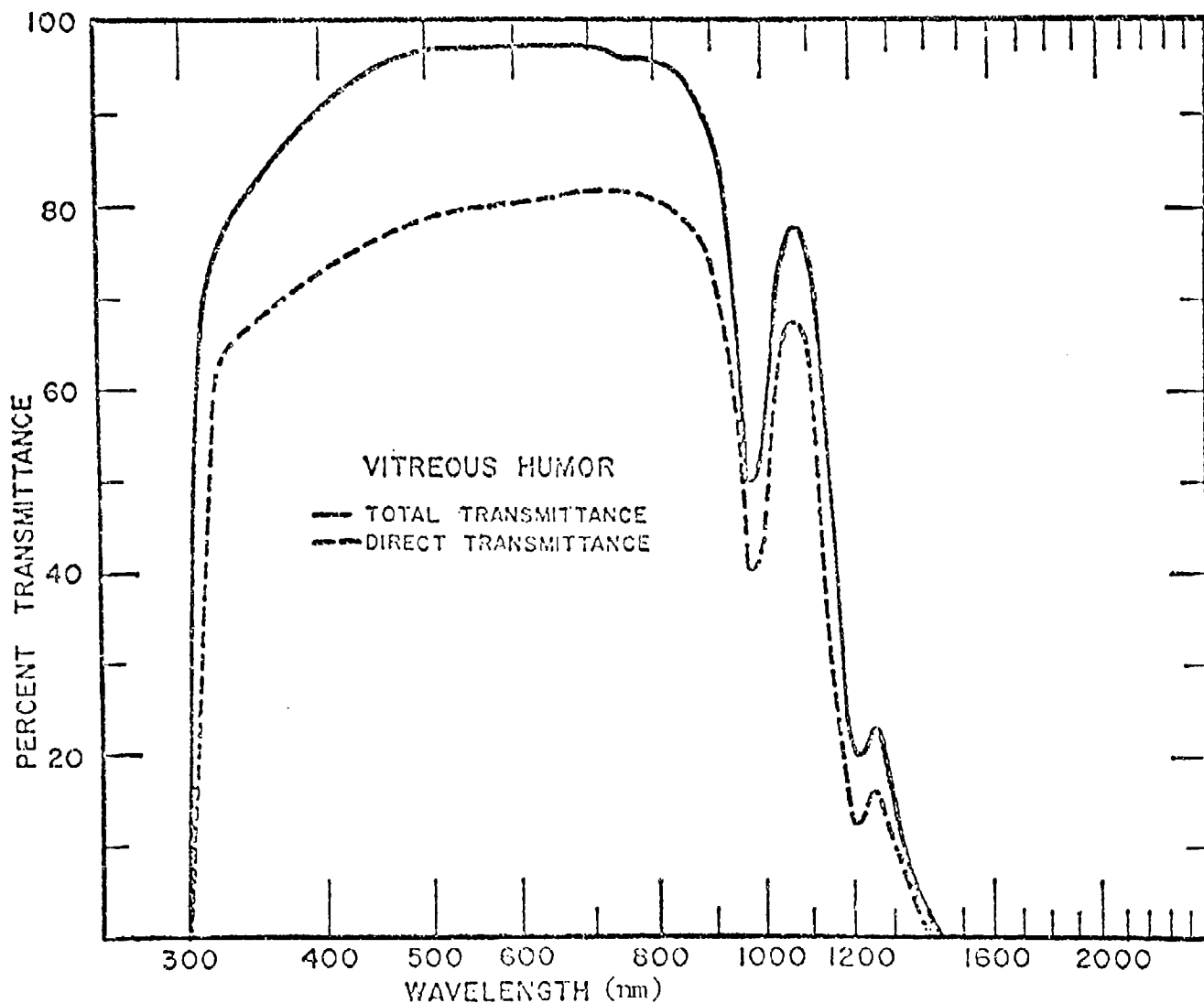


Figure G-17 TRANSMITTANCE OF THE VITREOUS HUMOR OF MAN

Using the data of Table G-8, Boettner has computed the percentage of the light incident on the human cornea which was transmitted through to the anterior surfaces of the aqueous, lens, vitreous and retina. The results are shown in Figure G-18 for direct transmittance, excluding forward scattering, for a young eye.

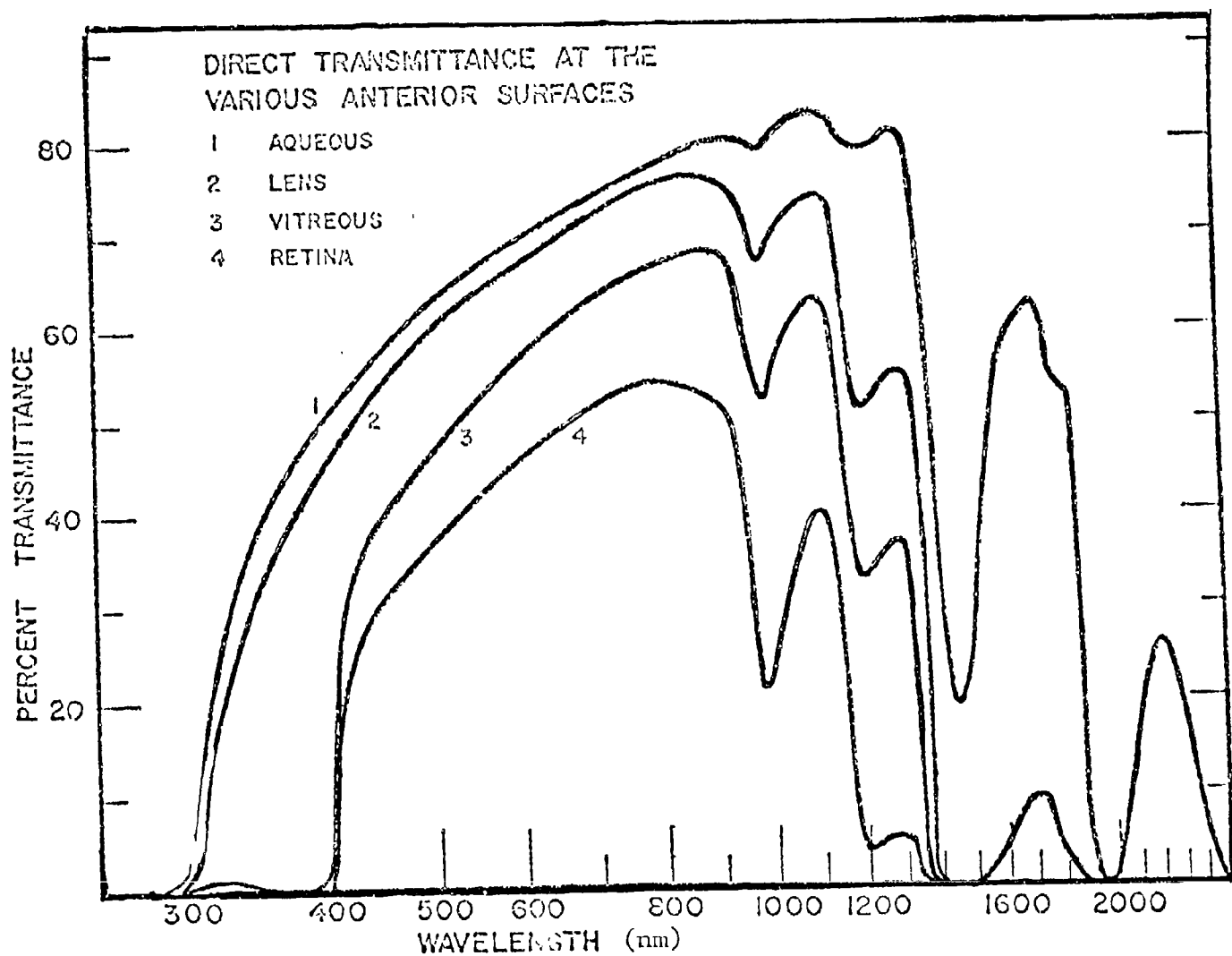


Figure G-18 CALCULATED DIRECT TRANSMITTANCE OF THE ENTIRE HUMAN EYE

Here the total transmittance for a young human eye is shown in Figure G-19 including the forward scattered radiation. The results were computed rather than measured. The data allow for the reflection losses at the air-cornea interface.

The data of Figures G-18 and G-19 are presented in tabular form in Table G-9.

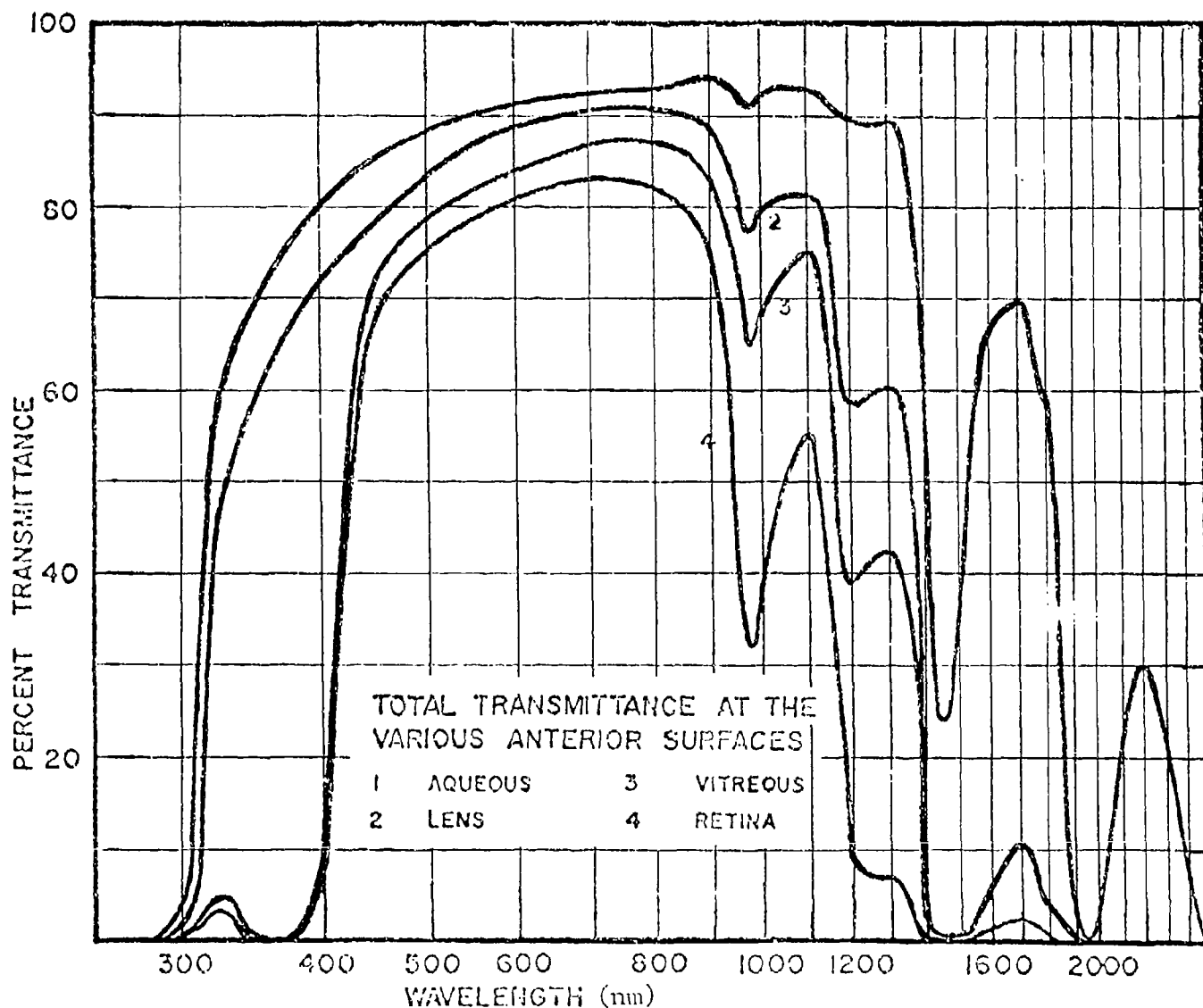


Figure G-19 CALCULATED TOTAL TRANSMITTANCE OF THE ENTIRE HUMAN EYE



Table G-9

PROGRESSIVE TRANSMISSION OF LIGHT THROUGH THE HUMAN OCULAR MEDIA (%)  
(percentage of light incident on the cornea which reaches the  
anterior surfaces of the components named)

Wavelength (nm)	Aqueous		Lens		Vitreous		Retina	
	Direct	Total	Direct	Total	Direct	Total	Direct	Total
280	< 0.1	< 0.1	< 0.1	< 0.1				
300	2.	8.5	0.3	1.5	0.0	0.0	0.0	0.0
320	26.5	59.	20.5	46.	1.5	4.	0.9	3.
340	34.5	66.5	28.5	55.	0.5	1.	0.3	1.0
360	42.	71.5	36.	61.5	0.1	0.4	< 0.1	0.4
380	47.	76.5	41.5	67.5	0.4	1.	0.3	0.9
400	51.	80.5	46.	72.5	5.5	10.	4.0	9.
420	54.	82.	49.	74.5	27.5	47.5	20.5	44.
440	57.	83.5	53.	77.	37.5	69.5	28.7	65.5
460	60.	85.	56.	79.5	41.5	74.	32.	70.0
480	62.	86.5	58.5	81.5	44.5	76.	35.	72.5
500	63.	88.	59.5	83.	46.5	78.	37.	75.
550	66.	90.	63.5	86.5	52.	82.	41.5	79.
600	69.5	91.	67.	88.	57.	83.5	46.	80.5
650	71.5	92.	69.5	89.5	60.5	85.5	49.	82.5
700	74.	93.	72.	90.5	63.5	87.	51.5	83.5
750	76.	93.	74.	90.5	65.5	87.	53.5	83.
800	77.5	93.	75.	90.	66.5	86.5	54.	82.
850	79.	93.5	76.	90.	68.	86.5	53.5	81.5
900	80.	93.5	75.5	88.5	68.	84.5	51.5	75.
950	79.5	93.	71.5	83.5	60.5	75.	36.	49.5
980	79.	91.5	66.5	77.5	52.5	64.5	21.5	32.
1000	80.	92.	69.5	80.	56.	69.	25.	38.5
1100	83.5	92.5	73.5	81.5	63.	75.	41.	55.
1200	78.5	89.5	51.4	58.5	33.	39.	4.	8.
1300	80.5	88.5	54.5	59.5	36.5	41.5	4.5	6.5
1400	39.	58.	0.2	0.3	< 0.1	< 0.1	0.0	0.0
1445	18.5	24.	0.0	0.0	0.0	0.0		
1500	27.	32.5	< 0.1	< 0.1	< 0.1	0.0		
1600	57.	66.5	5.	6.	0.5	0.9		
1700	62.5	69.5	9.5	10.5	1.0	1.5		
1800	54.5	60.5	3.	3.5	0.2	0.2		
1900	3.	5.	0.0	0.0	0.0	0.0		
1950	0.0	0.5	0.0	0.0				
2000	1.	3.	0.0	0.0				
2100	16.5	21.5	< 0.1	< 0.1				
2200	26.	30.5	< 0.1	< 0.1				
2300	17.5	20.5	< 0.1	< 0.1				
2400	5.5	8.	0.0	0.0				
2500	0.0	0.5						

Boettner (6) made some transmission measurements on complete human eyes from which the sclera and fundus had been removed. The results for the 7 year eye are in reasonable agreement with the computed values. Also shown are the percentage of 566 nm radiation scattered outside a cone of 1° total angle. The scatter profile for the 7 year human eye is shown on the next page.

Table G-10  
SUMMARY OF TOTAL PERCENT TRANSMITTANCE MEASUREMENTS

	Scatter*	466 (nm)	566 (nm)	666 (nm)	800 (nm)
August 14, 1963					
7-year male	29		79.0 (600 nm)	82.5	
April 27, 1964					
51-year female	40	56.5	79.0	81.0	
June 18, 1964					
53-year female	39	38.0	65.0	71.0	71.0
October 22, 1964					
45-year male	37	46.0	69.0	84.0	64.0
February 19, 1965					
52-year male	30	41.0	69.0	79.0	67.0
Calculated Transmission		68	78	82	81

\*Percent of 566 nm scattered outside of a 1 degree cone, except 7-year male, which was measured at 600 nm.

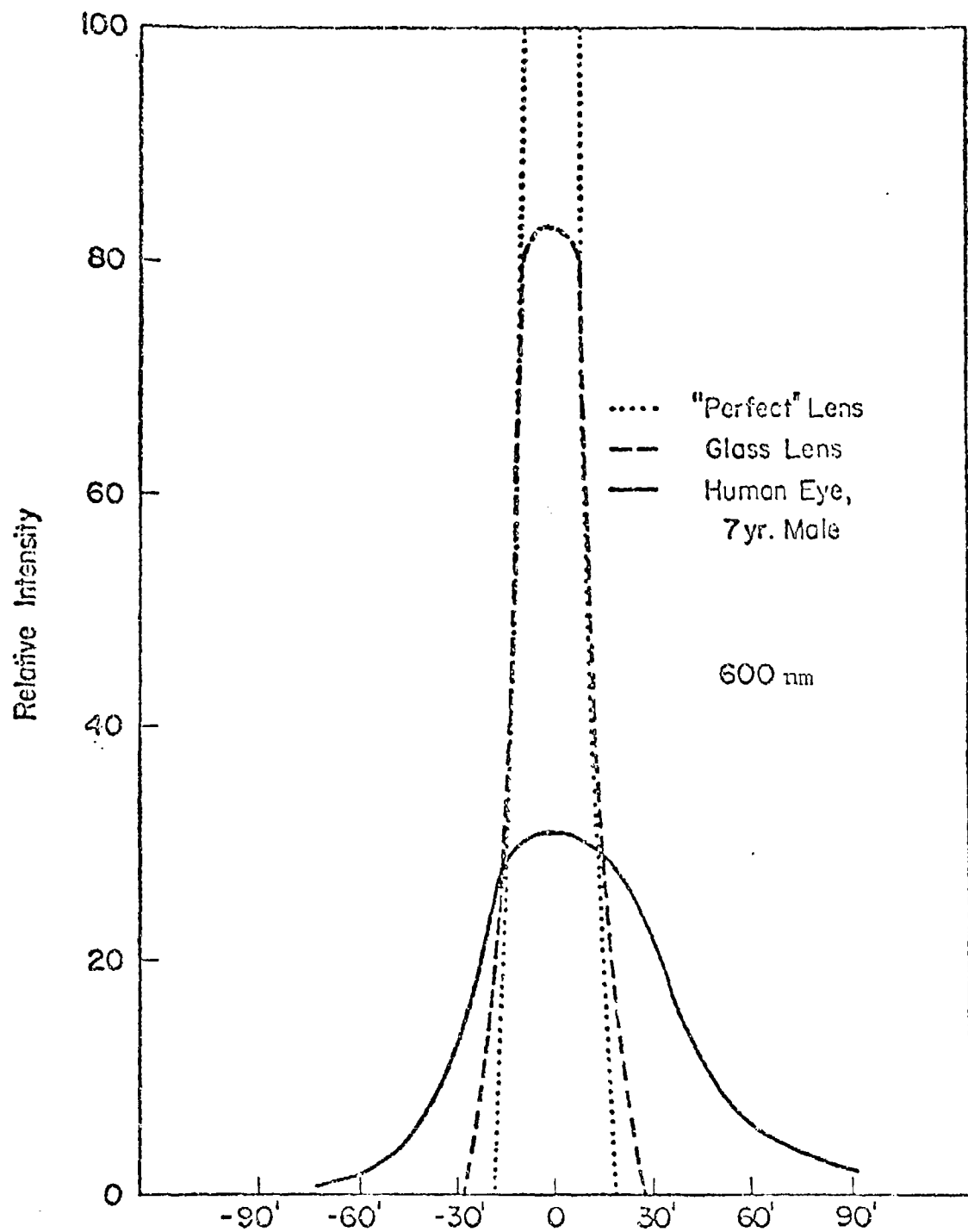


Figure G-20 SCATTER PROFILE OF A HUMAN EYE, GLASS LENS, AND "PERFECT" LENS

Earlier measurements on the transmission of the ocular media of the human eye were made by Ludvigh and McCarthy (36) measurements were made by Alpern et al (37) in vivo. A comparison of these two sets of measurements with those of Boettner is given below.

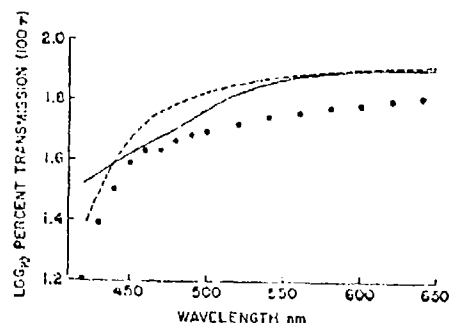


Figure C-21 The mean spectral transmittance curve for the three eyes (solid line) compared to in vitro measurements of Boettner and Wolter (10) (dotted line) and of Ludvigh and McCarthy (filled circles) (36)

Ruddock (38) has examined the effect of age upon the transmission of the human ocular media, the curve below showing the ratio of transmissions of 63 year old versus 21 year old eyes. The results are shown in Figure G-22.

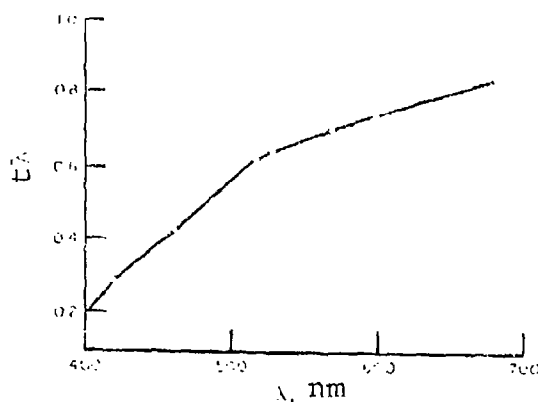


Figure G-22 The transmission of the ocular media as a function of wavelength. The values of  $t_\lambda$  represent the transmission of the media in a 63-year-old observer relative to a 21-year-old observer (for whom  $t_\lambda$  is unity at each wavelength)

The ocular media transmissions reported by Boettner (6) and Geeraets and Berry (9) are compared by Sliney and Freasier (39) as shown in the curves of Figure G-23. He claims that much of the discrepancy could be explained by differences in the size of the image upon the retina.

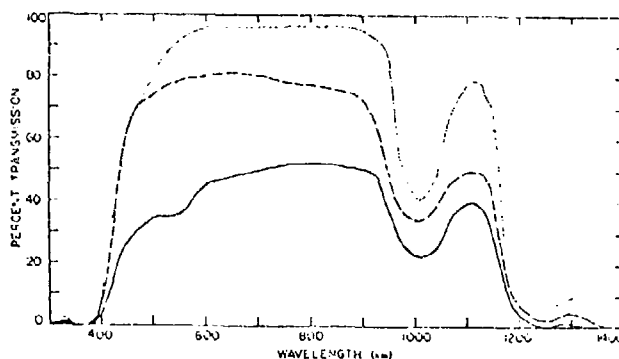


Figure G-23 Spectral transmission of the ocular media of the human eye. Upper curve was total transmission obtained by Geeraets and Berry using twenty-eight enucleated eyes. Lower two curves by Boettner and Wolter were obtained by combining separately measured transmission factors for the cornea, aqueous, lens, and vitreous for nine human eyes. Lowest curve is direct transmission obtained by eliminating forward scattered light, whereas middle curve was obtained by collecting total light transmitted.

Norren (40), in comparing all available sources of data for human eyes, arrived at the curve of Figure G-24 as a best estimate of the transmission of the ocular media between 400 and 700 nm. This appears to be a curve for direct transmission.

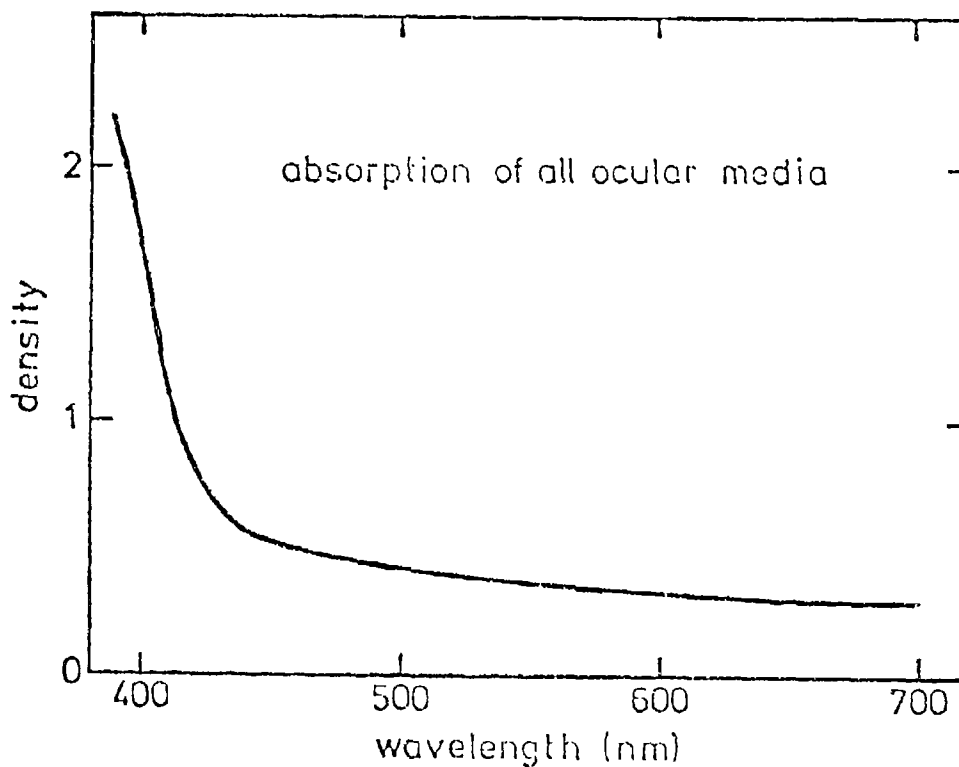


Figure G-24 PROPOSED COURSE OF THE SPECTRAL ABSORPTION OF ALL OCULAR MEDIA FOR AN AVERAGE 30 YEARS OLD OBSERVER

## 2.5 TRANSMISSION THROUGH THE OCULAR MEDIA

The data of Boettner (6,10) shown graphically in Figs. G-12, G-13, G-16 and G-17 are presented here in tabular form.

Table G-8

TRANSMISSION OF THE INDIVIDUAL OCULAR MEDIA							
Wavelength (nm)	Cornea		Aqueous	Lens		Vitreous	
	Direct	Total		Direct	Total	Direct	Total
	0.0	0.0	< 0.1				
280	< 0.1	< 0.1	0.1			0.0	0.0
300	2.0	8.5	17.5	0.0	0.0	1.0	1.5
320	27.	60.5	78.	6.5	9.	57.	74.
340	35.	68.	83.	2.	2.	64.	79.
360	43.	73.	86.	0.5	0.5	68.	83.
380	48.	78.5	88.5	1.0	1.5	71.	87.
400	52.	82.5	90.	12.	14.	73.	90.
420	55.	84.	91.	56.	63.5	74.5	92.5
440	58.5	85.5	92.	71.	90.	76.	94.
460	61.5	87.	93.5	74.	93.	77.	94.5
480	63.5	88.5	93.5	76.	93.5	78.5	95.5
500	64.5	90.	94.	78.5	94.	79.5	96.
550	67.5	92.	96.	82.	95.	80.	96.5
600	70.5	93.	96.5	85.	95.	80.5	96.5
650	73.	94.	97.5	87.	95.5	81.	97.
700	76.	95.	97.5	88.	96.	81.	96.
750	78.	95.	97.5	88.	96.	81.5	95.5
800	79.5	95.	97.	88.5	96.	81.5	95.
850	81.	95.5	96.5	89.5	96.	79.	94.5
900	82.	95.5	94.5	90.	95.5	75.5	88.
950	81.5	95.	90.	84.5	90.	59.5	66.
980	81.	93.5	84.5	79.	83.	41.	49.5
1000	82.	94.	87.	80.5	86.	44.5	56.
1100	85.5	94.5	88.	86.	92.	65.	73.5
1200	80.5	91.5	65.5	64.5	66.5	12.	20.5
1300	82.5	90.5	67.	67.	69.5	12.5	16.
1400	40.	59.5	0.5	1.5	4.	< 0.1	2.5
1445	19.	25.	0.0	0.0	0.0		
1500	27.5	33.	0.1	0.2	0.5		
1600	58.5	68.	9.0	9.5	14.5		
1700	64.	71.	15.	11.5	15.5		
1800	56.	62.	6.	5.5	6.5		
1900	3.	5.	0.	0.0	0.0		
1950	0.0	0.5	0.				
2000	1.	3.	< 0.1				
2100	17.	22.	< 0.1				
2200	26.5	31.	0.2				
2300	18.	21.	< 0.1				
2400	5.5	8.	0.0				
2500	0.0	0.5					



Boettner (6,10) measured the total transmission and the transmission with scattering excluded for human lenses of various ages. The results are shown in Figure G-16.

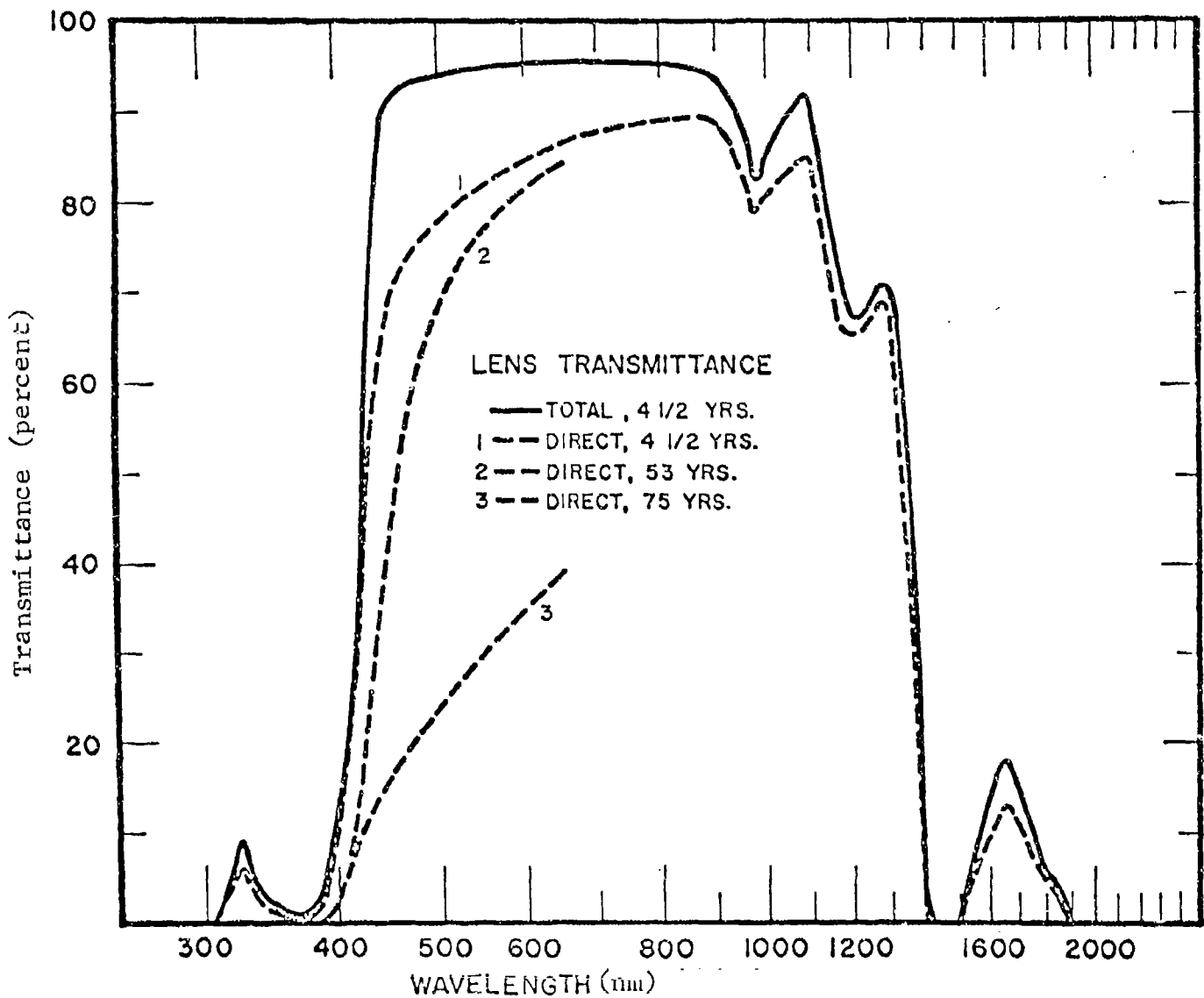


Figure G-16 TRANSMITTANCE OF THE HUMAN LENS

## 2.6 FUNDUS

Geeraets and Berry (9) made a series of measurements on the fundus tissues of man, rhesus monkey and rabbit. The spectral reflectances for each are shown in Figure G-25. Note that for man because the eyes had aged 24-28 hours post mortem the nervous retina had swollen and clouded and had to be excised. Even so the data for man show considerable scatter.

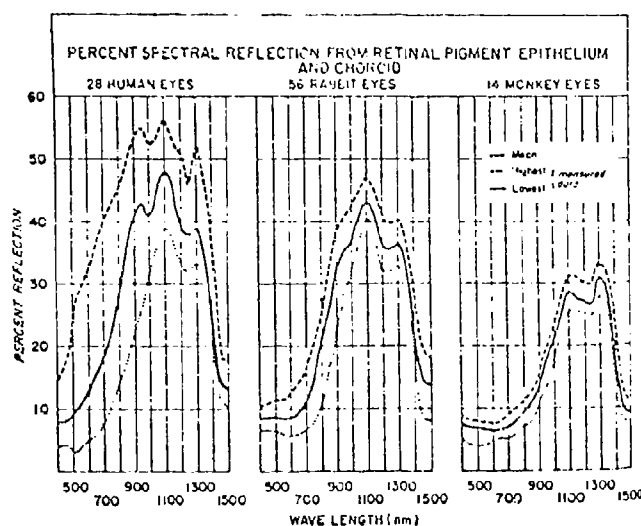


Figure G-25 REFLECTION COEFFICIENTS FOR THE HUMAN P.E. & CHOROID, WITH COMPARISONS WITH THE COMPLETE FUNDI OF THE RABBIT AND RHESUS MONKEY

Geeraets and Berry (9) measured the spectral absorption of the combined pigment epithelium and choroid in man. The absorptions are shown in Figure G-26 as percentages of the light incident upon the cornea. The solid curve is the more useful, since it has been corrected for the reflection from the fundus.

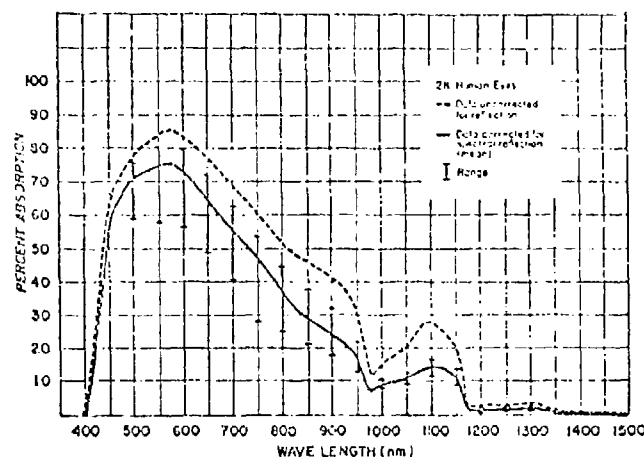


Figure G-26 ABSORPTION IN HUMAN P.E. & CHOROID, AS A PERCENTAGE OF THE LIGHT INCIDENT ON THE CORNEA

The earlier work of Geeraets et al (8) does not appear to be corrected for reflection from the fundus, but is included here because of the dearth of data for man. Figure G-27 shows, for the human eye, the range in value of the absorptions of the pigment epithelium and the choroid. Figure G-28 shows the absorption in the lightest pigment epithelium as a percentage of the light incident on the cornea.

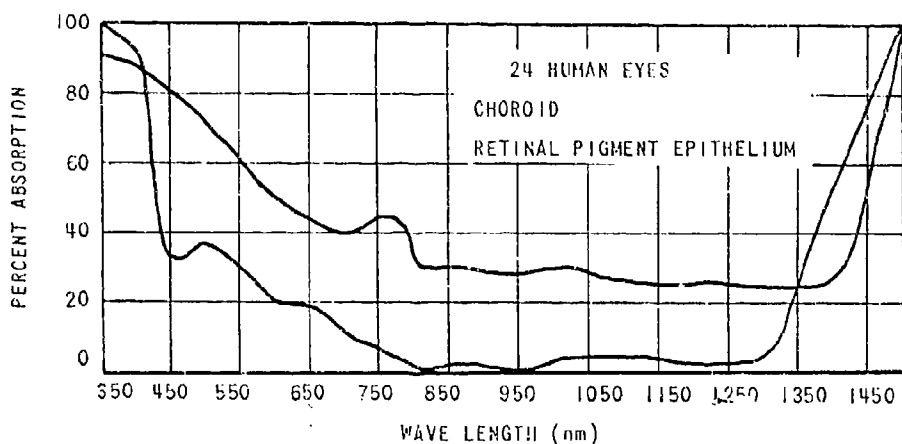


Figure G-27 Range of absorption in human retinal pigment epithelium (area between solid lines) and choroid

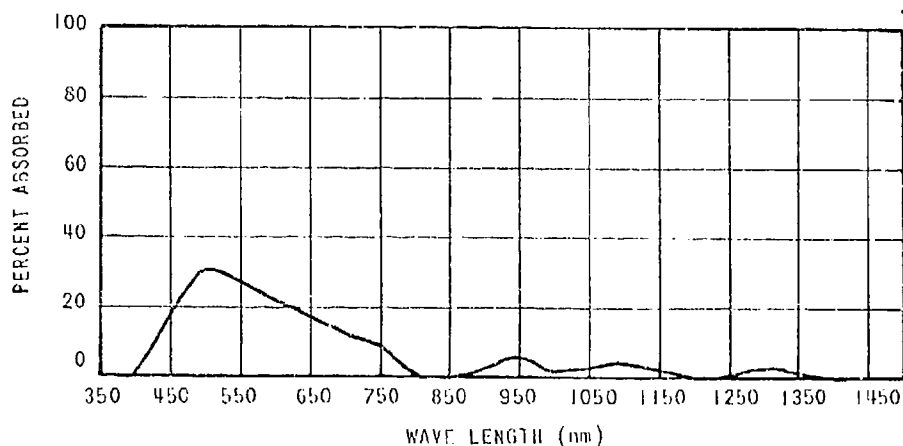


Figure G-28 Curves showing absorption in lightest human retinal pigment epithelium for light incident on the cornea

Figures G-29, G-30 and G-31 show the Geeraets measurements of the absorption of the darkest human pigment epithelium, the lightest human choroid and the darkest human choroid, in each case as percentages of the light incident on the cornea.

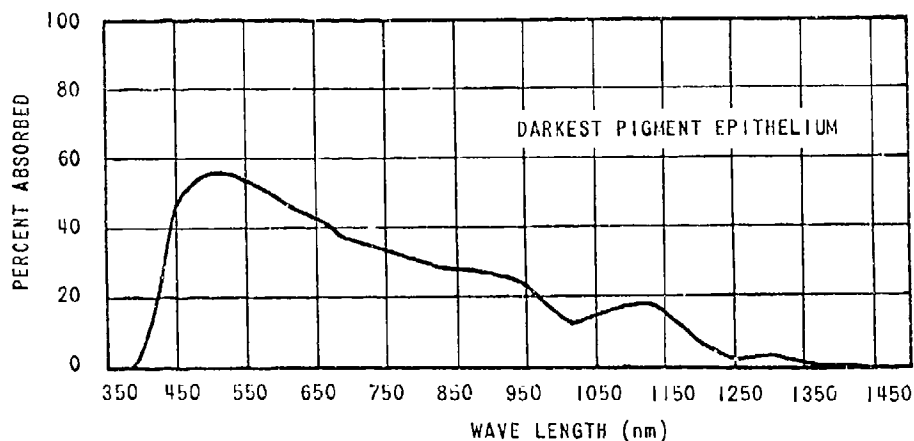


Figure G-29 Curve showing absorption in darkest human retinal pigment epithelium for light incident on the cornea

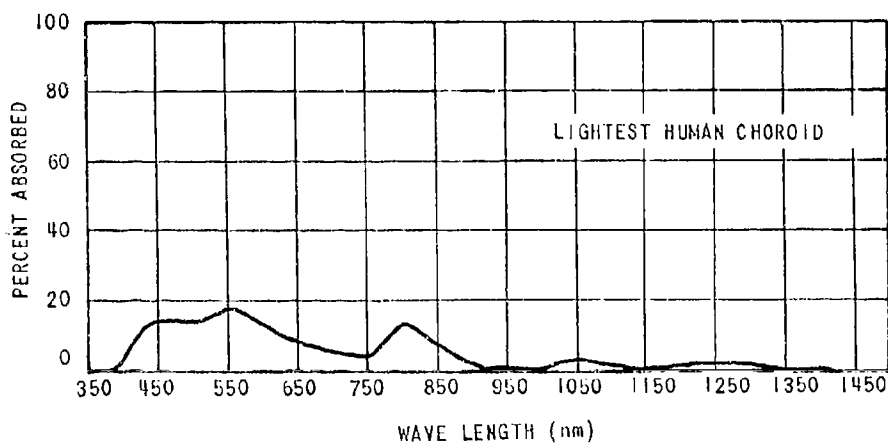


Figure G-30 Curve showing absorption in lightest human choroid for light incident on the cornea

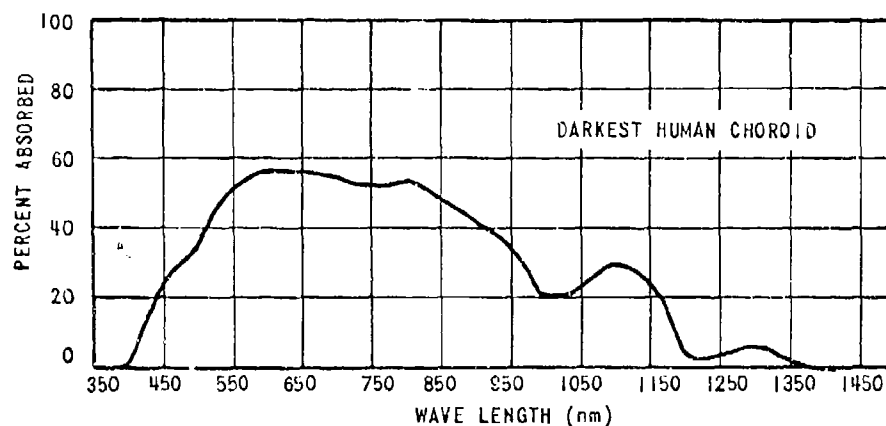


Figure G-31 Curve showing absorption in darkest human choroid for light incident on the cornea

Sliney and Freasier (39) used the Geeraets spectral absorption measurements for man and multiplied them by the ocular media transmittances due to Geeraets, and Boettner's lowest curve to show the range in values for the absorbed dose in the retina plus choroid as a percentage of the light incident on the cornea. These results are shown in Fig. G-32.

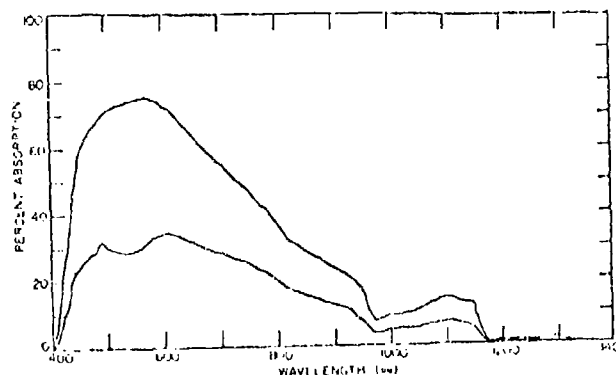


Figure G-32 Spectral absorbed dose in retina and choroid relative to spectral corneal exposure as a function of wavelength. Retina and choroid spectral absorption values corrected for fundus reflection obtained by Geeraets and Berry were multiplied by corresponding transmission spectral factors of the ocular media from Geeraets (upper) and Boettner (lower)

Coogan et al (41) claims that the rhesus monkey is a poor surrogate for man in terms of laser damage to the fundus, because the human pigment epithelium is much more heavily pigmented which renders it more prone to damage. However, human pigment is located towards the rear of the PE rather than at the front as with monkeys. Also threshold data available indicate the monkey retina is more sensitive to laser radiation than that of humans. The rhesus choroid is the more heavily pigmented, but this is not the primary site of laser-induced damage. However, the spectral absorption characteristics of the two fundi may differ slightly, since man has fuscine mixed with his melanin, the rhesus monkey does not.

The rabbit is a good surrogate, as demonstrated by Geeraets et al (7) who showed via the curves below that the fundal absorptions of man and the rabbit are similar if the pigmentation density can be matched.

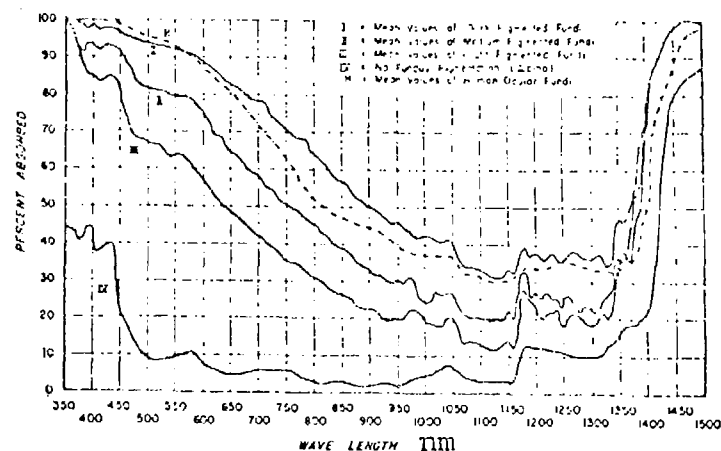


Figure G-33 Percentage of the energy incident on the fundus which is absorbed, for one human individual and for rabbits of 4 different pigmentation classes. The human fundus here lacked the nervous retina

## 2.7 Sclera

Smith and Stein (42) have made measurements on the human sclera over the range 0.5 to 2.5  $\mu\text{m}$ . Their interest was in laser damage via transscleral beams so their measurements were made on anterior portions of the sclera, viewed from outside. Figure G-34 shows the spectral reflection from the sclera alone, while Fig. G-35 shows the spectral transmission. The spectral absorption, derived for each wavelength by subtracting the reflectance plus transmission from 100%, is shown in Fig. G-36.

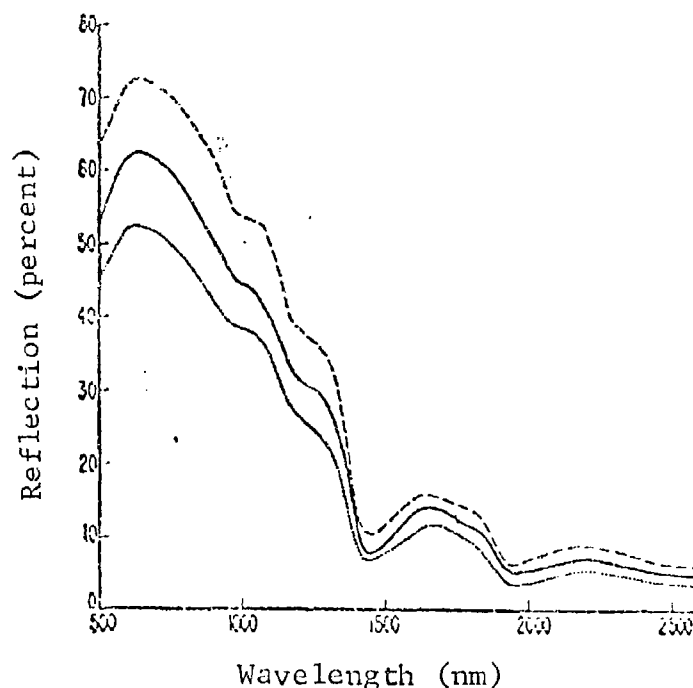


Figure G-34 SPECTRAL REFLECTION FROM THE HUMAN SCLERA



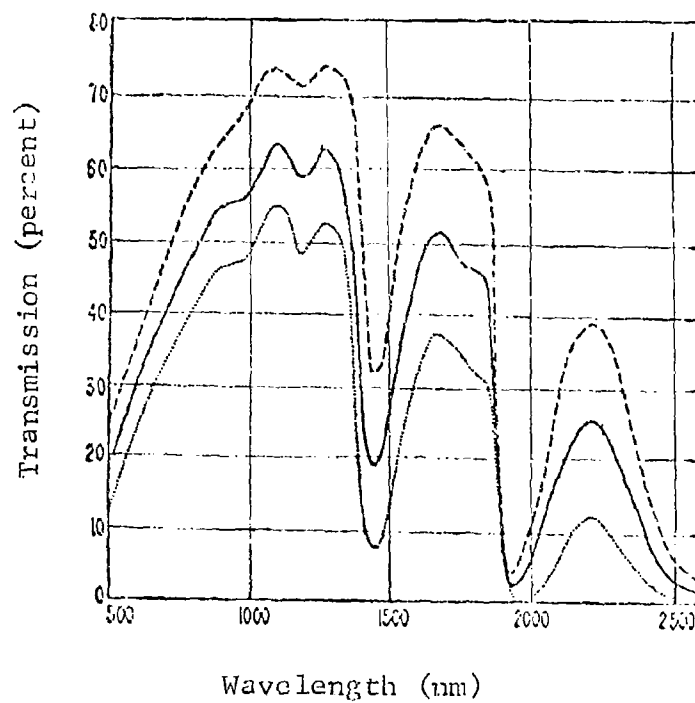


Figure G-35 TRANSMISSION THROUGH THE HUMAN SCLERA

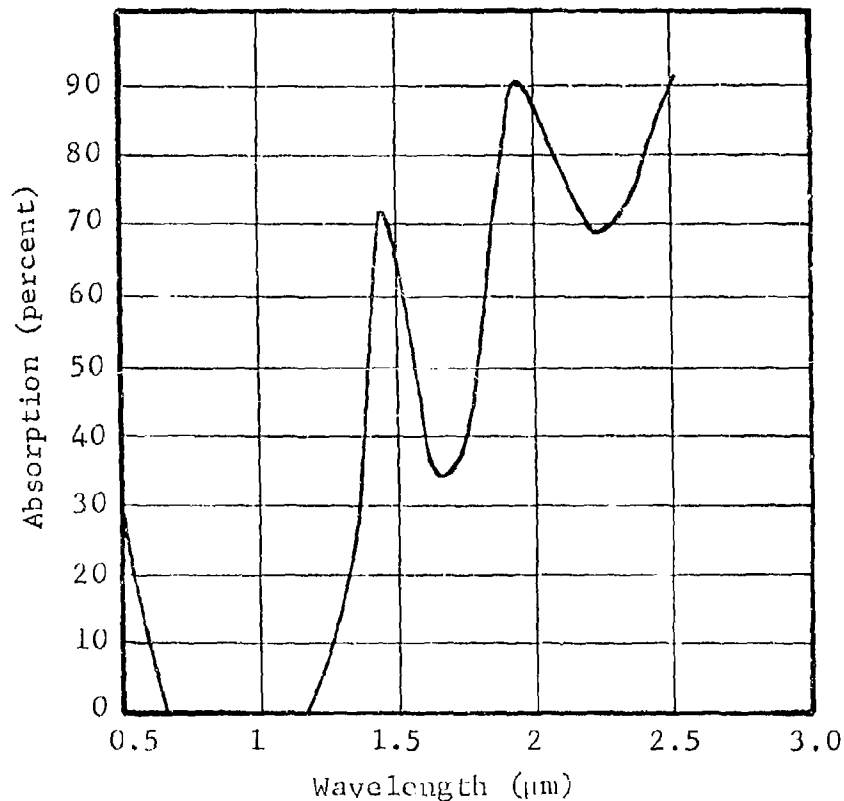


Figure G-36 SPECTRAL ABSORPTION IN THE HUMAN SCLERA

Alpern et al (37) measured the reflectance from the outside of the sclera of living human eyes, as shown in Fig. G-37. They covered only 0.4 to 0.65  $\mu\text{m}$ . These reflectances are all below 40%, thus considerably below Smith and Stein's measurements.

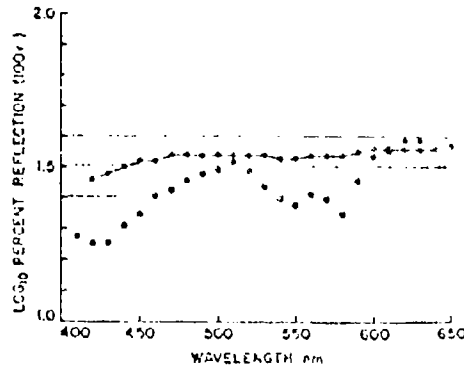


Figure G-37 Spectral reflectance of the sclera. Open circles are measurements made by reflecting light from the outside of a living human eye. Filled circles are the measurements made by reflecting light from the inside of an enucleated monkey eye which has been carefully denuded of pigment epithelium and underlying choroid.

APPENDIX H  
RETINAL IRRADIANCE PROFILE

## RETINAL IRRADIANCE PROFILE

1. INTRODUCTION

The determination of retinal irradiance for axial plane or spherical beams can be performed using the Fourier transform properties of imaging systems. Accordingly, the Fourier transform of the image distribution is given by the product of the Fourier transforms of the object distribution and of the point spread function (impulse response) of the eye.

$$I(f_x, f_y) = H(f_x, f_y) \cdot O(f_x, f_y) \quad (H-1)$$

An inverse transformation of  $I$  then provides the desired image distribution  $H(x, y)$ . In the case of laser sources the radiation is coherent. The physical quantities are the (complex) amplitudes, and the coherent transfer function. The retinal intensity distribution is obtained by squaring the absolute values of the calculated amplitude distribution obtained from the Fourier transform of  $I(f_x, f_y)$ . Appropriate scaling of the object amplitude is required and the transfer function must include the effects of aberration and pupil size as well as the effects of the retina not being conjugate to the object plane.

An equivalent and, in the case of this program, preferable procedure is to view the problem in terms of scalar diffraction theory, in particular the Fresnel approximation. An excellent discussion of this topic can be found in the book by Goodman (43) Taking the appropriate result from this we can express the amplitude in the retinal plane as

$$U(x_R, y_R) = \iint h(x_R, y_R; x, y) U(x, y) dx dy \quad (H-2)$$

where  $U(x, y)$  is the amplitude at the exit pupil and

$$h(x_R, y_R, x, y) = \frac{\exp i k z}{i \lambda z} \exp \left\{ i \frac{k}{2z} [(x_R - x)^2 + (y_R - y)^2] \right\} \quad (H-3)$$

We can therefore write

$$U(x_R, y_R) = \frac{\exp ikz}{i\lambda z} \exp \left[ i \frac{k}{2z} (x_R^2 + y_R^2) \right].$$

$$\iint \left\{ U(x, y) \exp \left[ \frac{ik}{2z} (x^2 + y^2) \right] \right\} \exp \left[ -\frac{ik}{z} (x_R x + y_R y) \right] dx dy \quad (H-4)$$

Aside from phase factors and constants, the retinal amplitude is the Fourier transform of the pupil amplitude multiplied by a quadratic phase term. The radiant intensity is then

$$H(x_R, y_R) = |U(x_R, y_R)|^2 \quad (H-5)$$

Thus the problem becomes one of specifying  $U(x, y)$ . We can separate this into two parts, one part determined by the experimental parameters, the others by the properties of the eye which are most conveniently described by the aberration function.

## 2. ABERRATION FUNCTION

The aberration function for the eye includes a number of contributions from different terms. In order to simplify the computation of this we shall use only the radially symmetric terms. The justification of this is two-fold. First, in experiments we assume that the subjects used are selected for minimal aberrations of the astigmatic kind and that coma is negligible because of nearly axial illumination. Secondly, the thermal calculations are based on radial symmetry. This reasoning leads us to characterization of the eye in terms of spherical aberration alone via an aberration function

$$C_1 \rho^2 + C_2 \rho^4 \quad (H-6)$$

where  $\rho$  = radius in pupil plane.

The spherical aberration term  $C_2 \rho^4$  is of the form  $\frac{2\pi C_2'}{\lambda} \rho^4$ . The coefficient  $C_2'$  for the human eye can be estimated in the following way. From Born and Wolf (Ref. 44) the longitudinal spherical aberration  $\Delta z$  is related to  $C_2'$  by

$$C_2' = \frac{\Delta z}{4a^2 f^2} \quad (H-7)$$

According to Lotmar (Ref. 45)  $\Delta z \approx -.1$  cm (.35 cm pupil radius) giving

$$\frac{2\pi}{\lambda} C_2' = -1.0 \cdot 10^4 \text{ cm}^{-4} \quad (H-8)$$

Lotmar's value corresponds to a longitudinal aberration of 3 diopters. Van Meeteren (Ref. 46) gives a value of 1 diopter which leads to

$$\frac{2\pi}{\lambda} C_2' \approx -3.0 \cdot 10^3 \text{ cm}^{-4} \quad (H-9)$$

We have used  $\lambda = 500.0$  nm for these calculations. Considering the range of variation found in human eyes we can choose the mean, where  $\lambda$  is in nanometers. El Hage and Berny (Ref. 47) have published aberration profiles which give values quite consistent with this choice. In the Retinal code  $C_2 = \text{CABER2}$  while  $2\pi C_2' = \text{CABER} - 3.0 \cdot 10^6 \text{ cm}^{-4} \text{ nm}$ .

### 3. DEFOCUSING FUNCTION

The experimental part of  $U(x,y)$  can be represented as

$$\sqrt{P(\rho)} \cdot F_1(\rho) \quad (H-10)$$

where  $P(\rho)$  is the intensity distribution at the cornea and  $F_1(\rho)$  is the phase distribution. On the assumption of an incident spherical wave the phase function is

$$\exp \left[ \frac{i2\pi n}{\lambda} W \right] \quad (H-11)$$

where  $n$  is the index of refraction, and  $W$  is proportional to the path difference between the actual wave front and the reference sphere centered at the retina--both evaluated at the pupil.

The phase function after taking the quadratic term in the diffraction integral into account depends only on the departure of the actual wavefront from a spherical wavefront converging toward the rating. Since our concern here is with spherical wavefronts that do not quite converge on the retina (i.e., defocus), we can write

$$w(\rho) = \frac{W}{a^2} \rho^2 \quad (H-12)$$

where  $W$  is the negative of the wavefront difference at the pupil radius  $a$ . The defocus parameter can be derived from Fig. H-1. The point  $I$  is the actual image,  $R$  is the retinal point and  $\rho$  is the pupil location from the second principal plane.

$$W = \overline{BI} - \overline{AI} \quad (H-13)$$

Solving the triangle (BRI) for  $BI$  gives

$$W = -f' - \Delta z \cdot (1 - \cos \alpha) + [f'^2 - (\Delta z)^2 \sin^2 \alpha]^{\frac{1}{2}} \quad (H-14)$$

$$\text{where } \tan \alpha = \frac{a}{f' + \Delta z}$$

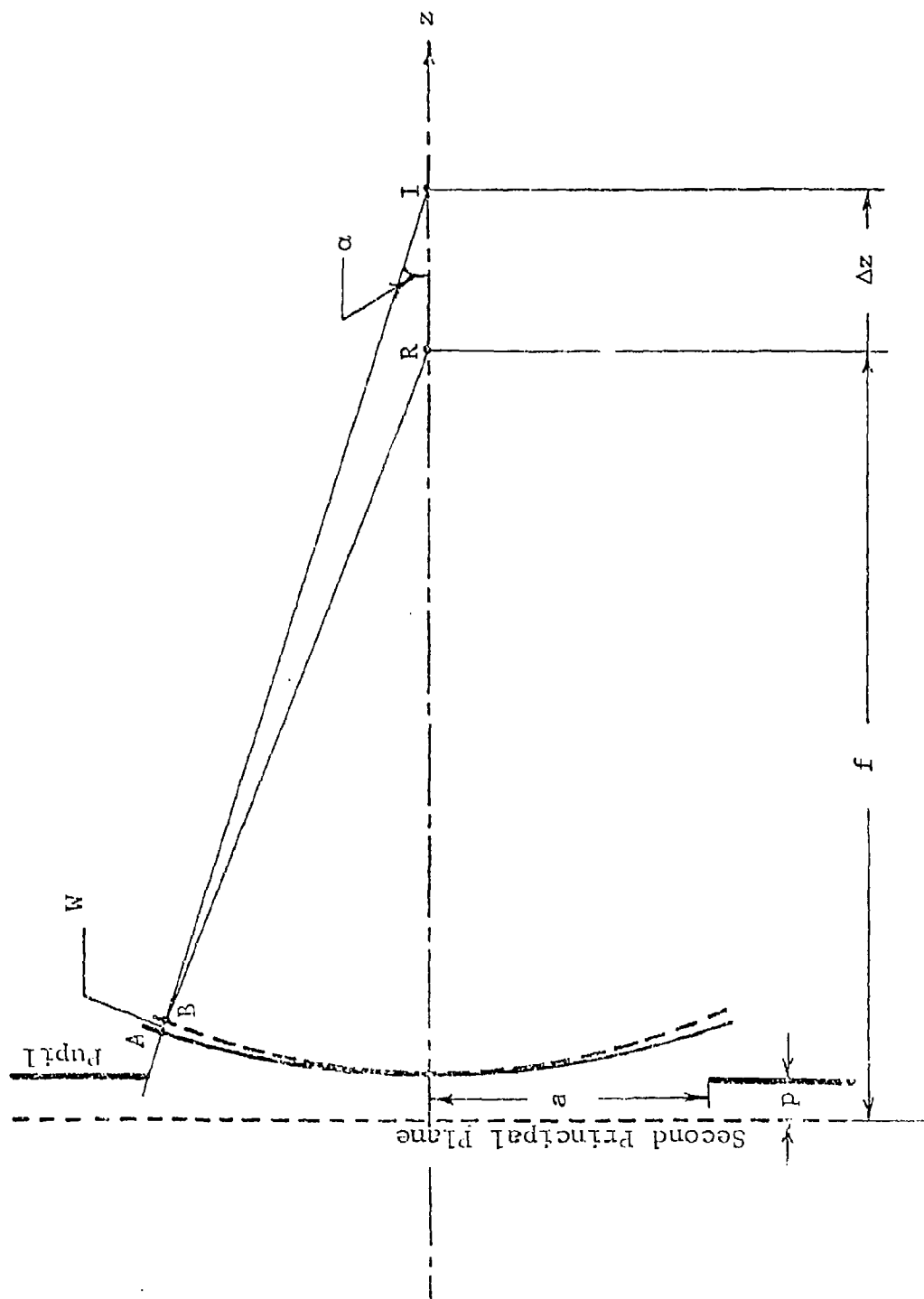


Fig. H-1 SCHEMATIC FOR EVALUATING  $W$



$$\Delta z = \frac{nz_0 f}{nz_0 - f} - f_0$$

(H-15)

a = pupil radius

f = back focal length (measured from second principal ~~plane~~ <sup>plane</sup>)

f' = f - p

n = index of refraction

p = distance between pupil and second principal ~~plane~~ <sup>plane</sup>

z<sub>0</sub> = distance of pupil from the waist of the laser beam

#### 4. CHROMATIC ABERRATION

Considering that fixed experimental geometries are used even through the wavelength changes we need to include the effect of the "chromatic aberrations" of the eye. In the application at hand this is the change in focal length with wavelength and if we include this in the defocus term we have accomplished our purpose.

The dependence of focal length is given by (Ref. 15)

$$f = f_0 \frac{n(n_0-1)}{n_0(n-1)} \quad (H-16)$$

where  $n = n(\lambda)$

$n_0 = n(\lambda_0)$  and  $\lambda_0$  is the wavelength at which the focal length of the eye is  $f_0$ .

The dependence of refractive index of water on wavelength can be obtained in tabular form from Irvine and Pollack (Ref. 48). Recent measurements (Ref. 49) have shown good agreement with the Irvine and Pollack compilation.

We have used the refractive index of water since the eye media consists mainly of water. As has been shown (Ref. 50) the calculated eye behaviour agrees with that determined experimentally at wavelengths above about 430 nm. The use of the water index at the short wavelengths results in an excessive focal length and is apparently due to the nonaqueous constituents particularly the lens. Using the Wald and Griffin data we can calculate the corresponding effective refractive index for use as the tabulated values below 500 nm.

The results are

$\lambda$	$n$
350	1.357
400	1.346
450	1.341

## 5. RETINAL IRRADIANCE

With the above functions the diffraction integral becomes

$$H(r, \theta) = \left| \frac{1}{\lambda F} \int_0^a \int_0^{2\pi} \sqrt{P(\rho)} \exp i \left[ C_0 \rho^2 + C_2 \rho^4 \right] \cdot \exp - \left[ \frac{2\pi i}{\lambda F} \cdot \rho \cdot r \cdot \cos(\phi - \theta) \right] \rho d\rho d\phi \right|^2 \quad (H-17)$$

where we have taken advantage of the symmetry and converted to cylindrical coordinates. Recognizing that

$$\frac{1}{2\pi} \int_0^{2\pi} \exp - \left[ \frac{2\pi i}{\lambda F} \cdot \rho \cdot r \cdot \cos(\phi - \theta) d\phi \right] = J_0 \left( \frac{2\pi \rho r}{\lambda F} \right) \quad (H-18)$$

the normalized profile becomes

$$\frac{H(r)}{H(0)} = \left| \frac{1}{\lambda F} \int_0^a \sqrt{P(\rho)} J_0 \left( \frac{2\pi r \rho}{\lambda F} \right) \exp i \left[ C_0 \rho^2 + C_2 \rho^4 \right] \rho d\rho \right|^2 \quad (H-19)$$

APPENDIX I  
GRID SYSTEM

## APPENDIX I

### GRID SYSTEM

#### 1. INTRODUCTION

In both models, polar coordinates  $r$  and  $z$  were chosen to assess the transport of heat within the eye. To conserve on computational times, the points at which temperatures are calculated are closely spaced in regions of greatest energy deposition. The mid-point of the grid shown in Fig. I-1 is located at  $i=M2+1$ ,  $j=1$  where  $i$  represents the index for points on the  $z$  axis while  $j$  represents the index for points on the  $r$  axis.

On the  $z$  axis, there are  $M1$  uniform increments on each side of the mid-point, while on the  $r$  axis there are a total of  $N1$  uniform increments starting at  $j=1$ . Beyond the uniform portion of the grid, it commences to expand so that each succeeding increment is a constant factor larger than the previous increment.

Choice of the grid network is based on the surface of the cornea being at  $z=0$  and the edge of the eye at  $r=RVL$ . Consideration is also given to the interfaces between eye media. For the Retinal model the thicknesses of the eye media are represented by TAV, TPE, TVL, TCH, TSC and TTS, where

TAV = thickness of all eye media from cornea  
to pigment epithelium, cm

TPE = thickness of the pigment epithelium, cm

TVL = thickness of the chorio-capillaris, cm

TCH = thickness of the choroid, cm

TSC = thickness of sclera, cm

TTS = thickness of tissues beneath eye, cm

Distances of the interfaces from the surface of the cornea, wherein  $z=0$ , are given by  $ZD(LI)$  starting with  $ZD(1)=0$ .

In the Corneal model the thicknesses of the various eye media are represented by  $TH(1)$ ,  $TH(2)$ , ...,  $TH(6)$ . Distances of the interfaces from the surface of the cornea are represented by  $ZD(LI)$  again starting with  $ZD(1)=0$  at the anterior surface of the cornea.

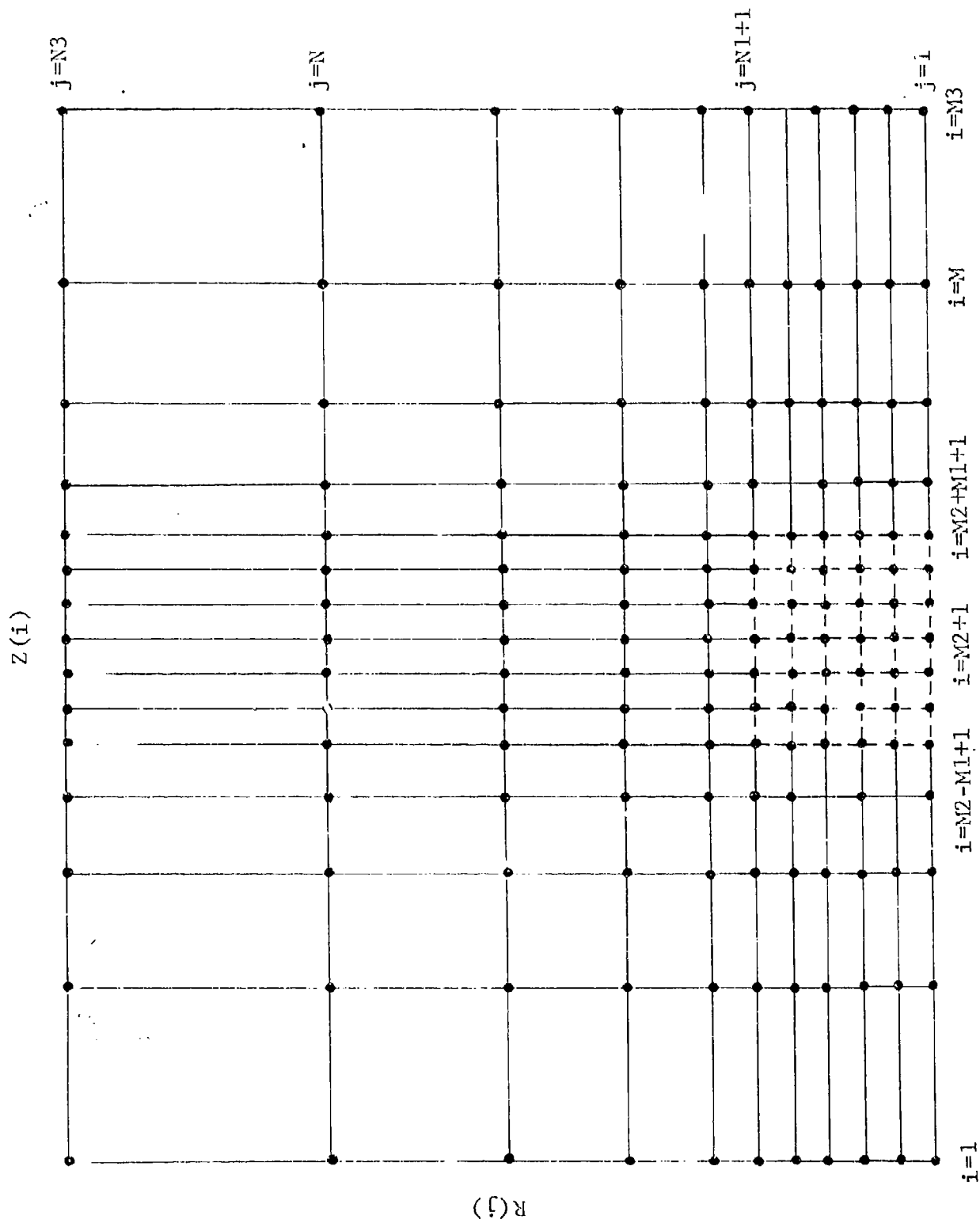


Figure I-1 GRID SYSTEM USED BY CORNEAL AND RETINAL MODELS

Next we shall discuss how the grid network was related to the various interfaces. In this regard, the only liberty one has once the number of grid points are selected, is the choice of two points with which to fix the grid.

## 2. RADIAL NETWORK

In both models, the first radial grid point was located on the axis of the eye (wherein  $j=1$ ) so that

$$R(1) = 0 \quad (I-1)$$

The edge of the eye at  $r=RVL$  is located halfway between  $R(N-1)$  and  $R(N)$ . Thus, there are two radial points, namely  $R(N)$  and  $R(N3)$  beyond eye. This situation prevails regardless of how many grid points are chosen.

## 3. AXIAL NETWORK

Choice of the axial grid work differs in the two models since the finer grid is always located in and about the region of greatest energy deposition.

### 3.1 Retinal Model

In the Retinal model, the anterior surface of the cornea is located halfway between  $Z(1)$  and  $Z(2)$ . On the other hand, the anterior surface of the pigment epithelium is located halfway between  $Z(M2-M1+1)$  and  $Z(M2-M1+2)$ . The first grid point in the pigment epithelium is at  $Z(M2-M1+2)$ .

### 3.2 Corneal Model

In the Corneal model, the grid work for  $z$  differs according to whether one wishes to assess corneal or lens damage. For the case of corneal damage, the finer grid is located at the front of the eye so that the corneal surface lies halfway between  $Z(M2-M1+1)$  and  $Z(M2-M1+2)$ . The last grid point  $Z(M3)$  is located so it coincides with  $ZD(7)$ .

For the case of lens damage, the fine grid is located in and about the lens. The surface of the tear layer is located halfway between  $Z(3)$  and  $Z(4)$ , while the anterior surface of the lens (at  $z=ZD(5)$ ) is located halfway between  $Z(M2-M1+1)$  and  $Z(M2-M1+2)$ .

#### 4. DETERMINATION OF EXPANSION FACTOR

Once one has chosen the number of nonuniform grid points with which to cover a given distance, the next problem is to assess the expansion factor by which the increments must be sequentially increased to arrive at the given distance. To illustrate the method, we will develop the expansion factor for the radial grid. The method is an extension of the technique used by Tech. Inc. (Refs. 1,52).

First, consider that one wishes to locate the edge of the eye ( $r=RVL$ ) halfway between  $R(N-1)$  and  $R(N)$ . Moreover, consider that there are  $N1$  uniform increments of size  $DR$  included within a total of  $N+1$  points. If we represent the expansion factor by  $R$ , then the distances  $P_1$  and  $P_2$  from the start of the last uniform increment at  $R(N1)$  to  $R(N-1)$  and  $R(N)$ , respectively, are given by

$$P_1 = \frac{R^{j-1}-1}{R-1} = 1 + R + R^2 \dots R^{j-2} \quad (I-2)$$

$$P_2 = \frac{R^j-1}{R-1} = 1 + R + R^2 \dots R^{j-1} \quad (I-3)$$

where  $j=N-N1$ . If we now add these two equations, and represent  $(P_1+P_2)/2$  by  $P$ , then

$$\frac{P \cdot 2(R-1)+2}{R+1} = R^{j-1} \quad (I-4)$$

Taking the logs of both sides and solving for the  $R$  on the right-hand side of Eq. I-4 yields

$$R = \exp(\log(\frac{2 \cdot (P \cdot (R-1)+1)}{R+1}) / (j-1)) \quad (I-5)$$

This equation can be solved for  $R$  by successive approximations. First one evaluates the right-hand side using an estimated value for  $R$ . The result represents the first approximation of  $R$ . The next approximation is made by substituting the newly found value for  $R$  back into the right-hand side of Eq. I-5. This process is continued until  $R$  ceases to change. Usually, about 10 approximations are required.



APPENDIX J

MEASURING UNCERTAINTIES IN PREDICTED LASER POWERS  
TO CAUSE DAMAGE

APPENDIX J  
MEASURING UNCERTAINTIES IN PREDICTED LASER POWERS  
TO CAUSE DAMAGE

In this appendix a methodology is described which measures the variability in the predictions of the laser of the Corneal and Retinal models caused by uncertainties in the input parameters. A computer program has been developed for this purpose. This appendix describes the problem, the methodology, and an example.

1. THE PROBLEM

Consider a mathematical model with  $n$  input parameters labeled as  $X_1, X_2, \dots, X_n$  and an output result  $Y$ . Hence,  $Y$  is related to the parameters  $X$  in some functional form as

$$Y = f(X_1, X_2, \dots, X_n) \quad (J-1)$$

1.1 Parameter Nominal Values

To use the mathematical model, one must specify values for the input parameters: these may be denoted as  $X_{10}, \dots, X_{n0}$ . Upon exercising the program a particular output result is obtained, say  $Y_0$ . In functional form

$$Y_0 = f(X_{10}, \dots, X_{n0}) \quad (J-2)$$

1.2 Uncertainty in Nominal Values

As a result of the fact that the nominal values  $X_{10}, \dots, X_{n0}$  probably deviate from their true values, the nominal values are in reality "most-likely" values of the parameters. To appreciate the consequence of uncertainties in the parameters, the limits over which each parameter may range must be specified.

1.3 Uncertainty in Output Result

Because of uncertainties in the input parameters, a corresponding uncertainty exists in the output results. The purpose of this appendix is to measure this uncertainty.

## 2. THE METHOD

To measure the variability in output results, there are three basic steps as follows:

- define the uncertainty in input parameter values,
- determine the variability in output results associated with each parameter's variability,
- combine all the uncertainties so that the output variability can be measured.

### 2.1 Variability in Input Parameter Values

In addition to the assigned nominal value for each parameter, the user must specify a pair of minimum and maximum values within which the time parameter value lies. The nominal value is assumed to be the most likely value for the parameter. With these three values the probability distribution produced by each parameter's variability can be estimated by use of the Beta probability distribution.

The Beta probability distribution takes on many shapes depending on two coefficients, namely a and b. In this application 19 possible combinations of a and b have been selected. These are (a=1,2,...,10 with b=10) and (a=10 with b=1,2,...,10). Some examples are cited in Fig. J-1. The case in which both a and b equal 10 is very near a normal distribution.

In a standardized Beta distribution, the variable range is from zero to one. The most likely value, which is hereafter called the mode, becomes

$$\text{Mode} = \frac{a-1}{a+b-2} \quad (\text{J-3})$$

It is the mode which is used to determine the coefficients for a particular parameter.

The corresponding standardized mode of the i-th parameter is found from

$$\text{Mode} = \frac{X_{i0} - X_i(\text{min})}{X_i(\text{max}) - X_i(\text{min})} \quad (\text{J-4})$$

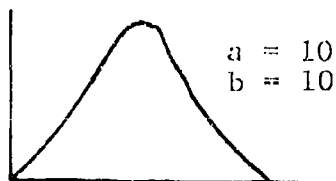
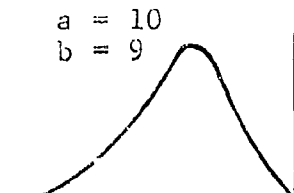
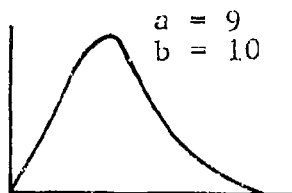
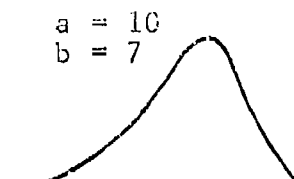
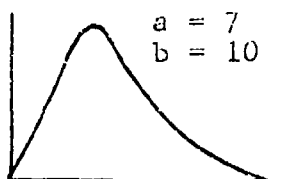
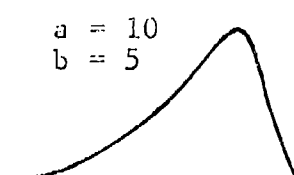
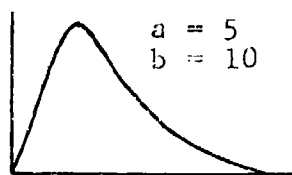
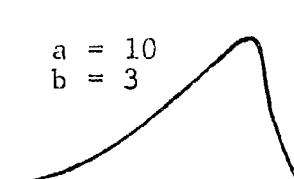
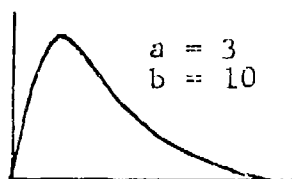
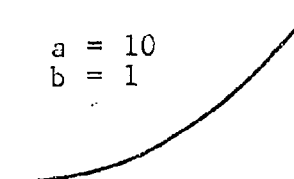
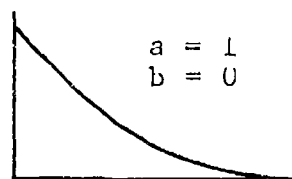


Fig. J-1 SOME EXAMPLES OF THE BETA PROBABILITY DENSITY

where

$X_{i0}$  = nominal value for parameter

$X_i(\min)$  = minimum possible value for parameter

$X_i(\max)$  = maximum possible value for parameter

Given the estimate of the mode in Eq. J-4, a search is conducted to find the closest of the 19 combinations of a and b which corresponds to Eq. J-3. Once found, the shape of the distribution for the i-th parameter is obtained.

Now with the shape of the i-th parameter value established, five representative values of  $X_i$  are selected. These are denoted as  $X_i(p)$  for  $p=0.1, 0.3, 0.5, 0.7, 0.9$ . Here p represents the 100 p-percentiles as shown in Figure J-2. The figure shows that the

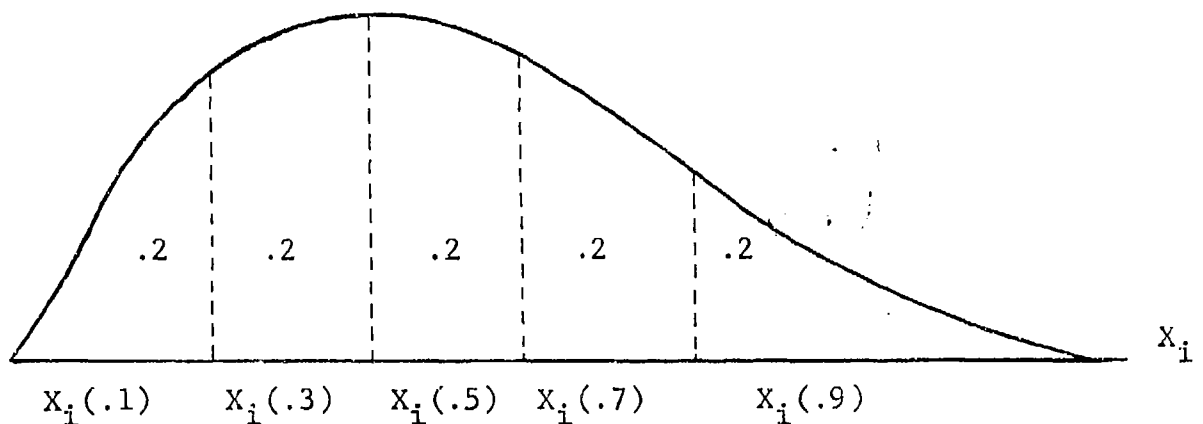


Fig. J-2 FIVE REPRESENTATIVE VALUES  
OF THE i-th PARAMETER VALUES

probability distribution for  $X_i$  is separated into five equal areas, each with a probability value of 0.2. The center point of  $X_i$  for the left-most such area becomes  $X_i(.1)$ . Next is  $X_i(.3)$ , and so forth.

In this fashion, five representative values for each of the n parameters are obtained. These now become

$$\begin{aligned} & (X_i(.1), X_i(.3), X_i(.5), X_i(.7), X_i(.9)), \dots \\ & (X_n(.1), X_n(.3), X_n(.5), X_n(.7), X_n(.9)) \end{aligned} \quad (J-5)$$

For the  $i$ -th parameter, the set of five values are selected in a fashion where they are each equally likely to occur.

## 2.2 Variability in Output Results per Parameter

Having selected the five representative values of each input parameter, it is now necessary to measure the effect that each of these values play on the output results. For this purpose the results from the sensitivity analysis is used. For convenience here a short review of the sensitivity analysis is given at this time.

In the sensitivity analysis each parameter is individually investigated to determine the effect on the output result. For the  $i$ -th parameter, a low and a high value are selected and labeled  $X_{i(LO)}$  and  $X_{i(HI)}$  where

$$X_{i(LO)} \leq X_{i0} \leq X_{i(HI)} \quad (J-6)$$

Corresponding values of  $Y$  are obtained by varying only the  $i$ -th parameter from its nominal value, i.e.

$$Y_{i(LO)} = f(X_{10}, \dots, X_{i(LO)}, \dots, X_{n0})$$

and

$$Y_{i(HI)} = f(X_{10}, \dots, X_{i(HI)}, \dots, X_{n0})$$

(J-7)

The results may be depicted as shown in Figure J-3.

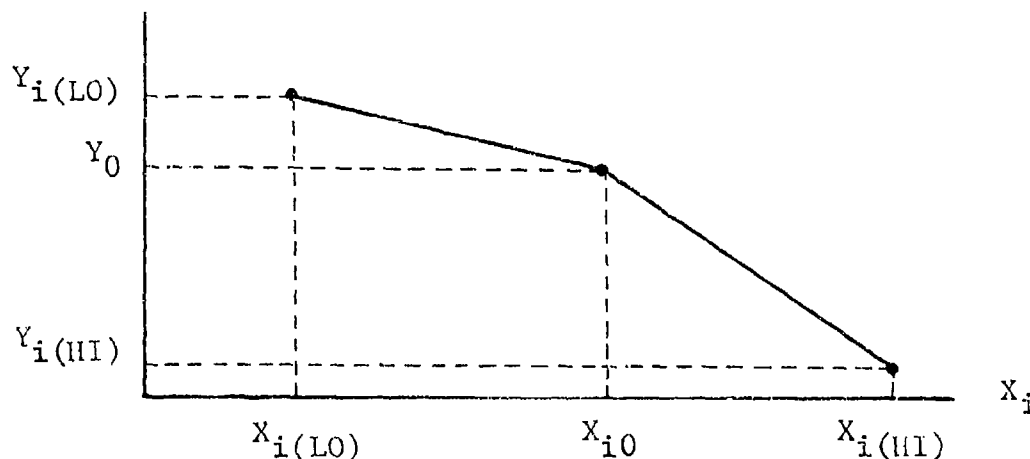


Fig. J-3 DISPLAY OF SENSITIVITY RESULTS  
FOR AN ARBITRARY PARAMETER

Now it is possible to estimate the sensitivity associated with the five values of parameter  $i$  by simple interpolation or extrapolation, whichever pertains. The results yield

$$(Y_i(.1), Y_i(.3), Y_i(.5), Y_i(.7), Y_i(.9))$$

and are obtained as depicted in Figure J-4. Note that  $X_{i(L0)}$  and

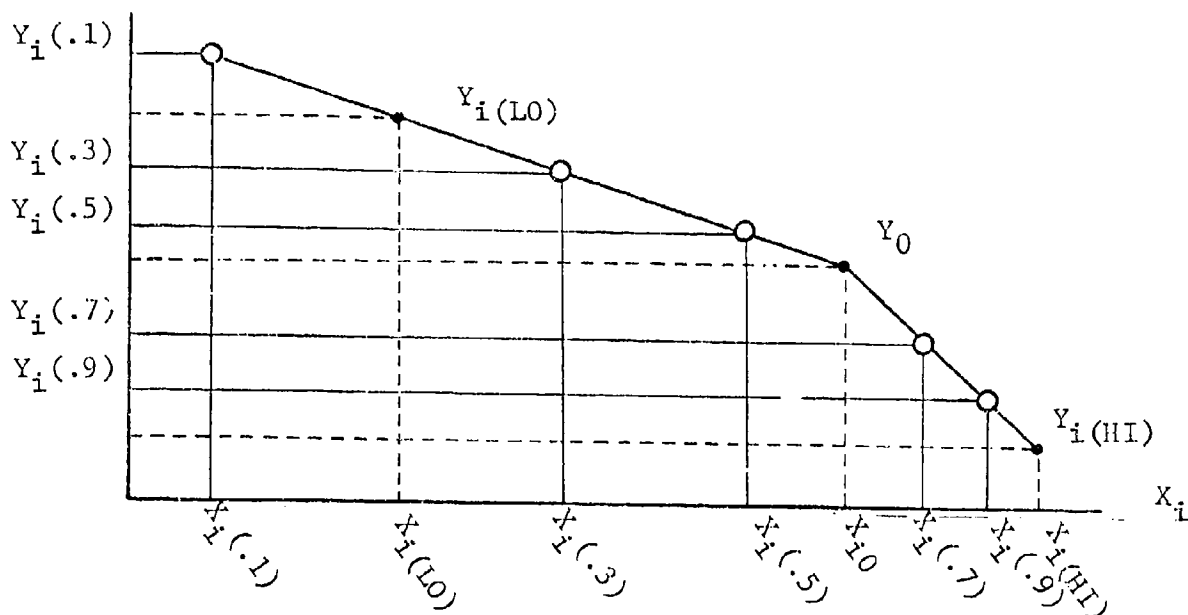


Fig. J-4 SELECTING  $Y_i(P)$

$X_{i(HI)}$  are not necessarily outside of the range containing  $X_i(.1)$  to  $X_i(.9)$ .

With the values of  $Y_i(p)$  now available, it is possible to calculate five deviates for each  $i$ , i.e.,

$$\Delta_i(p) = (Y_i(p) - Y_0) \quad \begin{matrix} i = 1, 2, \dots, n \\ p = .1, \dots, .9 \end{matrix} \quad (J-8)$$

Note that for the  $i$ -th parameter, that the five associated deviates are equally likely to occur.

### 2.3 Applying All Combinations

Now variables to  $Y=Y_0$  can be obtained by selecting all combinations of the deviates and applying them to the expression

$$Y = Y_0 + \Delta_1(p_1) + \Delta_2(p_2) + \dots + \Delta_n(p_n) \quad (J-9)$$

where  $P_i = .1, .3, .5, .7, .9$  for  $i=2 \dots n$ . The frequency distribution of  $Y$  from all of the combinations yields the estimate of the uncertainty in the output result.



APPENDIX K

NOMENCLATURE, SAMPLE DATA, CODE LISTING, AND  
SAMPLE RUN FOR RETINAL MODEL

C \*\*\* NOMENCLATURE FOR RETINAL MODEL

C -----  
C A(I,1),A(I,2),

C A(I,3) COEFFICIENTS OF FINITE DIFFERENCE EQUATIONS,Z ELEMENTS

C AAV ABSORPTION COEFFICIENT FOR EYE MEDIA FROM CORNEA TO  
C RETINA,PER CM

C AB(1,1), PRODUCTS OF ABSORPTION COEFFICIENTS AND THICKNESSES OF

C AB(I,2),... SUCCESSIVE EYE MEDIA BETWEEN ZH(I-1) AND ZH(I)

C ABR(I,L1) SUM OF AB(I,1),AB(I,2)... OF MEDIA BETWEEN ZH(I-1)  
C AND ZD(L1)

C ABS(L) ABSORPTION COEFFICIENTS ASSOCIATED WITH L-TH EYE  
C MEDIA BETWEEN ZD(L) AND ZD(L+1),PER CM

C ACH ABSORPTION COEFFICIENT FOR CHOROID,PER CM

C AP FRACTION OF HEAT DEPOSITED IN GRANULATED PE THAT IS  
C ABSORBED BY GRANULES

C APE ABSORPTION COEFFICIENT FOR PIGMENT EPITHELIUM,PER CM

C ASC ABSORPTION COEFFICIENT FOR SCLERA,PER CM

C AVL ABSORPTION COEFFICIENT FOR CHORIO-CAPILLARIS,PER CM

C ATS ABSORPTION COEFFICIENT FOR TISSUES BENEATH EYE,PER CM

C B(J,1),B(J,2),

C 2(J,3) COEFFICIENTS OF FINITE DIFFERENCE EQUATIONS,R ELEMENTS

C BT TIME INTERVAL,SEC

C BB CHANGES IN A AND B MATRIX ELEMENTS DUE TO BLOOD FLOW  
C IN TISSUES SURROUNDING EYE

C BV(J,1)... CHANGES IN A AND B MATRIX ELEMENTS DUE TO BLOOD FLOW  
C IN CHORIO-CAPILLARIS

C CABER CONSTANT USED TO EVALUATE SPHERICAL ABERRATION  
C CONSTANT CABER2 = CZ

C CABER2 SPHERICAL ABERRATION CONSTANT,1/CM<sup>4</sup>

C CFLOW TOTAL BLOOD FLOW TO CHORIO-CAPILLARIS,GM/SEC

C CON(I) THERMAL CONDUCTIVITY AT DEPTH Z(I),CAL/CM-SEC-C

C CONX(L) THERMAL CONDUCTIVITIES FOR L-TH EYE MEDIA,CAL/CM-SEC-C

C CQ RATIO OF PREDICTED TO ACTUAL LASER POWER,  
C INITIALLY ESTIMATED AND THEN REFINED BY DAMAGE CALC.

C CXC(J) ARRAYS USED TO EVALUATE TEMPERATURES USING MATRIX  
C CXR(I) ELEMENTS

C CUT NORMALIZED INTENSITY OF LASER BEAM AT R=RIM

C DAMAGE(L1, COEFFICIENTS FOR RATE OF THERMAL DAMAGE,RATE=  
C L2) EXP(DAMAGE(1,1)-DAMAGE(1,2)/(VC(273+T0)) FOR TEMPERA-  
C TURES BELOW 50 C, AND RATE=EXP(DAMAGE(2,1)-DAMAGE(2,2)/  
C (VC+273+T0)) FOR TEMPERATURES ABOVE 50 C

C DFLOW(L1) RADIAL DISTANCES AT WHICH BLOOD FLOW IS DESCRIBED,CM

C DIM MAX. NUMBER OF ELEMENTS USED TO COMPUTE THERMAL EFFECTS  
C OF GRANULES

C DPULSE DURATION OF INDIVIDUAL PULSES,SEC. ALWAYS HELD FIXED

C DR R INCREMENT IN UNIFORM PART OF GRID, CM

C DT FIRST TIME INTERVAL FOR SINGLE-PULSE TEMPERATURE CALC.

C SUCCESSIVE INTERVALS INCREASED BY FACTOR XC,SEC

C DTSTM TEMPERATURE INCREMENT TO BE ADDED TO TSTEAM CONSIDERING  
C AVER.GRANULE TEMPERATURE AS HYPOTHETICAL DAMAGE  
C CRITERION

C DX SIZE OF GRID USED TO CALC. GRANULE TEMPERATURE RISES,CM

C DXC(J) ARRAYS USED TO EVALUATE TEMPERATURES RISES

C DXR(I)

C DZ

C EDT1 Z INCREMENT IN UNIFORM PART OF GRID, CM

C TO WHICH TIME IS RAISED TO SPECIFY NUMBER OF CYCLES  
C TO WHICH BASIC TEMPERATURE CALCULATIONS ARE REPEATED  
C TO ENSURE STABILITY

C EDT2 ADDITIVE FACTOR TO SPECIFY NUMBER OF CYCLES TO WHICH  
C SINGLE-PULSE TEMPERATURE CALC. ARE REPEATED TO ENSURE

C		STABILITY
C	FA(L)	AREA FROM R=0 TO R=(L-.5)*RINT,CM2---FOR CALC. IRREGULAR
C		PROFILES
C	FC	FOCAL LENGTH OF CORNEA,=3.12 CM FOR HUMANS,=2.43 CM
C		FOR MONKEYS
C	FL	FOCAL LENGTH OF LENS AT WAVELENGTH WAVELENGTH,CM
C	FLO	SECOND PRINCIPAL FOCAL LENGTH AT WAVELENGTH OF 500
C		NM,=2.242 CM FOR HUMANS,=1.684 FOR MONKEYS
C	FLOWI(J),	FLOW OF BLOOD INTO UNIT VOLUME OF VASCULAR LAYER AT R(J),
C		GM/CM3-SEC
C	FLOWX(J)	PRODUCT OF RAC AND FLOW OF BLOOD PER UNIT AREA IN R
C		DIRECTION AT R(J),CM/CM-SEC
C	FP(L)	TOTAL LASER POWER BETWEEN R=0 AND R=(L-.5)*RINT---
C		FOR CALC. IRREGULAR PROFILES
C	FTIME(L)	FACTORS BY WHICH EXPOSURE TIME IS MULTIPLIED TO YIELD
C		SUFFICIENT TIME FOR DAMAGE TO OCCUR,GIVEN AS FUNCTION
C		OF PULSE WIDTH
C	FXC(J)	ARRAYS USED TO EVALUATE TEMPERATURES
C	FXR(I)	
C	HR(J)	NORMALIZED RETINAL IRRADIANCE AT R(J),CAL/CM2-SEC
C	I	INDEX OF AXIAL GRID POINTS Z(I)
C	IAB(I,J)	INDICES CONTROLLING WHICH I,J ELEMENTS TO INCORPORATE BB
C		CHANGES TO A AND B MATRIX ELEMENTS
C	IBLOOD(L1)	INDICES DESIGNATING DZ ELEMENTS ASSOCIATED WITH CHORIO
C		CAPILLARIS,L1=1,2,...,NVL
C	ID1,ID2	I INDICES FOR PRINTING AT DEPTHS Z(I) WHERE I=IPE+ID1 TO
C		IPE+ID2
C	IFIL	INDEX CONTROLLING USE OF SPREAD FUNCTION,SET=1 TO USE
C		FUNCTION OTHERWISE SET=0
C	IG	I INDEX INDICATING LOCATION OF GRANULES
C	IGX	INDEX INDICATING WHETHER HUMAN OR MONKEY,IF MONKEY SET=0,
C		IF HUMAN SET=1
C	II(I)	NUMBER OF INTERFACES(ZD) BETWEEN ZH(I-1) AND ZH(I),
C		PLUS 1
C	I13	I INDEX OF V(I13,J) TEMPERATURE CURVE(J VARYING) TO MARK
C		ON 3-D PLOTS
C	IKX	NUMBER OF TIMES TEMPERATURE CALC. ARE REPEATED FOR
C		PURPOSES OF STABILITY
C	IMAX	I INDEX AT WHICH PEAK TEMPERATURES OCCUR
C	IN	NUMBER OF PULSES GROUPED TOGETHER FOR DAMAGE CALCULATIONS
C	INX	NUMBER OF GROUPS OF PULSES CONSIDERED DURING EXPOSURE
C		TO LASER
C	INXX	NUMBER OF GROUPS OF PULSES CONSIDERED DURING AND
C		FOLLOWING EXPOSURE TO LASER
C	IPA	INITIAL GRID POINT IN CORNEA
C	IPC	INITIAL GRID POINT IN CHOROID
C	IPE	INITIAL GRID POINT IN PIGMENT EPIYTHELIUM
C	IPROF	INDEX DESCRIBING LASER PROFILE,UNIFORM IF=0,GAUSSIAN IF=1
C		IRREGULAR IF=2
C	IPS	INITIAL GRID POINT IN SCLERA
C	IPT	INITIAL GRID POINT IN TISSUES BENEATH EYE
C	IPV	INITIAL GRID POINT IN CHORIO-CAPILLARIS
C	ITYPE	K INTERVAL AT WHICH VC(I,J,K) IS PRINTED
C	IV(I)	INDICES CONTROLLING I VALUES AT WHICH TO INCORPORATE BV
C		CHANGES TO A AND B MATRIX ELEMENTS
C	IX(L)	I INDICES ASSOCIATED WITH INITIAL GRID POINT (Z) IN L-TH
C		EYE MEDIA
C	IZ(I)	INDEX L OF FIRST INTERFACE ZD(L) BEYOND ZH(I-1)
C	J	INDEX FOR RADIAL GRID POINTS R(J)
C	JD1,JD2	J INDICES FOR PRINTING, WILL PRINT J=JD1 TO JD2

C	JM	MAXIMUM J INDEX AT WHICH DAMAGE ASSESSMENTS ARE TO BE MADE
C		*DEPENDS ON VALUE CHOSEN FOR RMAX
C	JVL	J INDEX FOR WHICH R(JVL) APPROXIMATES RVL
C	JO(L)	BESSEL FUNCTION OF 0 ORDER
C	K	INDEX FOR TIMES XT(K)
C	KM	INTEGER SUCH THAT XT(KM)=DPULSE
C	KT	MAXIMUM NUMBER OF EXPANDING TIMES XT(K)
C	KTT(L)	NUMBER OF TIME STEPS WITH WHICH TO REACH TOTAL TIME
C	KTYPE	NUMBER OF TIMES AT WHICH 3D TEMPERATURE DRAWINGS ARE DESIRED
C		--- FOR NO DRAWINGS SET KTYPE=0
C	KTYPEO	CONTROL INDEX WHICH WHEN SET =1 WILL PREEMPT CARD
C		PUNCHING WHILE MAINTAINING PRINT OUTS OF TEMPERATURES
C		AT SELECTED TIMES AND POINTS---SET =0 FOR CARD PUNCHING.
C	KX	TOTAL NUMBER OF TIME INTERVALS FROM PULSE TO PULSE
C	LESION	LESION RADIUS,CM
C	LI,LII	NUMBER OF RADIAL INTERVALS USED TO INTEGRATE SPREAD
C		FUNCTION
C	LIM	NUMBER OF RADIAL INTERVALS FROM R=0 TO R=RIM OR LESION
C	LIMAX	I INDEX DESCRIBING RANGE OF I OVER WHICH TO ASSESS DAMAGE,
C		RANGE=IMAX=LIMAX TO IMAX+LIMAX
C	LLT,LLG	INDICES USED TO CONTROL CALC. OF THRESHOLD POWER
C	LPA	LAST GRID POINT IN VITREOUS HUMOR
C	LPC	LAST GRID POINT IN CHOROID
C	LPE	LAST GRID POINT IN PIGMENT EPITHELIUM
C	LPS	LAST POINT IN SCLERA
C	LPT	NUMBER OF INCREMENTAL PULSES BT IN DPULSE
C	LPV	LAST POINT IN CHORIO-CAPILLARIS
C	LR	NUMBER OF POINTS DESCRIBING IRREGULAR LASER PROFILE
C	LY	INDEX OF NUMBER OF TIME INTERVALS BT
C	LTMAX	TIME INDEX(TIME=LTMAX*BT) BEYOND WHICH EXCESS
C		TEMPERATURE RISE OF GRANULES IS DISSIPATED
C	LTT	TIME INDEX USED FOR K IN SUBROUTINE MXGRAN
C	LX(L)	I INDICES ASSOCIATED WITH LAST GRID POINT (Z) IN L-TH
C		EYE MEDIA
C	L1,L2,L3...	DUMMY VARIABLES USED IN COMPUTATIONS
C	M	NO. OF GRID SPACES IN Z DIRECTION(EVEN)
C	M1	HALF OF NUMBER OF UNIFORMLY THICK Z INCREMENTS(LESS THAN M/2)
C	M2	HALF THE NO. OF GRID SPACES IN Z DIRECTION
C	M3	NO. OF GRID POINTS IN Z DIRECTION (M+1)
C	N	NO. OF GRID SPACES IN R DIRECTION
C	NA(L)	REFRACTIVE INDEX AS FUNCTION OF WAVELENGTH
C		(350+50*(L-1)) NM
C	NB	REFRACTIVE INDEX AT WAVELENGTH OF 500 NM=NA(4)
C	NC	REFRACTIVE INDEX AT WAVELENGTH WAVEL
C	NP	NUMBER OF TIME INTERVALS WITHIN DPULSE,USED FOR DAMAGE
C		CALCULATIONS
C	NPL	TOTAL NUMBER OF PULSES IN EXPOSURE
C	NPT(L)	NUMBER OF INCREMENTAL TIMES USED TO SUBDIVIDE DPULSE
C	NPULSE(L)	NUMBER OF PULSES ASSOCIATED WITH L-TH TEST EXPOSURE
C	NTEST	NUMBER OF TEST EXPOSURES WHICH CAN DIFFER IN REPETITION
C		RATES OR NUMBER OF PULSES
C	N1	NUMBER OF UNIFORMLY THICK R INCREMENTS(LESS THAN N)
C	N3	NO. OF GRID POINTS IN R DIRECTION (N+1)
C	N4	NO. OF GRID POINTS IN UNIFORM PART OF GRID IN R DIRECTION
C	PC	DISTANCE OF PUPIL FROM CORNEA,=.40 CM FOR HUMANS,
C		=.36 CM FOR MONKEYS
C	PO	NUMBER OF INCREMENTAL PULSES CAUSING NEGLIGBLE TEMPER-
C		ATURE RISES IN GRANULE CALC.
C	POW,POX	LASER POWER ON CORNEAL PLANE,WATTS
C	PP	DISTANCE BETWEEN PUPIL AND SECOND PRINCIPAL PLANE,CM

C	PR(J)	CALCULATED OR MEASURED RETINAL IRRADIANCE PROFILE
C		NORMALIZED TO UNITY AT R(1)=0.
C	PT	TOTAL NUMBER OF ELEMENTS USED TO CALC. GRANULE TEMPERATURES
C	PYIME	UNIFORM TIME INTERVAL USED TO SUBDIVIDE DPULSE FOR MULTIPLE PULSES
C	PUPIL	PUPIL RADIUS,CM
C	PX(L)	IRREGULAR LASER PROFILE AT POINTS RX(L)
C	QD(I,J)	LASER POWER REQUIRED TO CAUSE IRREVERSIBLE DAMAGE AT Z(I),R(J),WATTS
C	QP	LASER INTENSITY ENTERING EYE AT R(1)=0,CAL/CM2-SEC
C	R(J)	RADIUS AT CO-ORDINATE J, CM
C	RCD	REFLECTION FROM CORNEA
C	REF(L)	FRACTION OF RADIATION REFLECTED AT Z=ZD(L)
C	REFL(L)	REFLECTED RADIATION FROM INTERFACE AT Z=ZD(L)
C	REPET(L)	REPETITION RATES ASSOCIATED WITH L-TH TEST EXPOSURE,PULSES/SEC
C	RGV	RANGE OF TEMPERATURE RISE(C) FOR 3-D AND 2-D PLOTS
C	RH(J)	RADIAL DISTANCE HALFWAY BETWEEN R(J) AND R(J+1)
C	RYM	IMAGE OR BEAM RADIUS, FOR GAUSSIAN PROFILES EQUALS RADIUS AT WHICH NORMALIZED PROFILE EQUALS CUT, FOR UNIFORM PROFILES EQUALS EXTENT OF PROFILE,CM
C	RINT	UNIFORM RADIAL INTERVALS,CM
C	RMAX	MAXIMUM RADIAL DISTANCE AT WHICH DAMAGE ASSESSMENTS ARE TO BE MADE
C	RN	MAXIMUM RADIAL DISTANCE,CM
C	RPE	FRACTION OF FRONT OF PE CONTAINING ALL GRANULES OR NONE
C	RRT	REFLECTION OFF OF RETINA
C	RSC	REFLECTION FROM SCLERA
C	RVL	RADIAL EXTENT OF EYE,CM
C	RX(L)	RADIAL DISTANCES ASSOCIATED WITH IRREGULAR LASER PROFILE PX(L)(SYMMETRIC IN R),CM
C	R1	STRETCHING FACTOR IN Z DIRECTION
C	R2	STRETCHING FACTOR IN R DIRECTION
C	S(I,J)	RATE OF HEAT DEPOSITION PER UNIT VOLUME AT Z(I),R(J), CAL/CM3-SEC
C	SHB	SPECIFIC HEAT OF BLOOD,CAL/GM-C
C	SIGMA	RADIUS AT WHICH NORMLIZED GAUSSIAN PROFILE EQUALS 1/E2
C	TAV	THICKNESS OF MEDIA FROM CORNEA TO VITREOUS HUMOR,CM
C	TC	TIME FROM START OF PULSE TO START OF NEXT PULSE,SEC
C	TCH	THICKNESS OF CHOROID,CM
C	TIME	MAXIMUM TIME LIMIT SET, SEC
C	TIMEX(L)	TIMES AT WHICH 3-D PLOTS ARE DESIRED,SEC
C	TOM	TRANSMITTANCE OF MEDIA FROM CORNEA THROUGH VITREOUS HUMOR
C	TPE	THICKNESS OF PIGMENT EPITHELIUM,CM
C	TS(L)	NORMALIZED TEMPERATURE RISES FOR GRANULES,C
C	TSC	THICKNESS OF SCLERA,CM
C	TSTEAM	GRANULE TEMPERATURE USED AS HYPOTHETICAL DAMAGE CRITERION,C
C	TVL	THICKNESS OF CHORIO-CAPILLARIS
C	TO	INITIAL TEMPERATURE OF EYE,C
C	V(I,J)	TEMPERATURE RISES AT Z(I),R(J) AT GIVEN TIME,C
C	VC(I,J,K)	TEMPERATURE RISES AT Z(I),R(J) AT TIME XT(K),C
C	VE(L,K,L1)	TEMPERATURE RISES AT Z(ID(L)),R(JD(L)) AT TIME XT(K),L1=1 FOR EYE MEDIA,AND L1=2 FOR GRANULES
C	VPX	TEMPERATURE RISES,C
C	VQ	TEMPERATURE RISE CAUSED BY ENERGY DEPOSITION WITHIN GRANULE DURING TIME INTERVAL PT,C
C	VSH(I)	VOLUMETRIC SPECIFIC HEAT AT Z(I),C*L/CM3-C
C	VSHX(L)	HEAT CAPACITY OF L-TH EYE MEDIA,CAL/CM3-C

```

C VZ(L,L6,L3, TEMPERATURE RISE AT TIME INTERVAL ZT(L3) AFTER
C L1) (L6=.5)*IN=.5 INCREMENTAL PULSES AT POINT Z(TD(L)),R(JD(L))
C ,L1=1 FOR EYE MEDIA AND L1=2 FOR GRANULES
C WAVELENGTH,NM
C XC STRETCHING FACTOR FOR TIME INTERVALS ASSOCIATED WITH
C SINGLE PULSE TEMPERATURE CALCULATIONS
C XCT(L) VALUES FROM WHICH EXPANSION FACTOR XC IS SELECTED BASED
C UPON PULSE WIDTH
C XFLOW RATE OF BLOOD FLOW TO TISSUES SURROUNDING EYE,GM/CM3-SEC
C XFLOWI(J) FLOW OF BLOOD INTO VASCULAR LAYER AT R=DFLOW(J),
C GM/CM2-SEC
C XFLOWO(J) FLOW OF BLOOD OUT OF VASCULAR LAYER AT R=DFLOW(J),
C GM/CM2-SEC
C XI(J) FLOW OF BLOOD INTO UNIT AREA OF VASCULAR LAYER HALF-
C WAY BETWEEN R(J) AND R(J+1),GM/CM2-SEC
C XO(J) FLOW OF BLOOD OUT OF UNIT AREA OF VASCULAR LAYER HALF-
C WAY BETWEEN R(J) AND R(J+1),GM/CM2-SEC
C XPD(K) NORMALIZED TEMPERATURE RISES OF GRANULES AT TIME XT(K)
C XT(K) TIMES FOLLOWING START OF EXPOSURE,INDICATED BY INDEX K
C ,SEC
C XX FRACTION OF LASERS ENERGY ENTERING EYE
C X1,X2,X3... DUMMY VARIABLES USED IN COMPUTATIONS
C Z(I) DISTANCE ALONG Z AXIS AT GRID POINT I,CM
C ZD(I) DEPTHS OF INTERFACES BETWEEN VARIOUS EYE MEDIA,CM
C ZH(I) AXIAL DISTANCES HALFWAY BETWEEN Z(I) AND Z(I+1),CM
C ZM HALF LENGTH OF Z AXIS, CM
C ZO DISTANCE OF PUPIL FROM LASERS WAIST,CM
C ZT(L3) TIME FROM START OF PULSE TO CENTER OF TIME INTERVALS
C USED TO PREDICT THERMAL DAMAGE FOR MULTIPLE PULSES
C ZTT(L3) LOG OF PRODUCT OF NUMBER OF PULSES/GROUP TIMES TIME
C INTERVALS AT WHICH DAMAGE CALC. ARE MADE
C ZTX(L3) TIME INTERVAL FROM START OF EACH PULSE AT WHICH
C GRANULE TEMPERATURES ARE TO BE CALCULATED
C *** DIMENSIONS OF VARIOUS ARRAYS USED IN PROGRAM
C -----
C COMMON DIMENSIONS A(M3,3),B(N3,3),BV(N3,3),CONX(6),CON(M3),DFLOW(6),
C HR(N3),IAB(M3,N3),IBLOOD(NVL),IV(M3),PR(N3),R(N3),S(M3,N3),TS(LTMAX),
C V(M3,N3),VC(M3,N3,KT),VSHX(6),VSH(M3),XFLOWI(N3),XFLOWO(N3),XPD(KT),
C XT(KT),Z(M3),ZD(8)
C *** MAIN PROGRAM
C DIMENSION CX(N3),CXR(M3),DAMAGE(2,2),DXC(N3),DXR(M3),FXC(N3),FXR(M3),
C ID(LIJ),JD(LIJ),KKT(38),NPT(38),NPULSE(NTEST),NRUN(NTEST),QD(M3,N3),
C REPET(NTEST),TIMEX(KTYPE),XCT(38),VE(LIJ,KT,2),VXX(M3,N3),VZ(LIJ,
C INXX,KX,2),ZT(KX),ZTT(KX),ZTX(KX)
C *** SUBROUTINE GRID
C IX(7),LX(7)
C *** SUBROUTINE IMAGE
C FA(LI+1),FP(LI+1),FX(LI+1),JU(32),PX(LR),RX(LR),XF1(LI+1),XF2(LI+1)
C *** SUBROUTINE HTXDEP
C AB(M3,3),ABR(M3,7),II(M3),IZ(M3),REF(8),REFL( ),ZH(M3)
C *** SUBROUTINE MXGRAN(ORIGINAL)
C T(7,7,7),TT(7,7,7)
C *** SUBROUTINE BLOOD
C FLOWI(N3),FLOWX(N3),RD(N3),RH(N3),XI(N3),XO(N3)

```

SAMPLE DATA FOR RETINAL MODEL USING EXPERIMENTALLY  
OBSERVED LASER PROFILE AT RETINA

```

-----
-----DATA CARDS 2-----
1.3 1.3 1.3 1.3 1.3 1.3 1.3 1.3 1.3 1.3
1.3 1.3 1.3 1.3 1.3 1.3 1.3 1.3 1.3 1.3
1.3 1.3 1.3 1.3 1.3 1.3 1.3 1.3 1.3 1.3
1.3 1.3 1.3 1.3 1.3 1.3 1.3 1.3 1.3 1.3
-----DATA CARD 4-----
.0025 5 0 0
-----DATA CARD 5-----
.0010 1 .0010
-----DATA CARD 6-----
1 2.01+2 1.35-1
-----DATA CARD 7-----
1.5-8
-----DATA CARD 8-----
1 11
-----DATA CARD 9-----
1.0+3
-----DATA CARD 10-----
1
-----DATA CARD 11-----
-1 2 1 5 4
-----DATA CARD 12-----
37. .10 1.
-----DATA CARD 13-----
.647 1425. 163. 163. 163. 163. .025 .070 .31 .333 530.0
-----DATA CARD 14-----
1.85 .0012 .0010 .0168 .1000 .7
-----DATA CARD 15-----
.00120 .00120 .00120 .00120 .00120 .00120
-----DATA CARD 16-----
1. 1. 1. 1. 1. 1.
-----DATA CARDS 17-----
1 3 5 7 10 14 18 21 25 28
30 31 32 33 34 35 36 37 38 39
40 41 42 43 44 45 46 47 48 49
50 51 52 53 54 55 56 57
-----DATA CARDS 18-----
1.2 1.2 1.2 1.2 1.2 1.2 1.2 1.2 1.2 1.2
1.2 1.2 1.2 1.2 1.15 1.15 1.15 1.15 1.15 1.15
1.15 1.15 1.15 1.15 1.15 1.15 1.15 1.15 1.1 1.1
1.1 1.1 1.1 1.1 1.1 1.1 1.1 1.1
-----DATA CARDS 19-----
35 35 35 35 35 35 36 36 37 37
38 38 39 39 40 40 41 42 42 43
44 45 46 47 48 49 50 51 52 52
53 54 55 56 57 57 58 58
-----DATA CARD 19A-----
.35+0

```

```

-----DATA CARD 20 -----
.92 .001 .024
-----DATA CARD 20A-----
1
-----DATA CARD 21 -----
2
-----DATA CARD 22 -----
.5-7 .5-6
-----DATA CARD 23 -----
10 11 10 1 2
-----DATA CARD 24 -----
6. 2191

```

-----DATA CARDS 25 -----											
8.000	7.359	6.815	6.349	5.944	5.590	5.277	4.999	4.749	4.523		
4.319	4.132	3.960	3.802	3.656	3.520	3.394	3.276	3.166	3.062		
2.965	2.874	2.787	2.706	2.629	2.557	2.488	2.423	2.361	2.303		
2.247	2.194	2.144	2.096	2.051	2.007	1.966	1.927	1.889	1.853		
1.819	1.786	1.755	1.725	1.697	1.670	1.644	1.619	1.595	1.572		
1.550	1.529	1.509	1.490	1.472	1.454	1.437	1.421	1.405	1.390		
1.376	1.362	1.349	1.336	1.324	1.312	1.301	1.290	1.280	1.270		
1.260	1.251	1.242	1.233	1.225	1.217	1.209	1.202	1.195	1.188		
1.181	1.175	1.169	1.163	1.157	1.152	1.147	1.141	1.137	1.132		
1.127	1.123	1.119	1.115	1.111	1.107	1.103	1.100	1.096	1.093		
1.090	1.087	1.084	1.081	1.078	1.075	1.073	1.070	1.068	1.066		
1.063	1.061	1.059	1.057	1.055	1.053	1.052	1.050	1.048	1.047		
1.045	1.043	1.042	1.041	1.039	1.038	1.037	1.035	1.034	1.033		
1.032	1.031	1.030	1.029	1.028	1.027	1.026	1.025	1.024	1.024		
1.023	1.022	1.021	1.021	1.020	1.019	1.019	1.018	1.017	1.017		
1.016	1.016	1.015	1.015	1.014	1.014	1.013	1.013	1.012	1.012		
1.012	1.011	1.011	1.010	1.010	1.010	1.009	1.009	1.009	1.008		
1.008	1.008	1.008	1.007	1.007	1.007	1.007	1.006	1.006	1.006		
1.006	1.006	1.005	1.005	1.005	1.005	1.005	1.005	1.004	1.004		
1.004	1.004	1.004	1.004	1.004	1.004	1.003	1.003	1.003	1.003		
1.002	1.002	1.002	1.002	1.002	1.002	1.002	1.002	1.002	1.002		
1.002	1.001	1.001	1.001	1.001	1.001	1.001	1.001	1.001	1.001		

```

-----DATA CARD 26 -----
149. 50000. 242. 80000. 100. 100.

```



# SAMPLE RUN OF RETINAL MODEL

R2= 4.8801  
R1= 3.1452 ZM= 2.8086

ID1= 9 ID2=12 JD1= 1 JD2= 5

R=

.0000	.0003	.0007	.0010	.0013	.0030	.0109	.0496	.2387	1.161
5.6637									

Z=

-.9575	.9575	1.5664	1.7599	1.8215	1.8411	1.8473	1.8493	1.8499	1.8501
1.8503	1.8505	1.8507	1.8509	1.8511	1.8513	1.8515	1.8517	1.8519	1.8521
1.8523	1.8529	1.8549	1.8611	1.8807	1.9423	2.1358	2.7447	4.6597	

PUPIL= .350

SIGMA= .250-02 RIM= .250-02

QP= .478+07 PK=

.100+01	.965+00	.867+00	.726+00	.566+00	.604-01	.297-16	.000	.000	.000
---------	---------	---------	---------	---------	---------	---------	------	------	------

HR=

.100+01	.965+00	.867+00	.726+00	.566+00	.604-01	.297-16	.000	.000	.000
---------	---------	---------	---------	---------	---------	---------	------	------	------

REPET=

.100+04
---------

NPULSE=

1
---

AAV= .1 ACH= 163. APE= 1425. ASC= 163. A7S= 163.  
AVL= 163. CFLOW= .0240 DPULSE= .150-07 DR= .333-03  
DT= .202-08 DZ= .200-03 IFIL=0 IPA= 2 IPC=21 IPE=10 IPS=25  
IPT=27 IPV=16 JVL= 9 KM= 6 KI=36 LIM= 3 LPA= 9 LPC=24  
LPE=15 LPS=26 LPV=20 M=28 MI= 6 N=10 NI= 4 NP= 5  
NTEST= 1 NVL= 5 POW= .201+03 PTIME= .000 QP= .478+07 RCU= .0250  
RIM= .0025 RPE= .3330 RRT= .0700 RVL= .700+00 SHB= .92  
TAV= .185+01 TCH= .168-01 TIME= .594-05 TOM= .8470 IPE= .120-02  
TSC= .100+00 TVL= .100-02 TO= 57.0 XC= 1.2 XFLOW= .0010

IKX= 1

FLOWI	.156+02	.156+02	.156+02	.156+02	.156+02	.156+02	.156+02	.156+02	.156+02
FLOWX	.000	.000	.000	.000	.000	.000	.000	.000	.000

ZH=

.104-06
.126+01
.166+01
.179+01
.183+01
.184+01
.185+01
.185+01
.185+01

.185+01  
 .185+01  
 .185+01  
 .185+01  
 .185+01  
 .185+01  
 .185+01  
 .185+01  
 .185+01  
 .185+01  
 .185+01  
 .185+01  
 .185+01  
 .185+01  
 .186+01  
 .187+01  
 .191+01  
 .204+01  
 .244+01  
 .370+01

AP#	.9206	APE1#	3952.79	APE2#	163.00	IG#10				
SE	.428+06	.413+06	.371+06	.311+06	.242+06	.259+05	.000	.000	.000	.000
SE	.401+06	.387+06	.348+06	.291+06	.227+06	.242+05	.000	.000	.000	.000
SE	.392+06	.379+06	.340+06	.285+06	.222+06	.237+05	.000	.000	.000	.000
SE	.390+06	.376+06	.338+06	.283+06	.221+06	.235+05	.000	.000	.000	.000
SE	.389+06	.375+06	.337+06	.282+06	.220+06	.235+05	.000	.000	.000	.000
SE	.389+06	.375+06	.337+06	.282+06	.220+06	.235+05	.000	.000	.000	.000
SE	.389+06	.375+06	.337+06	.282+06	.220+06	.235+05	.000	.000	.000	.000
SE	.389+06	.375+06	.337+06	.282+06	.220+06	.235+05	.000	.000	.000	.000
SE	.103+11	.992+10	.892+10	.746+10	.582+10	.621+09	.000	.000	.000	.000
SE	.466+10	.450+10	.404+10	.338+10	.264+10	.281+09	.000	.000	.000	.000
SE	.124+09	.120+09	.108+09	.903+08	.704+08	.751+07	.000	.000	.000	.000
SE	.120+09	.116+09	.104+09	.875+08	.682+08	.727+07	.000	.000	.000	.000
SE	.117+09	.113+09	.101+09	.847+08	.660+08	.704+07	.000	.000	.000	.000
SE	.113+09	.109+09	.979+08	.819+08	.639+08	.682+07	.000	.000	.000	.000
SE	.109+09	.105+09	.948+08	.793+08	.618+08	.660+07	.000	.000	.000	.000
SE	.106+09	.102+09	.917+08	.768+08	.598+08	.639+07	.000	.000	.000	.000
SE	.102+09	.988+08	.888+08	.743+08	.579+08	.618+07	.000	.000	.000	.000
SE	.991+08	.957+08	.860+08	.719+08	.561+08	.598+07	.000	.000	.000	.000
SE	.959+08	.926+08	.832+08	.696+08	.543+08	.579+07	.000	.000	.000	.000
SE	.913+08	.881+08	.792+08	.663+08	.516+08	.551+07	.000	.000	.000	.000
SE	.795+08	.767+08	.690+08	.577+08	.450+08	.480+07	.000	.000	.000	.000
SE	.522+08	.504+08	.453+08	.379+08	.295+08	.315+07	.000	.000	.000	.000
SE	.158+08	.152+08	.137+08	.114+08	.891+07	.951+06	.000	.000	.000	.000
SE	.465+06	.449+06	.403+06	.338+06	.263+06	.281+05	.000	.000	.000	.000
SE	.199+03	.192+03	.173+03	.145+03	.113+03	.000	.000	.000	.000	.000
SE	.000	.000	.000	.000	.000	.000	.000	.000	.000	.000
SE	.000	.000	.000	.000	.000	.000	.000	.000	.000	.000

TIME# .202-08 K# 2 POWER# .201+03WATTS  
 RF# .00000 .00033 .00067 .00100 .00133  
 Z# -.00010 .0 .0 .0 .0  
 Z# .00010 20.7 20.0 18.0 15.0 11.7  
 Z# .00030 9.4 9.1 8.1 6.8 5.3  
 Z# .00050 .3 .2 .2 .2 .1

TIME# .443-08 K# 3 POWER# .201+03WATTS

TIME= .734-08 K= 4 POWER= .201+03WATTS

TIME= .108-07 K= 5 POWER= .201+03WATTS

R=	.00000	.00033	.00067	.00100	.00133
Z=	.00010	.0	.0	.0	.0
Z=	.00010	111.2	107.3	96.5	80.7
Z=	.00030	50.4	48.7	43.7	36.6
Z=	.00050	1.4	1.3	1.2	1.0

TIME= .150-07 K= 6 POWER= .201+03WATTS

R=	.00000	.00033	.00067	.00100	.00133
Z=	.00010	.0	.0	.0	.0
Z=	.00010	154.2	148.8	133.7	111.9
Z=	.00030	69.9	67.5	60.6	50.7
Z=	.00050	1.9	1.8	1.6	1.4

TIME= .200-07 K= 7 POWER= .201+03WATTS

TIME= .260-07 K= 8 POWER= .201+03WATTS

TIME= .333-07 K= 9 POWER= .201+03WATTS

R=	.00000	.00033	.00067	.00100	.00133
Z=	.00010	.1	.1	.0	.0
Z=	.00010	154.1	148.7	133.6	111.8
Z=	.00030	69.9	67.5	60.6	50.7
Z=	.00050	1.9	1.9	1.7	1.4

TIME= .419-07 K=10 POWER= .201+03WATTS

TIME= .523-07 K=11 POWER= .201+03WATTS

TIME= .648-07 K=12 POWER= .201+03WATTS

R=	.00000	.00033	.00067	.00100	.00133
Z=	.00010	.1	.1	.1	.1
Z=	.00010	153.8	148.4	133.4	111.7
Z=	.00030	69.9	67.5	60.6	50.8
Z=	.00050	2.0	1.9	1.7	1.4

TIME= .798-07 K=13 POWER= .201+03WATTS

TIME= .978-07 K=14 POWER= .201+03WATTS

TIME= .119-06 K=15 POWER= .201+03WATTS

R=	.00000	.00033	.00067	.00100	.00133
Z=	.00010	.3	.2	.2	.2
Z=	.00010	153.4	148.1	133.1	111.4
Z=	.00030	69.9	67.5	60.7	50.8
Z=	.00050	2.1	2.0	1.8	1.5

TIME= .145-06 K=16 POWER= .201+03WATTS

TIME= .176-06 K=17 POWER= .201+03WATTS

TIME= .214-06 K=18 POWER= .201+03WATTS

R=	.00000	.00033	.00067	.00100	.00133
Z=	.00010	.5	.4	.4	.3
Z=	.00010	152.8	147.4	132.5	110.9

Z= .00030	70.0	67.5	60.7	50.8	39.6
Z= .00050	2.3	2.2	2.0	1.7	1.3

TIME= .258-06 K=19 POWER= .201+03WATTS

TIME= .312-06 K=20 POWER= .201+03WATTS

TIME= .376-06	K=21	POWER= .201+03WATTS			
R= .00000	.00033	.00067	.00100	.00133	
Z= -.00010	.8	.8	.7	.6	.5
Z= .00010	151.6	146.3	131.4	110.0	85.8
Z= .00030	70.0	67.6	60.7	50.8	39.6
Z= .00050	2.6	2.5	2.3	1.9	1.5

TIME= .454-06 K=22 POWER= .201+03WATTS

TIME= .546-06 K=23 POWER= .201+03WATTS

TIME= .658-06	K=24	POWER= .201+03WATTS			
R= .00000	.00033	.00067	.00100	.00133	
Z= -.00010	1.4	1.4	1.2	1.0	.8
Z= .00010	149.6	144.3	129.7	108.6	84.7
Z= .00030	70.1	67.7	60.8	50.9	39.7
Z= .00050	3.2	3.1	2.7	2.3	1.8

TIME= .791-06 K=25 POWER= .201+03WATTS

TIME= .951-06 K=26 POWER= .201+03WATTS

TIME= .114-05	K=27	POWER= .201+03WATTS			
R= .00000	.00033	.00067	.00100	.00133	
Z= -.00010	2.4	2.4	2.1	1.8	1.4
Z= .00010	146.3	141.1	126.8	106.2	82.8
Z= .00030	70.3	67.8	60.9	51.0	39.8
Z= .00050	4.1	4.0	3.6	3.0	2.3

TIME= .137-05 K=28 POWER= .201+03WATTS

TIME= .165-05 K=29 POWER= .201+03WATTS

TIME= .198-05	K=30	POWER= .201+03WATTS			
R= .00000	.00033	.00067	.00100	.00133	
Z= -.00010	4.1	4.0	3.6	3.0	2.3
Z= .00010	140.8	135.7	122.0	102.2	79.8
Z= .00030	70.4	67.9	61.0	51.1	39.9
Z= .00050	5.7	5.5	4.9	4.1	3.2

TIME= .238-05 K=31 POWER= .201+03WATTS

TIME= .286-05 K=32 POWER= .201+03WATTS

TIME= .343-05	K=33	POWER= .201+03WATTS			
R= .00000	.00033	.00067	.00100	.00133	
Z= -.00010	6.8	6.6	5.9	5.0	3.9
Z= .00010	132.1	127.2	114.4	95.8	74.9
Z= .00030	70.5	67.8	61.0	51.1	39.9
Z= .00050	8.2	7.9	7.1	6.0	4.7

TIME= .412-05 K=34 POWER= .201+03WATTS

TIME= .495-05 K=35 POWER= .201+03WATTS

TIME= .594-05 K=36 POWER= .201+03WATTS

K=	.00000	.00033	.00067	.00100	.00133
Z= .00010	10.9	10.5	9.5	7.9	6.2
Z= .00010	118.9	114.4	102.9	86.2	67.5
Z= .00030	69.9	67.2	60.5	50.7	39.7
Z= .00050	12.1	11.7	10.5	8.8	6.9

DIM= 6.00 LTMAX=2191 DX= .250-04 BI= .300-06

XPDS

1.00	8.00	8.00	7.97	7.94	7.87	7.81	7.68	7.49	7.31
7.14	6.92	6.68	6.40	6.11	5.77	5.43	5.05	4.68	4.31
3.93	3.55	3.18	2.82	2.49	2.17	1.90	1.66	1.46	1.31
1.19	1.11	1.05	1.02	1.01	1.00				

WAVELENGTH= 530.NM TSTEAM= 100. DAMAGE= 149. 50000. 242. 80000

NRUN= 11 PULSE WIDTH= .150-07 NUMBER OF PULSES= 1  
BEAM RADIUS= .250-02CM LESION RADIUS= .100-02CM

TSTEAM= 100.

K=	.00000	.00033	.00067	.00100	.00133
Z= .00010 QD=	.113+02	.117+02	.130+02	.155+02	.199+02

TSTEAM= 200.

K=	.00000	.00033	.00067	.00100	.00133
Z= .00010 QD=	.288+02	.298+02	.332+02	.396+02	.509+02

TSTEAM= 300.

K=	.00000	.00033	.00067	.00100	.00133
Z= .00010 QD=	.470+02	.487+02	.542+02	.647+02	.830+02

TSTEAM= 400.

K=	.00000	.00033	.00067	.00100	.00133
Z= .00010 QD=	.531+02	.550+02	.612+02	.731+02	.938+02

TSTEAM= 500.

K=	.00000	.00033	.00067	.00100	.00133
Z= .00010 QD=	.531+02	.550+02	.612+02	.731+02	.938+02

Z= .100-03CM RADIAL EXTENT OF IRREVERSIBLE DAMAGE= .100+03CM

# MAIN PROGRAM OF RETINAL MODEL

```

1.  COMMON A(20,3),AP,AAV,ACH,APF,ASC,ATS,AVL,R(11,3),RB,RV(11,3),
2.  1CONX(6),CON(29),CUT,DIM,DFLOW(6),DPULSE,DR,DT,DTX,DZ,FL,HR(11),
3.  2IAB(29,11),IRLOUD(6),IFIL,IG,IGX,IHT,IPA,IPC,IPE,IPOF,IPS,IPT,
4.  3IPV,IV(29),JVL,LIM,LPA,LPC,LPE,LPS,LPV,LPX,LTMAX,K,KM,KT,M,M1,M2,
5.  4M3,N,N1,N3,N4,NVL,POX,PR(11),PTIME,QR,R(11),RCO,RIM,RN,RPE,RRT,
6.  SRVL,RSC,S(29,11),SHB,TAV,TCH,TOM,TPE,TVL,TS(2200),TSC,TTS,V(29,11)
7.  6,VC(29,11,60),VSH(29),VSHX(6),WAVEL,XC,XFLOW,XFLOWI(6),XFLOWO(6),
8.  7XPD(60),XT(60),Z(29),ZD(8),ZM
9.  DIMENSION CXC(11),CXR(29),DAMAGE(2,2),DXC(11),DXR(29),FTIME(38),
10.  1FXC(11),FXR(29),JD(50),JD(50),KIT(38),NPT(38),NPULSE(7),NRUN(7),
11.  2QD(29,11),REPET(7),TIMEX(5),XCT(38),VE(20,60,2),VXX(29,11),
12.  3VZ(20,26,8,2),ZT(8),ZTT(8),ZTX(8)
13.  REAL LFSTOM
14.  2 FORMAT(10F7.3)
15.  3 FORMAT(F7.4,3I7)
16.  4 FORMAT(11F7.2)
17.  5 FORMAT(10I7)
18.  6 FORMAT(F7.2,I7,2F7.2)
19.  7 FORMAT(10E7.2)
20.  8 FORMAT(17,3E7.2)
21.  READ(5,4)(FTIME(L),L=1,38)
22.  READ(5,3)RIM,LIM,IFIL,IGX
23.  READ(5,6)KMAX,LIMAX,LESION
24.  *** SET VALUES FOR N,N1,N3,N4, AND DR
25.  N1=4
26.  N=N1+6
27.  N3=N+1
28.  N4=N1+1
29.  READ(5,8)IPOF,POW,CUT
30.  DR=LESION/LIM
31.  IF(IPOF.EQ.0)DR=RIM/(LIM-.5)
32.  READ(5,7)DPULSE
33.  READ(5,5)NTEST,(NRUN(L),L=1,NTEST)
34.  READ(5,7)(REPET(L),L=1,NTEST)
35.  READ(5,5)(NPULSE(L),L=1,NTEST)
36.  READ(5,5)ID1,ID2,JD1,JD2,ITYPE
37.  LPX=1
38.  IF(NTEST.EQ.1.AND.NPULSE(1).EQ.1)LPX=0
39.  IF(DPULSE.GT..3E-8)GO TO 10
40.  *** ADJUST POWER AND PULSE WIDTH FOR EXPOSURES WITH PULSES LESS THAN
41.  *** .3E-8 SEC
42.  POW=POW*DPULSE/.3E-8
43.  DPULSE=.3E-8
44.  10 READ(5,4)TO,FD11,ED12
45.  READ(5,4)TOM,APF,AVL,ACH,ASC,ATS,RCO,RRT,RSC,RPE,WAVEL
46.  READ(5,4)TAV,TPE,TVL,TCH,TSC,RVL
47.  AAV=-ALOG(TOM)/TAV
48.  READ(5,4)(CONX(L),L=1,6)
49.  READ(5,4)(VSHX(L),L=1,6)
50.  READ(5,5)(NPT(L),L=1,38)
51.  READ(5,2)(XCT(L),L=1,38)
52.  READ(5,5)(KIT(L),L=1,38)
53.  *** COMPUTE DI,KM,KT,MP,PTIME,TIME, AND XC
54.  L1=ALOG(DPULSE)/.69315+29.
55.  IF(L1.LT.1)L1=1
56.  IF(L1.GT.38)L1=38
57.  IF(LPX.EQ.1)GO TO 11

```

2  
4  
5

6

7

8

9

10

11

12

13

14

15

16

17

18

19

# MAIN(RETINAL)

```

58. *** ---SINGLE PULSED EXPOSURES
59.   XC=XCT(L1)
60.   NP=NPT(L1)
61.   KT=KTT(L1)
62.   DT=DPULSE*(XC-1.)/(XC**NP-1.)
63.   TIME=DT*(XC**KT-1.)/(XC-1.)
64.   GO TO 13
65. *** ---MULTIPLE PULSED EXPOSURES
66.   11 XC=1.4
67.   NP=5
68.   X1=0.
69.   DO 12 L=1,NTEST
70.   IF(X1.LT.NPULSE(L)/RFPET(L))X1=NPULSE(L)/RFPET(L)
71.   12 CONTINUE
72.   TIME=FTIME(L1)*X1
73.   DT=DPULSE*(XC-1.)/(XC**NP-1.)
74.   KT=ALOG(1.+TIME*(XC-1.)/DT)/ALOG(XC)+1.
75.   PTIME=DPULSE/NP
76.   13 KT=KT+1
77.   KM=NP+1
78.   IF(KT.GT.59)WRITE(6,14)KT
79.   14 FORMAT(1H0,3HKT=,I3,2X,22HTIME DIMENSION TOO LOW)
80.   IF(KT.GT.59)STOP
81. *** CALC. DZ AND I INDICES
82.   M1=7.-6.*(DPULSE**,1)
83.   IF(M1.LT.1)M1=1
84.   M=2*M1+16
85.   M2=M/2
86.   M3=M+1
87.   IPE=M2-M1+2
88.   DZ=TPE/M1-1.F=25
89.   IPA=2
90. *** STORE AXIAL DISTANCES TO INTERFACES OF EYE
91.   ZD(1)=1.E-25
92.   ZD(2)=TAV
93.   ZD(3)=ZD(2)+RPE*TPE
94.   ZD(4)=ZD(3)+(1.-RPF)*TPE
95.   ZD(5)=ZD(4)+TVL
96.   ZD(6)=ZD(5)+TCH
97.   ZD(7)=ZD(6)+TSC
98.   ZD(8)=ZD(7)+10.
99.   CALL GRID
100.  NVL=LPV-IPV+1
101. *** CALCULATE AND STORE I,J INDICES AT WHICH TEMPERATURES ARE PRINTED
102.  ID1=ID1+IPF
103.  ID2=ID2+IPF
104.  IF(ID1.LT.IPA)ID1=IPA
105.  IF(ID2.GT.M)ID2=M
106.  IF(JD2.GT.N)JD2=N
107.  WRITE(6,15)ID1,ID2,JD1,JD2
108.  15 FORMAT(1H0,4HID1=,I2,3X,4HID2=,I2,3X,4HJD1=,I2,3X,4HJD2=,I2)
109.  WRITE(6,18)(R(J),J=1,N3)
110.  18 FORMAT(1H0,2HR=/(1X,10F8.4))
111.  WRITE(6,19)(Z(I),I=1,M3)
112.  19 FORMAT(1H0,2HZ=/(1X,10F8.4))
113.  DO 20 L1=1,NVL
114.  20 IBLOOD(L1)=IPV+L1-1

```

CALL

# MAIN (RETINAL)

```

115. *** CALC. NORMALIZED LASER PROFILES---
116.   DO 21 L=1,N3
117.   21 HR(L)=0.
118.   POW=POW
119.   CALL IMAGE
120.   WRITE(6,26)QP,(PR(L),L=1,N)
121.   26 FORMAT(1H0,3HQP=,E8.3,3X,3HPR=/(1X,10EA,3))
122.   DO 27 J=1,N3
123.   DO 27 I=1,M3
124.   V(I,J)=1.E-10
125.   27 S(I,J)=0.
126.   WRITE(6,28)(HR(J),J=1,N)
127.   28 FORMAT(1H0,3HHR=/(1X,10EA,3))
128.   READ(5,2)SHB,XFLOW,CFLOW
129. *** SET BLOOD FLOW RATES ENTERING AND LEAVING VASCULAR LAYER AS
130. *** FUNCTION OF RADIAL DISTANCE
131.   X2=CFLOW/(3.1416*RVL*RVL)
132.   DFLOW(1)=0.
133.   X4=0.
134.   DO 30 L1=2.6
135.   X4=X4+.1
136.   30 DFLOW(L1)=X4
137.   DO 31 L1=1.6
138.   XFLOWI(L1)=X2
139.   31 XFLOWO(L1)=X2
140.   WRITE(6,32)(REPET(L),L=1,NTEST)
141.   32 FORMAT(1H0,6HREPET=/(1X,10FA,3))
142.   WRITE(6,33)(NPULSE(L),L=1,NTEST)
143.   33 FORMAT(1H0,7HNPULSE=/(1X,10IA))
144.   DO 34 T=1,M3
145.   DO 34 J=1,N3
146.   34 VC(I,J,1)=1.E-10
147.   WRITE(6,35)AAV,ACH,APE,ASC,ATS,AVL,CFLOW,DPULSE,DR,DT,DZ,IFIL,IPA,
148.   1,IPC,IPE,IPS,IP1,IPV,JVL,KM,KT,LIM,LPA,LPC,LPE,LPS,LPV,M,M1,N,N1,
149.   2NP,NTEST,NVL,POW,PTIME,QP,RCD,RIM,RPE,RRT,RVL,SHB,TAV,TCH,TIME,
150.   3TOM,TPE,TSC,TVL,T0,XC,XFLOW
151.   35 FORMAT(1H0,4HAAV=,F7.1,2X,4HACH=,F7.0,2X,4HAPE=,F7.0,2X,4HASC=,F7.
152.   10,2X,4HATS=,F7.0/1X,4HAVL=,F7.0,2X,6HCFLOW=,F7.4,2X,7HDPULSE=,E8.3
153.   2,2X,3HDR=,E8.3/1X,3HDT=,E8.3,2X,3HDZ=,E8.3,2X,5HTFIL=,I1,2X,4HTPA=
154.   3,12,2X,4HIPC=,I2,2X,4HIPF=,I2,2X,4HIPS=,I2/1X,4HTPT=,I2,2X,4HIPV=,
155.   4I2,2X,4HJVL=,I2,2X,3HKM=,I2,2X,3HKT=,I2,2X,4HLIM=,I2,2X,4HLPA=,I2,
156.   52X,4HLPC=,I2/1X,4HLPE=,I2,2X,4HLPS=,I2,2X,4HLPV=,I2,2X,2HM=,I2,2X,
157.   63HM1=,I2,2X,2HN=,I2,2X,3HN1=,I2,2X,3HNP=,I2/1X,6HNTEST=,I2,2X,4HNV
158.   7L=,I2,2X,4HPO=,E8.3,2X,6HPTIME=,E8.3,2X,3HQP=,E8.3,2X,4HRCO=,F7.4
159.   8/1X,4HRIM=,E8.4,2X,4HRPE=,F7.4,2X,4HRRT=,F7.4,2X,4HRVL=,E8.3,2X,4H
160.   9SHB=,F7.2/1X,4HTAV=,E8.3,2X,4HTCH=,E8.3,2X,5HTIME=,E8.3,2X,4HTOM=,
161.   1F7.4,2X,4HTPE=,E8.3/1X,4HTSC=,E8.3,2X,4HTVL=,E8.3,2X,3HTO=,F5.1,2X
162.   2,3HXC=,F5.1,2X,6HXFLOW=,F7.4)
163.   READ(5,8)KTYPE0
164.   READ(5,8)KTYPE
165.   L1=KTYPE
166.   IF(KTYPE.EQ.0) L1=1
167.   READ(5,7)(TIMEX(K),K=1,L1)
168.   READ(5,5)II1,II2,II3,JJ1,JJ2
169. *** START OF TEMPERATURE CALCULATIONS FOR ONE PULSE. TO BE USED EITHER
170. *** FOR MULTIPLE OR SINGLE PULSED EXPOSURES
171. -----

```

CALI  
---

20

---

---

---

---

---

20A

21

22

23



# MAIN (RETINAL)

```

172.      XT(1)=0.
173.      DTX=DT
174.      KTX=KT+1
175.      DO 36 K=2,KTX
176.      XT(K)=XT(K-1)+DT
177. 36    DT=XC*DT
178.      IKX=TIME**FDT1+EDT2
179.      IF(IKX.LT.1)IKX=1
180.      XX=2*IKX
181.      WRITE(6,37)IKX
182. 37    FORMAT(1H0,4HIKX=,I2)
183.      K=2
184.      IHT=2
185.      IYPEX=ITYPE
186.      CALL BLOOD
187. 38    DT=XT(K)-XT(K-1)
188.      IF(K.GT.KM)GP=0.
189.      CALL HTXDEP
190.      IF(K.GT.2)GO TO 41
191.      DO 40 I=IPA,M
192.      WRITE(6,39)(S(I,J),J=1,N)
193. 39    FORMAT(1H ,2HS=,10E8.3)
194.      40 CONTINUE
195.      41 WRITE(6,42)XT(K),K,PDW
196.      42 FORMAT(1H0,5HTIME=,E8.3,3X,2HK=,I2,3X,6HPOWER=,E8.3,5HWATTS)
197.  *** CALCULATE TEMPERATURE RISE (MATRIX REDUCTION ALGORITHM)
198.      IK=1
199.  *** COLUMNS (NORMAL) -----
200.      43 DO 45 I=IPA,M
201.      W=XX*VSH(I)/DT
202.      DO 44 J=1,N
203.      FXC(J)=W+CON(I)*R(J,2)-BV(J,2)*IV(I)-BR*IAR(I,J)
204.      IF(J.GT.1)FXC(J)=FXC(J)+(CON(I)*R(J,1)+BV(J,1)*IV(I))*CXC(J-1)
205.      CXC(J)=- (CON(I)*R(J,3)+BV(J,3)*IV(I))/FXC(J)
206.      SUM=(W-(A(I,2)-BV(J,2)*IV(I)-BR*IAR(I,J))*V(I,J)+A(I,1)*V(I-1,J)+
207.      1A(I,3)*V(I+1,J)+S(I,J)
208.      DXC(J)=SUM/FXC(J)
209.      IF(J.GT.1)DXC(J)=(SUM+(CON(I)*R(J,1)+BV(J,1)*IV(I))*DXC(J-1))/FXC(
210.      1J)
211.      44 CONTINUE
212.      VX=0.
213.      DO 45 L=1,N
214.      J=N+1-L
215.      VX=DXC(J)-CXC(J)*VX
216.      45 VXX(I,J)=VX
217.      DO 46 I=JPA,M
218.      DO 46 J=1,N
219.      46 V(I,J)=VXX(I,J)
220.  *** ROWS (NORMAL) -----
221.      CXR(JPA-1)=0.
222.      DO 50 J=1,N
223.      DO 48 I=IPA,M
224.      W=XX*VSH(I)/DT
225.      FXR(I)=W+A(I,2)-BV(J,2)*IV(I)-BR*IAR(I,J)+A(I,1)*CXR(I-1)
226.      CXR(I)=-A(I,3)/FXR(I)
227.      SUM=(W-(CON(I)*R(J,2)-BV(J,2)*IV(I)-BR*IAR(I,J))*V(I,J)+(CON(I)*
228.      1B(J,3)+BV(J,3)*IV(I))*V(I,J+1)+S(I,J)

```

# MAIN (RETINAL)

```

229. IF(J.GT.1)SUM=SUM+(CON(I)*R(J,1)+BV(J,1)*IV(T))*V(T,J-1)
230. DXR(I)=SUM/FXR(I)
231. IF(I.GT.IPA)DXR(I)=(SUM+A(T,1)*DXR(I-1))/FXR(I)
232. 48 CONTINUE
233. VX=0.
234. DO 50 L=IPA,M
235. I=M+IPA-L
236. VX=DXR(I)-C(R(I))*VX
237. VC(I,J,K)=VX
238. 50 VXX(I,J)=VX
239. DO 51 I=IPA,M
240. DO 51 J=1,N
241. 51 V(I,J)=VXX(I,J)
242. IK=IK+1
243. *** RECYCLE TEMPERATURE CALCULATIONS
244. IF(IK.LE.IKX)GO TO 43
245. IF(K.EQ.KM)GO TO 62
246. IF(ITYPEX.LT.ITYPE.AND.K.LT.KT)GO TO 64
247. 62 WRITE(6,63)(R(J),J=JD1,JD2)
248. 63 FORMAT(1H,10X,2HR=,9F8.5/13X,30H-----)
249. DO 65 I=ID1,ID2
250. X1=Z(I)-Z(IPE)+DZ/2.
251. WRITE(6,64)X1,(VC(I,J,K),J=JD1,JD2)
252. 64 FORMAT(1H,2HZ=,F8.5,2X,9F8.1)
253. 65 CONTINUE
254. ITYPEX=0
255. 66 K=K+1
256. ITYPEX=ITYPEX+1
257. IF(K.LF.KT)GO TO 38
258. *** READ NORMALIZED TEMPERATURE RISES TS OF GRANULES FOR .3E-8 PULSE
259. *** AND CALCULATE NORMALIZED RISFS XPD FOR ACTUAL PULSE
260. READ(5,6)DJM,LTMAX
261. 70 FORMAT(1H0,61H DIMENSION OF ARRAYS ASSOCIATED WITH ARGUMENT LIJ IS
262. 1 TOO SMALL)
263. DO 71 L=1,LTMAX
264. 71 TS(L)=1.
265. READ(5,2)(TS(L),L=1,LTMAX,10)
266. CALL MXGRAN
267. DO 72 L=1,K1
268. 72 XPD(L)=AP*XPD(L)+1.-AP
269. READ(5,4)(DAMAGE(L2,1),DAMAGE(L2,2),L2=1,2),TSTEAM,DTSTM
270. WRITE(6,73)WAVELENGTH,TSIFAM,DAMAGE(1,1),DAMAGE(1,2),DAMAGE(2,1),
271. 1 DAMAGE(2,2)
272. 73 FORMAT(1H0,11HWAVELENGTH=,F6.0,2HNM,3X,7HTSTEAM=,F6.0,3X,7HDAMAGE=
273. 1,4F9.0)
274. *** CALCULATE I,J INDICES AT WHICH DAMAGE CALCULATIONS ARE TO BE MADE
275. JM=0
276. DO 74 J=1,N
277. IF(R(J).LT.RMAX+.000001)JM=J+1
278. 74 CONTINUE
279. X1=0.
280. DO 75 I=IPA,M
281. IF(VC(I,1,KM).GT.X1)IMAX=I
282. IF(VC(I,1,KM).GT.X1)X1=VC(I,1,KM)
283. 75 CONTINUE
284. L=0
285. ID1=IMAX-LIMAX

```

# MAIN (RETINAL)

```

286.      I02=IMAX+LIMAX
287.      DO 76 I=I01,I02
288.      DO 76 J=1,JM
289.      L=L+1
290.      ID(L)=I
291. 76    JD(L)=J
292.      LIJ=(I02-I01+1)*JM
293.      IF(LIJ.GT.20)WRITE(6,70)
294.      IF(LIJ.GT.20)STOP
295.      IF(LPX.EQ.0)GO TO 125
296. ***  TEMPERATURE AND DAMAGE EVALUATIONS FOR MULTIPLE PULSES
297.      -----
298. ***  EVALUATE  TEMPERATURE RISES WITH AND WITHOUT GRANULES
299.      DO 77 L=1,LIJ
300.      I=ID(L)
301.      J=JD(L)
302.      VE(L,1,1)=0.
303.      VE(L,1,2)=0.
304.      DO 77 K=2,KT
305.      VE(L,K,1)=VC(I,J,K)
306.      VE(L,K,2)=VC(I,J,K)
307.      IF(1.NE.IG)GO TO 77
308.      VE(L,K,2)=XPD(K)*VC(I,J,K)
309.      IF(VE(L,K,1).LT..0)VE(L,K,1)=0.
310.      IF(VE(L,K,2).LT..0)VE(L,K,2)=0.
311. 77    CONTINUE
312.      X60=(XC-1.)/DIX
313.      X61=ALOG(XC)
314.      XSTEAM=1STEAM
315.      DO 108 L13=1,NTEST
316.      X3=NPULSEF+(NPULSEF(L13)-1)/REPET(L13)
317.      WRITE(6,78)NRUN(L13),X3,DPULSE,NPULSEF(L13),RPF1(L13)
318. 78    FORMAT(1H0,5HNPUN=,I3,2X,13HTRAIN LENGTH=,E8.3,3HSEC,2X,12HPULSE W
319.      1IDTH=,E8.3,2X,3HSEC/1X,17HNUMBER OF PULSES=,I5,3X,16HREPETITION RA
320.      2TE=,E8.3,10HPULSES/SEC)
321.      IF(1F1L.EQ.0)GO TO 80
322.      WRITE(6,79)RTM,LFSTION
323. 79    FORMAT(1H ,12HBEAM RADIUS=,E8.3,2HCM,5X,14HLESION RADIUS=,E8.3,2HC
324.      1M)
325.      GO TO 82
326. 80    WRITE(6,81)RTM,LESTION
327. 81    FORMAT(1H ,13HIMAGE RADIUS=,E8.3,2HCM,5X,14HLESION RADIUS=,E8.3,2HC
328.      1CM)
329. 82    TC=1./REPET(L13)
330.      NPL=NPULSE(L13)
331.      KX=NP+3
332.      IN=1
333. 83    IF(NPL/IN.LI.20)GO TO 84
334.      IN=IN+2
335.      GO TO 83
336. 84    X1=NPL
337.      INX=.5+X1/IN
338.      L1=ALOG(DPULSE)/.69315+29.
339.      IF(L1.LI.1)L1=1
340.      INXX=FTIME(L1)*INX
341. ***  STORE TIME INTERVALS AND LOGS OF INTERVALS FOR DAMAGE CALCULATIONS
342.      ZIX(1)=PTIME

```

# MAIN (RETINAL)

```

343. ZT(1)=PTIME/2.
344. ZTT(1)=ALOG(IN*PTIME)
345. DO 85 L3=2,NP
346. ZTT(L3)=ALOG(IN*PTIME)
347. ZTX(L3)=ZTX(L3-1)+PTIME
348. 85 ZT(L3)=ZT(L3-1)+PTIME
349. L1=NP+1
350. X3=(TC-DPULSE)/(KX-NP)
351. ZTX(L1)=DPULSE+X3
352. ZT(L1)=DPULSE+X3/2.
353. ZTT(L1)=ALOG(IN*X3)
354. L1=L1+1
355. DO 86 L3=L1,KX
356. ZTT(L3)=ALOG(IN*X3)
357. ZTX(L3)=ZTX(L3-1)+X3
358. 86 ZT(L3)=ZT(L3-1)+X3
359. *** CALCULATE TEMPERATURE RISES ASSOCIATED WITH L3-TH TIME INTERVAL
360. *** FOLLOWING (L6=.5)*IN=.5 PULSE
361. DO 95 L=1,L1J
362. DO 95 L3=1,KX
363. X1=0.
364. X2=0.
365. L1=1+IN/2
366. L7=1
367. 87 X3=(L7-1)*TC+ZT(L3)
368. K=ALOG(X3*X60+1.)/X61+1.
369. X5=VE(L,K,1)+(X3-XT(K))*(VE(L,K+1,1)-VE(L,K,1))/(XT(K+1)-XT(K))
370. X1=X1+X5
371. X3=(L7-1)*TC+ZTX(L3)
372. K=ALOG(X3*X60+1.)/X61+1.
373. X2=X2+VE(L,K,2)+(X3-XT(K))*(VE(L,K+1,2)-VE(L,K,2))/(XT(K+1)-XT(K))
374. IF(X5.LT..0001*X1)GO TO 88
375. L7=L7+1
376. IF(L7.LE.L1)GO TO 87
377. 88 VZ(L,L3,1)=X1
378. VZ(L,L3,2)=X2
379. DO 93 L6=2,INXX
380. IF(X5.LT..0001*X1)GO TO 91
381. X1=VZ(L,L6-1,L3,1)
382. X2=VZ(L,L6-1,L3,2)
383. L2=L1+1
384. L1=L1+IN
385. L7=L2
386. 90 X3=(L7-1)*TC+ZT(L3)
387. K=ALOG(X3*X60+1.)/X61+1.
388. X5=VE(L,K,1)+(X3-XT(K))*(VE(L,K+1,1)-VE(L,K,1))/(XT(K+1)-XT(K))
389. X1=X1+X5
390. X3=(L7-1)*TC+ZTX(L3)
391. K=ALOG(X3*X60+1.)/X61+1.
392. X2=X2+VE(L,K,2)+(X3-XT(K))*(VE(L,K+1,2)-VE(L,K,2))/(XT(K+1)-XT(K))
393. IF(X5.LT..0001*X1)GO TO 91
394. L7=L7+1
395. IF(L7.LE.L1)GO TO 90
396. 91 VZ(L,L6,L3,1)=X1
397. 93 VZ(L,L6,L3,2)=X2
398. L1=INX+1
399. DO 94 L6=L1,INXX

```

# MAIN (RETINAL)

```

400.      LB=L6-1NX
401.      VZ(L,L6,L3,1)=VZ(L,L6,L3,1)-VZ(L,L8,L3,1)
402.      94 VZ(L,L6,L3,2)=VZ(L,L6,L3,2)-VZ(L,L8,L3,2)
403.      95 CONTINUE
404.      *** DAMAGE CALCULATIONS -----
405.      TSTEAM=XSTEAM
406.      XQ=0.
407.      96 WRITE(6,130)TSTEAM
408.      DO 104 L=1,LIJ
409.      I=ID(L)
410.      J=JU(L)
411.      IF(VZ(L,1NX,NP,1).LT..001)QD(I,J)=1.F+20
412.      IF(VZ(L,1NX,NP,1).LT..001)GO TO 104
413.      L9=10.*(1.4+EXP(-.0014*DPULSE))/VZ(L,1NX,NP,1)
414.      CQ=L9+1.
415.      X10=70.*(1.4+EXP(-.0014*DPULSE))/VZ(L,1NX,NP,1)
416.      IF(L9.EQ.0)CQ=X10
417.      LLT=0
418.      LGT=0
419.      99 DAMC=0.
420.      L6=1
421.      100 DO 101 L3=1,KX
422.      X3=0.
423.      IF(VZ(L,L6,L3,2)*CQ.GT.TSTEAM-T0)X3=1.F+30
424.      IF(VZ(L,L6,L3,2)*CQ.GT.TSTEAM-T0)GO TO 101
425.      X50=VZ(L,L6,L3,1)*CQ+273.+T0
426.      IF(X50.LT.317.)GO TO 101
427.      X1=ZTT(L3)+DAMAGE(1,1)-DAMAGE(1,2)/X50
428.      IF(X50.GT.323.)X1=ZTY(L3)+DAMAGE(2,1)-DAMAGE(2,2)/X50
429.      IF(X1.GT.0.)X3=1.01
430.      IF(X1.GT.0.)GO TO 101
431.      X3=EXP(X1)
432.      101 DAMC=DAMC+X3
433.      IF(DAMC.GT.1.)GO TO 102
434.      *** INCREASE TIME INDICES AND CONTINUE
435.      L6=L6+1
436.      IF(L6.LE.1NXX)GO TO 100
437.      *** ADJUST LASER POWER TO YIELD THRESHOLD DAMAGE AT GIVEN POINT
438.      IF(LGT.EQ.1)CQ=1.02*CQ
439.      IF(LGT.EQ.1)GO TO 103
440.      LLT=1
441.      CQ=1.04*CQ
442.      GO TO 99
443.      102 IF(LLT.EQ.1)CQ=.98*CQ
444.      IF(LLT.EQ.1)GO TO 103
445.      LGT=1
446.      CQ=.96*CQ
447.      GO TO 99
448.      103 QD(I,J)=CQ*POX
449.      104 CONTINUE
450.      WRITE(6,63)(R(J),J=1,JM)
451.      DO 106 I=ID1,ID2
452.      X1=Z(I)-Z(TPE)+DZ/2.
453.      WRITE(6,105)X1,(QD(I,J),J=1,JM)
454.      105 FORMAT(1H ,2H Z=,F7.5,1X,3HQD=,8E8.3)
455.      106 CONTINUE
456.      X2=(XQ-QD(IMAX,1))/QD(IMAX,1)

```

# MAIN (RETINAL)

```

457.      X3=X2*X2
458.      IF(X3.LT..0001)GO TO 108
459.      TSTEAM=TSTEAM+DTSTM
460.      XQ=QD(IMAX+1)
461.      GO TO 96
462. 108  CONTINUE
463.      IF(KTYPE.EQ.0)GO TO 174
464. ***  CALCULATE AND STORE TEMPERATURES FOR PLOTTING TEMPERATURE PROFILES
465.      TC=1./REPET(1)
466.      NPL=NPULSE(1)
467.      DO 123 L15=1,KTYPE
468.      IF(TIMEX(L15).GT.XT(KT))GO TO 123
469.      RGV=0.
470.      L2=TIMFX(L15)/TC
471.      DTIME=TIMEX(L15)-L2*TC
472.      L2=L2+1
473.      DO 116 I=II1,II2
474.      DO 116 J=JJ1,JJ2
475.      X1=0.
476.      DO 113 L6=1,L2
477.      K=ALOG((DTIME+(L6-1)*TC)*X60+1.)/X61+1.
478.      X2=(DTIME+(L6-1)*TC-XT(K))/(XT(K+1)-XT(K))
479. 113  X1=X1+VC(I,J,K)+X2*(VC(I,J,K+1)-VC(I,J,K))
480.      V(I,J)=X1
481.      L3=L2-NPL
482.      IF(L3.LE.0)GO TO 115
483.      X1=0.
484.      DO 114 L6=1,L3
485.      K=ALOG((DTIME+(L6-1)*TC)*X60+1.)/X61+1.
486.      X2=(DTIME+(L6-1)*TC-XT(K))/(XT(K+1)-XT(K))
487. 114  X1=X1+VC(I,J,K)+X2*(VC(I,J,K+1)-VC(I,J,K))
488.      V(I,J)=V(I,J)+X1
489. 115  IF(V(I,J).GT.RGV)RGV=V(I,J)
490. 116  CONTINUE
491.      IF(KTYPEQ.EQ.1)GO TO 121
492.      WRITE(1,117)NRUN(1),NPULSE(1),REPET(1)
493. 117  FORMAT(2I7,F7.1)
494.      WRITE(1,118)DPULSE,WAVEL,RIM
495. 118  FORMAT(10E8,3)
496.      WRITE(1,119)II1,II2,II3,JJ1,JJ2
497. 119  FORMAT(5I7)
498.      WRITE(1,119)N3,M3
499.      WRITE(1,120)(R(J),J=1,N3)
500. 120  FORMAT(10F7,4)
501.      WRITE(1,120)(Z(I),I=1,M3)
502.      WRITE(1,118)TIMEX(L15)
503. 121  DO 122 I=II1,II2
504.      WRITE(6,124)(V(I,J),J=JJ1,JJ2)
505.      IF(KTYPEQ.EQ.1)GO TO 122
506.      WRITE(1,124)(V(I,J),J=JJ1,JJ2)
507. 122  CONTINUE
508. 123  CONTINUE
509. 124  FORMAT(10F7,1)
510.      GO TO 174
511. ***  DAMAGE CALCULATIONS FOR SINGLE PULSE
512. -----
513. 125  WRITE(6,126)NRUN(1),DPULSE,NPULSE(1)

```

# MAIN (RETINAL)

```

514. 126 FORMAT(1H0,5HNRUN=,I3,2X,12HPULSE WIDTH=,E8.3,2X,17HNUMBER OF PULS
515. 1ES=,I5)
516. IF(IF11.EQ.0)GO TO 127
517. WRITE(6,79)RIM.LESION
518. GO TO 128
519. 127 WRITE(6,81)RIM.LESION
520. 128 XQ=0.
521. 129 *WRITE(6,130)TSTEAM
522. 130 FORMAT(1H0,7HYSTEAM=,F7.0/1X,10H-----)
523. DO 138 I=ID1,ID2
524. DO 138 J=1,JM
525. IF(VC(I,J,KM).LT..001)QD(I,J)=1.E+20
526. IF(VC(I,J,KM).LT..001)GO TO 138
527. L9=10.*(1.4+EXP(-.0014*DPULSE))/VC(I,J,KM)
528. CQ=L9+1.
529. X10=70.*(1.4+EXP(-.0014*DPULSE))/VC(I,J,KM)
530. IF(L9.EQ.0)CQ=X10
531. LLT=0
532. LGT=0
533. 131 DAMC=0.
534. K=2
535. 132 X13=ALOG(XT(K)-XT(K-1))
536. VPX=(VC(I,J,K)+VC(I,J,K-1))/2.
537. X3=0.
538. IF(I.NE.IG)GO TO 133
539. IF(VPX*XPDK)*CQ.GT.TSTEAM-T0)X3=1.E+30
540. IF(VPX*XPDK)*CQ.GT.TSTEAM-T0)GO TO 134
541. 133 X50=VF*(CQ+273.+T0
542. IF(X50.LT.317.)GO TO 134
543. X1=X13+DAMAGE(1,1)-DAMAGE(1,2)/X50
544. IF(X50.GT.323.)X1=X13+DAMAGE(2,1)-DAMAGE(2,2)/X50
545. IF(X1.GT.0.)X3=1.01
546. IF(X1.GT.0.)GO TO 134
547. X3=EXP(X1)
548. 134 DAMC=DAMC+X3
549. IF(DAMC.GE.1.)GO TO 135
550. K=K+1
551. IF(K.LT.KT)GO TO 132
552. *** ADJUST LASER POWER TO YIELD THRESHOLD DAMAGE AT GIVEN POINT
553. IF(LGT.EQ.1)CQ=1.02*CQ
554. IF(LGT.EQ.1)GO TO 136
555. LLT=1
556. CQ=1.04*CQ
557. GO TO 131
558. 135 IF(LLT.EQ.1)CQ=.98*CQ
559. IF(LLT.EQ.1)GO TO 136
560. LGT=1
561. CQ=.96*CQ
562. GO TO 131
563. 136 QD(I,J)=CQ*POX
564. 138 CONTINUE
565. WRITE(6,63)(R(J),J=1,JM)
566. DO 143 I=ID1,ID2
567. X1=Z(I)-7(IPE)+D7/2.
568. WRITE(6,105)X1,(QD(I,J),J=1,JM)
569. 143 CONTINUE
570. X2=(XQ-QD(IMAX,1))/QD(IMAX,1)

```

# MAIN (RETINAL)

```

571.      X3=X2*X2
572.      IF(X3.LT..0001)GO TO 150
573.      TSTEAM=TSTEAM+DISIM
574.      XU=QD(IMAX,1)
575.      GO TO 129
576. 150 IF(KTYPE.EQ.9)GO TO 174
577. *** CALCULATE AND STORE TEMPERATURES FOR PLOTTING PROFILE
578.      DO 170 LIS=1,KTYPE
579.      RGV=0.
580.      DTIME=TIME*(XC-1.)/DTX+1.)/ALOG(XC)+1.
581.      K=ALOG(DTIME*(XC-1.)/DTX+1.)/ALOG(XC)+1.
582.      IF(K+1.GT.K1)GO TO 170
583.      X1=(DTIME-XT(K))/(XT(K+1)-XT(K))
584.      DO 166 I=1I1,I12
585.      DO 166 J=JJ1,JJ2
586.      V(I,J)=VC(T,J,K)+X1*(VC(T,J,K+1)-VC(T,J,K))
587.      IF(V(I,J).GT.RGV)RGV=V(I,J)
588. 166 CONTINUE
589.      IF(KTYPE.EQ.1)GO TO 167
590. *** CALCULATE AND STORE TEMPERATURES FOR PLOTTING PROFILE
591.      WRITE(1,117)NRUN(1),NPULSE(1),REPET(1)
592.      WRITE(1,118)DPULSE,KAVFL,RIM
593.      WRITE(1,119)I1,I12,J13,JJ1,JJ2
594.      WRITE(1,119)N3,M3
595.      WRITE(1,120)(R(J),J=1,N3)
596.      WRITE(1,120)(Z(I),I=1,M3)
597.      WRITE(1,118)TIME*(XC-1.)/DTX+1.)/ALOG(XC)+1.
598. 167 DO 168 I=I1,I12
599.      WRITE(6,124)(V(I,J),J=JJ1,JJ2)
600.      IF(KTYPE.EQ.1)GO TO 168
601.      WRITE(1,124)(V(I,J),J=JJ1,JJ2)
602. 168 CONTINUE
603. 170 CONTINUE
604. *** INTERPOLATE AXIAL EXTENT OF DAMAGE
605. 174 IS=0
606.      IS=0
607.      IF(I01.EQ.I02)GO TO 182
608.      DO 175 I=I01,I02
609.      LI=I01+I02-1
610.      IF(QD(LI,1).GT.POX)IS=LI
611.      IF(QD(LI,1).LT.POX)IS=LI
612.      IF(QD(I,1).GT.POX)I7=I
613.      IF(QD(I,1).LT.POX)I8=I
614. 175 CONTINUE
615.      IF(I5.EQ.0)WRITE(6,176)
616. 176 FORMAT(1H0,45HDEPTHS OF DAMAGE BEYOND BOTH SPECIFIED DEPTHS)
617.      IF(I5.EQ.0)GO TO 182
618.      IF(I6.EQ.0)GO TO 190
619.      IF(I5.GE.I6)GO TO 178
620.      X2=ALOG(QD(I6,1)/QD(I5,1))/(Z(I6)-Z(I5))
621.      X1=QD(I5,1)
622.      X3=ALOG(POX/X1)/X2+Z(I5)-Z(IPE)+DZ/2.
623.      WRITE(6,177)X3
624. 177 FORMAT(1H0,24HMINIMUM DEPTH OF DAMAGE=,E8.3,2HCM)
625. 178 IF(I8.GE.I7)GO TO 182
626.      X2=ALOG(QD(I8,1)/QD(I7,1))/(Z(I8)-Z(I7))
627.      X1=QD(I7,1)

```



# MAIN (RETINAL)

```

628.      X3=ALOG(POX/X1)/X2+Z(17)-Z(1PE)+DZ/2.
629. 180  WRITE(6,181)X3
630. 181  FORMAT(1H0,24HMAXIMUM DEPTH OF DAMAGE=,E8.3,2HCM)
631. ***  INTERPOLATE RADIAL EXTENT OF IRREVERSIBLE DAMAGE AT SPECIFIED DEPTHS
632. 182  DO 189 I=ID1,ID2
633.      J1=0
634.      X3=Z(1)-7(1PE)+DZ/2.
635.      DO 183 J=1,JM
636.      IF(POX.GT.QD(I,J))J1=J
637. 183  CONTINUE
638.      X20=0.
639.      IF(J1.EQ.0)GO TO 187
640.      IF(J1.EQ.JM)WRITE(6,185)X3,R(JM)
641. 185  FORMAT(1H0,2HZ=,F8.3,2HCM,5X,36HRADIAL EXTENT OF DAMAGE GREATER TH
642.      1AN,E8.3,2HCM)
643.      IF(J1.EQ.JM)GO TO 189
644.      X2=ALOG(QD(I,J1+1)/QD(I,J1))/(R(J1+1)-R(J1))
645.      X1=QD(I,J1)
646.      X20=ALOG(POX/X1)/X2+R(J1)
647. 187  WRITE(6,188)X3,X20
648. 188  FORMAT(1H0,2HZ=,F8.3,2HCM,5X,37HRADIAL EXTENT OF IRREVERSIBLE DAMA
649.      1GE=,E8.3,2HCM)
650. 189  CONTINUE
651.      STOP
652. 190  WRITE(6,191)
653. 191  FORMAT(1H0,31HNO DAMAGE---LASER POWER TOO LOW)
654.      STOP
655.      END

```

# SUBROUTINE GRID(RETINAL)

```

1. SUBROUTINE GRID
2. *** GRID COMPUTES THE COEFFICIENTS IN PARTIAL DIFFERENTIAL EQUATIONS A AND B
3. *** RADIAL AND AXIAL COORDINATES, R AND Z, AND ASSIGNS CONDUCTIVITY AND
4. *** VOLUMETRIC SPECIFIC HEAT TO GRID
5. COMMON A(29,3),AP,AAV,ACH,APE,ASC,ATS,AVL,R(11,3),RB,BV(11,3),
6. 1CONX(6),CUN(29),CUT,DIM,DFLOW(6),DPULSE,DR,DT,DTX,DZ,FL,HR(11),
7. 2IAB(29,11),1HLODD(6),IFIL,IG,IGX,IHT,IPA,IPC,IFE,IPROF,IPS,IPT,
8. 3IPV,IV(29),JVL,LIM,LPA,LPC,LPE,LPS,LPV,LPX,LTMAX,K,KM,KT,M,M1,M2,
9. 4M3,N,N1,N3,N4,NVL,POX,PR(11),PTIME,QP,R(11),RCO,RIM,RN,RPE,RRT,
10. 5RVL,RSC,S(29,11),SHB,TAV,TCH,TOM,TPE,TVL,TS(2200),TSC,TTS,V(29,11)
11. 6,VC(29,11,60),VSH(29),VSHX(6),WAVEL,XC,XFLOW,XFLOWI(6),XFLOWO(6),
12. 7XPD(60),XT(60),Z(29),ZD(R),ZM
13. DIMENSION IX(7),LX(7)
14.
15. R(1)=0.
16. CK=N-N1
17. CP=RVL/DR-N1+1.
18. X1=2.
19. 180 R2=EXP(ALOG(2.*(CP*(X1-1.)+1.)/(X1+1.))/(CK-1.))
20. IF(R2/X1.GT..99999.AND.R2/X1.LT.1.00001)GO TO 183
21. X1=R2
22. GO TO 180
23. 183 WRITE(6,184)R2
24. 184 FORMAT(1H,3HR2=,F8.4)
25. RN=DR*(N1-1.+(R2*(CK+1.)-1.)/(R2-1.))
26. *** CALCULATE RADIAL SPACE STEPS R(J)
27. DO 185 J=2,N4
28. 185 R(J)=DR*(J-1)
29. X1=R2*DR
30. DO 186 J=N4,N
31. R(J+1)=R(J)+X1
32. 186 X1=R2*X1
33. *** CALCULATE COEFFICIENTS B OF FINITE DIFFERENCE EQNS.
34. X1=2./(DR*DR)
35. DO 187 J=2,N1
36. B(J,1)=.25*(2*J-3)*X1/(J-1)
37. B(J,2)=X1
38. 187 B(J,3)=X1-B(J,1)
39. X2=DR
40. X1=R2*DR
41. DO 188 J=N4,N
42. B(J,2)=2./(X1*X2)
43. B(J,1)=(2./X2-1./R(J))/(X1+X2)
44. B(J,3)=B(J,2)-B(J,1)
45. X2=R2*X2
46. 188 X1=R2*X1
47. B(1,1)=0.
48. B(1,2)=2./(DR*DR)
49. B(1,3)=B(1,2)
50. DO 189 J=1,N
51. IF(R(J).LI.RVL)JVL=J
52. 189 CONTINUE
53. *** CALCULATE AXIAL SPACE STEPS Z(J)
54. CK=M2-M1+1
55. X1=2.
56. 190 CP=2.*TAV/DZ+1.-(X1*(CK-1.)-1.)/(X1-1.)
57. R1=EXP(ALOG(CP*X1-CP+1.)/CK)

```

# GRID(RETINAL)

```

58. IF(R1/X1.GT..99999.AND.R1/X1.LT.1.00001)GO TO 192
59. X1=R1
60. GU TO 190
61. 192 ZM=((R1**CK-1.)/(R1-1.)+M1-1.)*DZ
62. WRITE(6,194)R1,ZM
63. 194 FORMAT(1H ,3HR1=,F8.4,2X,3HZM=,F8.4)
64. X1=0Z
65. X2=X1
66. DO 195 I=2,M2
67. Z(M2+I)=7M+X2
68. Z(M2+2-I)=ZM-X2
69. IF(1.GT.M1)X1=R1*X1
70. 195 X2=X2+X1
71. Z(1)=0.
72. Z(M2+1)=ZM
73. Z(M+1)=2.*ZM
74. X1=Z(1PE)-DZ/2.-ZD(2)
75. DO 196 I=1,M3
76. 196 Z(I)=Z(1)-X1
77. L3=IPA
78. DO 200 L=1,7
79. L1=0
80. DO 197 I=1PA,M3
81. IF(Z(1).LT.ZD(L+1))L3=I
82. IF(Z(1).LT.ZD(L).OR.Z(I).GE.ZD(L+1))GO TO 197
83. L2=1
84. L1=L1+1
85. 197 CONTINUE
86. IF(L1.EQ.0)IX(L)=L3
87. IF(L1.EQ.0)LX(L)=L3
88. IF(L1.GT.0)IX(L)=L2+1-L1
89. IF(L1.GT.0)LX(L)=L2
90. 200 CONTINUE
91. IPV=IX(4)
92. IPC=IX(5)
93. IPS=IX(6)
94. IPT=IX(7)
95. LPA=LX(1)
96. LPE=LX(3)
97. LPV=LX(4)
98. LPC=LX(5)
99. LPS=LX(6)
100. LPT=M3
101. *** SET CONDUCTIVITY CON AND HEAT CAPACITY VSH FOR VARIOUS EYE MEDIA
102. DO 203 I=1,LPA
103. CON(I)=CONX(1)
104. 203 VSH(I)=VSHX(1)
105. DO 204 I=1PE,LPE
106. CON(I)=CONX(2)
107. 204 VSH(I)=VSHX(2)
108. DO 205 I=1PV,LPV
109. CON(I)=CONX(3)
110. 205 VSH(I)=VSHX(3)
111. DO 206 I=1PC,LPC
112. CON(I)=CONX(4)
113. 206 VSH(I)=VSHX(4)
114. DO 207 I=1PS,LPS

```

# GRID(RETINAL)

```

115.      CON(I)=CONX(5)
116. 207  VSH(I)=VSHX(5)
117.      DO 208 I=IPT,M3
118.      CON(I)=CONX(6)
119. 203  VSH(I)=VSHX(6)
120. ***  CALCULATE COEFFICIENTS A OF FINITE DIFFERENCE EQNS.
121.      DO 210 I=IPA,M
122.      X1=Z(I+1)-Z(I-1)
123.      X2=(CON(I-1)-CON(I+1))/(X1*X1)
124.      X3=2.*CON(I)/X1
125.      A(I,1)=X2+X3/(Z(I)-Z(I-1))
126.      IF(I.EQ.IPA)A(I,1)=0.
127.      A(I,3)=-X2+X3/(Z(I+1)-Z(I))
128. 210  A(I,2)=A(I,1)+A(I,3)
129.      RETURN
130.      END

```

# SUBROUTINE IMAGE (RETINAL)

```

1.  SUBROUTINE IMAGE
2.  *** IMAGE COMPUTES THE RETINAL IRRADIANCE PROFILE
3.  COMMON A(29,3),AP,AAV,ACH,ΔPE,ASC,ATS,AVL,R(11,3),RB,BV(11,3),
4.  1CONX(6),CUN(29),CUT,DIM,DFLOW(6),DPULSF,DR,DT,DTX,DZ,FL,HR(11),
5.  2IAB(29,11),HLOUD(6),IFIL,IG,IGX,IHT,IPA,IPC,IPE,IPROF,IPS,IPT,
6.  3IPV,IV(29),JVL,LIM,LPA,LPC,LPE,LPS,LPV,LPX,LTMAX,K,KM,KT,M,M1,M2,
7.  4M3,N,N1,N3,N4,NVL,POX,PR(11),PTIME,QP,R(11),RCN,RIM,RN,RPE,RRT,
8.  5KVL,RSC,S(29,11),SHB,TAV,TCH,TOM,TPE,TVL,TS(2200),TSC,TTS,V(29,11)
9.  6,VC(29,11,60),VSH(29),VSHX(6),WAVEL,XC,XFLOW,XFLOWI(6),XFLOWO(6),
10.  7XPD(60),XI(60),Z(29),ZD(R),ZM
11.  DIMENSION FA(501),FF(501),FX(501),FY(501),JO(32),NA(22),PX(30),
12.  1RX(30),XF1(501),XF2(501)
13.  REAL JO,NA,NR,NC
14.  DO 200 J=1,N
15.  200 PX(J)=0.
16.  LI=500
17.  L11=LI
18.  DO 201 L=1,LI
19.  201 FX(L)=0.
20.  READ(5,202)PUPIL
21.  202 FORMAT(10E8,3)
22.  WRITE(6,203)PUPIL
23.  203 FORMAT(1H0,6HPUPIL=,F7.3)
24.  RINT=PUPIL/(LI-1)
25.  IF(IPROF.EQ.1)GO TO 214
26.  IF(IPROF.EQ.0)GO TO 219
27.  *** INTERPOLATE IRREGULAR LASER PROFILE (SYMMETRIC IN R) AT INTERVALS
28.  *** OF RINT STARTING AT R=0
29.  READ(5,205)LR
30.  205 FORMAT(17)
31.  READ(5,206)(RX(L),L=1,LR)
32.  206 FORMAT(10E7,3)
33.  READ(5,206)(PX(L),L=1,LR)
34.  X1=PX(1)
35.  DO 207 L=1,LR
36.  207 PX(L)=PX(L)/X1
37.  X5=0.
38.  X6=0.
39.  DO 208 L=2,LR
40.  X2=(PX(L)-PX(L-1))/(RX(L)-RX(L-1))
41.  X1=PX(L)-X2*RX(L)
42.  X3=X1*(RX(L)*RX(L)-RX(L-1)*RX(L-1))/2.
43.  X4=X2*(RX(L)*RX(L)*RX(L)-RX(L-1)*RX(L-1)*RX(L-1))/3.
44.  IF(RX(L).GT.PUPIL)X6=X6+6.2832*(X3+X4)
45.  208 X5=X5+6.2832*(X3+X4)
46.  QP=POX*.23906*(1.-RCN)/X5
47.  XX=(X5-X6)/X5
48.  IF(RX(LR).LT.PUPIL)L11=RX(LR)/RINT+1
49.  L2=2
50.  X1=0.
51.  DO 213 L=1,L11
52.  210 IF(RX(L2).GT.X1)GO TO 212
53.  L2=L2+1
54.  IF(L2.LE.LR)GO TO 210
55.  GO TO 213
56.  212 X2=(X1-RX(L2-1))/(RX(L2)-RX(L2-1))
57.  FX(L)=PX(L2-1)+X2*(PX(L2)-PX(L2-1))

```

194

---

194\*

194\*\*

194\*\*

# IMAGE (RETINAL)

```

58. 213 X1=X1+RINT
59.     GO TO 223
60. *** CALCULATE GAUSSIAN LASER PROFILE AT INTERVALS OF RINT STARTING AT R=0
61. 214 SIGMA=RIM*SQRT(-2./ALOG(CUT))
62.     WRITE(6,215)SIGMA,RIM
63. 215 FORMAT(1H0,6HSIGMA=,F8.3,5X,4HRIM=,E8.3)
64.     QP=2.*POX*.23906*(1.-RCO)/(3.1416*SIGMA*SIGMA)
65.     XA=1.-EXP(-2.*PUPIL*PUPIL/(SIGMA*SIGMA))
66.     IF(IFIL.EQ.1)GO TO 217
67.     DO 216 J=1,N
68.     X3=2.*R(J)*R(J)/(SIGMA*SIGMA)
69.     IF(X3.GT.80.)GO TO 216
70.     PR(J)=EXP(-X3)
71. 216 CONTINUE
72.     GO TO 276
73. 217 X1=0.
74.     DO 218 L=1,LII
75.     X3=2.*X1*X1/(SIGMA*SIGMA)
76.     FX(L)=0.
77.     IF(X3.GT.80.)GO TO 218
78.     FX(L)=EXP(-X3)
79. 218 X1=X1+RINT
80.     GO TO 227
81. *** SPECIFY UNIFORM LASER PROFILE FROM R(1) TO R(LIM)
82. 219 QP=POX*.23906*(1.-RCO)/(3.1416*RIM*RIM)
83.     XX=1.
84.     IF(RIM.GT.PUPIL)XA=PUPIL*PUPIL/(RIM*RIM)
85.     IF(IFIL.EQ.1)GO TO 221
86.     DO 220 J=1,LIM
87. 220 PR(J)=1.
88.     GO TO 276
89. 221 L1=RIM/RINT
90.     RINT=RIM/L1
91.     LII=RIM/RINT+1
92.     DO 222 L=1,LII
93. 222 FX(L)=1.
94.     GO TO 227
95. *** CALCULATE TOTAL AREA FA(L) AND PORTION OF LASERS POWER BETWEEN R=0
96. *** AND (L-.5)*RINT
97. 223 IF(IFIL.EQ.1)GO TO 227
98.     FP(1)=3.1416*FX(1)*RINT*RINT/4.
99.     FA(1)=3.1416*RINT*RINT/4.
100.    DO 224 L=2,LII
101.    X1=(L-.5)*RINT
102.    X2=(L-1.5)*RINT
103.    FP(L)=FP(L-1)+FX(L)+3.1416*(X1*X1-X2*X2)
104. 224 FA(L)=FA(L-1)+3.1416*(X1*X1-X2*X2)
105. *** CALCULATE PROFILE PR(J)
106.    X1=0.
107.    X2=0.
108.    DO 225 J=1,N
109.    X3=(R(J)+R(J+1))/(2.*RINT)+.5000001
110.    IF(X3.LT.1.)X3=1.0000001
111.    L2=X3
112.    IF(L2.GE.LTI)GO TO 225
113.    X4=X3-L2
114.    X5=FP(L2)+X4*(FP(L2+1)-FP(L2))

```

# IMAGE (RETINAL)

```

115.      X6=FA(L2)+X4*(FA(L2+1)-FA(L2))
116.      PR(J)=(X5-X1)/(X6-X2)
117.      X1=X5
118.      X2=X6
119.225  CONTINUE
120.      GO TO 276
121.***  SPREAD FUNCTION CALCULATIONS
122.227  READ(5,202)Z0,FLO,FC,NB,CABER,PP,PC      19R*
123.      CABER2=CABER/WAVEL
124.      READ(5,228)(JD(L),L=1,32)              19R**
125.228  FORMAT(10F8.5)
126.      READ(5,228)(NA(L),L=1,22)              19R**
127.      X1=(WAVEL-350.)/50.+1.
128.      L1=X1
129.      X2=X1-L1
130.      NC=NA(L1)+X2*(NA(L1+1)-NA(L1))
131.      X1=(NB-1.)*NC/(NB*(NC-1.))
132.      FL=FLO*X1
133.      X2=Z0/FLO
134.      X0=NC*Z0*X1/(NC*X2-X1)-FLO
135.      X3=1.-PC*(NC*Z0-FC)/(NC*Z0*FC)
136.      DO 230 L=1,L1
137.      IF(L.GT.LII)GO TO 230
138.      X1=(L-1)/X3+1.000001
139.      L1=X1
140.      X2=X1-L1
141.      IF(L1+1.GT.LI)FY(L)=0.
142.      IF(L1+1.GT.LI)LII=L
143.      IF(L1+1.GT.LI)GO TO 230
144.      FY(L)=(FX(L1)+X2*(FX(L1+1)-FX(L1)))/(X3*X3)
145. 230  CONTINUE
146.      DO 231 L=1,LII
147. 231  FX(L)=FY(L)
148.      X5=ATAN(PUPIL/(FLO-PP+X0))
149.      X6=1.-COS(X5)
150.      X7=SIN(X5)*SIN(X5)
151.      FF=FLO-PP
152.      DO 23 L=1,LII
153.      X4=(L-1)*RINT
154.      X1=6.2832*NC*(-1+X6*X0+SQRT(FF*FF-X7*X0*X0))*X4*X4/(WAVEL*1.F-7*
155.      1PUPIL*PLPIL)
156.      X2=CABER2*X4*X4*X4*X4
157.      XF1(L)=SQRT(FX(L))*COS(X1+X2)
158. 234  XF2(L)=SQRT(FX(L))*SIN(X1+X2)
159.      WRITE(6,235)RINT,Z0,FLO,CABER,CABER2,PP,PC,NB,NC,WAVEL,FC
160. 235  FORMAT(140,5HRINT=,E8.3,3X,3HZ0=,E8.3,3X,4HFLO=,F6.3,3X,6HCABER=,
161.      1F8.3,3X,7HCCABER2=,F7.0/1X,3HPP=,F6.3,3X,3HPC=,F6.3,3X,3HNB=,F7.3,
162.      23X,3HNC=,F7.3,3X,6HWAVEL=,1.3HFC=,F6.3)
163.      DO 260 J=1,N
164.      X1=6.2832*PR(J)/(WAVEL*1.F-7*FF)
165.      X2=0.
166.      X3=0.
167.      DO 255 L=1,LII
168.      X4=X1*(L-1)*RINT
169.      IF(L.EQ.1)X4=X1*.25*RINT
170.      IF(X4.GT.3.)GO TO 250
171.      X5=X4/.1+1.000001

```

# IMAGE (RETINAL)

```

172.      L1=X5
173.      X1=X5-L1
174.      X7=J0(L1)+X5*(J0(L1+1)-J0(L1))
175.      GO TO 251
176. 250   X6=3./X4
177.      X8=.79788456-.00000077*X6-.00552740*X6*X6-.00009512*X6*X6*X6+
178.      1.00137237*X6*X6*X6*X6-.00072805*X6*X6*X6*X6*X6+.00014476*X6*X6*X6*
179.      2X6*X6*X6
180.      X9=X4-.78539816-.04166397*X6-.00003954*X4*X6+.00262573*X4*X6*X4-
181.      1.00054125*X6*X6*X6*X4-.00029333*X6*X6*X6*X6*X6+.00013558*X6*X6*X6*
182.      2X6*X6*X6
183.      X7=X8*COS(X9)/SQRT(X4)
184. 251   IF(L.GT.1)GO TO 252
185.      X2=X2+X7*.25*(3.*XF1(1)+XF1(2))* .25*PRINT*.5*PRINT
186.      X3=X3+X7*.25*(3.*XF2(1)+XF2(2))* .25*PRINT*.5*PRINT
187.      GO TO 255
188. 252   X2=X2+X7*XF1(L)*(L-1)*PRINT*PRINT
189.      X3=X3+X7*XF2(L)*(L-1)*PRINT*PRINT
190. 255   CONTINUE
191. 260   HR(J)=X2*X2+X3*X3
192.      X1=HR(1)
193.      DO 270 J=1,N
194. 270   HR(J)=HR(J)/X1
195.      X1=.0002
196.      X2=3.1416*X1*X1/4.
197.      J=2
198.      X4=HR(1)*X2
199.      L1=2
200. 271   IF(X1.LT.HR(J)+.0000001)GO TO 272
201.      J=J+1
202.      GO TO 271
203. 272   X5=(X1-HR(J-1))/(HR(J)-HR(J-1))
204.      X6=HR(J-1)+X5*(HR(J)-HR(J-1))
205.      X7=6.*(L1-1)*X2
206.      X4=X4+X6*X7
207.      L1=L1+1
208.      X1=X1+.0002
209.      IF(X1.LE..1)GO TO 271
210.      QP=.23906*XX*POX*(1.-PCQ1/X4
211.      WRITE(6,275)(HR(J),J=1,N)
212. 275   FORMAT(1H0,3HHR=/(1X,10E4.3))
213.      RETURN
214. 276   DO 280 J=1,N
215. 280   HR(J)=PR(J)
216.      RETURN
217.      END

```



## SUBROUTINE HTXDEP (RETINAL)

```

1. SUBROUTINE HTXDEP
2. *** HTXDEP COMPUTES RATE OF HEAT DEPOSITION AT VARIOUS POINTS I,J
3. COMMON A(29,3),AP,AAV,ACH,APE,ASC,ATS,AVL,R(11,3),RB,BV(11,3),
4. 1CUNX(6),CUN(29),CUT,DIM,DFLOW(6),DPULSE,DR,DT,DTX,DZ,FL,HR(11),
5. 2IAB(29,11),IBLQUD(6),IFIL,IG,IGX,IHT,IPA,IPC,IPE,IPROF,IPS,IPT,
6. 3IPV,IV(29),JVL,LIM,LPA,LPC,LPE,LPS,LPV,LPX,LTMAX,K,KM,KT,M,M1,M2,
7. 4M3,N,N1,N3,N4,NVL,PUX,PR(11),PTIME,QP,P(11),RCO,RIM,RN,RPE,RRT,
8. 5RVL,RSC,S(29,11),SHB,TAV,TCH,TOM,TPE,TVL,TS(2200),TSC,TTS,V(29,11)
9. 6,VC(29,11,60),VSH(29),VSHA(6),WAVEL,XC,XFLOW,XFLOWI(6),XFLOWO(6),
10. 7XPD(60),XI(60),Z(29),ZD(A),ZM
11. DIMENSION AB(29,3),ARR(29,7),APS(7),II(29),I7(29),PEF(A),REFL(A),
12. 1ZH(29)
13. IF(IHT.EQ.0)RETURN
14. IF(WP.LI.1.E-25)GO TO 340
15. IF(IHT.EQ.1)RETURN
16. LZ=7
17. LZ0=LZ-1
18. LZ1=LZ+1
19. DO 280 I=1,M
20. II(I)=0
21. IZ(I)=0
22. ZH(I)=(Z(I)+Z(I+1))/2.
23. DO 279 LI=1,3
24. 279 AB(I,LI)=0.
25. DO 280 LI=1,LZ
26. 280 ARR(I,LI)=0.
27. DO 282 LI=1,LZ
28. REF(LI)=0.
29. 282 REFL(LI)=0.
30. REF(2)=ARR
31. REF(6)=RSC
32. REF(LZ1)=0.
33. WRITE(6,283)(ZH(I),I=1,M)
34. 283 FORMAT(1H0,3HZH=/(1X,E8,3))
35. *** EVALUATE ABSORPTION CONSTANTS APE1 AND APE2 FOR FRONT AND REAR OF PE.
36. *** WELL AS IG INDICATING I INDEX WHERE GRANULES ARE LOCATED
37. IF(IGX.EQ.1)GO TO 284
38. APE1=(APE-ACH*(1.-RPE))/RPE
39. APE2=ACH
40. AP=(EXP(-ACH*APE*TPE)-EXP(-APE1*RPE*TPE))/(1.-EXP(-APE1*RPE*TPE))
41. IG=IPE
42. GO TO 285
43. 284 APE1=ACH
44. APE2=(APE-ACH*RPE)/(1.-RPE)
45. AP=(EXP(-ACH*(1.-RPE)*TPE)-EXP(-APE2*(1.-RPE)*TPE))/(1.-EXP(-APE2*
46. 1(1.-RPE)*TPE))
47. IG=LPE-(1.001-RPE)*(LPE-IPF+1)+.5
48. 285 WRITE(6,289)AP,APE1,APE2,IG
49. 289 FORMAT(1H0,3HAP=,F7.4,3X,SHAPE1=,F8.2,3X,SHAPE2=,F8.2,3X,3HIG=,I2)
50. ABS(1)=AAV
51. ABS(2)=APE1
52. ABS(3)=APE2
53. ABS(4)=AVL
54. ABS(5)=ACH
55. ABS(6)=ASC
56. ABS(7)=ATS
57. LI=2

```

## HTXDEP (RETINAL)

```

58.      DO 306 I=IPA,M
59. 295  IF(ZH(I-1).LT.ZD(L1))GO TO 296
60.      L1=L1+1
61.      GO TO 295
62. 296  IF(ZH(I).GE.ZD(L1))GO TO 299
63. ***  NO ZD BETWEEN ZH(I-1) AND ZH(I)
64.      AB(I,1)=ABS(L1-1)*(ZH(I)-ZH(I-1))
65.      II(I)=1
66.      IZ(I)=L1
67.      IF(L1.GT.LZ)GO TO 306
68.      DO 297 L2=L1,LZ
69. 297  ABR(I,L2)=AB(I,1)
70.      GO TO 306
71. 299  IF(ZH(I).GE.ZD(L1+1))GO TO 303
72. ***  ONLY ZD(L1) BETWEEN ZH(I-1) AND ZH(I)
73.      AB(I,1)=ABS(L1-1)*(ZD(L1)-ZH(I-1))
74.      AB(I,2)=ABS(L1)*(ZH(I)-ZD(L1))
75.      ABR(I,L1)=AB(I,1)
76.      II(I)=2
77.      IZ(I)=L1
78.      L3=L1+1
79.      IF(L3.GT.LZ)GO TO 306
80.      DO 300 L2=L3,LZ
81. 300  ABR(I,L2)=AB(I,1)+AB(I,2)
82.      GO TO 306
83. ***  ZD(L1) AND ZD(L1+1) BETWEEN ZH(I-1) AND ZH(I)
84. 303  AB(I,1)=ABS(L1-1)*(ZD(L1)-ZH(I-1))
85.      AB(I,2)=ABS(L1)*(ZD(L1+1)-ZD(L1))
86.      AB(I,3)=ABS(L1+1)*(ZH(I)-ZD(L1+1))
87.      ABR(I,L1)=AB(I,1)
88.      ABR(I,L1+1)=AB(I,1)+AB(I,2)
89.      II(I)=3
90.      IZ(I)=L1
91.      L3=L1+2
92.      IF(L3.GT.LZ)GO TO 306
93.      DO 304 L2=L3,LZ
94. 304  ABR(I,L2)=AB(I,1)+AB(I,2)+AB(I,3)
95. 306  CONTINUE
96.      DO 314 I=IPA,M
97.      IF(AB(I,1).GT.10.)AB(I,1)=10.
98.      IF(AB(I,2).GT.10.)AB(I,2)=10.
99.      IF(AB(I,3).GT.10.)AB(I,3)=10.
100.     DO 314 L=2,LZ
101.     IF(ABR(I,L).GT.10.)ABR(I,L)=10.
102. 314  CONTINUE
103. ***  DEPOSITION BY INCOMING BEAM
104.     X2=0F
105.     L1=2
106.     DO 317 I=IPA,M
107.     L2=II(I)
108.     X3=X2
109.     X2=X2*FXP(-AB(I,1))
110.     X4=0.
111.     IF(L2.EQ.1)GO TO 315
112.     L3=IZ(I)
113.     X4=X2*REF(L3)
114.     X2=X2*(1.-REF(L3))*EXP(-AB(I,2))

```

# HTXDEP (RETINAL)

```

115.      IF(L2.EQ.2)GO TO 315
116.      X4=X4+X2*REF(L3+1)
117.      X2=X2*(1.-REF(L3+1))*EXP(-AB(I,3))
118. 315  IF(X2.LT.1.E-10)X2=0.
119.      DO 317 J=1,JVL
120.      S(I,J)=(X3-X2-X4)*HR(J)/(ZH(I)-ZH(I-1))
121.      IF(S(I,J).LT.1.E-10/DPULSE)S(I,J)=0.
122. 317  CONTINUE
123. ***  CALCULATION OF REFLECTED INTENSITIES BY VARIOUS INTERFACES STARTING
124. ***  WITH FIRST INTERNAL INTERFACE
125.      X2=QP
126.      DO 322 L1=1,L20
127.      X3=ABS(L1)*(ZD(L1+1)-ZD(L1))
128.      IF(X3.GT.10.)X3=10.
129.      X2=X2*EXP(-X3)
130.      REFL(L1+1)=X2*REF(L1+1)
131. 322  X2=X2*(1.-REF(L1+1))
132.      DO 327 L1=2,LZ
133.      I=IPA
134. 324  IF(ZH(I).GT.ZD(L1))GO TO 325
135.      I=I+1
136.      IF(I.LF.M)GO TO 324
137.      GO TO 327
138. 325  X2=REFL(L1)
139.      DO 326 L3=IPA,I
140.      X3=X2
141.      L4=I+IPA-L3
142.      X2=X2*EXP(-ABR(L4,L1))
143.      DO 326 J=1,JVL
144.      S(L4,J)=S(L4,J)+(X3-X2)*HR(J)/(ZH(L4)-ZH(L4-1))
145.      IF(S(L4,J).LT.1.E-10/DPULSF)S(L4,J)=0.
146. 326  CONTINUE
147. 327  CONTINUE
148.      IHT=1
149.      RETURN
150. ***  NO HEAT DEPOSITION.BEAM OFF
151. 340  DO 342 I=1,M3
152.      DO 342 J=1,N3
153. 342  S(I,J)=0.
154.      IHT=0
155.      RETURN
156.      END

```

## SUBROUTINE MXGRAN (RETINAL)

```

1. SUBROUTINE MXGRAN
2. *** THIS ROUTINE COMPUTES CONSEQUENCE OF GRANULAR ABSORPTION ON TEMPERATURE
3. *** VARIATIONS IN PE (USED ONLY ONCE)
4. COMMON A(29,3),AP,AAV,ACH,APE,ASC,ATS,AVL,B(11,3),BB,BV(11,3),
5. 1CUNX(6),CUN(29),CUT,DIM,DFLOW(6),DPULSE,DR,DT,DTX,DZ,FI,HR(11),
6. 2IAB(29,11),18LOOD(6),IFIL,IG,IGX,IHT,IPA,IPC,IPE,IPOF,IPS,IPT,
7. 3IPV,IV(29),JVL,LIM,LPA,LPC,LPE,LPS,LPV,LPX,LTMAX,K,KM,KT,M,M1,M2,
8. 4M3,N,N1,N3,N4,NVL,POX,PR(11),PTIME,QP,P(11),PCO,PRM,PN,RPE,RPT,
9. 5RVL,RSC,S(29,11),SHB,TAV,TCH,TOM,TPE,TVL,TS(22001),TSC,TTS,V(29,11)
10. 6,VC(29,11,60),VSH(29),VSHX(6),WAVEL,XC,XFLOW,XFLOWT(6),XFLOWO(6),
11. 7XPD(60),X1(60),Z(29),ZD(9),ZM
12. L5=1
13. IF(DPULSE.GT.1.0E-5)GO TO 494
14. DX=.000025
15. BT=.3E-8
16. WRITE(6,405)DIM,LTMAX,DX,BT
17. 405 FORMAT(1H0,4HDIM=,F7.2,2X,6HLTMAX=,14,2X,3HDX=.E8,3,2X,3HBT=.E8,3)
18. LPT=DPULSE/.3E-8
19. L7=LTMAX-10
20. DO 410 L=1,L7,10
21. L1=L+1
22. L2=L+9
23. X1=TS(L)
24. X2=TS(L+10)-X1
25. X3=0.
26. DO 410 L3=L1,L2
27. X3=X3+.1
28. 410 TS(L3)=X1+X3*X2
29. LIT=2
30. XPD(1)=1.0
31. IF(LPT.GE.LTMAX)GO TO 472
32. *** CASE FOR LPT LESS THAN LTMAX-----
33. 440 IF(XT(LIT).GE..3E-8)GO TO 442
34. XPD(LIT)=TS(1)
35. LIT=LIT+1
36. GO TO 440
37. 442 TIMEX=XT(LIT)
38. XX=TIMEX/BT+.000001
39. LX=XX
40. PT=LX
41. IF(LX.GT.LPT)PT=LPT
42. PO=0.
43. IF(LX.GT.LTMAX)PO=LX-LTMAX
44. IF(LX.GT.LPT)GO TO 443
45. L1=1
46. L2=LX
47. GO TO 446
48. 443 IF(LX.GT.LTMAX)GO TO 444
49. L1=LX+1-LPT
50. L2=LX
51. GO TO 446
52. 444 IF(LX.LT.LTMAX+LPT)GO TO 445
53. L5=LIT
54. GO TO 494
55. 445 L1=LX-LPT+1
56. L2=LTMAX
57. 446 X2=PO

```

# MXGRAN(RETINAL)

```

58.      DO 448 L3=L1,L2
59. 448  X2=X2+TS(L3)
60.      XPD(LTT)=X2/PT
61.      LTT=LTT+1
62.      IF(LTT.LE.KT)GO TO 442
63.      GO TO 496
64.      *** CASE FOR LTMAX LESS THAN LPT-----
65. 472  TIMEX=XI(LTT)
66.      XX=TIMEX/BT+.000001
67.      LX=XX
68.      PT=LX
69.      IF(LX.GT.LPT)PT=LPT
70.      PO=0.
71.      IF(LX.GT.LTMAX)PO=LX-LTMAX
72.      IF(LX.GT.LPT)GO TO 473
73.      L1=1
74.      L2=LX
75.      IF(LX.GT.LTMAX)L2=LTMAX
76.      GO TO 475
77. 473  IF(LX.LT.LTMAX+LPT)GO TO 474
78.      L5=LTT
79.      GO TO 494
80. 474  L1=LX-LPT+1
81.      L2=LTMAX
82. 475  X2=PO
83.      DO 476 L3=L1,L2
84. 476  X2=X2+TS(L3)
85.      XPD(LTT)=X2/PT
86.      LTT=LTT+1
87.      IF(LTT.LE.KT)GO TO 472
88.      GO TO 496
89.      *** END CALCULATION IF TEMPERATURES VERY UNIFORM
90. 494  IF(L5.GT.KT)GO TO 496
91.      DO 495 L1=L5,KT
92. 495  XPD(L1)=1.
93. 496  WRITE(6,497)(XPD(L1),L1=1,KT)
94. 497  FORMAT(1H0.4HXPD=/(1X,10F8.2))
95.      RETURN
96.      END

```

# SUBROUTINE BLOOD(RETINAL)

```

1.  SUBROUTINE BLOOD
2.  SUBROUTINE COMPUTES CHANGES OF MATRIX ELEMENTS A AND B DUE TO BLOOD
3.  COMMON A(29,3),AP,AAV,ACH,APF,ASC,ATS,AVL,R(11,3),RB,BV(11,3),
4.  1CUNX(6),CON(29),CUT,DIM,DFLOW(6),DPULSE,DR,DT,DTX,DZ,FL,HR(11),
5.  2IAB(29,11),IRLOUD(6),IFIL,IG,IGX,IHY,IPA,IPC,IPE,IPROP,IPS,IPT,
6.  3IPV,IV(29),JVL,LIM,LPA,LPC,LPE,LPS,LPV,LPX,LYMAX,K,KK,KT,M,M1,M2,
7.  4M3,N,N1,N3,N4,NVL,POX,PR(11),PTIME,QP,R(11),RCO,RIM,RN,RPE,RRT,
8.  5RVL,RSC,S(29,11),SHB,TAV,TCH,TOM,TPE,TVL,TSC(200),TSC,TTS,V(29,11)
9.  6,VC(29,11,60),VSH(29),VSHX(6),WAVEL,XC,XFLOW,XFLOWI(6),XFLOWO(6),
10. 7XPD(60),XI(60),Z(29),ZD(R),ZM
11.  DIMENSION FLOWI(11),FLOWX(11),RD(11),RH(11),XI(11),XO(11)
12. *** INITIAL EVALUATION OF PARAMETERS AND ARRAYS
13.  DO 800 J=1,N3
14.  BV(J,1)=0.
15.  BV(J,2)=0.
16.  BV(J,3)=0.
17.  FLOWI(J)=0.
18. 800 FLOWX(J)=0.
19.  RH(1)=R(2)/2.
20.  DO 803 J=2,JVL
21. 803 RH(J)=(R(J)+R(J+1))/2.
22.  L2=2
23.  DO 810 J=1,JVL
24. 805 IF(DFLOW(L2).GT.RH(J))GO TO 806
25.  L2=L2+1
26.  GO TO 805
27. 806 X1=DFLOW(L2)-DFLOW(L2-1)
28.  X2=RH(J)-DFLOW(L2-1)
29.  X3=X2/X1
30.  X1(J)=XFLOWI(L2-1)+X3*(XFLOWI(L2)-XFLOWI(L2-1))
31. 810 XO(J)=XFLOWO(L2-1)+X3*(XFLOWO(L2)-XFLOWO(L2-1))
32.  FLOWX(1)=0.
33.  DO 812 J=2,JVL
34. 812 FLOWX(J)=FLOWX(J-1)+(XI(J-1)-XO(J-1))*(R(J)*R(J)-R(J-1)*R(J-1))/
35.  1(2.*TVL)
36.  FLOWX(JVL+1)=FLOWX(JVL)
37.  L2=2
38.  FLOWI(1)=XFLOWI(1)/TVL
39.  DO 820 J=2,JVL
40. 814 IF(DFLOW(L2).GT.R(J))GO TO 816
41.  L2=L2+1
42.  GO TO 814
43. 816 X4=DFLOW(L2)-DFLOW(L2-1)
44.  X5=R(J)-DFLOW(L2-1)
45.  X6=X5/X4
46. 820 FLOWI(J)=(XFLOWI(L2-1)+X6*(XFLOWI(L2)-XFLOWI(L2-1)))/TVL
47.  WRITE(6,21)(FLOWI(J),J=1,JVL)
48. 821 FORMAT(1H,6HFLOWI=/(1X,10F8.3))
49.  WRITE(6,22)(FLOWX(J),J=1,JVL)
50. 822 FORMAT(1H,6HFLOWX=/(1X,10F8.3))
51.  DO 823 J=2,JVL
52. 823 RU(J)=1./(R(J)*(R(J+1)-R(J-1)))
53. *** CALCULATE CHANGES IN MATRIX ELEMENTS A AND B DUE TO BLOOD FLOW
54.  BV(1,1)=0.
55.  BV(1,2)=-SHB*FLOWI(1)/2.
56.  BV(1,3)=0.
57.  BB=-SHR*XFLOW/2.

```

# BLOOD (RETINAL)

```

58.      DO 825 J=2,JVL
59.      BV(J,1)=SHB*RD(J)*FLOWX(J)
60.      BV(J,2)=SHB*RD(J)*(FLOWX(J-1)-FLOWX(J+1))/2.-SHB*FLOWI(J)/2.
61. 825  BV(J,3)=-SHB*RD(J)*FLOWX(J)
62.      DO 835 I=IPA,M
63. 835  IV(I)=0
64.      DO 840 L3=1,NVL
65.      L4=IBLOOD(L3)
66. 840  IV(L4)=1
67.      DO 845 I=IPA,LPG
68.      DO 842 J=1,JVL
69. 842  IAB(I,J)=0
70.      IF(JVL.EQ.N)GO TO 845
71.      L1=JVL+1
72.      DO 843 J=L1,N
73. 843  IAB(I,J)=1
74. 845  CONTINUE
75.      DO 850 I=IPT,M
76.      DO 650 J=1,N
77. 850  IAB(I,J)=1
78.      RETURN
79.      END

```

APPENDIX L

NOMENCLATURE, SAMPLE DATA, CODE LISTING, AND  
SAMPLE RUN FOR CORNEAL MODEL



# C \*\*\* NOMENCLATURE FOR CORNEAL MODEL

-----

C A(I,1),A(I,2),

C A(I,3) COEFFICIENTS OF FINITE DIFFERENCE EQUATIONS,Z ELEMENTS

C AB(I,1), PRODUCTS OF ABSORPTION COEFFICIENTS AND THICKNESSES OF

C AB(I,2),... SUCCESSIVE EYE MEDIA BETWEEN ZH(I-1) AND ZH(I)

C ABR(I,L1) SUM OF AB(I,1),AB(I,2)... OF MEDIA BETWEEN ZH(I-1) AND ZD(L1)

C ABS(L) ABSORPTION COEFFICIENTS ASSOCIATED WITH L-TH EYE

C MEDIA BETWEEN ZD(L) AND ZD(L+1),PER CM

C AP FRACTION OF HEAT ABSORBED BY MEDIA THAT IS ABSORBED BY PARTICLES OR PIGMENTS

C B(J,1),B(J,2),

C B(J,3) COEFFICIENTS OF FINITE DIFFERENCE EQUATIONS,R ELEMENTS

C CON(I) THERMAL CONDUCTIVITY AT DEPTH Z(I),CAL/CM-SEC-C

C CONX(L) THERMAL CONDUCTIVITIES FOR L-TH EYE MEDIA,CAL/CM-SEC-C

C CQ RATIO OF PREDICTED TO ACTUAL LASER POWER, INITIALLY ESTIMATED AND THEN REFINED BY DAMAGE CALC.

C CXC(J) ARRAYS USED TO EVALUATE TEMPERATURES

C CUT NORMALIZED INTENSITY OF LASER BEAM AT R=RIM

C DAMAGE(L1, COEFFICIENTS FOR RATE OF THERMAL DAMAGE,RATE=

C L2) EXP(DAMAGE(1,1)-DAMAGE(1,2)/(VC(273+T0)) FOR TEMPERA-

C TURES BELOW 50 C, AND RATE\*EXP(DAMAGE(2,1)-DAMAGE(2,2)/(VC+273+T0)) FOR TEMPERATURES ABOVE 50 C

C DIM MAX. NUMBER OF ELEMENTS USED TO COMPUTE THERMAL EFFECTS OF PARTICLES OR PIGMENTS

C DPULSE DURATION OF INDIVIDUAL PULSES,SEC. ALWAYS HELD FIXED

C DR R INCREMENT IN UNIFORM PART OF GRID, CM

C DT FIRST TIME INTERVAL FOR SINGLE-PULSE TEMPERATURE CALC,

C SUCCESSIVE INTERVALS INCREASED BY FACTOR XC,SEC

C DTSTM TEMPERATURE INCREMENT TO BE ADDED TO TSTEAM CONSIDERING PEAK PARTICLE TEMPERATURE AS HYPOTHETICAL DAMAGE CRITERION

C DXC(J) ARRAYS USED TO EVALUATE TEMPERATURES RISES

C DXR(I)

C DZ Z INCREMENT IN UNIFORM PART OF GRID, CM

C EDT1 POWER TO WHICH TIME IS RAISED TO SPECIFY NUMBER OF CYCLES TO WHICH BASIC TEMPERATURE CALCULATIONS ARE REPEATED TO ENSURE STABILITY

C EDT2 ADDITIVE FACTOR TO SPECIFY NUMBER OF CYCLES TO WHICH SINGLE-PULSE TEMPERATURE CALC. ARE REPEATED TO ENSURE STABILITY

C FA(L) AREA FROM R=0 TO R=(L-.5)\*RINT,CM2---FOR CALC. IRREGULAR PROFILES

C FC FOCAL LENGTH OF CORNEA,=3.12 CM FOR HUMANS,=2.43 CM FOR MONKEYS

C FP(L) TOTAL LASER POWER BETWEEN R=0 AND R=(L-.5)\*RINT---FOR CALC. IRREGULAR PROFILES

C FTIME(L) FACTORS BY WHICH EXPOSURE TIME IS MULTIPLIED TO YIELD SUFFICIENT TIME FOR DAMAGE TO OCCUR,GIVEN AS FUNCTION OF PULSE WIDTH

C FXC(J) ARRAYS USED TO EVALUATE TEMPERATURES

C FXR(I)

C HR(J) NORMALIZED IRRADIANCE ENTERING EYE AT R(J),CAL/CM2-SEC

C I INDEX OF AXIAL GRID POINTS Z(I)

C ID1,ID2 I INDICES FOR PRINTING AT DEPTHS Z(I) WHERE I=IP1+ID1 TO IP1+ID2

C IG I INDEX INDICATING LOCATION OF PARTICLES

C II(I) NUMBER OF INTERFACES(ZD) BETWEEN ZH(I-1) AND ZH(I), PLUS 1

C	I13	I INDEX OF V(I13,J) TEMPERATURE CURVE(J VARYING) TO MARK
C		ON 3-D PLOTS
C	IKX	NUMBER OF TIMES TEMPERATURE CALC. ARE REPEATED FOR
C		PURPOSES OF STABILITY
C	ILENS	INDEX INDICATING WHETHER TO CONSIDER CORNEAL BURNS OR
C		LENS BURNS, FOR CORNEA SET ILENS=0, FOR LENS SET ILENS=1
C	IMAX	I INDEX AT WHICH PEAK TEMPERATURES OCCUR
C	IN	NUMBER OF PULSES GROUPED TOGETHER FOR DAMAGE CALCULATIONS
C	INX	NUMBER OF GROUPS OF PULSES CONSIDERED DURING EXPOSURE
C		TO LASER
C	INXX	NUMBER OF GROUPS OF PULSES CONSIDERED DURING AND
C		FOLLOWING EXPOSURE TO LASER
C	IP	I INDEX OF FIRST Z(I) IN CORNEA OR LENS
C	IPROF	INDEX DESCRIBING LASER PROFILE, UNIFORM IF=0, GAUSSIAN IF=1
C		, IRREGULAR IF=2
C	IP1,IP2,...	I INDICES ASSOCIATED WITH INITIAL GRID POINTS ALONG Z
C		AXIS IN SUCCESSIVE EYE MEDIA STARTING WITH I=IP1 IN
C		CORNEA, OUTER BOUNDARY OF CORNEA AT $(Z(IP1-1)+Z(IP1))/2$
C	ITYPE	K INTERVAL AT WHICH VC(I,J,K) IS PRINTED
C	IX(L)	I INDICES ASSOCIATED WITH INITIAL GRID POINT (Z) IN L-TH
C		EYE MEDIA
C	IZ(I)	INDEX L OF FIRST INTERFACE ZC(L) BEYOND ZH(I-1)
C	J	INDEX FOR RADIAL GRID POINTS R(J)
C	JD1,JD2	J INDICES FOR PRINTING, WILL PRINT J=JD1 TO JD2
C	JM	MAXIMUM J INDEX AT WHICH DAMAGE ASSESSMENTS ARE TO BE MADE
C		, DEPENDS ON VALUE CHOSEN FOR RMAX
C	JVL	J INDEX FOR WHICH R(JVL) APPROXIMATES RVL
C	K	INDEX FOR TIMES XT(K)
C	KM	INTEGER SUCH THAT XT(KM)=DPULSE
C	KT	MAXIMUM NUMBER OF EXPANDING TIMES XT(K)
C	KTT(L)	NUMBER OF TIME STEPS WITH WHICH TO REACH TOTAL TIME
C	KTYPE	NUMBER OF TIMES AT WHICH 3D TEMPERATURE DRAWINGS ARE DESIRED
C		--- FOR NO DRAWINGS SET KTYPE=0
C	KTYPEO	CONTROL INDEX WHICH WHEN SET =1 WILL PREEMPT CARD
C		PUNCHING WHILE MAINTAINING PRINT OUTS OF TEMPERATURES
C		AT SELECTED TIMES AND POINTS---SET =0 FOR CARD PUNCHING.
C	KX	TOTAL NUMBER OF TIME INTERVALS FROM PULSE TO PULSE
C	LESION	LESION RADIUS, CM
C	LI	NUMBER OF RADIAL INTERVALS USED TO INTEGRATE PROFILE
C	LIM	NUMBER OF RADIAL INTERVALS FROM R=0 TO R=RIM OR LESION
C	LIMAX	I INDEX DESCRIBING RANGE OF I OVER WHICH TO ASSESS DAMAGE,
C		RANGE=IMAX TO IMAX+LIMAX
C	LLT,LLG	INDICES USED TO CONTROL CALC. OF THRESHOLD POWER
C	LP1,LP2...	I INDICES ASSOCIATED WITH LAST GRID POINTS(Z) IN
C		SUCCESSIVE EYE MEDIA(SEE IP1,IP2...)
C	LR	NUMBER OF POINTS DESCRIBING IRREGULAR LASER PROFILE
C	LT	INDEX OF NUMBER OF TIME INTERVALS BT
C	LTMAX	TIME INDEX(TIME=LTMAX*BT) BEYOND WHICH EXCESS
C		TEMPERATURE RISE OF PARTICLES IS DISSIPATED
C	LX(L)	I INDICES ASSOCIATED WITH LAST GRID POINT (Z) IN L-TH
C		EYE MEDIA
C	LZ	NUMBER OF DIFFERENT EYE LAYERS OR MEDIA
C	L1,L2,L3...	DUMMY VARIABLES USED IN COMPUTATIONS
C	M	NO. OF GRID SPACES IN Z DIRECTION(EVEN)
C	M1	HALF OF NUMBER OF UNIFORMLY THICK Z INCREMENTS(LESS THAN M/2)
C	M2	HALF THE NO. OF GRID SPACES IN Z DIRECTION
C	M3	NO. OF GRID POINTS IN Z DIRECTION (M+1)
C	N	NO. OF GRID SPACES IN R DIRECTION
C	NB	REFRACTIVE INDEX AT WAVELENGTH OF 500 NM
C	NC	REFRACTIVE INDEX AT WAVELENGTH WAVEL

C	NP	NUMBER OF TIME INTERVALS WITHIN DPULSE, USED FOR DAMAGE CALCULATIONS
C	NPL	TOTAL NUMBER OF PULSES IN EXPOSURE
C	NPT(L)	NUMBER OF INCREMENTAL TIMES USED TO SUBDIVIDE DPULSE
C	NPULSE(L)	NUMBER OF PULSES ASSOCIATED WITH L-TH TEST EXPOSURE
C	NTEST	NUMBER OF TEST EXPOSURES WHICH CAN DIFFER IN REPETITION RATES OR NUMBER OF PULSES
C	N1	NUMBER OF UNIFORMLY THICK R INCREMENTS (LESS THAN N)
C	N3	NO. OF GRID POINTS IN R DIRECTION (N+1)
C	N4	NO. OF GRID POINTS IN UNIFORM PART OF GRID IN R DIRECTION
C	PC	DISTANCE OF PUPIL FROM CORNEA, =.40 CM FOR HUMANS, =.36 CM FOR MONKEYS
C	POW,POX	LASER POWER ON CORNEAL PLANE, WATTS
C	PR(J)	CALCULATED OR MEASURED RETINAL IRRADIANCE PROFILE NORMALIZED TO UNITY AT R(1)=0.
C	PTIME	UNIFORM TIME INTERVAL USED TO SUBDIVIDE DPULSE FOR MULTIPLE PULSES
C	PUPIL	PUPIL RADIUS, CM
C	PX(L)	IRREGULAR LASER PROFILE AT POINTS RX(L)
C	QD(I,J)	LASER POWER REQUIRED TO CAUSE IRREVERSIBLE DAMAGE AT Z(I), R(J), WATTS
C	QP	LASER INTENSITY ENTERING EYE AT R(1)=0, CAL/CM <sup>2</sup> -SEC
C	R(J)	RADIUS AT CO-ORDINATE J, CM
C	REF(L)	FRACTION OF RADIATION REFLECTED AT Z=ZD(L)
C	REFL(L)	REFLECTED RADIATION FROM INTERFACE AT Z=ZD(L)
C	REPET(L)	REPETITION RATES ASSOCIATED WITH L-TH TEST EXPOSURE, PULSES/SEC
C	RGV	RANGE OF TEMPERATURE RISE(C) FOR 3-D AND 2-D PLOTS
C	RH(J)	RADIAL DISTANCE HALFWAY BETWEEN R(J) AND R(J+1)
C	RIM	IMAGE OR BEAM RADIUS, FOR GAUSSIAN PROFILES EQUALS RADIUS AT WHICH NORMALIZED PROFILE EQUALS CUT, FOR UNIFORM PROFILES EQUALS EXTENT OF PROFILE, CM
C	RINT	UNIFORM RADIAL INTERVALS, CM
C	RMAX	MAXIMUM RADIAL DISTANCE AT WHICH DAMAGE ASSESSMENTS ARE TO BE MADE
C	RN	MAXIMUM RADIAL DISTANCE, CM
C	R1	STRETCHING FACTOR IN Z DIRECTION
C	R2	STRETCHING FACTOR IN R DIRECTION
C	RX(L)	RADIAL DISTANCES ASSOCIATED WITH IRREGULAR LASER PROFILE PX(L) (SYMMETRIC IN R), CM
C	S(I,J)	RATE OF HEAT DEPOSITION PER UNIT VOLUME AT Z(I), R(J), CAL/CM <sup>3</sup> -SEC
C	SIGMA	RADIUS AT WHICH NORMLIZED GAUSSIAN PROFILE EQUALS 1/E <sup>2</sup>
C	TC	TIME FROM START OF PULSE TO START OF NEXT PULSE, SEC
C	TH(L)	THICKNESS OF EYE MEDIA INDICATED BY L, CM
C	TIME	MAXIMUM TIME LIMIT SET, SEC
C	TIMEX(L)	TIMES AT WHICH 3-D PLOTS ARE DESIRED, SEC
C	TSTEAM	GRANULE TEMPERATURE USED AS HYPOTHETICAL DAMAGE CRITERION, C
C	T0	INITIAL TEMPERATURE OF EYE, C
C	V(I,J)	TEMPERATURE RISES AT Z(I), R(J) AT GIVEN TIME, C
C	VC(I,J,K)	TEMPERATURE RISES AT Z(I), R(J) AT TIME XT(K), C
C	VE(L,K,L1)	TEMPERATURE RISES AT Z(ID(L)), R(JD(L)) AT TIME XT(K), L1=1 FOR EYE MEDIA, AND L1=2 FOR PARTICLES OR PIGMENTS
C	VpX	TEMPERATURE RISES, C
C	VSH(I)	VOLUMETRIC SPECIFIC HEAT AT Z(I), CAL/CM <sup>3</sup> -C
C	VSHX(L)	HEAT CAPACITY OF L-TH EYE MEDIA, CAL/CM <sup>3</sup> -C
C	VZ(L,L6,L3, L1)	TEMPERATURE RISE AT TIME INTERVAL ZT(L3) AFTER (L6-.5)*IN-.5 INCREMENTAL PULSES AT POINT Z(ID(L)), R(JD(L))

```

C      ,L1=1 FOR EYE MEDIA AND L1=2 FOR PARTICLES
C      WAVEL      WAVELENGTH,NM
C      XC          STRETCHING FACTOR FOR TIME INTERVALS ASSOCIATED WITH
C                   TECH. INCORP. TEMPERATURE CALCULATIONS
C      XCT(L)      VALUES FROM WHICH EXPANSION FACTOR XC IS SELECTED BASED
C                   UPON PULSE WIDTH
C      XPD(K)      NORMALIZED TEMPERATURE RISES OF GRANULES AT TIME XT(K)
C      XT(K)       TIMES FOLLOWING START OF EXPOSURE, INDICATED BY INDEX K
C                   ,SEC
C      XX          FRACTION OF LASERS ENERGY ENTERING EYE
C      X1,X2,X3,... DUMMY VARIABLES USED IN COMPUTATIONS
C      Z(I)        DISTANCE ALONG Z AXIS AT GRID POINT I,CM
C      ZCUN(I,J)   FACTOR BY WHICH LASERS INTENITIES(NORMAL BEAM) ARE
C                   MULTIPLIED TO ACCOUNT FOR REFRACTION,USED FOR LENS BURNS
C      ZD(I)       DEPTHS OF INTERFACES BETWEEN VARIOUS EYE MEDIA,CM
C      ZH(I)       AXIAL DISTANCES HALFWAY BETWEEN Z(I) AND Z(I+1),CM
C      ZM          HALF LENGTH OF Z AXIS, CM
C      ZO          DISTANCE OF PUPIL FROM LASERS WAIST,CM
C      ZT(L3)      TIME FROM START OF PULSE TO CENTER OF TIME INTERVALS
C                   USED TO PREDICT THERMAL DAMAGE FOR MULTIPLE PULSES
C      ZTT(L3)     LOG OF PRODUCT OF NUMBER OF PULSES/GROUP TIMES TIME
C                   INTERVALS AT WHICH DAMAGE CALC. ARE MADE
C      ZTX(L3)     TIME INTERVAL FROM START OF EACH PULSE AT WHICH
C                   PARTICLE TEMPERATURES ARE CALC..
C
C *** DIMENSIONS OF VARIOUS ARRAYS USED IN PROGRAM
C -----
C      COMMON DIMENSIONS A(M3,3),ABS(LZ),R(N3,3),CUNX(6),CUN(M3),HR(N3),
C      R(N3),REF(LZ+1),TH(LZ),TS(M3,N3),S(LTMAX),VC(M3,N3,KT),VSHX(6),VSH(M3),
C      XPD(KT),XT(KT),Z(M3),ZD(LZ+1)
C *** MAIN PROGRAM
C      DIMENSION CXC(N3),CXR(M3),DAMAGE(2,2),DXC(N3),DXR(M3),FXC(N3),FXR(M3),
C      ID(LIJ),JD(LIJ),KKT(38),NPT(38),NPULSE(NTST),QD(M3,N3),REPET(NTST),
C      TIMEX(KTYPE),XCT(38),V(M3,N3),VE(LIJ,KT,2),VXX(M3,N3),VZ(LIJ,INXX,KX,2),
C      ZT(KX),ZTT(KX)
C *** SUBROUTINE GRID
C      IX(6),LX(6)
C *** SUBROUTINE IMAGE
C      FA(LI+1),FP(LI+1),FX(LI+1),JO(32),PX(LR),RX(LR),XF1(LI+1),XF2(LI+1)
C *** SUBROUTINE HTXDEP
C      AB(M3,3),ABR(M3,LZ),II(M3),IZ(M3),REFL(LZ+1),ZH(M3)

```

# SAMPLE DATA FOR CORNEAL MODEL

```

-----DATA CARD 1-----
.055 .100
-----DATA CARDS 2-----
13.7 13.0 12.3 11.7 11.1 10.5 9.9 9.3 8.8 8.3
7.8 7.4 6.9 6.5 6.1 5.7 5.3 4.9 4.5 4.2
3.9 3.6 3.3 3.0 2.7 2.4 2.1 1.9 1.7 1.6
1.5 1.4 1.3 1.3 1.2 1.2 1.2 1.1
-----DATA CARD 3-----
6
-----DATA CARD 4-----
.064 3 0 0
-----DATA CARD 5-----
.05000 0 .05000
-----DATA CARD 6-----
1 4.00-1 1.35-1
-----DATA CARD 7-----
2.5-2
-----DATA CARD 8-----
1 8
-----DATA CARD 9-----
1.41
-----DATA CARD 10-----
1
-----DATA CARD 11-----
4 8 1 5 5
-----DATA CARD 12-----
37. .18 1.
-----DATA CARDS 13-----
1863. 1863. 1863. 1863. 1863. 1863. .025 .0 .0 .0
0. 0. 2727.
-----DATA CARD 14-----
.0006 .0580 .2900 .3500 1.1570 1.0000 .700
-----DATA CARD 15-----
.00120 .00120 .00120 .00120 .00120 .00120
-----DATA CARD 16-----
1. 1. 1. 1. 1. 1.
-----DATA CARDS 17-----
1 3 5 7 10 14 18 21 25 28
30 31 32 33 34 35 36 37 38 39
40 41 42 43 44 45 46 47 48 49
50 51 52 53 54 55 56 57
-----DATA CARDS 18-----
1.2 1.2 1.2 1.2 1.2 1.2 1.2 1.2 1.2 1.2
1.2 1.2 1.2 1.2 1.15 1.15 1.15 1.15 1.15 1.15
1.15 1.15 1.15 1.15 1.15 1.15 1.15 1.15 1.1 1.1
1.1 1.1 1.1 1.1 1.1 1.1 1.1 1.1
-----DATA CARDS 19-----
58 58 58 58 58 58 58 58 58 58
38 38 39 39 40 40 41 42 42 43
44 45 46 47 48 51 50 51 52 52
53 54 55 56 57 57 58 58
-----DATA CARD 19A-----
.35+0
-----DATA CARD 19A*-----

```

3		-----DATA CARD 19A**-----
.0+0 .29-1 .8-1		-----DATA CARD 19A***-----
1.+0 .135+0 .0+0		-----DATA CARD 19B -----
3.0+2 2.430+0 .36+0 1.336+0		-----DATA CARD 20 -----
1		-----DATA CARD 21 -----
2		-----DATA CARD 22 -----
2.-8 1.-7		-----DATA CARD 23 -----
8 8 8 1 1		-----DATA CARD 24 -----
6. 11		-----DATA CARD 25 -----
1. 1.		-----DATA CARD 26 -----
149. 50000. 242. 80000. 100. 100.		

# SAMPLE RUN OF CORNEAL MODEL

.39000+02	.60000+01	4	10	.16667-01	.19284+01
.39000+02	.60000+01	4	10	.16667-01	.19099+01
.39000+02	.60000+01	4	10	.16667-01	.19048+01
.39000+02	.60000+01	4	10	.16667-01	.19034+01
.39000+02	.60000+01	4	10	.16667-01	.19030+01
.39000+02	.60000+01	4	10	.16667-01	.19029+01
.39000+02	.60000+01	4	10	.16667-01	.19029+01
.39000+02	.60000+01	4	10	.16667-01	.19029+01
.39000+02	.60000+01	4	10	.16667-01	.19029+01

R2= 1.9029

.11959+04	.10000+02	11	2	.36000-01	.10560+01	.88115-03	.20315+01
.11959+04	.10000+02	11	2	.36000-01	.10560+01	.88115-03	.20377+01
.11959+04	.10000+02	11	2	.36000-01	.10560+01	.88115-03	.20390+01
.11959+04	.10000+02	11	2	.36000-01	.10560+01	.88115-03	.20392+01
.11959+04	.10000+02	11	2	.36000-01	.10560+01	.88115-03	.20393+01
.11959+04	.10000+02	11	2	.36000-01	.10560+01	.88115-03	.20393+01

R1= 2.0393 ZM= 1.0547

ID1=11 ID2=14 JD1= 1 JD2= 5

R=

.0000	.0167	.0333	.0500	.0667	.0984	.1587	.2736	.4921	.9076
1.6992									

Z=

-1.0534	-.5159	-.2523	-.1231	-.0597	-.0286	-.0134	-.0059	-.0022	-.0004
.0004	.0013	.0022	.0031	.0049	.0065	.0160	.0313	.0623	.1257
.2550	.5185	1.0560							

PUPIL= .350

SIGMA= .640-01 RIM= .640-01

WP= .145+02 HR=

.100+01	.873+00	.581+00	.295+00	.114+00	.881-02	.447-05	.129-15	.000	.000
---------	---------	---------	---------	---------	---------	---------	---------	------	------

REPET=

.100+02

NPULSE=

1

ABS= 1863. 1863. 1863. 1863. 1863. 1863. AP= .000  
 DPULSE= .250-01 DR= .167-01 DT= .106-04 DZ= .881-03 IP1=11 IP2=17  
 IP3=17 IP4=18 IP5=18 IP6=19 JVL= 9 KM= 43 KT= 47 LIM= 3 LP1=16  
 LP2=17 LP3=18 LP4=18 LP5=19 LP6=23 M=22 M1= 2 N=10 N1= 4 NP=42  
 NTEST= 1 POW= .400+00 PTIME= .000 QP= .145+02  
 REF= .025 .000 .000 .000 .000 .000 RIM= .640-01  
 RVL= .700 Th= .900-02 .900-02 .900-02 .900-02 .200-01  
 .100+01 TIME= .438-01 T0= 37.0 XC= 1.15

IKX= 1

ZH=

-.785+00-.384+00-.188+00-.914-01-.442-01  
 -.210-01-.964-02-.407-02-.134-02 .745-.08  
 .881-03 .176-02 .264-02 .398-02 .671-02  
 .123-01 .236-01 .468-01 .940-01 .190+00  
 .387+00 .787+00

S=	.133+05	.116+05	.771+04	.391+04	.151+04	.117+03	.594-01	.000	.000	.000
S=	.257+04	.225+04	.149+04	.758+03	.293+03	.227+02	.115-01	.000	.000	.000
S=	.499+03	.435+03	.290+03	.147+03	.567+02	.439+01	.223-02	.000	.000	.000
S=	.724+02	.632+02	.420+02	.213+02	.822+01	.637+00	.323-03	.000	.000	.000
S=	.318+01	.277+01	.184+01	.933+00	.360+00	.279-01	.000	.000	.000	.000
S=	.971-02	.847-02	.562-02	.284-02	.110-02	.851-04	.000	.000	.000	.000
S=	.000	.000	.000	.000	.000	.000	.000	.000	.000	.000
S=	.000	.000	.000	.000	.000	.000	.000	.000	.000	.000
S=	.000	.000	.000	.000	.000	.000	.000	.000	.000	.000
S=	.000	.000	.000	.000	.000	.000	.000	.000	.000	.000
S=	.000	.000	.000	.000	.000	.000	.000	.000	.000	.000
S=	.000	.000	.000	.000	.000	.000	.000	.000	.000	.000

TIME= .106-04 K= 2 POWER= .400+00WATTS  
 R= .00000 .01667 .03333 .05000 .06667  
 Z= .00044 .1 .1 .1 .0 .0  
 Z= .00132 .0 .0 .0 .0 .0  
 Z= .00220 .0 .0 .0 .0 .0  
 Z= .00308 .0 .0 .0 .0 .0

TIME= .228-04 K= 3 POWER= .400+00WATTS

TIME= .369-04 K= 4 POWER= .400+00WATTS

TIME= .530-04 K= 5 POWER= .400+00WATTS

TIME= .716-04 K= 6 POWER= .400+00WATTS

TIME= .929-04 K= 7 POWER= .400+00WATTS  
 R= .00000 .01667 .03333 .05000 .06667  
 Z= .00044 1.2 1.0 .7 .3 .1  
 Z= .00132 .3 .3 .2 .1 .0  
 Z= .00220 .1 .1 .0 .0 .0  
 Z= .00308 .0 .0 .0 .0 .0

TIME= .117-03 K= 8 POWER= .400+00WATTS

TIME= .146-03 K= 9 POWER= .400+00WATTS

TIME= .178-03 K=10 POWER= .400+00WATTS



TIME= .216-03 K=11 POWER= .400+00WATTS  
 TIME= .258-03 K=12 POWER= .400+00WATTS  
 R= .00000 .01667 .03333 .05000 .06667  
 Z= .00044 3.0 2.6 1.7 .9 .3  
 Z= .00132 1.0 .8 .6 .3 .1  
 Z= .00220 .2 .2 .1 .1 .0  
 Z= .00308 .0 .0 .0 .0 .0

TIME= .308-03 K=13 POWER= .400+00WATTS

TIME= .365-03 K=14 POWER= .400+00WATTS

TIME= .430-03 K=15 POWER= .400+00WATTS

TIME= .505-03 K=16 POWER= .400+00WATTS

TIME= .591-03 K=17 POWER= .400+00WATTS  
 R= .00000 .01667 .03333 .05000 .06667  
 Z= .00044 6.0 5.2 3.5 1.8 .7  
 Z= .00132 2.6 2.3 1.5 .8 .3  
 Z= .00220 .8 .7 .5 .2 .1  
 Z= .00308 .2 .2 .1 .1 .0

TIME= .691-03 K=18 POWER= .400+00WATTS

TIME= .805-03 K=19 POWER= .400+00WATTS

TIME= .936-03 K=20 POWER= .400+00WATTS

TIME= .109-02 K=21 POWER= .400+00WATTS

TIME= .126-02 K=22 POWER= .400+00WATTS  
 R= .00000 .01667 .03333 .05000 .06667  
 Z= .00044 10.6 9.3 6.2 3.1 1.2  
 Z= .00132 5.9 5.2 3.4 1.7 .7  
 Z= .00220 2.6 2.3 1.5 .8 .3  
 Z= .00308 .9 .8 .5 .3 .1

TIME= .146-02 K=23 POWER= .400+00WATTS

TIME= .169-02 K=24 POWER= .400+00WATTS

TIME= .196-02 K=25 POWER= .400+00WATTS

TIME= .226-02 K=26 POWER= .400+00WATTS

TIME= .261-02 K=27 POWER= .400+00WATTS  
 R= .00000 .01667 .03333 .05000 .06667  
 Z= .00044 17.4 15.2 10.1 5.1 2.0  
 Z= .00132 11.6 10.1 6.8 3.4 1.3  
 Z= .00220 6.7 5.8 3.9 2.0 .8  
 Z= .00308 3.4 2.9 2.0 1.0 .4

TIME= .301-02 K=28 POWER= .400+00WATTS

TIME= .347-02 K=29 POWER= .400+00WATTS

TIME= .400-02 K=30 POWER= .400+00WATTS

TIME= .462-02 K=31 POWER= .400+00WATTS

TIME= .532-02 K=32 POWER= .400+00WATTS

R=	.00000	.01667	.03333	.05000	.06667	
Z=	.00044	27.2	23.7	15.8	8.0	3.1
Z=	.00132	20.0	17.9	12.0	6.1	2.4
Z=	.00220	14.2	12.4	8.3	4.2	1.6
Z=	.00308	9.2	8.0	5.3	2.7	1.1

TIME= .613-02 K=33 POWER= .400+00WATTS

TIME= .706-02 K=34 POWER= .400+00WATTS

TIME= .812-02 K=35 POWER= .400+00WATTS

TIME= .935-02 K=36 POWER= .400+00WATTS

TIME=	.108-01	K=37	POWER=	.400+00WATTS		
R=	.00000		.01667	.03333	.05000	.06667
Z=	.00044	41.0	35.7	23.8	12.2	4.7
Z=	.00132	33.8	29.4	19.7	10.0	3.9
Z=	.00220	26.4	23.0	15.3	7.8	3.1
Z=	.00308	19.9	17.3	11.6	5.9	2.3

TIME= .124-01 K=38 POWER= .400+00WATTS

TIME= .143-01 K=39 POWER= .400+00WATTS

TIME= .164-01 K=40 POWER= .400+00WATTS

TIME= .189-01 K=41 POWER= .400+00WATTS

TIME=	.217-01	K=42	POWER=	.400+00WATTS		
R=	.00000		.01667	.03333	.05000	.06667
Z=	.00044	60.5	52.6	35.2	18.0	7.1
Z=	.00132	53.0	46.0	30.8	15.8	6.2
Z=	.00220	44.7	38.8	26.0	13.4	5.3
Z=	.00308	37.1	32.2	21.6	11.1	4.4

TIME=	.250-01	K=43	POWER=	.400+00WATTS		
R=	.00000		.01667	.03333	.05000	.06667
Z=	.00044	65.3	56.6	38.0	19.5	7.7
Z=	.00132	57.6	50.0	33.5	17.2	6.8
Z=	.00220	49.3	42.7	28.7	14.7	5.8
Z=	.00308	41.5	35.9	24.1	12.4	4.9

TIME= .288-01 K=44 POWER= .400+00WATTS

TIME= .331-01 K=45 POWER= .400+00WATTS

TIME= .381-01 K=46 POWER= .400+00WATTS

TIME=	.438-01	K=47	POWER=	.400+00WATTS		
R=	.00000		.01667	.03333	.05000	.06667
Z=	.00044	32.1	27.5	18.7	9.9	4.0

Z=	.00132	31.0	26.5	18.1	9.5	3.9
Z=	.00220	30.4	26.1	17.8	9.4	3.8
Z=	.00308	29.7	25.5	17.3	9.1	3.7

WAVELENGTH= 2727.0NM TSTEAM= 100. DAMAGE= 149. 50000. - 242. - 8000

NRUN= 8 PULSE WIDTH= .250-01 NUMBER OF PULSES= 1  
 BEAM RADIUS= .640-01CM LESION RADIUS= .500-01CM

TSTEAM= 100.

R= .00000 .01667 .03333 .05000 .06667  
 Z= .00044 QD= .173+00 .199+00 .297+00 .579+00 .147+01

TSTEAM= 200.

R= .00000 .01667 .03333 .05000 .06667  
 Z= .00044 QD= .173+00 .199+00 .297+00 .579+00 .147+01

Z= .441-03CM RADIAL EXTENT OF IRREVERSIBLE DAMAGE= .408-01CM

# MAIN PROGRAM OF CORNEAL MODEL

```

1.  COMMON A(23,3),ABS(6),AP,B(11,3),CON(23),CONX(6),CUT,DTM,DPULSE,
2.  1DR,DT,DTX,DZ,HR(11),IG,IHT,ILENS,IPOF,IP1,IP2,IP3,IP4,IP5,IP6,
3.  2JVL,LIM,LP1,LP2,LP3,LP4,LP5,LP6,LPX,LTMAX,LZ,K,KT,M,M1,M2,M3,N,
4.  3N1,N3,N4,POX,PTIME,QP,R(11),REF(7),RIM,RN,RVL,S(23,11),TH(6),
5.  4TS(2200),V(23,11),VC(23,11,60),VSH(23),VSHX(6),XC,WAVEL,XPD(60),
6.  5XT(60),Z(23),ZCON(23,11),ZD(8),ZM
7.  DIMENSION CXC(11),CXR(23),DAMAGE(2,2),DXC(11),DXR(23),FTIME(38),
8.  1FXC(11),FXR(23),ID(50),JD(50),KTT(38),NPT(38),NPULSE(7),NRUN(7),
9.  2QD(23,11),REPET(7),TIMEX(5),XCT(38),VE(20,60,2),VXX(23,11),
10. 3VZ(20,26,8,2),ZT(8),ZTT(8),ZTX(8)
11.  REAL LESION
12.  3 FORMAT(F7.4,3I7)
13.  4 FORMAT(10F7.2)
14.  5 FORMAT(10I7)
15.  6 FORMAT(F7.2,I7,2F7.2)
16.  7 FORMAT(10E7.2)
17.  8 FORMAT(I7,3E7.2)
18.  READ(5,4)DZ1,DZ2
19.  READ(5,4)(FTIME(L),L=1,38)
20.  READ(5,5)LZ
21.  READ(5,3)RIM,LIM,IG,ILENS
22.  READ(5,6)RMAX,LIMAX,LESION
23.*** SET VALUES FOR N,N1,N3,N4, AND DR
24.  N1=4
25.  N=N1+6
26.  N3=N+1
27.  N4=N1+1
28.  READ(5,8)IPOF,POW,CUT
29.  DR=LESION/LIM
30.  IF(IPOF.EQ.0)DR=RIM/(LIM-.5)
31.  READ(5,7)DPULSE
32.  READ(5,5)NTEST,(NRUN(L),L=1,NTEST)
33.  READ(5,7)(REPET(L),L=1,NTEST)
34.  READ(5,5)(NPULSE(L),L=1,NTEST)
35.  READ(5,5)ID1,ID2,JD1,JD2,1TYPE
36.  LPX=1
37.  IF(NTEST.EQ.1.AND.NPULSE(1).EQ.1)LPX=0
38.  IF(DPULSE.GT..3E-8)GO TO 10
39.*** ADJUST POWER AND PULSE WIDTH FOR EXPOSURES WITH PULSES LESS THAN
40.*** .3E-8 SEC
41.  POW=POW*DPULSE/.3E-8
42.  DPULSE=.3E-8
43. 10 READ(5,4)10,EDT1,EDT2
44.  READ(5,4)(ABS(L),L=1,LZ),(REF(L1),L1=1,LZ),WAVEL
45.  READ(5,4)(TH(L),L=1,LZ),RVL
46.  READ(5,4)(CONX(L),L=1,LZ)
47.  READ(5,4)(VSHX(L),L=1,LZ)
48.  READ(5,5)(NPT(L),L=1,38)
49.  READ(5,4)(XCT(L),L=1,38)
50.  READ(5,5)(KTT(L),L=1,38)
51.*** COMPUTE DT,KM,KT,NP,PTIME,TIME, AND XC
52.  L1=ALOG(DPULSE)/.69315+29.
53.  IF(L1.LT.1)L1=1
54.  IF(L1.GT.38)L1=38
55.  IF(LPX.EQ.1)GO TO 11
56.*** ---SINGLE PULSED EXPOSURES
57.  XC=XCT(L1)

```

1  
2  
3  
4  
5  
  
6  
  
7  
8  
9  
10  
11  
  
12  
13  
14  
15  
16  
17  
18  
19

# MAIN (CORNEAL)

```

58. NP=NPT(L1)
59. KT=KTT(L1)
60. DT=DPULSE*(XC-1.)/(XC**NP-1.)
61. TIME=DT*(XC**KT-1.)/(XC-1.)
62. GO TO 13
63.*** ---MULTIPLE PULSED EXPOSURES
64. 11 XC=1.4
65. NP=5
66. X1=0.
67. DO 12 L=1,NTEST
68. IF(X1.LT.NPULSE(L)/REPET(L))X1=NPULSE(L)/REPET(L)
69. 12 CONTINUE
70. TIME=FTIME(L1)*X1
71. DT=DPULSE*(XC-1.)/(XC**NP-1.)
72. KT=ALOG(1.+TIME*(XC-1.)/DT)/ALOG(XC)+1.
73. PTIME=DPULSE/NP
74. 13 KT=KT+1
75. KM=NP+1
76. IF(KT.GT.59)WRITE(6,14)KT
77. 14 FORMAT(1H0,3HKT=,I3,2X,22HTIME DIMENSION TOO LOW)
78. IF(KT.GT.59)STOP
79.*** CALC. DZ AND I INDICES
80. M1=2
81. M=2*M1+18
82. M2=M/2
83. M3=M+1
84. DZ=DZ1*(DPULSE**DZ2)/SQRT(ABS(1))
85. IF(ILENS.EQ.1)DZ=DZ1*(DPULSE**DZ2)/SQRT(ABS(4))
86.*** STORE AXIAL DISTANCES TO INTERFACES OF EYE
87. ZD(1)=1.F-25
88. ZD(2)=ZD(1)+TH(1)
89. ZD(3)=ZD(2)+TH(2)
90. ZD(4)=ZD(3)+TH(3)
91. ZD(5)=ZD(4)+TH(4)
92. ZD(6)=ZD(5)+TH(5)
93. ZD(7)=ZD(6)+TH(6)
94. ZD(8)=ZD(7)+10.
95. CALL GRID
96.*** CALCULATE AND STORE I,J INDICES AT WHICH TEMPERATURES ARE PRINTED
97. ID1=ID1+IP1
98. ID2=ID2+JP1
99. IF(ID1.LT.IP1)ID1=IP1
100. IF(ID2.GT.M)ID2=M
101. IF(JD2.GT.N)JD2=N
102. WRITE(6,15)ID1,ID2,JD1,JD2
103. 15 FORMAT(1H0,4HID1=,I2,3X,4HID2=,I2,3X,4HJD1=,I2,3X,4HJD2=,I2)
104. WRITE(6,18)(R(J),J=1,N3)
105. 18 FORMAT(1H0,2HHR=/(1X,10F8.4))
106. WRITE(6,19)(7(I),I=1,M3)
107. 19 FORMAT(1H0,2HZ=/(1X,10F8.4))
108.*** CALC. NORMALIZED LASER PROFILES---
109. POX=POW
110. CALL IMAGE
111. WRITE(6,26)GP,(HR(L),L=1,N)
112. 26 FORMAT(1H0,3HGP=,E8.3,3X,3HHR=/(1X,10E8.3))
113. DO 27 J=1,N3
114. DO 27 I=1,M3

```

# MAIN (CORNEAL)

```

115. V(I,J)=1.E-10
116. 27 S(I,J)=0.
117. WRITE(6,32)(REPET(L),L=1,NTEST)
118. 32 FORMAT(1H0,6HREPET=/(1X,10E8.3))
119. WRITE(6,33)(NPULSE(L),L=1,NTEST)
120. 33 FORMAT(1H0,7HNPULSE=/(1X,10I8))
121. DO 34 J=1,M3
122. DO 34 J=1,M3
123. 34 VC(I,J,1)=1.E-10
124. WRITE(6,35)(ABS(L),L=1,6),AP,DPULSF,DR,DT,DZ,IP1,IP2,IP3,IP4,IP5,
125. 1IP6,JVL,KM,KT,LIM,LP1,LP2,LP3,LP4,LP5,LP6,M,M1,N,N1,NP,NTEST,POW.
126. 2PTIME,QP,(REF(I1),L1=1,L7),RIM,RVL,(TH(L2),L2=1,LZ),TIME,TO,XC
127. 35 FORMAT(1H0,4HARS=,6F9.0,2X,3HAP=,F6.3/1X,7HDPULSF=,E8.3,2X,3HDR=,
128. 1E8.3,2X,3HDT=,E8.3,2X,3HDZ=,E8.3,2X,4HIP1=,I2,2X,4HIP2=,I2/1X,
129. 24HIP3=,I2,2X,4HIP4=,I2,2X,4HIP5=,I2,2X,4HIP6=,I2,2X,4HJVL=,I2,2X,
130. 33HKM=,I3,2X,3HK1=,I3,2X,4HLIM=,I2,2X,4HLP1=,I2/1X,4HLP2=,I2,2X,
131. 44HLP3=,I2,2X,4HLP4=,I2,2X,4HLP5=,I2,2X,4HLP6=,I2,2X,
132. 52HM=,I2,2X,3HM1=,I2,2X,2HN=,I2,2X,3HN1=,I2,2X,3HNP=,I2/1X,6HNTFST=
133. 6,I2,2X,4HPOW=,E8.3,2X,6HPTIME=,E8.3,2X,3HQP=,E8.3/1X,4HREF=,6F9.3,
134. 72X,4HRIM=,F8.3/1X,4HRLV=,F7.3,2X,3HTH=,5E10.3/1X,E10.3,2X,5HTIME=,
135. 8E8.3,2X,3HTO=,F6.1,2X,3HXC=,F6.2)
136. READ(5,8)KTYPEO
137. READ(5,8)KTYPE
138. L1=KTYPE
139. IF(KTYPE.EQ.0)L1=1
140. READ(5,7)(TIMEX(K),K=1,L1)
141. READ(5,5)I11,I12,I13,JJ1,JJ2
142.*** START OF TEMPERATURE CALCULATIONS FOR ONE PULSE. TO BE USED EITHER
143.*** FOR MULTIPLE OR SINGLE PULSED EXPOSURES
144. -----
145. XT(1)=0.
146. DTX=DT
147. KTX=KT+1
148. DO 36 K=2,KTX
149. XT(K)=XT(K-1)+DT
150. 36 DT=XC*DT
151. IKX=TIME**EDT1+EDT2
152. IF(IKX.LT.1)IKX=1
153. XX=2*IKX
154. WRITE(6,37)IKX
155. 37 FORMAT(1H0,4HIKX=,I2)
156. K=2
157. IHT=2
158. IYPEX=ITYPE
159. 38 DT=XT(K)-XT(K-1)
160. IF(K.GT.KM)QP=0.
161. CALL HTXDEP
162. IF(K.GT.2)GO TO 41
163. DO 40 I=IP1,M
164. WRITE(6,39)(S(I,J),J=1,N)
165. 39 FORMAT(1H ,2HS=,10F8.3)
166. 40 CONTINUE
167. 41 WRITE(6,42)XT(K),K,POW
168. 42 FORMAT(1H0,5HTIME=,E8.3,3X,2HK=,I2,3X,6HPOWER=,E8.3,5HWATTS)
169.*** CALCULATE TEMPERATURE RISE(MATRIX REDUCTION ALGORITHM)
170.*** COLUMNS(NORMAL)-----
171. IK=1

```

# MAIN (CORNEAL)

```

172. 43 DO 45 I=IP1,M
173.     W=XX*VSH(I)/DT
174.     DO 44 J=1,N
175.     FXC(J)=W+CON(I)*B(J,2)
176.     IF(J.GT.1)FXC(J)=FXC(J)+CON(I)*B(J,1)*CXC(J-1)
177.     CXC(J)=-CON(I)*B(J,3)/FXC(J)
178.     SUM=(W-A(I,2))*V(I,J)+A(I,1)*V(I-1,J)+A(I,3)*V(I+1,J)+S(I,J)
179.     DXC(J)=SUM/FXC(J)
180.     IF(J.GT.1)DXC(J)=(SUM+CON(I)*B(J,1)*DXC(J-1))/FXC(J)
181. 44 CONTINUE
182.     VX=0.
183.     DO 45 L=1,N
184.     J=N+1-L
185.     VX=DXC(J)-CXC(J)*VX
186. 45 VXX(I,J)=VX
187.     DO 46 I=IP1,M
188.     DO 46 J=1,N
189. 46 V(I,J)=VXX(I,J)
190.*** ROWS(NORMAL)-----
191.     CXR(IP1-1)=0.
192.     DO 50 J=1,N
193.     DO 48 I=IP1,M
194.     W=XX*VSH(I)/DT
195.     FXR(I)=W+A(I,2)+A(I,1)*CXR(I-1)
196.     CXR(I)=-A(I,3)/FXR(I)
197.     SUM=(W-CON(I)*B(J,2))*V(I,J)+CON(I)*B(J,3)*V(I,J+1)+S(I,J)
198.     IF(J.GT.1)SUM=SUM+CON(I)*B(J,1)*V(I,J-1)
199.     DXR(I)=SUM/FXR(I)
200.     IF(I.GT.IP1)DXR(I)=(SUM+A(I,1)*DXR(I-1))/FXR(I)
201. 48 CONTINUE
202.     VX=0.
203.     DO 50 I=IP1,M
204.     I=M+IP1-L
205.     VX=DXR(I)-CXR(I)*VX
206.     VC(I,J,K)=VX
207. 50 VXX(I,J)=VX
208.     DO 51 I=IP1,M
209.     DO 51 J=1,N
210. 51 V(I,J)=VXX(I,J)
211.     IK=IK+1
212. ** RECYCLE TEMPERATURE CALCULATIONS
213.     IF(IK.LE.IKX)GO TO 43
214.     IF(K.EQ.KM)GO TO 62
215.     IF(ITYPEX.LT.ITYPE.AND.K.LT.KT)GO TO 66
216. 62 WRITE(6,63)(R(J),J=JD1,JD2)
217. 63 FORMAT(1H ,10X,2HR=,9F8.5/13X,30H-----)
218.     DO 65 I=ID1,ID2
219.     WRITE(6,64)Z(I),(VC(I,J,K),J=JD1,JD2)
220. 64 FORMAT(1H ,2H2=,F8.5,2X,9F8.1)
221. 65 CONTINUE
222.     ITYPEX=0
223. 66 K=K+1
224.     ITYPEX=ITYPEX+1
225.     IF(K.LE.K1)GO TO 38
226. *** READ NORMALIZED TEMPERATURE RISES TS OF GRANULES FOR .3E-8 PULSE
227. *** AND CALCULATE NORMALIZED RISES XPD FOR ACTUAL PULSE
228. 70 FORMAT(1H0,61HDIMENSION OF ARRAYS ASSOCIATED WITH ARGUMENT LIJ IS

```

# MAIN (CORNEAL)

```

229. 1TOD SMALL)
230. READ(5,6)DIM,LTMAX
231. DO 71 L1=1,LTMAX
232. 71 TS(L1)=1.
233. READ(5,4)(TS(L),L=1,LTMAX,10)
234. CALL MXGRAN
235. DO 72 L=1,KT
236. 72 XPD(L)=AP*XPD(L)+1.-AP
237. READ(5,4)(DAMAGE(L2,1),DAMAGE(L2,2),L2=1,2),TSTEAM,DTSTM
238. WRITE(6,73)WAVEL,TSTEAM,DAMAGE(1,1),DAMAGE(1,2),DAMAGE(2,1),
239. 1DAMAGE(2,2)
240. 73 FORMAT(1H0.11HWAVELENGTH=,F7,1,2HNM,3X,7HTSTFAM=,F6,0,3X,7HDAMAGE=
241. 1,4F9,0)
242.*** CALCULATE I,J INDICES AT WHICH DAMAGE CALCULATIONS ARE TO BE MADE
243. JM=0
244. DO 74 J=1,N
245. IF(R(J).LT.RMAX+.000001)JM=J+1
246. 74 CONTINUE
247. X1=0.
248. DO 75 I=IP1,M
249. IF(Z(I).LT..0006)GO TO 75
250. IF(VC(I,1,KM).GT.X1)IMAX=I
251. IF(VC(I,1,KM).GT.X1)X1=VC(I,1,KM)
252. 75 CONTINUE
253. L=0
254. ID1=IMAX-LIMAX
255. IF(ID1.LT.IP1)ID1=IP1
256. ID2=IMAX+LIMAX
257. DO 76 I=ID1,ID2
258. DO 76 J=1,JM
259. L=L+1
260. ID(L)=I
261. 76 JD(L)=J
262. LIJ=(ID2-ID1+1)*JM
263. IF(LIJ.GT.20)WRITE(6,70)
264. IF(LIJ.GT.20)STOP
265. IF(LPX.EQ.0)GO TO 125
266.*** TEMPERATURE AND DAMAGE EVALUATIONS FOR MULTIPLE PULSES
267. -----
268.*** EVALUATE TEMPERATURE RISES WITH AND WITHOUT GRANULES
269. DO 77 L=1,LIJ
270. I=ID(L)
271. J=JD(L)
272. VE(L,1,1)=0.
273. VE(L,1,2)=0.
274. DO 77 K=2,KT
275. VE(L,K,1)=VC(I,J,K)
276. VE(L,K,2)=VC(I,J,K)
277. IF(I.NE.1G)GO TO 77
278. VE(L,K,2)=XPD(K)*VC(I,J,K)
279. 77 CONTINUE
280. X60=(XC-1.)/DTX
281. X61=ALOG(XC)
282. XSTEAM=TSTEAM
283. DO 108 L13=1,NTEST
284. X3=DPULSE+(NPULSE(L13)-1)/REPET(L13)
285. WRITE(6,78)NRUN(L13),X3,DPULSE,NPULSE(L13),RFPFT(L13)

```



# MAIN(CORNEAL)

```

286. 78 FORMAT(1H0.5HNRUN=,I3,2X,13HTRAIN LENGTH=,F8.3,3HSFC,2X,12HPULSE W
287. 11DTH=,F6.3,2X,3HSEC/1X,17HNUMBER OF PULSES=,I5,3X,16HREPEITION RA
288. 21E=,F8.3,10HPULSES/SFC)
289. WRITE(A,79)RIM,LFSION
290. 79 FORMAT(1H ,12HBEAM RADIUS=,F8.3,2HCM,5X,14HLESTON RADIUS=,F8.3,2HC
291. 1M)
292. TC=1./REPET(L13)
293. NPL=NPULSE(L13)
294. KX=NP+3
295. LN=1
296. 83 IF(NPL/IN.LT.20)GO TO 84
297. IN=IN+2
298. GO TO 83
299. 84 X1=NPL
300. INX=.5+X1/IN
301. L1=ALOG(DPULSE)/.69315+20.
302. IF(L1.LT.1) L1=1
303. INXX=PTIME(L1)*INX
304. *** STROKE TIME INTERVALS AND LOGS OF INTERVALS FOR DAMAGE CALCULATIONS
305. ZIX(1)=PTIME
306. ZI(1)=PTIME/2.
307. ZIT(1)=ALOG(IN*PTIME)
308. DO 85 L3=2,NP
309. ZIT(L3)=ALOG(IN+PTIME)
310. ZTX(L3)=ZTX(L3-1)+PTIME
311. 85 ZI(L3)=ZT(L3-1)+PTIME
312. L1=NP+1
313. X3=(TC-DPULSE)/(KX-NP)
314. ZIX(L1)=DPULSE+X3
315. ZI(L1)=DPULSE+X3/2.
316. ZIT(L1)=ALOG(IN*X3)
317. L1=L1+1
318. DO 86 L3=L1,KX
319. ZIT(L3)=ALOG(IN*X3)
320. ZTX(L3)=ZTX(L3-1)+X3
321. 86 ZI(L3)=ZI(L3-1)+X3
322. *** CALCULATE TEMPERATURE RISES ASSOCIATED WITH L3-TH TIME INTERVAL
323. *** FOLLOWING (L6+.5)*IN=.5 PULSE
324. DO 95 L=1,L1
325. DO 95 L3=1,KX
326. X1=0.
327. X2=0.
328. L1=1+IN/2
329. L7=1
330. 87 X3=(L7-1)*TC+ZT(L3)
331. K=ALOG(X3+X60+1.)/X61+1.
332. X5=VE(L,K,1)+(X3-XT(K))*(VE(L,K+1,1)-VE(L,K,1))/(XT(K+1)-XT(K))
333. X1=X1+X5
334. X3=(L7-1)*TC+ZTX(L3)
335. K=ALOG(X3+X60+1.)/X61+1.
336. X2=X2+VE(L,K,2)+(X3-XT(K))*(VE(L,K+1,2)-VE(L,K,2))/(XT(K+1)-XT(K))
337. IF(X5.LT..0001*X1)GO TO 88
338. L7=L7+1
339. IF(L7.EQ.L1)GO TO 87
340. 88 VZ(L,1,L3,1)=X1
341. (L,1,L3,2)=X2
342. DO 93 L6=2,INXX

```

# MAIN (CORNEAL)

```

343. IF(X5.LT..0001*X1)GO TO 91
344. X1=VZ(L,L6-1,L3,1)
345. X2=VZ(L,L6-1,L3,2)
346. L2=L1+1
347. L1=L1+IN
348. L7=L2
349. 90 X3=(L7-1)*TC+ZT(L3)
350. K=ALOG(X3*X60+1.)/X61+1.
351. X5=VE(L,K,1)+(X3-XT(K))*(VE(L,K+1,1)-VF(L,K,1))/(XT(K+1)-XT(K))
352. X1=X1+X5
353. X3=(L7-1)*TC+ZTX(L3)
354. K=ALOG(X3*X60+1.)/X61+1.
355. X2=X2+VE(L,K,2)+(X3-XT(K))*(VE(L,K+1,2)-VF(L,K,2))/(XT(K+1)-XT(K))
356. IF(X5.LT..0001*X1)GO TO 91
357. L7=L7+1
358. IF(L7.LE.L1)GO TO 90
359. 91 VZ(L,L6,L3,1)=X1
360. 93 VZ(L,L6,L3,2)=X2
361. L1=INX+1
362. DO 94 L6=L1,INXX
363. L6=L6-INX
364. VZ(L,L6,L3,1)=VZ(L,L6,L3,1)-VZ(L,L8,L3,1)
365. 94 VZ(L,L6,L3,2)=VZ(L,L6,L3,2)-VZ(L,L8,L3,2)
366. 95 CONTINUE
367. *** DAMAGE CALCULATIONS -----
368. TSTEAM=XSTEAM
369. XQ=0.
370. 96 WRITE(6,129)TSTEAM
371. DO 104 L=1,LIJ
372. I=ID(L)
373. J=JD(L)
374. IF(VZ(L,INX,NP,1).LT..001)GD(I,J)=1.E+20
375. IF(VZ(L,INX,NP,1).LT..001)GO TO 104
376. L9=10.*(1.4+EXP(-.0014*DPULSE))/VZ(L,INX,NP,1)
377. CQ=L9+1.
378. X10=70.*(1.4+EXP(-.0014*DPULSE))/VZ(L,INX,NP,1)
379. IF(L9.EQ.0)CQ=X10
380. LLT=0
381. LGT=0
382. 99 DAMC=0.
383. L6=1
384. 100 DO 101 L3=1,KX
385. X3=0.
386. IF(VZ(L,L6,L3,2)*CQ.GT.TSTEAM-T0)X3=1.E+30
387. IF(VZ(L,L6,L3,2)*CQ.GT.TSTEAM-T0)GO TO 101
388. X50=VZ(L,L6,L3,1)*CQ+273.+T0
389. IF(X50.LT.317.)GO TO 101
390. X1=ZTT(L3)+DAMAGE(1,1)-DAMAGE(1,2)/X50
391. IF(X50.GT.323.)X1=ZTT(L3)+DAMAGE(2,1)-DAMAGE(2,2)/X50
392. IF(X1.GT.0.)X3=1.01
393. IF(X1.GT.0.)GO TO 101
394. X3=EXP(X1)
395. 101 DAMC=DAMC+X3
396. IF(DAMC.GT.1.)GO TO 102
397. *** INCREASE TIME INDICES AND CONTINUE
398. L6=L6+1
399. IF(L6.LE.INXX)GO TO 100

```

# MAIN(CORNEAL)

```

400. *** ADJUST LASER POWER TO YIELD THRESHOLD DAMAGE AT GIVEN POINT
401. IF(LGT.EQ.1)CQ=1.02*CQ
402. IF(LGT.EQ.1)GO TO 103
403. LLT=1
404. CQ=1.04*CQ
405. GO TO 99
406. 102 IF(LLT.EQ.1)CQ=.98*CQ
407. IF(LLT.EQ.1)GO TO 103
408. LGT=1
409. CQ=.96*CQ
410. GO TO 99
411. 103 QD(I,J)=CQ*POX
412. 104 CONTINUE
413. WRITE(6,63)(R(J),J=1,JM)
414. DO 106 I=ID1,ID2
415. WRITE(6,105)Z(I),(QD(I,J),J=1,JM)
416. 105 FORMAT(1H,2HZ=,F7.5,1X,3HQD=,8E8.3)
417. 106 CONTINUE
418. X2=(XQ-QD(IMAX,1))/QD(IMAX,1)
419. X3=X2*X2
420. IF(X3.LT..0001)GO TO 108
421. TSTEAM=TSTEAM+DTSIM
422. XQ=QD(IMAX,1)
423. GO TO 96
424. 108 CONTINUE
425. IF(KTYPE.EQ.0)GO TO 174
426. *** CALCULATE AND STORE TEMPERATURES FOR PLOTTING TEMPERATURE PROFILES
427. TC=1./REPET(1)
428. NPL=NPULSE(1)
429. DO 123 L15=1,KTYPE
430. IF(TIMEX(L15).GT.XT(KT)) GO TO 123
431. RGV=0.
432. L2=TIMEX(L15)/TC
433. DTIME=TIMEX(L15)-L2*TC
434. L2=L2+1
435. DO 116 I=II1,II2
436. DO 116 J=JJ1,JJ2
437. X1=0.
438. DO 113 L6=1,L2
439. K=ALOG((DTIME+(L6-1)*TC)*X60+1.)/X61+1.
440. X2=(DTIME+(L6-1)*TC-XT(K))/(XT(K+1)-XT(K))
441. 113 X1=X1+VC(I,J,K)+X2*(VC(I,J,K+1)-VC(I,J,K))
442. V(I,J)=X1
443. L3=L2-NPL
444. IF(L3.LE.0)GO TO 115
445. X1=0.
446. DO 114 L6=1,L3
447. K=ALOG((DTIME+(L6-1)*TC)*X60+1.)/X61+1.
448. X2=(DTIME+(L6-1)*TC-XT(K))/(XT(K+1)-XT(K))
449. 114 X1=X1+VC(I,J,K)+X2*(VC(I,J,K+1)-VC(I,J,K))
450. V(I,J)=V(I,J)+X1
451. 115 IF(V(I,J).GT.RGV)RGV=V(I,J)
452. 116 CONTINUE
453. IF(KTYPEQ.EQ.1)GO TO 121
454. WRITE(1,117)NRUN(1),NPULSE(1),REPET(1)
455. 117 FORMAT(2I7,F7.1)
456. WRITE(1,118)CPULSE,WAVEL,RIM

```

# MAIN(CORNEAL)

```

457. 118 FORMAT(10E8.3)
458.  WRITE(1,119)II1,II2,II3,JJ1,JJ2
459. 119 FORMAT(5I7)
460.  WRITE(1,119)N3,M3
461.  WRITE(1,120)(R(J),J=1,N3)
462. 120 FORMAT(10F7.4)
463.  WRITE(1,120)(Z(I),I=1,M3)
464.  WRITE(1,118)TIMEX(L15)
465. 121 DO 122 I=II1,II2
466.  WRITE(6,128)(V(I,J),J=JJ1,JJ2)
467.  IF(KTYPED.F0.1)GO TO 122
468.  WRITE(1,128)(V(I,J),J=JJ1,JJ2)
469. 122 CONTINUE
470. 123 CONTINUE
471.  GO TO 174
472. *** DAMAGE CALCULATIONS FOR SINGLE PULSE
473.  -----
474. 125 WRITE(6,126)NRUN(1),DPULSE,NPULSE(1)
475. 126 FORMAT(1H0.5HNRUN=,I3.2X,1PHPULSE WIDTH=,E8.3,2X,17HNUMBER OF PULS
476. 1ES=,I5)
477.  WRITE(6,79)RIM,LFSION
478.  XQ=0.
479. 127 WRITE(6,129)TSTEAM
480. 128 FORMAT(10F7.1)
481. 129 FORMAT(1H0.7HTSTEAM=,F7.0/1X,10H-----)
482.  DO 138 I=ID1,ID2
483.  DO 138 J=1,JM
484.  IF(VC(I,J,KM).LT..001)QD(I,J)=1.E+20
485.  IF(VC(I,J,KM).LT..001)GO TO 138
486.  L9=10.*(1.+EXP(-.0014*DPULSE))/VC(I,J,KM)
487.  CQ=L9+1.
488.  X10=70.*(1.+EXP(-.0014*DPULSE))/VC(I,J,KM)
489.  IF(L9.F0.0)CQ=X10
490.  LLT=0
491.  LGT=0
492. 130 DAMC=0.
493.  K=2
494. 131 X13=ALOG(XT(K)-XT(K-1))
495.  VPX=(VC(I,J,K)+VC(I,J,K-1))/2.
496.  X3=0.
497.  IF(1.NE.IG)GO TO 133
498.  IF(VPX*XPD(K)*CQ.GT.TSTEAM-T0)X3=1.E+30
499.  IF(VPX*XPD(K)*CQ.GT.TSTEAM-T0)GO TO 134
500. 133 X50=VPX*CQ+273.+T0
501.  IF(X50.LT.317.)GO TO 134
502.  X1=X13+DAMAGE(1,1)-DAMAGE(1,2)/X50
503.  IF(X50.GT.323.)X1=X13+DAMAGE(2,1)-DAMAGE(2,2)/X50
504.  IF(X1.GT.0.)X3=1.01
505.  IF(X1.GT.0.)GO TO 134
506.  X3=EXP(X1)
507. 134 DAMC=DAMC+X3
508.  IF(DAMC.GE.1.)GO TO 135
509.  K=K+1
510.  IF(K.LT.KT)GO TO 131
511. *** ADJUST LASER POWER TO YIELD THRESHOLD DAMAGE AT GIVEN POINT
512.  IF(LGT.F0.1)CQ=1.02*CQ
513.  IF(LGT.E0.1)GO TO 136

```

MAIN (CORNEAL)

```

514.      LLT=1
515.      CQ=1.04*CQ
516.      GO TO 130
517. 135  IF(LLT.EQ.1)CQ=.98*CQ
518.      IF(LLT.EQ.1)GO TO 136
519.      LGT=1
520.      CQ=.96*CQ
521.      GO TO 130
522. 136  QD(I,J)=CQ*POX
523. 138  CONTINUE
524.      WRITE(6,63)(R(J),J=1,JM)
525.      DO 143 I=I1,I2
526.      WRITE(6,105)Z(I),(QD(I,J),J=1,JM)
527. 143  CONTINUE
528.      X2=(XQ-QD(IMAX,1))/QD(IMAX,1)
529.      X3=X2*X2
530.      IF(X3.LT..0001)GO TO 150
531.      TSTEAM=TSTEAM+DTSIM
532.      XQ=QD(IMAX,1)
533.      GO TO 127
534. ***  CALCULATE AND STORE TEMPERATURES FOR PLOTTING PROFILE
535. 150  IF(KTYPE.EQ.0)GO TO 174
536.      DO 170 L15=1,KTYPE
537.      DTIME=TIMEX(L15)
538.      K=ALOG(DTIME*(XC-1.)/DTX+1.)/ALOG(XC)+1.
539.      IF(K+1.GT.KT)GO TO 170
540.      X1=(DTIME-XT(K))/(XT(K+1)-XT(K))
541.      RGV=0.
542.      DO 166 I=I1,I2
543.      DO 166 J=J1,JJ2
544.      V(I,J)=VC(I,J,K)+X1*(VC(I,J,K+1)-VC(I,J,K))
545.      IF(V(I,J).GT.RGV)RGV=V(I,J)
546. 166  CONTINUE
547.      IF(KTYPEQ.FQ.1)GO TO 167
548.      WRITE(1,117)NRUN(1),NPULSE(1),REPET(1)
549.      WRITE(1,118)DPULSE,WAVEL,RIM
550.      WRITE(1,119)I1,I2,I3,JJ1,JJ2
551.      WRITE(1,110)N3,M3
552.      WRITE(1,120)(R(J),J=1,N3)
553.      WRITE(1,120)(Z(I),I=1,M3)
554.      WRITE(1,118)TIMEX(L15)
555. 167  DO 168 I=I1,I2
556.      WRITE(6,128)(V(I,J),J=JJ1,JJ2)
557.      IF(KTYPEQ.FQ.1)GO TO 168
558.      WRITE(1,128)(V(I,J),J=JJ1,JJ2)
559. 168  CONTINUE
560. 170  CONTINUE
561. ***  INTERPOLATE AXIAL EXTENT OF DAMAGE
562. 174  IP=M2+2-M1
563.      IF(ILENS.EQ.0)IP=1P1
564.      I5=0
565.      I6=0
566.      IF(ID1.EQ.ID2)GO TO 182
567.      DO 175 I=ID1,ID2
568.      L1=ID1+ID2-I
569.      IF(QD(L1,1).GT.POX)I5=L1
570.      IF(QD(L1,1).LT.POX)I6=L1

```

# MAIN(CORNEAL)

```

571. IF(QD(I,1).GT.POX)I7=1
572. IF(QD(I,1).LT.POX)I8=1
573. 175 CONTINUE
574. IF(I5.EQ.0)WRITE(6,176)
575. 176 FORMAT(1H0.45HDEPTHS OF DAMAGE BEYOND BOTH SPECIFIED DEPTHS)
576. IF(I5.EQ.0)GO TO 182
577. IF(I6.EQ.0)GO TO 190
578. IF(I5.GE.I6)GO TO 178
579. X2=ALOG(QD(I6,1)/QD(I5,1))/(Z(I6)-Z(I5))
580. X1=QD(I5,1)
581. X3=ALOG(POX/X1)/X2+Z(I5)-Z(IP)+DZ/2.
582. WRITE(6,177)X3
583. 177 FORMAT(1H0.24HMINIMUM DEPTH OF DAMAGE=,E8.3,2HCM)
584. 178 IF(I8.GE.I7)GO TO 182
585. X2=ALOG(QD(I8,1)/QD(I7,1))/(Z(I8)-Z(I7))
586. X1=QD(I7,1)
587. X3=ALOG(POX/X1)/X2+Z(I7)-Z(IP)+DZ/2.
588. 180 WRITE(6,181)X3
589. 181 FORMAT(1H0.24HMAXIMUM DEPTH OF DAMAGE=,E8.3,2HCM)
590. *** INTERPOLATE RADIAL EXTENT OF IRREVERSIBLE DAMAGE AT SPECIFIED DEPTHS
591. 182 DO 189 I=ID1,ID2
592. J1=0
593. X3=Z(I)-7(IP)+DZ/2.
594. DO 183 J=1,JM
595. IF(POX.GT.QD(I,J))J1=J
596. 183 CONTINUE
597. X20=0.
598. IF(J1.EQ.0)GO TO 187
599. IF(J1.EQ.JM)WRITE(6,185)X3,R(JM)
600. 185 FORMAT(1H0.2HZ=,E8.3,2HCM,5X,36HRADIAL EXTENT OF DAMAGE GREATER TH
601. 1AN,E8.3,2HCM)
602. IF(J1.EQ.JM)GO TO 189
603. X2=ALOG(QD(I,J1+1)/QD(I,J1))/(R(J1+1)-R(J1))
604. X1=QD(I,J1)
605. X20=ALOG(POX/X1)/X2+R(J1)
606. 187 WRITE(6,188)X3,X20
607. 188 FORMAT(1H0.2HZ=,E8.3,2HCM,5X,37HRADIAL EXTENT OF IRREVERSIBLE DAMA
608. 1GE=,E8.3,2HCM)
609. 189 CONTINUE
610. STOP
611. 190 WRITE(6,191)
612. 191 FORMAT(1H0.31HNO DAMAGE---LASER POWER TOO LOW)
613. STOP
614. END

```

END UT TIME: 1.793 SECONDS.

OF IN

T/IN KRI111

# SUBROUTINE GRID(CORNEAL)

```

1. SUBROUTINE GRID
2. *** GRID COMPUTES THE COEFFICIENTS IN PARTIAL DIFFERENTIAL EQUATIONS A AND
3. *** RADIAL AND AXIAL COORDINATES, R AND Z, AND ASSIGNS CONDUCTIVITY AND
4. *** VOLUMETRIC SPECIFIC HEAT TO GRID
5. COMMON A(23,3),ARS(6),AP,B(11,3),CON(23),CONX(6),CUT,DIM,DPULSE,
6. 1DR,DT,DTX,DZ,HR(11),IG,IHT,I LENS,IPROF,IP1,IP2,IP3,IP4,IP5,IP6,
7. 2JVL,LIM,LP1,LP2,LP3,LP4,LP5,LP6,LPX,LTMAX,LZ,K,KT,M,M1,M2,M3,N,
8. 3N1,N3,N4,POX,PTIME,QP,R(11),REF(7),RIM,RN,RVL,S(23,11),TH(A),
9. 4TS(2200),V(23,11),VC(23,11,60),VSH(23),VSHX(6),XC,WAVEL,XPD(60),
10. 5XT(60),Z(23),ZCON(23,11),ZD(8),ZM
11. DIMENSION IX(6),LX(6)
12.
13. R(1)=0.
14. CK=N=N1
15. CP=RVL/DR=N1+1.
16. X1=2.
17. 180 R2=EXP(ALOG(2.*(CP*(X1-1.)+1.)/(X1+1.))/(CK-1.))
18. IF(R2/X1.GT..999999.AND.R2/X1.LT.1.000001)GO TO 183
19. X1=R2
20. WRITE(6,182)CP,CK,N1,N,DR,X1
21. 182 FORMAT(1H0,2E10.5,2I7,2E10.5)
22. GO TO 180
23. 183 WRITE(6,184)P2
24. 184 FORMAT(1H ,3HR2=,F8.4)
25. RN=DR*(N1-1.+(R2**((CK+1.))-1.)/(R2-1.))
26. *** CALCULATE RADIAL SPACE STEPS R(J).
27. DO 185 J=2,N4
28. 185 R(J)=DR*(J-1)
29. X1=R2*DR
30. DO 186 J=N4,N
31. R(J+1)=R(J)+X1
32. 186 X1=R2*X1
33. *** CALCULATE COEFFICIENTS B OF FINITE DIFFERENCE EQNS.
34. X1=2./(DR*DR)
35. DO 187 J=2,N1
36. B(J,1)=.25*(2*J-3)*X1/(J-1)
37. B(J,2)=X1
38. 187 B(J,3)=X1-R(J,1)
39. X2=DR
40. X1=R2*DR
41. DO 188 J=N4,N
42. B(J,2)=2./(X1*X2)
43. B(J,1)=(2./X2-1./R(J))/(X1+X2)
44. B(J,3)=B(J,2)-B(J,1)
45. X2=R2*X2
46. 188 X1=R2*X1
47. B(1,1)=0.
48. B(1,2)=2./(DR*DR)
49. B(1,3)=B(1,2)
50. DO 189 J=1,N
51. IF(R(J).LT.RVL)JVL=J
52. 189 CONTINUE
53. *** CALCULATE AXIAL SPACE STEPS Z(I)
54. X1=2.
55. IP1=4
56. IF(I LENS.EQ.0)IP1=M2-M1+2
57. CK=M2-M1+3-IP1

```

# GRID (CORNEAL)

```

58.      IF (ILENS.EQ.0) CK=M2-M1+1
59. 190  CP=2.*ZD(4)/DZ+1.-(X1**CK-1.)/(X1-1.)
60.      IF (ILENS.EQ.0) CP=ZD(7)/DZ-2.*M1+1.5
61.      R1=EXP(ALOG(CP*X1-CP+1.)/CK)
62.      IF (R1/X1.GT..999999.AND.R1/X1.LT.1.000001) GO TO 193
63.      X1=R1
64.      WRITE(6,191) CP,CK,M2,M1,ZD(4),ZD(7),DZ,X1
65. 191  FORMAT(1H0,2E10.5,2I7,4E10.5)
66.      GO TO 190
67. 193  CK=M2-M1+1
68.      ZM=((R1**CK-1.)/(R1-1.)+M1-1.)*DZ
69.      WRITE(6,194) R1,ZM
70. 194  FORMAT(1H ,3HR1=,F8.4,2X,3HZM=,F8.4)
71.      X1=DZ
72.      X2=X1
73.      DO 195 I=2,M2
74.          Z(M2+I)=ZM+X2
75.          Z(M2+2-I)=ZM-X2
76.          IF (I.GT.M1) X1=R1*X1
77. 195  X2=X2+X1
78.          Z(1)=0.
79.          Z(M2+1)=ZM
80.          Z(M+1)=2.*ZM
81.          X1=(Z(IP1-1)+Z(IP1))/2.
82.          DO 196 I=1,M3
83. 196  Z(I)=Z(I)-X1
84.          L3=IP1
85.          DO 200 L=1,6
86.              L1=0
87.              DO 197 I=IP1,M3
88.                  IF (Z(I).LT.ZD(L+1)) L3=I
89.                  IF (Z(I).LT.ZD(L).OR.Z(I).GE.ZD(L+1)) GO TO 197
90.                  L2=I
91.                  L1=L1+1
92. 197  CONTINUE
93.          IF (L1.EQ.0) IX(L)=L3
94.          IF (L1.EQ.0) LX(L)=L3
95.          IF (L1.GT.0) IX(L)=L2+1-L1
96.          IF (L1.GT.0) LX(L)=L2
97. 200  CONTINUE
98.          IP2=IX(2)
99.          IP3=IX(3)
100.         IP4=IX(4)
101.         IP5=IX(5)
102.         IP6=IX(6)
103.         LP1=LX(1)
104.         LP2=LX(2)
105.         LP3=LX(3)
106.         LP4=LX(4)
107.         LP5=LX(5)
108.         LP6=M3
109. ***  SET CONDUCTIVITY CON AND HEAT CAPACITY VSH FOR VARIOUS EYE MEDIA
110.      DO 203 I=1,LP1
111.          CON(I)=CONX(1)
112. 203  VSH(I)=VSHX(1)
113.      DO 204 I=IP2,LP2
114.          CON(I)=CONX(2)

```



# GRID(CORNEAL)

```

115. 204 VSH(I)=VSHX(2)
116.      DO 205 I=IP3,LP3
117.      CON(I)=CONX(3)
118. 205 VSH(I)=VSHX(3)
119.      DO 206 I=IP4,LP4
120.      CON(I)=CONX(4)
121. 206 VSH(I)=VSHX(4)
122.      DO 207 I=IP5,LP5
123.      CON(I)=CONX(5)
124. 207 VSH(I)=VSHX(5)
125.      DO 208 I=JP6,M3
126.      CON(I)=CONX(6)
127. 208 VSH(I)=VSHX(6)
128. *** CALCULATE COEFFICIENTS A OF FINITE DIFFERENCE EQNS.
129.      DO 210 I=IP1,M
130.      X1=Z(I+1)-Z(I-1)
131.      X2=(CON(I-1)-CON(I+1))/(X1*X1)
132.      X3=2.*CON(I)/X1
133.      A(I,1)=X2+X3/(Z(I)-Z(I-1))
134.      IF(I.EQ.IP1)A(I,1)=0.
135.      A(I,3)=-X2+X3/(Z(I+1)-Z(I))
136. 210 A(I,2)=A(I,1)+A(I,3)
137.      RETURN
138.      END

```

# SUBROUTINE IMAGE(CORNEAL)

```

1.  SUBROUTINE IMAGE
2.  COMMON A(23,3),ARS(6),AP,B(11,3),CON(23),CONX(6),CUT,DIM,DPULSF,
3.  1DR,DT,DTX,DZ,HR(11),IG,IHT,I LENS,IPROF,IP1,IP2,IP3,IP4,IP5,IP6,
4.  2JVL,LIM,LP1,LP2,LP3,LP4,LP5,LP6,LPX,LTMAX,LZ,K,KT,M,M1,M2,M3,N,
5.  3N1,N3,N4,POX,PTIME,QP,R(11),REF(7),RTM,RN,RVL,S(23,11),TH(A),
6.  4TS(2200),V(23,11),VC(23,11,60),VSH(23),VSHX(6),XC,WAVEL,XPD(60),
7.  5XT(60),Z(23),ZCON(23,11),ZD(8),ZM
8.  DIMENSION FA(501),FP(501),FX(501),PX(30),RX(30)
9.  REAL NC
10.  LI=500
11.  DO 200 J=1,N3
12.  200 HR(J)=0.
13.  LII=LI
14.  DO 201 L=1,LI
15.  201 FX(L)=0.
16.  READ(5,202)PUPIL
17.  202 FORMAT(10E8,3)
18.  WRITE(6,203)PUPIL
19.  203 FORMAT(1H0,6HPUPIL=,F7.3)
20.  RINT=PUPIL/(LI-1)
21.  IF(IPROF.EQ.1)GO TO 214
22.  IF(IPROF.EQ.0)GO TO 219
23.  *** INTERPOLATE IRREGULAR LASER PROFILE(SYMMETRIC IN R) AT INTERVALS
24.  *** OF RINT STARTING AT R=0
25.  READ(5,205)LR
26.  205 FORMAT(I7)
27.  READ(5,206)(RX(L),L=1,LR)
28.  206 FORMAT(10E7,3)
29.  READ(5,206)(PX(L),L=1,LR)
30.  X1=PX(1)
31.  DO 207 L=1,LR
32.  207 PX(L)=PX(L)/X1
33.  X5=0.
34.  DO 208 L=2,LR
35.  X2=(PX(L)-PX(L-1))/(RX(L)-RX(L-1))
36.  X1=PX(L)-X2*RX(L)
37.  X3=X1*(RX(L)*RX(L)-RX(L-1)*RX(L-1))/2.
38.  X4=X2*(RX(L)*RX(L)*RX(L)-RX(L-1)*RX(L-1)*RX(L-1))/3.
39.  208 X5=X5+6.2832*(X3+X4)
40.  QP=POX*.23906*(1.-REF(1))/X5
41.  IF(RX(LR).LT.PUPIL)LII=RX(LR)/RINT+1
42.  L2=2
43.  X1=0.
44.  DO 213 L=1,LII
45.  210 IF(RX(L2).GT.X1)GO TO 212
46.  L2=L2+1
47.  IF(L2.LE.LR)GO TO 210
48.  GO TO 213
49.  212 X2=(X1-RX(L2-1))/(RX(L2)-RX(L2-1))
50.  FX(L)=PX(L2-1)+X2*(PX(L2)-PX(L2-1))
51.  213 X1=X1+RINT
52.  GO TO 222
53.  *** CALCULATE GAUSSIAN LASER PROFILE AT EACH VALUE OF R(J)
54.  214 SIGMA=R1M*SQRT(-2./ALOG(CUT))
55.  WRITE(6,216)SIGMA,P1M
56.  216 FORMAT(1H0,6HSIGMA=,E8.3,5X,4HR1M=,E8.3)
57.  DO 217 J=1,N

```

19A

---

19A\*

19A\*\*

19\*\*\*

---

# IMAGE (CORNEAL)

```

58.      X3=2.*R(J)*R(J)/(SIGMA*SIGMA)
59.      IF(X3.GT.80.)GO TO 217
60.      HR(J)=EXP(-X3)
61. 217  CONTINUE
62.      QP=2.*POX*.23906*(1.-REF(1))/(3.1416*SIGMA*SIGMA)
63.      GO TO 250
64. *** SPECIFY UNIFORM LASER PROFILE FROM R(1) TO R(LTM)
65. 219  DO 220 J=1,LIM
66. 220  HR(J)=1.
67.      QP=POX*.23906*(1.-REF(1))/(3.1416*PIM*PIM)
68.      GO TO 250
69. *** CALCULATE TOTAL AREA FA(L) AND PORTION OF LASERS POWER BETWEEN R=0
70. *** AND (L-.5)*RINT
71. 222  FP(1)=3.1416*FX(1)*RINT*RINT/4.
72.      FA(1)=3.1416*RINT*RINT/4.
73.      DO 224 L=2,LJI
74.      X1=(L-.5)*RINT
75.      X2=(L-1.5)*RINT
76.      FP(L)=FP(L-1)+FX(L)+3.1416*(X1*X1-X2*X2)
77. 224  FA(L)=FA(L-1)+3.1416*(X1*X1-X2*X2)
78. *** CALCULATE NORMALIZED PROFILE HP(J)...HR=1 AT R=0
79.      X1=0.
80.      X2=0.
81.      DO 225 J=1,N
82.      X3=R(J)/RINT+.5000001
83.      IF(X3.LT.1.)X3=1.0000001
84.      L2=X3
85.      IF(L2.GE.LJI)GO TO 225
86.      X4=X3-1.2
87.      X5=FP(L2)+X4*(FP(L2+1)-FP(L2))
88.      X6=FA(L2)+X4*(FA(L2+1)-FA(L2))
89.      HR(J)=(X5-X1)/(X6-X2)
90.      X1=X5
91.      X2=X6
92. 225  CONTINUE
93.      X1=HR(1)
94.      DO 227 J=1,N
95. 227  HR(J)=HR(J)/X1
96. 250  DO 297 I=1,P1,M
97.      DO 297 J=1,N
98. 297  ZCON(I,J)=0.
99.      READ(5,202)Z0,FC,PC,NC
100.     Z1=NC*Z0*FC/(NC*Z0-FC)
101.     DO 301 I=1,P1,M
102.     X0=1.-Z(I)/Z1
103.     ZCON(1,1)=1./(X0*X0)
104.     L=2
105.     DO 301 J=2,N
106.     X1=R(J)/X0
107. 298  IF(X1.LT.R(L))GO TO 299
108.     L=L+1
109.     IF(L.LE.N)GO TO 298
110.     GO TO 301
111. 299  X2=(X1-R(L-1))/(R(L)-R(L-1))
112.     ZCON(I,J)=0.
113.     IF(HR(J).LT.1.E-20)GO TO 301
114.     ZCON(I,J)=(HR(L-1)+X2*(HR(L)-HR(L-1)))/(HR(J)*X0*X0)
115. 301  CONTINUE
116.     RETURN

```

# SUBROUTINE HTXDEP (CORNEAL)

```

1. SUBROUTINE HTXDEP
2. *** HTXDEP COMPUTES RATE OF HEAT DEPOSITION AT VARIOUS POINTS I,J
3. COMMON A(23,3),ABS(6),AP,B(11,3),CON(23),CONX(6),CUT,DIM,DPULSE,
4. 1DR,DT,DTX,DZ,HR(11),IG,IHT,IENS,IPOF,IP1,IP2,IP3,IP4,IP5,IP6,
5. 2JVL,LIM,LP1,LP2,LP3,LP4,LP5,LP6,LPX,LTMAX,LZ,K,KT,M,M1,M2,M3,N,
6. 3N1,N3,N4,POX,PTIME,QP,R(11),REF(7),RIM,RN,RVL,S(23,11),TH(6),
7. 4TS(2200),V(23,11),VC(23,11,60),VSH(23),VSHX(6),XC,WAVEL,XPD(60),
8. 5XT(60),Z(23),ZCON(23,11),ZD(8),ZM
9. DIMENSION AB(23,3),ABR(23,6),II(23),IZ(23),REFL(6),ZH(23)
10. IF(IHT.EQ.0)RETURN
11. IF(QP.LT.1.E-25)GO TO 340
12. IF(IHT.EQ.1)RETURN
13. AP=1.
14. LZ0=LZ-1
15. LZ1=LZ+1
16. REF(LZ1)=0.
17. DO 290 I=1,M
18. II(I)=0
19. IZ(I)=0
20. ZH(1)=(Z(1)+Z(I+1))/2.
21. DO 289 L1=1,3
22. 289 AB(I,L1)=0.
23. DO 290 L1=1,LZ
24. 290 ABR(I,L1)=0.
25. DO 292 L1=1,LZ
26. 292 REFL(L1)=0.
27. WRITE(6,293)(ZH(I),I=1,M)
28. 293 FORMAT(1H0.3HZH=/(1X,5E8.3))
29. L1=2
30. DO 306 I=IP1,M
31. 295 IF(ZH(I-1).LT.ZD(L1))GO TO 296
32. L1=L1+1
33. GO TO 295
34. 296 IF(ZH(I).GE.ZD(L1))GO TO 299
35. *** NO ZD BETWEEN ZH(I-1) AND ZH(I)
36. AB(I,1)=ABS(L1-1)*(ZH(I)-ZH(I-1))
37. II(I)=1
38. IZ(I)=L1
39. IF(L1.GT.LZ)GO TO 306
40. DO 297 L2=L1,LZ
41. 297 ABR(I,L2)=AB(I,1)
42. GO TO 306
43. 299 IF(ZH(I).GE.ZD(L1+1))GO TO 303
44. *** ONLY ZD(L1) BETWEEN ZH(I-1) AND ZH(I)
45. AB(I,1)=ABS(L1-1)*(ZD(L1)-ZH(I-1))
46. AB(I,2)=ABS(L1)*(ZH(I)-ZD(L1))
47. ABR(I,L1)=AB(I,1)
48. II(I)=2
49. IZ(I)=L1
50. L3=L1+1
51. IF(L3.GT.LZ)GO TO 306
52. DO 300 L2=L3,LZ
53. 300 ABR(I,L2)=AB(I,1)+AB(I,2)
54. GO TO 306
55. *** ZD(L1) AND ZD(L1+1) BETWEEN ZH(I-1) AND ZH(I)
56. 303 AB(I,1)=ABS(L1-1)*(ZD(L1)-ZH(I-1))
57. AB(I,2)=ABS(L1)*(ZD(L1+1)-ZD(L1))

```

```

58. AB(I,3)=ABS(L1+1)*(ZH(I)-ZD(L1+1))
59. ABR(I,L1)=AB(I,1)
60. ABR(I,L1+1)=AB(I,1)+AB(I,2)
61. II(I)=3
62. IZ(I)=L1
63. L3=L1+2
64. IF(L3.GT.LZ)GO TO 306
65. DO 304 L2=L3,LZ
66. 304 ABR(I,L2)=ABR(I,1)+ABR(I,2)+ABR(I,3)
67. 306 CONTINUE
68. DO 314 I=IP1,M
69. IF(ABR(I,1).GT.10.)ABR(I,1)=10.
70. IF(ABR(I,2).GT.10.)ABR(I,2)=10.
71. IF(ABR(I,3).GT.10.)ABR(I,3)=10.
72. DO 314 L=2,LZ
73. IF(ABR(I,L).GT.10.)ABR(I,L)=10.
74. 314 CONTINUE
75. *** DEPOSITION BY INCOMING BEAM
76. X2=QP
77. L1=2
78. DO 317 I=IP1,M
79. L2=II(I)
80. X3=X2
81. X2=X2*EXP(-AB(I,1))
82. X4=0.
83. IF(L2.EQ.1)GO TO 315
84. L3=IZ(I)
85. X4=X2*REF(L3)
86. X2=X2*(1.-REF(L3))*EXP(-AB(I,2))
87. IF(L2.EQ.2)GO TO 315
88. X4=X4+X2*REF(L3+1)
89. X2=X2*(1.-REF(L3+1))*EXP(-AB(I,3))
90. 315 IF(X2.LT.1.E-10)X2=0.
91. DO 317 J=1,JVL
92. S(I,J)=(X3-X2-X4)*HR(J)*ZCON(I,J)/(ZH(I)-ZH(I-1))
93. IF(S(I,J).LT.1.E-6/DPULSE)S(I,J)=0.
94. 317 CONTINUE
95. *** CALCULATION OF REFLECTED INTENSITIES BY VARIOUS INTERFACES STARTING
96. *** WITH FIRST INTERNAL INTERFACE
97. X2=QP
98. DO 322 L1=1,LZ0
99. X3=ABS(L1)*TH(L1)
100. IF(X3.GT.10.)X3=10.
101. X2=X2*EXP(-X3)
102. REFL(L1+1)=X2*REF(L1+1)
103. 322 X2=X2*(1.-REF(L1+1))
104. DO 327 L1=2,LZ
105. I=IP1
106. 324 IF(ZH(I).GT.7D(L1))GO TO 325
107. I=I+1
108. IF(I.LE.M)GO TO 324
109. GO TO 327
110. 325 X2=REFL(L1)
111. DO 326 L3=IP1,I
112. X3=X2
113. L4=1+IP1-L3
114. X2=X2*EXP(-ABR(L4,L1))

```

# HTXDEP (CORNEAL)

```

115.      DO 326 J=1,JVL
116.      S(L4,J)=S(L4,J)+(X3-X2)*HR(J)*7CON(L4,J)/(ZH(L4)-ZH(L4-1))
117.      IF(S(L4,J).LT.1.E-6/DPULSE)S(L4,J)=0.
118.326  CONTINUE
119.327  CONTINUE
120.      IHT=1
121.      RETURN
122.*** NO HEAT DEPOSITION, BEAM OFF
123.340  DO 342 I=1,M3
124.      DO 342 J=1,N3
125.342  S(I,J)=0.
126.      IHT=0
127.      RETURN
128.      END

```

# SUBROUTINE MXGRAN(CORNEAL)

```

1.  SUBROUTINE MXGRAN
2.  *** THIS ROUTINE COMPUTES CONSEQUENCE OF GRANULAR ABSORPTION ON TEMPERATURE
3.  *** VARIATIONS IN PE(USED ONLY ONCE)
4.  COMMON A(23,3),ABS(6),AP,R(11,3),CON(23),CONV(6),CUT,DIM,DPULSE,
5.  1DR,DT,DTX,DZ,HR(11),IG,IHT,I LENS,IPROF,IP1,IP2,IP3,IP4,IP5,IP6,
6.  2JVL,LIM,LP1,LP2,LP3,LP4,LP5,LP6,LPX,LIMAX,LZ,K,KT,M,M1,M2,M3,N,
7.  3N1,N3,N4,POX,PTIME,QP,R(11),REF(7),RIM,RN,RVL,S(23,11),TH(6),
8.  4TS(2200),V(23,11),VC(23,11,60),VSH(23),VSHX(6),XC,WAVEL,XPD(60),
9.  5XT(60),Z(23),ZCON(23,11),ZD(8),ZM
10.  DO 495 L1=1,KT
11.  495 XPD(L1)=1.
12.  RETURN
13.  END

```

APPENDIX M

USER MANUAL FOR PREPARING 2-D AND 3-D ILLUSTRATIONS  
OF TEMPERATURE RISE PROFILES



## 1. INTRODUCTION

The computer program documented herein was developed by IIT Research Institute to display two and three dimensional temperature rise profile surfaces as a function of radial and axial coordinates. The methodology chosen was to start with temperature data for selected points from either the Corneal or Retinal Models. This information was then used to build a general three dimensional point array of plotting information. Finally, a generalized package is used to yield any desired view of this three dimensional data. This documentation pertains mainly to the use of this system and in less detail, to the documentation of the system itself.

## 2. EXAMPLE OF THE USE OF THE SYSTEM

A sample input deck to this system is shown in Table 1 with each data card preceded by annotated comments. The deck shown consists of two separate decks. Cards 1 through 14 contain information defining the data supplied by the Corneal or Retinal Models. Cards 15 through 35 contain individual plot commands. In particular, cards numbered 23, 25, 31 and 34 contain specific commands to plot while other cards provide auxiliary information concerning the screen size and desired view of the object. The last card (card 35) is necessary to properly close the plot file. The four plots generated by these commands are shown in Figs. M-1 through M-4.

## 3. SYSTEM DESCRIPTION

The entire program consists of approximately 1500 cards of FORTRAN source divided into a main program and twelve subroutines. It is assumed that this package is also supported by the subset of CALCOMP software consisting of the subroutines PLOTS, PLOT, NUMBER and SYMBOL. The FORTRAN is ANSI FORTRAN, and should be directly portable between computers. The package was developed on a UNIVAC 1108 and tested on an IBM 370 computer.

Table M-i

## SAMPLE USER INPUT DECK WITH COMMENTS

1.	3	7	1.0						
2.	1.+3	5.15+2	2.5-3						
3.	8	12	10	1	6				
4.	11	17							
5.	.0000	.0010	.0020	.0030	.0040	.0078	.0224	.0783	.2918 1.1082
6.	4.2287								
7.	-.8862	.8862	1.5110	1.7313	1.8090	1.8363	1.8460	1.8494	1.8506 1.8518
8.	1.8522	1.8649	1.8922	1.9699	2.1902	2.8150	4.5874		
9.	1.0+1								
10.	4.8	4.0	3.3	2.8	2.5	1.6			
11.	8.5	7.3	5.9	4.5	3.4	1.5			
12.	16.7	13.3	8.9	5.6	3.7	1.5			
13.	8.4	7.3	5.8	4.4	3.4	1.5			
14.	2.8	2.7	2.5	2.3	2.0	1.3			

COMMAND DATA FOR PLOTTING

- 15. ● Dump summary of all 3D points
- DUM
- Set viewing distance at 30 in. for perspective
- 16. DIST 30.
- Set lower left of screen, 4.1 inches left and 3.1 up, plus re-scaling of object to 8 in. wide, 6 in. deep and 6 in. long
- 17. SCRN -4.1 -3.1 8. 6.
- Re-scale object to fill screen
- 18. BOX 1. 1.
- Pitch object -90 degrees
- 19. PITCH -90.
- Yaw object -65 degrees
- 20. YAW -65.

Table M-1 (contd)

SAMPLE USER INPUT DECK WITH COMMENTS

21.	• Pitch object 25 degrees PITC 25.
22.	• Scale view to fill .9 of screen BOX .9
23.	• Set center of picture 10 in. forward and 6 in. up and plot PLOT 10. 6.
24.	• Dash hidden lines HIDE 2.
25.	• Set center of picture 10 in. forward and 6 in. up and plot PLOT 10. 6.
26.	• Suppress hidden line option HIDE
27.	• Re-initialize the matrix to give an X-Y view (isometric) REIN
28.	: Pitch object -90 degrees for an X-Z view PITC -90
29.	• Request isometric view (viewing distance of blank or zero is interpreted as request for isometric view) DIST
30.	• Scale view to fill 0.9 of the available X and Y dimensions of screen BOX 0.9 0.9
31.	• Advance 10 in. in X, 6 in. up in Y and plot PLOT 10. 6.

Table M-1 (concl)  
SAMPLE USER INPUT DECK WITH COMMENTS

32.	YAW	-90.	• Yaw by -90 degrees to give Y-Z view
33.	BOX	0.9 0.9	• Scale view to fill 0.9 of the available Y and Z dimensions of screen
34.	PLOT	10. 6.	• Advance 10 in. in X, 6 in. in Y and plot
35.	PLOT		• Terminate the plot tape

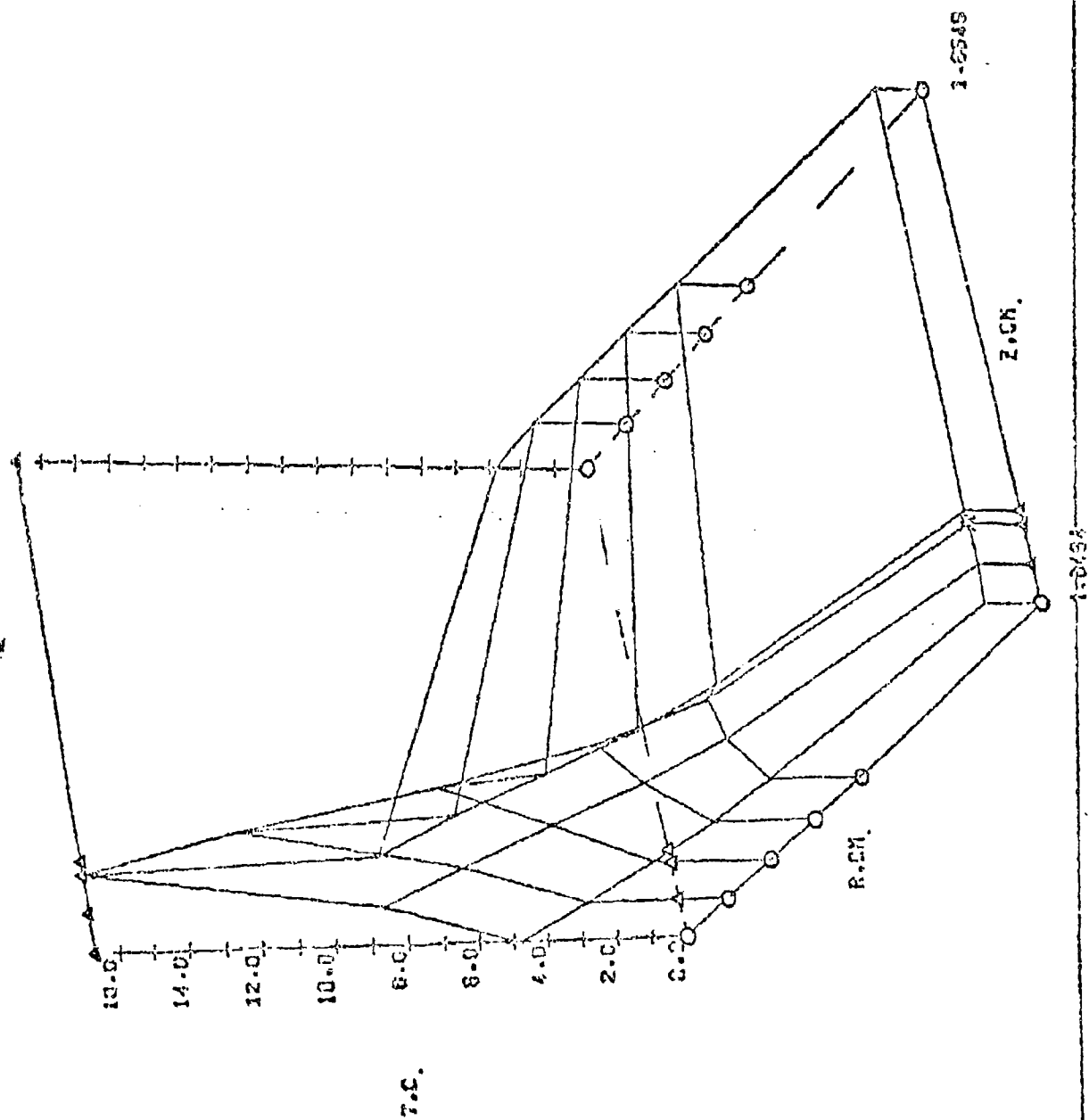


Fig. M-1 THREE DIMENSIONAL VIEW OF TEMPERATURE RISES

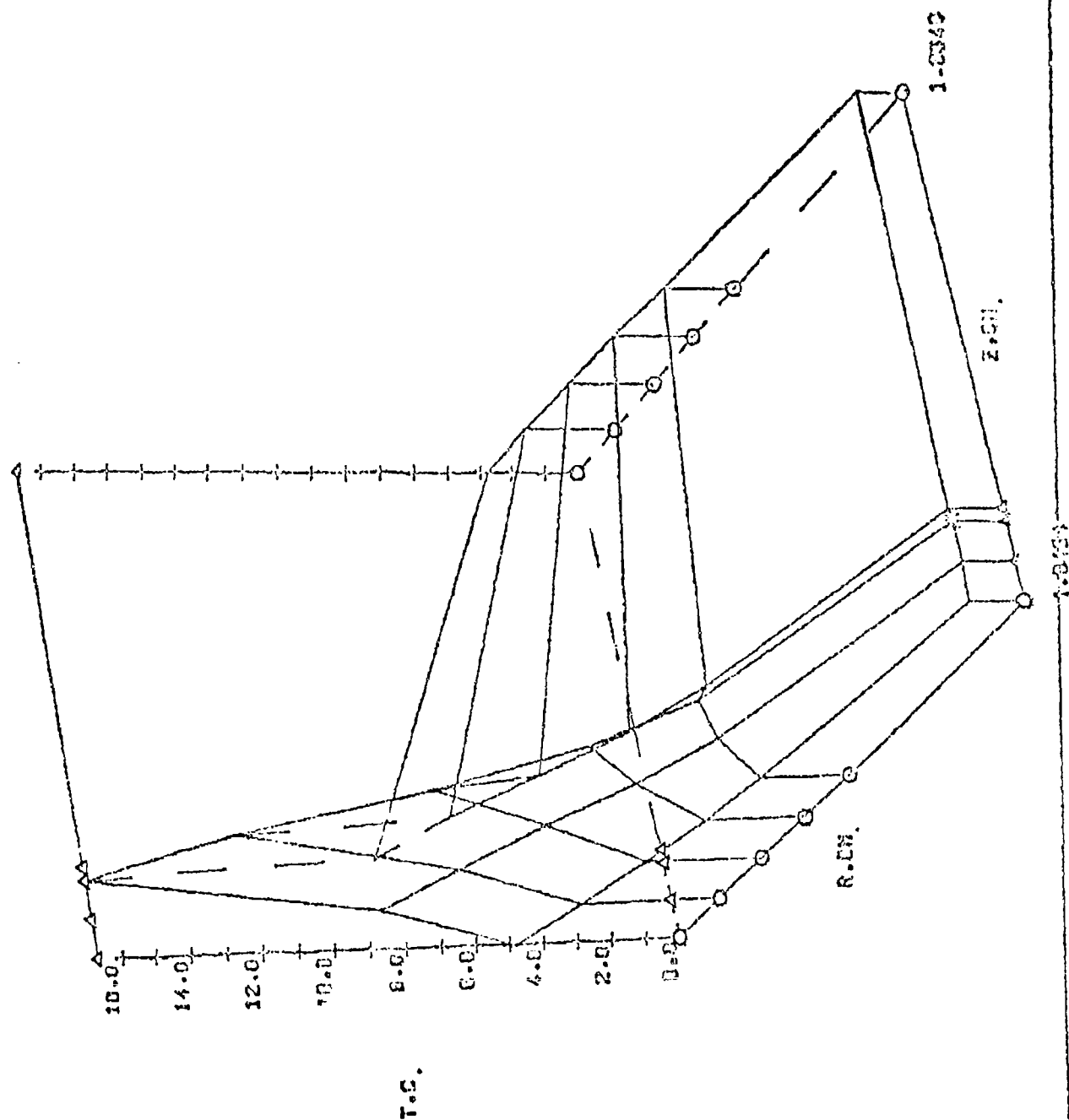


Fig. M-2 THREE DIMENSIONAL VIEW OF TEMPERATURE RISES WITH HIDDEN LINES

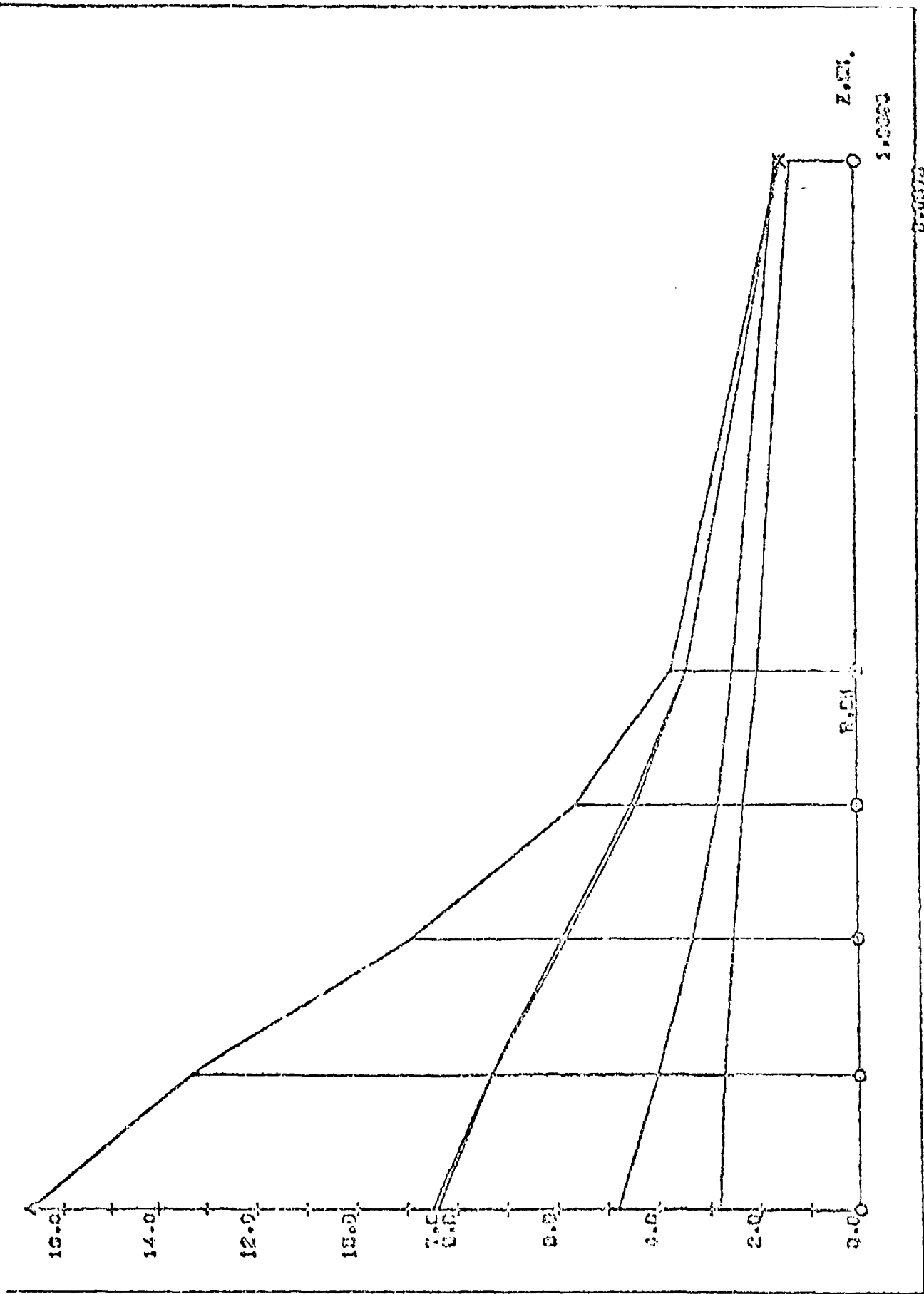


Fig. M-3 2D TEMPERATURE PROFILES (X,Z) IN RADIAL DIRECTION

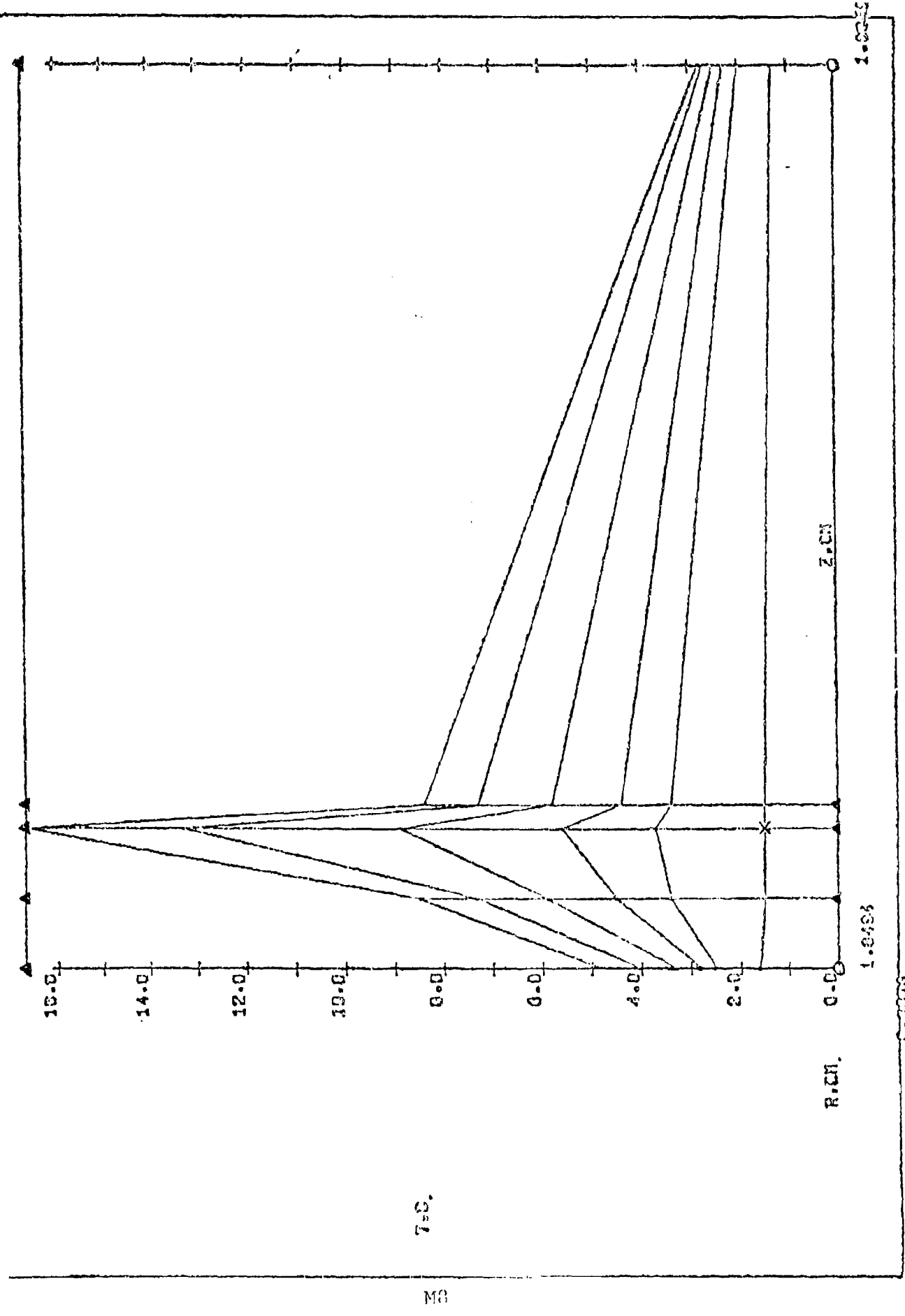


Fig. M-4 2D TEMPERATURE PROFILES (Y,Z) IN AXIAL DIRECTION



The processing flow and subroutine structure of the system are shown in Fig. M-5. The processing is divided into three parts. The first part of the main program (called COLUMN) reads temperature data generated by the Corneal or Retinal Models and prints a summary of this data. The second part of the program builds a consolidated array of three-dimensional point data. This array is arranged in the specific format for subsequent plotting and contains not only the criss-cross gridwork of scientific data, but all axial and labelling data as well. The subroutine POLSUR and its subsidiaries PCROSS and EQUIV are used to build the mesh points into a criss-cross pattern of plotting strokes with embedded normals to be used in hidden line views. The routines SYMCON (for symbol control) and AXES (for generated 3D axial information) are used to generate axial stroke lines and symbol and numeric size and positioning information.

At this point the main program relinquishes control to the subroutine 'READIN'. This subroutine is structured to read general plot information and to plot current views of the three-dimensional object. The READIN routine can be used to generate as many plots of the data as desired. In the particular example documented in Section 2, two general perspective space-views and two isometric plane views were all obtained from the same user input deck.

The Subroutine 'READIN' calls the principal plotting routine - namely 'SSPLOT'. The 'SSPLOT' routine in turn calls CALCOMP software and four other subroutines - namely, the 'WINDOW' routine to zoom in on a localized area of a plot, the 'MMULT' routine to multiply 4x4 matrices to produce a consolidated matrix containing all the scaling and positioning data relating to the current view of the object; the 'PERSPT', routine to generate a 4x4 matrix in response to a user's request for translation, rotation or scaling and a dummy 'OFFSET' routine. The 'OFFSET' routine has no function in the CALCOMP version of this system. However, at ILTRI a real 'OFFSET' routine is used to control a Tektronix Graphics terminal in a CALCOMP interface mode.

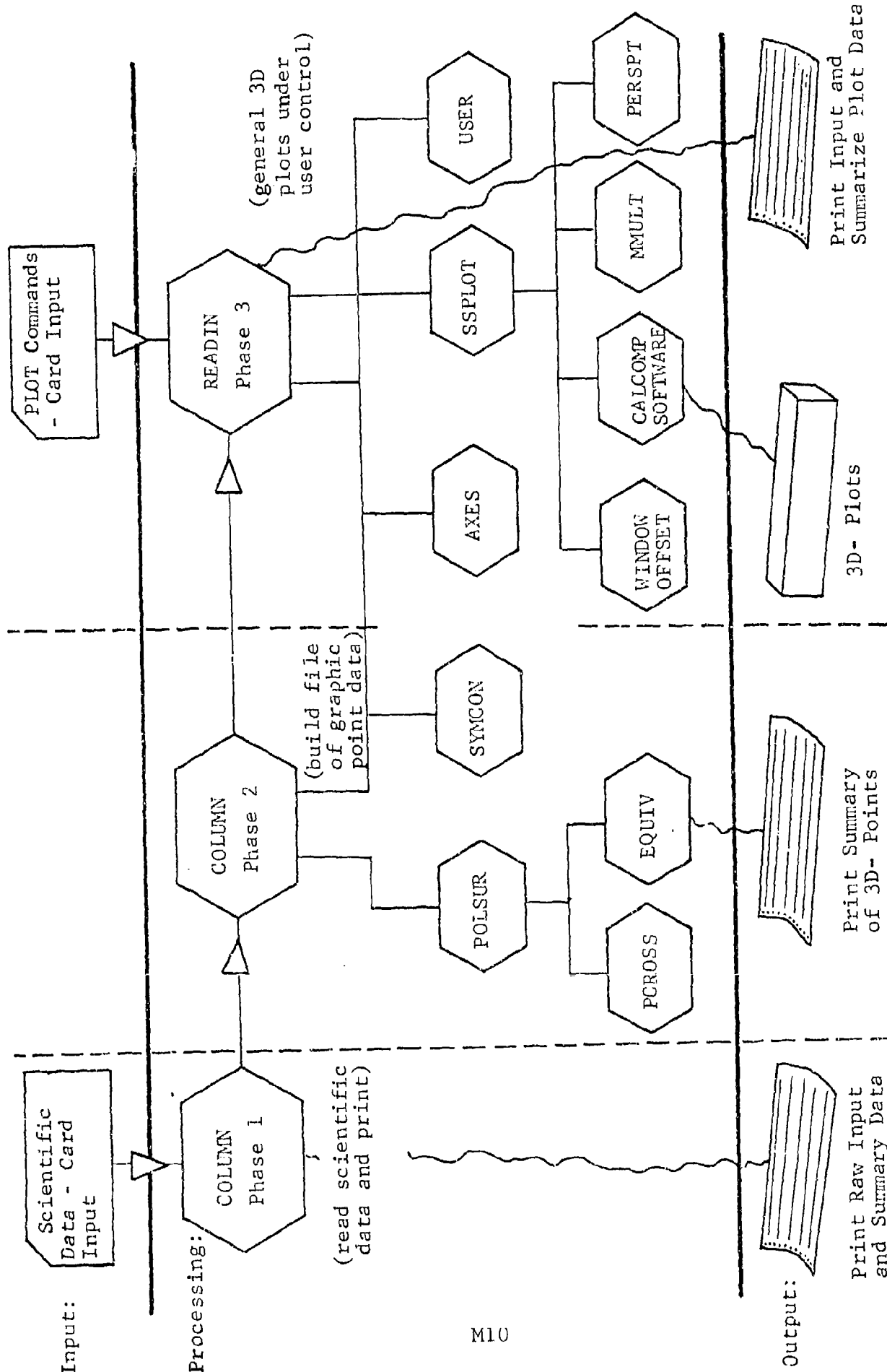


Fig. M-5 SYSTEM PROCESSING STRUCTURE

As shown in Fig. M-5 all phases of this program yield summary print data to aid the user in verifying not only his input, but also the results of intermediate processing. A listing of the entire code is at the rear of this appendix.

#### 4. DETAILED USER INPUT TO THE PLOT PROGRAM

The user's interface with the plotting portion of this program is controlled by the subroutine 'READIN'. This program is designed to read and list cards under a uniform format and to immediately execute the user's command indicated. The uniform format for all cards is shown below.

Columns	Columns	Columns	Columns	Columns	
1 - 4	11 - 20	21 - 30	31 - 40	41 - 50	etc.
Key word left-justified	First Parameter	Second Parameter	Third Parameter	Fourth Parameter	

A keyword in alphanumeric format is entered in Columns 1 - 4. Parameters - as applicable - are entered as floating point numbers in fields 10 characters wide starting with column 11. Of course, a blank entry is always read as a floating number with value zero. A user's card is always printed as read and if the keyword does not match the dictionary of keywords a clear diagnostic is produced and processing terminates.

Certain conventions should be described relative to the philosophy for viewing the object. A single matrix stores all of the user's consolidated requests for rotations, scaling and translation of the object. At program start this matrix, without any other information, would plot an isometric x-y view of the object where the user's numbers (x, y and z) are all interpreted as real inches. Of course, if x and y coordinates are in hundredths of a centimeter and temperature rise is in full degrees, such a view, if there is space on the plotter, would be little more than a vertical line because of disparity between coordinate magnitudes. Accordingly, the data can be scaled to fill a desired viewing area and to allow for proportional

scaling of axes. Rotated spatial views of the object are obtained by successive simple commands to roll, pitch or yaw the object from the initial viewing position. These commands are usually employed only after the 'BOX' command which centers the object on the origin and allows more reasonable application of successive rotational commands.

The viewer considers that the permanent x-axis lies to a horizontal right direction, the y-axis is vertical and up and the permanent z-axis is coming out toward him. If the viewer enters a command to roll  $45^\circ$ , the object will perform a  $45^\circ$  movement clockwise in the viewing plane. If he commands it to pitch  $45^\circ$  the object will rotate around the x-axis so that the top part of the screen will come toward him. If the viewer commands the object to yaw  $45^\circ$  the object will rotate around the permanent y-axis so that right most portion of the screen will move away from him. All of these commands are based on a right hand rule to determine orientation. Good three-dimensional views are usually built-up by a succession of three-rotational commands (such as in example 2).

The above gives some insight into the positioning philosophy of this model. What follows is a detailed description of each input command for the plotting system.

#### Keyword

1	11	21	31	41	51
P	a	x	y	z	w

The symbol 'P' denotes that a point or vector is being added to the data base of point P. Here P consists of a two digit real number of the form AB. The tens digit 'A' defines the mode in which the vector stroke to the current point should be plotted as follows:

- A = 0 maintain current mode
- A = 1 plot solid lines through succeeding points
- A = 2 plot dashed lines through succeeding points
- A = 3 plot only the points themselves
- A = 4 plot a string of dashed points through succeeding points

In case A = 5, the entry is not a point, but a vector attached to the previous point (this is used in hidden line views).

The units digit B carries the following interpretations:

- B = 0 plot no special symbol at the point
- B = 1 plot a Calcomp centered symbol at the point -  
the value of the symbol is held in w.
- B = 2 plot a floating number at the point -  
the value of the number is in w.
- B = 3 plot an alphanumeric label at the point. The  
label is held in the word w.  
(note: since the card parameters are all read  
under a floating point format, this option cannot  
be obtained through an input card).

The second, third and fourth parameters are x, y, z coordinates of a point and the w-coordinate carries the meaning as indicated in the explanation of the 'B' digit value.

In the present application of the model, this point array is built-up automatically in the COLUMN program and the user is not required to input data under this format.

#### INIT

The 'INIT' command initializes all plot data including zeroing out all point arrays). It also initializes the plot buffer. Plotting cannot occur until the INIT routine is called, either directly or indirectly. (Please note that in the 'COLUMN' model this command is called automatically at the beginning of the run).

#### ROLL           A

The 'ROLL' command indicates that the object should move counterclockwise in the viewing plane by an angle A.

#### PITC           A

The pitch command indicates that the object should 'pitch' by A degrees around the horizontal axis

#### YAW            A

This command indicates that the object should 'yaw' by A degrees (i.e., rotate around the fixed y-axis).

SCAL            A            B            C

This command rescales the current object. If the factors B and C are both zero, then all three dimensions are rescaled uniformly by the factor A. Otherwise, the x, y, and z coordinates are independently scaled by the factors A, B, and C respectively.

TRAN           A            B            C

The command 'TRAN' effects a translation of the current object position through a sector (A,B,C). It should be noted that all of the previous commands are cumulative - that is, they operate on the current transformed position and scale of the object.

DIST           A            B            x            y

The distance command adjusts the distance of the observer from the object. If no parameters or else zero parameters are input, the projection will simply be parallel. If only one non-zero parameter A is input, then the distance of the observer from the origin of coordinates and of the projection plane from the viewer are both interpreted as A units. Otherwise A is the distance of the viewer from the origin and B is the distance of the paper (on which the object is projected) from the viewer. Optionally third and fourth parameters (x and y, may be added to allow the viewer to shift his viewing position.

REIN

This command, mnemonic for re-initialize, is entered to restart the transformation matrix from the position of an identity transformation. All of the previously built up results from roll, pitch, yaw, scale, box and translation commands are lost.

HIDE           A

The 'HIDE' command is used to turn the hidden line calculation on or off. If parameter A is zero, the hidden line calculation is turned off. If A is 1.0, hidden lines are removed and if A is 2.0 hidden lines are dashed. The hidden line calculation can only be effected where normal vectors have been entered and depends simply on whether the normal is leaning away from or toward the observer.

SIGN           A

The SIGN command can be used to reverse the sense of surface normals entered in the data base.

WIND           A           B           C           D

The 'WINDOW' command is used to turn the window option on or off and to set the parameters for windowing. A and B are lower left hand coordinates of the windowed area and C and D are width and height of the window area in terms of display coordinates. In particular, if a SCREEN option is in effect, then the origin of coordinates is at the center of the screen. The Window option is not modal - it is only in effect for the plot command immediately following. However, it can be reactivated by entering a 'WIND' card with no parameters. In this case, 'WINDOW' will be switched on again and the old window parameters will be used. The window option does result in a permanent change of the display matrix whenever the 'Screen' option is in effect. In this case, the windowed area is automatically blown up to fill the Screen area. Otherwise "Window" merely acts to scissor unwanted parts of a plot.

SCRN           A           B           C           D           E

The 'Screen' command sets up the physical size of the display area and draws a border around that area for every plot. The screen command is modal, and remains in effect until it is

turned off. The parameters A and B describe the coordinates of the lower left corner of the screen and C and D describe the width and height. These units are all in inches. If no window command is in effect, then the screen acts as an automatic window area for scissoring the plot lines. A fifth parameter E may also be entered. In this case, the user defines a three-dimensional geometric box so that the object can subsequently be rescaled to fill that box.

BOX            A            B            C

The 'BOX' command causes the object to fill a fraction of the screen area. The object is first centered on its center of gravity and then rescaled from there to fill a proportion of the available viewing area. In case only one parameter, A, is entered, a single scale is applied to all three axes. If all three parameters are entered, then the object is scaled to fill the specified x, y, z screen width. The BOX command is used frequently to attain 'full' views of an object after rotation.

FACT            A

The factor command simply blows up or shrinks all plotting by the factor A.

PLOT            A            B            C

The plot command causes the current view of the object to be actually plotted. Parameters A and B define the relative x and y-advance on the Calcomp for a new origin of coordinates. If the parameter C is entered with a negative value the plot file is terminated. The plot file must always be explicitly terminated.

USER

The user command is simply designed to allow a user to branch to his own input routine. Of course the user would have to supply the coding to effect such input. In its present form, the 'USER' subroutine is a dummy subroutine.



PRIN

This is presently a dummy statement - eventually it may be used to control the level and amount of print information.

END

This word terminates the READIN program and allows control to pass to a higher level routine.

DUM

This word requests a summary of the current number of points in the data base and of the x-y-z range of the data.

LISTING OF CODE FOR 3D PLOTS

DATA(0)

## SAMPLE INPUT DATA

1.	3	7	1.0							
2.	1.+3	5.15+2	2.5-3							
3.	8	12	10	1	6					
4.	11	17								
5.	.0000	.0010	.0020	.0030	.0040	.0078	.0224	.0783	.2918	1.1082
6.	4.2287									
7.	-.8862	.8862	1.5110	1.7313	1.8090	1.8363	1.8460	1.8494	1.8506	1.8518
8.	1.8522	1.8649	1.8922	1.9699	2.1902	2.8150	4.5874			
9.	1.0+1									
10.	4.8	4.0	3.3	2.8	2.5	1.6				
11.	8.5	7.3	5.9	4.5	3.4	1.5				
12.	16.7	13.3	8.9	5.6	3.7	1.5				
13.	8.4	7.3	5.8	4.4	3.4	1.5				
14.	2.8	2.7	2.5	2.3	2.0	1.3				
15.	DUM									
16.	DIST	30.								
17.	SCRN	-4.1	-3.1	8.	6.	6.				
18.	BOX	1.	1.	1.						
19.	PITC	-90.								
20.	YAW	-65.								
21.	PITC	25.								
22.	BOX	.9								
23.	PLOT	10.	6.							
24.	HIDE	2.								
25.	PLOT	10.	6.							
26.	HIDE									
27.	REIN									
28.	PITC	-90.								
29.	DIST									
30.	BOX	0.9	0.9							
31.	PLOT	10.	6.							
32.	YAW	-90.								
33.	BOX	0.9	0.9							
34.	PLOT	10.	6.							
35.	PLOT			-1.						

COLUMN

1.	C	III,II2	I VALUES DESIGNATING RANGE OF Z(I) VALUES FOR PLOTTING,	
2.	C		RANGE=Z(III) TO Z(II2)	
3.	C	JJ1,JJ2	J VALUES DESIGNATING RANGE OF R(J) VALUES FOR PLOTTING,	
4.	C		RANGE=R(JJ1) TO R(JJ2)	
5.	C	R(J)	ORDINATE,CM	
6.	C	RGR	RANGE OF R VALUES TO BE PLOTTED,CM	
7.	C	RGV	RANGE OF TEMPERATURE VALUES TO BE PLOTTED,C	
8.	C	RGZ	RANGE OF Z VALUES TO BE PLOTTED,CM	
9.	C	TIMEX	TIME AT WHICH TEMPERATURE RISE VALUES ARE PLOTTED,SEC	
10.	C	V(I,J)	TEMPERATURE RISE AT TIME TIMEX(K),C	
11.	C	Z(I)	ABSISSA,CM	
12.		REAL LA		
13.		COMMON/PLBAS1/ P(4,3001),ICON(3001),NUM,NUMAX		
14.		COMMON/PLBAS2/AP(16),AV(16),CP(16),DAT(8)		
15.		DIMENSION LA(4)		
16.		DIMENSION RR(100),PT(3),RP(100)		
17.		DIMENSION R(11),V(23,11),Z(23)		
18.		DATA LA/4HZ,CM,4HR,CM,4H T,C,4HRUN=		
19.		DAT(1)=1.0		
20.		CALL SSPLIT		
21.		READ(5,9)NRUN,NPULSE,REP ET		1
22.		9 FORMAT(2I7,F7.1)		
23.		READ(5,10)DPULSE,WAVEL,RIM		2
24.		10 FORMAT(3E8.3)		
25.		READ(5,11)III,II2,II3,JJ1,JJ2		3
26.		11 FORMAT(5I7)		
27.		READ(5,11)N3,M3		4
28.		READ(5,12)(R(J),J=1,N3)		5
29.		12 FORMAT(10F7.4)		
30.		READ(5,12)(Z(I),I=1,M3)		6
31.		READ(5,10)TIMEX		7
32.		DO 15 I=III,II2		
33.		READ(5,14)(V(I,J),J=JJ1,JJ2)		8
34.		14 FORMAT(10F7.2)		
35.		15 CONTINUE		
36.	C ***	START OF PROGRAM FOR PLOTTING		
37.		RGR=R(JJ2)-R(JJ1)		
38.		RGZ=Z(II2)-Z(III)		
39.		RGV=0.		
40.		DO 20 I=III,II2		
41.		DO 20 J=JJ1,JJ2		
42.		IF(V(I,J).GT.RGV)RGV=V(I,J)		
43.		20 CONTINUE		
44.		WRITE(6,21)RGZ,RGR,RGV		
45.		21 FORMAT(1H0,4HRGZ=,E8.3,2X,4HRGR=,E8.3,2X,4HRGV=,E8.3)		
46.		DO 23 I=III,II2		
47.		WRITE(6,22)I,(V(I,J),J=JJ1,JJ2)		
48.		2 FORMAT(1H0,2HI=,I2/(1X,10F7.2))		
49.		23 CONTINUE		
50.	C ***	PLOT ROUTINE		
51.		30 CONTINUE		
52.	C			
53.	C-----	SET UP FOR PLOT		
54.	C			
55.		IDIF=II2-III+1		
56.		JDIF=JJ2-JJ1+1		
57.		NM=1		

COLUMN(0)

```
58.      DO 100 N=1, IDIF
59.      DO 100 M=1, JDIF
60.      I1=I11+N-1
61.      J1=JJ1+M-1
62.      P(1,NM)=R(J1)
63.      P(2,NM)=Z(I1)
64.      P(3,NM)=V(I1,J1)
65.      ICON(NM)=10
66.      IF (M.NE.1) ICON(NM)=0
67.      NM=NM+1
68.      100 CONTINUE
69.      DO 200 M=1, JDIF
70.      DO 200 N=1, IDIF
71.      J1=JJ1+M-1
72.      I1=I11+N-1
73.      P(1,NM)=R(J1)
74.      P(2,NM)=Z(I1)
75.      P(3,NM)=V(I1,J1)
76.      ICON(NM)=10
77.      IF (N.NE.1) ICON(NM)=0
78.      NM=NM+1
79.      200 CONTINUE
80.      NUMAX=3000
81.      NUM=NM-1
82.      CALL POLSUR(JDIF, IDIF)
83.      DO 150 MM=1, JDIF
84.      M=JJ1+MM-1
85.      NUM=NUM+1
86.      P(1,NUM)=R(M)
87.      P(2,NUM)=Z(I11)
88.      P(3,NUM)=0.0
89.      ICON(NUM)=10
90.      NUM=NUM+1
91.      P(1,NUM)=R(M)
92.      P(2,NUM)=Z(I11)
93.      P(3,NUM)=V(I11,M)
94.      ICON(NUM)=0
95.      150 CONTINUE
96.      DO 160 MM=1, JDIF
97.      M=JJ1+MM-1
98.      NUM=NUM+1
99.      P(1,NUM)=R(M)
100.     P(2,NUM)=Z(I12)
101.     P(3,NUM)=0.0
102.     ICON(NUM)=10
103.     NUM=NUM+1
104.     P(1,NUM)=R(M)
105.     P(2,NUM)=Z(I12)
106.     P(3,NUM)=V(I12,M)
107.     ICON(NUM)=0
108.     160 CONTINUE
109.     DO 170 NN=1, IDIF
110.     NUM=NUM+1
111.     N=NN+I11-1
112.     P(1,NUM)=R(JJ2)
113.     P(2,NUM)=Z(N)
114.     P(3,NUM)=0.0
```

COLUMN(0)

```
115.      ICON(NUM)=10
116.      NUM=NUM+1
117.      P(1,NUM)=R(JJ2)
118.      P(2,NUM)=Z(N)
119.      P(3,NUM)=V(N,JJ2)
120.      ICON(NUM)=0
121.      170  CONTINUE
122.      NUM=NUM+1
123.      P(1,NUM)=R(JJ2)
124.      P(2,NUM)=Z(II3)
125.      P(3,NUM)=V(II3,JJ2)
126.      P(4,NUM)=11.
127.      ICON(NUM)=31
128.      NUM=NUM+1
129.      P(1,NUM)=R(JJ1)
130.      P(2,NUM)=Z(II1)-RGZ*0.25
131.      P(3,NUM)=RGV*0.5
132.      P(4,NUM)=LA(3)
133.      ICON(NUM)=32
134.      NUM=NUM+1
135.      P(1,NUM)=R(JJ2)+RGR*0.1
136.      P(2,NUM)=Z(II1)+RGZ*0.5
137.      P(3,NUM)=0.0
138.      P(4,NUM)=LA(1)
139.      ICON(NUM)=32
140.      NUM=NUM+1
141.      P(1,NUM)=R(JJ1)+RGR*0.5
142.      P(2,NUM)=Z(II1)-RGZ*0.1
143.      P(3,NUM)=0.0
144.      P(4,NUM)=LA(2)
145.      ICON(NUM)=32
146.      CALL SYMCON(.07,4,-1.1,-1.2)
147.      NUM=NUM+1
148.      P(1,NUM)=R(JJ2)
149.      P(2,NUM)=Z(II1)
150.      P(3,NUM)=0.0
151.      P(4,NUM)=R(JJ2)
152.      ICON(NUM)=33
153.      C----- X-AXIS AT Y=Z(II1)
154.      RP(1)=JDIF
155.      DO 300 KK=1,JDIF
156.      IJ=KK*2
157.      JK=JJ1+KK-1
158.      RP(IJ)=R(JK)
159.      IJ=IJ+1
160.      RP(IJ)=-1
161.      300  CONTINUE
162.      PRINT 398
163.      398  FORMAT(10X,' X-AXIS')
164.      PRINT 399,(RP(LL),LL=1,IJ)
165.      399  FORMAT(5X,10F10.4)
166.      PT(1)=R(JJ1)
167.      PT(2)=Z(II1)
168.      PT(3)=0
169.      LAB=1
170.      CALL AXES(RP,PT,LAB,2,1)
171.      C----- X-AXIS AT Y=Z(II2)
```

I COLUMN(0)

```

172.      PT(1)=R(JJ1)
173.      PT(2)=Z(II2)
174.      PT(3)=0
175.      LAB=1
176.      CALL AXES(RP,PT,LAB,2,2)
177.      CALL SYMCON(0.07,4,1.1,-1.2)
178.      C----- Y-AXIS AT X=R(JJ1)
179.      RP(1)=IDIF
180.      DO 301 KK=1,IDIF
181.      IJ=KK*2
182.      JK=II1+KK-1
183.      RP(IJ)=Z(JK)
184.      IJ=IJ+1
185.      RP(IJ)=-1
186.      301 CONTINUE
187.      PRINT 397
188.      397 FORMAT(10X,' Y-AXIS')
189.      PRINT 399,(RP(LL),LL=1,IJ)
190.      PT(1)=R(JJ1)
191.      PT(2)=Z(II1)
192.      PT(3)=0
193.      LAB=2
194.      CALL AXES(RP,PT,LAB,2,2)
195.      C----- Y-AXIS AT TOP OF V
196.      PT(1)=R(JJ1)
197.      PT(2)=Z(II1)
198.      PT(3)=RGV
199.      LAB=2
200.      CALL AXES(RP,PT,LAB,2,1)
201.      C----- Y-AXIS AT X=R(JJ2)
202.      PT(1)=R(JJ2)
203.      PT(2)=Z(II1)
204.      PT(3)=0
205.      RP(3)=1
206.      RP(IJ)=1
207.      LAB=2
208.      CALL AXES(RP,PT,LAB,2,1)
209.      C----- Z-AXIS AT X=R(JJ1), Y=Z(II1)
210.      CALL SYMCON(0.07,1,-1.1,1.2)
211.      RP(1)=RGV+1.
212.      RR(1)=RGV+1
213.      II=RR(1)+1
214.      DO 302 KK=1,II
215.      IJ=KK*2
216.      RP(IJ)=KK-1
217.      RR(IJ)=KK-1
218.      IJ=IJ+1
219.      RR(IJ)=(-1)**(KK+1)
220.      RP(IJ)=-1.
221.      302 CONTINUE
222.      PRINT 396
223.      396 FORMAT(10X,' Z-AXIS')
224.      PRINT 399,(RR(LL),LL=1,IJ)
225.      PT(1)=R(JJ1)
226.      PT(2)=Z(II1)
227.      PT(3)=0
228.      LAB=3

```

COLUMN(0)

```
229.      CALL AXES(RR,PT,LAB,2,1)
230.      PT(1)=R(JJ1)
231.      PT(2)=Z(II2)
232.      PT(3)=0.
233.      LAB=3
234.      CALL AXES(RP,PT,LAB,2,1)
235.      DO 299 LL=1,NUM
236.      PRINT 199,LL,ICON(LL),P(1,LL),P(2,LL),P(3,LL)
237.      199 FORMAT(5X,I5,5X,I5,5X,3F15.4)
238.      299 CONTINUE
239.      C
240.      C----- END OF PLOT SETUP
241.      C
242.      WRITE(6,35)WAVEL,NPULSE
243.      35 FORMAT(1H0,11HWAVELENGTH=,E8.3,2HCM,10X,17HNUMBER OF PULSES=,I5)
244.      WRITE(6,36)DPULSE,RIM
245.      36 FORMAT(1H0,12HPULSE WIDTH=,E8.3,10X,13HIMAGE RADIUS=,E8.3)
246.      WRITE(6,37)REPET
247.      37 FORMAT(1H0,16HREPETITION RATE=,E8.3,10HPULSES/SEC)
248.      C
249.      WRITE(6,40)
250.      40 FORMAT(1H0,17HAXIAL DISTANCE,CM)
251.      WRITE(6,41)
252.      41 FORMAT(1H0,18HRADIAL DISTANCE,CM)
253.      WRITE(6,42)
254.      42 FORMAT(1H0,25HTEMPERATURE RISE,DEGREE C)
255.      WRITE(6,43) TIMEX,NRUN
256.      43 FORMAT(1H0,27HTEMPERATURE RISE PROFILE AT,E8.3,8HSEC(RUN=,I3,1H))
257.      CALL PLOT(0.,0.,-3)
258.      HT=.07
259.      A=TIMEX
260.      B=NRUN
261.      CALL SYMBOL(0.,1.,HT,29H TEMPERATURE RISE PROFILE AT ,0.,29)
262.      XX=29*HT
263.      CALL NUMBER(XX,1.,HT,A,0.0,7)
264.      XX=XX+12*HT
265.      CALL SYMBOL(XX,1.,HT,12HSEC -- RUN= ,0.0,12)
266.      XX=XX+12*HT
267.      CALL NUMBER(XX,1.,HT,B,0.0,0)
268.      CALL READIN(IRR)
269.      STOP
270.      END
```



PCROSS(0)

```
1.      SUBROUTINE PCROSS(PA,PR,PC,V,IS)
2.      DIMENSION PA(3),PB(3),PC(3),V(3)
3.      DIMENSION VX(3),VY(3)
4.      DO 10 I=1,3
5.      VX(I)=PB(I)-PA(I)
6.      VY(I)=PC(I)-PA(I)
7.      10 CONTINUE
8.      V(1)=VX(2)*VY(3)-VX(3)*VY(2)
9.      V(2)=-(VX(1)*VY(3)-VX(3)*VY(1))
10.     V(3)=VX(1)*VY(2)-VX(2)*VY(1)
11.     SUM=0.0
12.     DO 20 I=1,3
13.     20 SUM=SUM+V(I)*V(I)
14.     SUM=SQRT(SUM)+1.0E-20
15.     DO 30 I=1,3
16.     30 V(I)=IS*V(I)/SUM
17.     RETURN
18.     END
```

EQUIV(0)

```
1. SUBROUTINE EQUIV(PA,PB)
2. DIMENSION PA(3),PB(3)
3. DO 10 I=1,3
4.   10 PA(I)=PB(I)
5. RETURN
6. END
```

POLSUR(0)

```
1.      SUBROUTINE POLSUR(M,N)
2.      COMMON/PLBAS1/P(4,3001),ICON(3001),NUM,NUMAX
3.      DIMENSION W(3,500)
4.      NCT=0
5.      DO 10 I=1,N
6.      DO 10 J=1,M
7.      NCT=NCT+1
8.      DO 10 L=1,3
9.      W(L,NCT)=P(L,NCT)
10.     CONTINUE
11.     NUM=0
12.     DO 20 N1=1,N
13.     NLO=N1
14.     MM=M-1
15.     DO 20 M1=1,MM
16.     MLO=M1
17.     NUM=NUM+1
18.     NA=M1+N1*M-M
19.     CALL EQUIV(P(1,NUM),W(1,NA))
20.     ICON(NUM)=0
21.     IF(M1.EQ.1) ICON(NUM)=10
22.     NUM=NUM+1
23.     NA=M1+1+(N1-1)*M
24.     CALL EQUIV(P(1,NUM),W(1,NA))
25.     ICON(NUM)=0
26.     NUM=NUM+1
27.     ISIGN=1
28.     IF(N1.NE.1) ISIGN=-1
29.     NA=MLO+(NLO-1)*M+1
30.     NB=NA-1
31.     NC=NA+ISIGN*M
32.     ISIGN=-ISIGN
33.     CALL PCROSS(W(1,NA),W(1,NB),W(1,NC),P(1,NUM),ISIGN)
34.     ICON(NUM)=50
35.     CONTINUE
36.     DO 30 M1=1,M
37.     MLO=M1
38.     NN=N-1
39.     DO 30 N1=1,NN
40.     NLO=N1
41.     NUM=NUM+1
42.     NA=M1+(N1-1)*M
43.     CALL EQUIV(P(1,NUM),W(1,NA))
44.     ICON(NUM)=0
45.     IF(N1.EQ.1) ICON(NUM)=10
46.     NUM=NUM+1
47.     NA=M1+(N1-1)*M+M
48.     CALL EQUIV(P(1,NUM),W(1,NA))
49.     ICON(NUM)=0
50.     NUM=NUM+1
51.     ISIGN=1
52.     IF(M1.EQ.M) ISIGN=-1
53.     NA=MLO+(NLO-1)*M+M
54.     NB=NA+ISIGN
55.     NC=NA-M
56.     ISIGN=-ISIGN
57.     CALL PCROSS(W(1,NA),W(1,NB),W(1,NC),P(1,NUM),ISIGN)
```

POLSUR(0)

58.

ICON(NUM)=50

59.

30 CONTINUE

60.

RETURN

61.

END

OFFSET(0)

```
1. SUBROUTINE OFFSET(XDUM,YDUM)
2. C--- DUMMY OFFSET ROUTINE FOR CALCOMP
3. RETURN
4. END
```

SYMCON(0)

```
1.      SUBROUTINE SYMCON(HH,NN,XX,YY)
2.      COMMON/PLBAS1/ P(4,3001),ICON(3001),NUM,NUMAX
3.      NUM=NUM+1
4.      DO 10 I=1,3
5.      10 P(I,NUM)=0.0
6.      P(4,NUM)=HH
7.      ICON(NUM)=71
8.      NUM=NUM+1
9.      DO 20 I=1,3
10.     20 P(I,NUM)=0.0
11.     P(4,NUM)=NN
12.     ICON(NUM)=72
13.     NUM=NUM+1
14.     DO 30 I=1,3
15.     30 P(I,NUM)=0.0
16.     P(4,NUM)=XX
17.     ICON(NUM)=73
18.     NUM=NUM+1
19.     DO 40 I=1,3
20.     40 P(I,NUM)=0.0
21.     P(4,NUM)=YY
22.     ICON(NUM)=74
23.     RETURN
24.     END
```

AXES(0)

```
1. SUBROUTINE AXES(R,PT,LAB,MODE,NCON)
2. COMMON/PLBAS1/ P(4,3001),ICON(3001),NUM,NUMAX
3. DIMENSION R(1),T(102)
4. DATA NT/100/
5. DIMENSION PT(3)
6. DATA BIG/1.0E+20/
7. C--- OBJECTIVE OF ROUTINE IS TO GENERATE AXIS DATA IN THE THREE
8. C--- DIMENSIONAL POINT DATA BASE
9. C--- INPUT IS THRU CALLING ARGUMENTS AS FOLLOWS
10. C--- LAB SHOULD BE 1 2 OR 3 DENOTING X, Y OR Z AXIS INFORMATION
11. C--- IF MODE IS 1 THEN R(1,2,3 AND 4) DENOTE RESPECTIVELY THE START,
12. C--- INCREMENT,NUMBER OF INCREMENTS AND INCREMENT FOR NUMBERING
13. C--- MODE=2 MEANS THAT THE TICK DATA IS STORED IN THE ARRAY R SO THAT
14. C--- R(1) IS THE NUMBER OF POINTS, R(2) IS THE VALUE FOR THE FIRST
15. C--- MARK, R(3) IS POSITIVE IF A NUMBER SHOULD BE PLOTTED, AND NEGATIVE
16. C--- OTHERWISE AND SO ON
17. C--- IN THE CASE OF EACH MODE, TICK DATA IS BUILT INTO THE LOCAL ARRAY
18. C--- T AS A BUFFER, AND THEN TRANSFERRED TO THE POINT ARRAY
19. GO TO (10,20),MODE
20. 10 CONTINUE
21. START=R(1)
22. AINC=R(2)
23. NO=R(3)
24. IVINC=R(4)
25. IRR=1
26. IF(NO.LE.0) GO TO 998
27. IRR=2
28. IF(NO.GT.NT/2) GO TO 998
29. T(1)=NO
30. SMIN=BIG
31. SMAX=-BIG
32. DO 11 I=1,NO
33. T(2*I)=START+(I-1)*AINC
34. T(2*I+1)=-1
35. SMIN=AMIN1(T(2*I),SMIN)
36. SMAX=AMAX1(T(2*I),SMAX)
37. IF(IVINC.LE.0) GO TO 10
38. IF(MOD(I,IVINC).EQ.1) T(2*I+1)=1.0
39. 11 CONTINUE
40. GO TO 100
41. 20 CONTINUE
42. NO=R(1)
43. IRR=3
44. IF(NO.LE.0) GO TO 998
45. IRR=4
46. IF(NO.GT.NT/2) GO TO 998
47. SMIN=BIG
48. SMAX=-BIG
49. DO 21 I=1,NO
50. T(2*I)=R(2*I)
51. T(2*I+1)=R(2*I+1)
52. 21 CONTINUE
53. 100 CONTINUE
54. JTEM=NUM
55. DO 110 I=1,NO
56. JTEM=JTEM+1
57. DO 120 J=1,3
```

AXES(0)

```
58.      120 P(J,JTEM)=PT(J)
59.      P(4,JTEM)=LAB
60.      P(LAB,JTEM)=T(2*I)
61.      IF(I.EQ.1) ICON(JTEM)=NCON*10+1
62.      IF(I.NE.1) ICON(JTEM)=1
63.      110 CONTINUE
64.      NUM=NUM+NO
65.      JTEM=NUM
66.      DO 130 I=1,NO
67.      IF(T(2*I+1).LT.0.0) GO TO 130
68.      NUM=NUM+1
69.      JTEM=JTEM+1
70.      DO 140 J=1,3
71.      140 P(J,JTEM)=PT(J)
72.      P(LAB,JTEM)=T(2*I)
73.      ICON(JTEM)=33.
74.      P(4,JTEM)=T(2*I)
75.      130 CONTINUE
76.      999 IRR=0
77.      RETURN
78.      998 WRITE(6,997) IRR
79.      997 FORMAT(/,' ERROR IN AXES ROUTINE. IRR= ',I6,/)
80.      RETURN
81.      END
```



# DECOD(0)

```

1.      SUBROUTINE DECOD(PP,VV,AA,JCON,ISYM,IVEC,I)
2.      COMMON/PLBAS1/ P(4,3001),ICON(3001),NUM,NUMAX
3.      COMMON/PLBAS2/ AP(16),AV(16),CP(16),DAT(7)
4.      COMMON/PLBAS3/ WINXL,WINYL,WINXW,WINYW,IWIN
5.      COMMON/PLBAS4/ SCRNXL,SCRNYL,SCRNXW,SCRNYW,ISCRN
6.      COMMON/PLBAS5/ SIGNOR,SNPLOT,IH
7.      COMMON/PLBAS7/HT,NDECFX,XLATE,YLATE
8.      DIMENSION PP(3),VV(3)
9.      IVEC=0
10.     IF(I.GE.NUMAX) GO TO 999
11.     IF(I.GT.NUM) GO TO 999
12.     DO 10 L=1,3
13.       10 PP(L)=P(L,I)
14.       AA=P(4,I)
15.       JCON=JCON(I)/10
16.       ISYM=ICON(I)-10*JCON
17.       IF(JCON.GE.5) GO TO 997
18.       IF(ISYM.GT.3) GO TO 999
19.       INEX=ICON(I+1)/10
20.       IVEC=0
21.       IF(INEX.NE.5) GO TO 998
22.       I=I+1
23.       DO 20 L=1,3
24.       20 VV(L)=P(L,I)
25.       IVEC=1
26.       998 CONTINUE
27.       RETURN
28.       999 CONTINUE
29.       I=-1
30.       RETURN
31.       997 CONTINUE
32.       IVEC=999
33.       IF(JCON.NE.7) RETURN
34.       IF(ISYM.EQ.1) HT=P(4,I)
35.       IF(ISYM.EQ.2) NDECFX=P(4,I)
36.       IF(ISYM.EQ.3) XLATE=P(4,I)
37.       IF(ISYM.EQ.4) YLATE=P(4,I)
38.       RETURN
39.       END

```

SSPLOT(0)

```
1.      SUBROUTINE SSPLOT
2.      COMMON/PLBAS1/ P(4,3001),ICON(3001),NUM,NUMAX
3.      COMMON/PLBAS2/ AP(16),AV(16),CP(16),DAT(7)
4.      COMMON/PLBAS3/ WINXL,WINYL,WINXW,WINYW,IWIN
5.      COMMON/PLBAS4/ SCRNXL,SCRNYL,SCRNXW,SCRNYW,SCRNZW,ISCRN
6.      COMMON/PLBAS5/ SIGNOR,SNPLOT,IH
7.      COMMON/PLBAS6/ DIMAGE,DORIG,DOBX,DOBY
8.      COMMON/PLBAS7/ HT,NDECFX,XLATE,YLATE
9.      C--- AP,AV ARE PROJECTIVE NON SINGULAR MATRICES WHICH RECORD THE
10.     C--- CURRENT POSITION OF THE POINT SET
11.     C--- IH THE HIDDEN LINE FLAG
12.     C--- ZVIEW IS DISTANCE OF VIEWERS EYE FROM PROJECTION(XY) PLANE
13.     C--- DAT CONTAINS THE COMMAND DATA FOR EXECUTING PIECES OF THIS ROUTI
14.     C--- SIGNOR THE SIGN APPLIED TO THE SURFACE NORMALS
15.     C--- P CONTAINS XYZ DATA OF POINTS,VECTORS AND SYMBOL DATA IN 4TH PLC
16.     C--- ICON CONTAINS TWO PACKED DIGITS AB WITH THE FOLLOWING MEANING
17.     C--- A=0, CONTINUE PRESENT MODE OF PLOTTING, A=1 START CONNECTING POIN
18.     C--- BY STRAIGHT LINES, A=2 CONNECT PTS BY DASHED LINES, A=4 PLOT POI
19.     C--- S ONLY, A=4 PLOT DASHED POINTS
20.     C--- B=0 PLOT NO SYMBOL, B=1 PLOT CENTERED SYMBOL WHOSE VALUE IS P(4,)
21.     C--- PLOT LITERAL STRING IN FIELD P(4,) B=3 PLOT NUMBER IN FIELD P(4,
22.     C--- SET UP WINDOW PARAMETERS
23.     DATA SMALL/1.0E-10/,SMAL/1.0E-8/
24.     DIMENSION AID(16),TP(16),BP(16)
25.     DIMENSION RWD(3),RCEN(3),RMIN(3),RMAX(3)
26.     DIMENSION IBUF(1000)
27.     DIMENSION PP(3),VV(3)
28.     DATA AID/1.0,4*0.0,1.0,4*0.0,1.0,4*0.0,1.0/
29.     IT=DAT(1)
30.     GO TO (10,20,30,40,50,60,70,80,90,100,110,120,130,140,150),IT
31.     C--- IT=1 INITIALIZE KEY VARIABLES WITH DEFAULT VALUES
32.     10 SIGNOR=1.0
33.     NUM=0
34.     IPRIN=0
35.     HT=0.14
36.     HT=0.07
37.     SWIDTH=8.25
38.     SHEIGT=6.5
39.     ISCRN=-1
40.     IWIN=-1
41.     SCRNXL=0.0
42.     SCRNYL=0.0
43.     SCRNXW=8.5
44.     SCRNYW=6.25
45.     SCRNZW=SCRNXW
46.     SXUNIT=1024.
47.     SYUNIT=760.0
48.     IH=0
49.     ZVIEW=0.0
50.     NERASE=0
51.     HT=0.07
52.     NDECFX=-1
53.     XLATE=-1.1
54.     YLATE=-1.1
55.     NUM=0
56.     CALL PLOTS(IBUF,1000,10)
57.     IPRIN=0
```

SSPLOT(0)

```
58.          DO 11 I=1,16
59.          BP(I)=AID(I)
60.          AP(I)=AID(I)
61.          11 AV(I)=AID(I)
62.          BP(11)=0.0
63.          C--- REPLACE INCREMENTAL VALUES WITH ABSOLUTE VALUES
64.          NUMAX=3000
65.          DO 13 L=1,NUMAX
66.          DO 14 K=1,4
67.          14 P(K,L)=0.0
68.          ICON(L)=0
69.          13 CONTINUE
70.          DOBX=0.0
71.          DOBY=0.0
72.          GO TO 999
73.          C--- 20,30 AND 40 ARE ROTATION COMMANDS
74.          C--- IT=2 XYROT OR ROLL
75.          20 DAT(1)=1.0
76.          CALL PERSPT(DAT,TP)
77.          CALL MMULT(AP,TP,CP,1)
78.          CALL MMULT(AV,TP,CP,1)
79.          GO TO 999
80.          C--- IT=3 YZROT OR PITCH
81.          30 DAT(1)=2.0
82.          CALL PERSPT(DAT,TP)
83.          CALL MMULT(AP,TP,CP,1)
84.          CALL MMULT(AV,TP,CP,1)
85.          GO TO 999
86.          C--- IT=4 ZXROT OR YAW
87.          40 DAT(1)=3
88.          CALL PERSPT(DAT,TP)
89.          CALL MMULT(AP,TP,CP,1)
90.          CALL MMULT(AV,TP,CP,1)
91.          GO TO 999
92.          C--- IT=5 SCALE
93.          50 DAT(1)=4
94.          CALL PERSPT(DAT,TP)
95.          CALL MMULT(AP,TP,CP,1)
96.          GO TO 999
97.          C--- IT=6 TRANSLATION
98.          60 DAT(1)=5
99.          CALL PERSPT(DAT,TP)
100.         CALL MMULT(AP,TP,CP,1)
101.         GO TO 999
102.         C--- IT=7 SETUP PROJECTION ONTO XYPLAN FROM VIEWERS POSITION
103.         70 DAT(1)=6
104.         ZVIEW=DAT(2)
105.         DIMAGE=DAT(2)
106.         DORIG=DAT(3)
107.         DOBX=DAT(4)
108.         DOBY=DAT(5)
109.         CALL PERSPT(DAT,BP)
110.         GO TO 999
111.         C--- REIDENTIFY THE TRANSFORMATION MATRICES
112.         80 DO 81 I=1,16
113.         AP(I)=AID(I)
114.         81 AV(I)=AID(I)
```

SSPLOT(0)

```
115.      GO TO 999
116.      C--- SETUP THE HIDDEN LINE FLAG
117.      90 IH=DAT(2)
118.      GO TO 999
119.      100 SIGNOR=DAT(2)
120.      GO TO 999
121.      110 CONTINUE
122.      IWIN=-1
123.      IF(DAT(2)**2+DAT(3)**2+DAT(4)**2+DAT(5)**2.LT.SMAL) GO TO 999
124.      IWIN=1
125.      WINXL=DAT(2)
126.      WINYL=DAT(3)
127.      WINXW=DAT(4)
128.      WINYW=DAT(5)
129.      GO TO 999
130.      C--- SCREEN PARAMETERS INTRODUCED
131.      120 CONTINUE
132.      ISCRN=-ISCRN
133.      IF(DAT(2)**2+DAT(3)**2+DAT(4)**2+DAT(5)**2.LT.SMAL) GO TO 999
134.      SCRNXL=DAT(2)
135.      SCRNYL=DAT(3)
136.      SCRNXW=DAT(4)
137.      SCRNYW=DAT(5)
138.      SCRNZW=DAT(6)
139.      ISCRN=1
140.      GO TO 999
141.      C--- BOX COMMAND, SCALE THE OBJECT TO FILL THE SCREEN
142.      130 CONTINUE
143.      IF(ISCRN.LT.0) GO TO 999
144.      PROA=DAT(2)
145.      PROB=DAT(3)
146.      PROC=DAT(4)
147.      C--- DETERMINE THE XYZ EXTENT OF THE TRANSFORMED OBJECT
148.      DO 131 L=1,3
149.      RMIN(L)=1.0E+20
150.      131 RMAX(L)=-1.0E+20
151.      I=0
152.      137 I=I+1
153.      IF(I.GT.NUM) GO TO 138
154.      CALL DECOD(PP,VV,AA,JCON,ISYM,IVEC,I)
155.      IF(IVEC.EQ.999) GO TO 137
156.      IF(I.LT.0) GO TO 999
157.      WW=PP(1)*AP(13)+PP(2)*AP(14)+PP(3)*AP(15)+AP(16)+SMALL
158.      DO 132 L=1,3
159.      L4=L*4
160.      PPP=(PP(1)*AP(L4-3)+PP(2)*AP(L4-2)+PP(3)*AP(L4-1)+AP(L4))/WW
161.      RMIN(L)=AMIN0(PPP,RMIN(L))
162.      RMAX(L)=AMAX0(PPP,RMAX(L))
163.      132 CONTINUE
164.      GO TO 137
165.      138 CONTINUE
166.      DO 133 L=1,3
167.      RCEN(L)=(RMIN(L)+RMAX(L))/2.0
168.      RWID(L)=RMAX(L)-RMIN(L)+SMALL
169.      DAT(L+1)=-RCEN(L)
170.      133 CONTINUE
171.      C--- CENTERISE THE OBJECT AROUND THE ORIGIN
```

SSPLOT(0)

```
172.      DAT(1)=5
173.      CALL PERSPT(DAT,TP)
174.      CALL MMULT(AP,TP,CP,1)
175.      C--- SCALE THE OBJECT INTO THE SCREEN AREA OR WINDOW AREA IF REQUESTED
176.      IF(ISCN.LE.0) GO TO 999
177.      A=1.0E+20
178.      SX=SCRNXW/RWID(1)*PROA
179.      IF(PROB.GT.0.0) GO TO 135
180.      A=SCRNYW/RWID(2)*PROA
181.      SX=AMIN1(SX,A)
182.      DAT(2)=SX
183.      DAT(3)=SX
184.      DAT(4)=SX
185.      GO TO 136
186.      135 CONTINUE
187.      SY=SCRNYW/RWID(2)*PROB
188.      DAT(2)=SX
189.      DAT(3)=SY
190.      DAT(4)=1.0
191.      IF(PROC.GT.0.0) DAT(4)=SCRNZW/RWID(3)*PROC
192.      136 CONTINUE
193.      DAT(1)=4
194.      CALL PERSPT(DAT,TP)
195.      CALL MMULT(AP,TP,CP,1)
196.      CALL MMULT(AV,TP,CP,1)
197.      IF(IWIN.LE.0) GO TO 999
198.      C--- APPLY A FURTHER TRANSLATION AND SCALE IF WINDOW IS IN EFFECT
199.      DAT(1)=5.
200.      DAT(2)=- (WINXL+WINXW/2.0)
201.      DAT(3)=- (WINYL+WINYW/2.0)
202.      DAT(4)=0.0
203.      CALL PERSPT(DAT,TP)
204.      CALL MMULT(AP,TP,CP,1)
205.      DAT(2)=SCRNXW/WINXW
206.      DAT(3)=SCRNYW/WINYW
207.      DAT(2)=AMIN1(DAT(2),DAT(3))
208.      DAT(3)=DAT(2)
209.      DAT(4)=DAT(2)
210.      DAT(4)=1.0
211.      DAT(1)=4.0
212.      CALL PERSPT(DAT,TP)
213.      CALL MMULT(AP,TP,CP,1)
214.      CALL MMULT(AV,TP,CP,1)
215.      WINXW=SCRNXW
216.      WINYW=SCRNYW
217.      WINXL=SCRNXL
218.      WINYL=SCRNYL
219.      GO TO 999
220.      C--- APPLY A STRAIGHT FACTOR TO ALL SUBSEQUENT PLTS
221.      140 CONTINUE
222.      IF(DAT(2).LE.SMAL) GO TO 999
223.      CALL FACTOR(DAT(2))
224.      GO TO 999
225.      C--- MAIN PLOT PROCESSING IS HERE
226.      150 CONTINUE
227.      IF(DAT(4).LT.0.0) CALL PLOT(0.,0.-3)
228.      IF(DAT(4).LT.0.0) CALL PLOT(DAT(2),DAT(3),999)
```

SSPLOT(0)

```

229.      IF(DAT(4).LT.0.0) GO TO 999
230.      CALL PLOT(DAT(2),DAT(3),-3)
231.      C--- OFFSET COMMAND FOR THE TEKTRONIX VERSION ONLY
232.      CALL OFFSET(4,125,3,25)
233.      151 CONTINUE
234.      CALL MMULT(AP,BP,CP,3)
235.      C--- SETUP THE WINDOW,SCREEN AND PLOT BOUNDARIES
236.      IF(IWIN.LE.0.AND.ISCRN.LE.0) GO TO 154
237.      IF(ISCRN.GT.0) GO TO 153
238.      IF(IWIN.LE.0) GO TO 154
239.      XL=WINXL
240.      YL=WINYL
241.      XW=WINXW
242.      YW=WINYW
243.      GO TO 152
244.      153 XL=SCRNXL
245.      YL=SCRNYL
246.      XW=SCRNXW
247.      YW=SCRNYW
248.      152 CONTINUE
249.      IF(DAT(2)**2+DAT(3)**2.GT.SMAL) CALL PLOT(XL+XW/2.0,YL+YW/2.0,3)
250.      CALL PLOT(XL,YL,3)
251.      CALL PLOT(XL+XW,YL,2)
252.      CALL PLOT(XL+XW,YL+YW,2)
253.      CALL PLOT(XL,YL+YW,2)
254.      CALL PLOT(XL,YL,2)
255.      154 CONTINUE
256.      MOVNOW=0
257.      IF(ISCRN.GT.0.OR.IWIN.GT.0) CALL WINDOW(XL,YL,XW,YW,MOVNOW)
258.      XLAS=0.0
259.      YLAS=0.0
260.      IPERM=0
261.      NPLT=0
262.      I=0
263.      301 I=I+1
264.      IF(I.GT.NUM) GO TO 302
265.      C--- MAIN PLOTTING LOOP
266.      X1=XLAS
267.      Y1=YLAS
268.      C--- DECODE THE NECESSARY POINT AND AUXILIARY DATA
269.      IA=I
270.      CALL DECOD(PP,VV,AA,JCON,ISYM,IVEC,IA)
271.      IF(IVEC.EQ.999) GO TO 301
272.      IF(IA.LE.0) GO TO 300
273.      I=IA
274.      IF(JCON*(5-JCON).NE.0) IPERM=JCON
275.      IF(IPERM.EQ.0) GO TO 300
276.      WNOW=PP(1)*CP(13)+PP(2)*CP(14)+PP(3)*CP(15)+CP(16)+SMALL
277.      XNOW=(PP(1)*CP(1)+PP(2)*CP(2)+PP(3)*CP(3)+CP(4))/WNOW
278.      YNOW=(PP(1)*CP(5)+PP(2)*CP(6)+PP(3)*CP(7)+CP(8))/WNOW
279.      X2=XNOW
280.      Y2=YNOW
281.      MOVNOW=2
282.      IF(IWIN.LT.0) GO TO 310
283.      C--- MAKE THE REQUIRED WINDOW CHECK
284.      MOVNOW=1
285.      CALL WINDOW(X1,Y1,X2,Y2,MOVNOW)

```

SPLOT(0)

```
286.      310 CONTINUE
287.      IF(MOVNOW.LT.0) GO TO 600
288.      IF(IH.EQ.0.OR.IVEC.LT.1) GO TO 320
289.      C--- MAKE THE HIDDEN LINE/SURFACE NORMAL CHECK
290.      VXNOW=VV(1)*AV(1)+VV(2)*AV(2)+VV(3)*AV(3)
291.      VYNOW=VV(1)*AV(5)+VV(2)*AV(6)+VV(3)*AV(7)
292.      VZNOW=VV(1)*AV(9)+VV(2)*AV(10)+VV(3)*AV(11)
293.      PXNOW=PP(1)*AP(1)+PP(2)*AP(2)+PP(3)*AP(3)+AP(4)
294.      PYNOW=PP(1)*AP(5)+PP(2)*AP(6)+PP(3)*AP(7)+AP(8)
295.      PZNOW=PP(1)*AP(9)+PP(2)*AP(10)+PP(3)*AP(11)+AP(12)
296.      IF(ABS(BP(15)).LT.0.0001) GO TO 330
297.      ZVIEW=-BP(16)/BP(15)
298.      D=(PXNOW-DOBX)*VXNOW+(PYNOW-DOBY)*VYNOW+(PZNOW-ZVIEW)*VZNOW
299.      D=D*SIGNOR
300.      IHCUR=0
301.      PRINT 311
302.      311 FORMAT(' PXNOW,PYNOW,PZNOW,VXNOW,VYNOW,VZNOW,DOBX,DOBY,ZVIEW,D')
303.      WRITE(6,312) 1,
304.      X PXNOW,PYNOW,PZNOW,VXNOW,VYNOW,VZNOW,DOBX,DOBY,ZVIEW,D
305.      312 FORMAT(1X,I4,3(1X,F9.3)),2X,F9.3)
306.      IF(D.GT.0.0) IHCUR=1
307.      GO TO 340
308.      330 IHCUR=0
309.      D=VZNOW*SIGNOR
310.      IF(D.LT.0.0) IHCUR=1
311.      340 CONTINUE
312.      320 CONTINUE
313.      IPERMN =IPERM
314.      IF(IH.EQ.0.OR.IVEC.LT.1) GO TO 350
315.      IF(IHCUR.EQ.0) GO TO 350
316.      IF(IH.EQ.2) GO TO 360
317.      C--- TOTALLY HIDDEN LINE
318.      IPERMN=0
319.      GO TO 350
320.      360 CONTINUE
321.      IF(IPERM.EQ.1) IPERMN =2
322.      IF(IPERM.EQ.2) IPERMN =4
323.      350 CONTINUE
324.      IF(IPERMN .EQ.0) GO TO 600
325.      IF((IPERMN-2)*(IPERMN-4).EQ.0.AND.JCON.EQ.0) GO TO 370
326.      NDASH=1
327.      UX=X2-X1
328.      UY=Y2-Y1
329.      GO TO 380
330.      370 CONTINUE
331.      D=SQRT((X2-X1)**2+(Y2-Y1)**2)
332.      NDASH=D/0.25
333.      NDASH=MAX0(3,NDASH)
334.      D1=D/NDASH
335.      UX=(X2-X1)/(D+SMALL)*D1
336.      UY=(Y2-Y1)/(D+SMALL)*D1
337.      C--- POSITION POINT AT START OF SEGMENT
338.      IF(MOVNOW.EQ.3.OR.MOVNOW.EQ.5) CALL PLOT(X1,Y1,3)
339.      IF(MOVNOW.EQ.3.OR.MOVNOW.EQ.5) NPLT=NPLT+1
340.      380 CONTINUE
341.      IF(IPERMN .GT.2) GO TO 420
342.      MOD0=-1
```

SSPLOT(0)

```
343.      DO 410 J=1,NDASH
344.      XX=X1+UX*J
345.      YY=Y1+UY*J
346.      MOD0=-MOD0
347.      IPLT=2
348.      IF(MOD0.LT.0) IPLT=3
349.      IF(JCON.NE.0) IPLT=3
350.      NPLT=NPLT+1
351.      CALL PLOT(XX,YY,IPLT)
352. 410 CONTINUE
353.      GO TO 500
354. 420 DO 430 J=1,NDASH
355.      XX=X1+UX*J
356.      YY=Y1+UY*J
357.      CALL PLOT(XX,YY,3)
358.      CALL PLOT(XX,YY,2)
359.      NPLT=NPLT+1
360. 430 CONTINUE
361.      GO TO 500
362. 500 CONTINUE
363.      IF(MOVNOW.EQ.4.OR.MOVNOW.EQ.5) GO TO 590
364.      IF(ISYM.EQ.0) GO TO 590
365.      GO TO (510,520,530),ISYM
366. 510 CONTINUE
367.      INT=AA
368.      CALL SYMBOL(X2,Y2,HT,INT,0.0,-2)
369.      GO TO 590
370. 520 CONTINUE
371.      NCHAR=4.0
372.      XLEFT=(XLATE-1.0)*0.5*NCHAR*HT
373.      YLEFT=(YLATE-1.0)*0.5*NCHAR*HT
374.      CALL SYMBOL(X2+XLEFT,Y2+YLEFT,HT,AA,0.0,4)
375.      GO TO 590
376. 530 CONTINUE
377.      SZ=2
378.      S1=ABS(AA)
379.      IF(S1.GT.SMAL) SZ=ALOG10(S1)
380.      IF(S1.LY.0.0001) GO TO 591
381.      SZ=ALOG10(S1)
382.      IF(SZ.GE.0.0) NDEC=1
383.      IF(SZ.LY.0.0) NN=SZ
384.      IF(SZ.LT.0.0) NDEC=NN+2
385.      IF(NDECFX.GE.0) NDEC=NDECFX
386.      IF(SZ.GE.0.0) NSIG=SZ+1.0+2.0
387.      IF(SZ.LT.0.0) NSIG=NDEC+2.0
388.      GO TO 592
389. 591 CONTINUE
390.      NSIG=3
391.      NDEC=1
392. 592 CONTINUE
393.      IF(AA.LT.0.0) NSIG=NSIG+1
394.      XLEFT=HT*NSIG*(XLATE-1.0)*0.5
395.      YLEFT=HT*NSIG*(YLATE-1.0)*0.5
396.      CALL NUMBER(X2+XLEFT,Y2+YLEFT,HT,AA,0.0,NDEC)
397. 590 CONTINUE
398.      XLAS=XNOW
399.      YLAS=YNOW
```



SSPLOT(0)

```
400.      GO TO 300
401.      600 CONTINUE
402.      300 CONTINUE
403.      GO TO 301
404.      302 CONTINUE
405.      WRITE(6,390) NPLT
406.      390 FORMAT(6X,'PLOT COMPLETED, TOTAL POINTS PLOTTED= ',I6)
407.      GO TO 999
408.      999 RETURN
409.      END
```

MMULT(0)

```
1.      SUBROUTINE MMULT(A,B,C,M)
2.      C--- CONSTRUCT C=A*B AND STORE THE RESULT IN A OR B
3.      DIMENSION A(16),B(16),C(16)
4.      DIMENSION ITEMP(4)
5.      DATA ITEMP/1,5,9,13/
6.      DO 10 IROW=1,4
7.      DO 10 ICOL=1,4
8.      KK=ITEMP(ICOL)
9.      SUM=0.0
10.     DO 11 K=1,4
11.     SUM=SUM+A(IROW+K-4)*B(KK+K-1)
12.     11 CONTINUE
13.     C(4*ICOL-4+IROW)=SUM
14.     10 CONTINUE
15.     IDEBUG=0
16.     IF(IDEBUG.EQ.0) GO TO 20
17.     WRITE(6,50)
18.     50 FORMAT(//)
19.     DO 30 I=1,4
20.     IL=I+12
21.     WRITE(6,40) (A(L),L=I,IL,4), (B(L),L=I,IL,4), (C(L),L=I,IL,4)
22.     40 FORMAT(' MMULT',4(1X,F8.3),3X,4(1X,F8.3),3X,4(1X,F8.3))
23.     30 CONTINUE
24.     20 CONTINUE
25.     IF(M.EQ.3) RETURN
26.     DO 12 I=1,16
27.     IF(M.EQ.1) A(I)=C(I)
28.     IF(M.EQ.2) B(I)=C(I)
29.     12 CONTINUE
30.     RETURN
31.     END
```

PERSPT(0)

```
1.      SURROUTINE PERSPT(DAT,B)
2.      C--- GENERATE A PROJECTIVE MATRIX B FROM A SIMPLE COMMAND DAT
3.      DIMENSION DAT(1),B(1),AID(16)
4.      DATA AID/1.0,4*0.0,1.0,4*0.0,1.0,4*0.0,1.0/
5.      DATA CDR/0.01745329251994/
6.      C--- DAT(1) CONTAINS THE COMMAND FLAG  =1=XYROT, 2=YZROT,
7.      C--- 3=ZXROT, 4=VARIABLE SCALE, 5=TRANS, 6=CENTER
8.      DO 10 I=1,16
9.          10 B(I)=AID(I)
10.         IFLAG=DAT(1)
11.         IF(IFLAG.GT.3) GO TO 50
12.         A=DAT(2)*CDR
13.         C=COS(A)
14.         S=SIN(A)
15.         GO TO (20,30,40),IFLAG
16.         20 B(1)=C
17.             B(2)=-S
18.             B(5)=S
19.             B(6)=C
20.             GO TO 100
21.         30 B(6)=C
22.             B(7)=-S
23.             B(10)=S
24.             B(11)=C
25.             GO TO 100
26.         40 B(1)=C
27.             B(3)=S
28.             B(9)=-S
29.             B(11)=C
30.             GO TO 100
31.         50 IFLAG=IFLAG-3
32.             GO TO (60,70,80), IFLAG
33.         60 W=DAT(3)**2+DAT(4)**2
34.             IF(W.LT.0.000001) GO TO 65
35.             B(1)=DAT(2)
36.             B(6)=DAT(3)
37.             B(11)=DAT(4)
38.             GO TO 100
39.         65 B(1)=DAT(2)
40.             B(6)=DAT(2)
41.             B(11)=DAT(2)
42.             GO TO 100
43.         70 B(4)=DAT(2)
44.             B(8)=DAT(3)
45.             B(12)=DAT(4)
46.             GO TO 100
47.         80 D=ABS(DAT(2))
48.             B(11)=0.0
49.             IF(D.GT.0.0001) B(15)=-1./DAT(2)
50.             D1=ABS(DAT(3))
51.             IF(D1.GT.0.0001.AND.D.GT.0.0001) B(16)= DAT(3)/DAT(2)
52.             B(4)=-DAT(4)
53.             B(8)=-DAT(5)
54.         100 CONTINUE
55.             IDEBUG=0
56.             IF(IDEBUG.EQ.0) RETURN
57.             WRITE(6,140)
```

PERSPT(0)

```
58.      140 FORMAT(//)
59.      DO 110 I=1,4
60.          IL=I+12
61.          WRITE(6,120) (B(J),J=I,IL,4)
62.      120 FORMAT(10X,'PERSPT',4(2X,F12.5))
63.      110 CONTINUE
64.      RETURN
65.      END
```

WINDOW(0)

```
1.      SUBROUTINE WINDOW(XA,YA,XB,YB,MOD)
2.      C--- ROUTINE TO EXAMINE THE CURRENT SEGMENT RELATIVE TO THE CURRENT
3.      C--- WINDOW
4.      C--- INPUT IF MOD IS 0 THEN XA,YA ARE LOWER LEFT CORNER OF NEW WINDOW
5.      C--- AND XB AND YB ARE THE WIDTH AND HEIGHT OF THE WINDOW
6.      C--- OTHER PARAMETERS ARE ALSO INITIALIZED IN THIS CASE
7.      C--- THE RETURN VALUE OF MOD IS -1
8.      C--- IF MOD IS 1 THEN XA,YA AND XB,YB REPRESENT END POINTS OF A LINE
9.      C--- SEGMENT WHICH SHOULD BE WINDOWED. IF MOD=-1 ON RETURN THE SEGMENT
10.     C--- DOES NOT INTERSECT THE WINDOW. IF MOD=2 THE INTERSECTION OCCURS
11.     C--- AND THE FIRST POINT DOES NOT CHANGE, WHILE IF MOD=3 THE FIRST P
12.     C--- HAS CHANGED. XA,YA,XB,YB MAY BE MODIFIED ON OUTPUT TO HOLD
13.     C--- CHANGED VALUES OF THE END POINTS
14.     C--- IF MOD IS LESS THAN -1, AN ERROR HAS OCCURRED
15.     DIMENSION PX(2),PY(2),PD(5),X(5),Y(5),IND(2,2)
16.     DATA IND/1,2,4,3/
17.     DATA SMAL/1.0E-20/
18.     LOGICAL AIN,BIN
19.     BET(A,B,C)=(B-A)*(C-B)
20.     IF(MOD)20,10,20
21.     C--- INITIALIZATION OF WINDOW PARAMETERS
22.     10 CONTINUE
23.     XL=XA
24.     YL=YA
25.     XW=XB
26.     YW=YB
27.     XU=XL+XW
28.     YU=YL+YW
29.     X(1)=XL
30.     X(2)=XL+XW
31.     X(3)=X(2)
32.     X(4)=XL
33.     X(5)=XL
34.     Y(1)=YL
35.     Y(2)=YL
36.     Y(3)=YL+YW
37.     Y(4)=Y(3)
38.     Y(5)=YL
39.     HXW=XW/2.0
40.     HYW=YW/2.0
41.     XC=XL+HXW
42.     YC=YL+HYW
43.     DC=HXW*HXW+HYW*HYW
44.     MOD=-1
45.     GO TO 999
46.     C--- BEGIN WINDOW CUTTING ACTION ON SEGMENT
47.     20 CONTINUE
48.     AX=BET(XL,XA,XU)
49.     AY=BET(YL,YA,YU)
50.     AIN=.TRUE.
51.     IF(AX.LT.0.0.OR.AY.LT.0.0) AIN=.FALSE.
52.     BX=BET(XL,XB,XU)
53.     BY=BET(YL,YB,YU)
54.     BIN=.TRUE.
55.     IF(BX.LT.0.0.OR.BY.LT.0.0) BIN=.FALSE.
56.     IF(AIN.AND.BIN) GO TO 100
57.     IF(AIN.OR.BIN) GO TO 200
```

WINDOW(0)

```
58.      GO TO 300
59.      C--- BOTH INSIDE
60.      100 CONTINUE
61.      MOD=2
62.      GO TO 999
63.      C--- ONE INSIDE/ ONE OUTSIDE
64.      200 CONTINUE
65.      IF(AIN) GO TO 210
66.      XX=XA
67.      YY=YA
68.      GO TO 220
69.      210 XX=XB
70.      YY=YB
71.      220 CONTINUE
72.      C--- CHOOSE THE MAIN CORNER REFERENCE POINT
73.      SX=XX-XC
74.      SY=YY-YC
75.      I=2
76.      J=2
77.      IF(SX.LT.0.0) I=1
78.      IF(SY.LT.0.0) J=1
79.      IS=IND(I,J)
80.      C--- SET UP THE EQN OF THE LINE SEGMENT
81.      A=YB-YA
82.      B=XA-XB
83.      C=XB*YA-XA*YB
84.      ISA=IS-1
85.      IF(IS.LT.1) ISA=4
86.      D1=A*X(IS)+B*Y(IS)+C
87.      D2=A*X(ISA)+B*Y(ISA)+C
88.      IF(D1*D2.GT.0.0) ISA=IS+1
89.      IF(ISA.GT.4) ISA=1
90.      ICUM=ISA+IS
91.      IF(ICUM.NE.5) GO TO 240
92.      XX=X(IS)
93.      YY=-(C+A*X(IS))/(B+SMAL)
94.      GO TO 250
95.      240 XX=-(C+B*Y(IS))/(A+SMAL)
96.      YY=Y(IS)
97.      250 CONTINUE
98.      IF(AIN) GO TO 260
99.      XA=XX
100.     YA=YY
101.     MOD=3
102.     GO TO 999
103.     260 CONTINUE
104.     XB=XX
105.     YB=YY
106.     MOD=4
107.     GO TO 999
108.     C--- THE CASE OF TWO POINTS OUTSIDE THE WINDOW
109.     300 CONTINUE
110.     IF(XA-XL.LT.0.0.AND.XB-XL.LT.0.0) GO TO 390
111.     IF(XA-XU.GT.0.0.AND.XB-XU.GT.0.0) GO TO 390
112.     IF(YA-YL.LT.0.0.AND.YB-YL.LT.0.0) GO TO 390
113.     IF(YA-YU.GT.0.0.AND.YB-YU.GT.0.0) GO TO 390
114.     A=YB-YA
```

WINDOW(0)

```
115.      B=XA-XB
116.      C=XB*YA-XA*YB
117.      ICUM=0
118.      PD(1)=A*X(1)+B*Y(1)+C
119.      DO 310 I=2,5
120.      PD(I)=A*X(I)+B*Y(I)+C
121.      IF(PD(I)*PD(I-1).LT.0.0) ICUM=ICUM+1
122. 310 CONTINUE
123.      IF(ICUM.EQ.0) GO TO 390
124.      NUM=0
125.      DO 340 I=1,4
126.      IF(PD(I)*PD(I+1).GT.0.0) GO TO 340
127.      NUM=NUM+1
128.      IF(NUM.GT.2) GO TO 340
129.      ICUM=I+1
130.      IF(ICUM.EQ.3.OR.ICUM.EQ.7) GO TO 350
131.      PY(NUM)=-(C+A*X(I))/(B+SMAL)
132.      PX(NUM)=X(I)
133.      GO TO 340
134. 350 PX(NUM)=-(C+B*Y(I))/(A+SMAL)
135.      PY(NUM)=Y(I)
136. 340 CONTINUE
137.      IF(NUM.LT.2) GO TO 998
138.      D1=(PX(1)-XA)**2+(PY(1)-YA)**2
139.      D2=(PX(2)-XA)**2+(PY(2)-YA)**2
140.      NUM1=1
141.      IF(D2.LT.D1) NUM1=2
142.      XA=PX(NUM1)
143.      YA=PY(NUM1)
144.      NUM2=2
145.      IF(NUM1.EQ.2) NUM2=1
146.      XB=PX(NUM2)
147.      YB=PY(NUM2)
148.      MOD=5
149.      GO TO 999
150. 390 CONTINUE
151.      MOD=-1
152. 999 CONTINUE
153.      RETURN
154. 998 MOD=-2
155.      GO TO 999
156.      END
```

USER(0)

```
1. SUBROUTINE USER
2. COMMON/PLBAS1/ P(4,3001),ICON(3001),NUM,NUMAX
3. COMMON/PLBAS2/ AP(16),AV(16),CP(16),DAT(7)
4. COMMON/PLBAS3/ WINXL,WINYL,WINXW,WINYW,IWIN
5. COMMON/PLBAS4/ SCRNXL,SCRNYL,SCRNXW,SCRNYW,ISCRN
6. COMMON/PLBAS5/ SIGNOR,SNPLOT,IH
7. RETURN
8. END
```



READIN(0)

```
1.      SUBROUTINE READIN(IRR)
2.      COMMON/PLBAS1/ P(4,3001),ICON(3001),NUM,NUMAX
3.      COMMON/PLBAS2/ AP(16),AV(16),CP(16),DAT(7)
4.      COMMON/PLBAS3/ WINXL,WINYL,WINXW,WINYW,IWIN
5.      COMMON/PLBAS4/ SCRNXL,SCRNYL,SCRNXW,SCRNYW,ISCRN
6.      COMMON/PLBAS5/ SIGNOR,SNPLOT,IH
7.      DIMENSION NAM(21)
8.      DATA NAM/ 4HP      ,4HINIT,4HROLL,4HPITC,4HYAW ,
9.      X      4HSCAL,4HTRAN,4HDIST,4HREIN,4HHIDE,
10.     X      4HSIGN,4HWIND,4HSCRN,4HBOX ,4HFACT,
11.     X      4HPLOT,4HUSER,4HPRIN,4HEND ,4HDUM ,
12.     X      4HAXIS /
13.      DATA NONAM/21/
14.      EQUIVALENCE (DAT(1),RDAR(1))
15.      DIMENSION RDAR(8)
16.      DIMENSION R(4),RMN(3),RMX(3),PT(3)
17.      1 READ(5,10,END=999) NAMM,(RDAR(L),L=2,8)
18.      10 FORMAT(A4,6X,7F10.4)
19.      IF(IPRIN.GT.0) GO TO 41
20.      WRITE(6,40) NAMM,(RDAR(L),L=2,8)
21.      40 FORMAT(1X,A4,6X,7F10.4)
22.      41 CONTINUE
23.      C--- COMPARE TO PRESTORED NAMES IN ORDER TO DETERMINE THE ACTION CODE
24.      DO 20 I=1,NONAM
25.      IF(NAMM.EQ.NAM(I)) GO TO 30
26.      20 CONTINUE
27.      C--- ERROR PATH -- INPUT WORD WAS NOT VALID
28.      IRR=1
29.      WRITE(6,50) NAMM,NAM
30.      50 FORMAT(/,' ERROR -- THE CODE NAME ',A5,1X,' WAS NOT VALID, VALID
31.      X NAMES ARE AS FOLLOWS',/,20(1X,A4))
32.      GO TO 999
33.      30 CONTINUE
34.      IF(I.EQ.1) GO TO 100
35.      IF(I.GT.1.AND.I.LT.17) GO TO 120
36.      IK=I-16
37.      GO TO (170,180,190,200,210),IK
38.      100 CONTINUE
39.      IF(RDAR(2).LT.-0.1.OR.RDAR(2).GT.99.) GO TO 110
40.      NUM=NUM+1
41.      DO 111 L=1,4
42.      111 P(L,NUM)=RDAR(L+2)
43.      ICON(NUM)=RDAR(2)
44.      GO TO 1
45.      110 CONTINUE
46.      NUM=RDAR(3)
47.      GO TO 1
48.      120 CONTINUE
49.      RDAR(1)=I-1
50.      CALL SSPLIT
51.      GO TO 1
52.      170 CONTINUE
53.      RDAR(1)=17
54.      CALL USER
55.      GO TO 1
56.      180 CONTINUE
57.      IPRIN=RDAR(2)
```

READIN(0)

```
58.      GO TO 1
59.      190 CONTINUE
60.      GO TO 999
61.      200 CONTINUE
62.      WRITE(6,201) NUM,NUMAX
63.      201 FORMAT(5X,'CURRENT NUMBER OF POINTS= ',I6,' AND MAXIMUM ALLOWED=
64.      X,I6)
65.      NUM1=MIN0(NUMAX,NUM)
66.      IF(NUM1.LE.0) GO TO 1
67.      WRITE(6,205)
68.      205 FORMAT(1X,10HCOORDINATE,10H LOW VAL ,10H HI VAL ,
69.      X 10H MEAN VAL ,10H WIDTH )
70.      DO 202 J=1,3
71.      RMIN=1.0E+20
72.      RMAX=-1.0E+20
73.      DO 203 L=1,NUM
74.      IF(ICON(L).GE.49) GO TO 203
75.      RMIN=AMIN1(RMIN,P(J,L))
76.      RMAX=AMAX1(RMAX,P(J,L))
77.      203 CONTINUE
78.      RMEAN=(RMAX+RMIN)/2.0
79.      DIF=RMAX-RMIN
80.      WRITE(6,204) J,RMIN,RMAX,RMEAN,DIF
81.      204 FORMAT(1X,'COORD ',I2,1X,4F10.3)
82.      202 CONTINUE
83.      GO TO 1
84.      210 CONTINUE
85.      IF(NUM.LE.0) GO TO 999
86.      DO 211 J=1,3
87.      RMIN=1.0E+20
88.      RMAX=-RMIN
89.      DO 212 I=1,NUM
90.      IF(ICON(I).GT.49) GO TO 212
91.      RMIN=AMIN1(RMIN,P(J,I))
92.      RMAX=AMAX1(RMAX,P(J,I))
93.      212 CONTINUE
94.      RMX(J)=RMAX
95.      RMN(J)=RMIN
96.      PT(J)=(RMIN+RMAX)/2.0
97.      IF(RDAR(2).GT.0.1) PT(J)=RMAX
98.      IF(RDAR(2).LT.-0.1) PT(J)=RMIN
99.      211 CONTINUE
100.     DO 213 J=1,3
101.     IF(RMX(J)-RMN(J).LT.0.0001) GO TO 213
102.     IF(RMX(J)-RMN(J).GT.1.0E+20) GO TO 213
103.     R(1)=RMN(J)
104.     R(2)=(RMX(J)-RMN(J))/5.0
105.     R(3)=6.0
106.     R(4)=5.0
107.     LAB=J
108.     CALL AXES(R,PT,LAB,1)
109.     213 CONTINUE
110.     GO TO 1
111.     999 CONTINUE
112.     RETURN
113.     END
```

APPENDIX N  
LITERATURE BIBLIOGRAPHY

- Thermal Models
- Optical Models
- Thermal Properties
- Blood Effects
- Burn Criteria
- Experimental Temperature Data
- Experimental Burn Data
- Melanin Granules
- Miscellaneous

CATEGORY - 1 - THERMAL MODELS

- 1- 1. ALLEN ET AL .CALCULATION OF RETINAL BURN AND FLASHBLINDNESS  
SAFE SEPARATION DISTANCES, TECHNOLOGY, INC., SAN  
ANTONIO, TEXAS LIFESCIENCES DIV. F41609-67-C-0040.  
156P. JAN 1968.
- 1- 2. ALLEN ET AL RESEARCH TO OBTAIN EYE EFFECTS DATA AND DEVELOP A  
MATHEMATICAL MODEL FOR EYE EFFECTS PREDICTIONS.  
FINAL REPORT 9 DEC 1970. USAFSAM CONTRACT F41609-  
70-C-0007, TECH., INC.
- 1- 3. ASCHOFF ET AL HEAT TRANSFER THROUGH THE SKIN AND ITS CHANGE  
DURING VASOCONSTRICTION. ARCH.F.D.GES.PHYSIOL.,  
249, (1948), P. 112.
- 1- 4. CHATO J C .ADVANCED HEAT TRANSFER IN  
BIOENGINEERING, CHAO, H. I. (ED.), UNIV. OF ILL.  
PRESS, 395 PP., 1969.
- 1- 5. CHATO J C .THERMAL PROBLEMS IN BIOTECHNOLOGY, ASME, 1968.
- 1- 6. CLARKE ET AL .AN EQUILIBRIUM THERMAL MODEL FOR RETINAL INJURY  
FROM OPTICAL SOURCES, APPLIED OPTICS, 8, 1051-  
1053.
- 1- 7. CLAUSING A M .NUMERICAL METHODS IN HEAT TRANSFER, THREE LECTURES
- 1- 8. DOUGLAS J ON THE NUMERICAL INTEGRATION OF HEAT CONDUCTION  
EQUATION BY IMPLICIT METHODS, J. SOC. INDUS.  
APPL. MATH., 3, 42 PP., 1955.
- 1- 9. DOUGLAS ET AL A GENERAL FORMULATION OF ALTERNATING DIRECTION  
METHODS, I., NUMER. MATH., 6, 428-453, 1964.
- 1- 10. HS J H .A MODEL FOR THE STUDY OF RETINAL DAMAGE DUE TO  
LASER RADIATION, U.S. ARMY TECHNICAL REPORT 3678.
- 1- 11. LAYES ET AL .THERMAL MODEL FOR RETINAL DAMAGE INDUCED BY PULSED  
LASERS, AEROSPACE MEDICINE, 39, 474-480.
- 1- 12. HILDEBRAND F P 1968. FINITE-DIFFERENCE EQUATIONS AND SIMU-  
LATIONS, ENGLEWOOD CLIFFS, PRENTICE-HALL.
- 1- 13. MAINSTER ET AL .RETINAL TEMPERATURE INCREASES PRODUCED BY INTENSE  
LIGHT SOURCES, JOURNAL OF THE OPTICAL SOC. OF  
AMER. VOL. 60 NO. 2, (FEB 1970).
- 1- 14. MAINSTER ET AL .TRANSIENT THERMAL BEHAVIOR IN BIOLOGICAL SYSTEM,  
HULL. MATH. BIOPHYSICS 32,303 (1970).
- 1- 15. MAYER ET AL .EYE BURN DAMAGE CALCULATION FOR AN EXO-ATMOSPHERIC  
NUCLEAR EVENT, J. OPT. SOC. AMER., 54, 678-683, 196

- 1- 16. MILLER ET AL RETINAL BURNS AND FLASHBLINDNESS, FINAL REPORT, CONTRACT F41609-68-C0023, VOL. 1, NOV 69, TECHNOLOGY INC., DDC AD 697425.
- 1- 17. NICKEL J A EVALUATION OF EYE HAZARDS FOR NUCLEAR DETONATIONS FINAL REPORT F41609-69-C--0049, SEP 1970, TECH. INC.
- 1- 18. O'BRIEN ET AL .A STUDY OF THE NUMERICAL SOLUTIONS OF PARTIAL DIFFERENTIAL EQUATIONS, AM. MATHEMATICAL SOCIETY, DEC., 1949.
- 1- 19. PEACEMAN ET AL THE NUMERICAL SOLUTION OF PARABOLIC AND ELLIPTIC DIFFERENTIAL EQUATIONS, J. SOC. INDUST. APPL. MATH., 3, 28-41.
- 1- 20. PENNES H H .ANALYSIS OF TISSUE AND ARTERIAL BLOOD TEMPERATURE IN THE RESTING HUMAN FOREARM, JOURNAL OF APPLIED PHYSIOLOGY, VOL. 1, NO. 2, AUG.1948,PP.93-122.
- 1- 21. ROULIER A .CALCULATION OF TEMPERATURE INCREASE IN THE EYE PRODUCED BY INTENSE LIGHT, BULL. MATH. BIOPHYS., 32, 405(1970)
- 1- 22. SAID ET AL .THE VARIATION WITH AGE OF THE SPECTRAL TRANSMISSIVITY OF THE LIVING HUMAN CRYSTALLINE LENS, GERONTOLOGIA, 5,213, 1959.
- 1- 23. SAULIYEV V K INTEGRATION OF EQUATIONS OF PARABOLIC TYPE BY THE METHOD OF NETS, NEW YORK, MACHILLAN., 1964.
- 1- 24. SCHMIDT ET AL SOME CALCULATIONS OF TEMPERATURE IN RETINAL BURN PROBLEMS, LABORATORY REPORT, DEPARTMENT OF BIOPHYSICS, MEDICAL COLLEGE OF VIRGINIA, JUNE 1964
- 1- 25. SHITZER ET AL .ANALYTICAL SOLUTIONS TO THE PROBLEM OF TRANSIENT HEAT TRANSFER IN LIVING TISSUE, U. OF I., URBANA, ILL., ASME, AUG, 1971.
- 1- 26. SKEEN ET AL .OCULAR EFFECTS OF NEAR INFRARED LASER RADIATION FOR SAFETY CRITERIA, TECHNOLOGY, INC., AF CONTRACT F41609-71-C-0016, PROJ 6301, TASK05, WORK UNIT 022, JUNE 1972.
- 1- 27. SKEEN ET AL .OCULAR EFFECTS OF REPETITIVE LASER PULSES, TECHNOLOGY, INC., AF CONTRACT F41609-71-C-0018, PROJ 6301, TASK 05, FINAL REPORT WORK UNIT 024, JUNE 30,1972.
- 1- 28. TAKATA ET AL .INVESTIGATION OF MEANS AND MATERIALS TO COMBAT THERMAL RADIATION FLASH BURNS,ARMOUR RESEARCH ENRON PROJECT D046, JAN., 1957.
- 1- 29. VOS J J .DIGITAL COMPUTATIONS OF TEMPERATURE IN RETINAL BURN PROBLEMS, INSTITUTE FOR PERCEPTION, RVO-TNO, REPORT NO. IZF, 1965-16, SOESTERBERG, THE NETHER-

LANDS, 1965.

1- 30. VOS J J

TEMPORARY AND PERMANENT LOSS OF VISUAL FUNCTIONS BY FLASHES AT NUCLEAR EXPLOSIONS: A THEORETICAL APPROACH, REPORT NO. 1959.7, INSTITUTE FOR PERCEPTION RVO-TNO (AD 332-551), 1959, SNESTERBERG, NETHERLANDS

1- 31. WEAVER ET AL

MATHEMATICAL MODEL OF SKIN EXPOSED TO THERMAL RADIATION, U.S. NAVAL AIR DEVELOPMENT CENTER, JOHNSVILLE, WARMINSTER, PENN., 18974 1969, AEROSPACE MED., 40(1), 24-30.

1- 32. WHITE T J

OBSERVER DISTANCES FOR NUCLEAR EVENTS, VOL. 1, (MODEL FOR OBSERVER DISTANCES FOR RETINAL BURN CRITERIA), DEFENSE NUCLEAR AGENCY CONTRACT REPORT DASIAC SR-125, 1973.

1- 33. WHITE ET AL

CHORIORETINAL THERMAL BEHAVIOR, BULL. MATH. BIOPHYSICS, 32, 315 (1970).

1- 34. WHITE ET AL

EVALUATION OF EYE HAZARDS FROM NUCLEAR DETONATION II., SAFE SEPARATION DISTANCE PREDICTIONS, USAF SCHOOL OF AEROSPACE MEDICINE, AEROSPACE MEDICAL DIV. (AFSC), BROOKS AIR FORCE BASE, TEXAS, NOV. 1969.

1- 35. WHITE ET AL

THE FEASIBILITY OF ANALOG OCULAR THERMAL SIMULATION, 1968, INTERIM REPORT 1, AF41(609)-68-C-0025.

1- 36. WRAY J L

MODEL FOR PREDICTION OF RETINAL BURNS, DASA - 1282, DEFENSE ATOMIC SUPPORT AGENCY, WASHINGTON 25, D.C., (1 FEB. 1962), (UNCLASSIFIED).

1- 37. YOUNG D

THE NUMERICAL SOLUTION OF ELLIPTIC AND PARABOLIC PARTIAL DIFFERENTIAL EQUATIONS, IN SURVEY OF NUMERICAL ANALYSIS, ED. J. TODD, NEW YORK, MCGRAW-HILL, 1962.

1- 38. ZARET M M

ANALYSIS OF FACTORS OF LASER RADIATION PRODUCING RETINAL CHANGE, FED. PROC., 24, 862-64, SUPP. 14, (1965).

1- 39. -----

THERMAL PROBLEMS IN BIOTECHNOLOGY, ASME, NEW YORK, DECEMBER 1968

CATEGORY - 2 - OPTICAL MODELS

- 2- 1. ALLEN ET AL .CALCULATION OF RETINAL BURN AND FLASHBLINDNESS  
SAFE SEPARATION DISTANCES, TECHNOLOGY, INC., SAN  
ANTONIO, TEXAS LIFESCIENCES DIV. F41609-67-C-0040.  
156P. JAN 1968.
- 2- 2. ALLEN ET AL RESEARCH TO OBTAIN EYE EFFECTS DATA AND DEVELOP A  
MATHEMATICAL MODEL FOR EYE EFFECTS PREDICTIONS.  
FINAL REPORT 9 DEC 1970. USAFSAM CONTRACT F41609-  
70-C-0007. TECH., INC.
- 2- 3. HARAKAT ET AL IMAGE OF AN INCOHERENTLY ILLUMINATED DISK, J. OPT.  
SOC. AM., 55, 881 (1965).
- 2- 4. BORN ET AL PRINCIPLES OF OPTICS (PERGAMON PRESS, NEW YORK,  
1970), 4TH ED. PP. 188-190.
- 2- 5. BOYNTON ET AL SOURCES OF ENTOPIC SCATTER IN THE HUMAN EYE  
J. OPT. SOC. AMER., VOL. 54, PP. 110-119 (1964).
- 2- 6. FAHS J H .A MODEL FOR THE STUDY OF RETINAL DAMAGE DUE TO  
LASER RADIATION, U.S. ARMY TECHNICAL REPORT 3678.
- 2- 7. KEENEY ET AL STUDIES ON HUMAN OCULAR PIGMENT, IN - EYE STRUCTURE  
II., SYMP., (J.W. ROSEN, ED.), 535-548, STUTTGART, SCHLA-  
UDER-VERLAG, 1965.
- 2- 8. FELDLEAD ET AL ANALOG SOLUTION OF LASER RETINAL COAGULATION, MED.  
ELECTRON. BIOL. ENGG., 3, 145-155.
- 2- 9. GURISCH R W .OPTICAL PERFORMANCE OF HUMAN EYE, J. OPT. SOC. AM.  
57, 407 (1967)
- 2- 10. HANSEN ET AL .A POST-CASE ANALYSIS OF CONTINUOUS WAVE HE-NE  
LASER HAZARDS TO THE EYE, APPL. OPT., 6, 1973-  
1975.
- 2- 11. HOPKINS H H .GEOMETRICAL-OPTICAL TREATMENT OF FREQUENCY  
RESPONSE, PROC. PHYS. SOC., B70, 1162 (1957).
- 2- 12. HOPKINS H H .THE APPLICATION OF FREQUENCY RESPONSE TECHNIQUES  
IN OPTICS. IMPERIAL COLLEGE OF SCIENCE AND TECH-  
NOLOGY, LONDON S.W.7, 1961.
- 2- 13. HOPKINS H H .THE NUMERICAL EVALUATION OF THE FREQUENCY RESPONSE  
DEPT. OF PHYSICS, IMPERIAL COLLEGE, LONDON,  
JUNE, 1957.
- 2- 14. JONES R C .ON THE POINT AND LINE SPREAD FUNCTIONS OF PHOTO-  
GRAPHIC IMAGES, JOURNAL OF THE OPTICAL SOCIETY OF  
AMERICA, VOL. 48, NO. 12, DEC., 1958.

- 2- 15. LINFOOT E H      FOURIER METHODS IN OPTICAL IMAGE EVALUATION. THE FOCAL PRESS, NEW YORK (1966).
- 2- 16. MAURICE D N      THE PHYSICS OF CORNEAL TRANSPARENCY IN DUKE-ELDER, W.S., AND PERKINS, E.S., EDITORS, THE TRANSPARENCY OF THE CORNEA, SPRINGFIELD, ILL., 1960, CHARLES C. THOMAS, PUBLISHER.
- 2- 17. MAYER ET AL      THE RISK OF EYEBURN FROM A NUCLEAR EVENT OUTSIDE THE ATMOSPHERE (U), DASA 1368-10, E.J. PLESSET ASSOCIATES, INC., LOS ANGELES, CALIFORNIA (1962) (SECRET-RESTRICTED DATA).
- 2- 18. NICKEL J A      EVALUATION OF EYE HAZARDS FOR NUCLEAR DETONATIONS, FINAL REPORT F41609-69-C-0049, SEP 1970 TECH. INC.
- 2- 19. DOUE S      RESPONSE FUNCTION OF THE EYE, J. APPL. PHYS., JAPAN, 28, 531-534., 1959.
- 2- 20. POLYAK S L      THE RETINA, U. OF CHICAGO PRESS, CHICAGO, ILLINOIS (1941).
- 2- 21. RAO ET AL      GAUSSIAN AND EXPONENTIAL APPROXIMATIONS OF THE MODULATION TRANSFER FUNCTION, J. OPT. SOC. AM., 57, 1159 (1967).
- 2- 22. ROHLER R      ERKLÄRUNG DER SEHSCHÄRFE UND DER KONTRASTSCHWELLEN FÜR KLEINE OBJEKT AUS DEM OPTISCHEN ABBILDUNGSEIGENSCHAFTEN DER AUGENMEDLEN, OPTIK, 19, 519 (1962). (CALCULATING LIGHT INTENSITY IN RETINAL IMAGE FOR HUMAN EYE FROM THE EXPERIMENTAL CONTRAST TRANSMISSION FUNCTIONS).
- 2- 23. ROULIER A      CALCULATION OF TEMPERATURE INCREASE IN THE EYE PRODUCED BY INTENSE LIGHT, BULL. MATH. BIOPHYS., 32, 403(1970)
- 2- 24. SKEEN ET AL      OCULAR EFFECTS OF NEAR INFRARED LASER RADIATION FOR SAFETY CRITERIA, TECHNOLOGY, INC., AF CONTRACT F41609-71-C-0016, PROJ 6301, TASK 05, WORK UNIT 022, JUNE 1972.
- 2- 25. SKEEN ET AL      OCULAR EFFECTS OF REPETITIVE LASER PULSES, TECHNOLOGY, INC., AF CONTRACT F41609-71-C-0018, PROJ 6301, TASK 05, FINAL REPORT WORK UNIT 024, JUNE 30, 1972.
- 2- 26. STILES ET AL      THE LUMINOUS EFFICIENCY OF RAYS ENTERING THE EYE PUPIL AT DIFFERENT POINTS, PROC. ROY. SOC., B, 112, 428-450.
- 2- 27. VAN NES ET AL      SPATIAL MODULATION TRANSFER IN THE HUMAN EYE, J. OPT. SOC. AM., 57, 401 (1967).
- 2- 28. VOS ET AL      CONTRIBUTION OF THE CORNEA TO ENTROPIC SCATTER, J. OPT. SOC. AMER., VOL. 53, PP. 869-873 (1963).



2- 29. WHITE T J

.OBSERVER DISTANCES FOR NUCLEAR EVENTS, VOL. 1,  
(MODEL FOR OBSERVER DISTANCES FOR RETINAL BURN  
CRITERIA), DEFENSE NUCLEAR AGENCY CONTRACT REPORT  
DASIAC SR-125, 1973.

2- 30. WHITE ET AL

.EVALUATION OF EYE HAZARDS FROM NUCLEAR DETONATION  
II., SAFE SEPARATION DISTANCE PREDICTIONS. USAF  
SCHOOL OF AEROSPACE MEDICINE, AEROSPACE MEDICAL  
DIV.(AFSC),BROOKS AIR FORCE BASE, TEXAS, NOV.1969.

2- 31. WHITE ET AL

THE FEASIBILITY OF ANALOG OCULAR THERMAL SIMULAT-  
ION, 1968, INTERIM REPORT 1, AF41(609)-6A-C-0023.

2- 32. WRAY J L

MODEL FOR PREDICTION OF RETINAL BURNS, DASA -  
1282, DEFENSE ATOMIC SUPPORT AGENCY, WASHINGTON  
25, D.C.,(1 FEB, 1962), (UNCLASSIFIED).

2- 33. ZARET M M

ANALYSIS OF FACTORS OF LASER RADIATION PRODUCING  
RETINAL CHANGE, FED. PROC.,24,562-64, SUPP. 14,  
(1965).

CATEGORY - 3 - THERMAL PROPERTIES

- 3- 1. BOERN ET AL .ENGINEERING RADIATION HEAT TRANSFER PROPERTIES OF HUMAN SKIN, UNIV. OF UTAH, SALT LAKE CITY, UTAH, ASME, AUG, 1971.
- 3- 2. BUEITNER, K .EFFECTS OF EXTREME HEAT AND COLD ON HUMAN SKIN - I. ANALYSIS OF TEMPERATURE CHANGES CAUSED BY DIFF. KINDS OF HEAT APPLN., JOURNAL OF APPLIED PHYSL. VOL. 3, 691-702, NO. 12, JUNE, 1951.
- 3- 3. CHAN ET AL .ALTERATIONS OF SOLUBLE RETINAL PROTEINS DUE TO THERMAL INJURY, ACTA OPHTHALMOLOGICA, SUPPL 76, 101 (1963).
- 3- 4. CHAS B T .ADVANCED HEAT TRANSFER, UNIVERSITY OF ILLINOIS PRESS, URBANA-CHICAGO-LONDON, 1969
- 3- 5. CHAU J C .ADVANCED HEAT TRANSFER IN BIOENGINEERING, CHAU, B. T. (ED.), UNIV. OF ILL. PRESS, 395 PP., 1969.
- 3- 6. CHAU J C .A SURVEY OF THERMAL CONDUCTIVITY DATA ON BIOLOGICAL MATERIALS, U. OF I. URBANA, ILL.
- 3- 7. CHAU J C .THERMAL PROBLEMS IN BIOTECHNOLOGY, ASME, 1968.
- 3- 8. CUNNINGHAM D .AN EVALUATION OF HEAT TRANSFER THROUGH THE SKIN IN THE HUMAN EXTREMITY, CH. 22, PHYSIOLOGICAL AND TEMPERATURE REGULATION, JAMES D. HARDY, CHAS. C. THOMAS PUBLISHER, SPRINGFIELD, ILL.
- 3- 9. HATFIELD H S .MEASUREMENT OF THE THERMAL CONDUCTIVITY OF ANIMAL TISSUE, PHYSIOLOGICAL SOCIETY PROCEEDINGS, P. 35P, MARCH 20-21, 1953.
- 3- 10. KIRKLAND R W .IN VIVO THERMAL CONDUCTIVITY VALUES FOR BOVINE AND CAPRINE OSSEOUS TISSUE, PROCEEDINGS, ANNUAL CONFERENCE ON ENGINEERING IN MEDICINE AND BIOLOGY, 9, BOSTON, MASS., 204 PP. (PRELIMINARY DATA), 1967.
- 3- 11. LENIZ C P .THERMAL CONDUCTIVITY OF MEATS, FATS, GELATIN GELS, AND ICE, FOOD TECHNOLOGY, 15, 5 1961, P. 243.
- 3- 12. LIPKIN ET AL .MEASUREMENT OF SOME THERMAL PROPERTIES OF HUMAN TISSUES, J. APPL. PHYSIOLOGY, 7, 212 PP., 1954.
- 3- 13. POWDER E .THE COEFFICIENT OF THERMAL CONDUCTIVITY OF BLOOD AND VARIOUS TISSUES, JOUR. GEN. PHYSIOLOGY, 45, 545 PP., 1962.
- 3- 14. POPPENDIEK H F .THERMAL AND ELECTRICAL CONDUCTIVITY OF BIOLOGICAL FLUIDS AND TISSUES, DDC AD 405.

608-768, 613-560, 624-897, 630-303, 630-712, 1964-  
66.

3- 15. ----- THERMAL PROBLEMS IN BIOTECHNOLOGY. ASME, NEW YORK,  
DECEMBER 1966

CATEGORY - 4 - OPTICAL PROPERTIES

- 4- 1. ALPERN ET AL .SPECTRAL TRANSMITTANCE OF VISIBLE LIGHT BY HUMAN EYE, J. OPT. SOC. AM. 55, 723-727, 1965.
- 4- 2. ANDERSON ET AL .LIGHT-ABSORBING AND SCATTERING PROPERTIES OF NON-HAEMOLYSED BLOOD, PHYS. MED. BIOL., 12, 2, 173-184, 1967.
- 4- 3. ANDERSON ET AL .REFLECTION AND TRANSMISSION OF LIGHT BY THIN FILMS OF NONHAEMOLYSED BLOOD, PHYS. MED. BIOL., 12, 2, 185-192, 1967.
- 4- 4. BOEITNER E A .SPECTRAL TRANSMISSION OF THE EYE, FINAL REPORT ON CONTRACT AF-41(609)-2966 FOR USAF SCHOOL OF AEROSPACE MEDICINE, 1967.
- 4- 5. BOEITNER E A .THE MEASUREMENT OF OCULAR ABSORPTION OF LASER RADIATION FOR CALCULATING PERSONNEL HAZARDS, QUARTERLY REPORT # 1, CONTRACT F41609-74-C-0008, THE AEROSPACE MEDICAL DIVISION, BROOKS AIR FORCE BASE, TEXAS, 1974.
- 4- 6. BOEITNER ET AL .TRANSMISSION OF THE OCULAR MEDIA, INVEST. OPHTHAL. 1, 776-783, 1962.
- 4- 7. BOYNTON ET AL .PHYSICAL MEASURE OF STRAY LIGHT IN EXCISED EYES, J. OPHTHAL. SOC. AMERICAN 44, 879, 1954.
- 4- 8. CAMPBELL ET AL .OPTICAL AND RETINAL FACTORS AFFECTING VISUAL RESOLUTION, J. PHYSIOL., 181, 576 (1965).
- 4- 9. CAMPBELL ET AL .OPTICAL QUALITY OF THE HUMAN EYE, J. PHYSIOL., 186, 558 (1966).
- 4- 10. CASTLEMAN ET AL .FEATURE EXTRACTION IN VISUAL EVOKED POTENTIAL ANALYSIS, TECH. REPORT NO. 72, BIO-MED. ENGR. RESEARCH LAB., (AUG 1969).
- 4- 11. CENTENO M .THE REFRACTIVE INDEX OF LIQUID WATER IN THE NEAR INFRARED SPECTRUM, J. OPT. SOC. AMER., 31, 245 (1941).
- 4- 12. CODGAN ET AL .A HISTOLOGIC COMPARISON OF THE HUMAN AND RHESUS MONKEY RETINAS AND ITS RELATION TO LASER PHOTOCOAGULATION, USAF SCHOOL OF AEROSPACE MEDICINE, AEROSPACE MEDICAL DIV. (AFSC BROOKS AIR FORCE BASE, TEXAS, SAM-TR.)
- 4- 13. COOPER ET AL .THE YELLOW COLOUR OF THE LENS OF MAN AND OTHER PRIMATES, J. PHYSIOL., 230, 411-417, 1969.
- 4- 14. COOPER ET AL .USE OF OPTICAL FIBRES FOR DETERMINATION OF IRRADIANCE AT THE RETINAL PLANE, ACTA OPHTHALMOLOGICA, SUPPLEMENTUM 76, DEPT. OF RESEARCH, N.Y. EYE AND EAR INFIRMARY, N.Y., 3, N.Y., MARCH, 1963.

- 4- 15. COREN ET AL DENSITY OF HUMAN LENS PIGMENTATION, IN VIVO MEASURES OVER EXTENDED AGE RANGE, VISION RES., 12, 343-346, 1972.
- 4- 16. CRAWFORD B H .THE SCOTOPIC VISIBILITY FUNCTION, PROC. PHYS. SOC., 62 B, 321-334, 1949.
- 4- 17. DARINALL H J A THE PHOTOBIOLOGY OF VISUAL PROCESSES IN THE EYE, (ED. H. JAYSON) ACADEMIC PRESS, NEW YORK, 1962.
- 4- 18. DARINALL ET AL SCOTOPIC LUMINOSITY CURVE AND THE ABSORPTION SPECTRUM OF VISUAL PURPLE, NATURE (LOND), 139, P. 409, 1937.
- 4- 19. DENTON E J LIGHT ABSORPTION BY THE INTACT RETINA, SYMPOSIUM FROM VISUAL PROBLEMS OF COLOR, (1), CHEMICAL PUBLISHING CO., NEW YORK, 1961.
- 4- 20. FEENEY ET AL STUDIES ON HUMAN OCULAR PIGMENT, IN - EYE STRUCTURE II, SYMP., (J. W. ROSEN, ED.), 535-548, STUTTGART, SCHAEFFER-VERLAG, 1965.
- 4- 21. GAMIRE ET AL .STIMULATED BRILLOUIN SCATTERING IN LIQUIDS, APL. PHYS. LETTERS 5, 84-86, 1964.
- 4- 22. GEERAETS ET AL .LIGHT REFLECTANCE FROM THE OCULAR FUNDUS, A.M.A. ARCH. OF OPHTH., 69, 612, 1963.
- 4- 23. GEERAETS ET AL .OCULAR SPECTRAL CHARACTERISTICS AS RELATED TO HAZARDS FROM LASERS AND OTHER LIGHT SOURCES, AM. J. OPHTHAL., 66, 15-20 (1968).
- 4- 24. GEERAETS ET AL .THE LOSS OF LIGHT ENERGY IN RETINA AND CHOROID, A.M.A. ARCH. OPHTH., 64, 606-615, 1960.
- 4- 25. GEERAETS ET AL .THE RELATIVE ABSORPTION OF THERMAL ENERGY IN RETINA AND CHOROID, INVEST. OPHTH. 1, 340 (1962).
- 4- 26. GOODMAN Z W .INTRODUCTION TO FOURIER OPTICS, MC GRAW HILL, NEW YORK, P. 60, 1968
- 4- 27. GUBISCH R W .OPTICAL PERFORMANCE OF HUMAN EYE, J. OPT. SOC. AM. 57, 407 (1967)
- 4- 28. GUNKEL ET AL CHANGES IN SCOTOPIC VISIBILITY THRESHOLDS WITH AGE ARCH. OPHTHAL. 69, 4-9, 1963.
- 4- 29. HALE G M ET AL OPTICAL CONSTANTS OF WATER IN THE 200 NM TO 200 MU WAVELENGTH REGION, APPLIED OPTICS, 12, 3, 555 (1973).
- 4- 30. JOHNSON C C .OPTICAL DIFFUSION IN BLOOD, IEEE TRANS. ON BIOMEDICAL ENGINEERING, VOL. BME-17, NO. 2, 129-133, APR. 1970.
- 4- 31. KINSEY V L .SPECTRAL TRANSMISSION OF THE EYE TO ULTRAVIOLET, ARCH. OPHTH. 39, 508 (1948)
- 4- 32. KRAMER ET AL .INFLUENCE OF OXYGEN SATURATION, ERYTHROCYTE CONCENTR

TRATION AND OPTICAL DEPTH UPON THE RED & NEAR-INFRARED LIGHT TRANSMITTANCE OF WHOLE BLOOD, AMERICAN JOURNAL OF PHYSIOLOGY, VOL. 165, 229-246, APRIL, 1951.

4- 33. KRAUSKOPF J

.LIGHT DISTRIBUTION IN HUMAN RETINAL IMAGES, J. OPT. SOC. AM., 52, 1046 (1962).

4- 34. LUDVIGH ET AL

.ABSORPTION OF THE VISIBLE LIGHT BY THE REFRACTIVE MEDIA OF THE HUMAN EYE, ARCH. OPHTH., 20, 37, 1937.

4- 35. MELLERIO J

LIGHT ABSORPTION AND SCATTER IN THE HUMAN LENS, VISION RES., 11, 141, 1971.

4- 36. MORGAN J

.INTRODUCTION TO GEOMETRICAL AND PHYSICAL OPTICS, MC GRAW HILL, NEW YORK, 1953, P.29

4- 37. NORREN D

.LITERATURE REVIEW OF HUMAN OCULAR ABSORPTION IN THE VISIBLE, INSTITUTE FOR PERCEPTION RVO-IVO, REPT IZF-1972-S.

4- 38. PITTS D G

.THE OCULAR ULTRAVIOLET ACTION SPECTRUM AND PROTECTION CRITERION, HEALTH PHYSICS, PERGAMON PRESS, VOL. 25 (DEC.), PP. 559-566, MARCH, 1973.

4- 39. PITTS D G

.TRANSMISSION OF THE VISIBLE SPECTRUM THROUGH THE OCULAR MEDIA OF THE BOVINE EYE, AM. J. OPTOM. & ARCH. AM. ACAD. OPTOM., 36, 269, 1959.

4- 40. POLYAK S L

THE RETINA, U. OF CHICAGO PRESS, CHICAGO, ILLINOIS (1941).

4- 41. PRINCE J H

SPECTRAL ABSORPTION OF THE RETINA AND CHOROID 340-1700 MU, REPORT RE PROJECT 1069, BROOKS AIR FORCE BASE, TEXAS, MARCH, 1962.

4- 42. ROBERTSON ET AL

LAMBERT ABSORPTION COEFFICIENTS OF WATER IN THE INFRARED, J. OPT. SOC. AMER., 61, 1316-1320, 1971.

4- 43. ROHLER R

.ERKLARUNG DER SEHSCHARFE UND DER KONTRASTSCHNELLEN FÜR KLEINE OBJEKTE AUS DEN OPTISCHEN ABBILDUNGSEIGENSCHAFTEN DER AUGENMEDIENT, OPTIK, 19, 519 (1962), (CALCULATING LIGHT INTENSITY IN RETINAL IMAGE FOR HUMAN EYE FROM THE EXPERIMENTAL CONTRAST TRANSMISSION FUNCTIONS).

4- 44. ROHLER ET AL

.BESTIMMUNG DER LICHTVERTEILUNG AUF DER NETZHAUT BEI ABBILDUNG EINFACHER TESTOBJEKTE, OPTIK, 23, 47 (1965), (MEASUREMENTS OF THE MODULATION TRANSMISSION FUNCTIONS OF HUMAN EYES).

4- 45. RUDDUCK K H

.THE EFFECT OF AGE UPON COLOUR VISION II., CHANGES WITH AGE IN LIGHT TRANSMISSION OF THE OCULAR MEDIA, VISION RES., 5, 47-58, 1964.

4- 46. SAID ET AL

.THE VARIATION WITH AGE OF THE SPECTRAL TRANSMISSIVITY OF THE LIVING HUMAN CRYSTALLINE LENS, GERONTOLOGIA, 3, 213, 1959.

- 4- 47. SLINNEY ET AL .EVALUATION OF OPTICAL RADIATION HAZARDS, VOL. 21, NO. 1 APPL. OPTICS (JAN 1973).
- 4- 48. SMITH ET AL .OCULAR HAZARDS OF TRANSCLERAL LASER RADIATION. AMER. JOUR. OPHTHAL., 66, P. 21, 1968.
- 4- 49. STILES ET AL .THE LUMINOUS EFFICIENCY OF RAYS ENTERING THE EYE PUPIL AT DIFFERENT POINTS, PROC. ROY. SOC., B, 112, 428-450.
- 4- 50. VAN DEN BRINK G MEASUREMENTS OF THE GEOMETRICAL ABERRATIONS OF THE EYE, VISION RES., 2, 233 (1962).
- 4- 51. WEALE R A LIGHT ABSORPTION BY THE LENS OF THE HUMAN EYE, OPT. ACTA, 1, 107-110, 1954.
- 4- 52. WEALE R A NOTES ON THE PHOTOMETRIC SIGNIFICANCE OF THE HUMAN CRYSTALLINE LENS, VISION RES., 1, 183-191, 1961.
- 4- 53. WESTHEIMER G .OPTICAL AND MOTOR FACTORS IN THE FORMATION OF THE RETINAL IMAGE, J.O.S.A., 53(1), 86-93., 1963.
- 4- 54. WESTHIMER ET AL .LIGHT DISTRIBUTION IN THE IMAGE FORMED BY THE LIVING HUMAN EYE, J. OPT. SOC. AMER., 52, 1040, (1962).
- 4- 55. WEISINGER ET AL .THE TRANSMISSION OF LIGHT THROUGH THE OCULAR MEDIA OF THE RABBIT EYE, AM. J. OPHTH., 42, 907 (1956).
- 4- 56. ZDROJNOWSKI ET AL .OPTICAL TRANSMISSION AND REFLECTION BY BLOOD, IEEE TRAN. ON BIOMEDICAL ENGINEERING, VOL. BME-17, NO. 2, 122-128, APRIL, 1970.
- 4- 57. ----- RELATIVE ABSORPTION THERMAL ENERGY IN RETINA AND CHOROID, INVEST. OPHTHAL., 1, (3), 340-347, 1962A.

CATEGORY - 5 - BLOOD EFFECTS

- 5- 1. BUTTNER R THE INFLUENCE OF BLOOD CIRCULATION ON THE TRANSPORT OF HEAT IN THE SKIN, STRAHLENTHERAPIE, 55 (1936), P. 333.
- 5- 2. CAMPBELL ET AL BLOOD VESSEL FORMATION IN THE CORNEA, BRIT. J. OPHTH. 33, 248, 1949.
- 5- 3. CHAUD J C THERMAL PROBLEMS IN BIOTECHNOLOGY, ASME, 1968.
- 5- 4. COOPER ET AL THE BLOOD FLOW IN SKIN AND MUSCLE OF THE HUMAN FOREARM, J PHYSIOL., 128, 258-267, 1955.
- 5- 5. CUNNINGHAM D AN EVALUATION OF HEAT TRANSFER THROUGH THE SKIN IN THE HUMAN EXTREMITY, CH. 22, PHYSIOLOGICAL AND TEMPERATURE REGULATION, JAMES D. HARDY, CHAS. C. THOMAS PUBLISHER, SPRINGFIELD, ILL.
- 5- 6. GEERAETS ET AL RATE OF BLOOD FLOW AND ITS EFFECT ON CHORIORETINAL BURNS, DEPT. OF OPHTHAMOLOGY AND BIOPHYSICS, THE MEDICAL COLLEGE OF VA., DEC. 1961.
- 5- 7. GORDY & DRABKIN DETERMINATION OF THE OXYGEN SATURATION OF BLOOD BY A SIMPLIFIED TECHNIQUE, APPLICABLE TO STANDARD EQUIPMENT, JOURNAL OF BIOLOGICAL CHEMISTRY, VOL. 227, 285-299, JULY-AUGUST, 1957.
- 5- 8. HAM ET AL THE RATE OF BLOOD FLOW AND ITS EFFECT ON CHORIORETINAL BURNS, ARCH. OPHTHAL., 68, 58-61, 1962B.
- 5- 9. HERIZMAN, ET AL REGIONAL DIFFERENCES IN THE BASAL AND MAXIMAL RATES OF BLOOD FLOW IN THE SKIN, J. APPL. PHYSIOL. 11 234-241, 1948.
- 5- 10. PENNES H H ANALYSIS OF TISSUE AND ARTERIAL BLOOD TEMPERATURE IN THE RESTING HUMAN FOREARM. JOURNAL OF APPLIED PHYSIOLOGY, VOL. 1, NO. 2, AUG. 1948, PP. 93-122.
- 5- 11. POPPENDIEK H F THERMAL AND ELECTRICAL CONDUCTIVITY OF BIOLOGICAL FLUIDS AND TISSUES, DDC AD NOS. 608-768, 613-560, 624-897, 630-303, 630-712, 1964-66.
- 5- 12. SENAY L C CUTANEOUS BLOOD FLOWS IN CALF, FOREARM, CHEEK, AND EAR DURING CHANGING AMBIENT TEMPERATURE. CONTRACT NO. AF.33(616)-7077, ST. LOUIS UNIV., MARCH, 1961.
- 5- 13. SHERWOOD R J 1955, TRANS. ASSOC. INDUS. MED. OFFICERS, 5, NO. 1, I. U.S. AIR FORCE, JULY 1951, STANDARD VALUES IN BLOOD, ED. E.C. ALBRITTON, TECH. REPORT NO.



6039, DAYTON, OHIO.

S- 14. SPELLS K E

.THE THERMAL CONDUCTIVITIES OF SOME BIOLOGICAL  
FLUIDS, IN MEDICINE AND BIOLOGY, S, 139-153.

S- 15. WILSON ET AL

.THE MEASUREMENT OF THE CHOROIDAL BLOOD FLOW IN THE  
RABBIT USING 85-KRYPTON, EXP. EYE RES., 16, 421-425,  
1973.

## CATEGORY - 6 -

## BURN CRITERIA

- 6- 1. ASHE ET AL .TIME-TEMPERATURE RELATIONSHIP WHICH PRODUCES HOT AIR BURNS OF HUMAN SKIN, ARMORED MED. RESEARCH LABS, FORT KNOX, KY, JULY, 1944.
- 6- 2. GOETTER, K .EFFECTS OF EXTREME HEAT AND COLD ON HUMAN SKIN - I. ANALYSIS OF TEMPERATURE CHANGES CAUSED BY DIFF. KINDS OF HEAT APPLN., JOURNAL OF APPLIED PHYSIOL. VOL. 3:691-702, NO. 12, JUNE, 1951.
- 6- 3. DAVIS I P THE HEATING OF SKIN BY RADIANT ENERGY- IN TEMPERATURE\* ITS MEASUREMENT AND CONTROL IN SCIENCE AND INDUSTRY(C.M.HERTZFELD,ED.),149-169,VOL.3,REINHOLD PUBLISHING CORPORATION,NEW YORK,1963.
- 6- 4. EHRENKRANZ ETAL HAZARDS FROM LASERS, LOS ALAMOS SCIENTIFIC LABORATORY, LADC-5764, 1962.
- 6- 5. FUGITT C H A RATE PROCESS THEORY OF THERMAL INJURY, HEADQUARTERS, ARMED FORCES SPECIAL WEAPONS PROJECT AFSWP-606.
- 6- 6. HAN ET AL .OCULAR HAZARDS FROM PICOSECOND PULSES OF Nd:YAG LASER RADIATION, SCIENCE, VOL.185, JULY 174, P.362
- 6- 7. HARDY, ET AL .SKIN TEMPERATURE AND CUTANEOUS PAIN DURING WARM WATER IMMERSION, J.H.PIERCE FNDN. LAB. AND DEPT. OF PHYSIOLOGY, YALE UNIV., NEW HAVEN, CONN., OCT., 1964.
- 6- 8. HENRIQUES F C .STUDIES OF THERMAL INJURY, ARCH. PATH. 43, 489-502 (1947).
- 6- 9. HENRIQUES ET AL .STUDIES THERMAL INJURY. I..OF CONDUCTION OF HEAT TO AND THROUGH SKIN AND THE TEMPERATURES ATTAINED THEREIN, A THEORETICAL AND EXPERIMENTAL INVESTIGATION, AMER. J. PATH., 23:531-550 (1947).
- 6- 10. KOHLIAD ET AL HAZARDS AND PHYSIOLOGICAL EFFECTS OF LASER RADIATION, THE LASER, NEW YORK ACAD. SC.,122,777, 1965.
- 6- 11. MARSHALL J THERMAL AND MECHANICAL MECHANISMS IN LASER DAMAGE TO THE RETINA,INVEST.OPHTHAL.,9:97-115,1970.
- 6- 12. MORITZ ET AL STUDIES OF THERMAL INJURY. II..THE RELATIVE IMPORTANCE OF TIME AND SURFACE TEMPERATURE IN THE CAUSATION OF CUTANEOUS BURNS, AMER. J. PATH., 23, 695-720 (1947).
- 6- 13. MORITZ ET AL .STUDIES OF THERMAL INJURY III..THE PATHOLOGY AND PATHOGENESIS OF CUTANEOUS BURNS - AN EXPERIMENTAL

STUDY, AM. JOURNAL OF PATHOLOGY, VOL. XXIII, NO. 6,  
NOV., 1947.

6- 14. MORITZ ET AL

.STUDIES OF THERMAL INJURY IV., AN EXPLORATION OF  
THE CASUALTY PRODUCING ATTRIBUTES OF CONFLAGRA-  
TIONS; LOCAL AND SYSTEMIC EFFECTS OF GENERAL CUTA-  
NEOUS EXPOSURE TO EXCESSIVE CIRCUMAMBIENT (AIR)  
AND CIRCUMADIENT HEAT OF VARYING DURATION AND  
INTENSITY, ARCH. OF PATHOLOGY, 43, 466-488, 1947.

6- 15. PEALOCK G R

SURFACE TEMPERATURE AS A PARAMETER IN ESTIMATING  
LASER INJURY THRESHOLDS, US ARMY MED. RES. LAB. REPORT  
733, FORT KNOX, KENTUCKY, 1967.

6- 16. PITTS D G

.THE OCULAR ULTRAVIOLET ACTION SPECTRUM AND  
PROTECTION CRITERION, HEALTH PHYSICS, PERGAMON  
PRESS, VOL. 25 (DEC.), PP. 559-566, MARCH, 1973.

6- 17. STOLL ET AL

.RELATIONSHIP BETWEEN PAIN AND TISSUE DAMAGE DUE  
TO THERMAL RADIATION, JOUR. APPL. PHYSIOLOGY, 14,  
P. 373, 1959.

6- 18. TAKATA ET AL

.INVESTIGATION OF MEANS AND MATERIALS TO COMBAT  
THERMAL RADIATION FLASH BURNS, ARMOUR RESEARCH PROJ.  
PROJECT D046, JAN., 1957.

6- 19. VOS J J

.A THEORY OF RETINAL BURN, DOLL. MATH. BIOPHYSICS,  
24, 115-128, 1962.

6- 20. VOS J J

.HEAT DAMAGE TO THE RETINA BY LASERS AND PHOTO-  
COAGULATORS, INST. OF PERCEPTION RVO-IND (SOESTER-  
BERG), 1964., OPHTHALMOLOGICA, 151, 652-654 (1966).

6- 21. WHITE T J

.OBSERVER DISTANCES FOR NUCLEAR EVENTS, VOL. 1,  
(MODEL FOR OBSERVER DISTANCES FOR RETINAL BURN  
CRITERIA), DEFENSE NUCLEAR AGENCY CONTRACT REPORT  
DASIAC SR-125, 1973.

6- 22. -----

THE PRODUCTION OF RADIATION BURNS ON THE RETINA  
AT THE THRESHOLD LEVEL OF DAMAGE: A LITERATURE  
SURVEY AND TENTATIVE MATHEMATICAL THEORY, R.A.P.  
INSTITUTE OF AVIATION MEDICINE, REPORT NO. FPRC/  
1222, (1964).

CATEGORY - 7 - EXPERIMENTAL TEMPERATURE DATA

- 7- 1. BUETTNER, K .EFFECTS OF EXTREME HEAT AND COLD ON HUMAN SKIN -  
I. ANALYSIS OF TEMPERATURE CHANGES CAUSED BY DIFF.  
KINDS OF HEAT APPLN., JOURNAL OF APPLIED PHYSL.  
VOL. 3, 691-702, NO. 12, JUNE, 1951.
- 7- 2. CAIN AND WELCH .MEASURED AND PREDICTED LASER-INDUCED TEMPERATURE  
RISES IN THE RABBIT FUNDUS, INVEST. OPHTHAL., VOL.  
13, NO. 1, P. 60-70, JANUARY, 1974.
- 7- 3. CAMPBELL ET AL .INTRAOCULAR TEMPERATURE CHANGES PRODUCED BY LASER  
COAGULATION, ACTA OPHTHAL., SUPPL., 76, 22-31.
- 7- 4. CROWDER J .MEASUREMENTS OF THE VITREOUS TEMPERATURE DURING  
PHOTOCOAGULATION IN THE RABBIT EYE, ACTA OPHTHAL.,  
SUPPL., 76, 32-40.
- 7- 5. DAVIS I P .IN VIVO TEMPERATURE MEASUREMENTS, ACTA  
OPHTHALMOLOGICA, SUPPL. 76, 41-50 (1963).
- 7- 6. DERKSEN ET AL TEMPERATURE\*ITS MEASUREMENT AND CONTROL IN SCIENCE  
AND INDUSTRY, J.D. HARDY, ED. (REINHOLD PUBLISHING  
CORPORATION, NEW YORK, 1963), VOL. 3, P. 171 FF.,  
PP. 171-175.
- 7- 7. FREEMAN AND FAT .ENVIRONMENTAL INFLUENCE ON OCULAR TEMPERATURE,  
INVEST. OPHTHAL., VOL. 12, (8), AUGUST 1973, P. 596-602
- 7- 8. KONTIAD ET AL .TEMPERATURE RISE AND PHOTOCOAGULATION OF RABBIT  
RETINAS EXPOSED TO THE CR LASER, AMER. J. OPHTHAL.  
62, 524-528 (1966).
- 7- 9. LUMHOLT S INVESTIGATIONS ON THE TEMPERATURE DISTRIBUTION IN  
THE SKIN DURING IRRADIATION WITH VISIBLE LIGHT,  
STRAHLENTHERAPIE, 35, 324 PP., 1930.
- 7- 10. NAJAC H ET AL .DIRECT THERMOCOUPLE MEASUREMENTS OF TEMPERATURE  
RISE AND HEAT CONDUCTION IN THE RABBIT RETINA,  
INVEST. OPHTHAL., 2, 32-36., 1963.
- 7- 11. NOYORI ET AL .OCULAR THERMAL EFFECTS PRODUCED BY PHOTOCOAGU-  
LATION, ARCH. OPHTHAL., 70, 817-822., 1963.
- 7- 12. SCHWARTZ ET AL .TEMPERATURE GRADIENTS IN THE RABBIT EYE, INVEST.  
OPHTHAL., VOL. 1, (1), AUGUST 1962, P. 513-521.
- 7- 13. WHITE ET AL CHORIORETINAL TEMPERATURE INCREASES FROM SOLAR  
OBSERVATION, BULL. MATH. BIOPHYS., 33, 1 (1970).

## CATEGORY - 8 -

## EXPERIMENTAL BURN INFORMATION

- 8- 1. ALLEN ET AL ECLIPSE BURNS IN HUMANS AND LABORATORY MEASUREMENT IN RABBITS, SAM-TR-66-45 (MAY) 1966.
- 8- 2. ALLEN ET AL PRODUCTION OF CHORIORETINAL BURNS BY NUCLEAR DETONATIONS AND TESTS OF PROTECTIVE DEVICES AND PHOTOGRAPHIC MATERIALS (U), POR 2014(WI-2014), OPERATION DOMINIC, PROJECT 4.1, MARCH 1965, (SECRET-FRD)
- 8- 3. ALLEN ET AL RESEARCH ON OCULAR EFFECTS PRODUCED BY THERMAL RADIATION, FINAL REPORT ON CONTRACT AF-41(609)-3099 FOR USAF SCHOOL OF AEROSPACE MEDICINE, 1967.
- 8- 4. ALEXANDER ET AL RESEARCH ON OCULAR EFFECTS PRODUCED BY THERMAL RADIATION, FINAL REPORT ON CONTRACT AF-41(609)-2906 FOR USAF SCHOOL OF AEROSPACE MEDICINE, 1966.
- 8- 5. BEATRICE ET AL Q-SWITCHED NEODYMIUM LASER RETINAL DAMAGE IN RHESUS MONKEY, MEMO REPORT M73-9-1, FRANKFORD ARSENAL, PHILADELPHIA, PA., MARCH, 1973.
- 8- 6. BEATRICE ET AL Q-SWITCHED RUBY RETINAL DAMAGE IN RHESUS MONKEY, REPORT R-2051, FRANKFORD ARSENAL, PHILADELPHIA, PA., SEPTEMBER, 1972.
- 8- 7. BEATRICE ET AL RETINAL DAMAGE BY Q-SWITCHED RUBY LASER FOR LARGE RETINAL SPOT DIAMETERS, MEMO REPORT M70-22-1, FRANKFORD ARSENAL, PHILADELPHIA, PA., JUNE, 1970.
- 8- 8. BEATRICE ET AL RETINAL DAMAGE THRESHOLDS COMPARISON OF 3 MM AND 8 MM DIAMETER Q-SWITCHED RUBY LASER, REPORT R-1956, FRANKFORD ARSENAL, PHILADELPHIA, PA., APRIL, 1970.
- 8- 9. BERGQVIST ET AL LASER IRRADIANCE LEVELS FOR RETINAL LESIONS, ACTA OPHTHAL, 43, 331-349, 1965.
- 8- 10. BERGQVIST ET AL RETINAL LESIONS PRODUCED BY Q-SWITCHED LASERS, ACTA OPHTHAL, 44, 853-863, 1966.
- 8- 11. BLACKWELL H R CONTRAST THRESHOLDS OF THE HUMAN EYE, J. OPT. SOC. AM. 36 (1946) 624-643.
- 8- 12. HURLAND ET AL THRESHOLD LEVELS FOR DAMAGE OF THE CORNEA FOLLOWING IRRADIATION BY A CONTINUOUS WAVE CARBON DIOXIDE (10.6 MU) LASER, NATURE (LOND.), 234, 151-152, 1971.
- 8- 13. BREDEMAYER ET AL RADIATION THRESHOLDS FOR CHORIORETINAL BURNS, AD 416 652 (MAT. TECH. INFORMATION SERVICE, SPRINGFIELD, VA. 22151), 1963.
- 8- 14. BRESNICK G OCULAR LASER THRESHOLDS FROM AN ARGON LASER.

DEPARTMENT OF THE ARMY, FRANKFORD ARSENAL,  
PHILADELPHIA, PA., PERSONAL COMMUNICATION, 1970.

- 8- 15. BROWN J L. EXPERIMENTAL INVESTIGATION OF FLASHBLINDNESS,  
HUMAN FACTORS, 503-516, OCTOBER 1964.
- 8- 16. BROWNELL ET AL. CO2 LASER INDUCED SKIN LESIONS, US ARMY MED. RES. LAB  
REPORT 769, FORT KNOX, KENTUCKY, 1968.
- 8- 17. BYRNES ET AL. CHORIORETINAL LESIONS DUE TO THERMAL RADIATION  
FROM THE ATOMIC BOMB, A. M. A. ARCH. OPHTH.,  
55, 904-914.
- 8- 18. CAMPBELL ET AL. OCULAR EFFECTS PRODUCED BY EXPERIMENTAL LASERS,  
AMER. JOUR. OPHTH., 66, 459 PP., 1968.
- 8- 19. CAMPBELL ET AL. THE THRESHOLD OF THE RETINA TO DAMAGE BY LASER  
ENERGY, ARCH. OPHTH., (CHICAGO) 76, 437-442 (1966).
- 8- 20. CHISUM G T. INTRAOCULAR EFFECTS ON FLASHBLINDNESS, AEROSPACE  
MEDICINE, 39, 850-858, 1968.
- 8- 21. CHISUM ET AL. FLASHBLINDNESS\* THE EFFECTS OF PREFLASH  
ADAPTATION AND PUPIL SIZE, AEROSPACE MEDICINE,  
38, 395-399, 1967.
- 8- 22. COOGAN ET AL. A HISTOLOGIC COMPARISON OF THE HUMAN AND RHESUS  
MONKEY RETINAS AND ITS RELATION TO LASER  
PHOTOCOAGULATION, USAF SCHOOL OF AEROSPACE  
MEDICINE, AEROSPACE MEDICAL DIV. (AFSC BROOKS AIR  
FORCE BASE, TEXAS, SAM-TR.)
- 8- 23. COOGAN ET AL. AN IMPROVED HISTOLOGIC TECHNIC FOR STUDYING  
PRIMATE RETINA, SAM-TR-69-53, BROOKS AIR FORCE  
BASE, TEX, USAF SCHOOL OF AEROSPACE MEDICINE,  
1969.
- 8- 24. COOGAN ET AL. HISTOLOGIC AND SPECTROPHOTOMETRIC COMPARISONS OF  
THE HUMAN AND RHESUS MONKEY RETINA AND PIGMENTED  
OCULAR FUNDUS, FINAL REPORT, CONTRACT F41609-71-C-  
0006, RUSH-PRESBYTERIAN ST. LUKES MEDICAL CENTER,  
CHICAGO, ILLINOIS, JANUARY, 1974.
- 8- 25. DEMOTT ET AL. AN EXPERIMENTAL STUDY OF RETINAL BURNS, OR-548,  
ROCHESTER, N.Y. UNIV., ATOM. ENERGY, PROJECT CONTR.  
W 7401, 49, 1959A, MAY 11.
- 8- 26. DEMOTT ET AL. IRRADIANCE THRESHOLDS FOR CHORIORETINAL LESIONS,  
A. M. A. ARCH. OPHTH., 62, 143/653, 1959 B.
- 8- 27. DERKSEN ET AL. BURNS TO SKIN BY MILLISECOND LIGHT PULSES, DASA RE.  
1532, US NAVAL APPL. SCI. LAB., BROOKLYN, NEW YORK, 1964
- 8- 28. DUNSKY ET AL. CORNEAL DAMAGE THRESHOLDS FOR HYDROGEN FLUORIDE &  
DEUTERIUM FLUORIDE CHEMICAL LASER, SAMTR-73-51, USAF  
SCHOOL OF AEROSPACE MEDICINE, BROOKS AIR FORCE BASE  
TEXAS, DECEMBER, 1973.

- 8- 29. DUNSKY ET AL .DETERMINATION OF REVISED AIR FORCE PERMISSIBLE EXPOSURE LEVELS FOR LASER RADIATION, SAM-TR-72-11, USAF SCHOOL OF AEROSPACE MEDICINE, BROOKS AIR FORCE BASE, TEXAS, 1972.
- 8- 30. DUPONT ET AL EFFECTS OF LASER RADIATION ON THE MAMMALIAN EYE, TRANS N.Y. ACAD. SCI., SERIES II, 28, 517-526.
- 8- 31. EBBERS R W RETINAL EFFECTS OF MULTIPLE PULSE GALLIUM ARSENIDE LASER, SAMTR-72-25, USAF SCHOOL OF AEROSPACE MEDICINE, BROOKS AIR FORCE BASE, TEXAS, NOVEMBER, 1972.
- 8- 32. EBBERS ET AL RETINAL DAMAGE THRESHOLDS FOR MULTIPLE PULSE LASER AEROSPACE MEDICINE, 44, 3, 317, MARCH, 1973.
- 8- 33. FINE ET AL .CORNEAL INJURY THRESHOLD TO CARBON DIOXIDE LASER IRRADIATION, AMER. J. OPHTHAL., 66, 1, 1-15, JULY, 1968.
- 8- 34. FINE ET AL PRELIMINARY OBSERVATIONS OF OCULAR EFFECTS OF HIGH POWER, CONTINUOUS CO2 LASER IRRADIATION, AMER. J. OPHTHAL., 64, 209-222, 1967.
- 8- 35. FRIEDMAN ET AL .THE RETINAL PIGMENT EPITHELIUM-IV., THE DAMAGING EFFECTS OF RADIANT ENERGY, ARCH. OPHTHAL., 80, 265-279.
- 8- 36. FRISCH ET AL COMPARATIVE STUDY OF ARGON AND RUBY RETINAL DAMAGE THRESHOLDS, MEMO REPORT 171-9-1, FRANKFORD ARSENAL, PHILADELPHIA, PA., APRIL, 1971.
- 8- 37. FRISCH ET AL RETINAL INJURY THRESHOLD FROM ARGON LASER RADIATION, MEMORANDUM REPORT M70-21-1, JOINT LASER SAFETY TEAM, FRANKFORD ARSENAL, PHILADELPHIA, PA., JUNE, 1970.
- 8- 38. GEERAETS W J .RETINAL INJURY BY RUBY AND NEODYMIUM LASER, ACTA OPHTHALMOLOGICA VOL. 45 1967.
- 8- 39. GEERAETS ET AL EXPOSURE DATA BASED ON MINIMAL LESIONS AFTER IRRADIATION OF DIFFERENT SITES OF THE HUMAN RETINA TO A WHITE LIGHT SOURCE, FINAL REPORT, DA 49 146 XZ 416, MEDICAL COLLEGE OF VIRGINIA (1970).
- 8- 40. GEERAETS ET AL LASER VERSUS LIGHT COAGULATOR: A FUNDUSCOPIC AND HISTOLOGIC STUDY OF CHORIORETINAL INJURY AS A FUNCTION OF EXPOSURE TIME. FED. PRDC. SUPPL. 14, 24, (1), III S-48-S-61.
- 8- 41. GEERAETS ET AL .RETINAL DAMAGE FROM HIGH INTENSITY LIGHT, ACTA OPHTHALMOLOGICA, SUPPLEMENTUM 76, 109-112.
- 8- 42. GIBBONS W D .RETINAL BURN THRESHOLD FOR EXPOSURE TO A FREQUENCY DOUBLED NEODYMIUM LASER, SAMIR-73-45, USAF SCHOOL OF AEROSPACE MEDICINE, BROOKS AIR FORCE BASE, TEXAS, NOV 1973.
- 8- 43. GIBBONS ET AL .OCULAR DAMAGE THRESHOLDS FOR REPETITIVE PULSED

ARGON LASER EXPOSURE, SAMR-74-1, USAF SCHOOL OF AEROSPACE MEDICINE, BROOKS AIR FORCE BASE, TEXAS, FEB 1974.

- 8- 44. GIBSON G L M      RETINAL DAMAGE FROM REPEATED SUBTHRESHOLD EXPOSURE USING RUBY LASER PHOTOCOAGULATOR, SAMR-70-59, USAF SCHOOL OF AEROSPACE MEDICINE, BROOKS AIR FORCE BASE TEXAS, OCTOBER, 1970.
- 8- 45. GOLDMAN ET AL      THE EFFECT OF REPEATED EXPOSURES TO LASER BEAMS, ACTA DERMATOVENER. (STOCKHOLM) 44, 264 1964.
- 8- 46. GORN ET AL      .RETINAL DAMAGE BY VISIBLE LIGHT, ARCH OPHTHAL., 77, 115-118 (JAN) 1967.
- 8- 47. GRAHAM ET AL      .RETINAL LESION AND VISUAL ACUITY IN THE RHESUS MONKEY, TECHNICAL REPORT, ARL 1R-69-3, 6571ST ARL, HULLMAN AFB (1969).
- 8- 48. GUERRY ET AL      .EXPERIMENTAL PRODUCTION OF FLASH BURNS IN THE RABBIT RETINA, TRANS AMER OPHTHAL SOC., 54, 259-273, 1956.
- 8- 49. HAM ET AL      .EFFECTS OF LASER RADIATION ON THE HAMALIAN EYE, DIVISION OF BIOPHYSICS, MED. COLLEGE VA.
- 8- 50. HAM ET AL      .ELECTRONICALLY PULSED LIGHT SOURCE FOR THE PRODUCTION OF RETINAL BURNS, AM. J. MED. ELECTRONICS, 2, 308-315 (1963).
- 8- 51. HAM ET AL      FLASH BURNS IN THE RABBIT AS A MEANS OF EVALUATING THE RETINAL HAZARD FROM NUCLEAR WEAPONS, AM. J. OPHTH. 46, 700 (1958).
- 8- 52. HAM ET AL      .FLASHBURNS IN THE RABBIT RETINA, AM. J. OPHTH., 46, 700-723, 1958.
- 8- 53. HAM ET AL      .OCULAR EFFECTS OF LASER RADIATION, PART 1, ACTA OPHTHALMOLOGICA VOL. 43, 1965.
- 8- 54. HAM ET AL      RETINAL BURN THRESHOLD FOR THE HELIUM-NEON LASER IN THE RHESUS MONKEY, ARCH. OPHTHALMOL., 84, 797-809 1970.
- 8- 55. HENSTREET H W      OCULAR HAZARDS OF PICOSECOND AND REPETITIVE PULSE LASERS, QUARTERLY REPORT NO. 1, CONTRACT F41609-73-C-0016, TECHNOLOGY, INC., SAN ANTONIO, TEXAS, MAY, 1973.
- 8- 56. HENSTREET H W      OCULAR HAZARDS OF PICOSECOND AND REPETITIVE PULSE LASERS, QUARTERLY REPORT NO. 2, CONTRACT F41609-73-C-0016, TECHNOLOGY, INC., SAN ANTONIO, TEXAS, AUG, 1973.
- 8- 57. JACOBSON ET AL      .THE EFFECTS OF THERMAL ENERGY ON ANTERIOR OCULAR TISSUES, AD 412 730 (NATL. TECH. INFORMATION SERVICE, SPRINGFIELD, VA. 22151), 1963, AMRL-TR-63-53
- 8- 58. JONES ET AL      .RUBY LASER EFFECTS ON THE MONKEY EYE, INVEST.



OPHTHAL., 5,474, 1966.

8- 59. KAPANY ET AL

.RETINAL PHOTOCOAGULATION BY LASERS, NATURE, 199, 146, 1963.

8- 60. KIMIHAKU ET AL

OCULAR THERMAL EFFECTS PRODUCED BY PHOTOCOAGULATION, LABORATORY SCIENCES, SOUTHBRIIDGE, MASS.

8- 61. KISSEN ET AL

.DEVELOPMENT OF CHORIORETINAL LESIONS PRODUCED BY PHOTOCOAGULATION, AMER J OPTHAL 52,487, 1961.

8- 62. KLEIN ET AL

THRESHOLD STUDIES AND REVERSIBLE DEPIGMENTATION IN RODENT SKIN, NEREM RECORD, 1965, VOL. 7,P. 108.

8- 63. KOHTIAO ET AL

.THRESHOLD LESIONS IN RABBIT RETINAS EXPOSED TO PULSED RUBY LASER RADIATION, OPTHALMOL. 62, 684 (1966).

8- 64. KUHN J G ET AL

.LASER INJURY IN SKIN, LAP. INVEST., 17,1-13 (1967).

8- 65. LANDERS ET AL

DETERMINATION OF VISIBLE THRESHOLD OF DAMAGE IN RETINA OF RHESUS MONKEY BY Q-SWITCHED RUBY LASER. MEMO REP. N69-26-1, FRANKFORD ARSENAL, PHILADELPHIA, PA., OCTOBER, 1969.

8- 66. LAPPIN P W

.OCULAR DAMAGE THRESHOLDS FOR THE HELIUM-NEON RED-NE LASER, ARCH. ENVIRON. HEALTH, 20,177-183, 1970.

8- 67. LAPPIN ET AL

.HISTOLOGIC EVALUATION OF OPHTHALMOSCOPICALLY SUB-VISIBLE RETINAL LASER EXPOSURES, INVEST. OPTHAL. 9,537-543 (1970).

8- 68. LAPPIN ET AL

.RELATIVE SENSITIVITY OF VARIOUS AREAS OF THE RETINA TO LASER RADIATION, ARCH. OPTHAL., 84,350-354 (1970).

8- 69. LEIDOWITZ ET AL

.CORNEAL INJURY PRODUCED BY CARBON DIOXIDE LASER RADIATION, ARCH. OPTHALMOL., 81,713-721, 1969.

8- 70. LEIDOWITZ ET AL

CORNEAL DAMAGE PRODUCED BY CO2 LASER RADIATION, US ARMY MED. RES. LAB. REPORT 787, FORT KNOX, KY., 1968.

8- 71. LEIDOWITZ ET AL

THE RETINAL PIGMENT EPITHELIUM RADIATION THRESHOLD ASSOCIATED WITH THE Q-SWITCHED RUBY LASER, ARCH. OPTHAL., 82,332, SEPTEMBER, 1969.

8- 72. LIESPERANCE ET

THRESHOLD OF THE RETINA TO DAMAGE BY ARGON LASER RADIATION, ARCH. OPTHALMOL., 81,583-588, 1969.

8- 73. MACDONALD ET AL

ERYTHROPSIA AND LIGHT TOXICITY THRESHOLDS, PRESENTED AT THE MEETING OF THE ASSOCIATION FOR RESEARCH IN VISION AND OPHTHALMOLOGY, SARASOTA, FLORIDA (1971).

8- 74. MAINSTER ET AL

.SPECTRAL DEPENDENCE OF RETINAL DAMAGE PRODUCED BY INTENSE LIGHT SOURCES, JOSE 60, 6,848 (JUN 1970).

- 8- 75. MARSHALL ET AL HISTOLOGY OF RETINAL LESIONS PRODUCED WITH Q-SWITCHED LASERS, EXP. EYE RES., 7, 225-230, 1968.
- 8- 76. MILLER ET AL .EVALUATION OF EYE HAZARDS FROM NUCLEAR DETONATIONS, 1. RETINAL BURN--ETC. (U) TECH. INC. SAN ANTONIO, TEXAS, LIFE SCIENCES DIV., NOV 1969.
- 8- 77. MILLER ET AL RETINAL BURNS AND FLASHBLINDNESS, FINAL REPORT, CONTRACT F41609-68-C0023, VOL. 1, NOV 69, TECHNOLOGY INC., DDC AD 697425.
- 8- 78. MILLER ET AL RETINAL BURN THRESHOLDS IN PRIMATES, INTERIM REPORT ON CONTRACT AF 41(609)-68-C-0023 FOR USAF SCHOOL OF AEROSPACE MEDICINE, 1968.
- 8- 79. NOELL ET AL RETINAL DAMAGE BY LIGHT IN RATS, INVEST. OPHTHALMOL. 5(5), 450-472, 1966.
- 8- 80. NOYORI ET AL .THE CHARACTERISTICS OF EXPERIMENTAL LASER COAGULATION OF THE RETINA, ARCH. OPHTH., 72, 254, 1964.
- 8- 81. PEABODY ET AL THRESHOLD DAMAGE FROM CO2 LASERS, ARCH. OPHTHALMOL., 82, 105-107, 1969.
- 8- 82. ROSE H W RESEARCH STUDY OF THE PRODUCTION OF RETINAL BURNS, TECH. REP. DASA-1279, DEFENSE ATOMIC SUPPORT AGENCY, WASHINGTON, D.C. 1961.
- 8- 83. ROSE ET AL .HUMAN CHORIORETINAL BURNS FROM ATOMIC FIREBALLS, ARCH. OPHTH., 55, 205-210, 1956.
- 8- 84. ROULIER A PHOTOCOAGULATION THROUGH THE GOLDMANN CONTACT GLASS. II, AN APPARATUS USING A QUASI-CONTINUOUS LASER SOURCE, ARCH. OPHTHAL., 79, 674-683, 1968.
- 8- 85. ROUNDS D E .EFFECTS OF LASER RADIATION ON CELL CULTURES, FED. PROC., 24, 8116-121, SUPP. 14 (1965).
- 8- 86. ROWE ET AL .INVESTIGATIONS OF OCULAR HAZARD FROM LASERS IN HUMAN SUBJECTS, DEPT. OF OPHTHALMOLOGY AND LASER LABORATORIES, UNIV. OF CINCINNATI, CIN., OHIO, MAY, 1972.
- 8- 87. SANDERS V E RESEARCH ON THE EYE EFFECTS OF LASER RADIATION, QUARTERLY REPORT NO. 2, CONTRACT F41609-73-C-0017, TECHNOLOGY, INC., SAN ANTONIO, TEXAS, AUGUST, 1973.
- 8- 88. SANIUS ET AL CHORIORETINAL LESIONS PRODUCED BY LASER ON MONKEY AND RABBITS, AMER. J. OPHTHAL., 61, 230-240 (1966).
- 8- 89. SHELIN ET AL EFFECTS OF HIGH INTENSITY RADIANT ENERGY ON SKIN. I, TYPE OF INJURY AND ITS RELATION TO ENERGY DELIVERY RATE, ARCH. PATH. (CHICAGO), 55, 265-279 (1957).
- 8- 90. STUCK B E CORNEAL DAMAGE THRESHOLDS FOR CARBON DIOXIDE LASER IRRADIATION, PRESENTED AT THE THIRD MEETING OF TICP

J-10 WORKING GROUP A (LASER HAZARDS), OTTAWA, CANADA,  
19-23 JUNE, 1972.

- 8- 91. TOWNES ET AL XENON PHOTOCOAGULATION OF THE PAPILLUMACULAR  
BUNDLE, AN EXPERIMENTAL STUDY, ARCH. OPHTHAL., 87,  
679-683 (1972).
- 8- 92. VASSILIADISE TAL OCULAR LASER THRESHOLD INVESTIGATIONS, FINAL REPORT  
ON CONTRACT F41609-70-C-0001, STANFORD RESEARCH IN-  
STITUTE, MENLO PARK, CALIFORNIA, JANUARY 1971.
- 8- 93. VASSILIADISE TAL RESEARCH ON OCULAR LASER THRESHOLDS, CONTRACT NO.  
F41609-68-C-0041, STANFORD RESEARCH INSTITUTE, MENLO  
PARK, CALIFORNIA, AUGUST, 1969.
- 8- 94. WATZKE ET AL. RUBY LASER PHOTOCOAGULATION OF THE PAPILLUMACULAR  
BUNDLE, AN EXPERIMENTAL STUDY, ARCH. OPHTHAL. 87,  
684-687 (1972).
- 8- 95. WILLIAMS ET AL. EXAMINATION OF THE CORNEA FOLLOWING EXPOSURE TO  
MICROWAVE RADIATION, AEROSPACE MEDICINE, APRIL, 1974.
- 8- 96. WOLBARSH ET AL. RETINA\*PATHOLOGY OF NEODYMIUM AND RUBY LASER BURNS  
SCIENCE, 150, 1453-1454, 1965.
- 8- 97. ZARET M M OCULAR EXPOSURE TO Q-SWITCHED LASER IRRADIATION,  
AFAL-TR-65-279, APR. 1966.
- 8- 98. ZARET M M OPHTHALMOLOGICAL EFFECTS OF INTENSE LIGHT BEAMS,  
AL-TR-64-217, WRIGHT-PATTERSON AIR FORCE BASE,  
OHIO, AVIONICS LABORATORY, 1964.
- 8- 99. ZARET ET AL LASER PHOTOCOAGULATION OF THE EYE, A.M.A. ARCH.  
OPHTH., 69, 97 (JAN. 1963).
- 8-100. ZARET ET AL OCULAR LESION, PRODUCED BY AN OPTICAL MASER  
(LASER), SCIENCE 134, 1525-1526, (10 NOV. 1961).
- 8-101. ZWENG ET AL. EXPERIMENTAL Q-SWITCHED RUBY LASER RETINAL DAMAGE,  
ARCH. OPHTHALMOL., 78, 634 (1967).
- 8-102. ZWENG ET AL HISTOLOGY OF HUMAN OCULAR COAGULATION, ARCH.  
OPHTHAL., 76, 11-15, 1966.
- 8-103. ----- HEAT DAMAGE TO THE RETINA BY LASERS AND  
PHOTOCOAGULATORS, 1966, OPHTHALMOLOGICA, 151,  
652-654.
- 8-104. ----- THE PRODUCTION OF RADIATION BURNS ON THE RETINA  
AT THE THRESHOLD LEVEL OF DAMAGE\* A LITERATURE  
SURVEY AND TENTATIVE MATHEMATICAL THEORY, R.A.P.  
INSTITUTE OF AVIATION MEDICINE, REPORT NO. FPRC/  
1222. (1964).

CATEGORY - 9 - MELANIN GRANULE EFFECTS

- 9- 1. COOGAN ET AL .A HISTOLOGIC COMPARISON OF THE HUMAN AND RHESUS MONKEY RETINAS AND ITS RELATION TO LASER PHOTOCOAGULATION, USAF SCHOOL OF AEROSPACE MEDICINE, AEROSPACE MEDICAL DIV. (AFSC BROOKS AIR FORCE BASE, TEXAS, SAN-TR.)
- 9- 2. DARTNALL H J A VISUAL PIGMENTS IN PHOTORECEPTORS - IN THE EYE (H. DAVSON, ED.), VOL. 2, 512-513, ACADEMIC PRESS, NEW YORK AND LONDON, 1962.
- 9- 3. DROCHMANS P MELANIN GRANULES\* THEIR FINE STRUCTURE, FORMATION AND DEGRADATION IN NORMAL AND PATHOLOGICAL TISSUES INT. REV. EXP. PATH., 2, 357-422, 1963.
- 9- 4. DROCHMANS P THE FINE STRUCTURE OF MELANIN GRANULES, IN - STRUCTURE AND CONTROL OF THE MELANOCYTE (G. DELLA PORTA & O. MUHLENBROCK, EDS.), SIXTH INTERNATIONAL PIGMENT CELL CONFERENCE, 90-95, BERLIN-HEIDELBERG-NEW YORK, SPRINGER-VERLAG, 1966.
- 9- 5. DROCHMANS P ULTRASTRUCTURE OF MELANIN GRANULES, IN - ADVANCES IN BIOLOGY OF SKIN, VOL. 8, THE PIGMENTARY SYSTEM (P. MONTAGNA & F. HU, EDS.), 169-177, OXFORD, PERGAMON PRESS, 1967.
- 9- 6. FEENEY ET AL STUDIES ON HUMAN OCULAR PIGMENT, IN - EYE STRUCTURE 11, SYMP. (J.W. ROSEN, ED.), 535-548, STUTTGART, SCHAEFFHAUER-VERLAG, 1965.
- 9- 7. FRANCOIS ET AL ELECTRON MICROSCOPIC OBSERVATIONS ON CHOROID, PIGMENT EPITHELIUM AND PECTEN OF THE DEVELOPING CHICK IN RELATION TO MELANIN SYNTHESIS, OPHTHALMOLOGICA (BASEL), 146, 415-431, 1963.
- 9- 8. HANSEN ET AL .MELANIN GRANULE MODELS FOR PULSED LASER INDUCED RETINAL INJURY, VOL. 7, NO. 1, APPLIED OPTICS 155.
- 9- 9. HUNTER ET AL MELANOGENESIS\* ULTRASTRUCTURAL HISTOCHEMICAL OBSERVATIONS ON ULTRAVIOLET IRRADIATED HUMAN MELANOCYTE INVEST. DERM., 51, 213-221, 1970.
- 9- 10. MOYER F H DEVELOPMENT, STRUCTURE AND FUNCTION OF THE RETINAL PIGMENT EPITHELIUM - IN THE RETINA (STRAATSMAN ET AL, EDS.), 1-30, REGENTS OF UC, LOS ANGELES, CAL., 1969.
- 9- 11. MOYER F H ELECTRON MICROSCOPIC OBSERVATIONS ON THE ORIGIN, DEVELOPMENT & GENETIC CONTROL OF MELANIN GRANULES IN THE MOUSE EYE - IN STRUCTURE OF THE EYE (G.R. SMI-LSER, ED.), 469-486, ACADEMIC PRESS, NEW YORK, 1961.
- 9- 12. PORTER ET AL STUDIES ON THE ENDOPLASMIC RETICULUM\* V. ITS FORM

AND DIFFERENTIATION IN PIGMENT EPITHELIAL CELLS  
OF THE FROG RETINA, J. BIOPHYS. BIOCHEM. CYTOL.,  
8,181-205, 1960.

9- 13. SEBROUYS M

STUDY OF THE ULTRASTRUCTURE OF THE RETINAL EPITHE-  
LIUM BY MEANS OF THE ELECTRONIC MICROSCOPE, AMER. J.  
OPHTHAL., 34, 989-992, 1951.

9- 14. SEIJI ET AL

CHEMICAL COMPOSITION & TERMINOLOGY OF SPECIALIZED  
ORGANELLES (MELANOSOMES AND MELANIN GRANULES) IN  
MAMMALIAN MELANOCYTES, NATURE (LOND), 1082-1084, 1963.

9- 15. SEIJI ET AL

SUBCELLULAR LOCALIZATION OF MELANIN BIOSYNTHESIS,  
ANN. N. Y. ACAD. SCI., 100, 497-533, 1963.

9- 16. SPITZNAS M

MORPHOGENESIS & NATURE OF THE PIGMENT GRANULES IN  
THE ADULT HUMAN RETINAL PIGMENT EPITHELIUM, Z. ZELL-  
LEBENSFORSCH., 122, 378-388, SPRINGER-VERLAG, 1971.

9- 17. TAKEUCHI H

MORPHOLOGICAL STUDIES OF THE PIGMENT GRANULES OF  
THE RETINA BY THE ELECTRON MICROSCOPE, JAP. J. OPH-  
THAL., 1, 100-106, 1957.

9- 18. TANIGUCHI Y

ULTRASTRUCTURE OF PIGMENT GRANULES OF RETINAL  
EPITHELIUM\* I., COW'S EYE, AMER. J. OPHTHALMOL., 48,  
221-230, 1959.

9- 19. WELLINGS ET AL

ELECTRON MICROSCOPIC STUDIES ON THE SUBCELLULAR  
ORIGIN AND ULTRASTRUCTURE OF MELANIN GRANULES IN  
MAMMALIAN MELANOMAS, ANN. N. Y. ACAD. SCI., 100, 548-568,  
1963.

9- 20. WELLINGS ET AL

ELECTRON MICROSCOPY OF HUMAN MALIGNANT, J. NAT.  
CANCER INSTITUTE, 24, 437-462, 1960.

9- 21. WELLINGS ET AL

ROLE OF GOLGI APPARATUS IN THE FORMATION OF MELA-  
NIN GRANULES IN HUMAN MALIGNANT MELANOMA, J. ULTRA-  
STRUC. RES., 3, 147-154, 1959.

CATEGORY - 0 - MISCELLANEOUS

- 0- 1. ALPEN ET AL      EFFECTS OF HIGH INTENSITY RADIANT ENERGY ON SKIN -  
II, QUANTITATIVE DEPENDENCE OF TISSUE INJURY ON  
DURATION OF EXPOSURE, ARCH. PATH. (CHICAGO) 55,  
280-285 (1953).
- 0- 2. DAER ET AL      LIGHT SENSITIVITY IN BIOLOGIC SYSTEMS;  
PHOTOOTOXICITY AND PHOTOALLERGY RELATED TO VISIBLE  
LIGHT, FED. PROC. 24, 15-21, SUPP. 14 (1965).
- 0- 3. BLANCHARD ET AL      A CASE OF ACCIDENTAL MACULAR PHOTOCOAGULATION BY  
LASER, BULL. SOC. OPHTHAL. 64, 751-756, 1964.
- 0- 4. BLUM H F      PHOTODYNAMIC ACTION AND DISEASES CAUSED BY LIGHT,  
(HAFNER PUBLISHING COMPANY, NEW YORK, 1964).
- 0- 5. BROWN ET AL      RELATION OF THRESHOLD CRITERION TO THE FUNCTIONAL  
RECEPTORS OF THE EYE, J. OPT. SOC. AMER. 47, 198-  
204, 1957.
- 0- 6. BRUMA M S      MECHANISM FOR ENERGY TRANSFER BETWEEN A FOCUSED  
LASER BEAM AND A TRANSPARENT MEDIUM INVOLVING  
ELECTROMAGNETIC FIELD GRADIENTS. (PRESENTED AT THE  
1964 SPRING MEETING OF THE OPTICAL SOCIETY OF  
AMERICA, WASHINGTON, D.C.) APRIL 1-3, 1964 (WF 15).
- 0- 7. BUETTNER K      EFFECTS OF EXTREME HEAT AND COLD ON HUMAN SKIN -  
III, NUMERICAL ANALYSIS AND PILOT EXPERIMENTS ON  
PENETRATING FLASH RADIATION EFFECTS, J. APPL.  
PHYSIOL. 5, 207-220 (1953).
- 0- 8. BUETTNER ET AL      EYE HAZARDS FROM AN ATOMIC BOMB, SIGHTSAVING REV.  
23, 1.
- 0- 9. BURKHALTER J H      MATERIAL EFFECTS OF LASER RADIATION AND BASIC  
INTERACTION PHENOMENA, FED. PROC. 24, 531-534, 1965
- 0- 10. BURNETT W D      LASER EYE HAZARD EVALUATION, SANDIA LABORATORIES  
SC-RR-67-563, AUG. 1967.
- 0- 11. CAMPBELL F W      THE DEPTH OF FIELD OF THE HUMAN EYE, OPTICA ACTA,  
4, 157-164., 1957.
- 0- 12. CAMPBELL ET AL      THE OPTICAL MASER AS A RETINAL COAGULATOR\* AN  
EVALUATION, TRANS AMER ACAD OPHTHAL OTOLARYING  
67, 58-67 (JAN-FEB) 1963.
- 0- 13. CARONE ET AL      GENERATION OF ACOUSTIC SIGNALS IN LIQUIDS IN ROBY-  
LASER-INDUCED THERMAL STRESS TRANSIENTS, APPLIED  
PHYS. LETTERS, 4, 95-97 (15 MARCH 1964).
- 0- 14. CHAN ET AL      LIGHT COAGULATION AND INTRAOCULAR MALIGNANT

TUMORS\*AN EXPERIMENTAL STUDY, ACTA OPHTHALMOLOGICA,  
MEDICAL COLL. OF VA., RICHMOND, MARCH, 1963.

- 0- 15. CLARKE ET AL .LASER EFFECTS ON THE EYE, ARCH. ENVIRON. HEALTH,  
18, 424-427.
- 0- 16. COOGAN ET AL LASERS\* THEIR TECHNICAL, BIOLOGIC AND AIR FORCE  
IMPLICATIONS, SAM-AMR-3-68.
- 0- 17. COURNEY L S .CONVERSION OF ELECTROMAGNETIC TO ACOUSTIC ENERGY  
BY SURFACE HEATING, J. ACOUS. SOC., VOL.40, 1966
- 0- 18. CURTIN ET AL REFLECTED LASER BEAM CAUSING ACCIDENTAL BURN OF  
RETINA, AMER. J. OPHTHAL., 65, 188-189, 1968.
- 0- 19. DANIELS F JR IN THERAPEUTIC ELECTRICITY AND ULTRAVIOLET  
RADIATION, S.H. LIGHT, ED. (HAVERLY PRESS,  
BALTIMORE, 1967), PP. 372-402.
- 0- 20. DAVIES ET AL .PROCEEDINGS OF THE U.S. ARMY NITICK LAB FLASH  
BLINDNESS SYMPOSIUM, ARMED FORCES--NATIONAL  
RESEARCH COUNCIL COMMITTEE ON VISION, AD 697793  
(NATL. TECH. INFORMATION SERVICE, SPRINGFIELD,  
VA. 22151), PP. 264, 1967.
- 0- 21. DAVSON H .THE EYE, 2ND ED., VOL. 1, ACADEMIC PRESS, NEW  
YORK, N.Y., 1969.
- 0- 22. DAVSON H .THE EYE, 2ND ED., VOL. 3, ACADEMIC PRESS, NEW YORK,  
N.Y., 1969.
- 0- 23. DERR ET AL .FREE RADICAL OCCURRENCE IN SOME LASER-IRRADIATED  
BIOLOGICAL MATERIALS, FED. PROC. 24, S99-103. SUPP.  
14 (1965).
- 0- 24. DUKE-ELDER A S TEXTBOOK OF OPHTHALMOLOGY, VOL. 1, 1938, VOL. 4,  
VOL. 6, 1949, ST. LOUIS, THE C.V. MOSBY COMPANY.
- 0- 25. DUNN F .PHYSICAL MECHANISMS OF THE ACTION OF INTENSE  
ULTRASOUND ON TISSUE, AMER. J. OF PHYSICAL MED.,  
37, 148-151, 1958.
- 0- 26. ECCLES ET AL EXPERIMENTAL PHOTO-RETINITIS, MED. J. AUSTRALIA 1,  
339-342,
- 0- 27. EL HAGE ET AL .J. OPT. SOC. AM., VOL. 63, P. 205, 1973
- 0- 28. ENOCH ET AL PHYSICAL AND OPTICAL CHANGES IN EXCISED RETINAL  
TISSUE, INVEST. OPHTH., VOL. 5, PP. 208-221  
(1966).
- 0- 29. EVERETT D RICKE THRESHOLD DISTANCES FOR RETINAL BURNS FROM LOW-  
YIELD NUCLEAR DETONATIONS, SCHOOL OF AEROSPACE  
MEDICINE, AEROSPACE MEDICAL DIVISION (AFSC),  
BROOKS AIR FORCE BASE, TEXAS.
- 0- 30. FANKHAUSER ET AL METHODS OF PHOTOCOAGULATION THROUGH THE GOLDMANN

CONTACT GLASS, MOD. OPHTHAL., 7, 256-272, 1968.

0- 31. FARRER ET AL

THE EFFECT OF THRESHOLD MACULAR LESIONS AND SUB-THRESHOLD MACULAR EXPOSURES ON VISUAL ACUITY IN THE RHESUS MONKEY, SUBMITTED FOR PUBLICATION IN THE JOURNAL OF AMERICAN INDUSTRIAL HYGIENE ASSOCIATION, 1969.

0- 32. FARRER ET AL

VISUAL ACUITY IN MONKEYS, VISION RES., 7, 745 (1967).

0- 33. FINE ET AL

BIOLOGICAL EFFECTS OF LASER RADIATION. IN ADVANCES IN BIOLOGICAL AND MEDICAL PHYSICS, VOL. 10, PP. 149-226. NEW YORK: ACADEMIC PRESS, 1965.

0- 34. FINE ET AL

HAZARDS & PROTECTIVE DEVICES ASSOCIATED WITH 10.6 MU RADIATION, PROC. 20TH ANNUAL CONFERENCE ON ENGG. IN MEDICINE AND BIOLOGY, BOSTON, MASSACHUSETTES, NOV. 13-16, 1967, P. 52.

0- 35. FINE ET AL

INTERACTION OF LASER RADIATION WITH BIOLOGICAL SYSTEMS. I. STUDIES ON INTERACTION WITH TISSUES, FED PROC. 24, 35-45, SUPP. 14 (1965).

0- 36. FINE ET AL

LASER IRRADIATION OF BIOLOGICAL SYSTEMS, IEEE SPECTRUM, 1, 81-90.

0- 37. FINE ET AL

MECHANISMS AND CONTROL OF LASER HAZARDS AND MANAGEMENT OF ACCIDENTS. PROC 2ND CONFERENCE ON LASER TECHNOLOGY, ILL. INSTITUTE OF TECH. CHICAGO, ILL., APR. 1965.

0- 38. FINE ET AL

MULLER'S CELLS AND THE MIDDLE LIMITING MEMBRANE OF THE HUMAN RETINA\* AN ELECTRON MICROSCOPIC STUDY, IN VEST. OPHTHAL., 1, 304, 1962.

0- 39. FLYNN A J

PHOTO-RETINITIS IN ANTI-AIRCRAFT LOOKOUTS, MED. J. AUSTRALIA, 2, 400.

0- 40. FREEMAN ET AL

AN EVALUATION OF THE RUBY LASER AS A RETINAL COAGULATING SOURCE, ANN. N.Y. ACADE. SCI., 122, 783-789, 1965.

0- 41. GAYDON A G

COLOR SENSATIONS PRODUCED BY ULTRAVIOLET LIGHT, PROC. PHYS. SOC., 50, 714-720, 1938.

0- 42. GEERAETS W J

IN LASER EYE EFFECTS, H.G. SPERLING, ED., ARMED FORCES - NATIONAL RESEARCH COUNCIL COMMITTEE ON VISION, AD 667-494 (NATL. TECH. INFORMATION SERVICE, SPRINGFIELD, VA. 22515), 1968.

0- 43. GEERAETS ET AL

ENZYME ACTIVITY IN THE COAGULATED RETINA\* A MEANS OF STUDYING THERMAL CONDUCTION AS A FUNCTION OF EXPOSURE TIME, ACTA OPHTHAL. (COPENHAGEN) SUPPL. 76, 79-93 (1963)

0- 44. GOLDMAN L

DERMATOLOGIC MANIFESTATIONS OF LASER RADIATION, FED. PROC. 24, S92-93, SUPP. 14 1965.



- 0- 45. GOLONAN ET AL LASER RADIATION OF MALIGNANCY IN MAN; CANCER, 18,533-545 (1965).
- 0- 46. GOODEVE ET AL THE PHOTSENSITIVITY OF VISUAL PURPLE SOLUTIONS & THE SCOTOPIC SENSITIVITY OF THE EYE IN THE ULTRA-VIOLET, PROC. R. SOC. B., 130,380-395, 1942.
- 0- 47. GORDON ET AL THE MASER-NEW TYPE OF AMPLIFIER, FREQUENCY STANDARD, AND SPECTROMETER, PHYS. REV., 99,1264-74.
- 0- 48. GOURNAY L S .CONVERSION OF ELECTROMAGNETIC TO ACOUSTIC ENERGY BY SURFACE HEATING, THE JOURNAL OF THE ACOUSTICAL SOCIETY OF AMERICA, VOL. 40, NO. 6, P. 1322-1330, 1966.
- 0- 49. GRAHAM ET AL VISION AND VISUAL PERCEPTION, WILEY AND SONS, NEW YORK (1966).
- 0- 50. GRIFFITH ET AL LIGHT AND ELECTRON MICROSCOPIC OBSERVATIONS IN A SUPERFICIAL CORNEAL DYSTROPHY\* PROBABLE EARLY REISBUCKLESI TYPE, AMER. J. OPHTHAL., 63, 1659, 1967.
- 0- 51. GUERRY ET AL .PHOTOCOAGULATION OF THE RETINA\* REPORT ON A SUCCESSFULLY TREATED CASE OF ANGIOMATOSIS RETINAE, AM. J. OPHTH., 46, 463., 1958.
- 0- 52. HAM ET AL .FLASHBURNS IN THE RABBIT RETINA, AM. J. OPHTH., 46, 700-723., 1958.
- 0- 53. HAM ET AL .OCULAR EFFECTS OF LASER RADIATION, PART 1, DASA REPORT 1574, 1964.
- 0- 54. HAM ET AL .OCULAR HAZARDS FROM LASER RADIATION, SYMPOSIUM ON THE PHYSIOLOGICAL AND BIOLOGICAL ASPECTS OF LASER RADIATION, 1 APRIL 1964, OPTICAL SOC. AM., WASHINGTON, D.C. (TO BE PUBLISHED) AND FED. PROC. 24, 5-97 (1965).
- 0- 55. HAM ET AL OPTICAL MASERS (LASERS), ACTA OPHTHALMOLOGICA, SUPPL. 76, 60 (1963).
- 0- 56. HAM ET AL STATEMENT BEFORE SPECIAL SUBCOMMITTEE ON RADIATION, JOINT COMMITTEE ON ATOMIC ENERGY, CONGRESS OF THE U.S. UNITED STATES GOVT. PRINTING OFFICE, PP. 248-249, WASHINGTON, D.C..
- 0- 57. HELSPER ET AL THE SYNERGISTIC EFFECT OF LASER RADIATION AND IONIZING RADIATION ON MALIGNANT TUMORS IN VIVO AND IN VITRO. AMER. J. ROENTGEN. 99, 446-449 (1967).
- 0- 58. HELWIG ET AL ANATOMICAL AND HISTOCHEMICAL CHANGES IN SKIN AFTER LASER IRRADIATION, FED. PROC., 24, 583-91, SUPP. 14, (1965).
- 0- 59. HESS ET AL .MESSENDE UNTERSUCHUNGEN UBER DIE GELBFÄRBUNG DER MENSCHLICHEN LINSE UND UBER IHREN EINFLUSS

AUF DAS SEHEN, ARCH. F. AUGENHEILK. 63, 164-166, 1909.

- 0- 60. HU C L ET AL THE THERMAL-CHEMICAL DAMAGE IN BIOLOGICAL MATERIAL UNDER LASER IRRADIATION, IEEE TRANS. BIOMED. ENG. 17, 3, 220 (1970)
- 0- 61. IRVINE ET AL .ICARUS, VOL. 5, P. 324, 1968.
- 0- 62. JACOBSON H EFFECT OF THERMAL ENERGY ON RETINAL FUNCTION, AMRL-DR-62-96, 6573TH AEROSPACE MEDICAL RESEARCH LABORATORIES, AEROSPACE MEDICAL DIVISION, WRIGHT-PATTERSON AIR FORCE BASE, OHIO, AUGUST, 1962.
- 0- 63. JAKUS M A FURTHER OBSERVATIONS ON THE FINE STRUCTURE OF THE CORNEA, INVEST. OPHTHAL., 1, 202, 1962.
- 0- 64. JONES R C ON THE THEORY OF THE DIRECTIONAL PATTERNS OF CONTINUOUS SOURCE DISTRIBUTIONS ON A PLANE SURFACE, J. OPT. SOC. AM., 16, 147 (1945).
- 0- 65. JONES ET AL LASER RADIATION EFFECTS ON THE MORPHOLOGY AND FUNCTION OF OCULAR TISSUE, SECOND ANNUAL REP. OADA-17-67-C-0019 (1968).
- 0- 66. JONES ET AL ON THE INFLUENCE OF THE REGION OF THE RETINA ON THE VISUAL ACUITY, J. OPT. SOC. AM., 37, 217 (1947).
- 0- 67. JONES ET AL .PHOTOGRAPHIC GRANULARITY AND GRAININESS, SOME CHARACTERISTICS OF THE VISUAL SYSTEM OF IMPORTANCE IN THE EVALUATION OF GRAININESS AND GRANULARITY, JOURNAL OF OPTICAL SOCIETY OF AMERICA, VOL. 37, NO. 4, APRIL, 1947.
- 0- 68. KETCHAM ET AL LASER RADIATION AS A CLINICAL TOOL IN CANCER THERAPY, FED. PROC., 24, S159-160, SUPP. 14 (1965).
- 0- 69. KINGSLAKE R APPLIED OPTICS AND OPTICAL ENGINEERING, VOL. IV, PART I, CHAP. 8 (RADIOMETRY BY F. E. NICODRUS), ACADEMIC PRESS, NEW YORK (1967).
- 0- 70. KLEIN ET AL INTERACTION OF LASER RADIATION WITH BIOLOGIC SYSTEMS. II., EXPERIMENTAL TUMORS, FED. PROC. 24, S-143-149, SUPP. 14 (1965).
- 0- 71. KLEIN ET AL .INTERACTION OF LASER RADIATION WITH BIOLOGIC SYSTEMS. III., STUDIES ON BIOLOGICAL SYSTEMS IN VITRO, FED. PROC. 24, S-104-110, 1966.
- 0- 72. KURABARA ET AL RETINAL DAMAGE BY VISIBLE LIGHT\* AN ELECTRON MICROSCOPIC STUDY, ARCH OPHTHAL 79, 69-78 (JAN) 1968.
- 0- 73. LAOR Y ET AL THE PATHOLOGY OF LASER RADIATION OF THE SKIN AND BODY WALL OF THE MOUSE. AMER. J. PATH., 47, 643-664 (1965).

- 0- 74. LEACH W M BIOLOGICAL ASPECTS OF ULTRAVIOLET RADIATION, A REVIEW OF HAZARDS RPH/DBE 70-5 (U.S. PUBLIC HEALTH SERVICE, BUREAU OF RADIOLOGICAL HEALTH, ROCKVILLE, MARYLAND, SEPT. 1970.)
- 0- 75. LENGVEL B A INTRODUCTION TO LASER PHYSICS, NEW YORK, JOHN WILEY AND SONS, 1967.
- 0- 76. LUTNAR W J. OPT. SOC. AM., VOL.61, P.1522, 1971
- 0- 77. MACKEEN ET AL LASER FOCUS 7(4), 29 (1971).
- 0- 78. MAINMAN T H STIMULATED OPTICAL RADIATION IN RUBY, NATURE 187, 493-4., 1959.
- 0- 79. MAINSTER M A DESTRUCTIVE LIGHT ADAPTATION, ANN. OPHTHAL., 2, 44 (1970).
- 0- 80. MAKADUS ET AL EFFECTS OF LASERS ON THE HUMAN EYE, JOURNAL, MAY 1968, PP. 257-271.
- 0- 81. MANDELBAUM ETAL PERIPHERAL VISUAL ACUITY, AM. J. OPHTHALMOLOGY, 30, 581 (1947).
- 0- 82. MCGUFF P E COMPARATIVE EFFECTS OF LASER AND/OR IONIZING RADIATION ON EXPERIMENTAL MALIGNANT TUMORS WITH REPORT OF SYNERGISTIC TUMORICIDAL EFFECT OF COMBINED LASER AND IONIZING RADIATION, ANN. BIOMEDICAL LASER CONFERENCE, 1ST, BOSTON, MASS., JUNE 1965.
- 0- 83. MCNEER K ET AL ELECTRORETINOGRAPHY AFTER LIGHT COAGULATION, ACTA OPHTHAL., (COPENHAVEN) SUPPL. 76, 94-100 (1963).
- 0- 84. MENDELSON ET AL STUDY OF BIOLOGICALLY INSIGNIFICANT FORCES FOLLOWING LASER IRRADIATION, FED. PROC. 24, S111-115, SUPP. 14 (1965).
- 0- 85. MEYER ET AL LIGHT COAGULATION, ST. LOUIS, THE C.V. MOSBY COMPANY, 1960.
- 0- 86. MILLER N D POSITIVE AFTERIMAGE AS A BACKGROUND LUMINANCE, J. OPT. SOC. AM., 56, 1616-1620, 1966.
- 0- 87. MILLER N D POSITIVE AFTERIMAGE FOLLOWING BRIEF HIGH INTENSITY FLASHES, J. OPT. SOC. AM., 56, 802-806, 1966.
- 0- 88. MILLER N D VISUAL RECOVERY FROM BRIEF EXPOSURES OF HIGH LUMINANCE, J. OPT. SOC. AM., 55, 1661-1669, 1965.
- 0- 89. MILLER N D VISUAL RECOVERY FROM HIGH INTENSITY FLASHES, ANNUAL PHASE REPORT, USAF CONTRACT AF41(609)-2426, JULY 1965.
- 0- 90. MINION ET AL UNCOLYSIS WITH LASER ENERGY COMBINED WITH CHEMOTHERAPY, NATURE (LONDON), 207, 140 (1965).
- 0- 91. MIRELS ET AL POWER AND EFFICIENCY OF A CONTINUOUS RF CHEMICAL

LASER, IEEE JOURNAL OF QUANTUM ELECTRONICS, QE-7, NO. 11, 501-507, 1971.

0- 92. NEWELL F W

INDUSTRIAL AND TRAUMATIC OPHTHALMOLOGY, A.H. KEENEY ET AL., EDS. (C.V. MOSBY COMPANY, SAINT LOUIS, 1964), PP. 158-187.

0- 93. NORTON ET AL

FLUORESCIN FUNDUS PHOTOGRAPHY: AN AID IN THE DIFFERENTIAL DIAGNOSIS OF POSTERIOR OCULAR LESIONS, TRANS. AMER. ACAD. OPHTHAL. OTOLARYNG., 68, 755-765, 1964.

0- 94. PALMER ET AL

J. OPT. SOC. AM., VOL. 64, P. 1107, 1974

0- 95. PARSONS JH

DISEASES OF THE EYE, MACMILLAN CO., 10TH ED., NEW YORK, N.Y., 1942.

0- 96. PEACOCK G R

SPOT SIZE AND BEAM PARAMETERS IN FUNDAMENTAL MODE LASER BEAMS, US ARMY MED. RES. LAB. REPORT 774, FORT KNOX, KENTUCKY, 1968.

0- 97. PONDER E

MEDICAL PHYSICS, VOL. 1, 597, ED. O. GLASSER, 1943 (CHICAGO, THE YEARBOOK PUBLISHERS, INC.)

0- 98. RATHKEY A S

ACCIDENTAL LASER BURN OF THE MACULA, ARCH. OPHTHAL., 74, 346-348, 1965.

0- 99. RICHNEY E O

PREDICTION OF EYE SAFE SEPARATION DISTANCES, PRESENTED AT AGARD SYMPOSIUM ON LOSS OF VISION FROM HIGH INTENSITY LIGHT, PARIS, FRANCE, MARCH 1966.

0-100. KITLER U L

THE SUN'S RETINA-BURNING POWER IN SPACE, PRESENTED AT THE SPACE MEDICAL SYMPOSIUM OF THE ELEVENTH INTERNATIONAL ASTRONAUTICAL CONGRESS, STOCKHOLM, AUG. 15-20, 1960.

0-101. ROSAN R C ET AL

CURRENT PROBLEMS IN LASER MICROPROBE ANALYSIS, FED. PROC., 24, S126-128, SUPP. 14 (1965).

0-102. ROUNDS ET AL

LASER RADIATION OF TISSUE CULTURE, ANN. N.Y. ACAD. SCI., 122, 713-727, ART. 2 (1965).

0-103. ROUNDS ET AL

THE POTENTIATION OF GAMMA RADIATION WITH ENERGY FROM A RUBY LASER, SAM-TR-65-41, JUNE 1965.

0-104. SALZMANN H

THE ANATOMY AND HISTOLOGY OF THE HUMAN EYEBALL, (UNIV. OF CHICAGO PRESS, CHICAGO, 1912), PP. 61-62.

0-105. SCHAWLOW ET AL

INFRARED AND OPTICAL MASERS, PHYS. REV., 112, 1940-49 (1958).

0-106. SHERMAN ET AL

THE APPLICATION OF LASER FOR THE SPECTROCHEMICAL ANALYSIS OF CALCIFIED TISSUES, ANN. N.Y. ACAD. SCI., 122, 767-772, ART. 2 (1965).

0-107. SLINNEY D H

IN LASER APPLICATIONS IN MEDICINE AND BIOLOGY, M.L. FOLBARSHT, ED. (PLENUM PRESS, NEW YORK,

- 1971), PP. 163-238.
- 0-108. SOLON ET AL. PHYSIOLOGICAL IMPLICATIONS OF LASER BEAMS, SCIENCE, 134, 1506-8 (10 NOV. 1961).
- 0-109. SPENCER ET AL. CONTINUOUS WAVE CHEMICAL LASERS, INT. J. CHEM. KINET., 1, 493-494, 1969.
- 0-110. SPENCER ET AL. PRELIMINARY PERFORMANCE OF A CONTINUOUS WAVE CHEMICAL LASER, APP. PHYS. LETTERS, 10, 6, 235-237, 1970.
- 0-111. SPIZNAS ET AL. OTHER SEGMENTS OF PHOTORECEPTORS AND THE RETINAL PIGMENT EPITHELIUM- INTERRELATIONSHIP IN HUMAN EYE ARCH. OPHTHAL., 84, 810-819, 1970.
- 0-112. STEIN ET AL. MEASUREMENT OF RETINAL IMAGE FOR LASER RADIATION IN RHESUS MONKEY, FINAL REPORT, FA1609-68-C-0038, EYE RESEARCH FOUNDATION OF BETHESDA, BETHESDA, MD (1970).
- 0-113. STREHLER B L. ON THE HISTOCHEMISTRY AND ULTRASTRUCTURE OF AGE PIGMENT - IN ADVANCES IN GERONTOLOGICAL RESEARCH, VOL. I, (B.L. STREHLER, ED.), 343-384, ACADEMIC PRESS, NEW YORK AND LONDON, 1964.
- 0-114. TAN K E W P. VISION IN THE ULTRAVIOLET, DRUKKERIJ ELINKWIJK-UTRECHT, 1971.
- 0-115. TENGROTH ET AL. LASER ACTION ON THE HUMAN EYE, ACTA OPHTHAL., 41, 595, 1963.
- 0-116. TIERHUNE R W. NON-LINEAR OPTICS, SOLID STATE DESIGN, 4, 38-46, 1963.
- 0-117. URBACH F. THE BIOLOGIC EFFECTS OF ULTRAVIOLET RADIATION (PERGAMON PRESS, NEW YORK, 1969), PP. 83-84, 327-436, 541-654.
- 0-118. VAN MEETEREN A. OPTICA ACTA, VOL. 21, P. 395, 1974.
- 0-119. VASSILIADIS A. IN LASER APPLICATIONS IN MEDICINE AND BIOLOGY, M.L. WOLHARSH, ED. (PLENUM PRESS, NEW YORK, 1971), PP. 125-162.
- 0-120. VASSILIADISE ET AL. INVESTIGATION OF RETINAL DAMAGE USING A Q-SWITCHED RUBY LASER, TECHNICAL REP., AIR FORCE AVIONICS LAB., AF33(615-5060), WRIGHT PATTERSON AIR FORCE BASE, OHIO, AUGUST, 1966.
- 0-121. VASSILIADISE ET AL. INVESTIGATION OF RETINAL HAZARD DUE TO PULSED XENON LAMP RADIATION, (STANFORD RESEARCH INSTITUTE, MENLO PARK, CALIF., 1970.)
- 0-122. VERHOEFF ET AL. THE PATHOLOGICAL EFFECTS OF RADIANT ENERGY ON THE EYE, PROC. AM. ACAD. ARTS & SCI., 51, 630-759, 1916.
- 0-123. VOS ET AL. SOME REFLECTIONS ON THE DANGER OF AND THE PROTECTION AGAINST NUCLEAR FLASHBLINDNESS AND RETINAL

BURNS, REPORT NO. IZF 1964-25, INSTITUTE FOR PER-  
CEPTION, KVO-IND (AD 456-728), 1966.

- 0-124. WALD AND GRIFFI J. OPT. SOC. AM., VOL.37, P.321, 1947
- 0-125. WALKER A M THE PATHOLOGICAL EFFECTS OF RADIANT ENERGY ON THE  
EYE\* A SYSTEMATIC REVIEW OF THE LITERATURE, PROC.  
AM. ACAD. ARTS & SCI., 51,760-817., 1916.
- 0-126. WEYMOUTH ET AL VISUAL ACUITY WITHIN THE AREA CENTRALIS AND ITS  
RELATION TO EYE MOVEMENTS AND FIXATION, AM. J.  
OPHTHALMOL., 11, 947 (1928).
- 0-127. WOLFF E ANATOMY OF THE EYE AND ORBIT (W.B. SAUNDERS COM-  
PANY, PHILADELPHIA, 1968), 6TH ED., CH. 2, PP.  
105-109.
- 0-128. WRIGHT W D .THE VISUAL SENSITIVITY OF NORMAL AND APHAKIC  
OBSERVERS IN THE ULTRA-VIOLET, ANN. PSYCHOL., 50,  
169-177, 1951.
- 0-129. ZWENG H C ACCIDENTAL M-SWITCHED LASER LESION OF HUMAN MACULA  
ARCH. OPHTHAL., 78, 596-599, 1967.
- 0-130. ZWENG ET AL CLINICAL EXPERIENCES WITH LASER PHOTOCOAGULATION,  
FED. PROC., 24, 565-70, SUPP. 14 (1965).
- 0-131. ----- AMERICAN CONFERENCE OF GOVERNMENTAL INDUSTRIAL  
HYGIENISTS, THRESHOLD LIMIT VALUES OF PHYSICAL  
AGENTS ADOPTED BY ACGIH FOR 1971 (ACGIH, BOX 1937,  
CINCINNATI, OHIO, 1971).
- 0-132. ----- LASER HEALTH HAZARDS CONTROL, AFM 161-H, U.S. DE-  
PARTMENT OF THE AIR FORCE, WASHINGTON, D.C., APRIL  
1969 AND SEPT. 1971.
- 0-133. ----- .LASERS\* THEIR TECHNICAL, BIOLOGIC, AND AIR FORCE  
IMPLICATIONS, AEROMEDICAL REVIEWS, 3-68, USAF  
SCHOOL OF AEROSPACE MEDICINE, BAFB, TEXAS, 1968.
- 0-134. ----- PAPERS READ BEFORE THE SECOND INTERNATIONAL LASER  
SAFETY CONFERENCE AND WORKSHOPS, CINCINNATI, MARCH  
24-25, 1969, ARCH. ENV. HEALTH, VOL.20, NO. 2,  
PP. 145-211, (FEBRUARY, 1970).
- 0-135. ----- PHOTOCOAGULATION THROUGH THE GOLDMANN CONTACT  
GLASS\* III, CLINICAL EXPERIENCE WITH AN APPARATUS  
USING A QUASI-CONTINUOUS LASER SOURCE, IBID., 664-  
696.
- 0-136. ----- PROCEEDINGS OF THE FIRST CONFERENCE ON LASER  
SAFETY, MARTIN COMPANY, ORLANDO, FLA., MAY 1966.
- 0-137. ----- SAFE USE OF LASERS, PROPOSED STANDARD Z-136 (AMER-  
ICAN NATIONAL STANDARDS INSTITUTE, NEW YORK 1972).